ERDC/CERL TR-15-16

US Army Corps
of Engineers®
Engineer Research and
Development Center

ERDC
INNOVATIVE SOLUTIONS
for a safer, better world

Basic Research in Military Construction

Development of Cold-Formed Steel Seismic Design Recommendations

James Wilcoski and Douglas A. Foutch

August 2015

Construction Engineering
Research Laboratory

The U.S. Army Engineer Research and Development Center (ERDC) solves the nation's toughest engineering and environmental challenges. ERDC develops innovative solutions in civil and military engineering, geospatial sciences, water resources, and environmental sciences for the Army, the Department of Defense, civilian agencies, and our nation's public good. Find out more at www.erdc.usace.army.mil.

To search for other technical reports published by ERDC, visit the ERDC online library at http://acwc.sdp.sirsi.net/client/default.

ERDC/CERL TR-15-16
August 2015

Development of Cold-Formed Steel Seismic Design Recommendations

James Wilcoski

Construction Engineering Research Laboratory
U.S. Army Engineer Research and Development Center
2902 Newmark Drive
Champaign, IL 61822

Douglas A. Foutch

Department of Civil and Environmental Engineering
University of Illinois at Urbana-Champaign
Urbana, IL 61801

Final report

Prepared for U.S. Army Corps of Engineers
Washington, DC 20314-1000

Under Project CFM-E021, "Inelastic Response Characterization of Building Systems"

Abstract

Cold-formed steel-wall construction is a versatile and affordable technology used extensively as the gravity- and lateral-load-resisting structural system for low-rise construction. Structural design guidance for cold-formed steel members was first published in 1946, but in the 1990s the Corps of Engineers imposed a moratorium on its own use of these systems after identifying detailing and construction practices that would prevent adequate ductile performance under seismic loading. At that time, the Corps initiated the first of several applied engineering and basic research studies to investigate light-gage steel design and construction methods that provide the required ductility while conforming with applicable steel-industry specifications. That research produced design guidelines that enabled the Corps to lift its moratorium, including two updates incorporating the results of follow-on studies.

This technical report, prepared with funding support from the National Institute of Standards and Technology, compiles for the first time the complete results of three Army Research, Development, Test, and Evaluation studies on cold-formed steel design and validation. The report includes detailed, updated design recommendations for ductile structural performance in seismic events and a sample design problem to illustrate application of the recommendations.

Contents

Figures and Tables

Figures

Tables

Preface

The research documented in this report was executed for Headquarters, U.S. Army Corps of Engineers (HQUSACE) under three Corps Research, Development, Test, and Evaluation (RDTE) projects:

- "Cold-Formed Steel Seismic Design Guidance" (approach and prototype shear panels), under Program Element 40162784AT41, "Military Facilities Engineering Technology"
- "Improved Cold-Formed Steel Seismic Design" (additional panel configuration and improved anchorage details), under Program Element 40162784AT41, "Military Facilities Engineering Technology"
- "Inelastic Response Characterization of Building Systems" (shake table model verification), under Program Element 611102T23, "Basic Research in Military Construction"

The compilation of results from these three projects as a comprehensive Technical Report was funded under an interagency agreement with the National Institute of Standards and Technology (NIST) under the project entitled "TechBrief Series 2013: Seismic Design of Cold-Formed Steel Shear Panels for Use in Low-Rise Construction." The HQUSACE technical monitors were Charles H. Gutberlet Jr., currently at CETAC-EC-TF; and Peter J. Rossbach, CECW-EI. The NIST Project Manager was Dr. John R. Hayes, with assistance from Steven McCabe.

The work was performed by the Materials and Structures Branch of the Facilities Division (CEERD-CFM), U.S. Army Engineer Research and Development Center, Construction Engineering Research Laboratory (ERDC-CERL). At the time of publication, Vicki L. Van Blaricum was Chief, CEERD-CFM; Michelle J. Hanson was Acting Chief, CEERD-CF; and Kurt Kinnevan (CEERD-CVT) was the Technical Director for Adaptive and Resilient Installations. The Deputy Director of ERDC-CERL was Dr. Kirankumar Topudurti and the Director was Dr. Ilker Adiguzel.

The authors express their appreciation to Patrick D. Lindsey, CENWO-ED-SH, whose background in cold-formed steel construction was critical to the development of test panel configurations. Mr. Lindsey and his staff also developed test panel drawings. The authors also express their apprecia-

tion to Gregory Ralph, Randy Daudet, and Thomas Lawson of Dietrich Industries and Dietrich Design Group, who donated materials for all test panels and offered guidance for practical anchorage configurations. Appreciation is expressed to Jay W. Larson, formerly with Bethlehem Steel Corporation and currently the director of construction standards with the American Iron and Steel Institute, for providing information on the material properties of ASTM A653 steel reported in Chapter 4. Appreciation is expressed to Hank Martin and others with the AISI Committee on Framing Standards, who have reviewed portions of this report. Appreciation is also expressed to Dr. Hayes who, while employed at ERDC-CERL, provided numerous informal reviews of portions of this work and, as manager of the ERDC-CERL seismic program, led several program-review meetings.

The Acting Commander of ERDC was LTC John T. Tucker III, and the Director was Dr. Jeffery P. Holland.

Unit Conversion Factors

Multiply	By	To Obtain
feet	0.3048	meters
cubic inches	1.6387064 E-05	cubic meters
inches	0.0254	meters
microinches	0.0254	micrometers
pounds (force) per square inch	6.894757	kilopascals
square inches	6.4516 E-04	square meters

PART I:
INTRODUCTION
AND
DESIGN RECOMMENDATION
DEVELOPMENT PROCESS

1 Introduction

1.1 Background

Cold-formed steel partition-wall construction first emerged as a replacement for wood stud-wall construction. It is now being used extensively as the gravity- and lateral-load-resisting structural system for low-rise construction. The American Iron and Steel Institute (AISI) has published structural design guidance for cold-formed steel members. The first specification was adopted in 1946. The current specification, AISI S100-07 (AISI 2007), includes seven parts: A–General Provisions; B–Elements; C–Members; D–Structural Assemblies and Systems; E–Connections and Joints; F–Tests for Special Cases; and G–Design of Cold-Formed Steel Structural Members and Connections for Cyclic Loading (Fatigue). Section A2.3 presents steel ductility requirements; these are material requirements only, where the ratio of tensile to yield strength, $F_u/F_y \geq 1.08$, and total elongation must be at least 10% for a 2 in. gage length and 7% for an 8 in. gage length, based on coupon tests. However, the AISI specification does not include guidance to ensure that the structural system provides adequate ductility. ASCE/SEI 7-10 (ASCE 2010) gives a response-modification coefficient, R, of 6.5 for bearing wall systems, light-framed (cold-formed steel) walls sheathed with wood structural panels rated for shear resistance or steel sheets, and a value of 4 for light-framed (cold-formed steel) wall systems using flat-strap bracing. For building frame systems, light-framed (cold-formed steel) walls sheathed with wood structural panels rated for shear resistance or steel sheets, the R value is even greater, at 7. This coefficient represents the inherent over-strength, global ductility capacity, redundancy, and energy-dissipation capacity of lateral-force-resisting systems (ATC 1995, 1997). Seismically induced lateral loads are divided by this coefficient, recognizing the structure's ability to continue resisting lateral loads after yielding. Therefore, the structural system must be proportioned and detailed to ensure such a ductile response.

The U.S. Army Corps of Engineers (USACE) has observed detailing and construction practices in cold-formed steel construction that would prevent adequate ductile performance under seismic loading. Consequently, the Corps imposed a moratorium on using cold-formed steel as the primary structural system in its own construction projects. However, because cold-formed steel construction is a cost-effective approach, Headquarters,

USACE, initiated an engineering study to investigate methods of cold-formed steel design and construction that will provide the required ductility. The results of that study led directly to the preparation of seismic design specifications and details for constructing shear wall panels using cold-formed steel. The first version of these ERDC-CERL design recommendations were published in 1998 in a document entitled *Design of Cold-Formed Load Bearing Steel Systems and Masonry Veneer/Steel Stud Walls* (TI 809-07, USACE 1998). Subsequently, that publication was updated with supporting studies and disseminated in two more forms. The issuance of those documents provided crucial design information that enabled the Corps to end the moratorium on cold-formed steel construction in its own projects.

The Corps of Engineers has withdrawn TI 809-07 and its successor documents in keeping with its practice of using established industry standards where feasible. However, complete documentation of the multi-year cold-formed steel studies executed for the Corps has never before been integrated and interpreted in a single ERDC-CERL technical report. This report presents in its entirety for the first time a fully updated edition of ERDC-CERL seismic design recommendations for cold-formed steel construction, including a design philosophy for ductile performance in seismic loading and complete details of all research supporting the development of the design recommendations.

1.2 Issues in cold-formed steel design and research studies

Seismic design with cold-formed steel has two problems that are inherent in the material itself: (1) its light gage thickness and (2) its strength variability. The general objective of seismic design guidance is to assure ductile building system performance in a large seismic event and elastic response in a small event or wind loading. Ductile building performance requires that selected ductile components yield while carrying loads and absorbing energy through significant plastic response. At the same time, potentially brittle failure modes, such as column buckling or connection failure, must be prevented.

The design challenge for cold-formed steel is to specify that building components—in particular, shear panel components—be proportioned relative to each other and detailed such that the ductile response is assured. In Corps CFS design, this challenge is met by designing the diagonal straps to

yield and respond plastically through significant displacement in order to avoid damaging brittle connections or causing the buckling of columns.

The U.S. Army Engineer Research and Development Center, Construction Engineering Research Laboratory (ERDC-CERL) was tasked by HQUSACE to perform a comprehensive investigation for the purpose of developing, refining, and validating design guidance for cold-formed steel structures that ensures ductile performance in response to anticipated seismic loads.

1.2.1 Previous studies

Two papers documenting effective thin shear wall ductile behavior were reviewed for the present study. Both are summarized below.

A paper by Caccese, Elgaaly, and Chen (1993) claims that "tremendous post-buckling strength can be achieved in a thin plate that is restrained at its boundaries and subjected to in-plane shear."[1] Their experimental study varied two parameters: panel thickness and beam-to-column connection (moment or shear-type). Six quarter-scale specimens were tested with panel thickness ranging from 0.0299 to 0.1046 in. The panel slenderness ratios (width/thickness) varied from 1639 to 468. The test specimens were loaded cyclically with a single in-plane horizontal load (i.e., no vertical loading) at the top of the shear wall. Three panels included moment-resisting beam/column connections, and two included shear beam/column connections. The type of beam/column connection had very little influence because the infill plate was continuously welded to the beams and columns, causing the shear connection to act as a moment-resisting connection. The inelastic behavior of thin plate panels is primarily controlled by the yielding of the plates (formation of a diagonal tension field), whereas the behavior of the heavier plate panels is controlled by the column response. Earlier seismic design guidance had required that steel plate shear walls be designed not to buckle, which heavily loads and fails the columns well before the plate optimal capacity can be developed. In fact, the test results imply that panel performance significantly improves if the thin sheet is designed to allow buckling and the formation of a diagonal tension field. Optimal performance is achieved when the sheet is allowed to buckle, yield, and form the diagonal tension field cyclically, ab-

[1] A companion paper in the same journal (Elgaaly, Caccese, and Du 1993) presents mathematical models for nonlinear cyclic and dynamic finite element analysis of these panel systems.

sorbing energy hysteretically, thereby reducing amplification of building response and justifying design guidance based on acceptable R coefficients. This type of guidance will prevent more brittle connection and frame member failures while reducing amplified building response. Caccese, Elgaaly, and Chen (1993) conclude that a building could be designed using thin steel-plate shear walls so it will respond elastically to minor seismic events or high winds. Then when subjected to a severe seismic event, thin plate walls would buckle, develop the tension field, absorb energy, and protect the building gravity-load-resisting system from collapse.

Another paper documenting related work (Driver et al. 1998a[2]) describes an experimental study of a single 50% scale, four-story single-bay steel plate shear wall specimen. Infill panel thickness was 0.189 in. in the bottom two stories and 0.134 in. in the top two stories. The panel slenderness ratio in the bottom stories was 635. The specimen had moment-resisting beam-to-column connections. Gravity loads were applied at the top of the wall and equal cyclic in-plane horizontal loads were applied at each floor level. Deflections in the bottom story reached nine times the yield deflection (ductility of 9) after 20 cycles of inelastic deflections. First yielding (δ_y) occurred at 0.33 in. at the boundary of the infill plate, as well as visible buckling. The first tear occurred at 1.00 in. ($3\delta_y$) in a weld at the corner of the infill panel, but this tear did not propagate in subsequent cycles. At 1.33 in. ($4\delta_y$), local buckling occurred at the interior column flanges of the first-floor beam/column connection and at an outside flange at the base of a column. At 1.66 in. ($5\delta_y$), tears as large as 4.7 in. were seen at the top corners of the bottom panel, and these tears propagated in subsequent cycles. In this cycle, the peak maximum base shear or ultimate capacity of the panel system was reached, and the load-carrying capacity decreased gradually with each cycle of increased deflection. This shear wall system was able to maintain capacity at least up to a ductility of 5 ($5\delta_y$). Load/deflection curves from these tests show excellent hysteretic energy-dissipating performance, with very limited pinching, at deflections as great as nine times the yield deflection. This lack of pinching is primarily due to the effectiveness of the moment frame in sustaining loads when the panel tension field is unloaded. The hysteresis envelopes demonstrate this panel is both very ductile and stable, with no sudden loss of stiffness until final

[2] A companion paper in the same journal (Driver et al. 1998b) describes the development of analytical tools for predicting the behavior of steel plate shear walls.

failure. The ability of this panel to sustain damage but maintain load by redistributing forces to other parts of the system provides excellent redundancy and hysteretic energy dissipation that will effectively prevent building collapse in very severe seismic motions. However, if failures of connections seen in these panels had occurred in cold-formed steel panels, the load capacity may have begun to drop more rapidly because the redistribution of loads may have been less effective in the thin materials.

Significantly, the shear-wall panels described in both of the papers summarized above were constructed with heavier hot-rolled frame members and infill steel plates (Caccese, Elgaaly, and Chen 1993; Driver et al. 1998a). The performance described in those papers is more difficult to achieve using panels constructed with cold-formed steel frames, given the characteristics of the lighter material as discussed above. For cold-formed steel frames, it is even more critical that design guidance ensures formation of a diagonal tension field in the thin steel sheet. Inelastic column response should be limited because of the potential for more brittle failure of the columns. The columns are made up of relatively thin studs or tubing in which the controlling failure mode can be local buckling, out-of-plane buckling or connection failures. Failure in other frame members, such as the top and bottom tracks, must also be prevented, as these can occur as brittle failure modes.

Both of the papers summarized above demonstrate that the desired ductile panel behavior can be achieved if the panel is thin enough relative to the frame, and connection capacity is sufficient to ensure the formation of a diagonal tension field in the panel.

1.2.2 Test setup issues for CFS panel design studies

For cold-formed steel wall panels, it is particularly important that gravity loading be accurately represented. The panel columns are constructed of relatively thin materials, so they are more vulnerable to local buckling than the hot-rolled frames tested in the studies cited above. The panel tests presented in Caccese, Elgaaly, and Chen (1993) did not include any net gravity loading, and neglecting that loading significantly reduces the potential for local column buckling. The panel test presented in Driver et al. (1998a) included gravity loads, but they were applied using post-tensioning rods at the columns. That should be an effective method of applying gravity loads when little axial deformation is expected, as with the heavy hot-rolled sections. When horizontal load is applied and the panel deforms significantly

horizontally, the diagonal tension field will form, placing the column on the side resisting the tension field in compression. This will cause shortening in the column resisting the tension field relative to the opposite column due to axial deformation. When the columns are made using thin CFS materials, they also will be vulnerable to local buckling that will cause further shortening and redistribution to the more stiffened portion of the column cross section. The column on this face will then shorten more than the other column due to both axial deformation and local buckling. In a real building, a stiff beam above the panel will cause redistribution of gravity loads away from the shortening column. Therefore, the top beam will tend to rotate, with the compression column shortening, and the tension (or reduced compression, if post-tensioned) column lengthening. This "bending" type deformation will be even more significant for tall, narrow walls (i.e., those with a large aspect ratio). In a real building, the top beam will be restrained from rotation by the relatively stiff top beam.

In the 1990s, the American Iron and Steel Institute (AISI) sponsored a multiphase experimental project to develop design values for lightweight cold-formed steel panels. The second phase of that work included development of values for diagonal-strap and full-panel sheet steel shear panels (Serrette 1997). The discussion here specifically addresses those panels designed with steel diagonal straps. (However, it also discusses full-panel sheets acting as the primary lateral load-resisting element, which were investigated in third and fourth phases of the AISI project.) The Serrette (1997) study tested panels with both monotonic static and cyclic loading. Many of the diagonal-strap panels failed by local buckling of the columns or tracks. The columns in those specimens were all built up by fastening two studs together, web to web. The studs used to fabricate these columns include knockouts in the webs for electrical conduit penetrations, etc. These studs are particularly vulnerable to local buckling where the knockout holes are located. Furthermore, the tracks at the tops of the panels buckled when they were pulled out of plane by column failure. These modes of failure would provide little ductility or structural paths for load redistribution. Better ductile performance could have been obtained had the diagonal straps been smaller relative to the frame members, using a proportional design approach. The test report acknowledged both types of failure as premature (Serrette 1997).

The non-ductile failures documented in Serrette (1997) prevented the development of diagonal strap capacity, and the subsequent strap yielding

that would provide a ductile response. That type of failure certainly will not support the ductile, energy-dissipating hysteretic performance needed to justify the ASCE 7 response modification coefficients of 4, 6.5, and 7. The hysteresis plots from the cyclic tests in Serrette (1997) demonstrate extreme pinching. In real seismic motions, after a large peak excursion, this type of panel will rack in the opposite direction with little resistance for several inches. Velocity will increase during this unrestrained motion until sudden resistance is again encountered, causing impact loading. The impact can result in very high accelerations that cause brittle failures at the connections of the lateral-load-resisting elements (diagonal straps or others). Therefore, although the plots in Serrette (1997) may show reasonable ductility, it is not an acceptable level to support a sufficiently ductile failure mode. An individual loading cycle will show very little area inside the hysteretic envelope, demonstrating that very little energy will be dissipated by the tested panel design. All full-sheet panels failed at the screw connections either by pulling through the edge of the sheet or pulling through the column studs. The screw connections again failed at a closer spacing, plus the columns failed by local buckling. As with hot-rolled structural steel designed in accordance with ANSI/AISC 360-10, ductile design of cold-formed steel should prevent failure in connections. Serrette (1997) acknowledged that the premature failure of the connections in the full-sheet configuration prevented the development of the desired tension field; similar to the diagonal-strap configuration discussed above, the full-sheet configuration resulted in severely pinched hysteresis plots.

The results of the Serrette (1997) study demonstrate the critical need for design guidance that will ensure acceptable ductile performance for CFS shear panels in light-steel construction projects managed by the Corps of Engineers. The hypothesis driving the research and design recommendations documented in the present report is that proportionate design should ensure ductile plastic yielding in the lateral-load-resisting system, which will absorb energy and redistribute forces. The use of cost-effective thinner steel makes it difficult to avoid the local buckling of column components that leads to brittle column or track failures. In order to achieve the desired ductile performance, design recommendations and test procedures should constrain out-of-plane deflections and the buckling that results from them.

1.2.3 Seattle District shear panel tests

In 1997, U.S. Army Engineer District Seattle (i.e., Seattle District) conducted strength tests on two shear wall panels that were used in the construction of a barracks building at Fort Lewis, WA (USACE 1997). The panels were tested to determine their shear strength following the cyclic load procedure specified in ASTM E 564-95, "Standard Practice for Static Load Test for Shear Resistance of Framed Walls for Buildings" (ASTM 1995). That procedure, however, is not appropriate for measuring the hysteretic behavior of structural systems. This is an important limitation because the hysteretic performance of shear wall panels is critical to determining the degree of pinching and acceptable ductility. The procedure given in ASTM E 564-95, section 6.3.3 (ASTM 1995), specifies that a preload of approximately 10% of the estimated ultimate load should be applied first for 5 minutes, then released for 5 minutes before reading the initial conditions. That step of the procedure is apparently intended to seat the panel. Any need to seat the panel in this way would indicate that the panel may rack with a very small load, suggesting that such a panel would have pinching equivalent to the initial condition offset. By design, ASTM E 564-95 does not measure this initial seating offset, so this most critical pinching measurement is not captured.

Also, this ASTM test protocol calls for loading the panels using load control with five cycles at one third, two thirds, and the full estimated ultimate load of the panel, but these increments of loading will not define the load/deflection hysteretic envelope effectively. Because the shear yield strength may be close to the ultimate load of a panel, the number of nonlinear cycles could be very small in this procedure. Therefore, this procedure is not appropriate for seismic testing where the hysteretic performance is essential to establishing values of acceptable ductility. Even in small seismic motions, the pinched hysteresis will cause the panels to deflect with almost no resistance, allowing velocity to increase until the seating deflection is overcome. At this point the lateral-load-resisting element and other panel components will be loaded with an impact, resulting in high accelerations and forces under which the panel may fail at even very low seismic motions. A well established stroke-control procedure for defining panel hysteretic performance would be much more appropriate. Two such procedures are the ATC-24 and SAC Phase 2 guidelines (ATC 1992; SAC 1997).

Even with concerns about the appropriateness of the test procedures, some observations can be made from the Seattle District tests. These panels were designed for an ultimate load of 40 kips. No gravity loads were applied in these tests. Neglecting gravity is nonconservative in relation to the columns, because the gravity-load effect will combine with the lateral-load effect to cause the columns to buckle at lower lateral loads. However, neglecting gravity should be conservative in relation to column anchors, because the greatest anchor uplift forces will occur when the lateral load is applied with no vertical load.

The Seattle District after-action report on this testing states that the test panel should exhibit ductile behavior by deflecting six times the design-load deflection (USACE 1997). Because of test equipment limitations, however, this deflection limit was not met. The report states "it was later agreed that this criteria [sic] could be modified, as the panel had exhibited adequate strength and behaved linearly to the working load (39 kips)." Because the design load was 13 kips, the desired factor of safety of 3.0 was achieved. Several assumptions underlying that conclusion must be questioned, however. First, meeting the ductility requirements should require test deflections that are at least equal to the design ductility value (6 in this case) times the yield deflection. The District evaluation assumed that test deflections could be the design ductility times the design-load deflection. Load-deflection plots for Panel 2 at the 50 kip load interval shows that panel yielding did not begin until deflections of approximately 0.6 in. were achieved. To meet the design ductility, the panel should have been deformed to deflections of at least 3.6 in. (6 x 0.6 in.), which equates to peak-to-peak deflections of 7.2 in. The panels should have been tested to deflections greater than 3.6 in. (i.e., greater than 7.2 in. peak-to-peak) to ensure that brittle failures do not occur soon after the required deflection is reached. In the final cycle, deflections only reached peak-to-peak levels of 2.3 in. (ductility of 2.0). Still, the design criteria show that ductility values, R_w, of 6.0 were used. The response modification coefficient, R, according to ASCE 7, is a measure not only of global ductility but also over-strength. As stated previously in the present report, seismically induced lateral loads are divided by this coefficient in recognition of the structural system's ability to continue resisting lateral loads after yielding. Therefore, a value of 2.0 for the ductility portion of the R coefficient can be justified based on these tests. The tests showed that these panels are significantly overdesigned because their yield strength is three times greater than their design lateral force. Because the tests were stopped prematurely due to equip-

ment limitations, true panel over-strength (ultimate lateral capacity over yield) and ductility are not known.

A more appropriate design approach, based on the experimental results achieved, would have increased the design capacity of the panel and reduced the R coefficient, resulting in essentially the same panel design. For example, the design capacity could have been increased to 37 kips (i.e., resistance factor for tensile members or tension field of a sheet, ϕ_t, of 0.95 times the panel yield capacity of 39 kips) and the R coefficient reduced to 2.0. Since the applied seismic loads in linear analysis procedures are inversely proportional to the R coefficient, the applied loads would have increased by a factor of 3 (R reduced from 6 to 2) from 13 kips to 39 kips. Even with this very large reduction in the R coefficient, the design capacity of 37 kips is only slightly lower than the applied loads, so the impact on design would be minimal. However, had the test been carried out to larger panel deformations without loss of capacity, a larger R coefficient (greater than 2) along with the greater panel capacity could have been justified, resulting in more economical design. The design used in the Seattle (USACE 1997) study, with either the low design capacity and R coefficient of 6 or the increased capacity and reduced R coefficient, will result in almost elastic response of the building in an earthquake, as is the case with any structural system that uses a very small R coefficient. In a large earthquake, this design will result in very high accelerations and potential for extensive damage to nonstructural components that are vulnerable to larger inertia forces. A much more practical approach would be to provide the basis for justifying larger ductility values, which in this case requires conducting cyclic tests to peak-to-peak deflections of 7.2 in.

Not only should panels be tested to much greater deflections to verify higher ductility, but the resulting hysteretic envelope must not be overly pinched in order that a degree of load resistance can be maintained throughout each load cycle. To obtain such plastic behavior, the initial yielding must take place in the primary lateral-load-resisting element (i.e., steel sheet in this case), not the frame or connections, which may fail in a more brittle manner and thus lead to ultimate collapse of the shear panel system. The tops of the panels used in the Seattle study (USACE 1997) were loaded using a 3 x 6 x 3/16 in. structural tubing top beam attached to the hydraulic ram. This tube is far more flexible in bending than the beam/floor slab in the field, and therefore will not properly represent the anchorage of the tension field nor the rotational restraint for the columns.

The 50 kip limit on the hydraulic ram prevented testing to the ultimate capacity of the panels. Failure of the test fixture (base plate, panel anchorage tension rod, and structural tube top beam) also prevented testing to the ultimate capacity of the panel. Warping, or elastic buckling in the steel sheet, first occurred at the 13 kip load cycle, which should also have resulted in the development of the panel tension field. However, the hysteretic envelopes do not show a clear softening of the panel that would result from significant yielding of the steel sheet. Also, Tables 1 and 2 of the test report (USACE 1997) give values of global shear stiffness for each cycle. These stiffness values at the greatest load cycles (50 kips) are only about 20% lower than at the first load cycles (13 kips). Therefore, it is difficult to justify a yield deflection before the 0.6 in. deflection defined above as a yield deflection (corresponding to a load of 36 kips). These tests appeared to have produced limited tension-field development in the steel sheet before any failure of the frame or connections. However, the panels were simply not loaded far enough to define the hysteretic behavior. Loading was limited by failures of the tension rod anchors, test frame, and load and deflection capacity of the test ram. The result is that the Seattle test results can only justify a ductility value of 2.0. It also appears that the steel sheet was much too heavy relative to the capacity of the frame, such that the development of a significant plastic tension field was prevented. Development of tension field plastic response could have formed the basis for much greater ductility values.

1.3 Research problem

The original research problem, which was investigated and addressed in the late 1990s, was to develop and validate a design for CFS shear panels that met established standards for ductile performance under seismic loading; and then to develop and specify detailed recommendations for implementing the design. Ensuring the ductile performance of this structural system would enable USACE to lift its moratorium on cold-formed steel construction. The key requirement was to provide proportional design specifications for the behavior of the primary lateral-load-resisting elements (diagonal straps) versus the columns, and detailing guidance that ensures acceptable ductile panel performance. The proportional specifications were developed to ensure significant plastic performance of the diagonal straps before brittle failure of either the columns or connections. The recommendations include the definition of a system response-modification coefficient, R, and deflection-amplification factor, C_d. They also account for the influence of system overstrength.

1.4 Objective

The objective of this project was to compile the results of the extensive research, development, and testing program that led to the development, validation, and specifications for shear panels that provide adequate ductility to cold-formed steel buildings during a seismic event. The documentation encompasses all research activities, an updated set of detailed design recommendations derived from the research, and an example problem that illustrates how to apply the design recommendations.

1.5 Approach

This multi-year research project encompassed the following major tasks:

1. Review of related work
2. Development of a design philosophy
3. Definition of promising panel configurations
4. Development of a preliminary design model
5. Design of prototype test shear panels and development of preliminary design recommendations
6. Definition of material properties and coupon test results
7. Pretest of predicted panel response based on preliminary design model and coupon test results
8. Definition of test configuration, procedures, and instrumentation
9. Test of prototype shear panels and documentation of performance
10. Model verification testing on shake table to account for dynamic effects
11. Modification of shear panel models
12. Development of design recommendations and example design problem

1.6 Scope

The report is presented in two parts:

- Part I documents ERDC-CERL investigations that provide the technical basis for developing the CFS seismic design recommendations.
- Part II presents the seismic design recommendations (Chapter 11) and a representative seismic design problem to illustrate how the recommendations are applied (Chapter 12).

The key requirement for these recommendations is to provide proportional design criteria for the behavior of the primary lateral-load-resisting el-

ements (diagonal straps) versus the columns, and detailing recommendations that will ensure acceptable ductile panel performance. The proportional recommendations should ensure significant plastic performance of the diagonal straps before brittle failure of either columns or connections. These recommendations include the definition of a system response modification coefficient, R, and deflection amplification factor, C_d. It also accounts for the influence of system over-strength.

The recommendations presented in Chapter 11 assume that the shear panels are adequately anchored to floor diaphragms above and below. Initially, panel anchorage was outside the scope of this study, and anchorage design was not an issue in the test panels. After initial prototype panel testing, however, it became clear that panel system performance could be improved with the proper anchorage configuration. Therefore, improved prototype shear panel configurations including anchorage details were tested, and anchorage design recommendations were written. To ensure a continuous load path for multiple-story buildings, shear panels installed above the ground floor must have shear panels installed at every story level below. It is also assumed that the diaphragms are sufficient to transfer loads between various shear panels located at a given floor level. The panels must be located such that the center of stiffness and center of mass align with each other in both horizontal directions.

Three levels of seismic design recommendations are provided:

1. Tabular data for prototype shear panels in terms of the maximum story shear and maximum and minimum gravity load. These terms are defined in Chapter 11, and the shear panel configurations and data are provided in Appendix C.
2. Detailed seismic design recommendations using shear panels with diagonal straps as the primary lateral-load-resisting element. These recommendations are provided in Chapter 11, and an example problem illustrating the recommendations is given in Chapter 12.
3. A test procedure and acceptance criteria for other shear panel configurations, which are provided in Appendix D.

1.7 Mode of technology transfer

The design recommendations presented in Chapter 11 would be appropriate to consider for incorporation into a future AISI standard on seismic design for light steel construction systems.

The spreadsheet program used in the example problem presented in Chapter 12 will be made available through the Network for Earthquake Engineering Simulation (NEES) Data Repository (http://nees.org/warehouse), a centralized resource for sharing and publishing earthquake engineering research data from experimental and numerical studies. The spreadsheet can be used as a shear-panel design-assistance tool.

2 Shear Panel Configurations Considered

Several shear panel configurations were considered. Only configurations using conventional building materials were given serious consideration in this program. Future studies that investigate the use of composite panels and other innovative materials, and evaluating their use in a similar manner as the conventional materials here, were contemplated but not investigated. Each panel consists of a cold-formed steel frame with columns at the edges and single interior studs spaced 16 in. on center. The top and bottom of the panels have a standard channel track. Table 2-1 shows a matrix of the panel configuration variables considered. The first variable is the column construction, where columns built up with studs and single structural tubes were considered. The second variable is the primary lateral load-resisting element, where diagonal steel straps and full panel steel sheets were considered. The last variable is the panel fastening system, where self-tapping screws and welded connections were considered. Input was gathered from the cold-formed steel industry on constructability and cost-effectiveness for each configuration so that the developed recommendations would focus on the most practical configurations. The following discussion of each configuration includes the feedback from industry.

The design of each panel configuration assumed all panels were rigidly anchored to the building diaphragm above and below. This rigid anchorage would prevent out-of-plane distortions at the top and bottom track and would keep the top track horizontal. For the panels tested in this program, all panel tracks were bolted to the top and bottom beam. Anchorage design was outside the scope of the initial panel configurations, but it soon became clear that anchorage behavior would significantly influence panel performance, so later panel configurations included anchorage details.

Table 2-1. Matrix of shear panel configurations considered.

Panel Configuration	Exterior Column Construction	Lateral-load-resisting Element	Panel Fastening System	Comments
A	Built-up Studs	Diagonal Steel Straps	Self-tapping Screws	Lowest capacity diagonal strap configuration
B	Structural Tubing	Diagonal Steel Straps	Self-tapping Screws	
C	Built-up Studs	Diagonal Steel Straps	Welded	

Panel Configuration	Exterior Column Construction	Lateral-load-resisting Element	Panel Fastening System	Comments
D	Structural Tubing	Diagonal Steel Straps	Welded	Highest capacity diagonal strap configuration
E	Built-up Studs	Full Panel Steel Sheet	Self-tapping Screws	
F	Structural Tubing	Full Panel Steel Sheet	Self-tapping Screws	
G	Built-up Studs	Full Panel Steel Sheet	Welded	
H	Structural Tubing	Full Panel Steel Sheet	Welded	Highest capacity full panel sheet configuration

2.1 Panel A

This should be the lowest-cost configuration of those shown in Table 2-1. It should also be the most similar to current construction practices using cold-formed steel. This panel configuration may be constructed entirely with carpenters in the field, avoiding the need for the additional trade participation of ironworkers[3]. This assumes the built-up columns may be welded without an ironworker, because the steel is 0.125 in. or less in thickness. Columns may be built up with several studs less expensively than a single structural tube because this avoids the need for ironworkers. Built-up columns would most likely be fabricated in the shop in an automated fashion (e.g., robotic welding), leading to even more cost-effective fabrication. The columns must be built up with the studs oriented to form a closed section. This will reduce, though not eliminate, the potential for local buckling. These columns are also vulnerable to local buckling due to the utility knockouts in the stud webs. The design recommendations presented in Chapter 11 recognize and account for this vulnerability. Test panel A1, A2, and A3 drawings show details for such a column (see Appendix A for all test panel drawings). Chapter 11 provides built-up column welding recommendations to ensure composite behavior of columns. The welds are simple intermittent groove welds, sized and spaced so as to provide the shear transfer needed to develop the full bending capacity of the composite column. The diagonal strap/column connections must be detailed to develop the full yield capacity of this strap. The column anchors at both the top and bottom of the panel must be detailed to transfer the shear and possible tension load in the column to the supporting diaphragms

[3] Phone conversation between Gregory Ralph of Dietrich Industries and James Wilcoski of ERDC-CERL, January 1998.

(beams or slabs).[4] These loads originate primarily from the tensile load in the connected diagonal strap. If properly detailed, this configuration should provide a cost-effective lateral-load-resisting shear panel and it warrants further evaluation.

The A2 test panel configuration included a nested stud, laid inside and parallel to the top and bottom track on both sides of the column. This stud was welded to the columns and tracks in which they rested. The nested stud was oriented with its web against the web of the channel track. This stud was also welded to the track along the edge of channel track flange. The nested studs increased the tensile and shear capacity of the column/track/anchor connection that would be insufficient with the track alone. Construction with the nested stud does not require an ironworker because the welds are less than the 0.125 in.

The A3 test panel is similar to the A1 panel, but uses an off-the-shelf anchor.

After the panel tests, the use of a nested stud was replaced with angle iron anchors on both sides of the columns. These anchors provide the needed shear and uplift resistance, as did the nested stud. The anchors must be welded to the columns, and this weld can also be made without an ironworker because the weld thickness is less than 0.125 in. The anchors also provide a good degree of moment resistance for the column, while the nested stud provided little. This moment resistance would reduce pinching of the hysteresis when loading cyclically, which may in turn lead to an increase in R, C_d, and system overstrength of the panel.

2.2 Panel B

This configuration is similar to Panel A, except the columns are hollow structural sections (HSS). The HSS thickness will normally be greater than 0.125 in. and the weld thickness for the connection to the anchor will equal the thickness of the column. Therefore an ironworker will normally be required, resulting in a cost increase. If the HSS columns are used, requiring an ironworker, welded diagonal strap-to-column connections become

[4] The column anchors for the A1, A2, and A3 test panels were designed as pinned connections, but later anchor guidance requires moment resistance (as used in C1 test panel).

more practical, which results in the Panel D configuration. Therefore, no further consideration was given to this configuration.

2.3 Panel C

This configuration is similar to Panel A with stiffened angle iron anchors, except that connections are welded. This configuration may also be more cost-effective than Panel A because of the numerous fasteners required in Panel A connections. The thickness of the stud material will be under 0.125 in., so an ironworker is not needed for either the welds at the diagonal strap-to-column or column-to-anchor connections. This configuration differs from the Panel D configuration only in that the columns are built up from studs rather than the single structural tube columns. This configuration would require more labor to weld the studs into a composite column section. However, it has an advantage over the Panel D configuration in that an ironworker is not required. Columns built up from heavy studs (e.g., 97 or 118 mil) could provide similar properties as very light HSS columns. The details for the C1 test panel are provided in Appendix A. This panel is most similar to the A2 panel, except that the connections of the diagonal straps to the columns are welded rather than screwed.

2.4 Panel D

This configuration uses HSS columns and welded connections. This panel should have the greatest capacity of the diagonal-strap configurations. The heavier thickness of the column material relative to the studs in Panel C should reduce the potential for local buckling. The welded connections should be less vulnerable to failure than the self-tapping screws, especially when subjected to the cyclic seismic load conditions. The details of Panels D1 and D2 are shown in Appendix A. The D1 panel uses nested studs to anchor the panel columns, while the D2 panel uses stiffened angle anchors. The D1 panel nested studs were intended to provide only a pinned connection for the columns that would resist the shear loads applied to the columns, while the D2 panel anchors provide a moment connection for the columns.

2.5 Panel E

This panel differs from the Panel A configuration in that a full steel sheet is used on one face of the panel for the primary lateral load-resisting element in place of the diagonal straps of Panel A. Each steel sheet configuration

relies on the sheet forming a diagonal tension field orientated at a 45-degree angle to the application of load. The optimal performance of these panels will be achieved when the panel height-to-width aspect ratio is approximately 1.0. This will allow the formation of the diagonal tension field at a 45 degree angle, in a way that this field transfers loads directly into the rigid anchor to the supporting beam above and below the shear panel. If this aspect ratio much greater than 1.0, the diagonal tension field will need to be resisted by the more flexible columns. If the aspect ratio is much lower than 1.0, the diagonal tension field will need to be resisted by the top and bottom track. These tracks should not be used to carry bending load by themselves. The bending resistance could be increased somewhat by adding a nested stud or column anchors to the interior of the columns similar to the D2 panel. Using the columns to resist the tension field would require very heavy columns relative to the sheet, to meet the requirement that the lateral-load-resisting element yield before the frame. For shear panels that cannot avoid this high aspect ratio, a horizontal compression member may be added at mid-height of the panel. This compression member would essentially allow the panel to act as one panel on top of the other so that two parallel tension fields would develop, one in the lower and one in the upper portion of the panel.

The sheet connection to the frame must have the capacity to resist the full yield tension field capacity of the sheet. The widest available coiled steel sheet in the United States is 60 in., so that any panel taller than 60 in. will have an aspect ratio that exceeds 1.0 unless two sheets are used together in a single panel. Using two sheets in a single panel will require welding the panels along the full length of their joint. If the sheet is to be welded, the entire panel should also be welded, resulting in either a Panel G or H configuration. Therefore the Panel E configuration is practically limited to 60 in. in width, which would result in an aspect ratio greater than 1.0.

The high aspect ratio requires that a mid-height horizontal compression member be added. The Panel E configuration then requires enough screws to develop the full yield tension field. A preliminary design of such a panel was developed using a very thin 22 gage (30 mil) steel sheet with yield strength of 33 ksi. Screws would be required around the entire panel perimeter, plus a very dense concentration at the corners and at mid-height of the columns to develop the tension field. This preliminary design called for about 1,100 #10-16 (Teks brand) self-tapping screws, on the side of the panel with the steel sheet. A heavier sheet, a higher sheet yield strength, or

a lower screw strength would have all required even more fasteners. The large numbers of required fasteners make the E configuration impractical.

2.6 Panel F

This configuration differs from Panel E in that the columns are structural tubing members. Similar to the Panel E configuration, this panel could be no wider than 60 in. and would therefore have a high aspect ratio and would require a mid-height horizontal compression member. It would also require a very large number of screws, and therefore would be impractical.

2.7 Panel G

This configuration differs from Panel E in that welded connections are used in place of the screws. Continuous welds are used to fasten the sheet to the frame, effectively developing the panel tension field. The welded connections would solve the problem of the very large numbers of fasteners. The welded connections also mean steel sheets could be welded together at the internal steel studs, so wider panels with aspect ratios smaller than 1.0 could be used. This eliminates the need for the mid-height horizontal compression member. The thickness of the stud material would be less than 0.125 in., so that an ironworker would not be needed for either the welds at the sheet-to-column or column-to-anchor connections. However, it was still assumed that the Panel H configuration could be constructed more effectively because it avoids welding built-up columns from studs. Therefore, this configuration has potential, but was not given further consideration here.

2.8 Panel H

The H configuration uses a full-panel steel sheet on one face, structural tubing columns, welded connections and anchors similar to those shown in panel D2. The steel sheet would be welded around its entire perimeter, to the columns at its sides and to the heavy tracks at the top and bottoms. The tracks would be greatly stiffened near the corners of the panel, where anchors, similar to those used in the C1 and D2 test panels (see Appendix A drawings), at the insides of the columns are against the tracks. This panel was judged to be the most practical of all steel sheet configurations for the reasons stated in the Panel E, F, and G discussion. Ideally, the panel width should be approximately equal to the panel height (aspect ratio equal to 1.0). However, the use of narrower panels with a mid-height hori-

zontal compression member could be investigated. If detailed properly, this panel should offer greater R and C_d values, plus better system overstrength than any diagonal strap configuration. This panel differs from Panel D in that it uses a steel sheet rather than diagonal straps. Under cyclic loading, at large deflections where the Panel D straps are significantly elongated, the straps will offer little resistance soon after a peak excursion. This is because the strap that had been in tension will buckle when unloaded, but the opposite diagonal strap had itself been stretched in the other direction, so it will remain buckled until the panel deflects significantly back in the other direction. In this condition, the Panel D columns must provide almost all the lateral resistance. The Panel H steel sheet on the other hand should pick up load soon after a peak excursion. The sheet buckled perpendicular to the tension field must be forced to straighten out picking up some load in the process. The sheet should not be attached to the intermediate studs at the interior of the sheet because spot welds or other connections at these locations could shock load the welded connection to the panel columns and tracks. The test results for the D1 panel reported in Chapter 7 show that spot welds between the diagonal straps and intermediate studs failed suddenly, shock loading the connections of the strap to the columns. This shock loading took place under very low-velocity cyclic testing. In a seismic event the shock loading could be more severe because several spot welds could fail at the same time on either a diagonal strap or steel sheet. Therefore, the sheet should not be welded to the intermediate studs because when the spot welds fail they could cause brittle failure of the perimeter sheet weld connections to the frame. Also, any improved capacity from these spot welds would be minimal.

The steel sheet, welded to both the column and track in the corners, further stiffens this connection (see Caccese 1993). The unbuckling of the sheet and moment resistance of the column to anchor connection will all provide some resistance, even after a peak excursion, while the sheet is still buckled. Panel tests are needed to measure the extent of this contribution, but this effect should reduce the pinched hystereses to some extent, making the energy dissipation greater in this panel than Panel D.

The same model developed for the diagonal strap configurations (Panels A, C, and D) could be used for the Panel H configuration once a method is developed to define the width of the diagonal tension field. The diagonal tension field would develop at close to a 45-degree angle. The diagonal

tension fields of panels with large aspect ratios (e.g., 50% taller than wide) would load the columns in bending. Such bending load on the columns would require very heavy columns relative to the thickness of the sheet. A more practical solution for panels with large aspect ratios is to add a mid-height compression member. A method for defining the width of the tension field was to be developed based on detailed Abaqus finite-element analysis and panel test results. However, the scope of this study did not permit testing Panel H test panels, so no further consideration was given to this configuration.

Based on the issues described for each panel above, all further panel evaluation focused on the A, C, and D configurations. These panels, plus the Panel H configuration, appear to be the most promising in terms of required ductile behavior, constructability, and cost-effectiveness.

3 Shear Panel Design Philosophy and Analytical Model

This chapter presents the design philosophy used in the development of cold-formed steel shear panel design that is presented in detail in Chapter 11. It also introduces analytical models that were used in the design of test panels.

3.1 Seismic-resistant building performance through ductile shear panel design

Design forces resulting from earthquake motions are determined partially on the basis of energy dissipation in the nonlinear range of response. Building codes provide response-modification coefficients, R, by which seismically induced lateral loads are divided. Design recommendations allow the use of R values between 2 and 7 for light-framed walls (ASCE/SEI 7-10, Table 12.2-1).

Ductile shear panel performance requires that the primary lateral load-resisting elements deform significantly while continuing to resist lateral loads. Diagonal straps perform this function for the shear panel configurations developed for detailed study. The thin tension-only diagonal straps will yield and continue to resist load as they elongate. As they are loaded cyclically, they will absorb energy hysteretically, thereby reducing amplification of building response and justifying design recommendations based on their R values. The diagonal straps must yield and elongate, within defined limits of lateral load, while other components that could fail in a brittle manner must be proportionately designed to remain elastic for the maximum loads that could be applied to them based on the diagonal strap strength. The diagonal straps effectively act a fuse to limit the loads applied to other components. This behavior will prevent damage through more brittle failures to connections and frame members while reducing amplified building response. A building can be designed to behave elastically to minor seismic events or high winds, yet respond inelastically to moderate or major seismic events in a way that protects the gravity-load-resisting system and prevents collapse. In a moderate earthquake, some plastic response may occur in the lateral-load-resisting elements, with little or no damage to the vertical or gravity-load-resisting elements. After

the event, building components can be inspected and the lateral-load-resisting elements can be replaced with no disruption of or shoring of the vertical load system (columns, anchors, or diaphragms). The shear panels are constructed so that the lateral-load-resisting elements are installed last so they could be more easily replaced after a damaging earthquake.

The thin materials used in cold-formed steel construction makes them particularly vulnerable to buckling and tearing. The large material strength variability also makes achieving ductile panel system behavior difficult because one must account for this variability in proportionate design that ensures significant diagonal strap yielding before column buckling or any brittle failures in the connections. When columns are built-up with light-gage studs, the columns are particularly vulnerable to local buckling at the knockouts cut in the webs of panel studs for penetration by building utilities. Panel columns may yield after significant plastic response in the straps, but they must not buckle. Limited local buckling of the columns is acceptable after this plastic response as long as it does not result in gross section collapse.

Chapter 11 defines design recommendations that address several possible modes of failure in the diagonal strap connections to the columns. Each mode of failure must have a minimum capacity that exceeds the maximum load that may be applied to them through the diagonal straps. The shear panels are anchored to the diaphragms above and below using fasteners that are connected to these columns. Chapter 11 defines an anchor configuration that can withstand limited inelastic response itself, but other potentially brittle modes of failure must be prevented. The recommendations in Chapter 11 define each mode of failure, and the brittle ones must have a minimum capacity that exceeds the maximum loads applied to them from the diagonal straps and columns acting as a moment frame.

The simple model presented here can be represented in a spreadsheet and used as a design aid. The models developed in this work were used to design test panels. After coupon tests to measure the real material properties of test panels, the models were used to develop pre-test predictions of panel response (see Chapter 5). Then the adequacy of the models and recommendations were evaluated based on actual test panel performance.

3.2 Cold-formed steel shear panel model

Figure 3-1 provides a schematic drawing of the analytical model. This model applies to the A, C, and D shear panel configuration defined in the previous chapter. The columns in the A and C configurations are built up with cold-formed steel studs that have utility knockouts in stud webs. In the built-up columns the knockouts will be in their flanges. The thin cold-formed steel flange that was already vulnerable to local buckling is now much more vulnerable both because of the reduced area and the unsupported flange along the knockout. Tests by others demonstrate that the studs are particularly vulnerable to local buckling at the knockouts (Serrette 1997). The reduced section area and greater vulnerability to local buckling is not taken into account in the simple models developed here, but the design guidance in Chapter 11 does account for it by defining an effective column cross-section for carrying axial loads. The columns may begin to buckle locally at the knockouts, but should have the reserve capacity to redistribute the loads to other parts of the column cross-section, preventing gross column collapse.

Figure 3-1. Schematic drawing of cold-formed steel shear panel model.

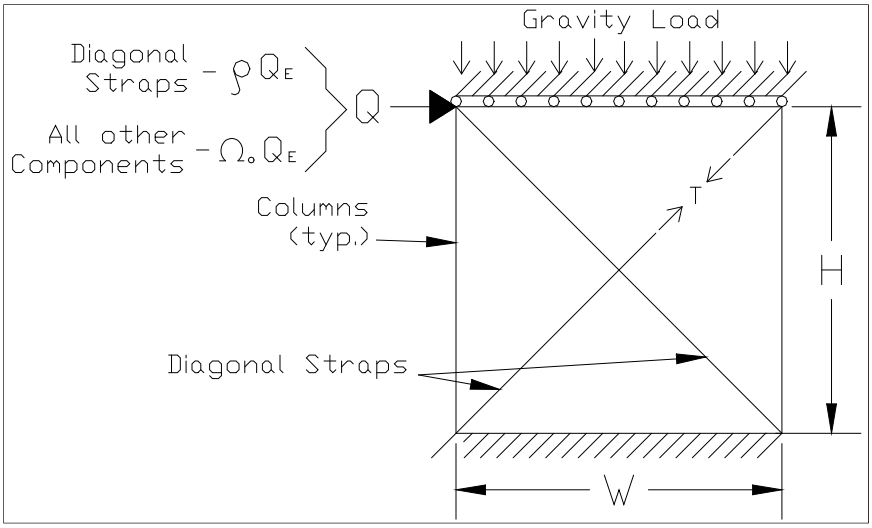

The load-deflection behavior of each shear wall panel is modeled based on spreadsheet calculations. The drawings for each test panel configuration (A1, A2, A3, C1, D1 and D2) are given in Appendix A. Each of these panels uses thin, flat diagonal-strap cross-braces as the lateral-load-resisting element. The design intent is that the diagonal straps carry the majority of the lateral load and provide for the needed panel ductility with significant plastic response. The supporting frame and connections must provide suf-

ficient capacity to resist the resultant forces, but should remain elastic until significant strap inelastic response.

Because the diagonal straps are quite thin, they are assumed to carry load in tension only. The initial test panels (A1, A2, and D1) had the diagonal straps fastened to the intermediate panel studs at 16 in. on center, so the straps would carry a very small load in compression. The thought was that this would widen the load-versus-deformation hysteresis loops slightly, because the straps would carry very small compressive loads when the panel begins to be unloaded after a peak excursion. This small contribution from the straps acting in compression was conservatively ignored, and they were designed as tension only members. After the initial panel test it was seen that the connections to the intermediate studs had a negative influence on panel performance. At large panel deformation, these connections would suddenly fail, shock loading the diagonal straps and their connections to the columns. It was decided that this shock loading could lead to a brittle failure of an already heavily loaded strap-to-column connection. These intermediate connections were eliminated from future test panels and should not be used in actual construction.

The shear panel frame columns will provide some lateral resistance, if the columns are able to act with the slabs above and below as moment frames. The column anchors are detailed to provide moment resistance for the eccentric loading of the diagonal strap and for the full moment capacity of the columns. However, though the anchors have the full moment capacity of the columns, the anchor stiffness will be less than fully fixed. The design recommendations presented in Chapter 11 neglect the column moment frame capacity. But the model developed here and used to predict panel performance in Chapter 5 defines panel capacity based on both the diagonal straps alone and with the columns acting as a fully fixed moment frame. The actual panel capacity should be somewhere between ignoring the moment frame and assuming it is fully fixed. The moment-frame capacity of the columns is very important for widening the hystereses loops, by carrying lateral load when the panel is unloaded after a peak excursion.

The intermediate studs between the panel columns will carry a small portion of the gravity load depending on the flexural stiffness of the diaphragms. The gravity load used in this model is assumed to be only that portion carried by the columns. After large lateral deflections, the axial capacity of the intermediate studs will decrease due to the P delta effects on

these very slender studs. Therefore, the axial capacity of these studs was conservatively ignored.

The following equations are used in the spreadsheet model. The lateral yield capacity of a shear panel based on the diagonal strap strength alone, Q_{sy}, is given by:

$$Q_{sy} = n_s b_s t_s F_{sy} \left(\frac{W}{\sqrt{H^2+W^2}}\right) \quad \text{(Eq 3-1)}$$

where

n_s = the number of diagonal straps in each direction, i.e., straps on 1 or 2 faces
b_s = the diagonal strap width
t_s = the diagonal strap thickness
F_{sy} = the strap yield strength
W = the overall width of the shear panel
H = the overall height of the panel.

The panel lateral deflection when the strap yields, δ_{sy}, is defined by:

$$\delta_{sy} = \frac{F_{sy}}{E}\sqrt{H^2+W^2}\left(\frac{\sqrt{H^2+W^2}}{W}\right) = \frac{F_{sy}}{E}\left(\frac{H^2+W^2}{W}\right) \quad \text{(Eq 3-2)}$$

where

E = the steel modulus of elasticity.

The panel initial lateral stiffness based on the diagonal strap stiffness alone, k_{sy}, is given by:

$$k_{sy} = \frac{Q_{sy}}{\delta_{sy}} = \frac{n_s b_s t_s F_{sy}\left(\frac{W}{\sqrt{H^2+W^2}}\right)}{\frac{F_{sy}}{E}\left(\frac{H^2+W^2}{W}\right)} = n_s b_s t_s E\left(\frac{W^2}{(H^2+W^2)^{3/2}}\right) \quad \text{(Eq 3-3)}$$

The lateral stiffness of two columns fixed at both their tops and bottoms in a shear panel, k_c, is:

$$K_c = \frac{24EI_x}{H^3} \quad \text{(Eq 3-4)}$$

where

I_x = the moment of inertia of an individual column in the plane of the shear panel.

The total lateral stiffness of the shear panel before strap yielding, k_T, is:

$$k_t = k_{sy} + k_c \quad \text{(Eq 3-5)}$$

The fully fixed column lateral force at strap yielding, Q_{csy}, is:

$$Q_{csy} = k_c \delta_{sy} \quad \text{(Eq 3-6)}$$

The total panel lateral force at strap yielding, Q_{Tsy}, is:

$$Q_{T_{sy}} = Q_{sy} + Q_{csy} \quad \text{(Eq 3-7)}$$

The maximum column axial load applied to the panel columns is based on the maximum yield stress in the diagonal straps, P_{vymax}, defined below:

$$P_{vymax} = \frac{GL_{max}}{2} + F_{symax} n_s b_s t_s \left(\frac{H}{\sqrt{H^2+W^2}}\right) \quad \text{(Eq 3-8)}$$

where

GL_{max} =the maximum gravity load per shear panel, defined in detail in Chapter 11.

F_{symax} =the maximum estimated yield stress in the diagonal straps, which is defined in detail in Chapter 11.

The column design capacity is defined in Chapter 11.

The maximum estimated yield force in the diagonal straps (in the axis of the straps), P_{symax}, is:

$$P_{symax} = F_{symax} n_s b_s t_s \quad \text{(Eq 3-9)}$$

The diagonal strap-to-column connections must be designed to resist the forces defined by Equation 3-9. This equation also defines the loads applied to the panel anchors that anchor the columns to the diaphragms.

Chapter 11 provides detailed design recommendations for these connections and anchors.

The combined shear capacity of the columns and anchors must exceed the maximum shear panel horizontal seismic force P_{hymax} defined in Equation 3-10:

$$P_{hymax} = F_{symax} n_s b_s t_s \left(\frac{W}{\sqrt{H^2+W^2}}\right) \quad \text{(Eq 3-10)}$$

This force is based on the load developed form the maximum yield strength of the diagonal straps. Chapter 11 defines the shear capacity of the columns and design of anchors to resist this load.

The shear capacity of the anchor bolts on both sides of each column must exceed the force P_{hymax} defined in Equation 3-10. Chapter 11 defines the anchor bolt shear capacity. Chapter 11 also defines applied tensile force per bolt and the several anchor design requirements for various potential modes of failure.

Chapter 11 further develops this model for cold-formed steel shear panel design purposes. Chapter 5 expands the model for that purpose to predict shear panel capacity to larger deformations where the column yields. The purpose for this is to provide a simple spreadsheet model that can be compared with cyclic test data reported in Chapter 7 and the shake table test results reported in Chapter 8. The test results in combination with comparisons with the predicted model should validate that the detailed recommendations presented in Chapter 11 can be relied upon to achieve the desired ductile behavior.

4 Material Properties and Coupon Test Results

4.1 Material properties

Actual expected yield and ultimate strength, not just design minimums, are very important for designing panels that will provide significant ductility from plastic response of the diagonal straps before damage to the panel columns or connections. Cold-formed steel suppliers may reroll materials to obtain a thinner product from a thicker one. The rerolling causes strain hardening, which may significantly increase the strength and the variability in strength. The degree of strength variability depends on the degree of strain hardening and makes design of shear panels with cold-formed steel difficult. The ratio or ultimate over yield strength (F_u/F_y) is also significantly reduced in the rerolling, and this ratio is critical if net section failure in connections is to be prevented. Also, strain hardening will significantly reduce the ductility or elongation of the material. Therefore, the recommendations here prohibit the use of rerolled materials for the diagonal straps, where the maximum yield and plastic behavior are critical. They also assume only virgin ASTM A653 or, better yet, ASTM A1003/A1003M Type H steel will be used (ASTM 2013a, 2013b).

The strength of even virgin ASTM A653 materials can vary significantly. The following information on ASTM A653 material properties was obtained from a 1995 in-house study conducted at Bethlehem Steel (Larson 1998). In this study, data were gathered from two galvanized coating lines where the conditions of the lines varied significantly so as to provide a good range of test results:

> ASTM A653 does not specify a maximum yield or tensile (ultimate) strength. Normally the concern in the high-strength end of the range is having enough ductility to form a part. A653 specifies a minimum elongation to satisfy this concern.
>
> 1) For Grade 33 (data also included Grade 40), the yield strength may vary between 1 and 2 times the minimum specified (i.e., 33 ksi), but is typically 1½ times the minimum specified.

2) For Grade 50, the yield strength may vary between 1 and 1½ times the minimum specified (i.e., 50 ksi), but is typically 1⅛ times the minimum specified.

3) For Grade 33 (data also included Grade 40), the tensile (ultimate) strength may vary between 1 and 1½ times the minimum specified (i.e., 45 ksi), but is typically 1¼ times the minimum specified.

4) For Grade 50, the tensile (ultimate) strength may vary between 1 and 1¼ times the minimum specified (i.e., 65 ksi), but is typically 11/16 times the minimum specified.

5) For Grade 33 (data also included Grade 40), the elongation (strain) may vary between 1 and 2 times the minimum specified (i.e., 20%), but is typically 1½ times the minimum specified.

6) For Grade 50, the elongation (strain) may vary between 1 and 3 times the minimum specified (i.e., 12%), but is typically 2¼ times the minimum specified.

Grade 50 would tend to significantly reduce the "over-strength" issue while providing adequate ductility. However, this information is based on an in-house Bethlehem Steel study and is not necessarily representative of the steel industry. Individual sample size (grade/coating) in this study varied from 30 to 717 coils. An individual sample may include several thicknesses for a given sample grade and coating.

Note minimum ductility requirements in AISI Specification S100-07, section A2.3.1 (AISI 2007a, 8): $F_u/F_y > 1.08$ and total elongation of at least 10% for a 2 in. gage length, based on ASTM A370 coupon test requirements (ASTM 2014b).

The section "Load and Resistance Factor Design, LRFD, Commentary on the LRFD Design Specification for Structural Steel Building" (AISC 2011), provides a good discussion on limit states and an overview of the probabilistic basis for the LRFD. The LRFD specification uses a general format given by the following equation (AISC 2011, Equation B3-1):

$$R_u \leq \emptyset R_n \qquad \text{(Eq 4-1)}$$

where

R_u = the required strength using LRFD load combinations
R_n = the nominal strength
ϕ = the resistance factor corresponding to R_n
ϕR_n = the design strength.

The left side of Equation 4-1 represents the required resistance computed by structural analysis based on the assumed loads. The right side of this equation represents a limiting structural capacity provided by the selected members or connection detail. The resistance factors, ϕ, reflect the fact that the loads, load effects on forces and moments, and the resistances can be determined to imperfect degrees of accuracy. The probabilistic basis for the LFRD attempts to define the mean and standard deviations of the load effects and resistance factors. The probability of a given limit state being reached (e.g., a material yielding or fracture occurring in a connection) is the probability that ϕR_n exceeds R_u, which is related to the mean and standard deviations of these.

The Bethlehem Steel study, excerpted above, provides some basis for the mean yield and ultimate strengths of cold-formed steel materials that can be related to certain limit states. Many of these limit states form the basis of the design provisions in Chapter 11. However, the authors are unaware of the standard deviations of these properties other than the large range of properties defined in the Bethlehem Steel study. Therefore, conservative assumptions had to be made to develop design recommendations based on this data that would prevent brittle modes of failure (limit states) by encouraging ductile modes of failure (diagonal strap yielding).

4.2 Coupon test results

To gain a better understanding of shear panel tests results, material tests were conducted on each of the primary components of the test panels. In order to design the panels it is important to know the material properties of critical panel elements such as the diagonal straps, columns, and anchor angles. Several coupons taken from these materials for each panel were tested in accordance with ASTM A370, *Standard Test Methods and Definitions for Mechanical Testing of Steel Products* (ASTM 2014b). The data obtained from each coupon are shown in Table 4-1 and Table 4-2. The results of the data were analyzed to determine average values for the yield

stress, F_y, yield strain, plateau stress, ultimate stress, F_u, and strain at the ultimate stress. These average results are shown in Table 4-3.

Table 4-1. Coupon test results for the A1, A2, and A3 panels.

Material	Thickness (in.)	Yield Strain (in/in)	Yield Stress (ksi)	Plateau Stress (ksi)	Strain at Ultimate (in/in)	Ultimate Stress (ksi)	Ultimate / Yield Stress	Elongation in 2 in.	Stress at Elongation (ksi)
A1 Diagonal Strap									
Coupon 1a	0.0496	0.0013	44.21	43.23	0.183	52.04	1.18	22.0%	51.10
Coupon 1b	0.0480	0.0011	45.60	43.02	0.134	54.24	1.19	20.0%	53.80
Coupon 1c	0.0472	0.0014	45.22	44.58	0.160	54.52	1.21	21.6%	52.90
Coupon 1d	0.0476	0.0014	46.06	44.58	0.164	54.63	1.19	20.0%	54.10
A1 Strap Average	0.0481	0.0013	45.27	43.85	0.160	53.86	1.19	20.9%	52.98
A1 Column Stud									
Coupon 2a	0.0453	0.0013	43.25	43.61	0.134	53.83	1.24	20.5%	53.43
Coupon 2b	0.0469	0.0013	41.27	42.48	0.145	52.16	1.26	19.8%	46.36
Coupon 2c	0.0496	0.0013	41.38	40.05	0.166	49.36	1.19	19.9%	46.41
Coupon 2d	0.0504	0.0013	40.19	39.38	0.158	48.44	1.21	20.1%	47.98
Coupon 2e	0.0504	0.0013	40.77	39.65	0.155	48.24	1.18	20.1%	41.93
A1 Stud Average	0.0485	0.0013	41.37	41.03	0.152	50.41	1.22	20.1%	47.22
A2 Diagonal Strap									
Coupon 3a	0.0720	0.0007	31.90	N/A	0.189	49.70	1.56	21.8%	49.40
Coupon 3b	0.0720	0.0012	32.39	N/A	0.180	49.54	1.53	20.2%	49.44
Coupon 3c	0.0709	0.0009	32.47	N/A	0.211	50.78	1.56	21.7%	50.59
Coupon 3d	0.0709	0.0014	32.12	N/A	0.207	50.83	1.58	21.0%	50.43
A2 Strap Average	0.0715	0.0010	32.22	N/A	0.197	50.21	1.56	21.2%	49.97
A2 Column Stud									
Coupon 4a	0.1004	0.0017	61.04	60.17	0.117	73.78	1.21	16.9%	14.72
Coupon 4b	0.1004	0.0018	60.03	60.04	0.116	72.90	1.21	15.5%	15.87
Coupon 4c	0.1004	0.0019	58.97	60.37	0.128	73.22	1.24	17.3%	2.91
Coupon 4d	0.1004	0.0020	60.74	60.34	0.114	72.88	1.20	16.6%	0.22
A2 Stud Average	0.1004	0.0018	60.19	60.23	0.119	73.20	1.22	16.6%	8.43
A3 Diagonal Strap									
Coupon 5a	0.0433	0.0019	59.95	N/A	0.029	62.50	1.04	4.0%	60.58
Coupon 5b	0.0433	0.0021	59.86	N/A	0.035	62.34	1.04	6.9%	54.99
Coupon 5c	0.0433	0.0022	60.46	N/A	0.029	62.81	1.04	4.9%	60.19
Coupon 5d	0.0429	0.0020	60.61	N/A	0.032	63.11	1.04	13.7%	44.73
Coupon 5e	0.0429	0.0024	60.49	N/A	0.031	63.05	1.04	12.2%	45.01
Coupon 5f	0.0437	0.0029	59.85	N/A	0.028	61.95	1.04	4.6%	61.22
A3 Strap Average	0.0432	0.0023	60.20	N/A	0.031	62.63	1.04	7.7%	54.45
A3 Column Stud									
Coupon 6a	0.0555	0.0014	39.83	39.31	0.178	49.09	1.23	20.3%	48.76
Coupon 6b	0.0547	0.0014	40.04	40.20	0.182	49.94	1.25	20.4%	49.80
Coupon 6c	0.0551	0.0015	44.12	43.02	0.166	50.76	1.15	20.3%	50.58
Coupon 6d	0.0555	0.0014	42.62	41.84	0.170	50.04	1.17	20.5%	49.86
Coupon 6e	0.0551	0.0011	42.32	42.48	0.155	50.42	1.19	20.2%	50.22
A3 Stud Average	0.0552	0.0014	41.79	41.37	0.170	50.05	1.20	20.3%	49.84

Table 4-2. Coupon test results for the C1, D1, and D2 panels.

Material	Thickness (in.)	Yield Strain (in/in)	Yield Stress (ksi)	Plateau Stress (ksi)	Strain at Ultimate (in/in)	Ultimate Stress (ksi)	Ultimate / Yield Stress	Elongation in 2 in.	Stress at Elongation (ksi)
C1 Diagonal Strap									
Coupon 7a	0.0693	0.0029	79.50	N/A	0.026	80.87	1.02	11.5%	55.49
Coupon 7b	0.0673	0.0029	81.91	N/A	0.057	84.55	1.03	13.6%	61.12
Coupon 7c	0.0677	0.0027	80.82	N/A	0.025	83.07	1.03	13.2%	64.64
Coupon 7d	0.0681	0.0026	80.91	N/A	0.026	83.01	1.03	13.4%	62.97
Coupon 7e	0.0681	0.0026	81.12	N/A	0.027	83.49	1.03	12.3%	62.89
Coupon 7f	0.0681	0.0030	81.55	N/A	0.016	82.71	1.01	3.9%	80.60
C Strap Average	0.0679	0.0028	81.26	N/A	0.030	83.37	1.03	11.3%	64.62
C1 Column Stud									
Coupon 8a	0.0980	0.0020	65.90	66.29	0.078	81.53	1.24	19.3%	10.32
Coupon 8b	0.0976	0.0021	66.81	67.34	0.096	82.73	1.24	18.6%	11.10
Coupon 8d	0.0976	0.0025	65.54	66.16	0.098	81.81	1.25	17.2%	37.43
Coupon 8e	0.0980	0.0020	66.73	67.45	0.081	82.68	1.24	16.7%	7.56
Coupon 8f	0.0980	0.0021	66.18	66.84	0.085	82.18	1.24	16.1%	52.25
C1 Stud Average	0.0979	0.0021	66.23	66.82	0.088	82.18	1.24	17.6%	23.73
C1 Anchor Angle									
Coupon 9a	0.4976	0.0014	48.71	48.76	0.182	72.35	1.49	19.9%	71.39
Coupon 9b	0.4937	0.0016	51.72	51.58	0.146	74.40	1.44	20.8%	72.08
Coupon 9c	0.4929	0.0015	50.62	50.42	0.153	73.30	1.45	20.0%	72.31
C1 Angle Average	0.4948	0.0015	50.35	50.25	0.160	73.35	1.46	20.2%	71.93
D1 Diagonal Strap									
Coupon 10a	0.1079	0.0013	36.42	N/A	0.111	47.49	1.30	20.1%	46.89
Coupon 10b	0.1091	0.0012	38.03	N/A	0.131	47.70	1.25	19.8%	46.64
Coupon 10c	0.1079	0.0012	38.49	N/A	0.104	47.75	1.24	19.9%	47.11
Coupon 10d	0.1071	0.0011	37.56	N/A	0.128	47.81	1.27	20.0%	47.18
Coupon 10e	0.1079	0.0014	37.64	N/A	0.126	47.91	1.27	0.6%	39.83
D1 Strap Average	0.1080	0.0012	37.63	N/A	0.120	47.73	1.27	16.1%	45.53
D2 Diagonal Strap									
Coupon 11a	0.1004	0.0014	54.97	55.07	0.149	72.26	1.31	20.9%	70.61
Coupon 11b	0.1000	0.0016	54.96	55.69	0.137	73.22	1.33	20.5%	56.35
Coupon 11c	0.0996	0.0015	55.70	55.98	0.153	73.36	1.32	20.2%	71.91
Coupon 11d	0.0996	0.0018	55.43	55.39	0.164	72.69	1.31	21.6%	71.60
Coupon 11e	0.0992	0.0021	56.18	56.10	0.141	73.20	1.30	21.4%	72.27
Coupon 11f	0.1004	0.0010	55.82	56.02	0.144	73.14	1.31	21.3%	70.55
D2 Strap Average	0.0998	0.0016	55.62	55.71	0.148	73.12	1.31	21.0%	68.88
D2 Column HSS									
Coupon 12a	0.1705	0.0012	49.85	N/A	0.116	63.14	1.27	13.5%	62.51
Coupon 12b	0.172	0.0012	54.45	N/A	0.138	65.33	1.20	20.3%	64.65
Coupon 12c	0.1740	0.0017	48.42	N/A	0.149	64.32	1.33	19.1%	63.11
Coupon 12d	0.1724	0.0016	48.89	N/A	0.159	64.30	1.32	23.3%	63.28
Coupon 12e	0.1728	0.0018	48.88	N/A	0.154	64.30	1.32	20.0%	63.06
D2 Column HSS	0.1724	0.0015	50.10	N/A	0.143	64.28	1.29	19.2%	63.32
D2 Anchor Angle									
Coupon 13a	0.4886	0.0011	50.08	49.85	0.130	72.66	1.45	19.9%	71.71
Coupon 13b	0.4909	0.0013	50.44	50.49	0.151	73.46	1.46	17.6%	72.61
Coupon 13c	0.4898	0.0014	49.44	49.76	0.146	72.58	1.47	18.8%	72.06
D2 Angle Average	0.4898	0.0013	49.98	50.03	0.142	72.90	1.46	18.8%	72.13

Table 4-3. Average coupon test results for all panel types.

Material	Thickness (in.)	Yield Strain (in/in)	Yield Stress (ksi)	Plateau Stress (ksi)	Strain at Ultimate (in/in)	Ultimate Stress (ksi)	Ultimate / Yield Stress	Elongation in 2 in.	Stress at Elongation (ksi)
A1 Diagonal Strap	0.0481	0.0013	45.27	43.85	0.160	53.86	1.19	20.9%	52.98
A1 Column Stud	0.0485	0.0013	41.37	41.03	0.152	50.41	1.22	20.1%	47.22
A2 Diagonal Strap	0.0715	0.0010	32.22	N/A	0.197	50.21	1.56	21.2%	49.97
A2 Column Stud	0.1004	0.0018	60.19	60.23	0.119	73.20	1.22	16.6%	8.43
A3 Diagonal Strap	0.0432	0.0023	60.20	N/A	0.031	62.63	1.04	7.7%	54.45
A3 Column Stud	0.0552	0.0014	41.79	41.37	0.170	50.05	1.20	20.3%	49.84
C1 Diagonal Strap	0.0679	0.0028	81.26	N/A	0.030	83.37	1.03	11.3%	64.62
C1 Column Stud	0.0979	0.0021	66.23	66.82	0.088	82.18	1.24	17.6%	23.73
C1 Anchor Angle	0.4948	0.0015	50.35	50.25	0.160	73.35	1.46	20.2%	71.93
D1 Diagonal Strap	0.1080	0.0012	37.63	N/A	0.120	47.73	1.27	16.1%	45.53
D2 Diagonal Strap	0.0998	0.0016	55.62	55.71	0.148	73.12	1.31	21.0%	68.88
D2 Column HSS	0.1724	0.0015	50.10	N/A	0.143	64.28	1.29	19.2%	63.32
D2 Anchor Angle	0.4898	0.0013	49.98	50.03	0.142	72.90	1.46	18.8%	72.13

The material properties are defined in ASTM A370 (ASTM 2014b). Yield stress and strain were found using a 0.2% offset method. After finding the intersection of the 0.2% offset line and the stress-strain curve, the value of strain was offset by subtracting 0.2% from the intersection point. The result is a bilinear plot that is an accurate representation of the real stress-strain relationship. The plateau stress, given in Table 4-1 through Table 4-3, occurs when necking takes place in the test specimen prior to strain hardening. Necking of the specimen produces an increase in strain at a nearly constant stress, thereby forming a plateau on the curve. To find a value for the plateau stress, the average of the stress was taken from the point where the necking starts to the point where strain hardening begins. The values for ultimate stress and strain at the ultimate stress were obtained by finding the maximum value of stress and the corresponding strain at that stress. The material properties obtained and shown in Table 4-1 through Table 4-3 provide a fairly complete description of the material behavior of each coupon.

Figure 4-1 through Figure 4-6 plot the stress versus strain for the most representative coupons of each material. For example, after analyzing all of the data obtained from the tests conducted on the A1 diagonal strap specimens, the curve labeled “A1 Diagonal Strap” in Figure 4-1 was chosen as the most representative for that particular material. The “A1 Diagonal Strap” curve corresponds to the actual curve of coupon 1c from Table 4-1. Although some of the coupon results varied, one could expect a typical panel element to behave as shown in Figure 4-1 through Figure 4-6. Figure 4-1 plots the coupon test results for all the materials used in the A configu-

ration panels. Figure 4-2 plots the same coupon data, but zooms in on the small strain region of up to 0.04 in./in., clearly showing material yielding and initial strain hardening. This region of small strains is of greatest interest because the test panels must reach large lateral deflections of 9.6 in. before the strap strains reach 0.04 in./in. Figure 4-3 and Figure 4-4 show similar plots for the C1 panel materials. Figure 4-5 and Figure 4-6 show these plots for the D configuration panels.

Table 4-1 and Table 4-2 show that A3 and C1 diagonal straps do not meet the required 1.08 ratio of ultimate over yield strength and the A3 straps do not meet the 10% elongation requirement for ASTM A 1003/A 1003M high-ductility steel (ASTM 2013b). The lack of a plateau in the stress-versus-strain plot and lack of increase in stress beyond yield for the A3 and C1 straps shown in Figure 4-1 and Figure 4-3 show they were strain hardened. The A2 straps may also have been somewhat strain hardened based on a lack of a plateau in Figure 4-1. Coupon tests of the A3, C1, and D2 strap materials were conducted before designing their test panels so that the panels could be designed where strap strength was equal to the maximum strength in accordance with the Bethlehem Steel study. For example, the measured yield strength of the A3 strap was 60.1 ksi, and the panel was designed as if the strap specified design strength was 30 ksi, as if Grade 33 material had been specified (see panel A3 strap specification in Figure A-7).

Table 4-3 shows the material thickness, yield strain, yield stress (F_y), ultimate stress (F_u), ratio of ultimate over yield stress, and elongation within the 2 in. coupon gage length for all the primary materials used in the cold-formed steel test panels except the D1 column hollow structural section, HSS.

Figure 4-1. Coupon test results for the A1, A2, and A3 panels.

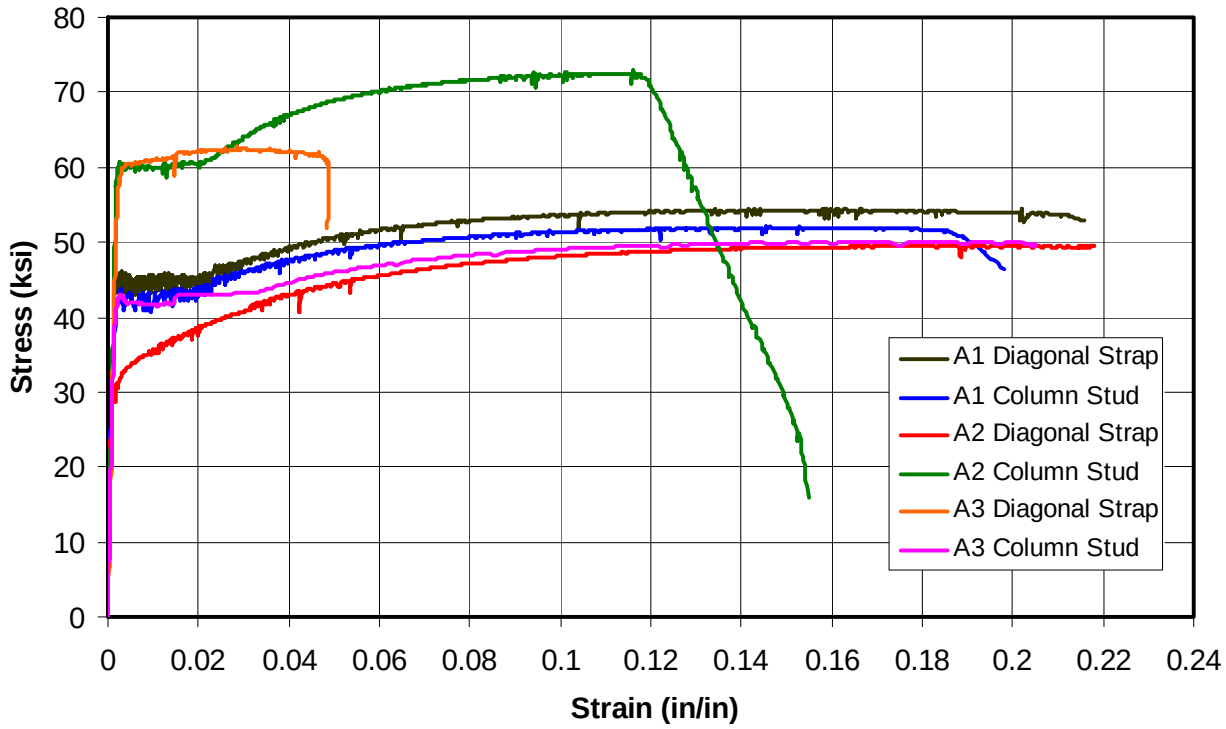

Figure 4-2. Coupon test results at small strains for the A1, A2, and A3 panels.

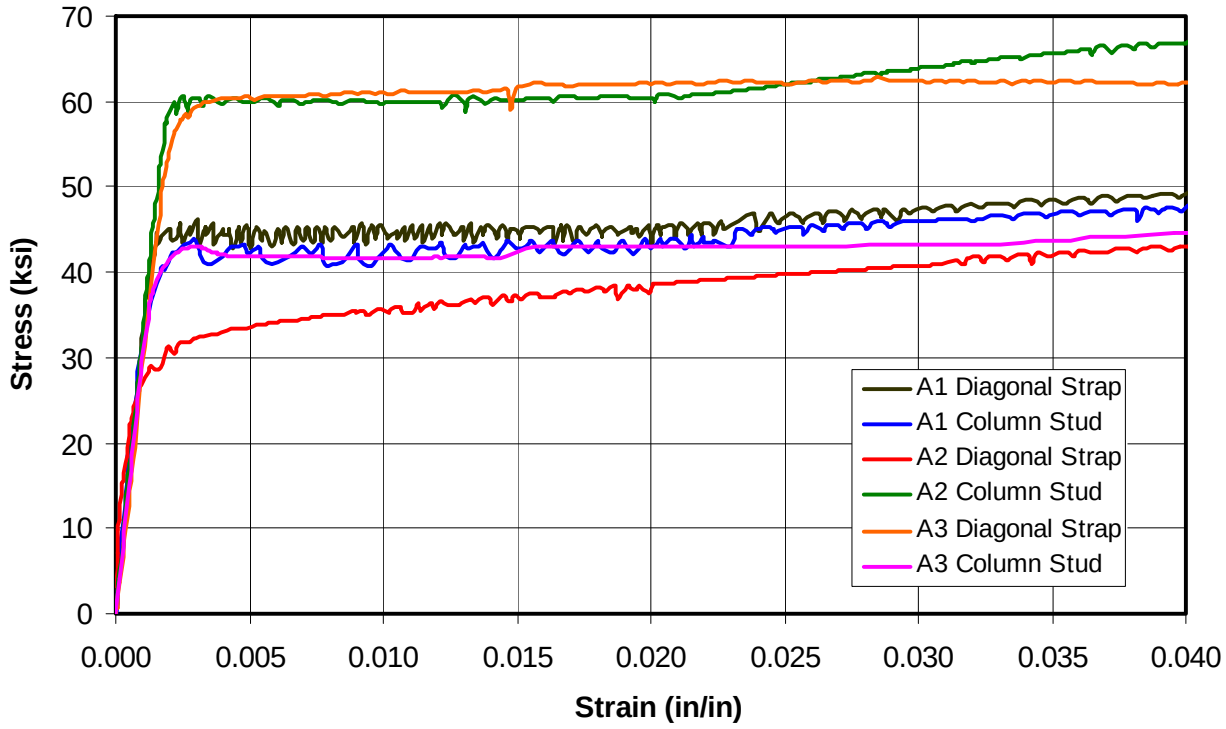

Figure 4-3. Coupon test results for the C1 panels.

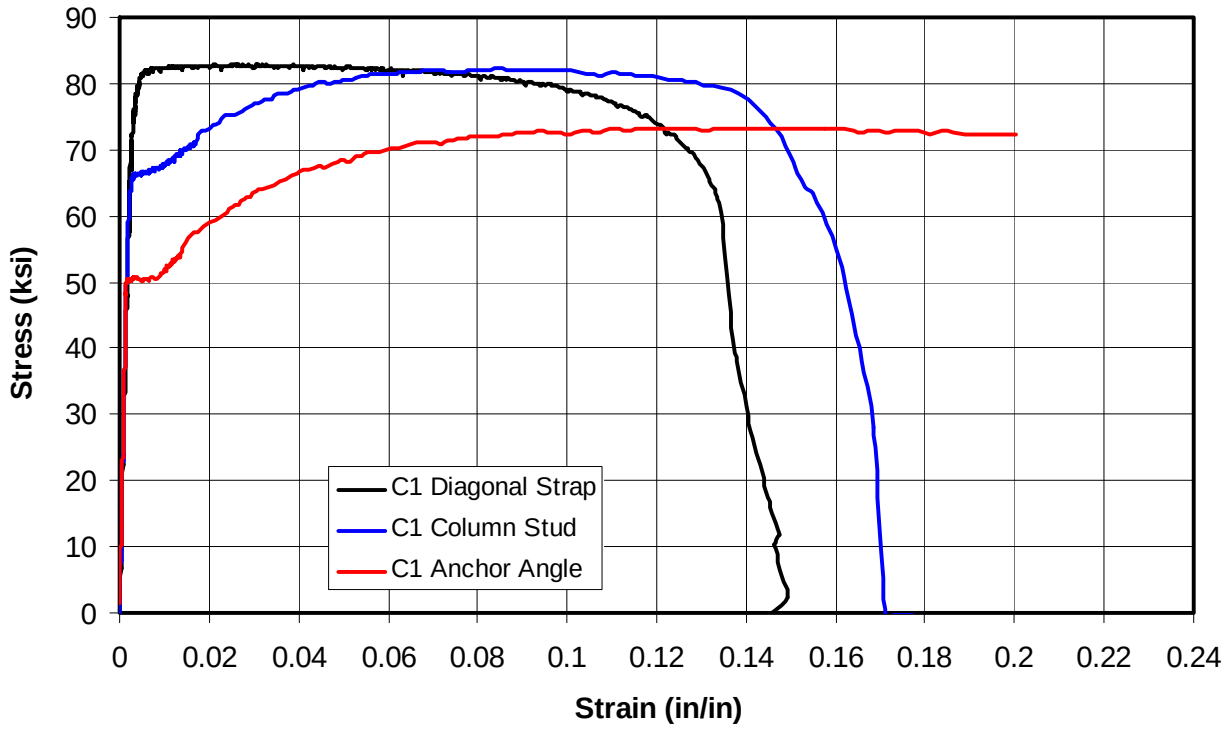

Figure 4-4. Coupon test results at small strains for the C1 panels.

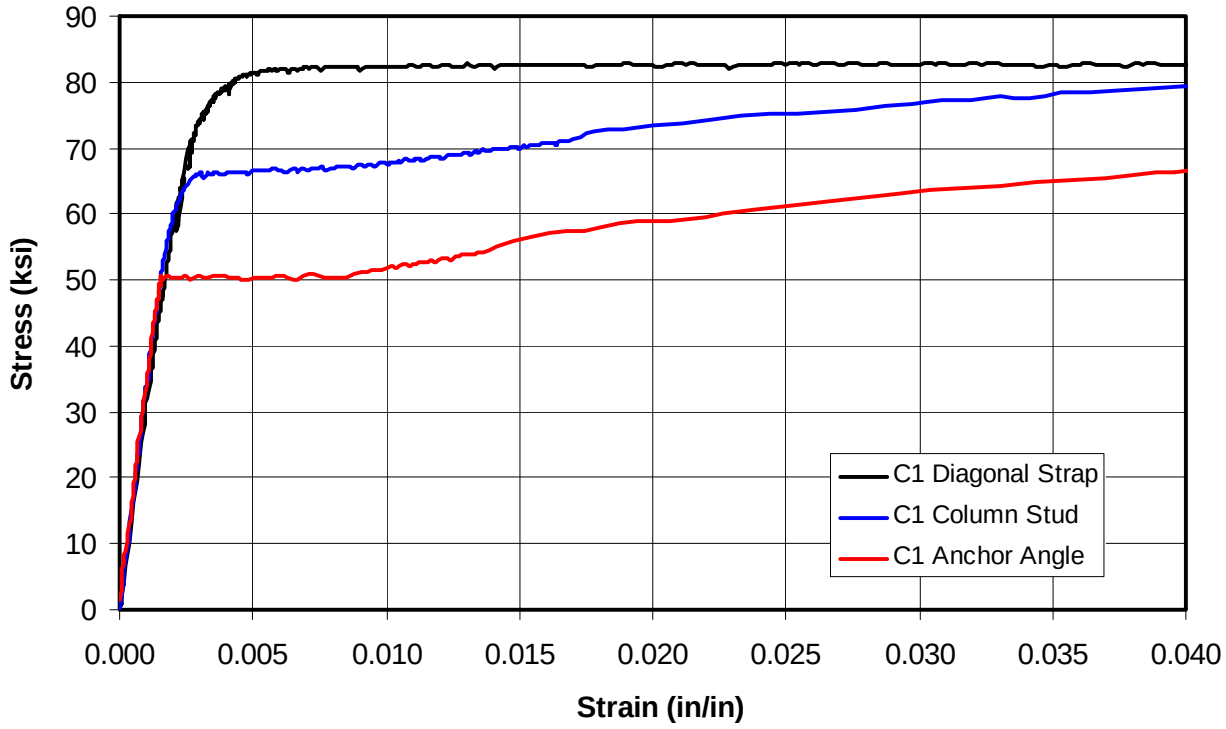

Figure 4-5. Coupon test results for the D1 and D2 panels.

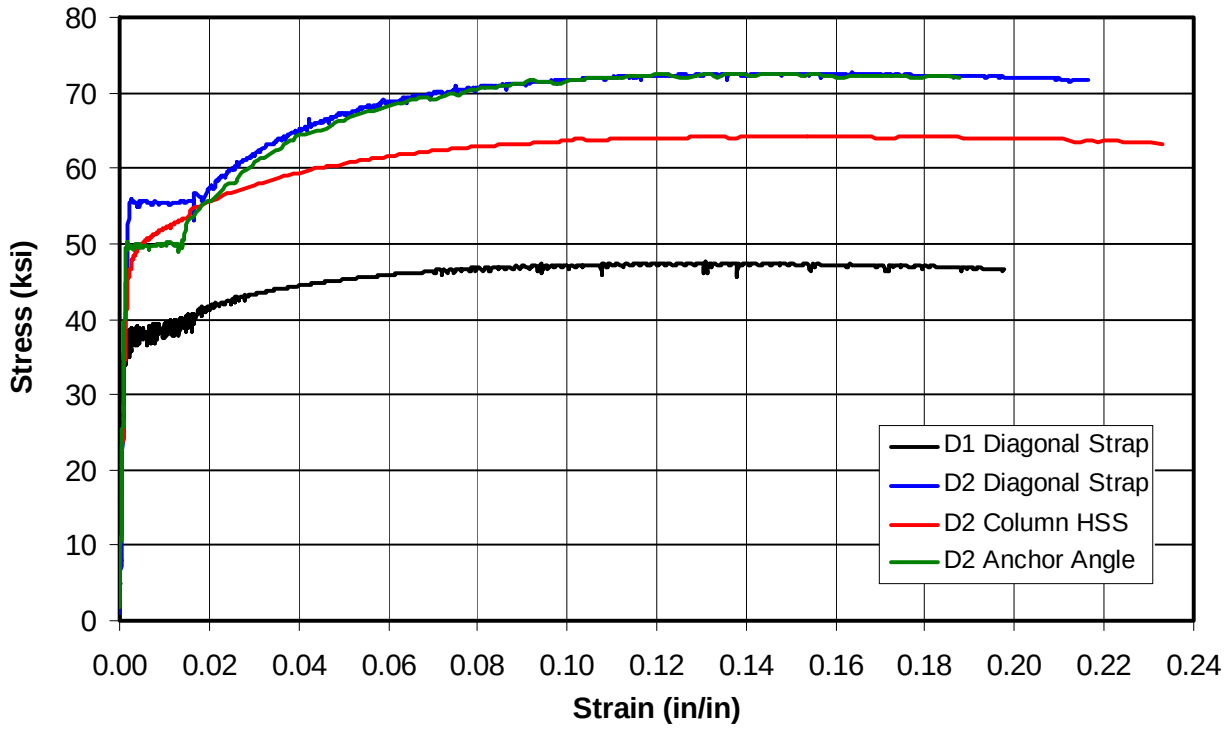

Figure 4-6. Coupon test results at small strains for the D1 and D2 panels.

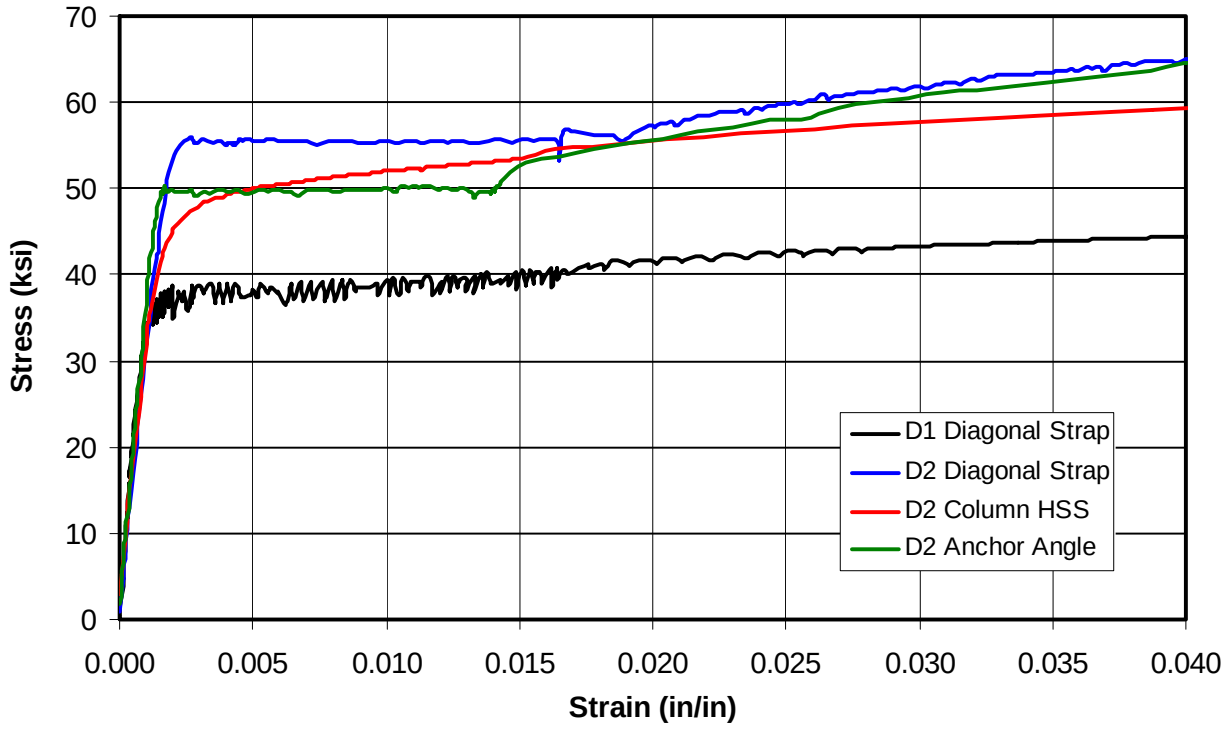

5 Predicted Panel Response Based on Analytical Model and Coupon Test Results

The model developed in Chapter 3 can be modified for predicting shear panel lateral-load-versus-deformation behavior. This model can be expanded to develop predicted envelopes of lateral load capacity versus deformation, which include data points at strap yielding and column yielding. The measured diagonal strap and column material properties presented in Chapter 4 are used in this model to predict panel behavior. These predictions can be compared with test data to evaluate the model.

When the shear panels are loaded laterally, they should behave linearly until the diagonal straps begin to yield. The first point on a plot of the predicted lateral load-versus-deformation plot is the lateral capacity of the diagonal strap alone at lateral yield deformation of the strap. The lateral capacity of a shear panel, based on the strap strength alone, Q_{sy}, when the strap begins to yield, was defined in Equation 3-1. The panel lateral deformation when the strap yields, δ_{sy}, was given in Equation 3-2. The diagonal strap properties and calculation of the strength and deformation values are shown in Table 5-1, and they are plotted in Figure 5-1 for each cyclically tested shear panel. Table 5-2 and Table 5-3 provide additional properties of the test panel straps and columns.

The second point on the plot is the total panel lateral force at strap yielding, Q_{Tsy}, defined in Equation 3-7. This adds the lateral resistance from the two panel columns assuming they are fully fixed at both their tops and bottoms, Q_{csy}, defined in Equation 3-6. The columns can act as a moment frame assuming they are anchored to the floor diaphragms above and below. The degree of fixity of the moment connections is unknown, so Q_{sy} becomes a lower estimate of panel capacity assuming the columns have pinned connections and Q_{Tsy} is an upper estimate of capacity assuming full column fixity. Values for Q_{Tsy} are shown in the third column of Table 5-4 for each test panel.

Table 5-1. Test panel diagonal strap properties and predicted lateral capacity.

Column Type	Panel Width W (in)	Panel Height H (in)	Strap Faces n_s (#)	Strap Width b_s (in)	Strap Thickness (ga)	Strap Thickness t_s (in)	Strap Initial Lat Stiffness k_s (k/in)	Yield Stress of Strap F_{sy} (ksi)	Capacity at Strap Lat Yield Q_{sy} (k)	Design Shear Strength $\phi_t Q_{sy}$ (k)	Lat Defl at Strap Yielding δ_{sy} (in)
A1	121	120	1	4	18	0.0481	17	45.3	6.2	5.9	0.375
A2	121	120	2	8	14	0.0715	98	32.2	26.2	24.8	0.267
A3	123	120	1	4	18	0.0432	15	60.2	7.5	7.1	0.498
C1	121	120	2	8	14	0.0679	93	81.3	62.7	59.5	0.673
D1	121	120	2	8	12	0.1080	148	37.6	46.1	43.8	0.311
D2	119	120	2	8	12	0.0998	136	55.6	62.5	59.4	0.460

Figure 5-1. Predicted lateral load-versus-deflection for all test panels.

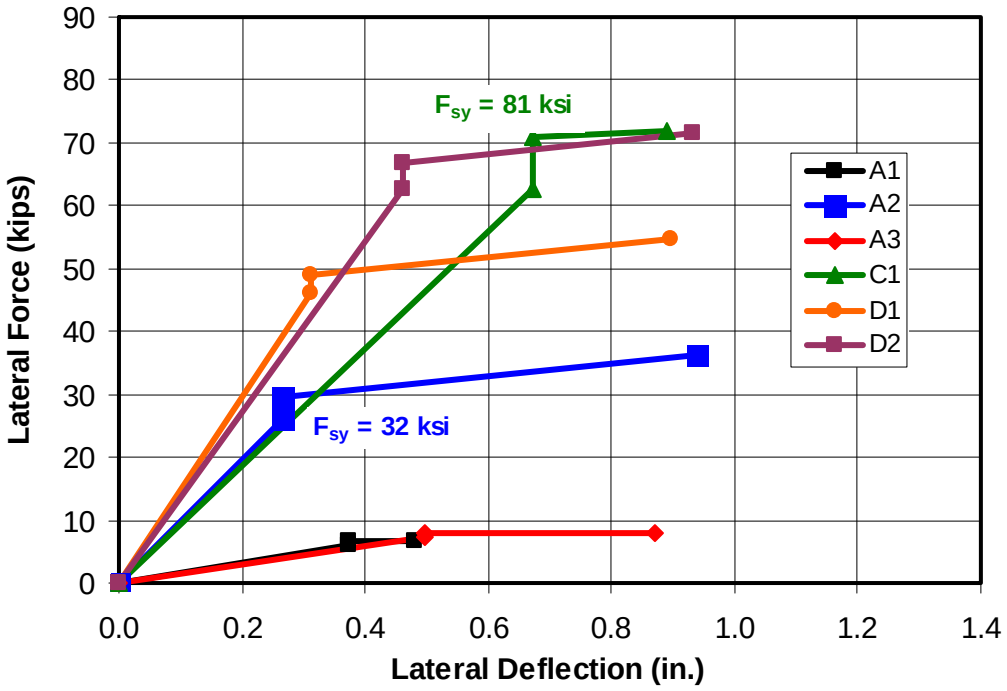

Table 5-2. Additional properties of test panel straps, gravity loads, and columns.

Column Type	Diagonal Strap Ult Stress F_{su} (ksi)	Max Ult Strap Stress F_{sumax} (ksi)	Max Gravity Load/ Panel GL_{max} = (kips)	Column Axial load at Strap Ult P_{vumax} (k)	Column Yield Stress F_{cy} (ksi)	Column Ultimate Stress F_{cu} (ksi)	Column Thickness (ga)	Column Thickness t_c (in)	Number of Studs /Column n	Panel Thickness /Column b_c (in)	Col Stud Flange Width b_f (in)	Column Depth h_c (in)
A1	53.9	53.9	27	20.8	41.4	49.9	18	0.0485	2	6.0	2.0	4.0
A2	50.1	50.1	27	53.8	60.3	72.9	12	0.1004	4	6.0	2.0	8.0
A3	62.5	62.5	10	12.5	41.8	49.9	16	0.0552	2	3.625	2.0	4.0
C1	82.5	82.5	30	78.4	66.3	82.0	12	0.0979	4	6.0	2.0	8.0
D1	47.6	47.6	27	71.4	45.1	53.7		0.1875	1	6.0	6.0	6.0
D2	72.6	72.6	30	97.4	50.0	64.0		0.1724	1	6.0	6.0	6.0

Table 5-3. Area and section modulus of test panels.

Column Type	Nominal Column Area A_c (in^2)	Distance to Extreme Fiber c (in)	In-Plane Mom of Inertia I_x (in^4)	Radius of Gyration r_y (in)
A1	0.97	2.00	2.75	1.68
A2	4.02	4.00	31.16	2.79
A3	0.84	2.00	2.10	1.58
C1	3.91	4.00	30.42	2.79
D1	4.27	3.00	23.8	2.36
D2	4.27	3.00	23.8	2.36

Table 5-4. Test panel predicted lateral capacities.

Column Type	Lat Defl at Strap Yielding δ_{sy} (in)	Capacity at Strap Lat Yield Q_{Tsy} (k)	Lat Defl at Col Yielding δ_{cy} (in)	Column Lat Cap @Yield Q_{cy} (k)	Total Lat Cap @CYield Q_{Tcy} (k)	Col Axial Stress @ Strap Yield f_{ca} (ksi)	Col Bend Stress @ Col Yield f_{cb} (ksi)	Col Comb Stress @ Col Yield f_{cr} (ksi)
A1	0.358	6.3	0.677	0.8	6.7	16.9	24.4	41.4
A2	0.268	29.7	1.038	13.0	39.3	6.6	53.7	60.3
A3	0.497	7.8	0.974	0.8	8.3	10.2	31.5	41.8
C1	0.670	71.0	1.001	12.3	75.1	11.8	54.5	66.3
D1	0.309	48.8	0.898	8.6	54.5	8.5	36.6	45.1
D2	0.463	67.5	0.927	8.9	71.9	11.0	39.0	50.0

The third point on Figure 5-1 is where the columns themselves yield. The columns have axial stresses coming from the gravity load and from the vertical component of the diagonal straps in tension that are connected to the top of the columns. The laterally deformed columns also have bending stresses from the P-delta effect of the vertical load and from the applied lateral load. The total lateral capacity at column yielding, Q_{Tcy}, includes braced frame and moment frame components, and are shown Equation 5-1. Values for Q_{Tcy} are shown in the second or center section of Table 5-4.

$$Q_{Tcy} = Q_{sy} + Q_{cy} \quad \text{(Eq 5-1)}$$

where

Q_{cy} = the lateral force carried by the columns at column yielding.

Q_{cy} is unknown in the above equation. To calculate Q_{cy}, the lateral displacement that would cause the column to yield is calculated. Yielding will occur when the combination of axial and bending stresses exceed the yield strength. The column total stress, f_{cr} at the extreme fiber is given by:

$$f_{cr} = f_{ca} + f_{cb} \quad \text{(Eq 5-2)}$$

where

f_{ca} = the column axial stress
f_{cb} = the column bending stress.

The column axial stress due to the gravity load and vertical component of the diagonal strap is determined by the following relationship:

$$f_{ca} = \frac{GL_{max} + F_{sy} n_s b_s t_s \left(\frac{H}{\sqrt{H^2+W^2}}\right)}{2A_c} \quad \text{(Eq 5-3)}$$

where

GL_{max} = the maximum gravity load per shear panel
A_c = the cross-sectional area of a single column.

The bending stress is due to the moment from both the P-delta effect of the vertical forces and lateral force carried by the columns, which is calculated as follows:

$$f_{cb} = \frac{Mc}{I} = \left[\left(GL_{max} + F_{sy} n_s b_s t_s \left(\frac{H}{\sqrt{H^2+W^2}}\right)\right)\delta_{cy} + \frac{Q_{cy} H}{2}\right]\frac{c}{2I_x} \quad \text{(Eq 5-4)}$$

where

δ_{cy} = the lateral deflection of the panel that causes the column to yield
c = the distance from the neutral axis of the column to the extreme fiber
I_x = the x-axis (in-plane) moment of inertia of a single column.

Equation 5-4 shows the bending stress in the columns is dependent on both δ_{cy} and Q_{cy}, and Equation 5-5 (below) shows the column lateral yield capacity, Q_{cy}, depends on δ_{cy}. Therefore, these values are determined iteratively, by selecting values of δ_{cy} until the total column stress, f_{cr} equals the column yield strength. In Equation 5-4 the GL_{max} value should be the total maximum gravity load supported by all of the columns whose lateral loads are resisted by the shear panel.

$$Q_{cy} = 2\frac{12EI_x\delta_{cy}}{H^3} \quad \text{(Eq 5-5)}$$

The columns yield before the straps begin to strain harden, so the strength of the straps used in these calculations should be their yield strength.

5.1 Panel A1

Table 5-1 and Figure 5-1 show that panels A1 and A3 have the smallest predicted capacity and stiffness of all the test panels. Table 5-4 indicates the A1 panel has only a 6% greater lateral capacity at column yield than at strap yield. This increase would be even smaller if the full moment capacity of the columns was not developed by the column-to-track connection. The panel lateral deflection at which the columns yield, δ_{cy}, is the smallest of all panels with a value of 0.68 in. The small increase in strength from the columns and the small ductility at column yielding indicate that the hysteretic envelope was expected to be badly pinched. These predictions assume full column fixity, and the columns are anchored with only screwed connections to the track above and below as shown in Appendix A, Figure A-3. These anchors were expected to be much closer to pinned than fixed, so the panel lateral capacity was expected be closer to the first point in Figure 3-1, and was not expected to increase as the panel deformed. The ultimate panel deformation however, should be much greater than the predicted deflection at column yielding at 0.68 in., because the pinned connections will reduce bending stresses on the columns.

5.2 Panel A2

Panel A2 is the same basic configuration as the A1 panel, but it uses much heavier materials. It has much greater predicted capacity and stiffness than the A1 panel. Table 5-4 shows this panel has 33% greater lateral capacity at column yield than at strap yield. This indicates that the column moment frame contribution to panel capacity is much greater than with the A1 panel. This is an upper estimate of column contribution, assuming full fixity of the column to nested stud-and-track connection. The heavy track and nested stud that is welded to the columns, as shown in Figure A-5, would greatly increase the moment resistance compared to the A1 panel. However, this connection detail was intended to provide shear resistance and only a limited moment connection, so the peak lateral capacity was expected to be closer to lateral capacity from the strap only, Q_{sy} (26.2 kips as shown in Table 5-1), than the capacity at column yield, Q_{Tcy} (39.3 kips in Table 5-4). This increase in strength from the columns and the larger pan-

el deformation at column yielding (1.038 in. in Table 5-4) indicate that the hysteretic envelope should not be as badly pinched as for Panel A1.

5.3 Panel A3

Figures A-6 and A-7 show the A3 panel configuration is almost identical to A1. The A3 panel is slightly wider (W = 123 in.), the strap actual thickness is slightly less (Table 5-1), and the strap strength is greater. The A3 column thickness is slightly greater, the yield strength is slightly greater and the ultimate strength is the same. The depth of the panels, which is the width of the columns were much less (b_c in Table 5-2 is only 3.625 in.) than for the A1 panel. The predicted lateral capacity from the strap only is greater for this panel because of the much greater strap strength. The gravity load applied to the panel (GL_{max} = 10 kips) is much less than for A1 (GL_{max} = 27 kips). Table 5-4 indicates the A3 panel has only a 12% greater lateral capacity at column yield than at strap yield. This greater contribution relative to the 6% for the A1 panels is because of the much smaller gravity load. The off-the-shelf anchors used in the A3 panels (Figure A-7), should provide slightly more moment resistance than the A1 panel had. However, fixity of the anchors was expected to be very small, so the peak lateral capacity of this panel was expected to be closer to yield capacity of the straps alone, Q_{sy} (7.5 kips in Table 5-1), than the capacity at column yield, Q_{Tcy} (8.3 kips in Table 5-4). This panel is much different from the A1 panel in that the columns and hold-down anchor uplift resistance are designed assuming the maximum yield (F_{symax}) and ultimate strength (F_{sumax}) of the diagonal straps equals the actual measured strength of the strap material. For the A3 panel the measured yield strength was 60.2 ksi, but the design yield strength was taken as 30 ksi to simulate the worst case loading condition when the diagonal strap yield strength equals twice the specified value for Grade 33 material (see beginning of Chapter 4). The purpose of this test was to evaluate the performance of the columns, connections, and anchors under the worst-case material strength variability of the strap. The panel should deform enough to develop the full yield strength of the straps, but it may not deform much beyond this because the strain-hardened straps that are not permitted in actual design may fracture at relatively small elongations.

5.4 Panel C1

Figures A-8 and A-9 show that the C1 panel is similar to the A2 panel, in that the diagonal straps and columns are the same size. The primary dif-

ferences are (1) the straps are welded rather than screwed to the columns; (2) the columns anchors are angle sections with stiffeners rather than heavy nested studs and tracks; and (3) that panel columns, connections, and anchors were designed assuming the strap coupon strength equaled the F_{symax}. This anchor detail should provide greater fixity for the columns to act as moment frames. The strap specification in Figure A-9 shows the C1 straps had a measured yield strength of 81 ksi, but the design yield strength was taken as 41 ksi to simulate the worst-case loading condition when the diagonal strap yield strength equals twice the specified value for Grade 33 material (see beginning of Chapter 4). This panel should deform enough to develop the full yield strength of the straps, but it may not deform much beyond this because of the strain-hardened straps. Figure 5-1 shows that the predicted capacity of this panel was much greater than the A2 panel even though the strap and column sizes are the same. This difference is because the strength of the C1 straps is much greater.

Table 5-4 indicates the C1 panel has 20% greater lateral capacity at column yield than at strap yield. Since the column fixity should be greater than for the A2 panel, the actual ultimate capacity should be much greater than when the straps yield, that is if the panel is able to deform significantly before fracturing the strain-hardened straps. The predicted yield capacity from the straps alone, Q_{sy}, is 62.7 kips (see Table 5-1), and the total capacity of the panel from straps and columns at column yield, Q_{Tcy}, is 75.1 kips (see Table 5-4).

5.5 Panel D1

The panel D configuration generally will have the highest capacity and stiffness because the panel columns are hollow structural sections of HSS, so that their thickness can be much greater than for columns built up from standard cold-formed steel studs. The panel D1 test panel uses HSS 6 x 6 x 3/16 in. columns, which is more than 80% thicker than the A2 or C1 column material. The D1 columns have a slightly greater section modulus ($S_x = I_x/c$ in Table 5-3), so they are generally stronger, but their moment of inertia, I_x, is lower, so they are less stiff than the A2 and C1 columns. This panel has the diagonal straps welded to the HSS columns and the anchors consist of heavy studs nested inside heavy tracks, as shown in Figures A-10 and A-11. The D1 panel has welded nested stud anchors, so the peak lateral capacity was expected to be closer to the lateral capacity from the strap only, Q_{sy} (46.1 kips in Table 5-1), than the capacity at column yield, Q_{Tcy} (54.5 kips in Table 5-4). These values indicate the D1 panel has 19% greater pre-

dicted capacity at column yield than from strap yield alone. However, the relatively small column fixity of the nested stud anchor connection should result in a relatively modest increase in capacity beyond yield and a fairly pinched hysteretic envelope.

5.6 Panel D2

Figures A-12 and A-13 show that the D2 panel is very similar to the D1 panel. The primary differences are (1) the columns anchors are angle sections with stiffeners rather than heavy nested studs and tracks; and (2) that panel columns, connections and anchors were designed assuming the strap coupon strength equaled the F_{symax}. This anchor detail should provide greater fixity for the columns to act as moment frames. The strap specification in Figure A-13 shows the D2 straps had a measured yield strength of 56 ksi, but the design yield strength was taken as 28 ksi to simulate the worst case loading condition when the diagonal strap yield strength equals twice the specified value. This panel should deform enough to develop the full yield strength of the straps. Figure 4-5 and Figure 4-6 show the D2 diagonal straps were not strain hardened. However, the worst-case loading condition may result in other panel failures not too long after diagonal strap yielding. But because the diagonal straps are not hardened, the panel should reach greater deformations than the C1 panel.

Table 5-1 and Table 5-4 indicate the D2 panel has 15% greater predicted lateral capacity at column yield (Q_{Tcy} = 71.9 kips) than at strap yield (Q_{sy} = 62.5 kips). The strength of the D2 column material is lower than for C1, so the yield capacity, Q_{cy}, of the D2 column is less. Since the column fixity should be good and the straps are not strain hardened, the actual ultimate panel capacity should be much greater than when the straps yield. The hysteretic envelope should be relatively wide.

6 Test Configuration, Procedures, and Instrumentation

Figure 6-1 shows the test frame and configuration used to test all monotonically and cyclically loaded cold-formed steel shear panels. This configuration includes the strong floor that supports the reaction wall and panel base beam. A large, 40 in. stroke horizontal actuator is mounted to the face of the reaction wall on one end and the load beam on the other end.

Figure 6-1. Test frame used for monotonic and cyclic shear panel testing.

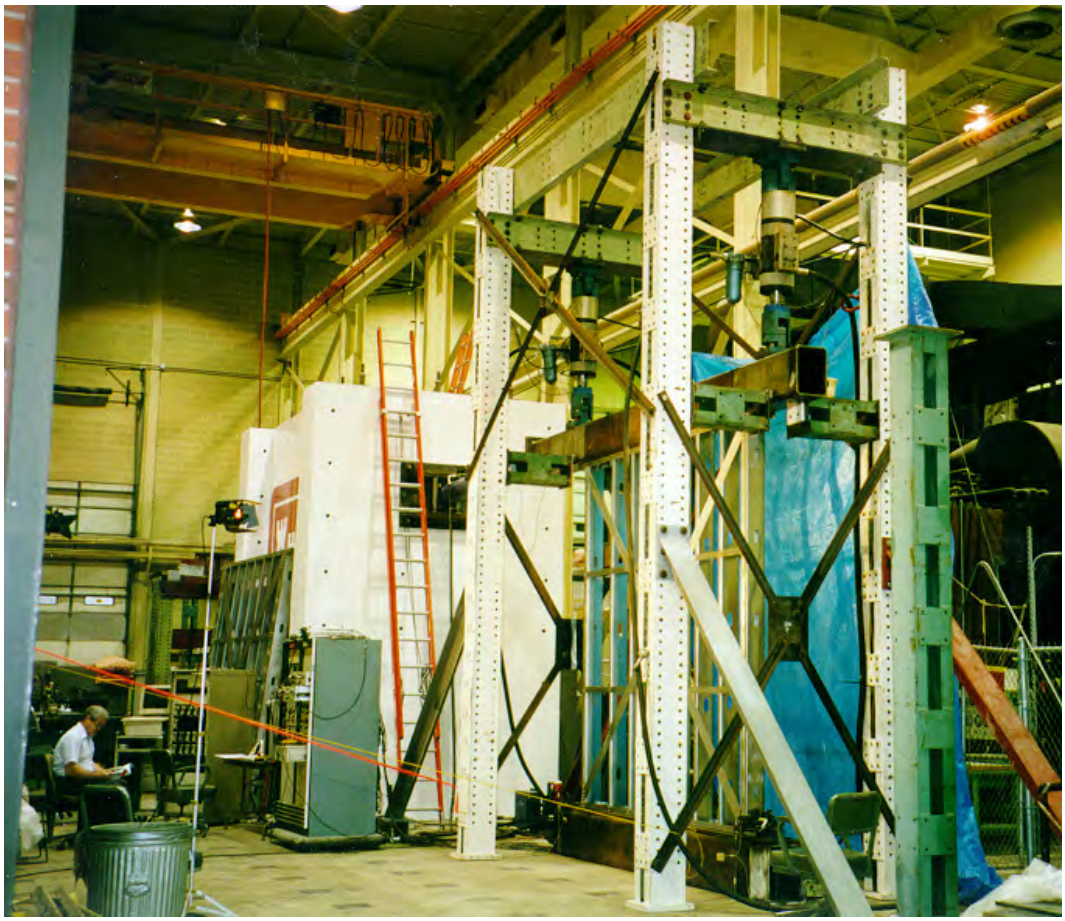

The figure also shows an A2 test panel installed in the frame. The bottom of the test panel is bolted to the top of the base beam, and the top of the panel is bolted to the bottom of the load beam. An additional steel frame was constructed around the test panel to support two vertical actuators which, in turn, provide vertical support for the load beam. The load beam is restrained against out-of-plane motions with Teflon® plates that bear

against the polished surfaces of the load beam. These plates are attached to the steel frame with short, horizontally oriented columns. The steel frame is braced to make it very rigid in order to prevent either in-plane or out-of-plane deformation. Figure 6-2 shows schematic drawings of in-plane and out-of-plane views of the test frame.

Figure 6-2. In-plane and out-of-plane views of the test frame.

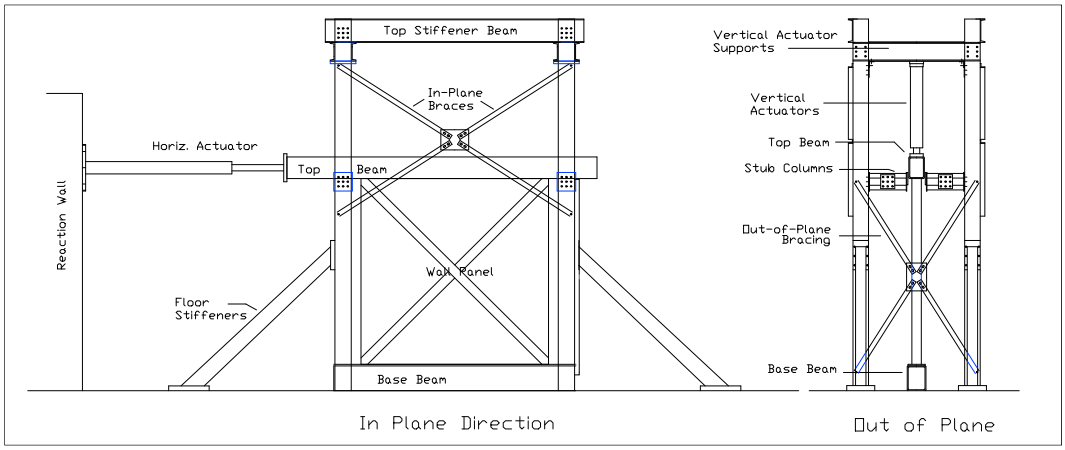

Partly because of the test configurations reported in Caccese et al. (1993) and Driver et al. (1998a), the test configuration used at ERDC-CERL was designed to prevent rotation of the top beam, allowing only pure shear and overall axial deformation of the panel. A constant axial load (2.5 kips/ft width, or 25 kips for a 10 ft wide panel) was applied to the top beam using two vertical actuators, and the top beam was not allowed to rotate. The top beam was allowed to deflect vertically at large horizontal deflection as the columns began to shorten or buckle. This vertical load was maintained so that when one column shortened, a portion of the vertical load was redistributed to the other shear panel column. This redistribution is similar to what will occur in a real building that has multiple shear panels in the same plane, connected on top by the floor diaphragm/floor beam. It is particularly important that the top beam be held horizontal after the columns begin to buckle and deform significantly vertically. The ability of the panels to sustain load even after severe damage is critical to determining panel ductility and seismic design recommendations. Also, the top beam and track/top beam connection must be very stiff to adequately anchor the tension field for sheet steel panels.

Vertical loads equal to the GL_{max} values in Table 5-2 (including the weight of the top beam) were applied to the panels using the vertical actuators. The total load of both vertical actuators was held constant in load control,

while the top beam was held horizontal with one actuator slaved to the other in stroke control. Stroke control was used to keep the deflection of the north actuator equal to that of the south actuator. This allowed the load to redistribute between the vertical actuators as needed to maintain the total load and horizontal orientation of the load beam. In a real earthquake the diaphragm on at the top of the wall would remain horizontal if it is rigid and two or more similar panels are installed in the same framing line.

For each panel configuration three specimens were tested, one was tested monotonically, and two were tested cyclically. The monotonic tests were conducted first to define the monotonic load-versus-deflection behavior through ultimate failure of each panel configuration. Monotonic tests also confirmed the calculated yield deflection, δ_y. The calculated yield deflection was the lateral deflection at which the diagonal strap would yield, defined in Equation 3-2. The calculated yield deflection based on the design yield strength was 0.273 in. for all panels. The calculated yield deflections based on the measured diagonal strap coupon yield strength were 0.375 in., 0.267 in., 0.498 in., 0673 in., 0.311 in., and 0.460 in. for test panels A1, A2, A3, C1, D1, and D2, respectively, as shown in the right column of Table 5-1. Recognizing that actual deflections would generally be greater, because of other sources of deformation in the panels, the yield deflection, δ_y, was set to 0.4 in. for all panels. This value agreed well with the observed yield deflection of the monotonically and cyclically loaded panels.

6.1 Monotonic test protocol

Lateral loads were applied using stroke control for both monotonic and cyclic tests. Monotonic tests were push-over tests in which the load was applied laterally at a constant stroke rate. A stroke rate of 0.5 in. per minute was used for the A1, A2, D1, and D2 monotonic tests, while a rate of 1.0 in. per minute was used for A3 and C1. The panels were loaded until ultimate failure or up to a maximum stroke of 15 in. The stroke rate is not critical, but should be slow enough to allow adequate time for making observations. The monotonic tests confirmed that panel yield consistently took place near 0.4 in.

6.2 Cyclic test protocol

The test protocol used should follow a standard method, so that test results can be compared with cyclic test results of other programs. Two simi-

lar cyclic test protocols were considered. Both use stroke control for cyclic testing to define hysteretic performance of building components. The first is the Applied Technical Council (ATC) 24, *Guidelines for Cyclic Seismic Testing of Components of Steel Structures* (ATC 1992). The second is the unpublished guidance, *SAC Testing Programs and Load Histories* (SAC n.d.). The ATC-24 guidance calls for a set number of cycles at deformations that are scaled to the measured or estimated panel yield deflections. The second and third columns in Table 6-1 show the deformations and number of cycles at those deformations scaled to a yield deflection of 0.4 in. and gives deformation values up to the 23rd load step, or deformation of 8.4 in. (for ATC-24 guidance).

Table 6-1. ATC-24 and modified SAC cyclic test steps based on 0.4 in. yield deformation.

Load Step #	ATC-24		SAC-2		Modified SAC (inches)
	Peak Deformation (inches)	Number of Cycles	Peak Deformation, ϑ (radians)	Number of Cycles, n	
1	0.2	3	0.00375	6	0.3
2	0.3	3	0.005	6	0.4
3	0.4	3	0.0075	6	0.6
4	0.8	3	0.01	4	0.8
5	1.2	3	0.015	2	1.2
6	1.6	2	0.02	2	1.6
7	2.0	2	0.03	2	2.4
8	2.4	2	0.04	2	3.2
9	2.8	2	0.05	2	4.0
10	3.2	2	0.06	2	4.8
11	3.6	2	0.07	2	5.6
12	4.0	2	0.08	2	6.4
13	4.4	2	0.09	2	7.2
14	4.8	2	0.10	2	8.0
15	5.2	2	0.11	2	8.8
16	5.6	2	0.12	2	9.6
17	6.0	2	0.13	2	10.4
18	6.4	2	0.14	2	11.2
19	6.8	2	0.15	2	12.0
20	7.2	2	0.16	2	12.8
21	7.6	2	0.17	2	13.6
22	8.0	2	0.18	2	14.4
23	8.4	2	0.19	2	15.0*

* Shear test panels at ERDC-CERL were tested monotonically and cyclically up to deformations as high as 15.0 in. (30 in. peak to peak). This deflection reached the rotation limit of the vertical actuators. Modification to the vertical actuator clevis would permit testing up to deformations of 40 in. peak-to-peak.

The SAC testing protocol is a modification of the earlier ATC-24 protocol. The SAC-recommended loading histories call for loading with a deformation parameter based on interstory drift angle, ϑ, defined as interstory height over interstory displacement. The commentary to the SAC document explains that the interstory drift angle of 0.005 radians corresponds to a conservative estimate of the value that would cause yield deformation. The interstory drift deformation that corresponds to an interstory drift of 0.005 radians is 0.63 in. (126 in. x 0.005). Because the SAC protocol was primarily developed for a different, more flexible structural system than the shear panels in this study (welded beam-to-column subassemblies), the interstory drift is modified (scaled) slightly so that the deformation at yield equals 0.4 in. Table 6-1 shows the SAC drift angles and corresponding modified SAC deformation values up through the maximum stroke limitation of the ERDC-CERL shear panel test facility (15 in.).

Most of the cyclic tests were conducted at a stroke rate of 6 in. per minute (Panels A2, D1, and D2). This rate was slow enough to allow adequate time to observe deterioration development while providing reasonable test duration for cyclic tests up to deformations of 15 in. Figure D-2 of Appendix D plots the modified SAC deformation time history up to the first cycle at 14.4 in., at a stroke rate of 6 in. per minute. A stroke rate of 3 in. per minute was used for Panel A1 cyclic tests, where the peak achieved deflections were lower and a slower rate was needed to observe the panel deterioration. A stroke rate of 12 in. per minute was used for both panel A3 cyclic tests and one panel C1 cyclic test.

6.3 Instrumentation

Table D-2 of Appendix D summarizes the purpose, type and location of all sensors used in the shear panel tests. This includes the force measured in the load cells and deflection measured in the LVDTs of the actuators. Figure D-1 of Appendix D shows the locations of all sensors on a schematic drawing.

Measurements taken by channels 7 through 9, as described in Table D-2 and Figure D-1, demonstrate that no significant slippage or uplift took place during any test. These values remained lower than 0.04 in. and 0.14 in., respectively, which are insignificant relative to the very large horizontal deflection. Therefore the horizontal deflection (DH) represents the shear panel deformation with no correction needed for slippage or rotation.

At very large horizontal deflections, the vertical actuators applied load to the top beam at a large angle. Both actuators always had the same angle and applied a net axial load to the top beam of GL_{max} minus the weight of the load beam and half the horizontal actuator (2.45 kips). At large angles, these actuators applied a horizontal component to the top beam that must be combined with the load in the horizontal actuator to calculate the total shear force, TSF. This total shear force can be expressed as

$$TSF = FH \pm FS(sin\theta) + FN(sin\theta) = FH \pm TVF(sin\theta) \quad \text{(Eq 6-1)}$$

where

FH = the horizontal actuator force
FS = the South actuator force
θ = the Vertical actuator angle (in radians) with respect to vertical
FN = the North actuator force
TVF = the total vertical actuator force
$\theta = \arctan\left(\frac{DH}{53"}\right)$ (Eq 6-2)
DH = the horizontal deflection

Lengths of the vertical actuators are 53 in.

Then the total shear force, TSF (when positive horizontal deflection is to the south), becomes:

$$TSF = FH - TVF\left(\sin\left(\arctan\left(\frac{DH}{53"}\right)\right)\right) \quad \text{(Eq 6-3)}$$

All panel test results plot this total shear force versus shear deflection.

7 Performance of Test Panels

Each of the shear panels shown in Table 7-1 were tested either monotonically or cyclically in the ERDC-CERL test frame shown in Figure 6-1. Drawings of each shear panel are shown in Figures A-2 through A-13 of Appendix A. Three specimens of each panel type were tested, with the first tested monotonically (e.g., panel A1a) and the other two tested cyclically (e.g., panels A1b and A1c). The test frame and test control procedure were evaluated by cyclically testing an extra A2 panel specimen (A2 Trial). Table 7-1 summarizes the results of all monotonically and cyclically tested shear panels. Tables in Appendix B provide details on damage progression with respect to lateral deformation for all these test panels. The following sections summarize the performance of each shear panel with plots of their total shear force, TSF (see Equation 6-1) versus horizontal deflection, DH (defined in Chapter 6).

Table 7-1. Summary of test panel performance.

Test Panel	Load Type	Load Rate (in./min)	Linear Shear Stiffness (kips/in.)	Shear Load at 0.4 in. Deflection (kips)	Lateral Deflection at Ultimate Shear Load (in.)	Ultimate Shear Load (kips)
A1a	Monotonic	0.5	13	4.0	1.1	5.2
A1b	Cyclic	3.0	13	4.0	1.2	5.9
A1c	Cyclic	3.0	13	4.3	1.2	6.5
A2a	Monotonic	0.5	49	18.7	7.8	36.4
A2 Trial	Cyclic	1.5	63	20.6	6.3	33.9
A2b	Cyclic	6.0	58	20.9	5.6	34.5
A2c	Cyclic	6.0	63	21.7	3.9	34.4
A3a	Monotonic	1.0	9	3.5	5.0	9.1
A3b	Cyclic	12	10	3.9	5.9	9.2
A3c	Cyclic	12	13	4.4	3.1	9.2
C1a	Monotonic	1.0	76	25.4	1.7	67.1
C1b	Cyclic	12	92	31.0	2.0	65.3
C1c	Cyclic	6	96	27.3	2.1	69.8
D1a	Monotonic	0.5	108	36.3	8.7	59.1
D1b	Cyclic	6.0	98	36.3	3.9	58.0
D1c	Cyclic	6.0	95	33.9	4.0	57.8
D2a (North)	Monotonic	0.5	69	24.4	1.7	64.2
D2a (South)	Monotonic	0.5	69	24.4	1.8	59.1
D2b	Cyclic	6.0	72	28.7	2.3	71.6
D2c	Cyclic	6.0	64	23.9	2.2	66.7

The A3, C1, and D2 test panels were all detail-validation test panels. A major concern about cold-formed steel construction is the impact of the large material strength variability. Therefore the A3, C1, and D2 test panels were all configured to evaluate the effectiveness of design recommendations in accounting for this variability. The most critical condition is when the diagonal straps have their maximum strength, and other panel components have their minimum design strength. In large seismic motions, the stronger diagonal straps would behave elastically until larger response motions of the building occur. The building response acceleration and resulting inertia forces would be greater with the stronger straps, loading the panel connections, columns, and anchors at higher levels. These components each have potentially brittle modes of failure that must be prevented. Chapter 11 accounts for this strap strength variability and provides recommendations that prevent brittle modes of failure, based partly on the results of these panel tests.

7.1 A1 test panel results

Figure 7-1 plots the measured lateral load versus deflection of the A1a, monotonically loaded shear panel. This figure also plots the predicted lateral load versus deflection for this panel, shown earlier in Figure 5-1. The top of this panel was pulled to the south (left in Figure A-2 of Appendix A). The A1 test panels performed poorly because the columns were not well anchored and did not have adequate shear capacity to resist the lateral forces applied by the diagonal straps. The A1 panel diagonal straps were connected to the columns at their ends with thirteen #10-16 screws as shown in Figure A-3. The columns were screwed to the track at both their top and bottoms using eight #10-16 screws as shown in the same figure. Table B-1 of Appendix B describes how this panel failed by the shear failure of the screws that connect the top of the south (left) column to the panel track on the same face as the diagonal strap.

Figure 7-1. A1a monotonic test panel measured and predicted lateral load versus deflection.

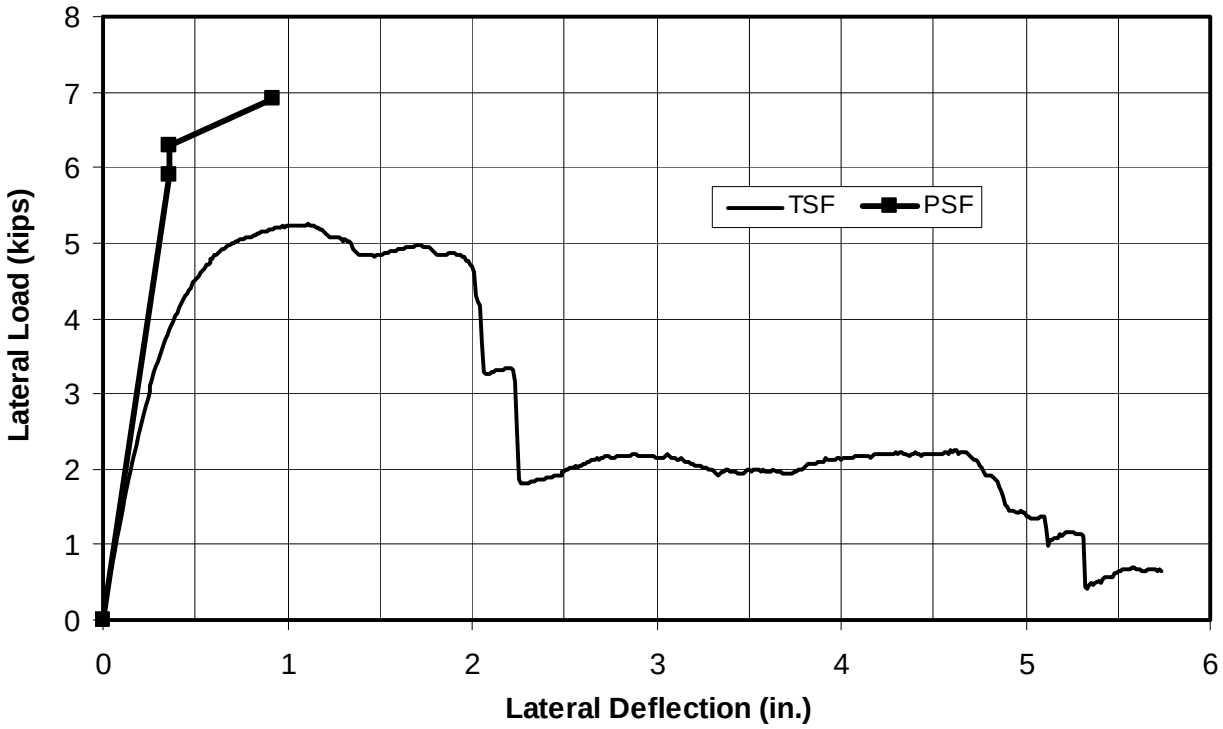

Figure 7-2 shows an overall view of the failed A1a test panel, where the panel failure was at the top of the left (south) column, which is the top left corner of the picture. The left side of the picture shows the scale of the panel. The screw connection failure was a combination of the shear failure of the screws themselves and tearing of the column at the screw connections (see Figure 7-3). The diagonal strap and column were both 43 mil (18 ga) in thickness, while the heavier track was 68 mil (14 ga), explaining why the tearing took place in the column where it was attached to the track with only eight screws. After the complete failure of this joint, at 2.1 in., the panel lateral resistance dropped dramatically, as shown in Figure 7-1. The diagonal straps were only installed on the front face of the panel. Figure 7-3 shows that after the screwed connection failure the column twisted so that a secondary load path developed from the front face diagonal strap through the twisting column and into the back-face column connection to the track. This column also continued to resist the vertical load applied to it without buckling. However, the screwed connection at the column-to-track joint is considered a brittle failure and is unacceptable performance. This panel configuration violates the recommendations presented in Chapter 11 on column and anchor shear capacity; following those recommendations would prevent the failure seen in this test panel.

Figure 7-2. Overall view of failed A1a monotonically tested shear panel.

Two secondary load paths developed after 2 in. of lateral deformation. The first was the diagonal strap to the twisted column to the back face track described earlier. The second was from the same strap to the intermediate studs, which carried a small amount of lateral load in weak-axis bending, to screwed connections to the track. The intermediate stud closest to the failed column connection was most efficient in resisting lateral load because the distance it spanned from the connection to the strap to its connection to the track was the least of the intermediate studs. Figure 7-1 shows that these secondary load paths develop only 42% of their ultimate capacity. Table B-1 indicates that shear failure of the screws at the back face of the top of the south column takes place at 5.0 in., explaining the large drop in resistance seen near 5 in. in Figure 7-1. The plot of the predicted lateral capacity is at strap yielding is greater than the ultimate measured capacity, indicating that the diagonal strap likely did not yield before the screwed connection began to fail.

Figure 7-3. Close-up view of column-to-track screw connection failure and column twisting in panel A1-a monotonic test.

Figure 7-4 plots the lateral load versus deflection of the A1b cyclically loaded shear panel. Comparison between the measured and predicted capacity in this figure indicates that the diagonal straps likely began to yield. Table B-2 indicates the straps began to yield at 0.4 in. Table B-2 shows that at 1.2 in. deflection the south column began to twist at the top track, indicating that the screwed connection between the column and track was beginning to fail similar to the A1a panel. Failure of the top south connection would have been due to lateral deflection to the south, which is positive deflection in Figure 7-4. The figure shows that lateral resistance began to drop dramatically due to this failure, decreasing from a peak of 5.9 kips to 3.4 kips at 1.5 in. When the panel was loaded in the other direction, just one screw sheared at the bottom south connection of the diagonal strap to the column at 1.2 in. lateral deflection. However, larger deformation cycles of 1.6 in. produced tearing in the south column at the screwed connection to the bottom track on the front face, which had the diagonal strap attach just inches above. Table B-2 indicates the top of the north column, buckled at 1.6 in. deflection in the same negative direction. At 3.2 in. positive deflection the south column screwed connection to the top track failed completely. Figure 7-4 shows almost complete loss of lateral capacity at 4.0 in of positive deflection, when the south column had twisted and torn to such

an extent that little lateral load was carried through the column to the back face of the top track. Finally, at 5.6 in. of lateral capacity the entire panel collapsed under gravity load.

Figure 7-5 shows the measured lateral load versus deflection of the cyclically loaded A1c panel, plus the predicted capacity. The failure of this panel began in an identical manner as the A1b cyclically loaded panel, where the screwed connections between the columns and tracks began. Since the failure occurred at the same lateral deflection and mode of failure was identical, it was decided to stop the test at 1.6 in. lateral deflection and take apart these joints so the development of damage in the column could be more closely inspected. Figure 7-5 shows that the measured capacity of this panel was almost identical to the A1b panel up to the point where the test was stopped.

Figure 7-4. A1b cyclic test panel measured and predicted lateral load versus deflection.

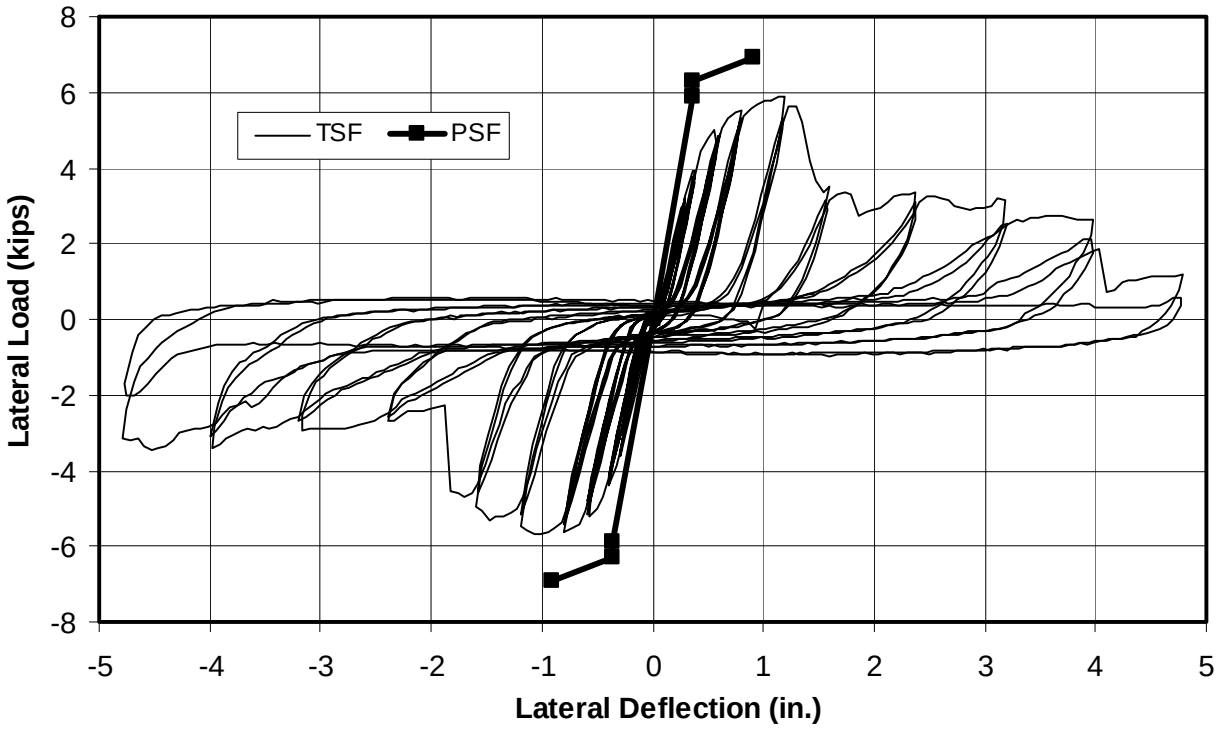

Figure 7-5. A1c cyclic test panel measured and predicted lateral load versus deflection.

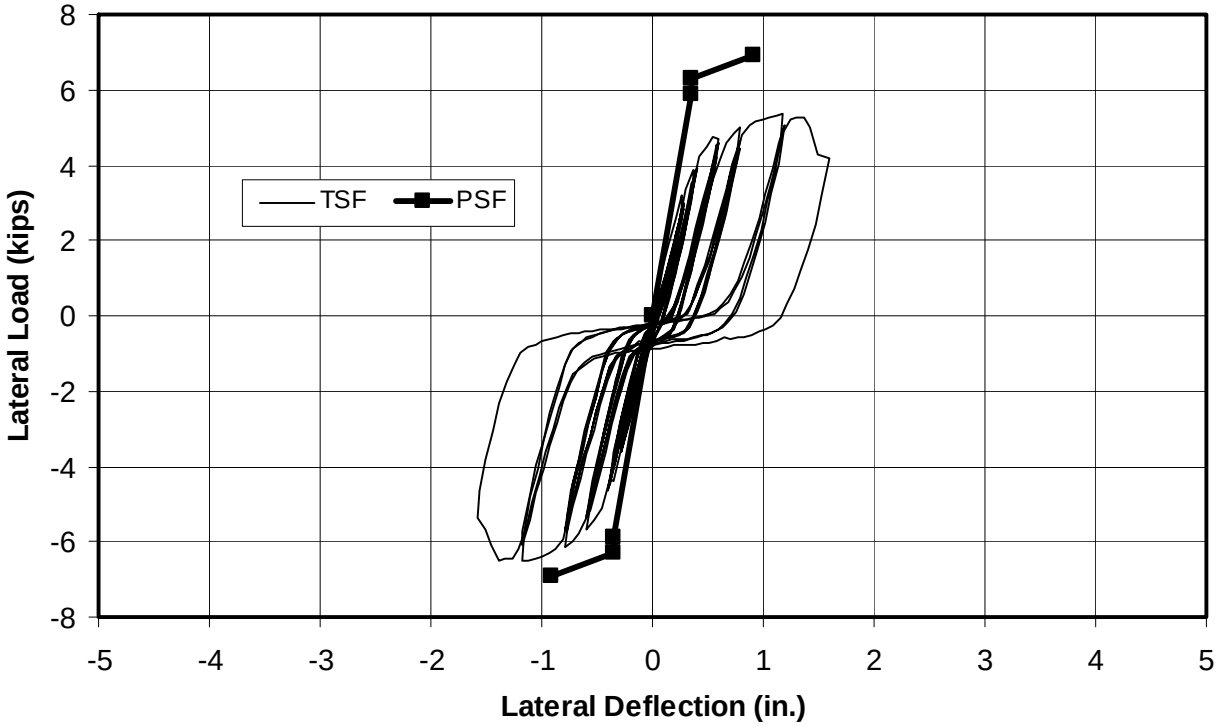

Figure 7-6 through Figure 7-9 show close-up pictures of the top or bottom of both columns at their connection to the top or bottom track. The diagonal straps were attached to only the front of the A1 panel, and these straps were removed from the column so the area of the column below the strap could be inspected. The screws between the tracks and columns were also removed and the tracks were pried back, exposing the condition of the columns behind the track. The joints shown in Figure 7-6 through Figure 7-9 are shown in ascending order of column damage. Figure 7-6 shows the top of the right (north) column. Just below the pried-up track shown at the top of this figure is the second row of screw holes that were screwed to the track. The next row of holes in the column were where the first row of screws were attached to the diagonal strap. The strap pulled in tension to the left and down at this joint, causing the lateral deformation in the column between these two rows of screw holes. Note that the column base metal is essentially undamaged at the screw holes and the only distress to this joint is the shear deformation. Figure 7-7 shows the bottom of the right column, where the column is deformed much more in shear between the row of screws that were attached to the top of the track and the row above that were attached to the bottom of the strap. The column here has buckled locally in a failure mode called *shear buckling*. At this point, the

screw holes have begun to elongate, but the column has not torn at the screw holes. Figure 7-8 shows the top of the left (south) column, where the opposite end of the diagonal strap that was attached to the joint in Figure 7-7 is anchored. Here the column has shear buckled even more than in Figure 7-7, and the column material has torn significantly starting at the screw holes. Note that elongation of the strap, and deformation of the joints in both Figure 7-7 and Figure 7-8 would have needed to deform laterally a total of 1.6 in. The amount of deformation in these joints suggests the straps may not have yielded. Figure 7-9 shows a view of the bottom of the left column where the damage was the greatest of all four. Here the shear buckling of the columns is the greatest, with much of the deformation due to the significant tearing through much of the front face of the column. The deformation in this joint was greater than the others, while the deformation in the joint connected to the opposite end of the same strap is the least (Figure 7-6), because the total of these joint deformations and strap elongation also needed to equal 1.6 in. in the lateral direction. Figure 7-9 shows the strap that was removed from the front face, and laid against the back face. This figure also shows the panel anchors, simply consisting of loose steel plates laid inside the heavy track and bolted down to the test frame. The figure shows that these plates were spaced about 0.5 in. from the exterior and 1 in. from the interior face of the column so they would not unintentionally brace the columns. This panel violates recommendations provided in Chapter 11 on the shear capacity of the columns and anchors. It also highlights the potential vulnerability of light-gage cold-formed steel materials to buckling or tearing, failures modes that must be prevented for ductile seismic design.

Figure 7-6. Top of right (north) column after A1c panel test.

Figure 7-7. Bottom of right (north) column after A1c panel test.

Figure 7-8. Top of left (south) column after A1c panel test.

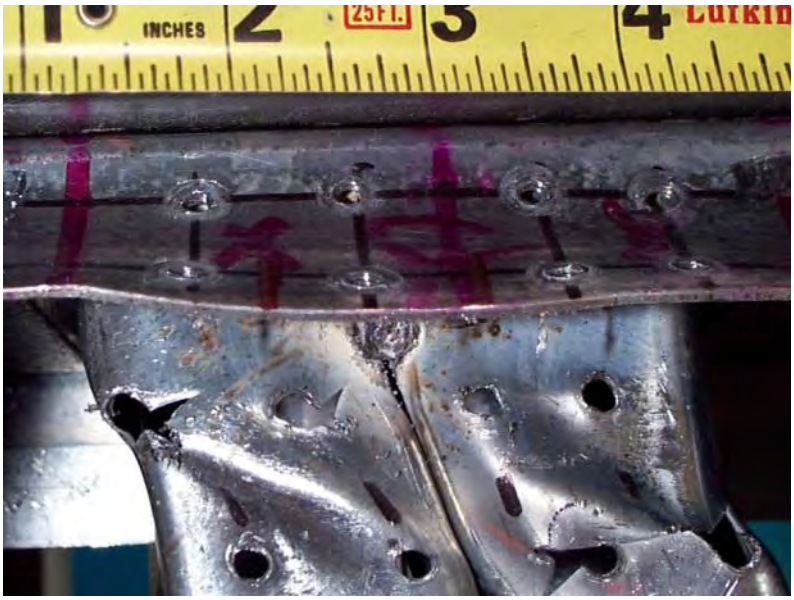

Figure 7-9. Bottom of left (south) column after A1c panel test.

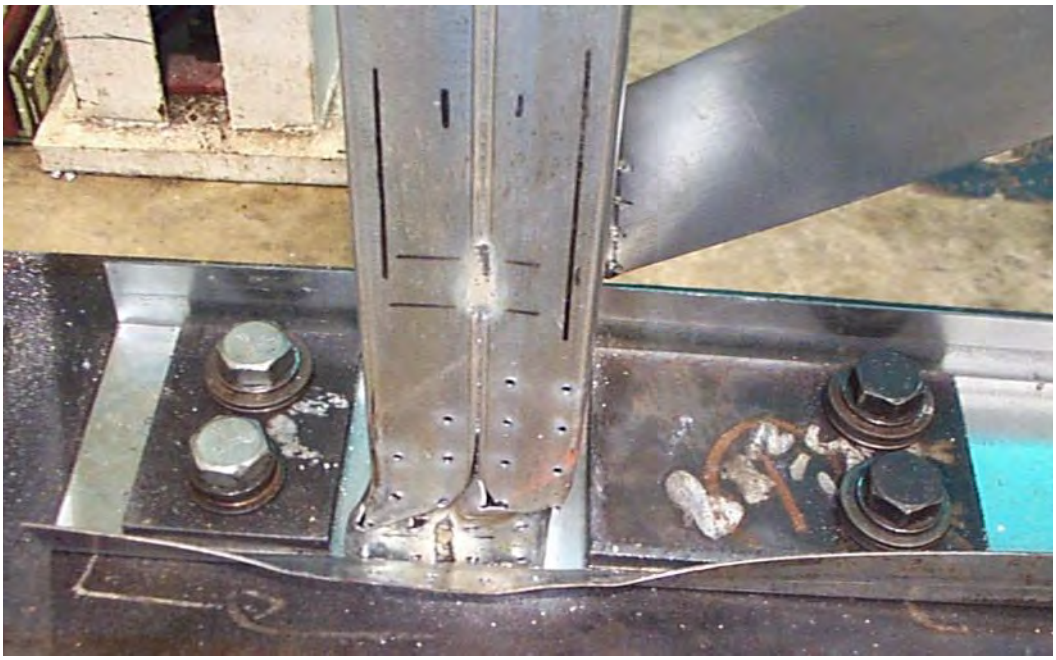

7.2 A2 test panel results

Figure 7-10 plots the measured lateral load versus deflection of the A2a, monotonically loaded shear panel. This figure also plots the predicted behavior shown in Figure 5-1. The top of this panel was pulled to the south (left in Figure A-4 of Appendix A). Figure 7-10 shows that the A2 shear panel deformed significantly without loss of lateral capacity, demonstrating excellent ductility. The panel lateral resistance was still 33.6 kips (92%

of the ultimate capacity) when the test was stopped at 15 in. of lateral deformation. Figure 7-10 shows this panel had significant over-strength, developing much greater resistance beyond yield capacity. Comparison between the measured and predicted capacity in Figure 7-10 suggests that much of this was due to the columns acting as a moment frame. However, the A2 diagonal strap coupon plots shown in Figure 4-1 and Figure 4-2 reveal that much of the increase in panel capacity was due to development of greater strap strength with increasing strain.

Figure 7-10. A2a monotonic test panel measured and predicted lateral load versus deflection.

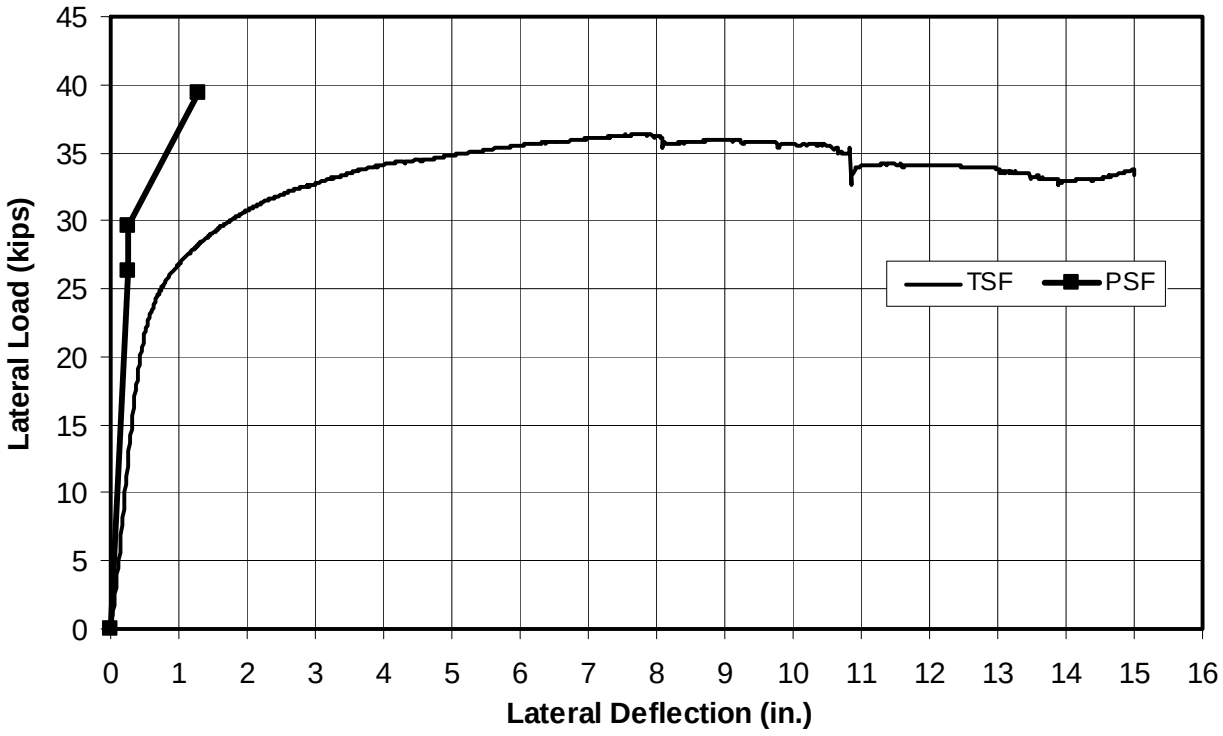

Using the coupon data in Figure 4-2, the strap stress is 32.2 ksi at a strain of 0.003 in./in., which equates to 26.1 kips panel capacity (Equation 3-1) at 0.72 in. lateral panel displacement (Equation 3-2). At larger strap strains, such as 0.03 in./in., the stress would be 40.7 ksi, which equates to 33.0 kips panel capacity at 7.2 in. panel displacement. These displacements are due to strap elongation only, but actual panel displacements would be greater due to rotation of the columns at their anchors. This demonstrates that most of the increase in panel capacity after yielding is due to increase strap stress, and a smaller portion is due to the columns acting as a moment frame. The predicted behavior shown in Figure 7-10 assumes no rotation in the column anchors. In fact, the A2 anchor detail

permits large rotations, so that the measured deformations are much greater than predicted.

Figure 7-10 shows that the strap begins to yield at about 0.5 in. lateral deformation and the panel is less stiff than predicted. This lack of stiffness is due to the joint rotation permitted at the column anchors. Table B-4 indicates that the panel anchors begin to fail with cracking at the column to nested stud welds, at the lips of the nested studs, at 2.1 in. deflection. These cracks progress to weld fracture at 2.9 in. deflection. The track and nested studs failed in shear with vertical base metal cracks along the columns. At 5.3 in. deflection, the welds at the back of the columns crack, and they completely fail at the bottom of the north column at 5.9 in. deflection. These failures at the column anchors do reduce the fixity of the columns, and do reduce the moment frame capacity of the column, but the overall panel capacity does not begin to drop until slight loss in capacity at 7.9 in. Screws between the straps and columns began to fail at 6.2 in, but this did not reduce panel capacity. The lips of the nested studs drove into the column material, causing local buckling and eventually puncturing the columns, but this did not reduce capacity.

An additional A2 panel (A2 Trial) was constructed and tested cyclically before any other shear panel in order to test the test frame, test procedure and control, and means for documenting the tests. This test revealed that the test control method was effective, loading cyclically as planned, while holding the load beam horizontal with the appropriate vertical load. The test also demonstrated that the data channels shown in Table D-2 and Figure D-1 were recording properly and that visual observations could be made while testing at a faster load rate than used in the A2 Trial panel test. Table 7-1 shows that the A2 Trial panel test used a load rate of 1.5 in/min, while the other A2 cyclically load panels used a rate of 6 in./min. This panel and the A2a monotonic panel were painted with a whitewash material (lime and water), so that yielding or other deformations of the panel could be clearly seen on the galvanized cold-formed steel material surfaces. The whitewash was applied after the panels were installed in the test frame because it is a brittle coating and would otherwise flake off during panel installation. These early tests revealed that panel deformation and failure modes were clearly visible, and these observations were not enhanced with the white-wash. Therefore, the whitewash material was not applied to other test panels.

Figure 7-11 plots the load-versus-deformation performance of the A2 Trial shear panel, along with the same predicted capacity shown in Figure 7-10. Table B-5 documents the panel observations, but the amplitude of panel deformation at which these observations were made were often not recorded in this trial test. In this panel greater damage occurred in the diagonal strap-to-column screwed connections than in the monotonically loaded panel. The damage to the screw connection (screw rotation and shear) also took place at smaller deformations than in the monotonic test. This difference may be due to the multiple cycles of load reversals on these fasteners, often referred to as *low-cycle fatigue*. This panel was tested to 15 in. in the positive direction without significant loss of capacity (see observations in Table B-5), but only to 9.6 in. in the negative direction. Figure 7-11 plots the measured capacity in both directions through the 9.6 in. cycles. The measured capacity shown in Figure 7-11 was slightly greater in this cyclic test than in the monotonic test (Figure 7-10) up to deflections of 2.0 in. Beyond 2.0 in. lateral deflection, the lateral capacity increased much less than it did in the monotonic test. It appears that the increase in capacity in the cyclic test was due to the increase in stress of the strap material as indicated in the coupon tests (Figure 4-2), while the additional contribution from the columns acting as a moment frame was much less than it was in the monotonic test. The nested stud and track anchors for the columns failed at lower deformations in this cyclic test than under the monotonic loading.

Figure 7-12 plots the load-versus-deformation performance of the cyclically loaded A2b test panel, along with the predicted capacity. Table B-6 documents the panel observations including detailed records of the lateral deformation at which various failures modes took place. Figure 7-12 shows that the panel capacity in the positive direction was slightly greater than in the negative direction, but the average of the two agrees with the A2 Trial panel values. Figure 7-12 shows that the A2b panel was tested cyclically to 15 in. in both directions, with no loss of lateral capacity.

Figure 7-11. A2 Trial cyclic test panel measured and predicted lateral load versus deflection.

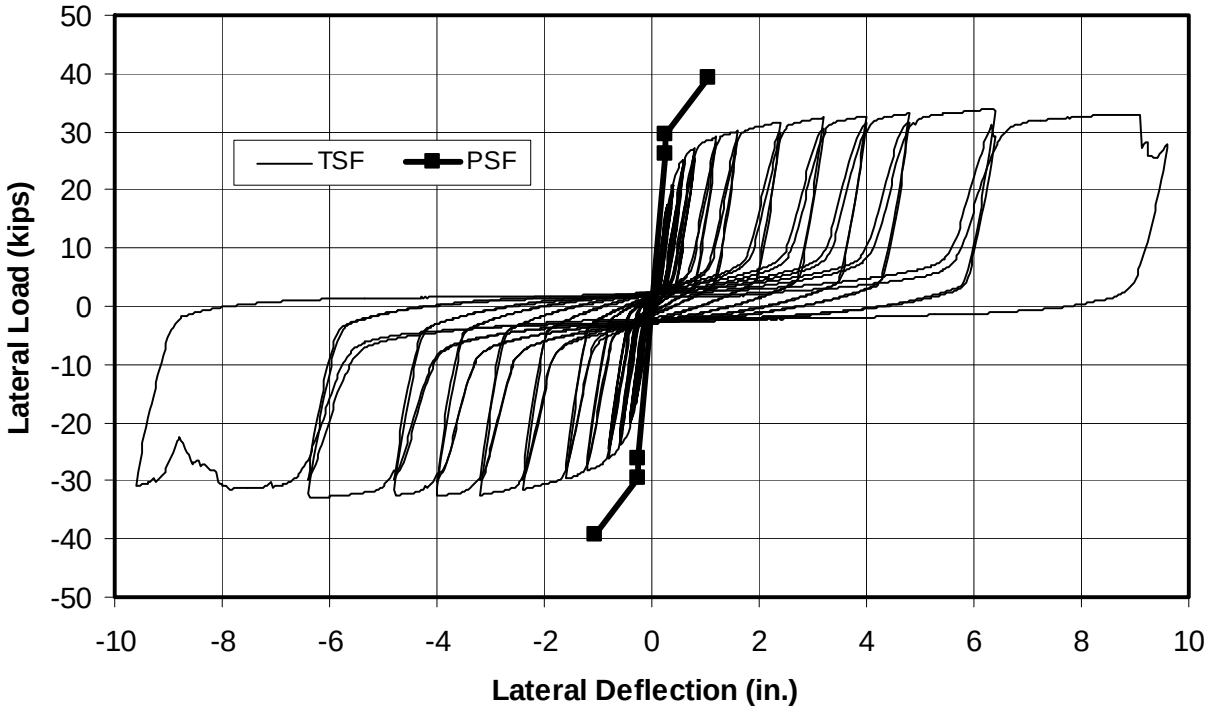

Figure 7-12. A2b cyclic test panel measured and predicted lateral load versus deflection.

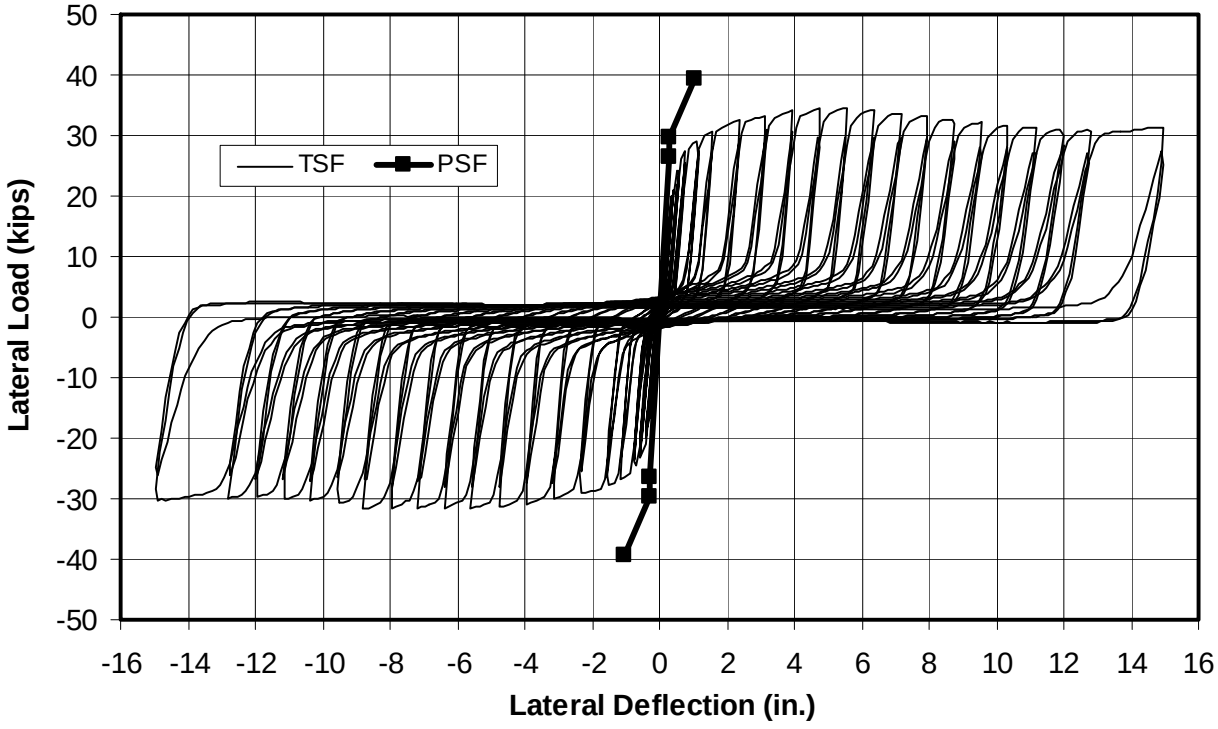

The diagonal straps of this panel began yielding at 0.4 in. lateral deflection; the welds joining the nested stud lips to the columns began to crack at 1.2 in.; these welds fractured at 2.4 in.; some tracks in the column anchors began to buckle at 3.2 in. while others failed in shear; the weld at the web of the track to the column fractured at 6.4 in.; and the tracks at these anchors fractured in shear at 6.4 in. Figure 7-13 shows a buckled track at the top of the north column after the end of the A2b test. A few diagonal strap-to-columns screws failed in shear early in the test, but these caused no reduction in capacity because the straps continued to yield and elongate throughout the length of the straps. A number of screws at the track-to-column connections failed, which led to a small reduction in the moment resistance of the column anchors.

Figure 7-13. Top of north column showing buckled track after the A2b cyclic test.

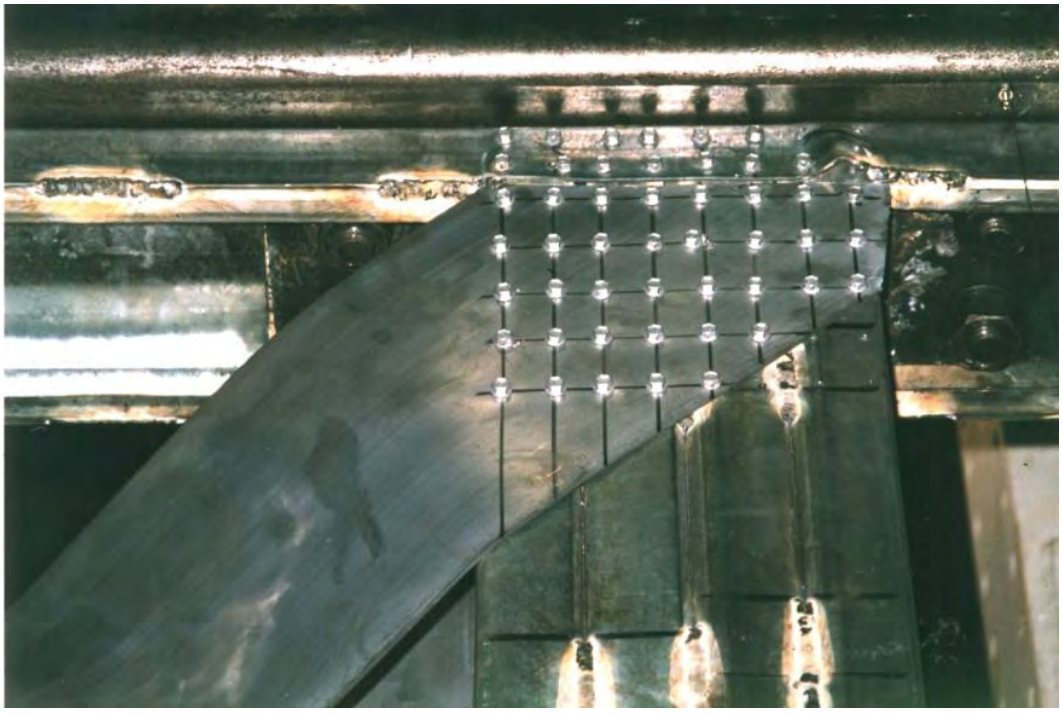

This panel reached its greatest average (of positive and negative) ultimate capacity of 33 kips at a lateral deformation of 5.6 in. This capacity included the effects of the increased strap stress at greater strains, plus a contribution of the columns acting as moment frames. After 5.6 in. deflection, the small decrease in capacity was due to the damage to the column anchors, which reduced the moment frame capacity, plus the increasing moment loading of these anchors due to the P-delta effects of the large deflection. Table 5-2 shows that the total vertical load, GL_{max}, was held at 27 kips, making the moment due to P-delta effects significant at large deflections.

Figure 7-14 plots the load-versus-deformation performance of the A2c test panel, along with predicted capacity. Table B-7 documents the panel observations and failure modes. Figure 7-14 shows that the panel capacity was slightly greater in the positive direction than the negative, and the average agreed well with the other two cyclically tested A2 panels. Figure 7-14 shows this panel was tested to 12.8 in. in both directions, with the only loss in capacity taking place at 11.8 in. in the negative direction. Table B-7 indicates this panel failed in a very similar manner as A2b, but with the degree of failure appearing to take place at smaller deformations. Table B-7 shows that the north column began to tear at the bottom anchor at 5.6 in. and on top at 6.4 in. At very large panel deformations, the nested stud lip punched through the interior face of the 12 gage columns. Figure 7-15 shows an overall view of the A2c panel deformed 12.8 in. in the negative direction at the end of this test. This panel provided excellent ductile behavior, resisting the full lateral load of the diagonal straps. However, the welding of a nested stud inside the track was considered an expensive way to provide column anchorage. The diagonal strap had a yield strength, F_{sy}, of only 32 ksi. Had this strength been much greater (see Chapter 4 on strength variability) it is likely that brittle modes of failure in the strap connections and anchor would have prevented the good ductility seen in these panels. Finally, the load-versus-deflection plots for this panel show very pinched hysteresis envelopes, indicating that the columns contribute very little lateral resistance when deforming in the opposite direction of a peak excursion in one direction. These panels would provide limited energy dissipation compared to panels with less-pinched hysterics from improved panel moment fame capacity.

Figure 7-14. A2c cyclic test panel measured and predicted lateral load versus deflection.

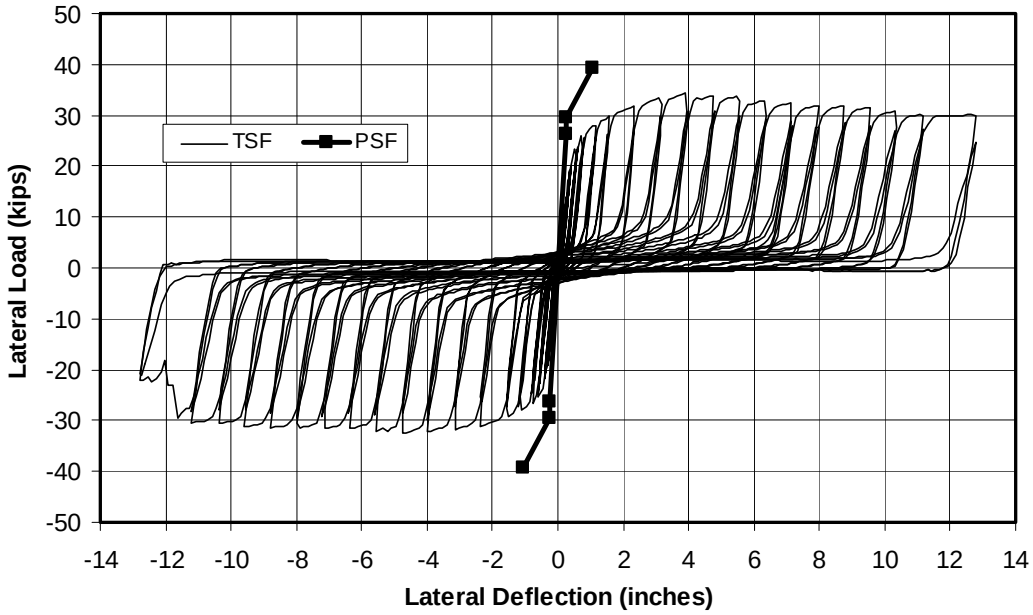

Figure 7-15. Overall view of the A2c panel, deformed 12.8 in. in the negative direction.

7.3 A3 test panel results

The A3 test panels used off-the-shelf hardware (Simpson Strong-Tie S/HD8) to anchor both the top and bottom of the panel columns. These

anchors were installed on both faces of each column as shown in Figures A-6 and A-7. Figure A-7 shows that each anchor was screwed to the columns with 18 #10-16 self-tapping screws, using the holes closest to the ends of the columns. Several additional screw holes were available, but only 18 were used because 18 were needed to resist the design uplift force assuming a design yield strength of the diagonal straps of 30 ksi. The actual strap yield strength was 60 ksi (see Table 4-1), but designing several components of this panel for a strap strength of only 30 ksi tested this panel for the maximum strength variability of the straps, providing the detail validation needed for this panel configuration. This panel used the same basic configuration as the A1 panel and had similar capacity. In addition to the off-the shelf anchors and strap strength variability design, this panel differed from A1 in that the total vertical load, GL_{max}, was much less at 10 kips (Table 5-2 shows a 27 kip load was applied to the A1 panel).

Figure 7-16 plots the measured lateral load versus deflection of the A3a monotonically loaded shear panel. This panel was first tested in the positive direction (left in Figure A-6). Detail A and Note 2 in Figure A-7 show that two screws (#10-16 Teks) were used on each side of the columns to lightly attach the track to the columns (one on either side of the individual studs). These screws were not intended as part of the panel design, but were added simply to fix the top and bottom tracks to the panel so it could be moved. The first half of Table B-8 shows that these nonstructural screws that connected the top of the south (left) column to the track began to fail at 1.3 in. lateral deflection, and these failures resulted in the spiked loss of capacity on the positive side of the plot in Figure 7-16. The measured data in Figure 7-16 shows that this panel did not reach its predicted yield capacity until a deflection of 1.9 in. and the shape of this plot at 1.9 in. also indicates yielding of the diagonal strap. Therefore, the screw connection failure began before strap yielding. Table B-8 shows major distortion of the top of this column above where the strap was screwed to the column at 2.8 in. deflection. The two screws between the front face of the track and the column provided the initial shear support for the column, but the intended design was for the anchors to provide this support. The thin material of the columns prevented the anchors from serving this purpose because the column buckled in shear once the screws to the tracks failed. The thin column material could only provide insignificant shear capacity in tension. The anchors at the in-plane interior side of the columns were intended to support the columns by the columns bearing up against them when the straps were loaded in tension. However, the columns buck-

led in shear, preventing the development of bearing resistance. The anchors on the in-plane exterior face were intended to provide hold-down resistance for both uplift and bending of the column. The screws connecting the anchors to the columns on the exterior face should not be relied upon to resist tensile force. However, these screws did not fail, but rather the thin column failed locally in bending between the screws and the column face. These off-the-shelf anchors may have worked had they been welded to the columns along their exterior vertical edge, where they meet the exterior side; and exterior face of the column, where the straps are attached. This would have resulted in the load applied to the columns by the diagonal straps being carried directly in tension through the columns to this anchor. However, such an anchor would provide little moment resistance, so if a welded anchor were used it would be even more effective to use a smaller version of the anchors used in the C1 shear panels (see Figure A-9). The screwed connection between the loaded diagonal strap and the top of the left column failed at 5.0 in. of lateral deflection. Figure 7-16 shows the test was stopped shortly after the failure of this connection.

Figure 7-16. A3a north and south monotonic test panel measured and predicted lateral load versus deflection.

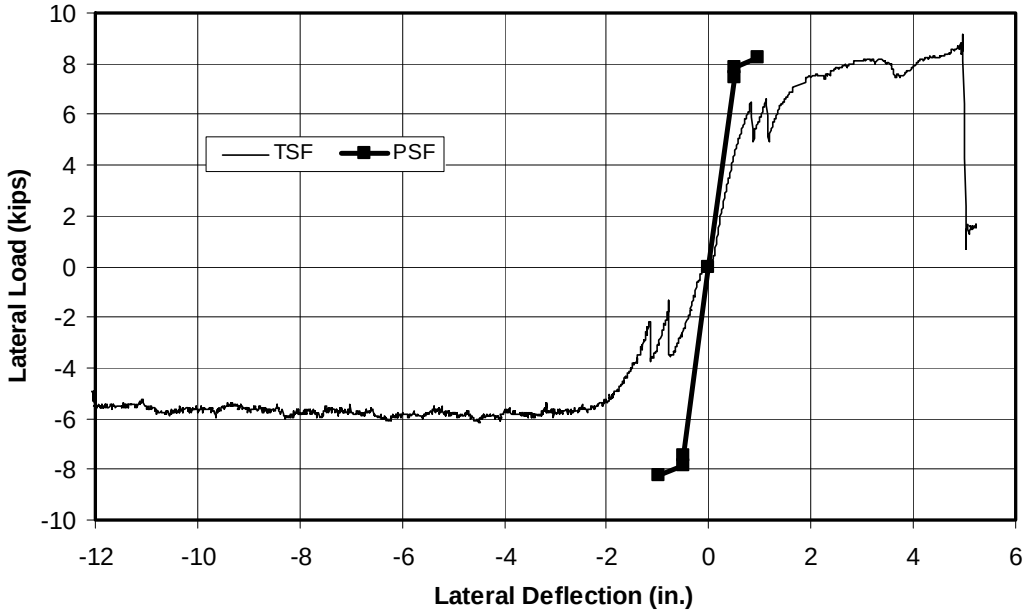

Figure 7-17 is a photograph of this test panel after the diagonal strap connection to the column had failed. Figure 7-18 zooms in on the details of this failed connection, showing the failure was a net area failure of the strap material between the screws. This figure also, shows the final condition of the column and anchor after the failures described above. These

include the two screws between the track and column; the shear buckling of the columns. After the column was buckled to the extent shown in this photograph, the screws between the exterior anchor and column pulled out, and some load was resisted in bearing when the column collapsed against the interior anchor. The anchors have not deformed on either side of the columns, so that the columns could still act as a moment frame with one anchor being in axial compression, while the other is in tension.

Figure 7-17. Overall view of A3a monotonically tested panel after it failed in the positive direction.

This panel was tested in the negative direction also by pulling the top of the panel to the north (right in Figure A-6). This provided a potentially useful second monotonic test since the diagonal strap, column connections, and anchors were essentially undamaged in this direction. The bottom half of Table B-8 documents the failure progression in this test, showing similar failure of the screwed connections between the tracks, followed by the columns and the shear buckling of the columns. However, the screws connecting the track to the column failed in shear, and shear buckling of the column took place at smaller lateral loads so that the diagonal strap never did yield in this second monotonic test. Figure 7-16 appears to show good ductile behavior when the panel is loaded in the negative direc-

tion, but in fact the performance in this direction is very poor because the modes of failure are highly variable in their capacity.

Figure 7-18. Close-up view of the A3a panel showing failed strap connection and column anchor.

Figure 7-19 shows the performance of the cyclically loaded A3b test panel, along with the predicted capacity. Table B-9 documents the failure progression, showing that the screws between the track and column failed at 0.45 in. when loading in the negative direction, and at 0.9 in. in the positive direction. These failures explain why the development of panel capacity was limited to about 6 kips at these deflections. The columns failed in shear buckling at 1.2 in. in the positive direction and at 1.8 in. in the negative direction. The measured capacity of this panel reaches the predicted yield strength of the straps alone (7.43 kips) at lateral deflections of 1.7 in. in the positive direction and 1.5 in. in the negative. The moment frame capacity of the slender, poorly anchored columns is very small, so it is clear that the diagonal straps yielded in both directions before 2.0 in. deflection.

The A3 strap coupon data in Figure 4-2 show that the strap stress increases only slightly above its yield value of 60.1 ksi, reaching an ultimate value of only 62.6 ksi. This ultimate stress value is reached at small strains of only 0.0285 in./in., which would equate to a lateral deformation due to strap

yielding of only 6.84 in. The straps would not have elongated to this extent especially since much of the panel deformation is due to deformation of the columns at their anchors. Still, the increase in panel capacity based on the ultimate strap stress is a reasonable upper bound, having a value of only 0.32 kips, which is an increase to 7.75 kips. The average of the maximum positive and negative panel capacity shown in Figure 7-19 is 8.82 kips, so the increase in strap strength accounts for only a small portion of the measured maximum capacity. The remaining increase in capacity must be from a combination of the columns acting as moment frames and both the deformed columns and interior studs acting as diagonal tensile trusses at large lateral deformations.

Figure 7-19. A3b cyclic test panel measured and predicted lateral load versus deflection.

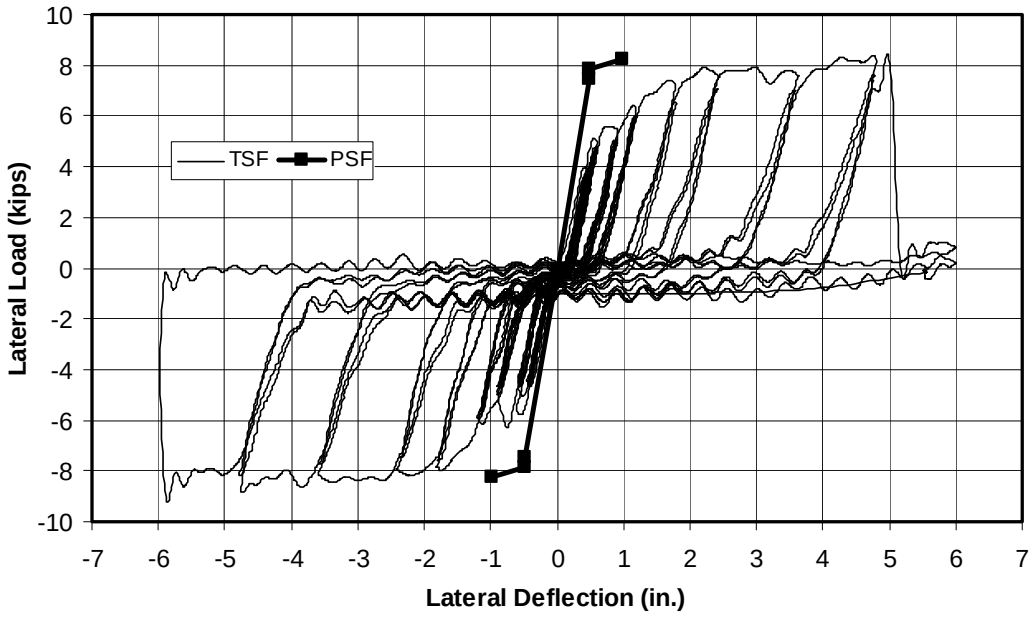

Figure 7-19 shows a sudden loss of capacity at 5.0 in. in the positive direction. This was caused by a net area failure across the screws that fastened the diagonal strap to the bottom of the north column. Figure 7-18 showed the same type of failure at the top of the south column of the A1a monotonically tested panel. The picture shows that the failure occurred between the screws, where the strap material between the screws ruptures. The load applied to this rupture surface is equal to yield stress of the strap times the gross area of the strap. The screw pattern used in this joint detail creates a critical rupture planes that are both vertical and horizontal along the screws so that the total failure plane is much larger than the width of

the straps. The load applied to this rupture surface is resisted by all the screws in the connection to the column. The strap stress is greatest at the rupture surface because the load on the strap decreases by the load picked-up by individual screws as the strap progresses into the joint. The strap yields locally near the screws along this rupture surface and the material elongates as the strains increase. As load increases on the strap, the stresses along this surface reach their ultimate value (62.6 ksi, shown in Table 4-1 for the A3 strap). The strap continues to elongate further locally, but the strength increases no further, until the local strap strains reach their ultimate values and the material fractures. The coupon data in Table 4-1 shows that the A3 coupons had an average strain at fracture of only 0.075 in./in. (elongation of 7.5%). The particular coupon specimen plotted in Figure 4-1 for the A3 straps shows an even smaller maximum strain of only 0.054 in./in. Even more important than the small maximum strain, Table 4-1 shows that this strain-hardened strap material had an ultimate-to-yield stress ratio of only 1.04, far below the required minimum of 1.08 for ASTM A1003/A 1003M, Type H material (ASTM 2013b). When the design recommendations presented in Chapter 11 are used on this test panel, it indicates that a net area failure should take place at this rupture surface, even when resistance factors are increased to 1.0, before the gross section of the strap yields. In actual panel construction, strain-hardened material would not be permitted in the straps, reducing the vulnerability to net area failures. This test demonstrates that if the recommendations presented on the design rupture strength in these connections in Chapter 11 are followed, net area failures can be prevented.

Figure 7-20 shows the performance of the cyclically loaded A3c test panel along with predicted capacity. Table B-10 documents the failure progression, showing that the bottom of the north column began to deform before complete failure of the screws between the track and column. At the other corners the screws between the track and column failed before significant column deformation.

Figure 7-20. A3c cyclic test panel measured and predicted lateral load versus deflection.

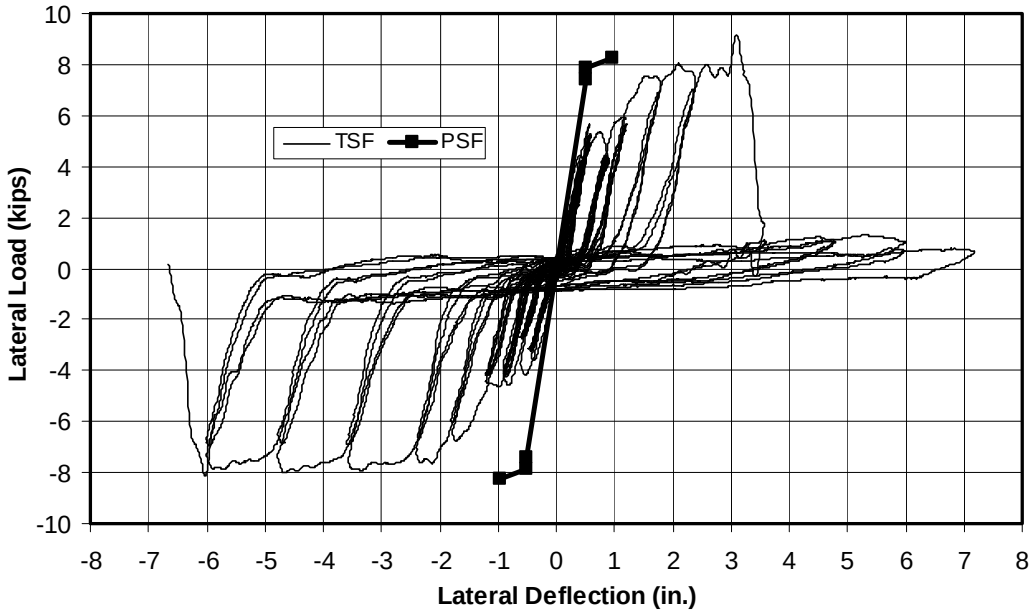

Figure 7-21 shows the bottom of the left column where column deformation permitted screw rotation so that they began to pull out from the strap. The column deformation also causes the strap to deform, creating additional stress concentrations at the critical rupture surface. The screw deformation at the strap column connection shown in Figure 7-21 is more typical than the lack of rotation seen in Figure 7-18.

Table B-10 shows that the strap at the bottom of the north (right) column had a net area failure at this joint, causing the loss of resistance seen in the positive direction in Figure 7-20 at 3.3 in. The strap at the top of the north column had a net area failure, causing the loss of capacity at 6.2 in. in the negative direction. The strap yield capacity is developed at similar deformations of 1.5 in. in the positive direction and 2.1 in the negative direction, as was seen in the A3b test. The measured capacity suggested the straps did yield, but much of the deformation of the panel was due to deformation of the columns where the straps were connected. Figure 7-20 shows that this panel reached an average peak capacity of 8.64 kips, well above the predicted capacity based on the strap yield strength (7.43 kips). This panel lost capacity in the positive direction at a smaller deformation of only 3.3 in., demonstrating the variability in this type of brittle failure. This panel provided fairly good ductile behavior, especially if the diagonal straps were constructed with the ASTM A1003/A 1003M, Type H material

(ASTM 2013b). The off-the-shelf anchors, which were screwed to the columns, were failures because they did not prevent shear buckling of the columns.

Figure 7-21. Bottom of left column of the A3c panel, showing column deformation and screw rotation.

7.4 C1 test panel results

The C1 test panels are another detail validation panel configuration. It is a heavier version of the A3 panel, but with the straps welded rather than screwed to the columns; and the anchors built up from L6 x 6 x 0.5 in. angle sections and a 0.75 in. triangular stiffener plate (see Figures A-8 and A-9 for details). The actual yield strength of the diagonal straps was 81 ksi, but several components of the panels were designed assuming a yield strength of 41 ksi in order to validate adequate ductile behavior for the maximum strap overstrength. Table 5-2 shows that the vertical load, GL_{max}, was held at 30 kips for all the C1 test panels. Figure 7-22 plots the

measured lateral load versus deflection for the C1a monotonically loaded shear panel. The predicted behavior, shown earlier in Figure 5-1, is also plotted.

Figure 7-22. C1a monotonic test panel measured and predicted lateral load versus deflection.

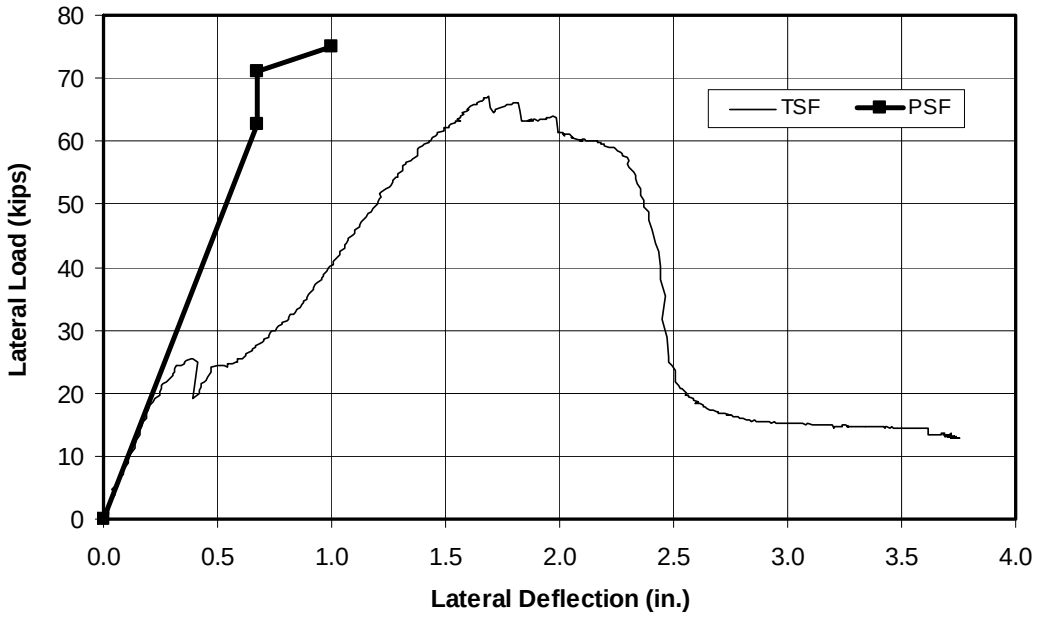

Detail A and Note 2 in Figure A-9 show that a 0.5 in. long tack weld was used to lightly attach the track to each side of the outer studs in the columns. These welds were not intended as part of the panel design, but were added simply to fix the top and bottom tracks to the panel so it could be moved, similar to the two screws in the A3 panels.

Table B-11 documents a few observations on the behavior of this panel. When the vertical load was being applied, one of the nonstructural welds failed and another failed at the top of the north column at 0.5 in. of lateral deflection, resulting in the drop in capacity seen in Figure 7-22. The plot shown in Figure 7-22 shows that the predicted yield strength of the strap alone was reached at 1.5 in. deflection. Figure 7-22 indicates that if the columns were fully fixed, the full lateral yield capacity of the columns would have been reached at only 1.0 in. of lateral deformation. Clearly the columns are not fully fixed, but this does indicate that the column moment frame contribution at the 1.5 in. lateral deflection should have been significant, indicating the straps very likely did not yield. If the straps had yielded, the shape of the plot of lateral load versus deflection would show a

gradual rolling over of the panel capacity. The sharp drop seen at 1.7 in. deflection indicates that minor brittle failures such as another nonstructural track weld failure may have occurred before strap yield was reached. These nonstructural weld failures, unfortunately shock loaded the panel, and may have led to earlier rupture of the diagonal straps.

The C1 panels had one strap in both diagonal directions on both the front and back face of the panel. Table B-11 shows that the diagonal strap on the front face began tearing near the bottom of the south column first, followed by the back face strap at the same location. Both straps tore gradually as the panel deformed laterally. Figure 7-22 shows a sudden loss of capacity at 2.3 in., when both straps would have been tearing. Figure 7-23 shows the front face of this connection after significant tearing of the strap. The lower tear in the strap began first, where the strap was welded to the left edge of this column, and the tear progressed along the weld and across the strap. As the strap crack pried open and rotated, the tear above it began from the top side of the strap. Figure 7-22 shows a complete loss of capacity at 3.7 in. deflection, when both straps failed completely.

Figure 7-23. Front face of the bottom of the south (left) column, showing strap tearing in the C1a panel.

Figure 4-3 shows that the C1 strap was severely strain hardened, so that the ultimate stress was almost no greater than yield. The elongation was reasonably good, but because the ultimate stress was not much greater than yield, there was little opportunity for the strap to deform and redistribute forces throughout the straps. The strap stress concentrations at the heat-affected zones of the welds provided an ideal location for a brittle fracture to begin and propagate through the strap. The recommendations developed in Chapter 11 would not permit the use of strain-hardened straps, because this material must be the ASTM A1003/A 1003M, Type H. This test was not a complete failure because it demonstrated that lateral load close to the yield strength of the panel could be resisted without brittle failures of the columns, connections, or anchors.

Figure 7-24 plots the performance of the C1b cyclically loaded panel. Table B-12 indicates that the track-to-column weld failures at 0.6 and 0.8 in. deflection caused the early loss of capacity seen in Figure 7-24. Table B-12 indicates that a small fracture began to form in the column material next to the vertical weld between the northeast edge of the bottom of the north column and the vertical edge of the anchor angle. The center-right side of Figure 7-25 shows this base metal fracture after the crack had opened.

Figure 7-24. C1b cyclic test panel measured and predicted lateral load versus deflection.

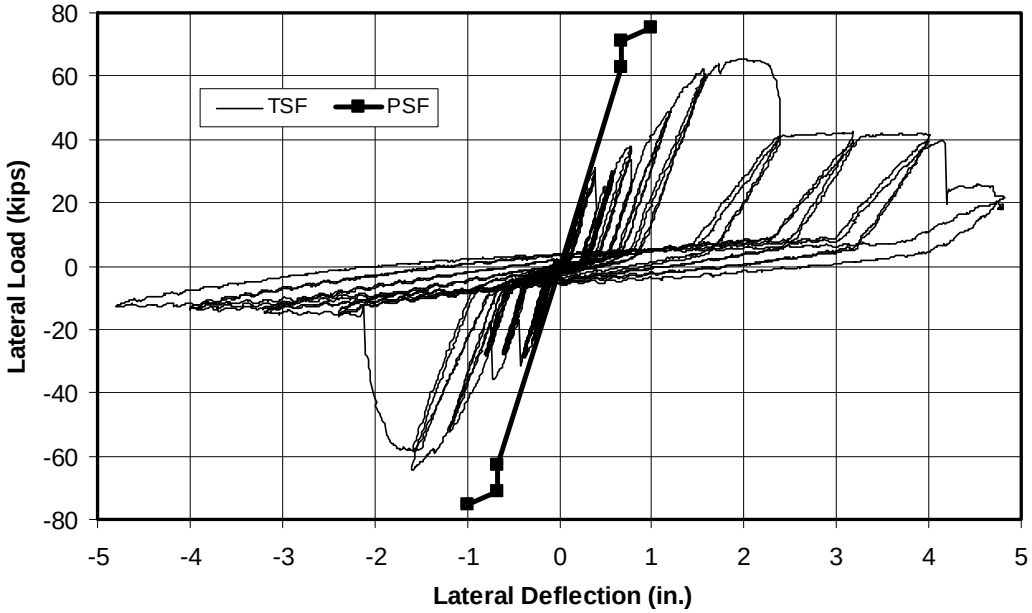

Figure 7-25. Base metal fracture of the bottom of the north column along the welded connection to the anchor.

This column tearing was clearly in the heat-affected zone of the weld to the anchor. Soon the diagonal straps began to fracture in the heat-affected zones of the welds to the columns. The strap failures near their connections led to the almost complete loss of capacity at 2.0 in. deflection in the negative direction, seen in Figure 7-24. The strap on the back face failed in the other direction in a similar manner, causing the large loss of capacity at 2.3 in. in the positive direction.

The sudden loss of capacity seen at 4.2 in. deflection in the positive direction is due to the development of a vertical tear in the column, along the top of the anchor angle shown in Figure 7-25. The column subsequently tore even further, leading to the loss in capacity seen at 4.8 in. Figure 7-26 shows that one end of three diagonal straps tore in the manner defined above, and the column tore near the anchor beginning at the front face of the bottom of the north (right) column.

Figure 7-26. Overall view of the C1b panel after failure of three straps and column.

This picture was taken a few seconds after the final failure of the strap at the bottom of the south (left) column, when the panel was displaced about 2.2 in. in the negative direction, where the top of the panel was displaced to the right. The peak measured capacity was only 65.3 kips at 2.0 in. deflection in the positive direction and 64.3 kips at 1.6 in. deflection in the negative direction. These ultimate capacities are only slightly greater than the predicted capacity of the strap alone at strap yield (62.8 kips), suggesting that the straps of this panel most likely did not yield in either direction.

Figure 7-27 plots the performance of the C1c cyclically loaded shear panel. Table B-13 indicates that the nonstructural track-to-column welds failed at 0.3 in. through 1.6 in., explaining the early loss of capacity seen at these deflections in Figure 7-27.

Figure 7-27. C1c cyclic test panel measured and predicted lateral load versus deflection.

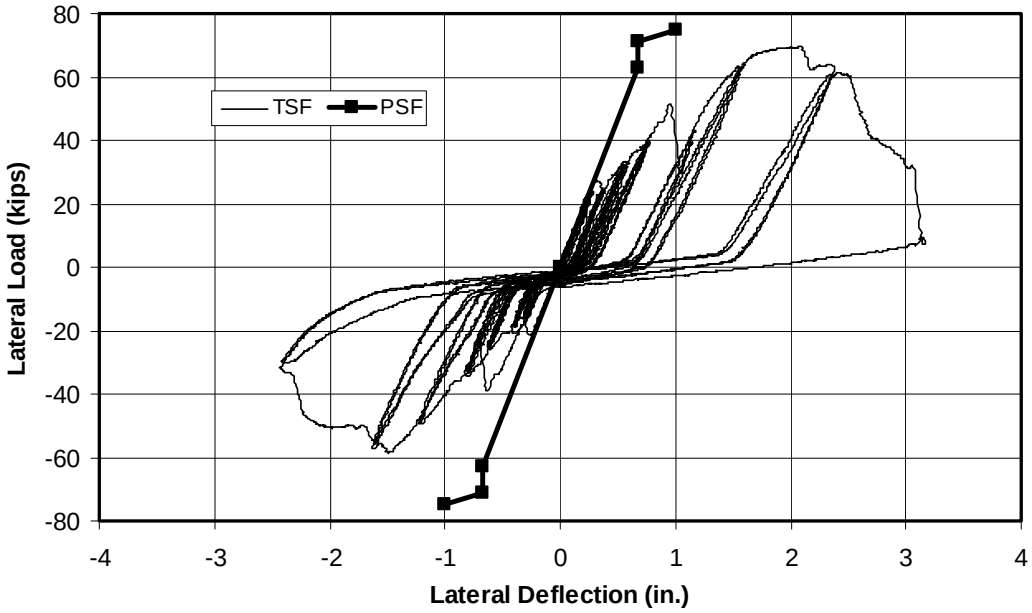

The peak measured capacity for this panel in the positive direction was 69.8 kips at 2.1 in. deflection, while the capacity in the negative direction was much less at 58.4 kips. This capacity in the positive direction is significantly greater than the predicted capacity of the strap alone at strap yield (62.8 kips), suggesting that the straps of this panel likely did yield when the panel deformed in this direction. The gentle rolling over of the plot (at 1.7 in.) without loss of capacity also suggests the diagonal straps yielded. The straps did begin to fracture at 1.5 in. deflection in the negative direction, and they also began to fracture in the positive direction at 2.2 in., so the strap yielding was relatively minor. Poor ductility was seen in the C1 panels because strain-hardened material was used in the straps. However, these panel tests demonstrate that panels designed in the C configuration (built-up columns, with welded strap connections and the type of anchors used in the C1 test panel) should perform in a ductile manner without brittle failures even at the maximum estimated strength in the diagonal straps.

7.5 D1 test panel results

The D configuration panels use hollow structural section (HSS) columns instead of the columns built up from studs used in the C1 test panels. The column material used in the D1 test panels is much thicker, 3/16 in., than the stud material that tore in the C1b test panel column (0.098 in). The

diagonal straps are welded to the columns like the C1 panel. The D1 test panels used a heavy track (97 mil or 12 gage) and nested studs (97 mil or 12 gage) welded inside the track and to the columns to provide column anchorage. These anchors were intended to resist shear loads on the columns, and provide only minimal resistance to rotation. Figures A-10 and A-11 provide the details on the design of this test panel. The D1 panel uses heavy 97 mil (12 gage) intermediate studs, as did the A2 panel. These are much heavier than the 33 mil (20 gage) intermediate studs used in the C1 test panels. The diagonal straps used in the D1 panel are 97 mil (12 gage) thick, which are heavier than those used in the A2 and C1 panels, though the strength of the strap material was only 37.6 ksi (see Table 5-1), much less than the 81.3 ksi strain-hardened material used in the C1 panel straps. Table 5-2 shows that the vertical load, GL_{max}, applied to the D1 test panels was 27 kips.

Figure 7-28 plots the measured lateral load versus deflection for the D1a monotonically loaded test panel. The predicted behavior plotted earlier in Figure 5-1 is also plotted for comparison. Table B-14 documents the progression of failure of this panel, showing that the straps began to visibly yield beginning at 0.95 in., while Figure 7-28 suggests they began to yield at 0.8 in. The coupon data in Figure 4-5 and Figure 4-6 show the D1 strap material had a fairly low yield strength (37.6 ksi in Table 4-2); the stress/strain plot plateaued until 0.008 in./in. strain, equivalent to 1.92 in. panel lateral deflection; and then increased fairly linearly until 0.035 in./in. strain, equivalent to 8.4 in. lateral deflection. Using the coupon data in Figure 4-6, the lateral capacity of the straps alone would have been 46.1 kips at strap yield, as plotted in Figure 7-28. At the strain of 0.035 in./in., the coupon stress was 43.9 ksi, which would have given a lateral capacity from the straps alone of 53.9 kips at a lateral deflection of 8.4 in., assuming no flexibility in the column anchors. However, Figure 7-28 shows that the D1a shear panel reached a peak capacity of 59.1 kips near the 8.4 in. deflection. Therefore, the columns acting as moment frames or the interior studs must have contributed at least 5.2 kips of lateral resistance (59.1 kips minus 53.9 kips). The nested stud and track column anchors would not have been very effective moment connections, so it is doubtful that even half the yield capacity of the columns could have been reached. Table 5-4 shows that the predicted yield capacity of both columns was 8.6 kips.

Figure 7-28. D1a monotonic test panel measured and predicted lateral load versus deflection.

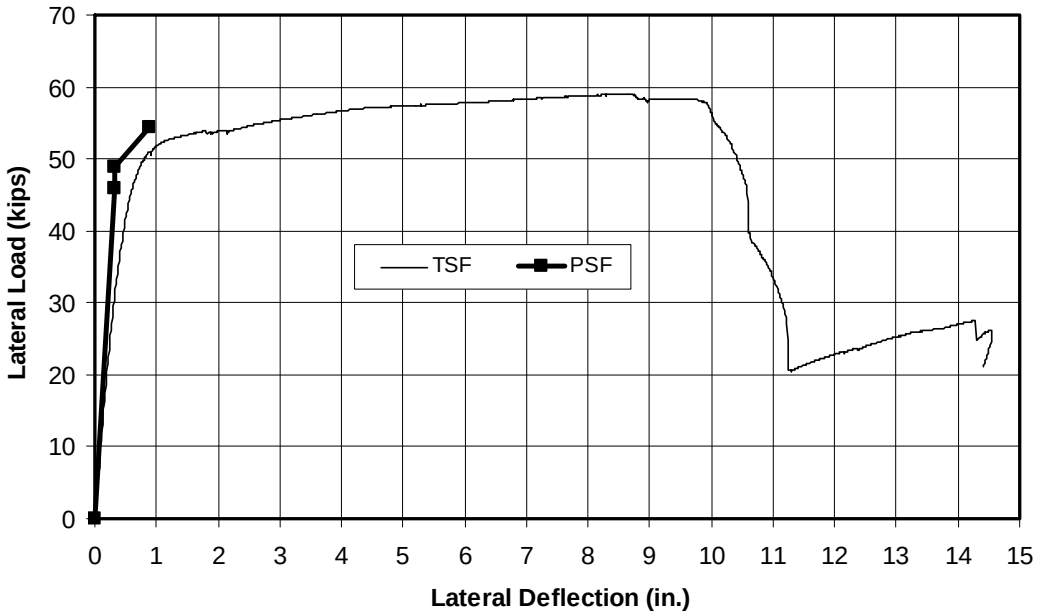

Figure A-10 shows that all 97 mil interior studs were connected to both the top and bottom tracks with 1 in. long weld along the lip of the track. Anchor bolts were installed close to each interior stud. The diagonal straps were also connected to the intermediate studs with 1 in. weld at both edges of the straps. The interior stud-to-track welds and stud-to-strap welds would have acted as pinned connections. These interior studs would have had some weak-axis bending capacity to resist lateral load applied by the straps in tension, especially for those studs closest to the columns, because of their short span. At very large lateral deflections, the interior studs would also resist lateral load in tension. Therefore, it is likely that the interior studs contributed a few kips to ultimate capacity of the D1a panel at the large deflection where the ultimate capacity was reached.

Table B-14 shows that cracks formed in the lips of the nested stud where it was welded to the columns at both the top of the south column and bottom of the north column, beginning at 1.0 in. deflection. The track below the outside edge of the bottom of the north column began prying up with the column at 1.4 in. deflection; this track tore vertically along this edge of the column at its back face at 2.1 in.; and tore through both faces at 4.0 in. Figure 7-29 is the back face of the bottom of the north column showing the pried-up and torn track. The failure in the lip of the nested stud where it is welded to the column is seen just above the track tear.

Figure 7-29. Back face of the bottom of the north column showing the pried-up and torn track at the center of the picture.

This tear is on the left side of the column. Just 0.5 in. to the left of the column, sitting inside the nested stud, is a 1 in. thick steel uplift plate that was bolted to the base beam restraining the nested stud and track anchor from rotation. These plates began to deform slightly in bending. The nested stud lips and flanges began buckling against the columns at the interior sides of the columns at 9.3 in. deflection. Table B-14 shows that all the damage up until 10 in. was to the anchors in nested studs or tracks. The moment capacity of these anchors decreased as the damage progressed, so the lateral loads would have gradually redistributed from the columns acting as a moment frame to the interior studs.

Table B-14 shows that the sudden loss of capacity near 10 in. deflection, seen in Figure 7-28, was due to diagonal strap tearing on the back face near the column, and by 11.2 in. the strap had torn through on the front face near the column. Significant loads were redistributed to the interior studs after the strap failures at the columns, so the panel still carried over 20 kips by the interior studs and columns. The stud weld connections to the track began to fail, and finally the welded strap connections to the interior studs failed at 14.5 in. After this failure the test was halted, although the panel resistance remained at 20 kips.

Figure 7-30 plots the lateral load-versus-deflection performance of the cyclically loaded D1b panel. Table B-15 indicates this panel fails in the same order as the D1a monotonically loaded panel. Figure 7-31 provides an overall view of the D1b panel at several inches of lateral deflection.

Figure 7-30. D1b cyclic test panel measured and predicted lateral load versus deflection.

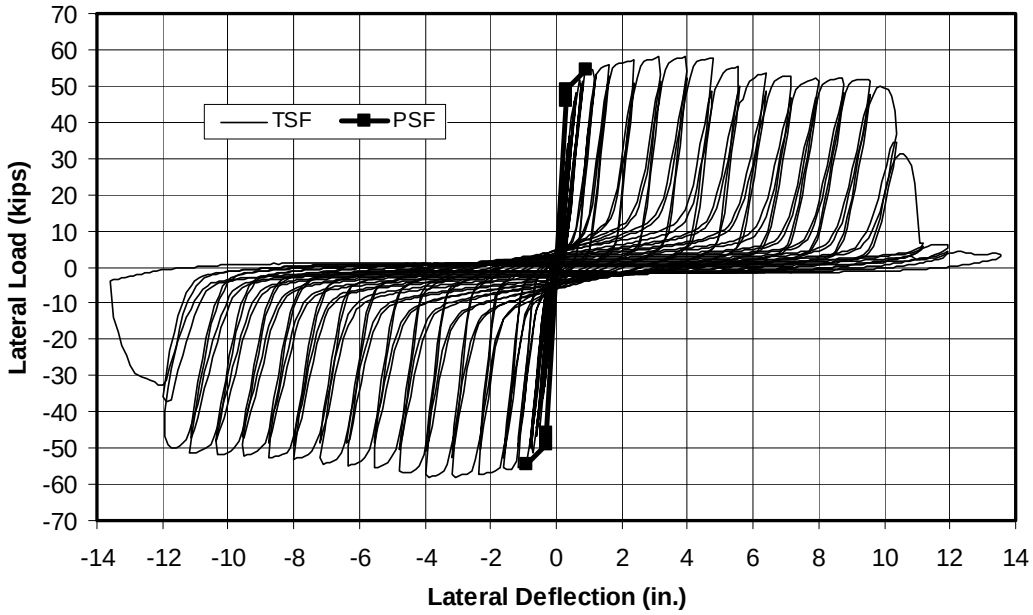

The progression of failure of all D1 test panel is summarized as follows:

- nested stud base metal failure near the welded connection between the nested stud lip and column
- bending of the track and nested stud anchor and bending of the 1 in. thick anchor plate
- shear tearing of the track and nested stud at the column
- track base metal failure near the welded connection between the track web and column
- fracture of the diagonal straps near the welds to the columns
- nested stud lip was driven into and buckled at the 3/16 in. thick column face.

Table B-15 indicates the strap weld connections to several interior studs began to fail at only 3.2 in. lateral deflection. This does not significantly reduce capacity immediately, but it does reduce the ability to redistribute forces from the straps to interior studs, particularly later in the test. This loss of ability can be seen in the gradual reduction in capacity beginning at 4 in. in Figure 7-30.

Figure 7-31. Overall view of the D1b test panel at several inches of lateral deflection.

The failure of the strap welded connections to the interior stud would shock load the strap-to-column connections, possibly causing earlier failures of the primary connections to the columns. Though strap connections to the interior studs provide a secondary load path, design recommendations in Chapter 11 discourage strap connections to these studs in order to avoid the shock loading. The interior studs can then be constructed with much lighter material, unless greater axial capacity is needed to resist gravity loads.

Table 7-1 and Table B-16 show that the performance and failure progression of the D1c cyclically tested shear panel was very similar to the D1b panel. However, the test data were not available for plotting.

7.6 D2 test panel results

The D2 test panels are another detail validation panel configuration. This panel used the same HSS columns used in the D1 panels, the straps were

welded to the columns, and the anchors were L8 x 6 x 0.5 in. angle sections with ¾ in. triangular stiffener plates (see Figures A-12 and A-13 for details). The actual yield strength of the diagonal straps was 56 ksi, but several components of the panels were designed assuming a yield strength of 28 ksi, in order to validate adequate ductile behavior for the maximum strap overstrength. Table 5-2 shows that the vertical load, GL_{max}, was held at 30 kips for all the D2 test panels. Figure 7-32 plots the measured lateral load versus deflection for the D2a monotonically loaded shear panel. This panel was tested monotonically, loading first to the north (positive) until failure and then to the south. The predicted behavior shown earlier in Figure 5-1 is also plotted. Detail A and Note 2 in Figure A-13 show that two 0.5 in. long tack welds were used to lightly attach the track to each face of the columns. These welds were not intended as part of the panel structural design, but were added simply to fix the top and bottom tracks to the panels so they could be moved.

Table B-17 shows that the nonstructural track welds of the D2a monotonically loaded panel failed at very small deflections of 0.7 in. when loaded in the positive (north) direction and 0.5 in. when loaded in the negative (south) direction. Figure 7-32 shows that the weld failures caused the temporary loss of resistance at these deflections. Had these nonstructural welds not existed, Figure 7-32 suggests the lateral resistance would have developed in a similar manner, but with a smaller slope or panel stiffness. Table B-17 shows that the when the panel was loaded to the north (positive in plot), the diagonal strap on the front face failed at 1.7 in., and the strap on the back face failed at 1.9 in., explaining the sudden loss in capacity seen in Figure 7-32. The predicted yield capacity of the straps alone was 63.0 kips, and the maximum capacity reached in the positive direction shown in Figure 7-32 was only 59.1 kips, indicating both diagonal straps most likely fractured before either yielded. The diagonal straps failed at similar amplitudes when the panel was loaded in the negative direction. The plot in the negative direction in Figure 7-32 suggests the strap on one face failed at 1.7 in. lateral deflection at a load of 64.2 kips, and the second failed at 1.8 in. and 36.7 kips.

Figure 7-32. D2a north and south monotonic test panel measured and predicted lateral load versus deflection.

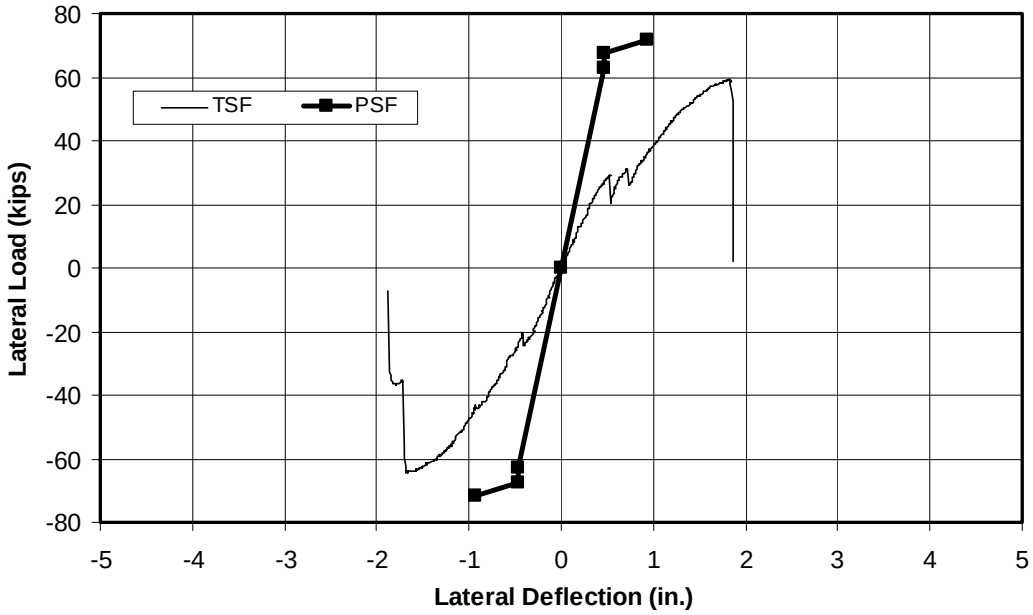

The peak capacity in the negative direction and the gentle decrease in slope just before this peak was reached suggest that both straps may have yielded. The reduced panel resistance that reached 36.7 kips suggested that one strap was still intact at 1.7 in., and that it failed soon after this. All of the diagonal strap failures in this panel began near the welds to the column, and then suddenly fractured through the center of the strap away from the weld. The panel capacity and ductility of this panel is clearly limited by the use of the strain-hardened straps. Had better quality straps been used, the straps would have yielded and elongated significantly, and the columns, connections, and anchors would most likely have continued to resist loads, providing good ductile performance with the columns providing a flexible but fairly strong secondary moment frame. The cyclic tests that follow support this claim.

Table B-18 shows that the cyclically loaded D2b shear panel failed in the same manner as the D2a panel, with the track weld failures followed by the fracture of the diagonal straps. However, the diagonal strap failures took place at larger panel deflections and larger measured capacities. Table B-18 and Figure 7-33 indicate that the back strap failed at 2.1 in. deflection in the positive direction, causing the panel resistance to drop to 40 kips, followed by later cycles where the front strap failed at 2.6 in and the resistance dropped to 11 kips. This table and figure show that the front strap

failed at 2.1 in. in the negative direction, causing the panel resistance to drop to 45 kips, followed by later cycles where the back strap failed at 3.5 in. and the resistance dropped to 13 kips.

Figure 7-33. D2b cyclic test panel measured and predicted lateral load versus deflection.

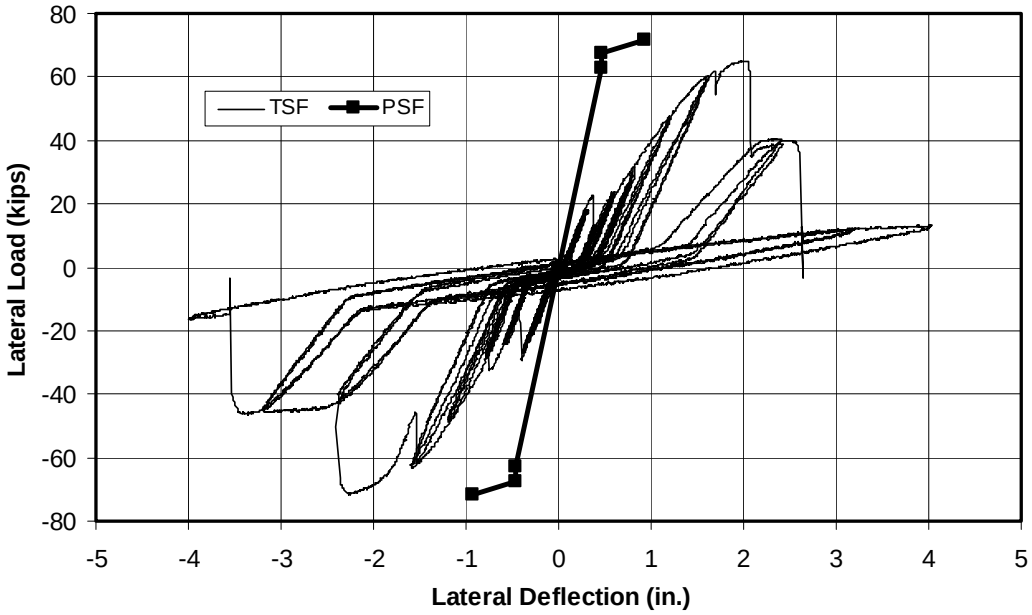

Figure 7-34 shows an overall photograph of this panel shortly after the front face strap failed at the bottom of the north (right) column at 2.6 in. in the positive direction. The straps near the bottoms of both columns show typical strap failure, where a crack in the strap begins near an edge of the strap near the welds to columns and progresses to the interior of the straps.

Figure 7-34. Overall view of the D2b test panel
after the front strap failed at the bottom of the north (right) column at 2.6 in.

In the positive direction, a peak capacity of 65.0 kips was reached at 2.0 in. deflection. This exceeds the predicted yield capacity of straps alone of 63.0 kips and the shape of the measured data in Figure 7-33 suggests that the straps had begun to yield in the positive direction. In the negative direction, a capacity of 71.6 kips was reached at 2.3 in. deflection. This peak capacity far exceeds the predicted yield capacity of the strap and is almost equal to the predicted total capacity of the panel when the straps are at their yield strength and the columns have begun to yield. The contribution of the interior studs is not included in the predicted strength, but that should be relatively small. The greater capacity in the negative direction, plus the gentle reduction in slope around 2 in. deflection indicate the straps have clearly yielded in the negative direction. The performance of the D2b panel shown in Figure 7-33 was not very ductile because of the strain-hardened straps, but this test clearly shows the straps yielded and no other brittle failures occurred in the columns, strap connections, or column anchors, showing that this detail validation test did demonstrate

that the recommendations presented in Chapter 11 will produce ductile performance. Figure 7-33 shows that after failure of both straps in both directions, the columns acting as moment frames and the interior studs develop lateral resistance of 13 kips in the positive direction and 16 kips in the negative direction. This demonstrates that columns and interior studs do provide somewhat of a redundant system that widens the hysteretic envelopes and should prevent building collapse even if the straps fail completely.

Table B-19 provides only a few observations on the failure of the D2c cyclically loaded panel. Still, these observations and the panel performance shown in Figure 7-35 indicate this panel behaved similarly to the D2b panel although its capacity and lateral deflection at failure were slightly lower.

Figure 7-35. D2c cyclic test panel measured and predicted lateral load versus deflection.

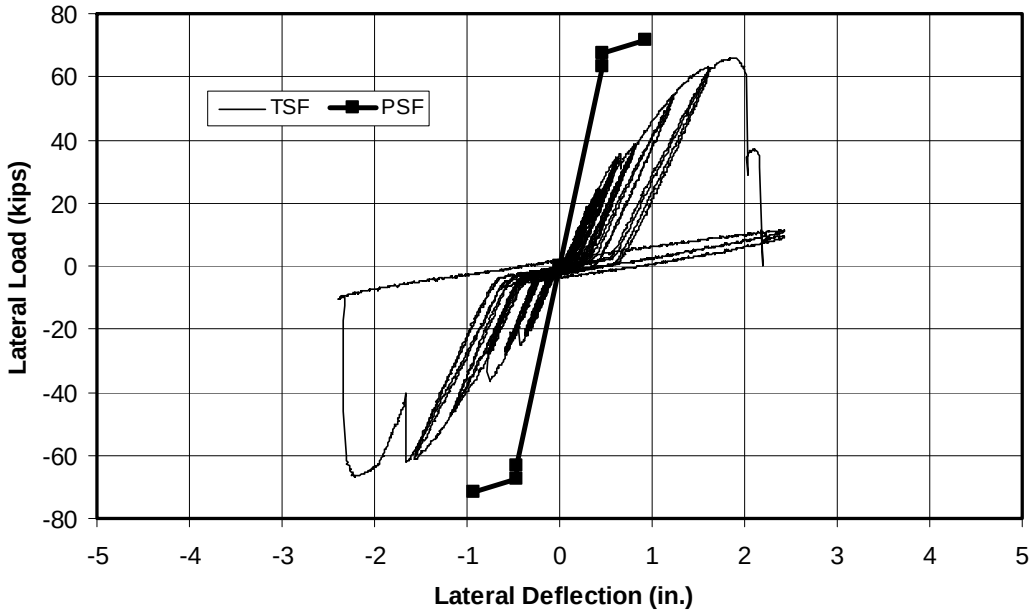

This panel reached a peak capacity of 65.8 kips at 1.9 in. deflection in the positive direction, exceeding the predicted yield capacity of the straps alone. This capacity, plus the plot shape, suggests the straps did yield in this direction. Figure 7-35 shows a strap on one face of the panel failed in this direction at 2.0 in., dropping the panel resistance to 36 kip, followed by failure of the strap on the other face at 2.2 in. The panel reached a peak capacity of 66.7 kips at 2.2 in. in the negative direction. This capacity and the plot shape also indicate the straps yielded in this direction. Both straps failed at 2.3 in. deflection.

These shear panel tests demonstrate that all three shear panel configurations with diagonal straps (A, C, and D) as the primary lateral-load-resisting element can be designed in a way that ensures effective ductile performance needed for resisting seismic loads. The tests of the lightweight A1 and A3 panels showed how critical it is to design the panels so the columns and anchors have adequate shear capacity for the maximum diagonal strap strength. The heavy nested stud and track that made up the anchors for the A2 and D1 shear panels did provide sufficient shear support for the panel columns. However, the extensive welding would be an expensive way to provide panel anchorage, and the anchors must have sufficient capacity for the maximum strength of the straps. The anchors used in the C1 and D2 panel configurations, however, would be relatively inexpensive. They can be designed for the strap overstrength and turn the columns into a true moment frame, making the panels a more redundant, more energy dissipating system. The off-the-shelf anchors used in the A3 panels could provide sufficient shear and hold-down resistance if they were welded to the columns, but a lighter version of the anchors used in the C1 panels would work better because they would make the columns moment frames. The C1 and D2 panel tests demonstrate shear panels designed using ASTM A1003/A 1003M, Type H strap material (ASTM 2013b), and other provisions described in Chapter 11 of this report can provide very ductile performance, even if the diagonal straps are at their maximum levels. The A3 panel tests demonstrate that lightweight panels can be designed that also have good ductile performance using practical anchor details, and this is illustrated in the example problem in Chapter 12.

8 Shake Table Model Verification Test

In October 2000, ERDC-CERL began a project to characterize the inelastic response of structural systems. Ductile behavior is critical to good structural performance of buildings in earthquakes. Current building code provisions recognize degrees of assumed ductile behavior through the use of a seismic response modification coefficient, R. Seismic loads used to design the vast majority of buildings (linear static or dynamic design) are inversely proportional to this coefficient. Values for these coefficients vary from a low of 1.25 (e.g., steel ordinary cantilever column systems) to a maximum of 8.0 (e.g., steel eccentrically braced frames) in ASCE/SEI 7-10, Table 12.2-1. These values are intended to represent the degree of ductility, overstrength, redundancy, and energy dissipation capacity of the structural system. These coefficients have a tremendous impact on the design of buildings, yet there is a no rational basis for defining the values. FEMA P-750, section C12.1.1, states "the R values in the standard are based largely on engineering judgment of the performance of the various materials and systems in past earthquakes. The R factor for a specific project should be chosen and used with care." The article, "A Rational Approach for Determining Response Modification Factors for Seismic Design of Building Using Current Code Provisions" (Foutch and Wilcoski 2005), proposes a rational approach for defining the R coefficient. This approach builds on the probabilistic procedures for design and assessment of steel moment-resisting frame buildings developed for the SAC project. This approach requires a series of nonlinear time-history analyses of representative building frames to determine what R coefficient is needed for a given structural system to achieve a 90% probability of collapse prevention for the 2% probability of exceedence in 50 year seismic hazard. The series of analysis cases with various ground motions and building configurations is needed to establish the probabilistic data. This nonlinear analysis is used to define both the deformation capacity and demand for each of the analysis cases that use ground motions representative of the seismic hazard.

The proposed procedure was applied to the cold-formed steel structural system, based on the seismic design recommendations presented in this report. The capacity is defined based on a hysteretic load-versus-deformation characterization of critical components of the lateral-load-resisting system. This hysteretic characterization is based on cyclic testing

in a laboratory. Full-scale cold-formed steel shear panels were tested at ERDC-CERL (see Chapter 7), and they provided very predictable hysteric behavior that could be readily modeled in the example analysis (see Chapter 5).

However, the static cyclic testing does not account for dynamic effects that will be experienced in real earthquakes. The hysteretic load-versus-deflection plots of cold-formed steel shear panels are severely pinched, because the main panel lateral-load-resisting elements are thin diagonal straps that only offer resistance under tensile load. After a deformation cycle that causes strap yielding, the panel will have little resistance until deformations have cycled in the opposite direction to amplitudes that the opposite straps become taut. While the straps are slack, the structure above the panel can develop significant velocity, and the straps can snap when they become taut again. This will cause large accelerations and apply large impulsive loads to the joints. The strap connections to the columns must not fail; the columns must not buckle; or the anchors of the columns must not fail. Any of those failures could be brittle, and are not represented by the ductile hysteretic behavior defined in the laboratory. Other structural systems that have pinched hysteretic envelopes may have similar issues.

The static cyclic tests also do not represent the large P-delta-related overturning moments that could result at large deformations of multistory building frames. Therefore shake table testing of a full-scale model was needed to evaluate the effectiveness of the nonlinear analysis in representing the dynamic response of structures at large deformations. This verification testing evaluated the ability to define the deformation demand and capacity of the lateral-load-resisting system. A new analytical procedure was developed for the SAC work called incremental dynamic analysis (IDA) for defining the deformation capacity, and this same procedure is used in the proposed approach for defining R coefficients for all structural systems. The IDA procedure was never experimentally validated for the SAC project. The verification testing should be at full scale to avoid introducing errors associated with scaling relationships and component behavior that will differ with much different scale section properties. This chapter documents a two-story, full-scale shake table verification model that was tested with one of the more severe ground motions used in the analysis presented in Foutch and Wilcoski (unpublished).

8.1 Shake table model configuration

Figure 8-1 shows a photograph of the cold-formed steel shake table model assembled on the ERDC-CERL Triaxial Earthquake and Shock Simulator (TESS shake table). The model is full scale, consisting of two framing lines of two-story cold-formed steel shear panels. Supplemental weight was added above and below the floor slabs.

Figure 8-2 shows an elevation view drawing of the model. This model was shaken with uniaxial motions, in the in-plane direction relative to this drawing. The model consists of two identical two-story, one bay wide frames, which are separated from each other by 154 in. on center in the out-of-plane direction. The second-story frame is identical to the first story, though the loads on first story are greater so that significant nonlinear response would occur on the first story only, where it could be more easily observed during the test. Figure 8-3 presents an out-of-plane view of this model, showing these two frames. A heavy reinforced concrete slab diaphragm was installed at the top of each floor level. The concrete slabs were 8 in. thick and 14.5 ft square. The slabs were designed to be very stiff, representing a beam at the top of the wall panels. Each slab weighed 21,000 lb. In a typical building shear panels might be installed in one of every 5 or 10 bays. Therefore, additional weights were added to the slabs in order to model the mass that might come from other bays of a typical building. All the available steel plate and lead weights at ERDC-CERL that could be easily installed to the model were evenly distributed on the two slabs. This was approximately 24,000 lb of steel plates and 40,000 lb of lead, plus channels to hold them in place. Figure 8-3 shows that 13,000 lb of steel weights (plates with channels) were attached to the bottom of each floor slab. This figure shows 22,700 lb of lead weights (lead plus steel channels) attached to the top of the first-floor slab and 23,200 lb at the top of the second floor slab. The weight of the shear panels was 400 lb, so that the effective model weight at the first floor was 57,500 lb (21,000 lb + 13,000 lb + 22,700 lb + 2 x 2 x 400 lb/2), and the effective weight at the second floor was 57,600 lb (21,000 lb + 13,000 lb + 23,200 lb + 2 x 400 lb/2). Figure 8-4 through Figure 8-7 are plan views of the first- and second-story slabs, showing the locations of the supporting channels and steel weights below the slabs and lead weights above the slabs. Figure 8-8 illustrates safety restraints built into the experiment to address the unlikely event of brittle failure of shear panel straps that might result in a collapse of the model. Figure 8-8 also shows the backup pipe columns that would “catch” the first-floor slab if the first-floor cold-formed steel columns buckled.

Figure 8-1. Photograph of the cold-formed steel verification model mounted on the ERDC-CERL TESS (viewed from northeast corner).

Figure 8-2. In-plane elevation drawing of the verification model.

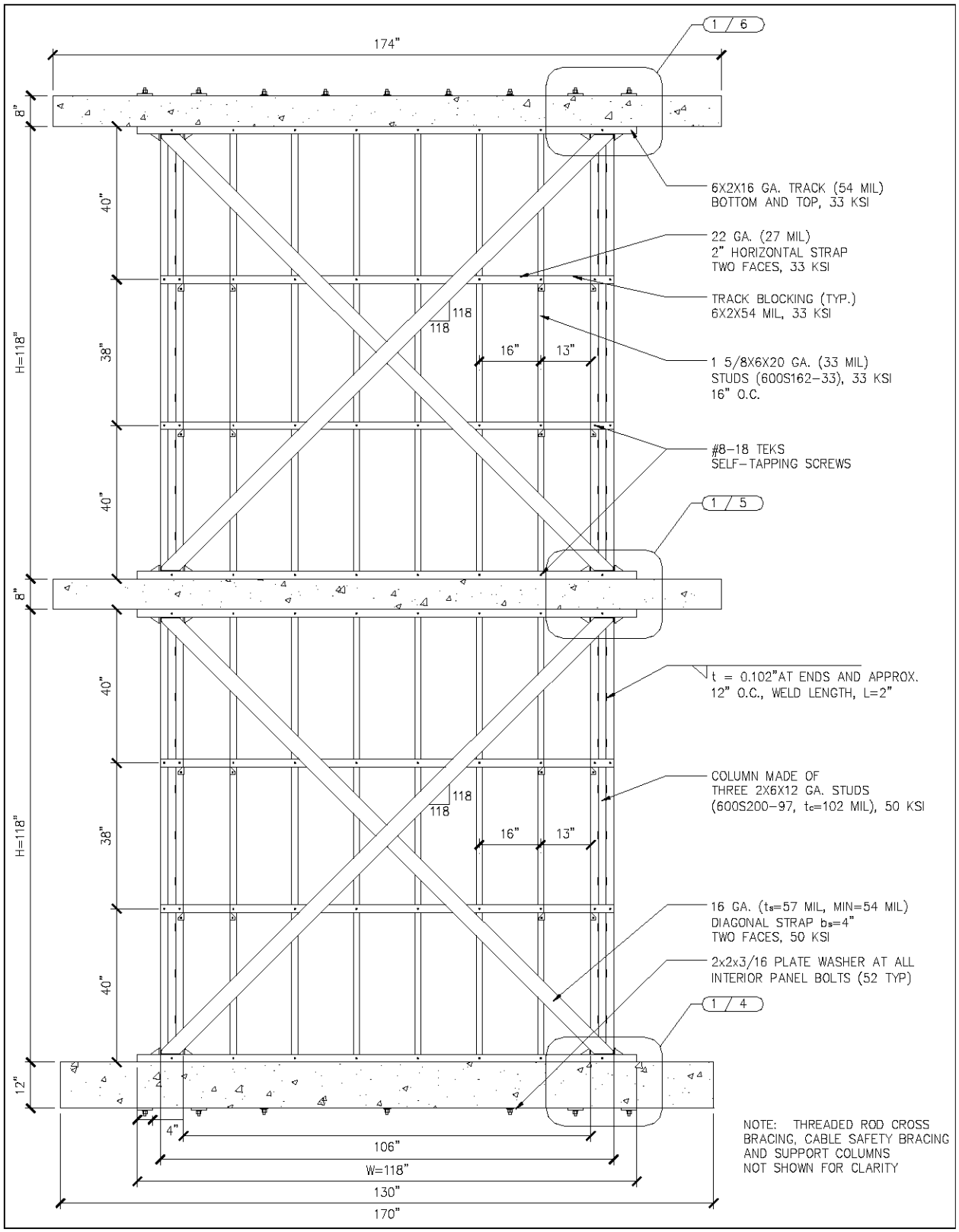

Figure 8-3. Out-of-plane elevation drawing of the verification model, showing weights.

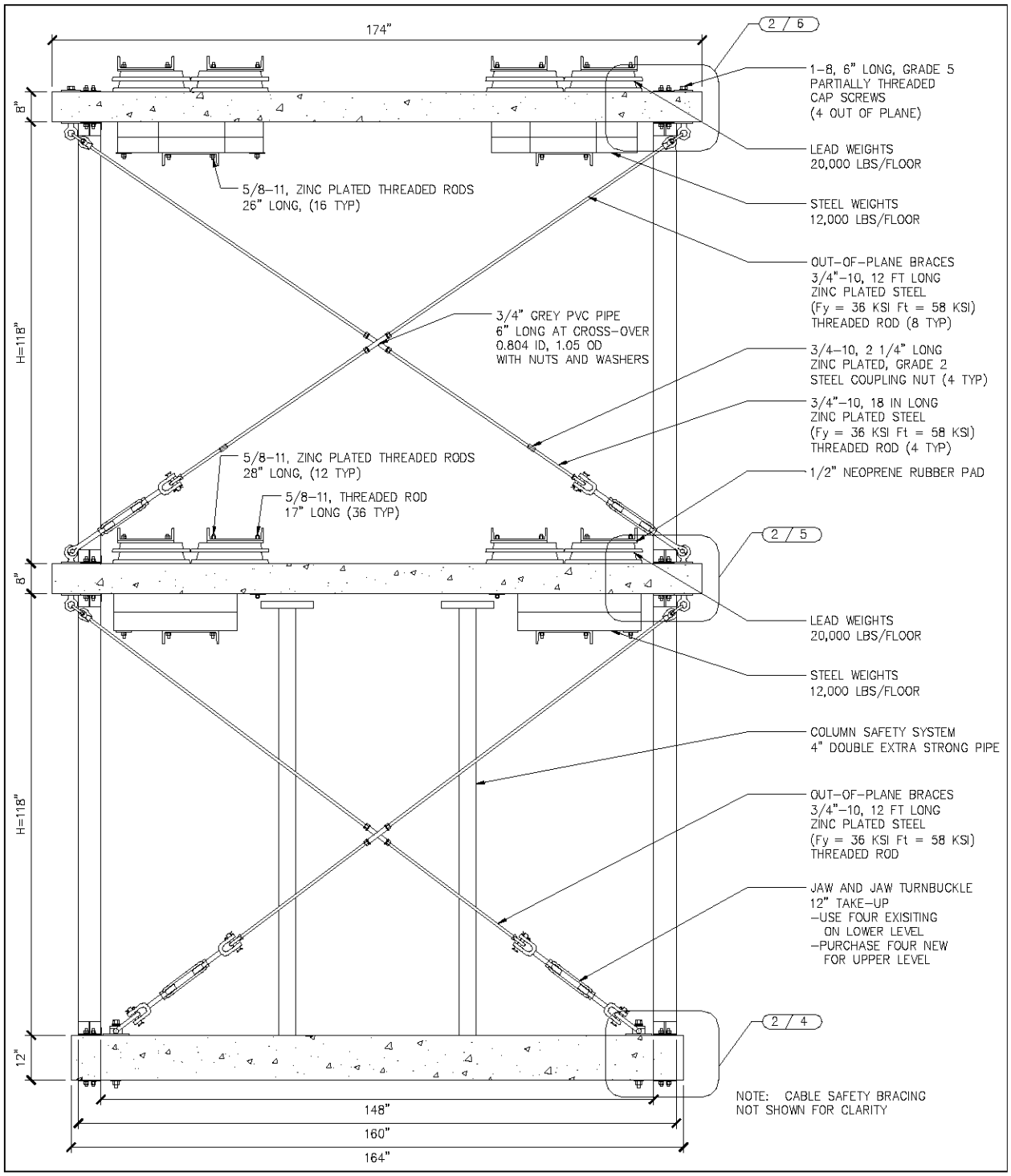

Figure 8-4. Plan view showing the steel plate weights below the first-story slab.

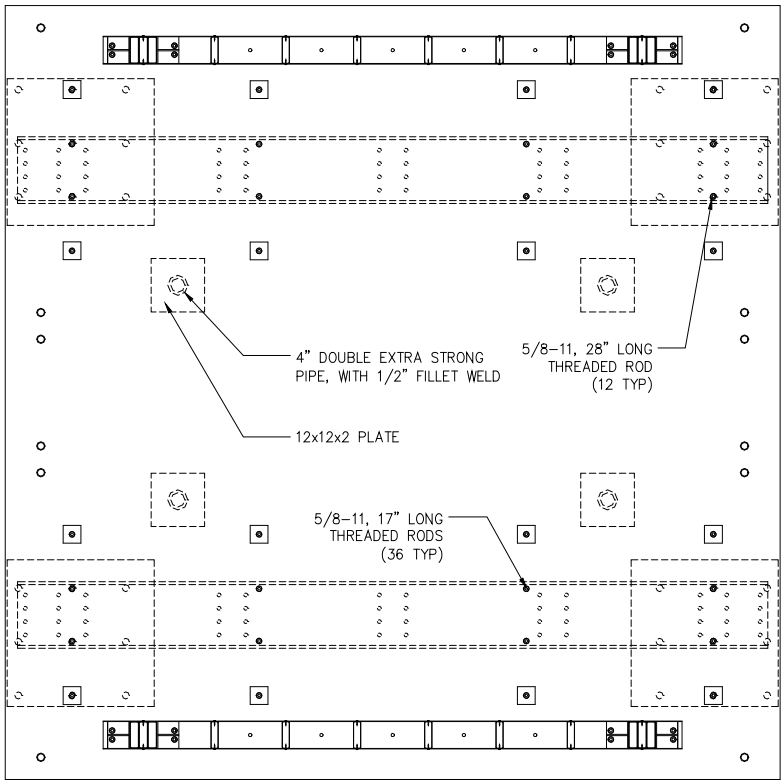

Figure 8-5. Plan view showing the lead weights above the first-story slab.

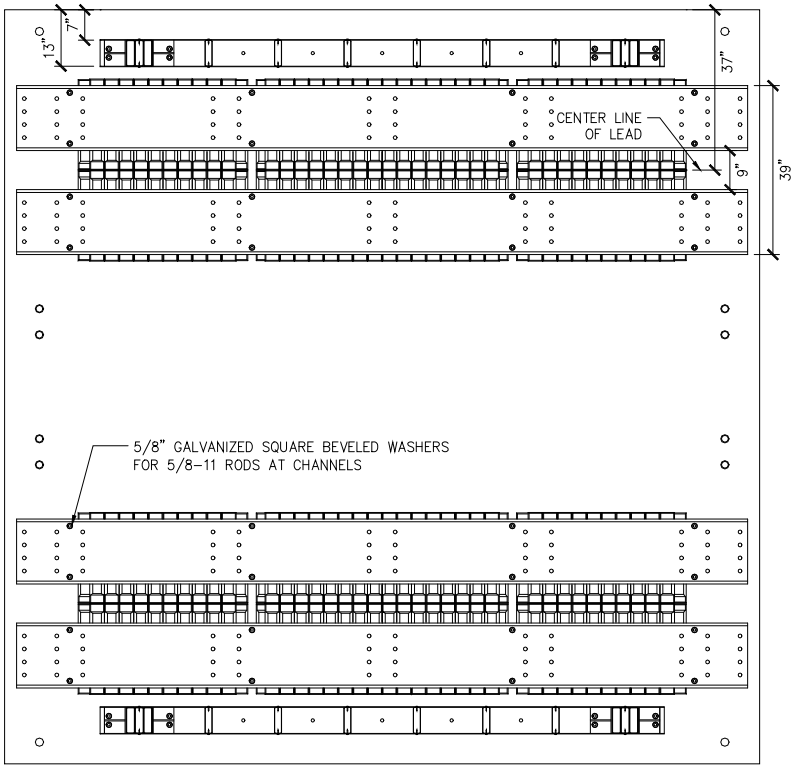

Figure 8-6. Plan view showing the steel plate weights below the second-story slab.

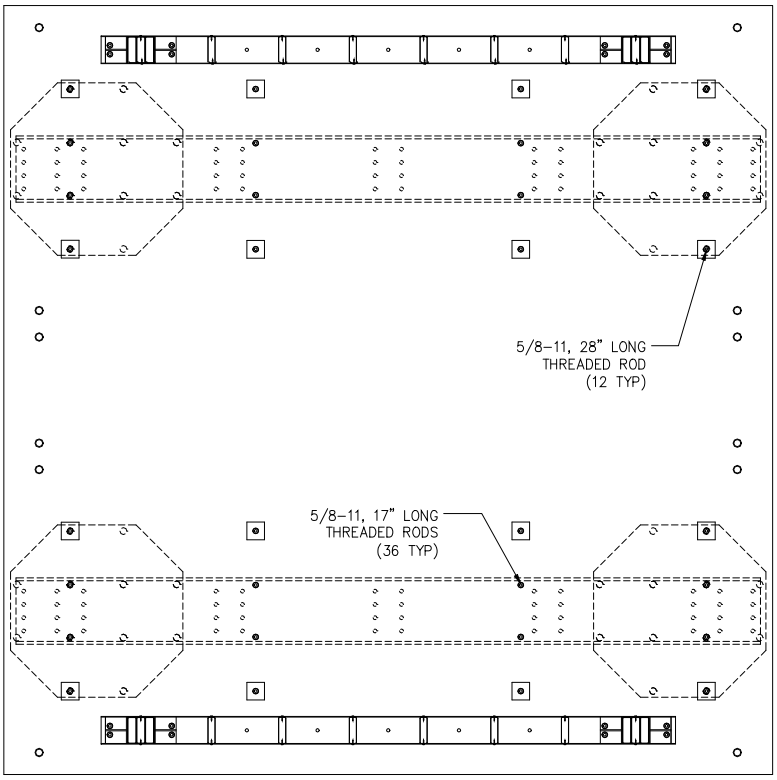

Figure 8-7. Plan view showing the lead weights above the second-story slab.

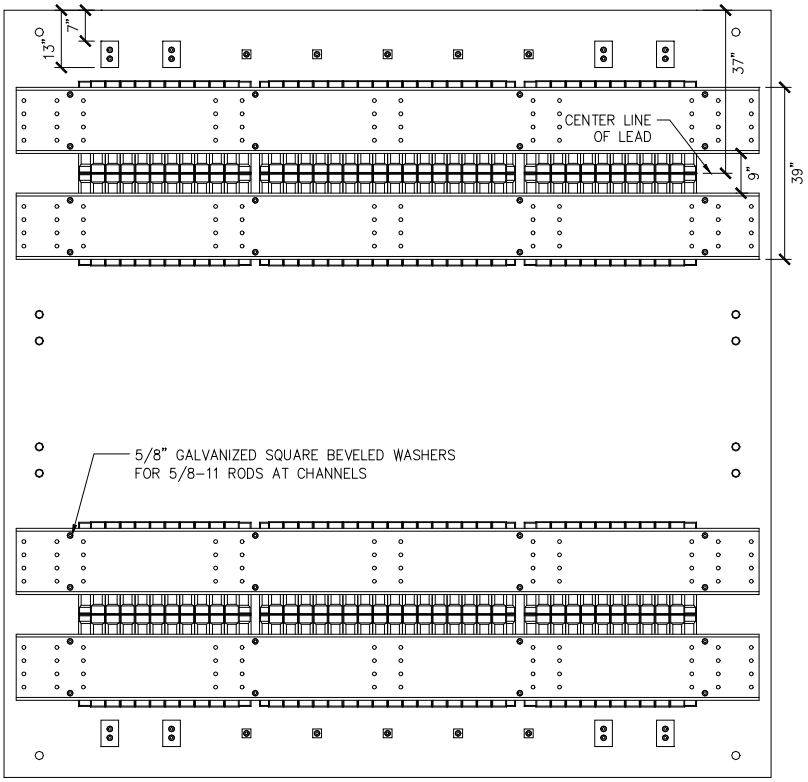

Figure 8-8. In-plane elevation view showing the floor slabs with safety cables (shear panels and weights not shown).

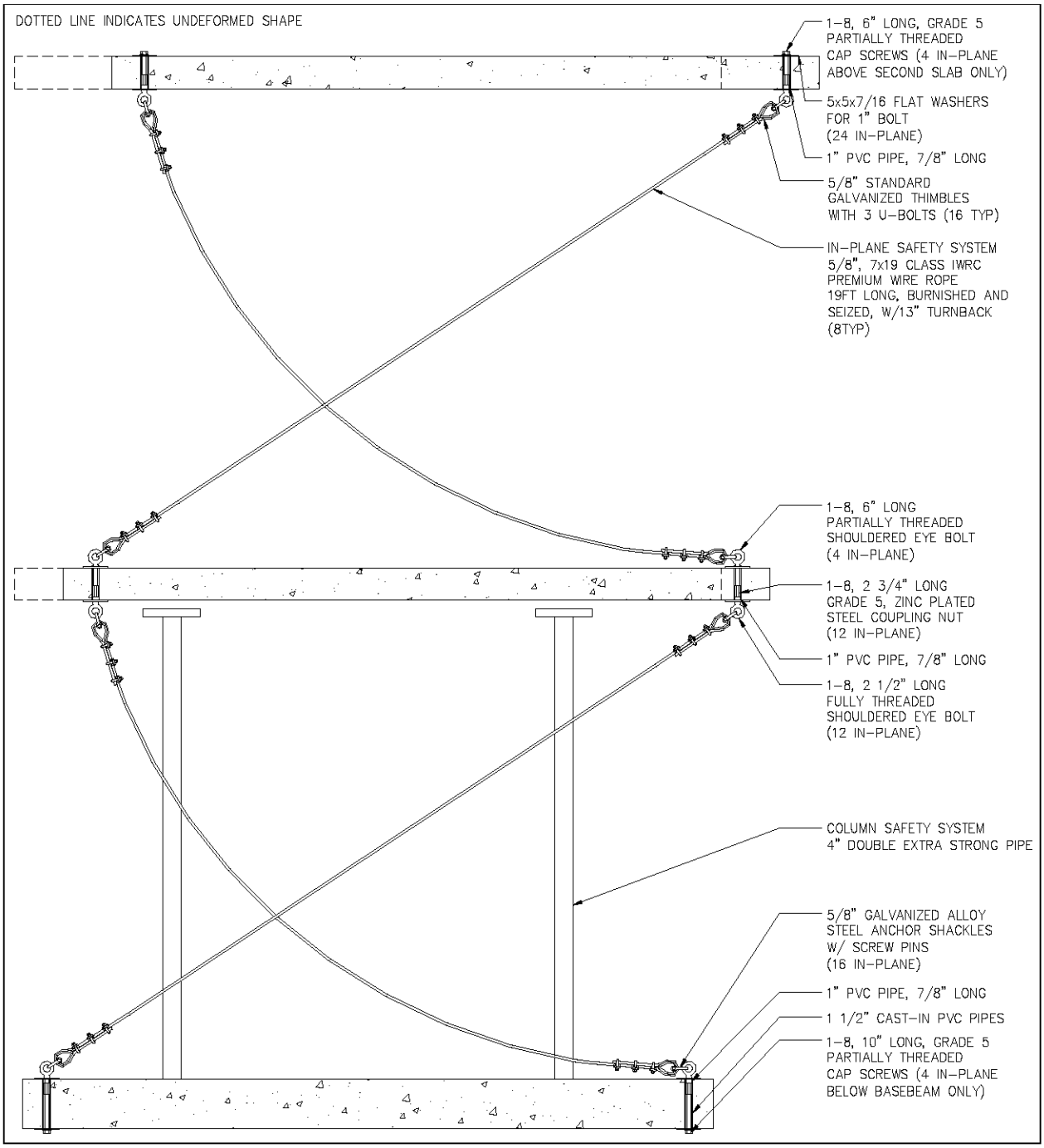

The weight estimates neglect the minimal additional weight of the hardware shown in Figure 8-3. The heavy slabs prevent flexural bending or in-plane rotation of the floor diaphragms, so that the single bay frame would provide similar frame response as a multiple bay building frame. The columns at the exterior edges of the frame were very stiff axially and had

moment connections to the slabs with through-bolts to the base beam below or slabs above.

Figure 8-3 shows that 0.75 in. threaded rod braces were installed out of plane to prevent unwanted out-of-plane model response. In the unlikely event that the panel diagonal straps were to fail in a brittle manner, loose cables were installed in the in-plane direction to "catch" the slabs. Two 5/8 in. diameter cables were installed in each direction at each floor level, and their lengths were such that they would become taut and carry load at 12 in. lateral deflection at each floor level. Figure 8-8 shows the floor slabs only (i.e., with shear panels and weights removed) at the 12 in. lateral deflection, when these cables would begin to restrain the slabs. In the very unlikely event that the model columns were to buckle and collapse, four 4 in. diameter double extra-strong pipe columns with 2 in. thick square plates welded to their tops and bottoms were installed below the first-floor slabs (see Figure 8-3 and Figure 8-8). The pipe column heights were such that the plates at the tops of the columns were 2 in. below the first-floor slab. Therefore this slab would need to drop 2 in. before making contact with these safety pipe columns. The safety columns were only installed at the first-floor level because the frames at the two levels are identical and the first-floor panel columns were loaded at almost twice the axial and bending loads as on the second floor.

8.2 Shake table model design

The shear panels installed in this model at both floor levels were full scale-wall panels designed for a base shear of 15.8 kips per panel, or 31.6 kips for both frames (see Table 8-1).

Table 8-1. Cold-formed steel diagonal strap design for shake table model.

Panel Level	Panel Width W (in)	Panel Height H (in)	Strap Faces n_s (#)	Strap Width b_s (in)	Strap Thickness (ga)	Strap Thickness t_s (in)	Strap Initial Lat Stiffness k_s (k/in)	Yield Stress of Strap F_{sy} (ksi)	Capacity at Strap Lat Yield Q_{sy} (k)	Design Shear Strength $\phi_t Q_{sy}$ (k)	Lat Defl at Strap Yielding δ_{sy} (in)	Applied Story Shear V_x (kips)	Elastic Lateral Defl δ_{xe} (in)	Defl Amp Factor C_d	Import Factor I	Design Story Drifts $\Delta = \delta_x$ (in)	Stability Coeff θ	Allow Story Drifts Δ_a (in)
2nd Fl	118	118	2	4	16	0.055	38	53.6	16.62	15.78	0.436	14.40	0.378	3.5	1.0	1.32	0.0100	2.36
1st Fl	118	118	2	4	16	0.055	38	53.6	16.62	15.78	0.436	21.58	0.567	3.5	1.0	1.98	0.0100	2.36

The diagonal straps were welded to the tops and bottoms of the columns as shown at the left sides of Figure 8-9 through Figure 8-11. These figures also show the column anchor details and out-of-plane details on their right sides. The connections and the columns themselves, plus the anchors to the base beam and floor slabs above, were all designed following the de-

sign recommendations presented in Chapter 11. However, these components were designed assuming the diagonal strap maximum strength was equal to the actual strength measured in coupon testing. They were also designed for the actual gravity load applied to the first-story panels (i.e., $Gl_{max} = GL_{min}$ = 115.1 kips/2 panels = 57.6 kips). The welded diagonal strap-to-column connections and the column anchors were then designed for the true loads applied to them based on the coupon material test results and actual gravity loads. These design assumptions provided an opportunity to evaluate actual shear panel performance under dynamic loading when critical components such as connections and anchors would be loaded the maximum that the design recommendations permit. They permit the evaluation of these potentially brittle components when the shear panels experience significant inelastic response. Section 8.4 presents tabular data on the shear panel design used to define the predicted lateral load-versus-deformation behavior.

The design recommendations in this Chapter 11 require the use of an R coefficient of 4. However, in order to test the nonlinear demand and capacity at large deformations, the cold-formed steel shear panels were undersized for the loads applied to them, based on an R coefficient of 4. Figure 8-12 shows one of the most severe synthetic records (SE32) used in the example analysis presented in Foutch and Wilcoski (unpublished). The model first mode of vibration was predicted to be just over 2 Hz. Figure 8-13 shows the SE32 record has a relatively level response-spectrum amplitude from 2.3 Hz down to 1 Hz. As the straps yield in the test, the effective natural frequency decreases so that the support motions below 2 Hz were expected to dominate the model response later in the test. The shake table model had to be tested in the shorter stroke direction of the TESS due to safety considerations. In this direction, the peak-to-peak stroke is limited to 5.5 in. The unfiltered record shown in Figure 8-12 has displacements that exceed the displacement limits of the TESS in this direction, so the record was high-pass filtered at 1.0 Hz to bring the maximum displacements down to within these limits. Figure 8-12 plots the 1.0 Hz high-pass filtered record with the unfiltered record, showing they match well. Figure 8-13 shows the response spectra for both the filtered and unfiltered records, showing the good fit above 1.0 Hz. Figure 8-14 shows the filtered and unfiltered acceleration records, zoomed in at the strong-motion portions between 16 and 40 seconds.

Figure 8-9. In-plane and out-of-plane connections and anchorage details at the second-story slab.

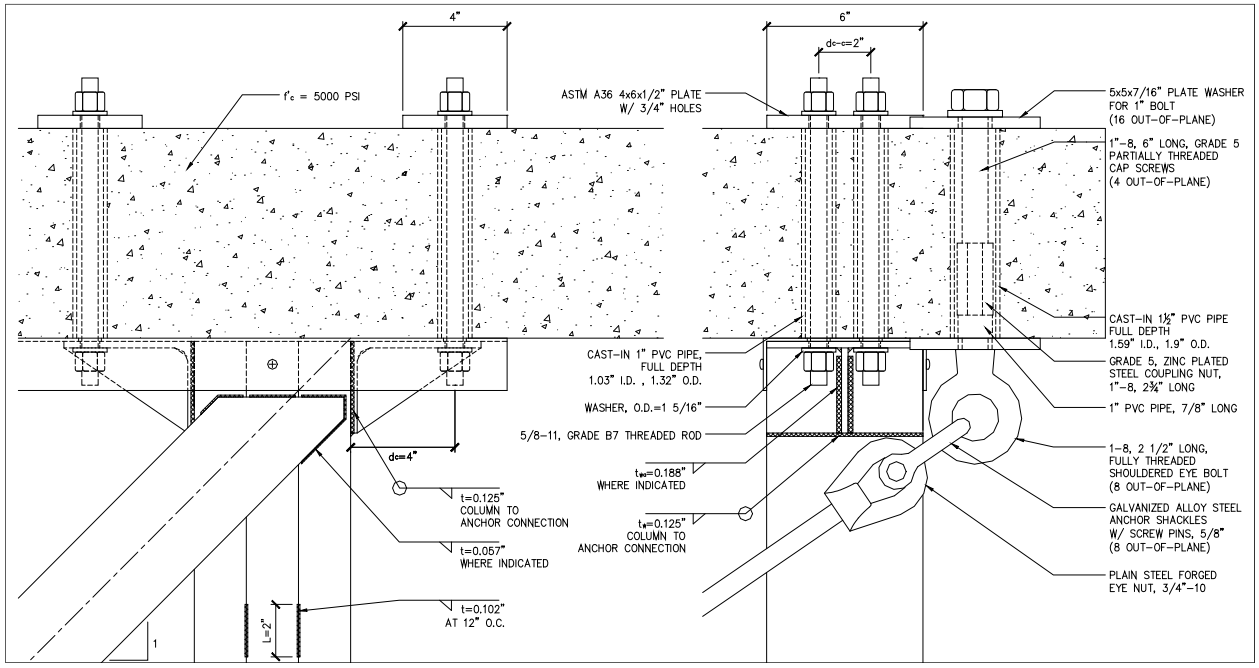

Figure 8-10. In-plane and out-of-plane connections and anchorage details at the first-story slab.

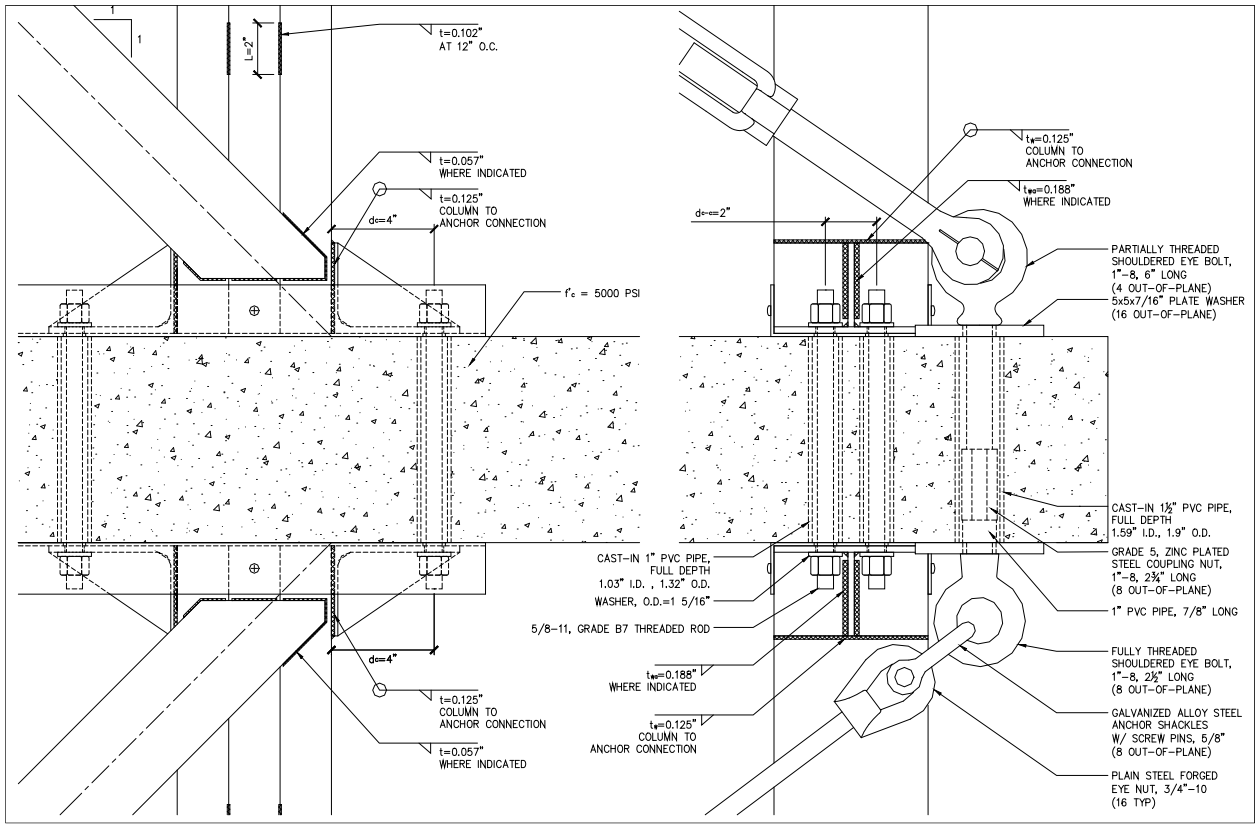

Figure 8-11. In-plane and out-of-plane connections and anchorage details at the base beam.

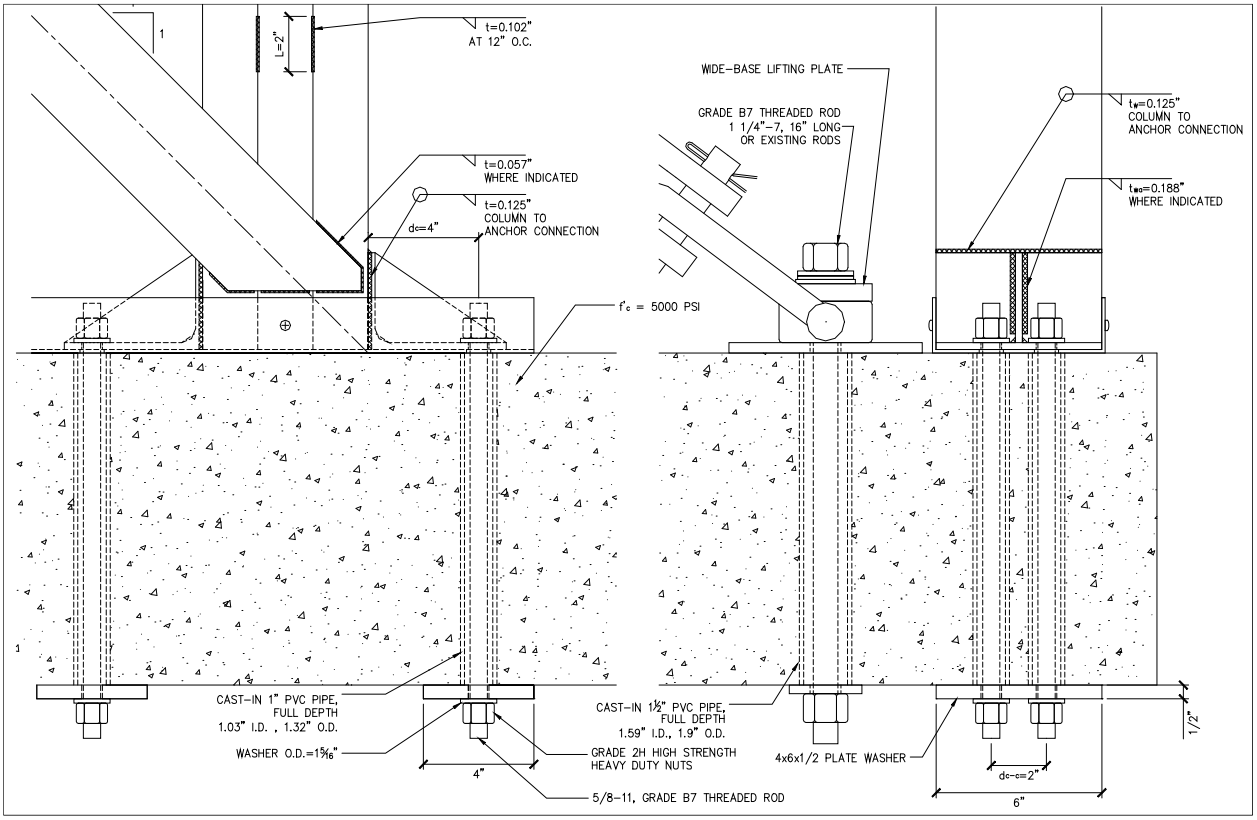

Figure 8-12. SE32 synthetic earthquake record and SE32 record filtered at 1.0 Hz.

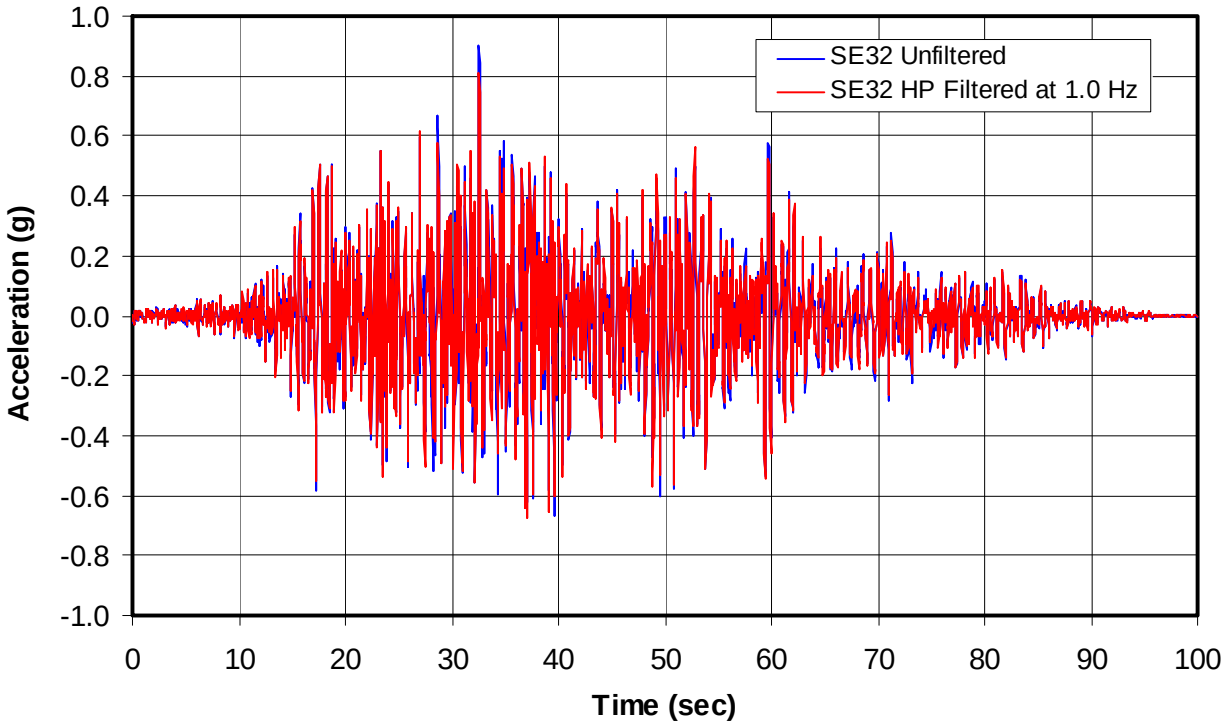

Figure 8-13. Response spectra plots of the SE32 unfiltered and filtered records.

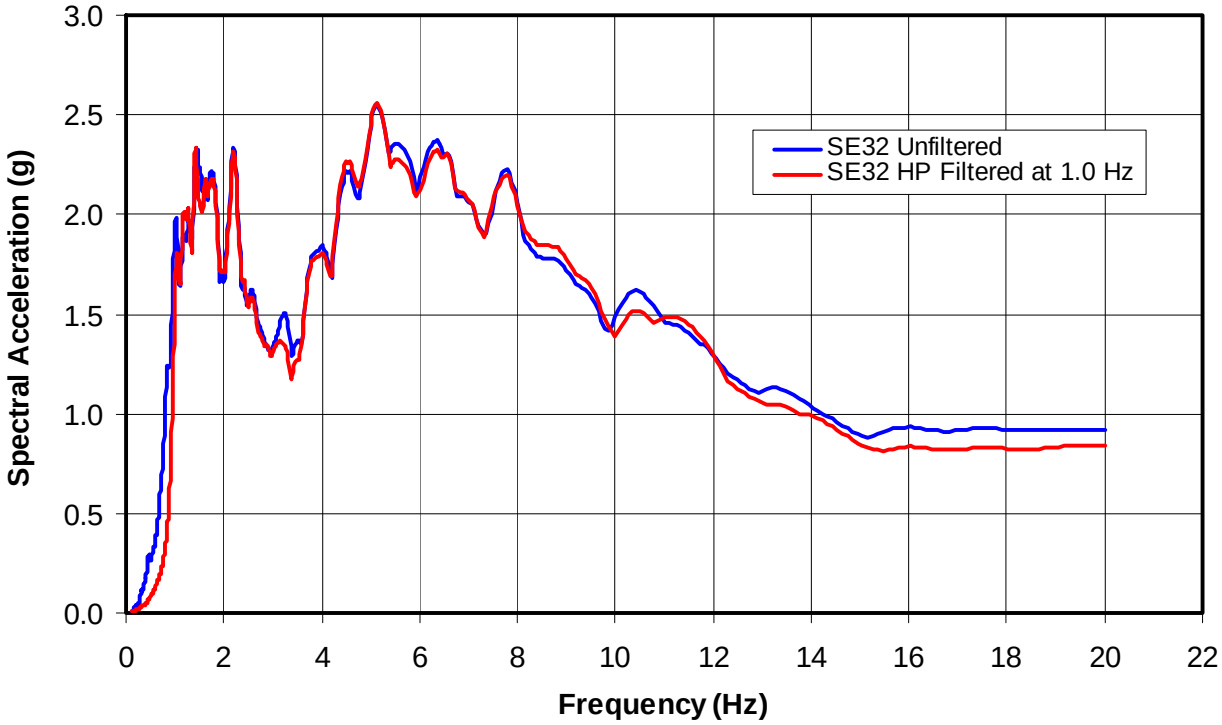

Figure 8-14. Strong motion portion of the SE32 unfiltered and filtered records.

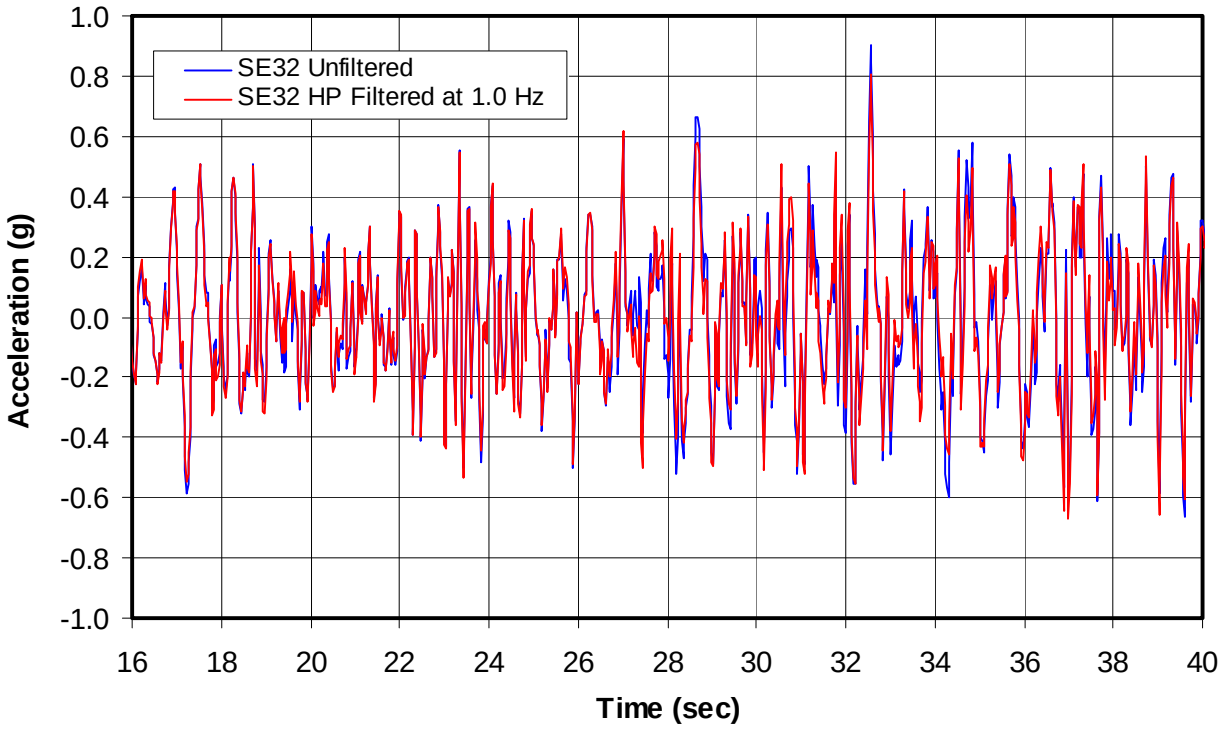

These records were double integrated to generate displacement time-history records. The strong-motion portions of these records are plotted in Figure 8-15 for both the filtered and unfiltered SE32 record, showing the large reduction of displacement amplitude in the filtered record.

Figure 8-15. Strong motion portion of the SE32 unfiltered and filtered displacement records.

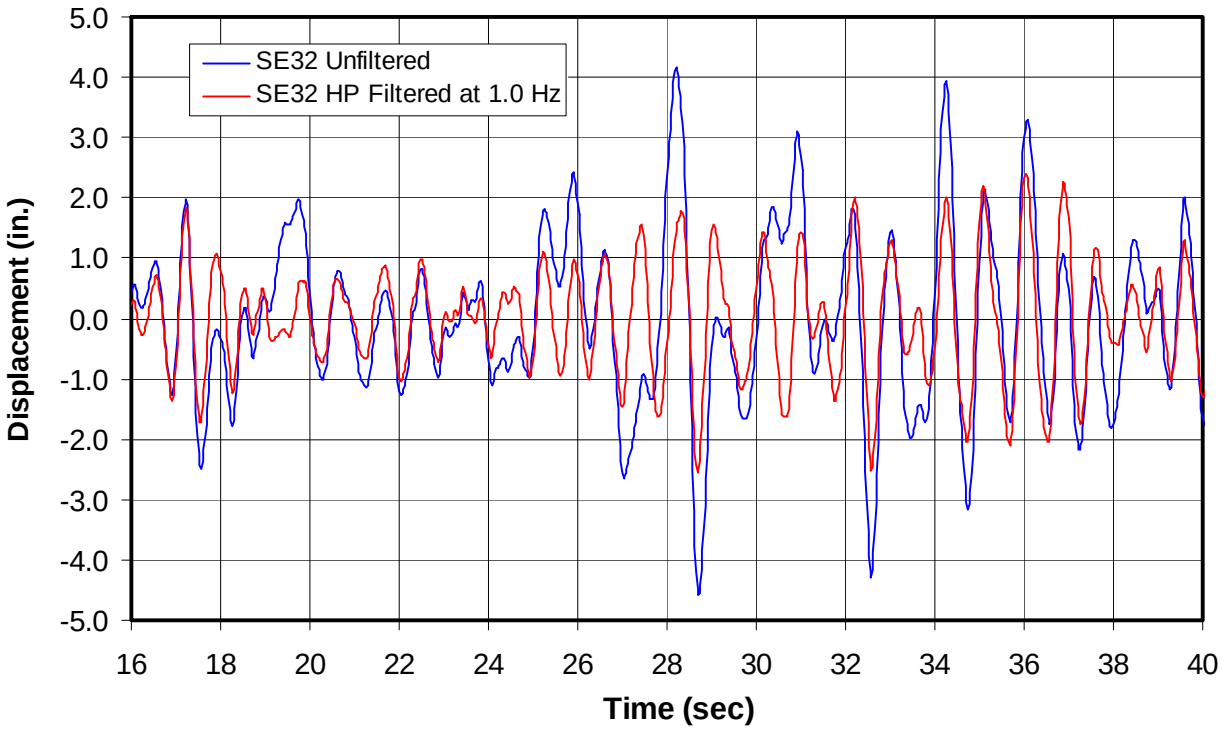

The unfiltered SE32 accelerometer waveform was developed to fit a design response spectrum that has a spectral response acceleration at short periods, S_{DS} of 1.5 g. Using the equivalent lateral force procedure, an R coefficient of 4, and an I of 1.0, the seismic base shear, V for this shake table model was estimated to be 21.6 kips per frame, or 43.2 kips for both frames ($V = S_{DS}I/R \times W$). Based on an R of 4, these first-story shear panels were significantly underdesigned. Table 8-2 summarizes these calculations based on the assumption that these frames are placed in the short direction of a building.

Table 8-2. Base shear and seismic story shears for shake table model.

Total Dead Load D_T= D+EW+IW (kips)	Total Floor Live Load L (kips)	Panel Level	Short Direction Total Weight W_S (k-mass)	Response Modification Factor R	Seismic Response Coefficient C_s (g)	Short Dir Base Shear V_S (kips)	Height at Floor Level h_{xS} or h_{xL} (ft)	Short Dir Vertical Distribution Factor C_{vxS}	Number Frames in Short Dir n_S	Short Dir Lateral Seismic Force/frame F_{xS} (kips)	Short Dir Seismic Story Shear V_{xS} (kips)
21	36.6	2nd	58				252	0.667	2	14.40	14.40
		Cumulative	58								14.40
21	36.5	1st	58				126	0.333	2	7.19	7.19
		Cumulative	115	4.00	0.375	43.2					21.58
			115	5.53	0.271	31.2					15.608

This applied load is 38% greater than the design capacity of the panels shown in Table 8-1. The last row in Table 8-2 shows that the R coefficient would need to be increased to 5.53 for the calculated first-story applied load to drop to the design capacity. The first-story shear panels were significantly undersized so they deform significantly, permitting the assessment of panel demand and capacity at very large drifts. This is needed to evaluate the ability to model nonlinear behavior at large drifts. The nonlinear analysis conducted using Drain 2DX predicts the panels will experience drifts of 5% of the story heights, which is almost 6 in. lateral drift in the first-story shear panels.

It must be noted that the purpose of the shake table test is to verify nonlinear analysis at large deformations, not to evaluate the performance of cold-formed steel shear panels. However, even though the cold-formed steel panels were significantly underdesigned for the loads that were be applied to them, the test should demonstrate very ductile behavior of this structural system, which is one of the benefits of cold-formed steel construction following the design recommendations presented in Chapter 11.

8.3 Model instrumentation

The shake table verification model was instrumented with accelerometers, displacement gages and strain gages. The instrument type and locations were selected to provide the model response measurements that could be compared directly with the calculated behavior from the DRAIN 2DX analysis.

8.3.1 Accelerometers

Table 8-3 gives the sensor names, locations, direction of measurement, full-scale range and resolution of measurement for each accelerometer.

Table 8-3. Shake table verification model accelerometers.

#	Sensor Name	Model Level	Sensor Coordinates* X (in.)	Y (in.)	Z (in.)	Sensor Direction	Full Scale (g)	Resolution (g)
0	ATx	TESS				Longitudinal (X)	4.0	0.00012
1	A1x	Basebeam	2	2	0	Longitudinal (X)	5.0	0.00015
2	A1y	Basebeam	2	2	0	Lateral (Y)	5.0	0.00015
3	A1z	Basebeam	2	2	0	Vertical (Z)	5.0	0.00015
4	A2x	Basebeam	168	2	0	Longitudinal (X)	5.0	0.00015
5	A2y	Basebeam	168	2	0	Lateral (Y)	5.0	0.00015
6	A2z	Basebeam	168	2	0	Vertical (Z)	5.0	0.00015
7	A3x	Basebeam	2	162	0	Longitudinal (X)	5.0	0.00015
8	A3y	Basebeam	2	162	0	Lateral (Y)	5.0	0.00015
9	A3z	Basebeam	2	162	0	Vertical (Z)	5.0	0.00015
10	A4z	Basebeam	168	162	0	Vertical (Z)	5.0	0.00015
11	A11x	1st Floor	2	2	126	Longitudinal (X)	5.0	0.00015
12	A11y	1st Floor	2	2	126	Lateral (Y)	5.0	0.00015
13	A11z	1st Floor	2	2	126	Vertical (Z)	5.0	0.00015
14	A12x	1st Floor	168	2	126	Longitudinal (X)	5.0	0.00015
15	A12y	1st Floor	168	2	126	Lateral (Y)	5.0	0.00015
16	A12z	1st Floor	168	2	126	Vertical (Z)	5.0	0.00015
17	A13x	1st Floor	2	162	126	Longitudinal (X)	5.0	0.00015
18	A13y	1st Floor	2	162	126	Lateral (Y)	5.0	0.00015
19	A13z	1st Floor	2	162	126	Vertical (Z)	5.0	0.00015
20	A14z	1st Floor	168	162	126	Vertical (Z)	5.0	0.00015
21	A21x	2nd Floor	2	2	252	Longitudinal (X)	5.0	0.00015
22	A21y	2nd Floor	2	2	252	Lateral (Y)	5.0	0.00015
23	A21z	2nd Floor	2	2	252	Vertical (Z)	5.0	0.00015
24	A22x	2nd Floor	168	2	252	Longitudinal (X)	5.0	0.00015
25	A22y	2nd Floor	168	2	252	Lateral (Y)	5.0	0.00015
26	A22z	2nd Floor	168	2	252	Vertical (Z)	5.0	0.00015
27	A23x	2nd Floor	2	162	252	Longitudinal (X)	5.0	0.00015
28	A23y	2nd Floor	2	162	252	Lateral (Y)	5.0	0.00015
29	A23z	2nd Floor	2	162	252	Vertical (Z)	5.0	0.00015
30	A24z	2nd Floor	168	162	252	Vertical (Z)	5.0	0.00015

*Accelerometer block base relative to the top northwest corner of the basebeam

The test was uniaxial, with the filtered SE32 synthetic earthquake motion (see Figure 8-12) in the longitudinal (X-direction) or in-plane direction with respect to the model drawings. Many accelerometers shown in Table 8-3 measured the desired longitudinal motions, including the input motion of shake table (ATX), base beam (A1x, A2x, and A3x), first floor (A11x, A12x, and A13x) and second floor (A21x, A22x, and A23x). Figure 8-16 through Figure 8-20 show all accelerometer locations. Table 8-3 and Figure 8-16 and Figure 8-17 show the second-floor accelerometers were located directly above the first-floor accelerometers, which are in turn directly above the base-beam accelerometers. The multiple accelerometers at each level were for measuring undesired torsional response (e.g., A21x and A23x on the second floor) and redundant measurement of the desired in-plane response (e.g., A21x and A22x, which were both on the west side (Y = 2 in.) of the second floor slab).

Figure 8-16. In-plane elevation drawing showing instrumentation.

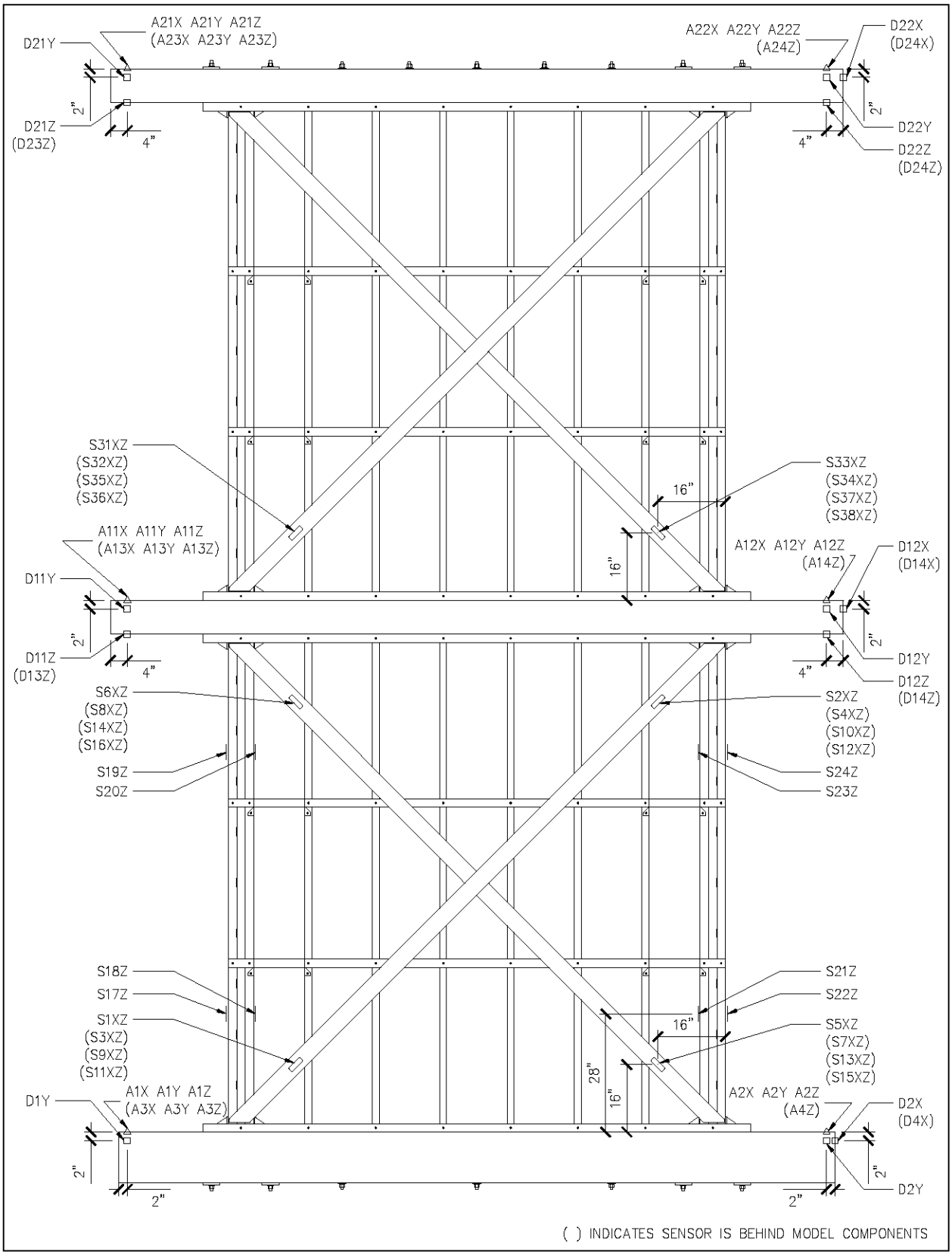

Figure 8-17. Out-of-plane elevation drawing showing instrumentation.

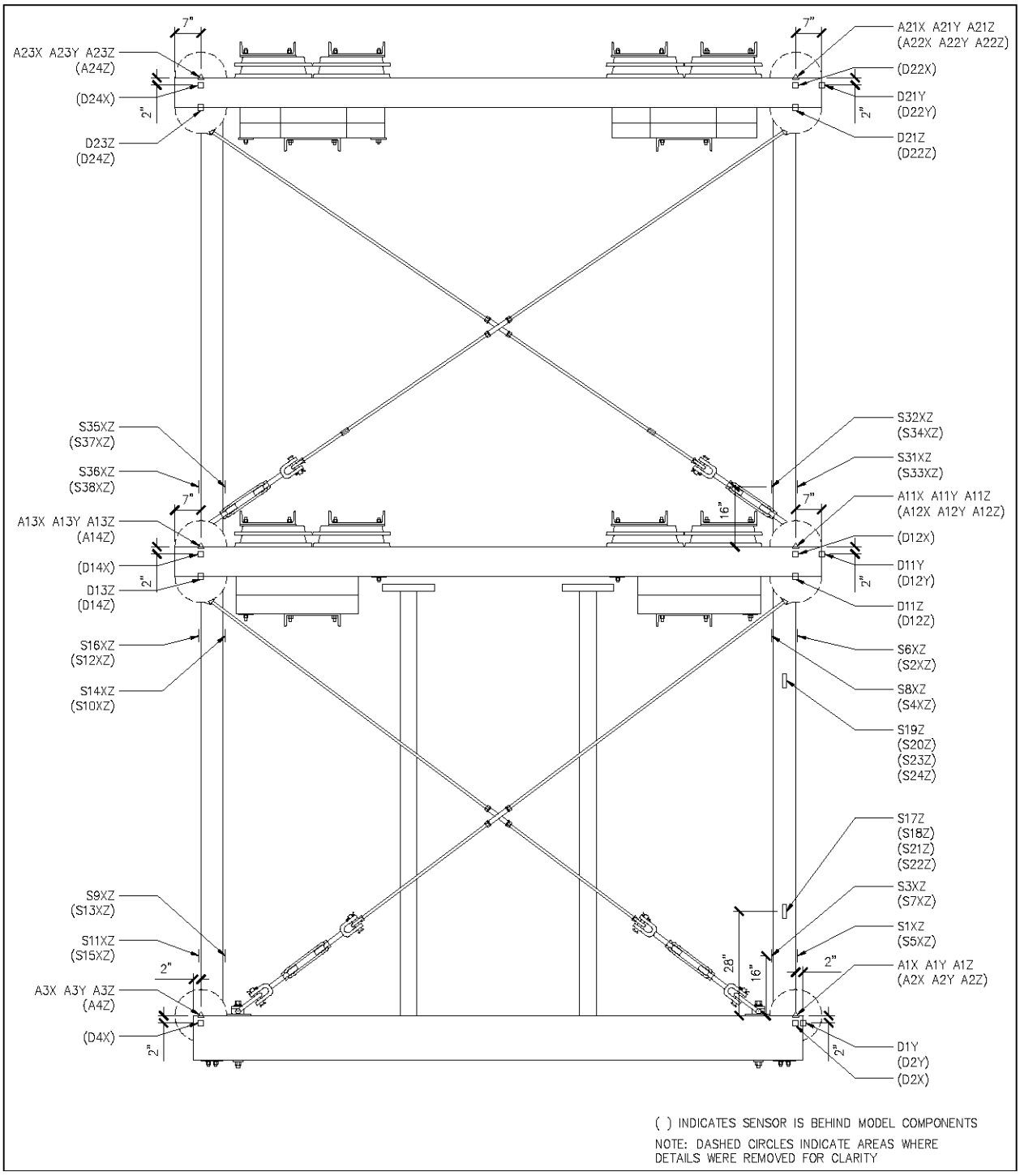

Figure 8-18. Plan view of the base beam showing instrumentation.

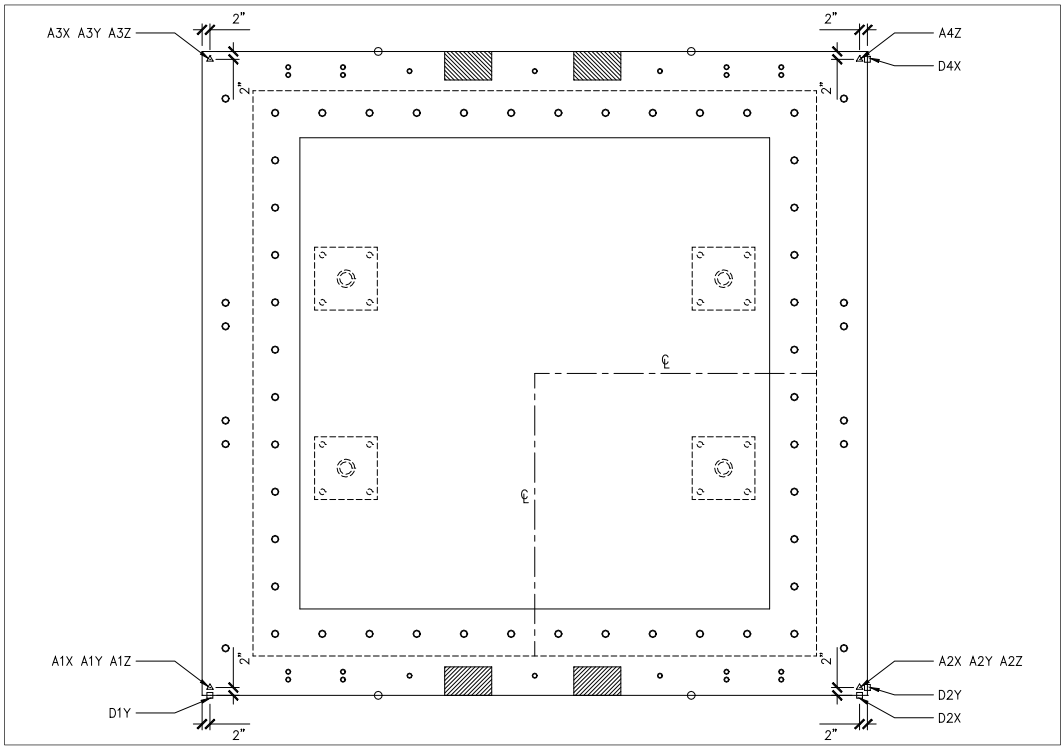

Figure 8-19. Plan view of the first-story slab showing instrumentation.

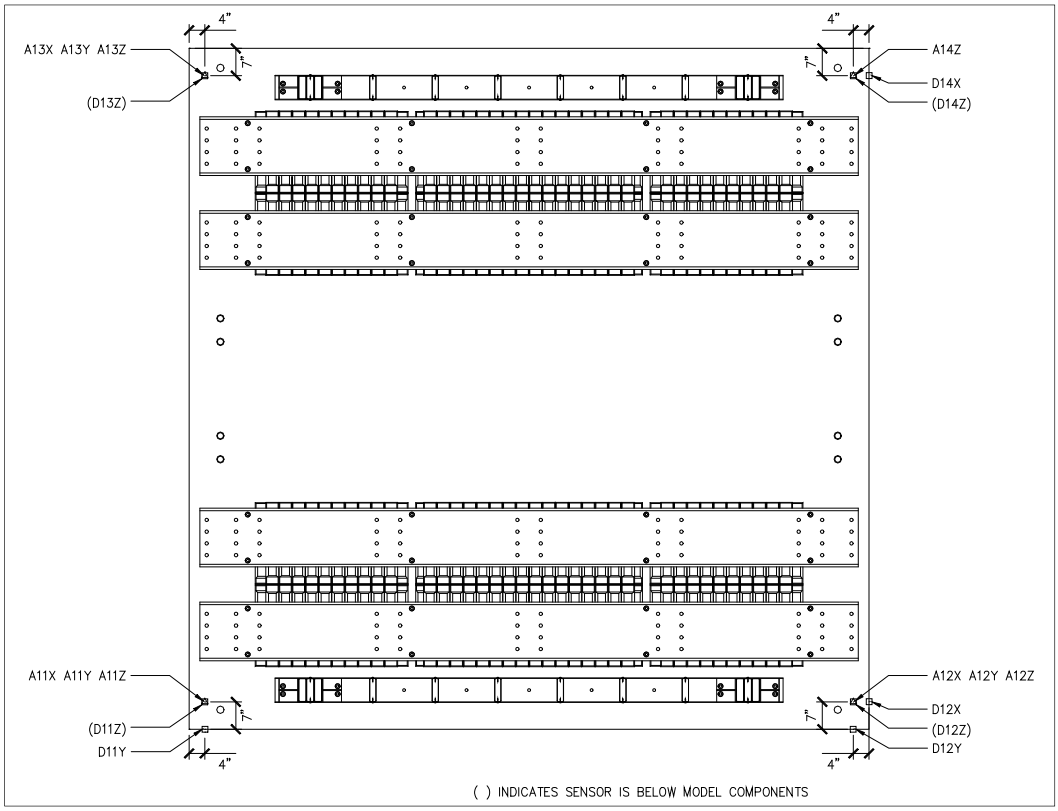

Figure 8-20. Plan view of the second-story slab showing instrumentation.

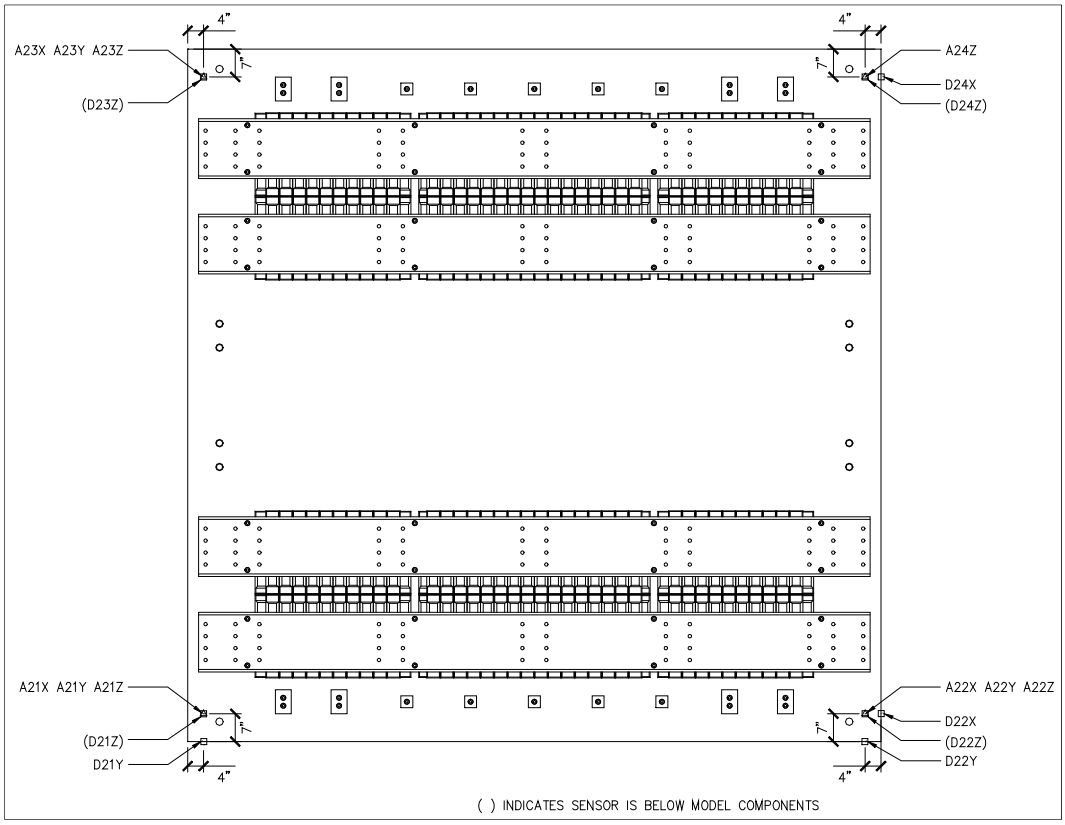

Other accelerometers were installed in the lateral (Y-direction) or out-of-plane direction to measure unwanted out-of-plane or torsional response. The model stiffness and mass distribution should have been very symmetric so that out-of-plane or torsional response would not be significantly induced. The out-of-plane threaded rods shown in Figure 8-3 were designed to restrain model response in this direction. The stiffness of this restraint was slightly less than the model stiffness in the in-plane direction. Therefore, the model was expected to have an out-of-plane mode of vibration with a frequency slightly less than the in-plane direction. This mode would be excited at low levels, but the levels of motion would be quite small because the mass and stiffness of the model were very symmetric and the model would not be excited out-of-plane. Still, the model would respond with relatively low levels of undesired rocking, torsion and out-of-plane motion. This motion was measured, so it could be accounted for when analyzing the response of the shake table model. The torsional and out-of-plane response should not be significant, and the rocking response can be accounted for in refined Drain 2DX analysis when comparing with predicted nonlinear response.

Some vertical response was expected of both the model and also the shake table surface itself. It was expected that the TESS surface would be driven somewhat by the very large overturning forces applied to it. The overturning motion of the TESS is unwanted but cannot be eliminated completely. The overturning flexibility of the TESS is due to the oil column and other flexibility associated with the vertical actuators. The TESS has tremendous overturning capacity and stiffness, with a total of nine 90 kip actuators, but the large overturning moment still causes unwanted vertical motions. The overturning moment applied to the TESS by testing to the filtered SE32 record is approximately 9900 k-in., calculated based on the seismic story shears per frame given in Table 8-2 (with an R of 4) times the two frames multiplied by the elevation of the floor slabs above the center of longitudinal actuators (12 in. below the TESS surface) (272 in. x 2 x 14.40 kip + 146 in. x 2 x 7.19 kip). The overturning capacity of the TESS is much greater at 25,920 k-in. (48 in. x 6 x 90 kips), showing that the TESS has more than adequate overturning capacity. However, due to the compressibility of the vertical actuator oil columns alone, the overturning stiffness, k_θ, can be roughly calculated to be 60,323,000 k-in. based on the oil column force per actuator, for a unit displacement times the number of actuators times the distance from the center of rocking divided by the rotation needed for a unit displacement (4 x 30 in^2 x 100 ksi /2.75 in. x 1 in. x 6 x 48 in./(1 in/48 in.)). If no compensation is made in the TESS control for oil compressibility, the overturning rotation may be approximately 0.000165 radians (9933 k-in./ 60,323,000 k-in.), which would result in 0.0097 in. (118 in./2 x 0.000166 radians) of unwanted vertical displacement, d_{VR}, at the exterior faces of the columns. This is a low estimate of vertical displacement because other sources of system flexibility increase displacements. However, these displacements are small relative to the large expected lateral deformation of the model. The polar moment of inertia of the model, J, was approximately 14,215 k-in.-sec^2 ($J = W/g \times r^2$ = (57.5 kip x (146 in.)^2 + 57.6 kip x (272 in)^2)/386 in./sec^2). From this, the rocking natural frequency, f_R, due to oil column compressibility alone was estimated to be 10 Hz ($f_R = 1/(2\pi) \times (k\theta/J)^{0.5} = 1/(2\pi) \times$ (60,323,000 k-in./14,215 k-in.-s2)$^{0.5}$). This was expected to be a high estimate of the overturning or rocking frequency of the system because of additional flexibility from the TESS system and the model itself. Still, this frequency was well above the model in-plane natural frequency, estimated to be 2 Hz. The vertical acceleration at the bottom of the model columns due to overturning, a_R, was estimated to be 0.107 g ($a_R = d_{VR}\omega^2$). The overturning-related lateral displacement, d_{Rx}, and acceleration, a_{Rx}, at the top of the model

were estimated to be 0.045 in. (272 in./(118 in./2) x 0.0097 in.) and 0.49 g (272 in./(118 in./2) x 0.107 g), respectively. However, because this estimated overturning frequency was much higher than the model frequency, the model could be isolated from the effects of this higher-frequency rocking. Still, the overturning response of the TESS was not well understood, and was measured with the vertical accelerometers shown in Table 8-3. The DRAIN 2DX analysis was repeated after the shake table test to adjust the predicted behavior in a way that accounts for TESS overturning. This correction was needed to facilitate valid comparisons. However, these approximations of expected overturning suggest the TESS overturning should not be large enough to interfere with the response of the model or the test verification purposes.

8.3.2 Displacement gages

Table 8-4 gives the sensor names, locations, direction of measurement, full-scale range and resolution for each displacement gage installed on the shake table model. The displacement gages, called cable-extension position transducers, use a wire under tension that coils into a box on one end and attaches to the model on the other. The longitudinal (X) and lateral (Y) displacement gages measured the model response relative to fixed references off the TESS surface. However, the vertical displacement gages measured the movement of the surface above to the level below (e.g., first-floor vertical displacement relative to the base beam below). These vertical displacements were expected to be very small relative to longitudinal displacements. Assuming no deformation in the cold-formed steel panel anchors, these measurements permit the calculation of the overall deformation history of individual panel diagonal straps, even at the largest nonlinear deformations. The strap deformation could not be easily measured directly with linear variable differential transducers (LVDTs) because of the extreme strap deformation in the first-story panels. Very small deformations were expected in the panel anchors relative to the panel straps, because of the direct load path between the straps, columns and anchors, and the linear response of the anchors and very large nonlinear response of the straps. The displacement gages also provided independent measurement of the overall model response relative to the accelerometers. Figure 8-16 through Figure 8-20, above, show the locations of all displacement gages.

Table 8-4. Shake table verification model displacement gages.

#	Sensor Name	Model Level	Sensor Coordinates* X (in.)	Y (in.)	Z (in.)	Sensor Direction	Full Scale (in.)	Resolution (g)
1	D1y	Basebeam	2	0	-2	Lateral (Y)	10.0	0.00031
2	D2x	Basebeam	168	0	-2	Longitudinal (X)	10.0	0.00031
3	D2y	Basebeam	170	2	-2	Lateral (Y)	10.0	0.00031
4	D4x	Basebeam	170	162	-2	Longitudinal (X)	10.0	0.00031
5	D11z	1st Floor	2	2	118	Vertical (Z)	10.0	0.00031
6	D12z	1st Floor	168	2	118	Vertical (Z)	10.0	0.00031
7	D13z	1st Floor	2	162	118	Vertical (Z)	10.0	0.00031
8	D14z	1st Floor	168	162	118	Vertical (Z)	5.0	0.00015
9	D11y	1st Floor	2	-5	124	Lateral (Y)	10.0	0.00031
10	D12x	1st Floor	172	2	124	Longitudinal (X)	10.0	0.00031
11	D12y	1st Floor	168	-5	124	Lateral (Y)	10.0	0.00031
12	D14x	1st Floor	172	162	124	Longitudinal (X)	10.0	0.00031
13	D21z**	2nd Floor	2	2	244	Vertical (Z)	5.0	0.00015
14	D22z**	2nd Floor	168	2	244	Vertical (Z)	5.0	0.00015
15	D23z**	2nd Floor	2	162	244	Vertical (Z)	5.0	0.00015
16	D24z**	2nd Floor	168	162	244	Vertical (Z)	5.0	0.00015
17	D21y	2nd Floor	2	-5	250	Lateral (Y)	10.0	0.00031
18	D22x	2nd Floor	172	2	250	Longitudinal (X)	10.0	0.00031
19	D22y	2nd Floor	168	-5	250	Lateral (Y)	10.0	0.00031
20	D24x	2nd Floor	172	162	250	Longitudinal (X)	10.0	0.00031

*Displacement (yo-yo) gage block base relative to top northwest corner of base beam.

**2nd floor vertical displacement gages run between the 1st and 2nd floor.

8.3.3 Strain gages

Table 8-5 presents the sensor names, locations, direction of measurement, full-scale range, and resolution for each strain gage installed on the shake table model. These sensors were installed on the cold-formed steel panel diagonal straps and columns. The shear panels were the same height and width, both dimensions being 118 in. An extension of the strap center lines extend through the exterior edge of the columns where they intersect the top and bottom of the panels at the concrete slab or base beam, as shown in Figure 8-9 through Figure 8-11. The center locations of all strain gages were 16 in. vertically and horizontally from this intersection, which placed them at the center of the strap cross-sections (see Figure 8-16). They were located this distance from the welded connection to the columns so that the stress and strains would be fairly uniform through the strap cross-sections. Near the welded connection these would not be uniform due to slight deformations of the anchors and columns and concentrations of stress and strain at the welds. The straps would also have some residual strains from the cold forming process and cutting to their 4 in. width. These residual strains may be quite different near the strap edges,

but should be fairly uniform along the length of the strap. The diagonal strap strain gages were primarily intended to measure the linear strains. As is explained later in the detailed test steps, these strain measurements were used to guide test levels for the linear shake table testing.

Table 8-5. Shake table verification model strain gages.

#	Sensor Name	Model Level	Sensor Coordinates* X (in.)	Y (in.)	Z (in.)	Sensor Direction	Full Scale** (mico in/in)	Resolution (mico in/in)
1	S1xz	1st Floor Straps	42	2	16	Long/Vert (XZ)	50000	1.53
2	S2xz	1st Floor Straps	128	2	102	Long/Vert (XZ)	50000	1.53
3	S3xz	1st Floor Straps	42	8	16	Long/Vert (XZ)	50000	1.53
4	S4xz	1st Floor Straps	128	8	102	Long/Vert (XZ)	50000	1.53
5	S5xz	1st Floor Straps	128	2	16	Long/Vert (-XZ)	50000	1.53
6	S6xz	1st Floor Straps	42	2	102	Long/Vert (-XZ)	50000	1.53
7	S7xz	1st Floor Straps	128	8	16	Long/Vert (-XZ)	50000	1.53
8	S8xz	1st Floor Straps	42	8	102	Long/Vert (-XZ)	50000	1.53
9	S9xz	1st Floor Straps	42	156	16	Long/Vert (XZ)	50000	1.53
10	S10xz	1st Floor Straps	128	156	102	Long/Vert (XZ)	50000	1.53
11	S11xz	1st Floor Straps	42	162	16	Long/Vert (XZ)	50000	1.53
12	S12xz	1st Floor Straps	128	162	102	Long/Vert (XZ)	50000	1.53
13	S13xz	1st Floor Straps	128	156	16	Long/Vert (-XZ)	50000	1.53
14	S14xz	1st Floor Straps	42	156	102	Long/Vert (-XZ)	50000	1.53
15	S15xz	1st Floor Straps	128	162	16	Long/Vert (-XZ)	50000	1.53
16	S16xz	1st Floor Straps	42	162	102	Long/Vert (-XZ)	50000	1.53
17	S17z	1st Floor West Columns	26	5	28	Vertical (Z)	5000	0.15
18	S18z	1st Floor West Columns	32	5	28	Vertical (Z)	5000	0.15
19	S19z	1st Floor West Columns	26	5	90	Vertical (Z)	5000	0.15
20	S20z	1st Floor West Columns	32	5	90	Vertical (Z)	5000	0.15
21	S21z	1st Floor West Columns	138	5	28	Vertical (Z)	5000	0.15
22	S22z	1st Floor West Columns	144	5	28	Vertical (Z)	5000	0.15
23	S23z	1st Floor West Columns	138	5	90	Vertical (Z)	5000	0.15
24	S24z	1st Floor West Columns	144	5	90	Vertical (Z)	5000	0.15
25	S31xz	2nd Floor Straps	42	2	142	Long/Vert (XZ)	50000	1.53
26	S32xz	2nd Floor Straps	42	8	142	Long/Vert (XZ)	50000	1.53
27	S33xz	2nd Floor Straps	128	2	142	Long/Vert (-XZ)	50000	1.53
28	S34xz	2nd Floor Straps	128	8	142	Long/Vert (-XZ)	50000	1.53
29	S35xz	2nd Floor Straps	42	156	142	Long/Vert (XZ)	50000	1.53
30	S36xz	2nd Floor Straps	42	162	142	Long/Vert (XZ)	50000	1.53
31	S37xz	2nd Floor Straps	128	156	142	Long/Vert (-XZ)	50000	1.53
32	S38xz	2nd Floor Straps	128	162	142	Long/Vert (-XZ)	50000	1.53

*Center of strain gage relative to the top northwest corner of the basebeam.
**The maximum strain measurement may be limited by bond failure of the brittle cement.

Pairs of strain gages were also installed near the top and bottom of the first-story west shear panel columns. For example, the lower-left corner of Figure 8-16 shows that one gage (S17z) was installed on the in-plane outside face and one (S18z) on the inside face, both 28 in. above the bottom of the column. A similar pair (S19z and S20z) was installed 28 in. below the

top of this same column. Similarly, the right side of Figure 8-16 shows that pairs of strain gages were installed near the bottom (S21z and S22z) and top (S23z and S24z) of the other column of this west shear panel. These pairs of sensors were used to measure the shear in the columns. The column shears should be uniform throughout their heights, so that the column moment near the column anchors can be estimated. These gages are placed far enough away from the column tops and bottoms, so that the strains should remain linear. These measurements were to be used to estimate when the columns yield.

8.4 Shear panel design details and predicted lateral load versus deflection

The model presented in Chapter 5 is also used here to predict the lateral load versus deflection of the shear panels used in the shake table model. Material tests were conducted on the steel used in the diagonal straps, columns, and column anchors by testing five coupons of each of these panel components. Figure 8-21 plots the stress-versus-strain results from a typical coupon test for each of these components. Each plot shown in Figure 8-21 is for a coupon that best represents the average of all five coupons tested for each component (straps, columns, and anchors).

Figure 8-21. Stress-versus-strain plots for shake table model shear panel materials.

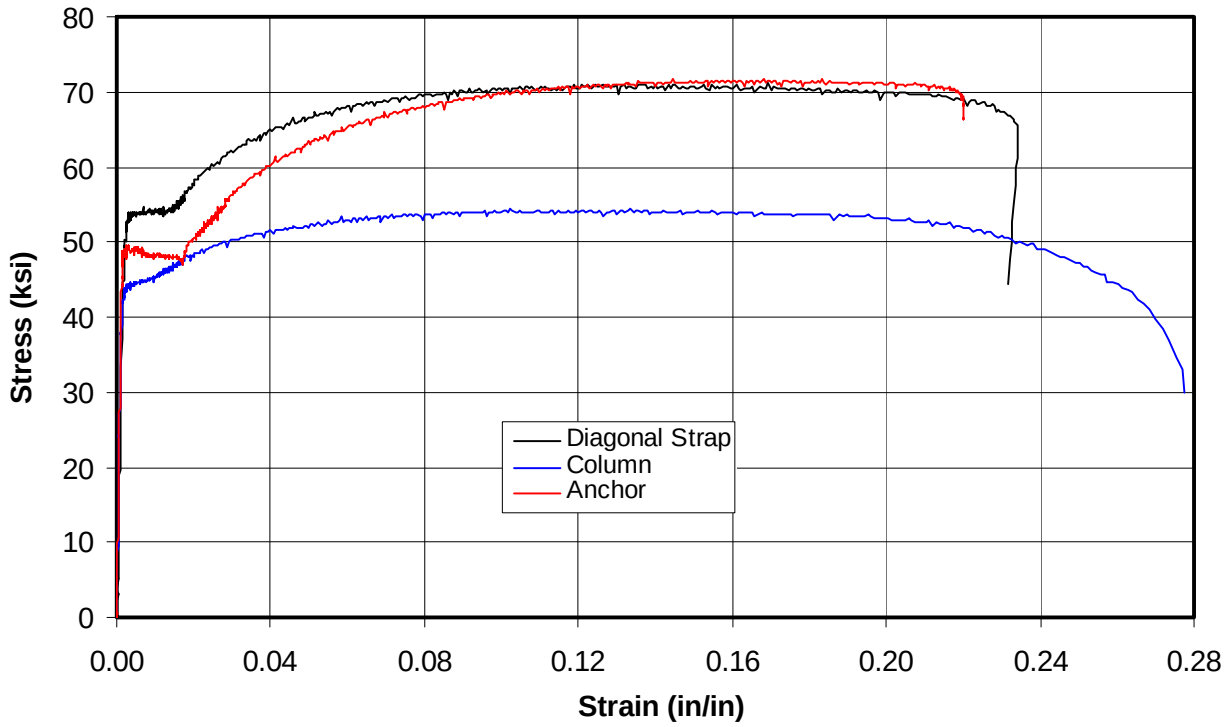

Figure 8-21 and Table 8-6 show that the material in the diagonal straps easily meets the required 1.08 ratio of ultimate over yield strength and the 10% elongation (0.10 in./in. strain) for ASTM A 1003/A 1003M high-ductility material (ASTM 2013b). Table 8-6 shows the material thickness, yield strain, yield stress, F_y, ultimate stress, F_u, ratio of ultimate over yield stress and elongation within 2 in. coupon gage length for the materials used in each component of the cold-formed steel shear panels. The thickness, yield stress, ultimate stress, ratio of ultimate over yield stress and elongation are average values from all five coupons tested for each panel component (diagonal straps, column studs and anchor angles). The yield stress was the average stress for all five coupons, at which a line drawn parallel to and offset 0.2% strain (0.002 in./in.) to the elastic region crosses the stress-versus-strain measured data. The yield strain in this table is the strain at which the representative coupon stress reached this average yield stress for the particular component. The elongation given in Table 8-6 is the average percentage of elongation over the 2 in. gage range at which the coupon ruptured for each material.

Table 8-6. Coupon test results for materials used in shake table model shear panels.

Material	Thickness (in.)	Yield Strain (in/in)	Yield Stress (ksi)	Ultimate Stress (ksi)	Ultimate / Yield Stress	Elongation in 2 in.
Diagonal Straps	0.055	0.0029	53.6	71.0	1.32	22.6%
Column Studs	0.116	0.0026	44.9	54.5	1.21	26.1%
Anchor Angle	0.257	0.0015	48.0	71.0	1.48	22.6%

Figure 8-22 plots the same material test data, but zooms in on the region of smaller strains that are still well beyond the greatest strains expected in the shake table test. The diagonal strap plot shows they begin to yield at a stress of 50 ksi. A yield strength, F_{sy}, of 53.6 ksi (design was 50 ksi) was used to calculate the panel capacity as shown in Table 8-7 (a repeat of Table 8-1 for convenience). The strain when the straps first begin to yield, ε_{sy}, should be 0.0017 in./in. (ε_s = 50 ksi/E). The straps initially yield at some unknown location that would most likely not be within the length of the strain gages. As strap yielding progressed locally, they would begin to strain harden at a strain of about 0.015 in./in. (see Figure 8-22). This would cause strap yielding throughout the length of strap between the columns. The first-story straps should be fairly uniformly yielded at the 0.015 in./in. strain when the first-story panel reaches about 3.2 in. drift (δ = 0.015 in./in. x ((106 in)^2 + (106 in)^2) / 106 in.).

Figure 8-22. Stress versus strain plots for shear panel materials, at small strains.

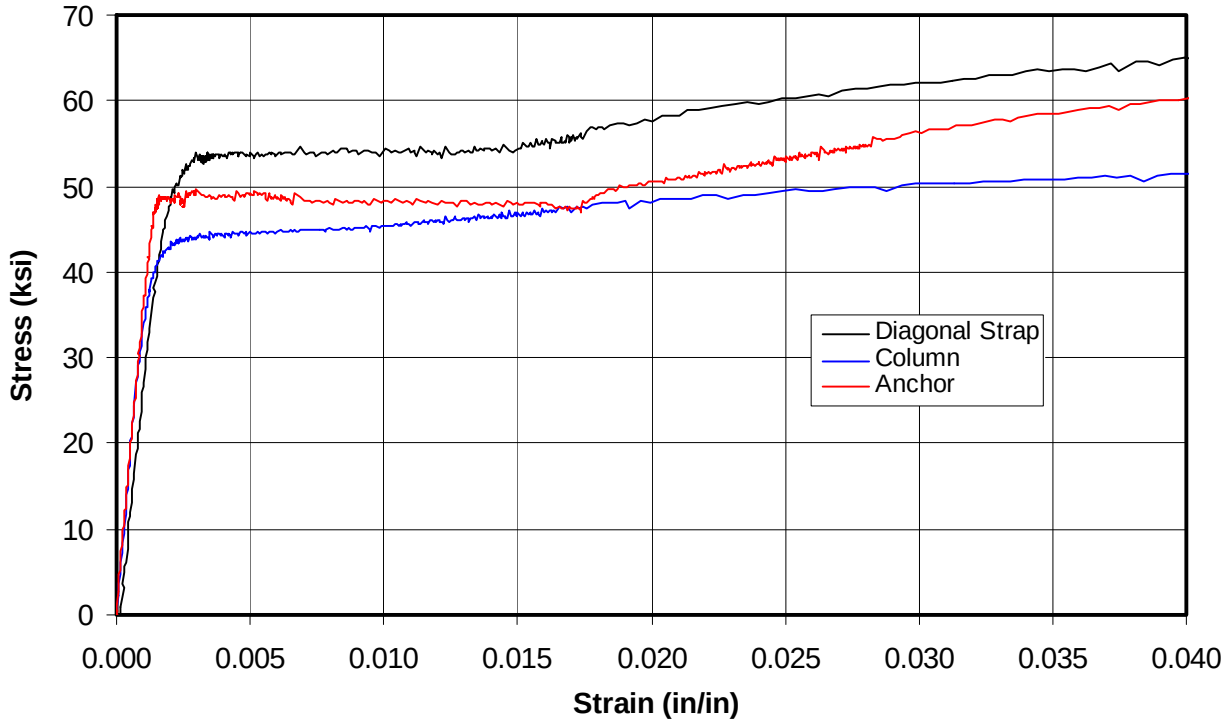

Table 8-7. Diagonal strap design for shake table model shear panels.

Panel Level	Panel Width W (in)	Panel Height H (in)	Strap Faces n_s (#)	Strap Width b_s (in)	Strap Thickness (ga)	Strap Thickness t_s (in)	Strap Initial Lat Stiffness k_s (k/in)	Yield Stress of Strap F_{sy} (ksi)	Capacity at Strap Lat Yield Q_{sy} (k)	Design Shear Strength $\phi_t Q_{sy}$ (k)	Lat Defl at Strap Yielding δ_{sy} (in)	Applied Story Shear V_x (kips)	Elastic Lateral Defl δ_{xe} (in)	Defl Amp Factor C_d	Import Factor I	Design Story Drifts $\Delta = \delta_x$ (in)	Stability Coeff θ	Allow Story Drifts Δ_a (in)
2nd Fl	118	118	2	4	16	0.055	38	53.6	16.62	15.78	0.436	14.40	0.378	3.5	1.0	1.32	0.0100	2.36
1st Fl	118	118	2	4	16	0.055	38	53.6	16.62	15.78	0.436	21.58	0.567	3.5	1.0	1.98	0.0100	2.36

This section presents the shake table model shear panel design details based on the panel configuration and details shown in Figure 8-2 and Figure 8-9 through Figure 8-11, and material properties shown in Table 8-7. Table 8-7 through Table 8-15 present the design details for both the first- and second-floor shear panels. The purpose of showing these details is that it shows the design demand and capacities for each of the panel components for both the first and second-story shear panels. These details will facilitate later discussion on panel performance observations and the adequacy of the design recommendations upon which these tables are based. Table 8-7 repeats the panel diagonal strap design details shown in Table 8-1. The first- and second-floor shear panels are identical, so their lateral deflection at strap yields, δ_{sy}, are both 0.436 in. in Table 8-7. Table 8-7 shows that design applied story shear V_x (21.58 kips) is much greater than the capacity at strap lateral yield, Q_{sy} (16.62 kips). This underdesign of the

shear panels was intentional so that significant nonlinear response would occur. As was mentioned earlier, the first-floor shear panels were designed as if an R coefficient of 5.53 were used.

Table 8-8 shows the diagonal strap ultimate strength, F_{su} and the maximum strap ultimate strength, F_{sumax}, equal each other, because they are the values measured in the coupon tests. Table 8-8 also shows the maximum gravity load per shear panel, GL_{max}, which is the total weight applied to each shear panels at both the first and second stories of the model. From these values the total compressive load applied to the columns, P_{vumax}, is shown. Table 8-8 shows the measured column yield and compressive strength, and thickness along with the other column properties. Table 8-9 shows the calculated column capacity, P, that exceeds the applied load, P_{vumax}. The left side of Table 8-10 summarizes the calculations used to determine the maximum intermittent weld spacing that will cause the column studs work together as a composite section. The intermittent weld length, L, is 2 in. and the maximum calculated spacing, s_{max}, is 11.7 in. and Figure 8-9 through Figure 8-11 show they were spaced slightly greater at 12 in. on center.

Table 8-8. Column design for shake table model shear panels.

Panel Level	Diagonal Strap Ult Stress F_{su} (ksi)	Max Ult Strap Stress F_{sumax} (ksi)	Max Gravity Load/ Panel GL_{max} = (kips)	Column Axial load at Strap Ult P_{vumax} (k)	Column Yield Stress F_{cy} (ksi)	Column Ultimate Stress F_{cu} (ksi)	Column Thickness (ga)	Column Thickness t_c (in)	Number of Studs /Column n	Panel Thickness /Column b_c (in)	Col Stud Flange Width b_f (in)	Column Depth h_c (in)
2nd Fl	71	71	28.8	36.4	44.90	54.50	12	0.116	3	6.0	2.0	6.0
1st Fl	71	71	57.6	50.8	44.90	54.50	12	0.116	3	6.0	2.0	6.0

Table 8-9. Column capacity calculations for shake table model shear panels.

Panel Level	Nominal Column Area A_c (in^2)	Distance to Extreme Fiber c (in)	In-Plane Mom of Inertia I_x (in^4)	In-Plane Radius of Gyration r_y (in)	Out-of-Plane Mom of Inertia I_y (in^4)	Out-of-Plane Radius of Gyration r_x (in)	Eff Length Factor K	Elastic Flexural Stress F_e (ksi)	λ_c	Nominal Axial Stress F_n (ksi)	Knockout hole dia d_h (in)	Flat Width w (in)	Slenderness factor λ	Eff Width b (in)	Eff Column Area A_e (in^2)	Column Design Strength P (kips)
2nd Fl	3.49	3.21	16.34	2.17	17.64	2.25	0.5	385	0.34	42.8	1.5	5.54	0.962	3.19	2.67	97.0
1st Fl	3.49	3.21	16.34	2.17	17.64	2.25	0.5	385	0.34	42.8	1.5	5.54	0.962	3.19	2.67	97.0

Table 8-10. Column intermittent weld design and combined axial and moment capacity.

Panel Level	Max Column Shear V_{cm} (kips)	Area on 1 Side of Crit Weld A (in^2)	Distance to Neutral Axis y (in)	Mom of Column Area Q (in^3)	Weld Shear/ Length q (k/in)	Intermittent Weld Length L (in)	Max o.c. Spacing s_{max} (in)	Strap Max Yield Stress F_{symax} (ksi)	Max Est Lat Defl at Strap Yield δ_{symax} (in)	Applied Moment @ δ_{symax} M_a (k-in)	Column Nominal Moment M_{nx} (k-in)	Column Interaction I
2nd Fl	3.9	2.32	1.62	3.8	0.9	2.0	11.7	53.6	0.436	105	263	0.631
1st Fl	3.9	2.32	1.62	3.8	0.9	2.0	11.7	53.6	0.436	111	263	0.747

The right side of Table 8-10 shows that the combination of axial load and moment on both columns, expressed in terms of an interaction expression, is well below 1.0. Table 8-11 summarizes the design of the welded diagonal strap connection to the columns. This shows that the maximum strap force, P_{su}, based on the measured ultimate strength of the straps is slightly greater than the welded connection capacity based on the measured ultimate strength of the thinner material welded (straps in this case). Figure 8-9 through Figure 8-11 show the weld capacity could have been increased by lengthening the weld along the longitudinal side of the straps. This was not done in order that the ability of these welds to perform without failure at their design limit could be tested, verifying the welded connection recommendations in the process.

Table 8-11. Welded connection design.

Panel Level	Max Est Ult Strap Force P_{su} (kips)	Fillet Weld Thickness t (in)	Longitudinal Weld Length L (in)	Longitudinal Weld Design Strength P_L (kips)	Long/Trans Weld Length L	Long/Trans Weld Design Strength P_{LT} (kips)	Welded Conn Total Capacity $(P_L+P_{LT})n_s$ (kips)
2nd Fl	31.1	0.055	3.25	5.2	5.16	10.1	30.7
1st Fl	31.1	0.055	3.25	5.2	5.16	10.1	30.7

The applied shear at the base of the columns, P_{humax}, is shown in Table 8-12. The total shear strength, V_T, far exceeds this applied load. In fact, the column shear capacity alone, V_C, without the anchor contribution to shear, exceeds this applied load. Therefore, the shear strength of the column and anchors were not close to being tested.

Table 8-12. Column and anchor shear design.

Panel Level	Column Shear Strength V_C (kips)	Strap Lat Ult Capacity $P_{humax}=A_0Q_E$ (kips)	Yield Stress of Angle F_{yA} (ksi)	Angle Thickness t_A (in)	Anchor Shear Strength V_A (kips)	Total Shear Strength V_T (kips)
2nd Fl	37.6	22.0	48	0.257	44.4	126.4
1st Fl	37.6	22.0	48	0.257	44.4	126.4

The panel anchors are most heavily loaded when the minimum gravity load is applied. For the shake table model, the gravity load does not change so that the minimum gravity load per shear panel, GL_{min}, equals the maximum gravity load per shear panel, GL_{max}. Table 8-13 shows that the height of the angles, H_A used in the anchors (3.5 in.) was sized so that the angle total weld strength, P_A, would barely exceed the maximum applied tensile force per anchor angle ($P_{vymax}/2 + P_M$) at the first-floor panel anchors. The shake table test then provided a good test of the design recommendations for the design of the welded connection between the columns and anchors.

Table 8-13. Shear panel anchor angle and plate design.

Panel Level	Min Gravity Load/ Panel GL_{min} (kips)	Anchor Uplift @ max Strap Yield P_{vymax} (kips)	Remaining Column Bending Cap M_{rem} (k-in)	Tensile Force Avail/angle P_M (kips)	Tensile Force/ Angle $P_{vymax}/2+P_M$ (kips)	Angle Horiz Weld Strength P_T (kips)	Col/Anchor Weld Thickness t_w (in)	Yield Stress F_{yA} (ksi)	Anchor Angle Size				Angle Vert Weld Strength P_G (kips)	Angle Tot Weld Strength P_A (kips)
										H_A (in.)		W_A (in.)	t_A (in.)	
2nd Fl	28.8	2.2	259.4	43.24	44.35	22.80	1/8	48	L	3.5	x	5.0	x 0.257	18.29	41.08
1st Fl	57.6	-12.2	283.6	47.27	41.19	22.80	1/8	48	L	3.5	x	5.0	x 0.257	18.29	41.08

Four, n_{AB} 5/8 in. diameter bolts were installed at each column anchor connection. Table 8-14 shows that bolt shear strength, P_v, far exceeded the applied shear per bolt, P_{hAB}. This table also shows the maximum tensile force per bolt, P_{tAB}, without prying action, and the bolt tensile design strength, P_t. Table 8-15 presents the total force per bolt when the effects of angle prying action are added, showing that this total force is still significantly less than the bolt tensile capacity. The significant difference in these values means that bolt strength in either shear or tension is not tested in the shake table test.

Table 8-14. Anchor moment and anchor bolt shear design.

Panel Level	# Anchor Bolts/col n_{AB} (in)	Anchor Bolt Dia d_{AB} (in)	Applied Shear/ Bolt P_{hAB} (kips)	Bolt Nom Shear Strength F_v (ksi)	Bolt Shear Design Strength P_v (kips)	Strap Max Yield Strength P_{symax} (kips)	Conn C/L Vert Dist from Base s_V (in)	Moment Arm of Dia Strap L_s (in)	Anchor Bolts to Column Face Spacing d_c (in)	Tensile Force/ Bolt $P_{tAB} = r_{ut}$ (kips)	Bolt Nom Tensile Strength F_t (ksi)	Bolt Design Strength $P_t = \phi r_n$ (kips)
2nd Fl	4	5/8	5.50	60	13.81	23.50	0.00	7.78	4.0	10.90	90	20.71
1st Fl	4	5/8	5.50	60	13.81	23.50	0.00	7.78	4.0	7.87	90	20.71

Table 8-15. Anchor bolt design with prying action.

Panel Level	Angle/stiff Weld Thickness t_{wA} (in)	Stiffener Plate Thickness t_S (in)	Washer Diameter OD (in)	Out-of-plane Space btw Bolts d_{c-c} (in)	a (in)	b (in)	a' (in)	b' (in)	ρ	β	δ	α'	Required Angle Thickness t_{req} (in)	No Prying Thickness t_c (in)	α	Factore Prying Force q_u (kips)	Force /bolt w/prying $r_{ut}+q_u$ (kips)
2nd Fl	3/16	1/4	1 5/16	2.00	1.09	0.88	1.41	0.56	0.40	2.25	0.87	1.00	0.285	0.537	1.491	2.46	13.36
1st Fl	3/16	1/4	1 5/16	2.00	1.09	0.88	1.41	0.56	0.40	4.08	0.87	1.00	0.242	0.537	0.757	1.25	9.12

The concrete slab was designed to be very stiff and strong, and also to provide significant weight for the model. The bolts are through-bolts, not anchor bolts, so the cone failure strength or edge distance capacity was not tested in the shake table model test. Because the concrete slab was quite heavy and well reinforced, the bending and shear modes of failure of this diaphragm were not tested in this model.

8.5 Predicted model behavior

The same model used in Chapter 5 to predict panel lateral load versus deflection capacity is used to predict the shake table model shear panel behavior. Table 8-7 through Table 8-15 summarize these calculated capacities based on the shear panel configurations and details shown in Figures 8-2, 8-9, 8-10, and 8-11, and material properties shown in Table 8-6. The lateral capacity shown in Table 8-7 is based on only the diagonal strap capacity. Since the column anchors are moment connections, the columns will act somewhat as a moment frame. If the columns were fully fixed at both top and bottom, the additional lateral capacity would increase significantly. Equation 3-7 in Chapter 3 gives an expression for lateral capacity of a shear panel at strap yield when the columns are fully fixed. The second and third columns of Table 8-16 show the lateral deflection at strap yielding, δ_{sy}, and the combined lateral capacity at strap yielding, Q_{Tsy}. This capacity is still less than the designed applied story shear, so significant nonlinear response was expected in the first-story panels. Figure 8-23 plots the shear panel predicted lateral capacity versus lateral deflection for both the first- and second-story shear panels. This plot assumes the columns

were fully fixed. Figure 8-23 plots lateral capacity with the diagonal strap only, Q_{sy} (first point on plot), and with the columns acting as a moment frame, Q_{Tsy} (second point), both with respect to the lateral deflection at strap yielding, δ_{sy}. The difference between Q_{Tsy} and Q_{sy} is the contribution of the moment frame, and since both capacities are based on the measured coupon strengths of the straps and columns, these plots can be used to compare with the measured panel response in the shake table test to evaluate the panel behavior and actual contribution of the columns acting as a moment frame.

Table 8-16. Lateral load versus deflection predictions for shake table model panels.

Panel Level	Lat Defl at Strap Yielding δ_{sy} (in)	Capacity at Strap Lat Yield Q_{scy} (k)	Lat Defl at Col Yielding δ_{cy} (in)	Column Lat Cap @Yield Q_{cy} (k)	Total Lat Cap @CYield Q_{Tcy} (k)	Col Axial Stress @ Strap Yield f_{ca} (ksi)	Col Bend Stress @ Col Yield f_{cb} (ksi)	Col Comb Stress @ Col Yield f_{cr} (ksi)
2nd Fl	0.436	19.64	0.861	5.96	22.58	6.51	38.39	44.90
1st Fl	0.436	19.64	0.723	5.00	21.62	10.64	34.27	44.90

Figure 8-23. Predicted lateral load versus deflection for shake table model shear panels.

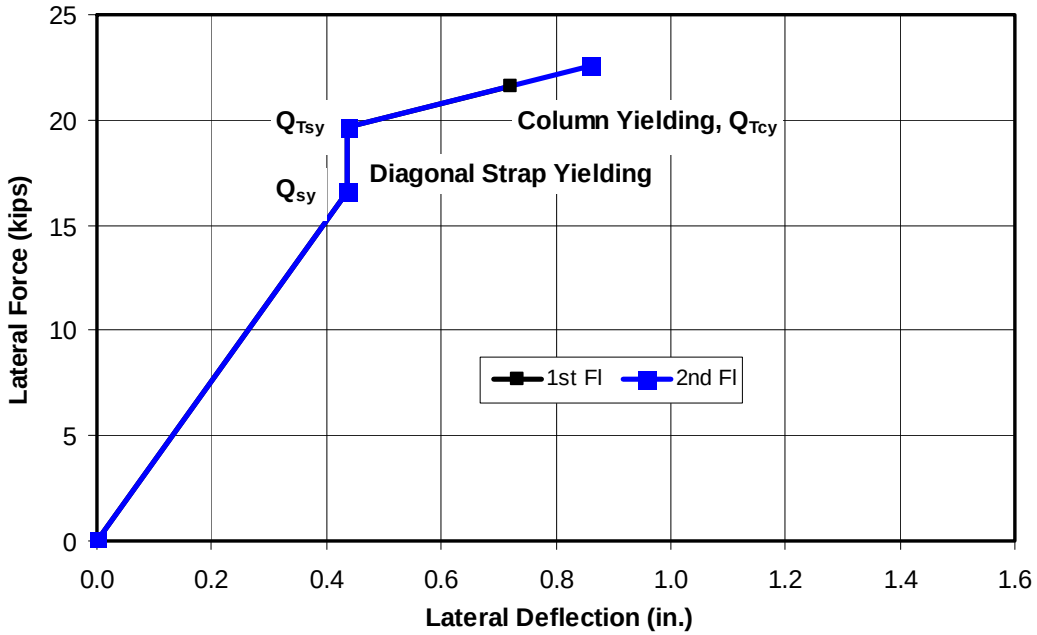

The second portion of Table 8-16 shows the calculation of the total panel lateral capacity at column yielding, Q_{Tcy}, defined in Equation 5-1, for both the first- and second-floor panels. Figure 8-23 plots these predicted capacities with respect to the panel lateral displacement at column yielding, δ_{cy}.

The predicted displacement at column yielding assumes the columns are fully fixed at both their top and bottoms. The columns will be less than fully fixed, so that actual column yielding will take place at larger displacements if at all. The panel capacity at column yielding should be less than those shown in Table 8-16 and Figure 8-23, because the increased deflection will increase moments due to P-delta effects, which would reduce the capacity available to resist lateral forces. Actual column behavior in the shake table model can be assessed based on the column strain gage measurements.

8.6 Test plan

Preliminary DRAIN 2DX analysis of the shake table model using the filtered SE32 record indicated the straps at the first-story panel would yield at only 11% of this record. This conservatively assumed strap yield strength of 47 ksi, which as shown in Figure 8-22, is the point where the strap coupon test results show the material first begins to yield. The column anchors were assumed fully fixed at their connection to the base beam and slab above. If the columns were not fully fixed, the straps could yield at even lower motion levels. Yielding of these straps should be the first nonlinear response of the model. At higher amplitudes, the columns should also yield. Figure 8-23 provided an estimate of predicted first-story panel capacity with respect to lateral deflection (drift). The model has two shear panels, and therefore it should have approximately twice the capacity shown in Figure 8-23.

Several shake table tests were planned prior to the full filtered SE32 test. The model was firmly bolted down to the TESS before testing. Rubber pads were taped to the intermediate studs, where the diagonal straps cross and between the crossing points of the opposing diagonal straps. These pads should not influence the panel behavior, but would reduce the distracting banging noise of the straps when they cycle between buckling and snapping in tension. All the instrumentation was installed prior to testing. The SE32 record used a time step of 0.025 sec, or a sampling rate of 40 Hz. The filtered SE32 record used to drive the shake table applied a smaller time step of 0.0125 sec (80 Hz sampling rate), by inserting interpolated acceleration levels, so that model behavior could be obtained at higher frequencies. Data were recorded with a time step of 0.008 sec (125 Hz sampling rate). The following steps summarize the planned tests:

1. Conduct uniaxial random vibration tests in each of the three translational directions (X, Y, and Z) and each of the three rotations (yaw, pitch, and roll). The amplitude of these motions was planned to begin at 0.02 g and then increase to about 0.05 g. The frequency range was to be 0.2 to 25 Hz, to ensure measuring any modes of vibration that may contribute to the response of this model. Transfer functions between the first- and second-floor slabs and base beam were to be used to determine the first and second modes of vibration in the X and Y direction. Transfer functions were to be used between the TESS accelerometers and the first and second slabs to determine the pitch, roll and yaw modes of vibration. For each mode of vibration, the damping was to be estimated based on the width of the transfer functions. Random testing might be repeated at higher levels as needed to achieve improved resolution. Understanding these modes may be important to understanding the desired response in the in-plane longitudinal direction. Lateral frequency should be slightly less than the in the longitudinal direction, because the out-of-plane stiffness provided by the threaded rods would be less than the shear panel stiffness.
2. First test at 2% of the filtered SE32 motions. This level may be large enough to provide very low measurements in all of the sensors. All data channels would be checked to confirm they were properly recording.
3. Test at 5% of the filtered SE32 motion. Check selected channels to confirm they were recording properly. Check overturning response of the model to confirm that it was within acceptable levels. Review more closely the strains in the first-story shear panels. They should be below 50% of their yield strain compared to the coupon strain data shown in Figure 8-22 (i.e., 0.0008 in./in.). The strains may be somewhat less because the straps are slightly slack when the model is not deformed, so the model has to rack over slightly to begin to strain them (e.g., 0.2 in.). This may cause a slight snapping effect, before yielding the straps. The strap strain levels should increase linearly with respect to test level, beyond the initial level needed to tighten them.
4. Test at 8% of the filtered SE32 record (i.e., 73% of the level estimated to cause yield). Review all the first-story strap strain data and predict the test level that should cause the average peak strain of all straps to reach 80% or the maximum of all straps to reach 90% of yield.
5. Test at the level of the filtered SE32 record that will cause all first-story straps to reach an average of 80% of yield, or the highest-strained strap reach 90% of yield. Review the achieved response levels for all data

channels. Compare these levels with predictions based on the DRAIN 2DX analysis results.

6. After reviewing step 5 data and comparing measured data with DRAIN 2DX analysis (this review was expected to take a day or two), test with the full filtered SE32 record. This test was expected to result in very large longitudinal displacements in the first-floor shear panel, estimated to be up to 6 in. This would cause significant yielding in the straps along their entire length and yielding of the columns near the anchors. The columns were expected to yield first at their compression face and possibly at their tensile face. No nonlinear response was expected in the second-story shear panels.
7. If the first-story shear panels did not experience significant nonlinear response and very large drifts that would permit the examination of P-delta effects, they were to be tested again using sinusoidal motions near the natural frequency of the model. This frequency would be much lower than the frequency of the undamaged model. This frequency would be estimated based on either uniaxial random tests or through transfer functions from the model response in the previous test. At low levels of random motion, the model would act as a very flexible moment frame, where only the columns contribute to the model lateral stiffness. At much greater levels of excitation, the model response becomes very nonlinear because the diagonal straps would become taut and then make the model much stiffer than with the columns alone. This increase stiffness though is only very temporary, creating an impact-loading effect. Therefore, further sinusoidal tests would be needed at the natural frequency of the model based on the low-level random motions, where only the columns contribute to the model stiffness and the frequency would be very low. The amplitude of these sinusoidal tests would start small and gradually increase. Safety considerations might limit these tests. The model was designed so that safety cables would “catch” the floor slabs once the first-floor drift reaches 12 in.

8.7 Modal test results

Shake table tests were conducted according to the above plan on 5 – 7 June 2002. Random tests (step 1) were initially conducted with a root-mean-squared (RMS) amplitude of 0.02 g. To achieve better resolution RMS amplitude was increased to 0.1 g for vertical, longitudinal (in-plane), and yaw (torsional) motions. The random motion levels were also increased to 0.05 g for lateral (out-of-plane), while pitch (in-plane rocking) and roll (out-of-plane rocking) were not increased beyond 0.02 g. Table

8-17 provides both the DRAIN2DX analysis predicted along with the measured frequencies and damping from these modal tests. One prediction model assumed a fixed base and another assumed that the foundation of the model was on a rotational spring, representing the pitch stiffness of the TESS. This rocking spring was represented in DRAIN2DX using vertical springs with a stiffness of 225 k/in. under each of the two columns. The vertical stiffness of the springs was defined such that the calculated frequency would match the measured first-mode measured frequency. Table 8-17 shows fixed-base frequency was greater (2.16 Hz) than the measured (1.65 Hz), while the pitch spring case matches the measured. Table 8-17 also shows that the measured out-of-plane (lateral) frequency was less than the in-plane, as was expected because of the relatively flexible threaded rods bracing the model in this direction. The calculated in-plane second mode frequency was greater than measured for both the fixed-base model and with the rocking spring, but the rocking spring value was closer. The lower-frequency measurements are most likely due to the fact that the shake table did pitch significantly, and the earlier DRAIN2DX model assumed a rigid base.

Table 8-17. Predicted and measured model frequencies and damping.

Mode of Vibration	Fixed Base		TESS Pitch Spring		Measured Frequency (Hz)	Measured Damping (% critical)
	Predicted Frequency (Hz)	Assumed Damping (% critical)	Predicted Frequency (Hz)	Assumed Damping (% critical)		
first Out-of-Plane					1.22	6.7
first In-Plane	2.12	4.0	1.64	6.0	1.65	7.2
first Torsion					2.02	4.0
second In-Plane	5.71	4.0	5.6	6.0	5.25	1.6

8.8 Linear seismic tests

Low-level shake table tests were then conducted at 2, 5, and 8% of the filtered SE32 record. Several data channels were checked to ensure data were being properly recorded. The measured strains from the 8% test showed that average strain measured in the first-story diagonal straps was 1,281 microstrain (75% of yield) and the peak value was 1,396 microstrain (82% of yield). These values were somewhat below the levels indicated in step 5 of the test plan (80% and 90%), but the linear tests ended at this level, because some of the strain measurements showed a slight offset during testing (maximum of 40 microstrain), suggesting that slight yielding of

the straps might have occurred. If yielding at this level took place across the entire length of a strap between the columns, it would only result in 0.006 in. strap elongation and a first-story lateral deflection of only 0.0085 in. This should have a very minor influence on later nonlinear testing.

8.8.1 Measured acceleration response

The acceleration and displacement data were examined to determine which data or combinations of them best represented the response of the model. The acceleration measured in the in-plane direction at A23x (top left corner in Figure 8-20) was much greater than measured at other locations on the second floor slab (at A21x and A22x). The out-of-plane accelerometers (A21y, A22y and A23y) or displacement gages (D21y and D22y) showed very little out-of-plane or torsional response. The in-plane displacements measured at the second floor (D22x and D24x) were very consistent with each other, confirming little torsional response. The acceleration recorded on the second floor were double integrated and corrected for any offsets, to provide displacement records that could be compared with the recorded displacement. The records from the A21x and A22x accelerometers were much less than the displacements measured by D22x and D24x. The displacement record from the A23x integrated record agreed very well with D22x and D24x. Therefore, the A23x acceleration measurements were the most representative of the second-floor acceleration.

The location of the A13x accelerometer on the first-floor slab is directly below A23x. The acceleration measured at this location was very similar to A12x, but significantly greater than at A11x (Figure 8-19 shows the location of all first-floor accelerometers). Similar to the second floor, the first-floor acceleration records were integrated to provide displacement records. The recorded displacements from the integrated A11x record were much lower than the recorded displacements at D12x and D14x, while those from both A12x and A13x agreed very well. Therefore, the A13x acceleration measurements were the most representative of the first-floor acceleration.

Figure 8-24 plots the measured acceleration at the TESS shake table (filtered ATx), first-story slab (A13x) and second-story slab (A23x). The ATx motions are an average of the longitudinal accelerometers inside the TESS. This plot shows the base motions (measured at the TESS) amplified significantly at the first-story slab, but slightly less at the second story. Figure 8-25 shows the same acceleration records, zoomed in on the 13–18 second

region. Figure 8-24 shows the model responded with slightly greater amplitudes between 50 and 51 seconds, but Figure 8-25 focuses on the 13–18 second region because the response is almost as great, plus the response in this region can be compared later to the nonlinear behavior, in the next test, during the same time region as the model begins to yield. Figure 8-24 and Figure 8-25 show the second-story slab (measured by the A23x accelerometer) responds at only slightly greater amplitudes than the first-story slab (A13x). Table 8-3 shows that the A13x and A23x accelerometers are directly above or below one another, located on the first- and second-floor slabs, respectively. Both the first- and second-floor accelerometers show the model responds in both the first (1.65 Hz) and second (5.25 Hz) modes of vibration of the model. The second-floor response is much more dominated by the first mode, while the first floor is influenced almost as much by the second mode, explaining why the first-floor acceleration is almost as great as the second floor.

Figure 8-24. Measured accelerations at the TESS, first-story, and second story in the 8% SE32 test.

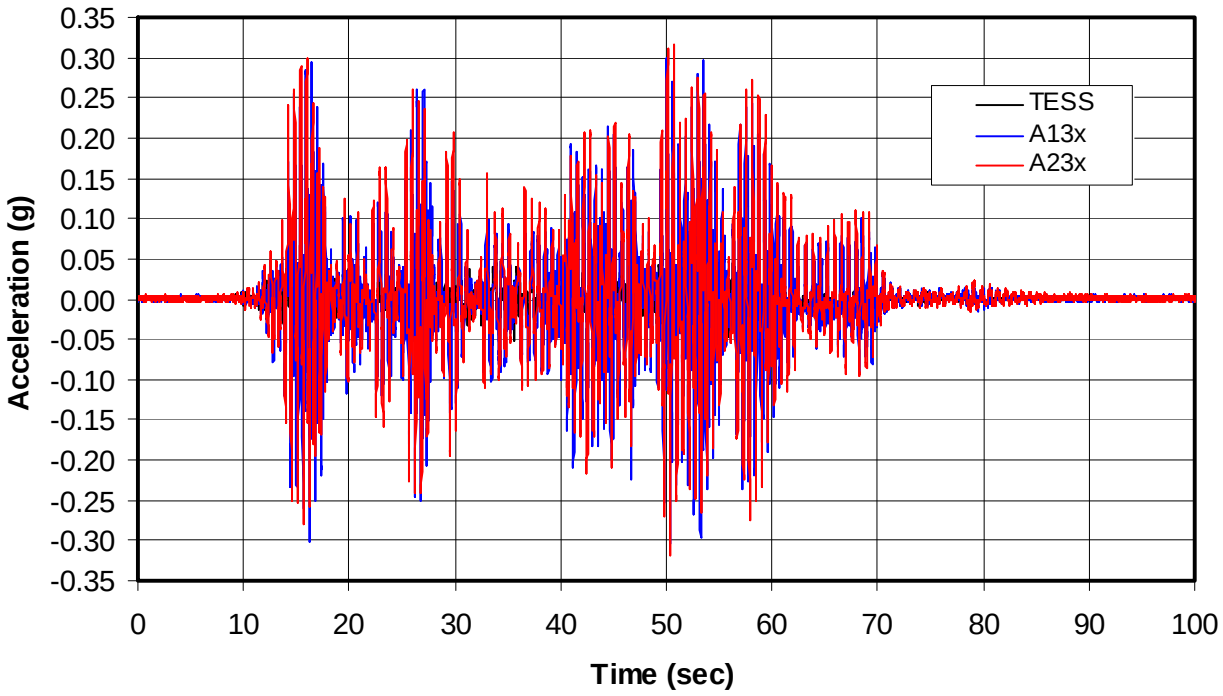

Figure 8-25. Accelerations at the TESS, first-story, and second story for 13–18 sec.

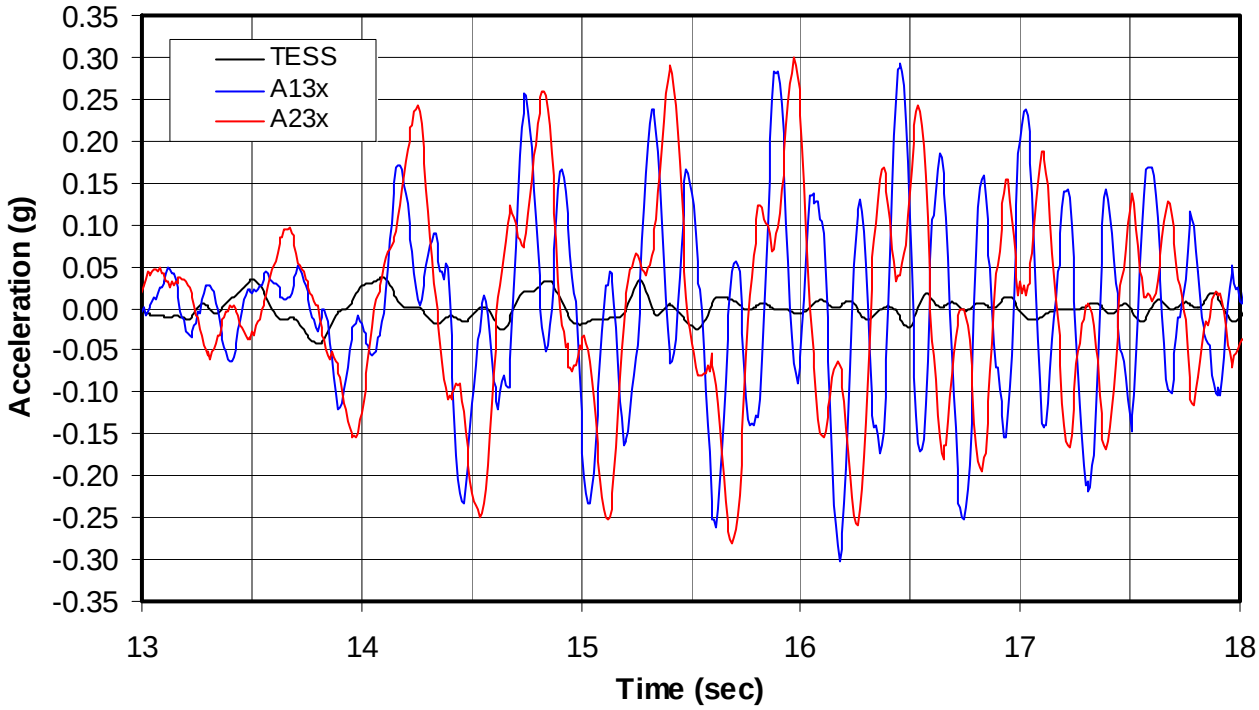

8.8.2 Measured displacement response

Figure 8-26 shows the displacements for the entire 8% SE32 test, measured at the base beam, first-floor level, and second-floor level. The displacement measurements define the behavior of the model better than the acceleration data because both displacement sensors on the same floor level provide measurements that are more consistent with each other than the accelerations. The base-beam displacements are the average of D2x and D4x (see Table 8-4 and Figure 8-16 and Figure 8-18); the first-floor displacements are the average of D12x and D14x; and the second-floor displacements are the average of D22x and D24x. Figure 8-26 also plots the pitch displacement, which is the in-plane rocking motion of the TESS. Figure 8-27 plots these displacements in the 13–18 second region of the 8% SE32 test.

Figure 8-26. Measured displacements at the base beam, first story and second story.

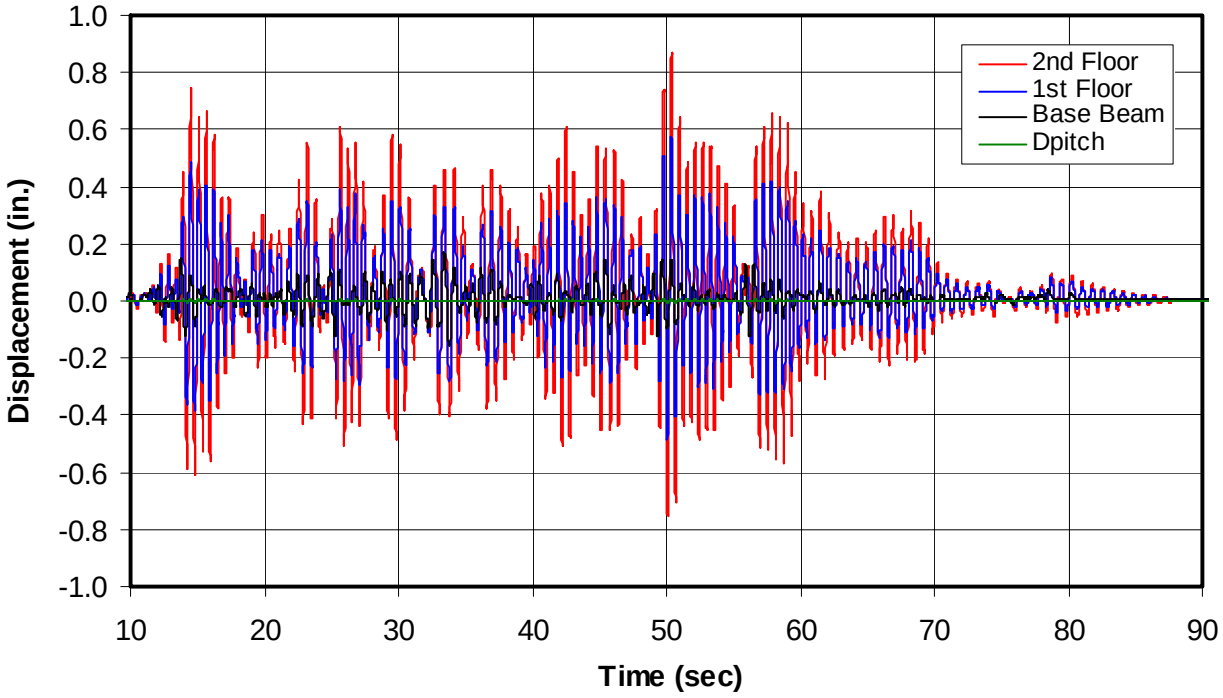

Figure 8-27. Displacements at the base beam, first story and second story, 13 through 18 seconds.

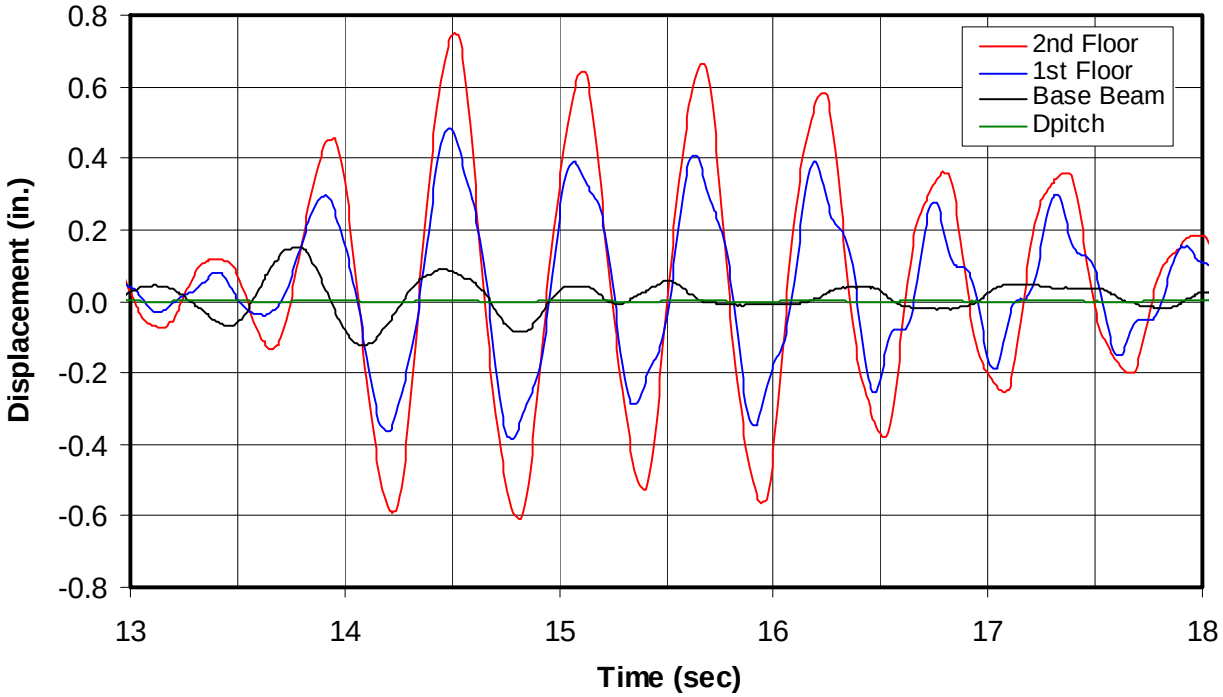

The pitch displacements were quite small in this test, but they do have a small influence on the measured displacements at the first- and second-story levels of the model. The first-floor lateral displacement relative to the base beam after correcting for the pitch motion of the TESS can be calculated as follows:

$$1stStoryDrift = 1stFlRel = 1stFloor - BaseBeam - (124" + 2")\frac{D_{pitch}}{48"} \quad \text{(Eq 8-1)}$$

As indicated in Equation 8-1, the first-story drift is identical to the first-floor relative displacement. D_{pitch} is the measured pitch displacement of the TESS. Vertical displacement of the TESS is measured with linear variable differential transducers (LVDTs) in each of the vertical actuators. There are a total of nine vertical actuators in a symmetric 3 x 3 pattern, spaced 48 in. both directions. The pitch displacement is the average vertical displacement on the three north actuators minus the average of the three south actuators divided by two. This pitch displacement is divided by 48 in. in Equation 8-1 to calculate the pitch rotation. This rotation is multiplied by the vertical distance between the base-beam displacement gages (Z = -2 in.) and first-floor displacement gages (Z = 124 in.). Similarly, the second-floor lateral displacement relative to the base beam can be calculated as follows:

$$2ndFlRel = 2ndFloor - BaseBeam - (250" + 2")\frac{D_{pitch}}{48"} \quad \text{(Eq 8-2)}$$

The second-story drift is the difference between the second-floor relative lateral displacement and first-floor relative lateral displacement, expressed as follows:

$$2ndStoryDrift = 2ndFlRel - 1stFlRel \quad \text{(Eq 8-3)}$$

Figure 8-28 plots the first floor (first-floor drift) and second-floor relative displacements for the portion of the test that caused significant model deformation. This plot shows that the largest model deformations take place between 13 and 18 seconds, and between 49 and 54 seconds. Figure 8-29 plots the story drifts for both the first and second stories calculated from the measured data according to Equations 8-1 and 8-3. This plot zooms into the 13–18 second region, and Figure 8-30 zooms into the 49–54 second region. Both plots in Figure 8-29 and Figure 8-30 show that the first-story drift is consistently greater than the second story.

Figure 8-28. Relative displacements and first-story drift.

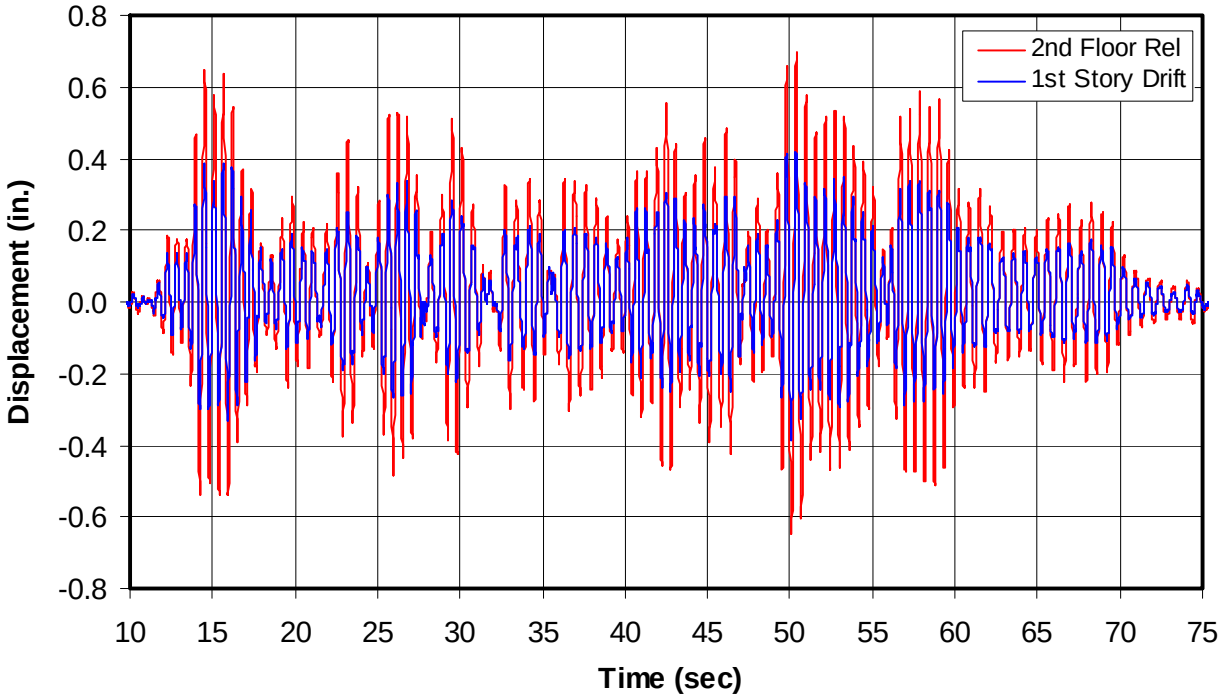

Figure 8-29. First- and second-story drifts, 13–18 seconds.

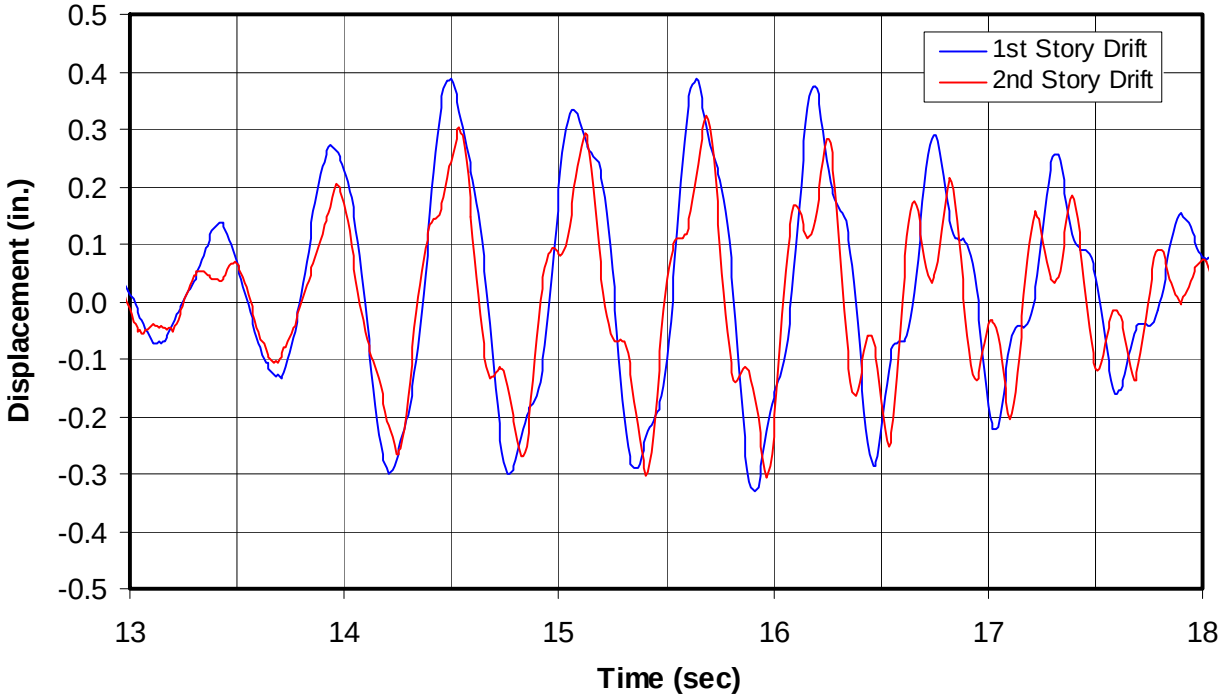

Figure 8-30. First- and second-story drifts, 49–54 seconds.

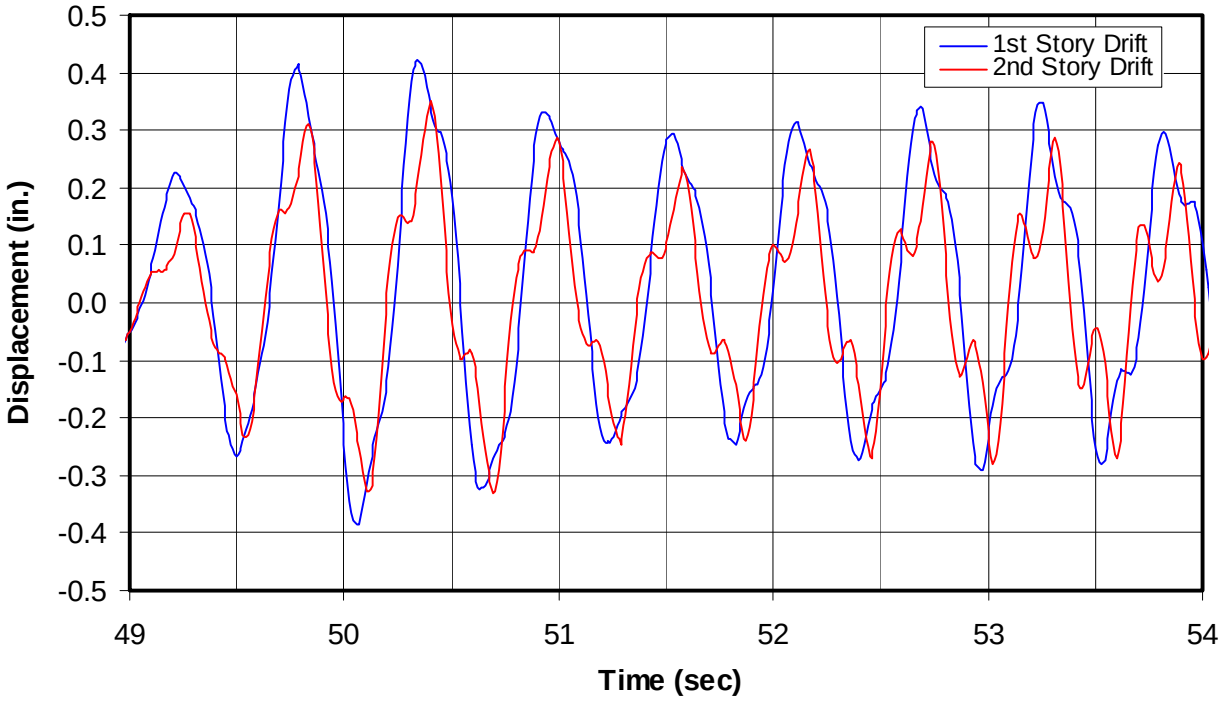

The drifts are somewhat greater in Figure 8-30, reaching peak amplitudes of 0.42 in. and 0.35 in. at the first and second stories, respectively, at 50.4 seconds. The greatest first-story drift (0.387 in.) measured during the first time region plotted in Figure 8-29 occurred at 14.496 seconds. This drift is the most critical deflection parameter defining the behavior of the model, and the amplitude at this time is almost as great as at 50.4 seconds. The deformed model shape is plotted at 14.496 seconds in Figure 8-31, because the model shape at this time can be compared with the behavior of the model at the same time region during the nonlinear test, documented later in this report. Figure 8-31 shows the absolute measured displacements, base beam, D_{pitch}, first floor, and second floor that were plotted in Figure 8-27, at 14.496 seconds, graphically showing the model displacement at that instant in time. Figure 8-31 also shows the relative displacements and drifts, illustrating the deformed shape of the model at this time of close to the greatest first-story drift. Table 8-7 showed that the calculated lateral deflection at strap yielding was 0.436 in., indicating that the first-story panels may have been on the verge of yielding in this test.

Figure 8-31. Model displacement and deformation
in the 8% SE32 test at 14.496 seconds.

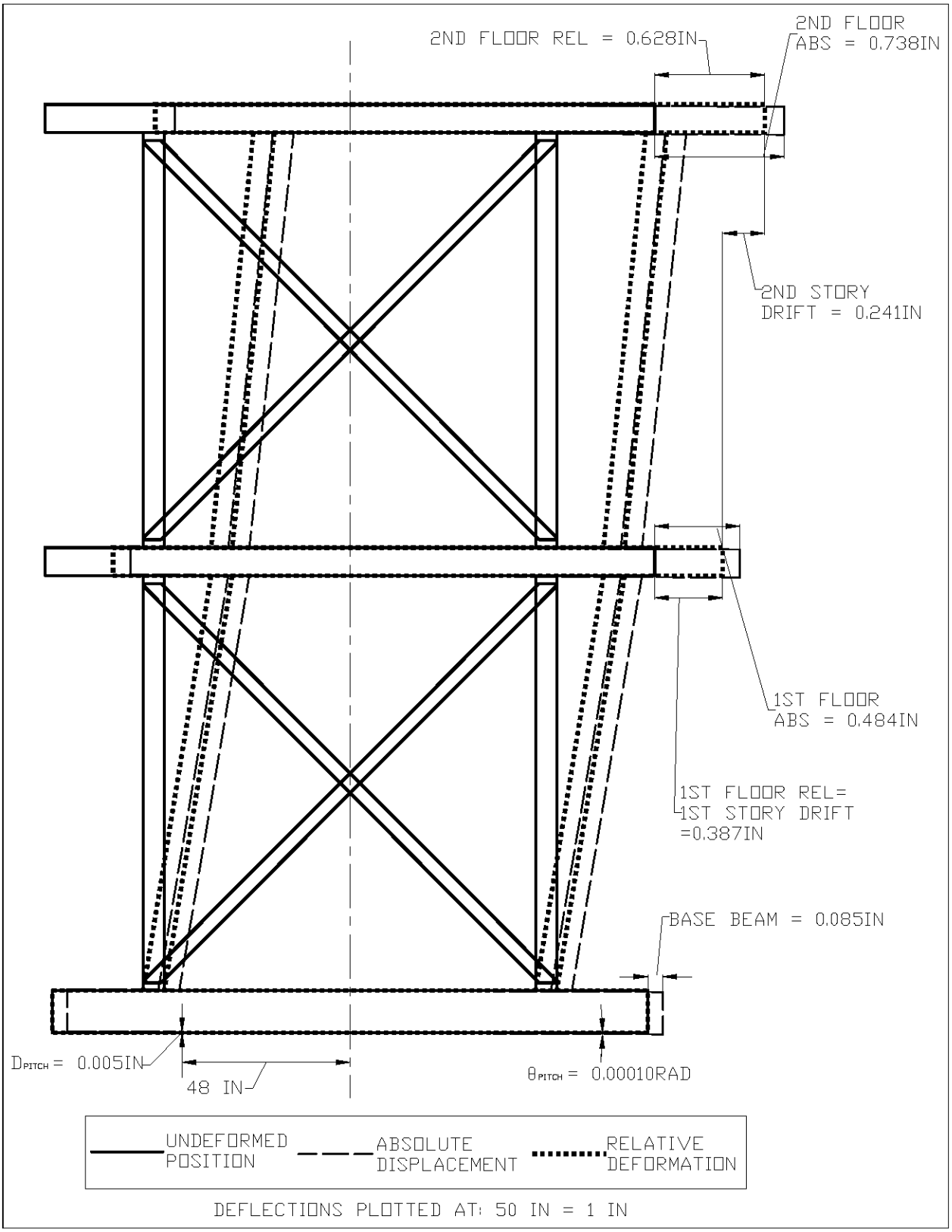

Since the mass of the model is well understood (57,500 lb at first floor and 57,600 lb at second floor, defined in section 8.1), inertia forces can be calculated based on the measured acceleration data presented in Figure 8-24 and Figure 8-25. These inertia forces can be used to estimate the applied lateral forces at both story levels, and they are used to develop plots of story shear versus story drift. These inertia forces are used to calculate the first-story shear per panel as follows:

$$1stStoryShear = \frac{57{,}500lb}{2} A13x + \frac{57{,}600lb}{2} A23x \qquad \text{(Eq 8-4)}$$

Similarly, the second-story shear per panel is calculated as follows:

$$2ndStoryShear = \frac{57{,}600lb}{2} A23x \qquad \text{(Eq 8-5)}$$

Figure 8-32 plots the first-story shear per panel with respect to the first-story drift. This figure also plots the shear versus drift for the second story, showing that both the story shear and drift were greater at the first story. These have been plotted along with the predicted lateral load versus deflection (see Figure 8-23). The portion of the predicted plot is only up to the point where the diagonal strap yields, and does not include any moment frame capacity contribution from the columns. The plots show that the shear panels on both levels have the same slope or lateral stiffness, because the panels were identical. Figure 8-33 shows the same story shear versus drift data, but for only the time region of 14.368–14.96 seconds, which includes the peak first-story drift that occurs at 14.496 seconds illustrated in Figure 8-31. The plots indicate essentially elastic behavior that agrees well with the predicted behavior, and it forms a basis for later comparison with the nonlinear behavior seen in the next test.

Figure 8-32. Story shear versus story drift
for both stories for the 8% SE32 test.

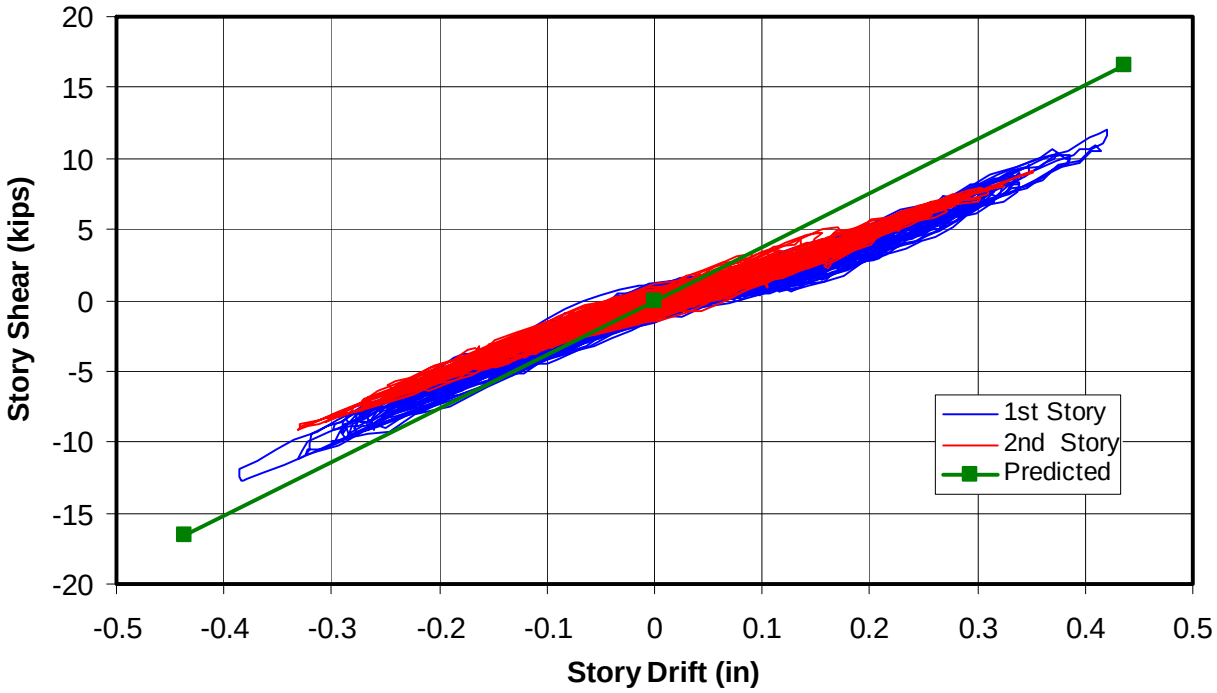

Figure 8-33. Story shear versus story drift
for 8% SE32 test, for 14.4–15 seconds.

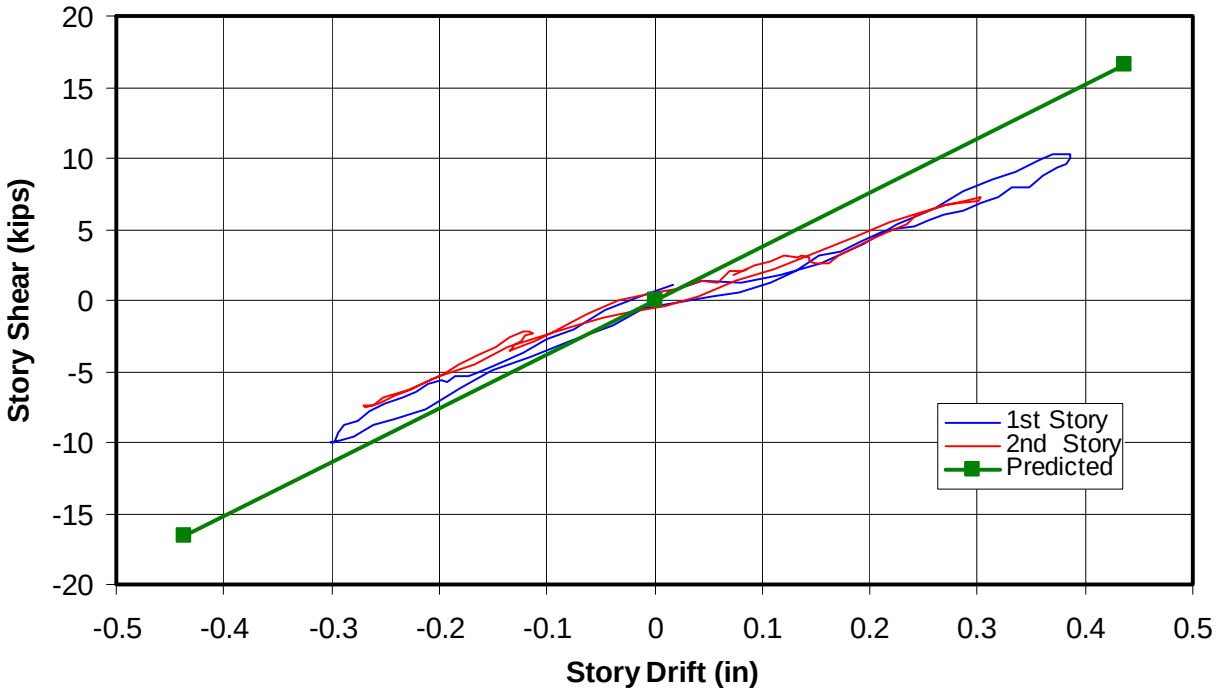

8.8.3 Measured strains

Figure 8-34 shows strains measured in one of the diagonal straps on the first-story shear panel (S13xz) and one on the second story (S36xz). These strain gages were selected because they have the greatest strains for their story level and yet their amplitudes are close to those values measured in other straps at their floors. Figure 8-16 showed that the S13xz gage was located at the lower south corner of the west face of the east shear panel, while the S36xz gage was located at the lower north corner of the east face of the east shear panel. The peak strain measured at the S13xz first-story strap was 1400 microinches/in., while the peak strain at the S36xz second-story strap was 997 microinches/in. Close inspection of the coupon data in Figure 8-22 showed that the straps began to yield at strains of 1700 microinches/in., indicating both first- and second-floor diagonal straps were significantly stressed but not about to yield.

Figure 8-34. Strains measured at first-story and second-story diagonal straps.

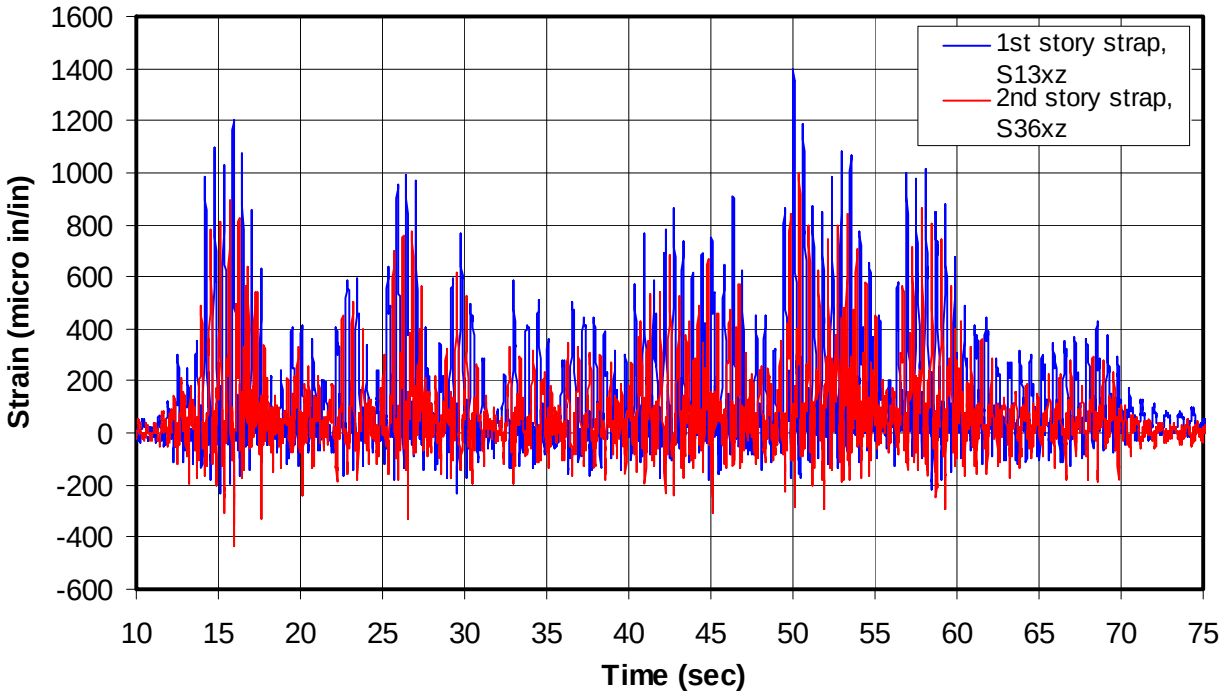

The straps were tension only, so the positive strains shown in Figure 8-34 were much greater than the small negative compressive strains, developed as the straps buckle. Figure 8-35 shows these strain measurements for the 13–18 second region. The maximum strain measured at the first-story strap, within the 13–18 second region (1201 microinches/in.), was significantly less than the maximum measured at 50 seconds. The strains for all

but one first-story diagonal strap remained below 90% in this region, relative to the peak strains measured near 50 seconds. For the second-story straps, the strains in this region generally reach 95% of the peak measured near 50 seconds.

Figure 8-35. Strains at the first-story and second-story straps, 13–18 seconds.

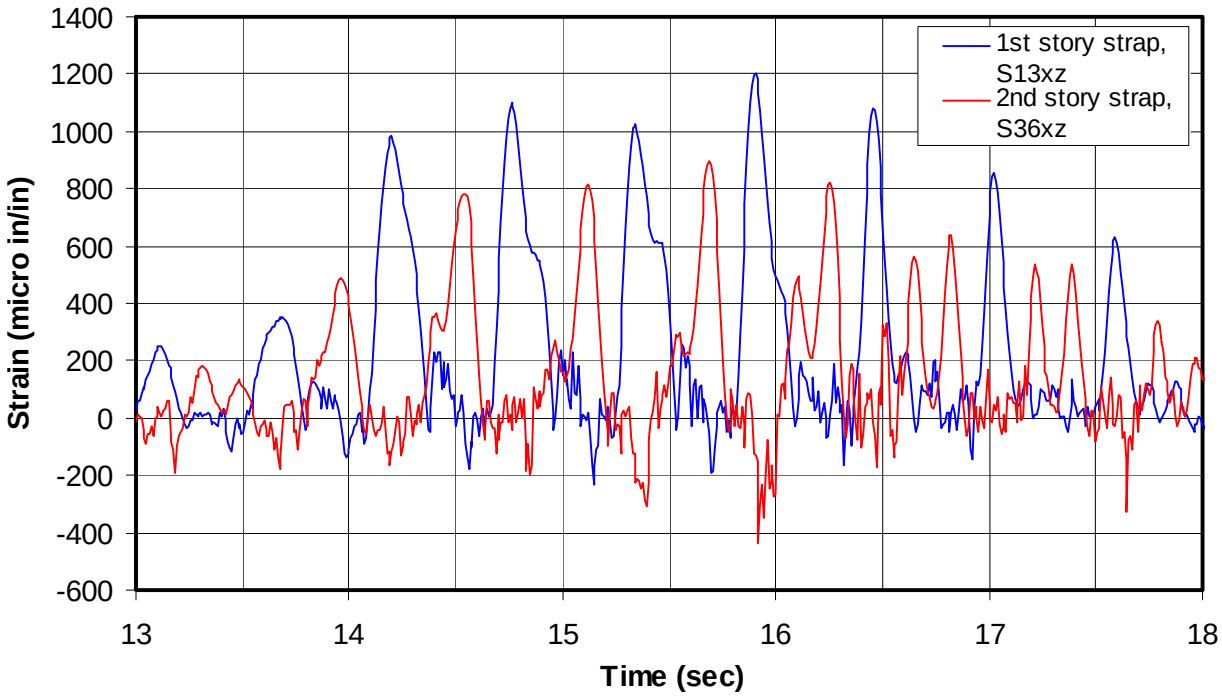

Figure 8-36 shows strains measured on the northwest column that have been reduced by 256 microinches/in. to account for an estimate of the strain in the columns due to gravity loading on the model. The reason for plotting an estimate of the true column strains, which have been offset by the effects of gravity, is to see if these strains overcome gravity and produce actual tensile strains and stresses in the columns at the locations of these gages. Inspection of all the column strain data for the 8% SE32 test shows that the effects of gravity are never overcome at the location of the gages, but projecting the decrease in compressive strains to the ends of the columns indicates small tensile strains and stresses occurred at the column tops and bottom. This strain correction assumes the columns equally distribute the load throughout their cross-section, and the intermediate studs carry a portion of the gravity load proportional to half their area relative to the columns (5.83 kips per panel). The much thinner intermediate studs (33 mil) were open C-sections and were therefore much more vul-

nerable to local buckling than the columns. Some intermediate studs did buckle during the placement of weights on the model before the test.

Figure 8-36. Strain measurements on the first-story northwest column.

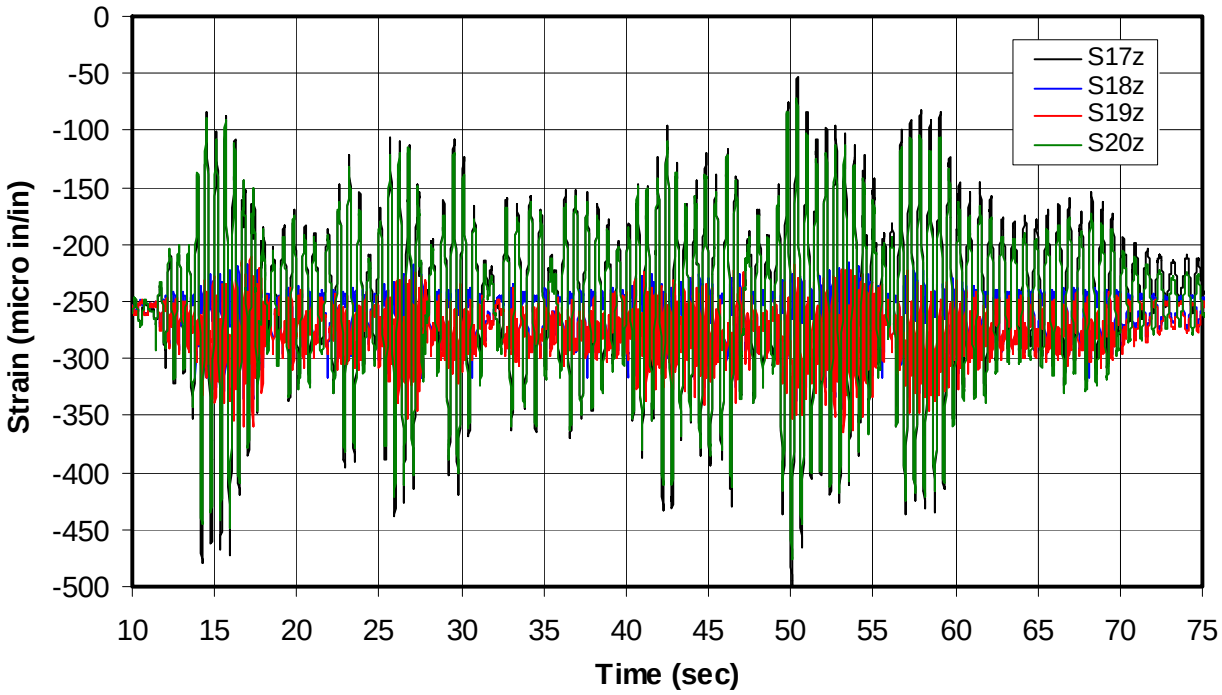

Figure 8-16 showed the S17z and S18z strain gages were 28 in. above the column bottom, at the outside and inside face of the column respectively, while S19z and S20z were at similar locations 28 in. below the column top. Figure 8-37 plots the same corrected strain measurements, zoomed in on the 13 through 18 second region of these records. Close inspection of the column coupon data plotted in Figure 8-22 indicates the columns begin to yield at strains of 1,300 microinches/in. This is much greater than the maximum compressive strains of 500 microinches/in. measured in the columns in the 8% SE32 test (Figure 8-36), indicating that the columns were far from yielding.

Figure 8-37. Strains on the first-story northwest column, for 13 to 18 seconds.

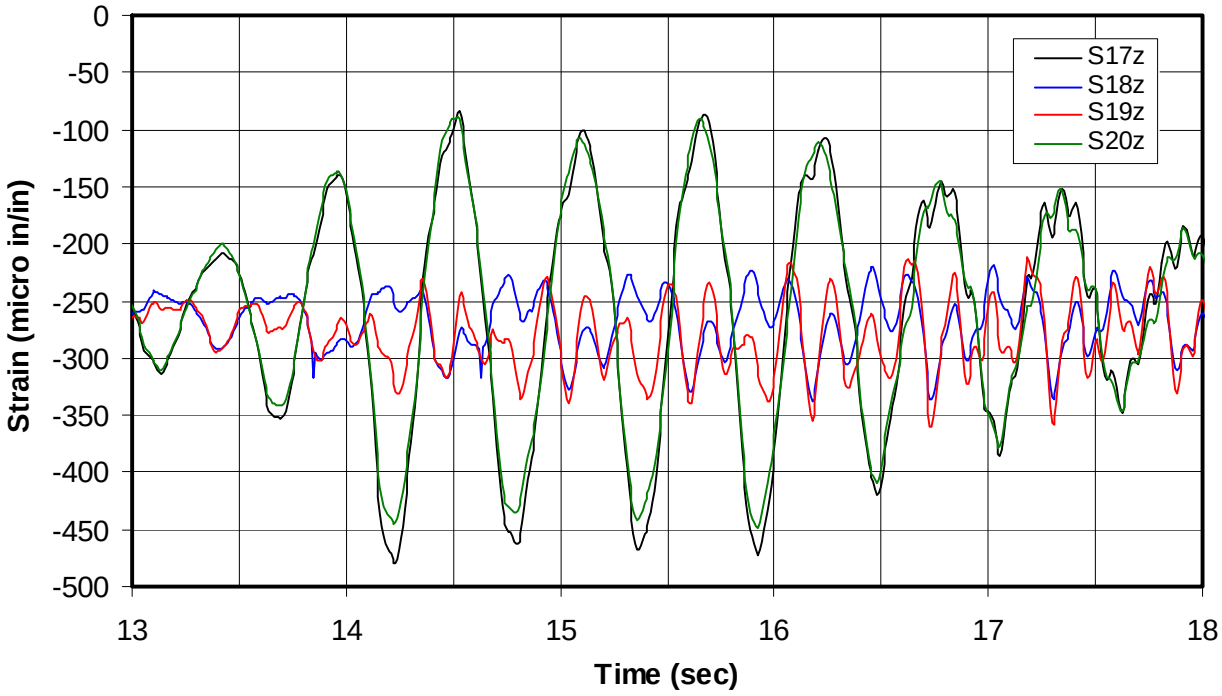

The strains measured near the bottom of the column (S17z and S18z) are out of phase with each other at the beginning of each cycle, because as the model racks in one direction, one strain gage measures an increase in strain while the other measures a decrease. When the model racks to the right (positive deflection), the deformed shape of the column, fixed at both its top and bottom, causes the strains at the bottom left face (S17z) to increase (reduction in compressive strains) while the strains at the right face (S18z) decrease further (e.g., 14.4 seconds in Figure 8-37). Figure 8-37 shows that when the model is racked to the right (e.g., at 14.4 seconds), the strains near the top, on the south face of this column (S20z), increase similar in phase and amplitude to S17z. The strains at the top-north face of this column (S19z) decease similar in phase and amplitude with S18z. These strains reflect the expected deformation of a column that is deformed laterally, while restrained from rotation at both top and bottom. When the model is racked to the right, the diagonal straps that connect the bottoms of the north (left) columns to the tops of the south columns are in tension. This loads the right columns with additional compressive load. At the same time the left column experiences a net increase in tensile strain because it is resisting the tensile load developed in the diagonal strap in the story above, plus it is resisting overall model overturning. This is consistent with the overall average increase in tensile strain in the left column

(S17z, S18z, S19z, and S20z), when the model is racked to the right (14.5 seconds in Figure 8-37). Close inspection of Figure 8-37 shows that the strains at S18z near the column bottom initially decrease out-of-phase with S17z as explained above, but then at 14.5 seconds the strain at S18z begins to increase due to the net tensile force applied to this column. The strain gages at both S17z and S18z experience a similar pattern of an initial strain change out of phase with the opposite side of the column due to column flexural deformation, followed by a change in strain that is in-phase with the opposite side of the column due to column overall axial deformation.

When the model racks to the left (e.g., at 14.7 seconds in Figure 8-37), the strains measured near the bottom of the column (S17z and Z18z) are again initially out of phase with each other, but with S17 experiencing a large decrease in strain (compressive strain) due to both the flexural deformation of the column and the net compressive axial load applied to the left (north) column, because the diagonal strap attached to its top is in tension. At 14.7 seconds the strain at S18z initially increases, out of phase with S17z, and then at 14.8 seconds begins to decrease, because of the overall increase in compressive load in this column. Similar response can be seen near the top of the column where S20z decreases in phase and amplitude with S17z, and S19z agrees with S18z. In general the strain at S18z appears to be more influenced by flexural deformation while S19z appears more influenced by axial deformation, though they are both similarly influence by the both deformations and are in phase with each other. Figure 8-38 provides similar column strain data for the southwest column (see Figure 8-16 for sensor locations) for the 13–18 second region. The strain measurements are greater on this column, and the strains near the bottom of the column are greater than on top. As expected, they do oscillate in a mirror image of those at the northwest column.

Figure 8-38. Strains on the first-story southwest column for 13–18 seconds.

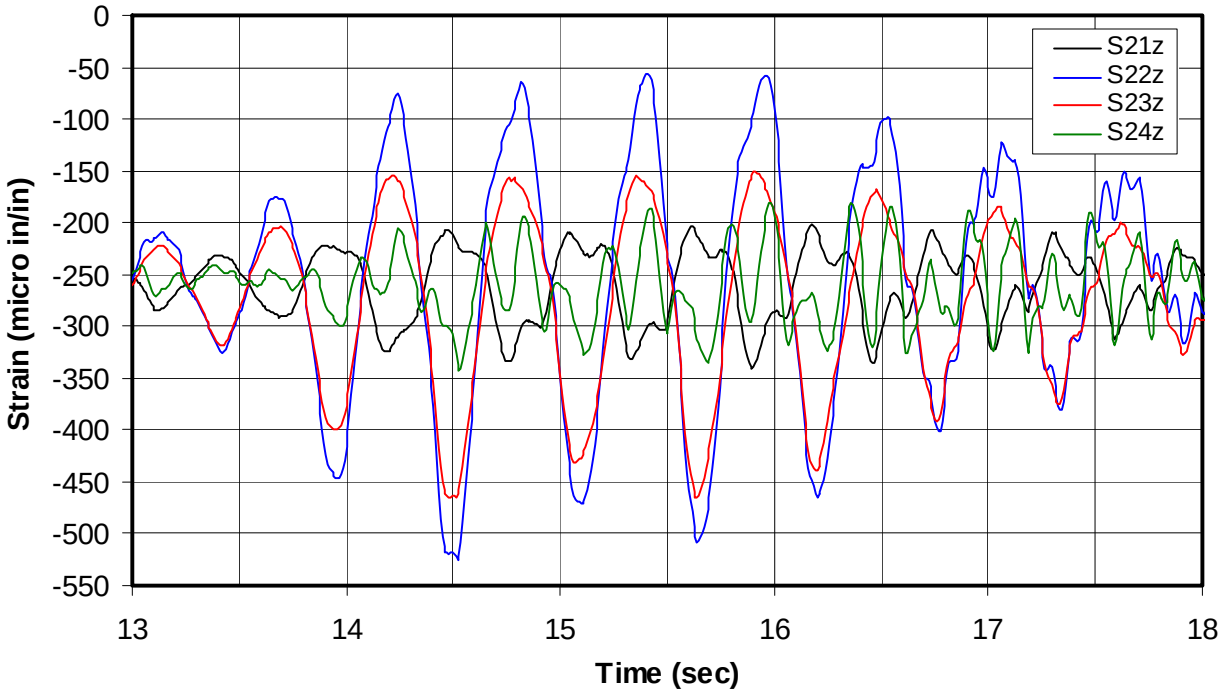

8.8.4 Column axial load, moments, and shears

These column strains can be used to estimate the column axial load, load carried in shear by the columns, and column moments at their tops and bottoms. Only the columns of the west shear panel on the first story were instrumented. The model experienced little torsional response, so the west side shear panel behavior should be representative of both sides. The first-story shear panels were more heavily loaded both laterally and vertically, so this panel is of greater interest. The axial load applied to the northwest (left) column, P_{aNW} is defined as follows:

$$P_{aNW} = \frac{(S17z+S18z+S19z+S20z)}{4} EA_c \qquad \text{(Eq 8-6)}$$

where

S17z, S18z, S19z and S20z are strains measured on the northwest column (see Figure 8-16), which have been corrected for the effects of gravity by decreasing their measurements by 256 microinches/in., and are plotted in Figures 8-36 and 8-37

E = modulus of elasticity of steel, which is 29,000 ksi

A_c = the column nominal area, which equals 3.49 sq in., as shown in Table 8-9.

The axial load applied to the southwest (right) column, P_{aSW}, is calculated in the same way using the strain gage data measured at S21z, S22z, S23z, and S24z (see Figure 8-38). Figure 8-39 and Figure 8-40 plot the applied axial load for both the north and south columns of the first-story west shear panel. Figure 8-40 shows the overall decrease in compressive load on the northwest column at 14.4 seconds, when the model is racked to the right. The increase in compressive load can also be seen in this figure when the model is racked to the left at 14.7 seconds.

Figure 8-39. Applied axial load for first-story west shear panel columns in the 8% SE32 test.

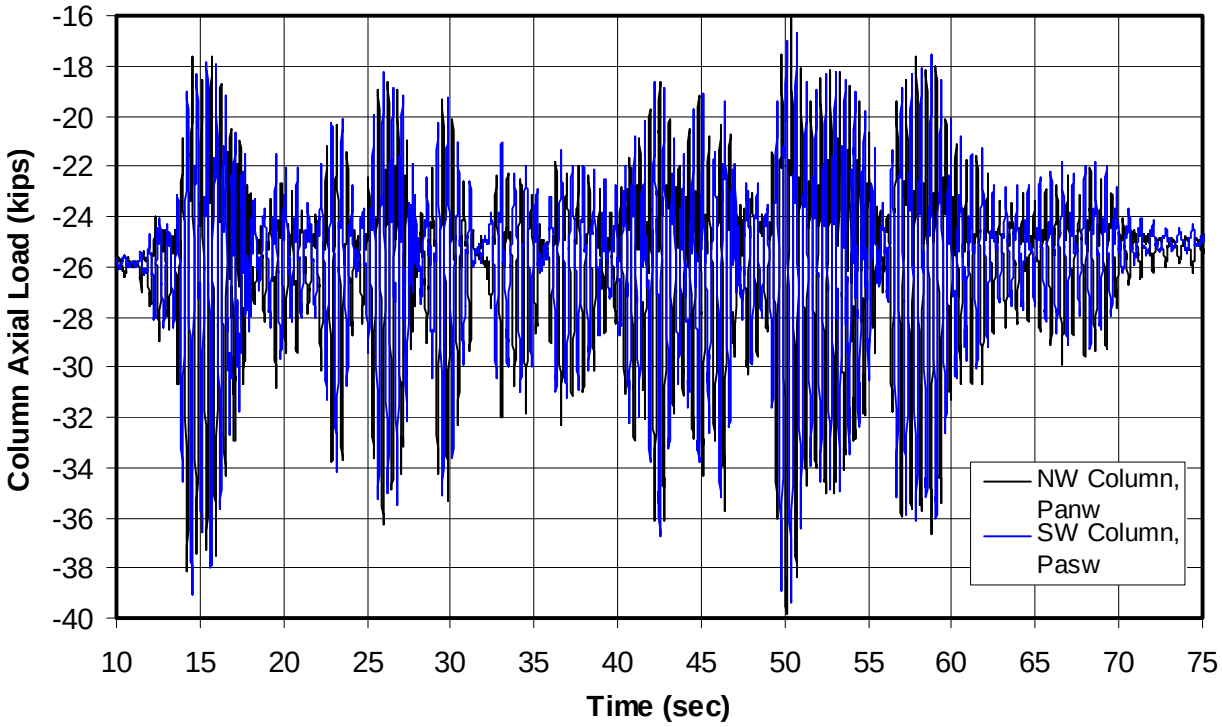

Figure 8-40. Axial load for first-story west panel columns, 8% SE32, 13–18 seconds.

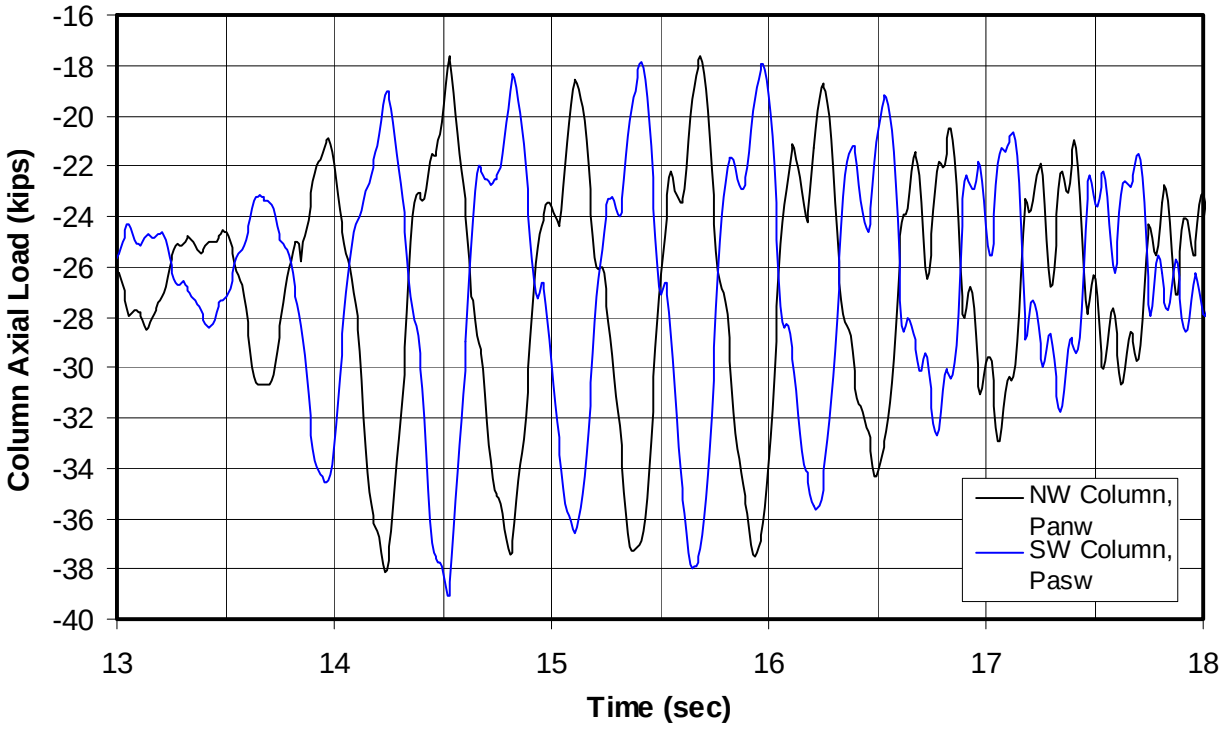

The diagonal strap connections to the columns and the column anchors are identical at their tops and bottoms. Figure 8-36, Figure 8-37, and Figure 8-38 show that the strains measured 28 in. above the bottom of the columns and 28 in. below their tops are similar. The overturning moment at the bottom of the columns is greater, so the difference in strains on opposite faces of the column should be greater near the bottom of the columns. Greater strains are more clearly seen on the bottom of the southwest column (S22z in Figure 8-38) than on the northwest column (S17z in Figure 8-37). The difference in strains measured near the ends of the columns can be linearly factored up to estimate the moment at the ends of the columns. The applied moment at the bottom of the northwest column, M_{anwb}, based on the strain data measured 28 in. above the bottom of the column, can be calculated as follows:

$$M_{anwb} = \frac{(S17z - S18z)}{2} E S_x \left[\frac{H}{H - 2(28in.)}\right] \quad \text{(Eq 8-7)}$$

where

S_x = the section modulus of the column, equal to 5.09 cu in., which equals Ix/c = 16.34 in.^{4}/3.21 in. as defined in Table 8-9.

H = the panel height, equal to 118 in.

Similarly, the applied moment at the top of the northwest column, M_{anwt}, based on the strain data measured 28 in. below the top of the column can be calculated as follows:

$$M_{anwt} = \frac{(S20z - S19z)}{2} ES_x \left[\frac{H}{H - 2(28in.)}\right] \quad \text{(Eq 8-8)}$$

The moment applied to top and bottom of the south (right) column, M_{aswt} and M_{aswb}, are calculated in the same way using the strain gage data measured at S21z, S22z, S23z, and S24z. Figure 8-41 and Figure 8-42 plot the moments applied to the top and bottom of both the north and south columns of the first-story west shear panel. The sign convention in these plots use the right hand rule so that the applied moment at both the top and bottom of the columns are positive when the model is deformed to the right (south). This results in the moments always being in phase with each other, facilitating comparison of their relative amplitudes.

Figure 8-41. Applied moment for first-story west shear panel columns in the 8% SE32 test.

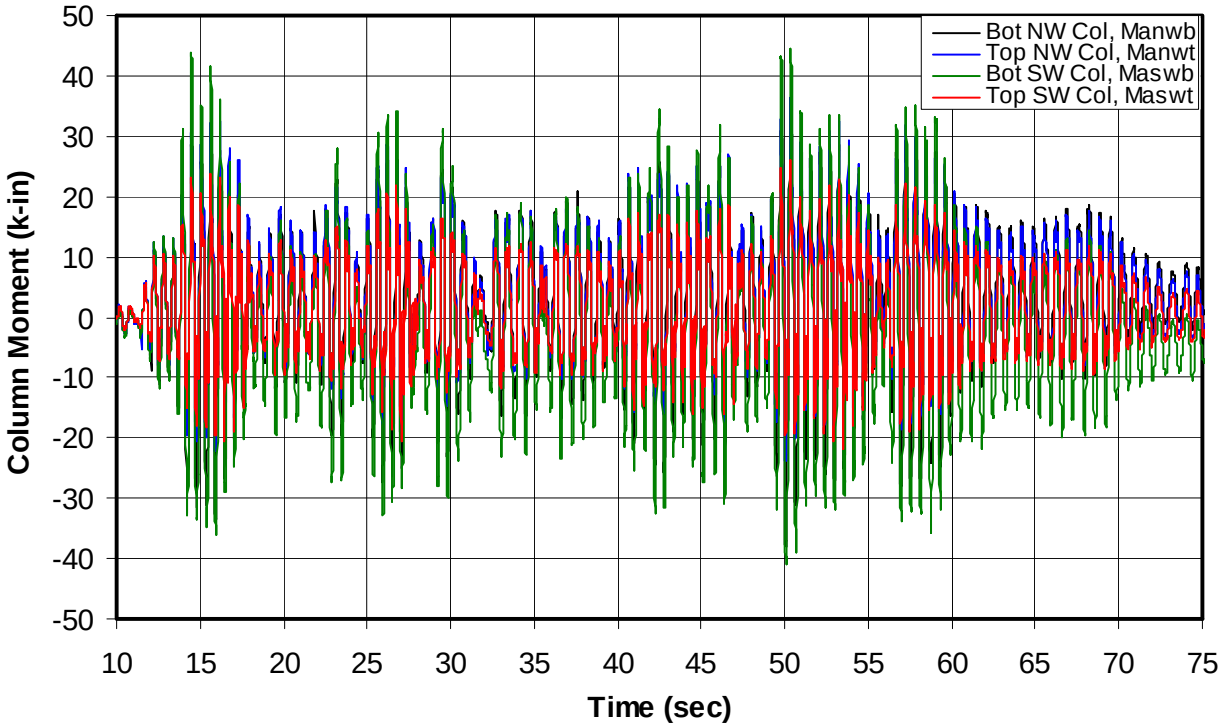

Figure 8-42. Moment for first-story west panel columns, 8% SE32, 13 through 18 seconds.

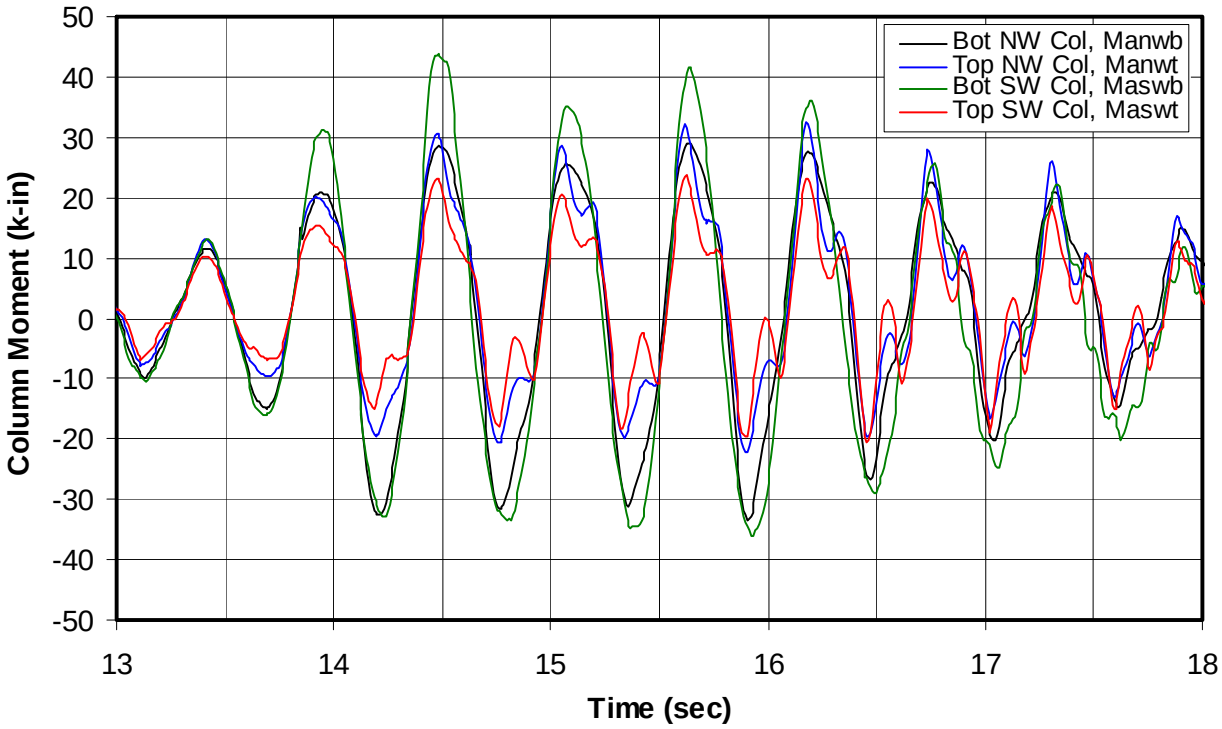

Normally the sign of at the bottom of the columns would be reversed. This shows the moments in the southwest column are consistently greater at the bottom than at the top. However, for the northwest column, when the model deforms to the right, the moments are greater at the column top.

The applied shear at the north column, V_{anw}, can be calculated as follows:

$$V_{anw} = \frac{(S17z - S18Z - S19Z + S20Z)}{2}\left[\frac{ES_x}{H - 2(28\ in)}\right] \qquad \text{(Eq 8-9)}$$

The shear applied to the south (right) column, V_{asw}, is calculated in the same way using the strain gage data measured at S21z, S22z, S23z, and S24z. Figure 8-43 and Figure 8-44 plot the applied shear at both the north and south columns of the first-story west shear panel. Figure 8-32 and Figure 8-33 (above) plotted the story shear per shear panel based on the inertia forces defined by the model acceleration and weight. This story shear at the first story carried by the columns is the total of the northwest and southwest column shear in Figure 8-43 and Figure 8-44, and the portion carried by the diagonal straps is the amount in Figure 8-32 and Figure 8-33 minus the total of the northwest and southwest columns.

Figure 8-43. Applied shear for first-story
west shear panel columns in the 8% SE32 test.

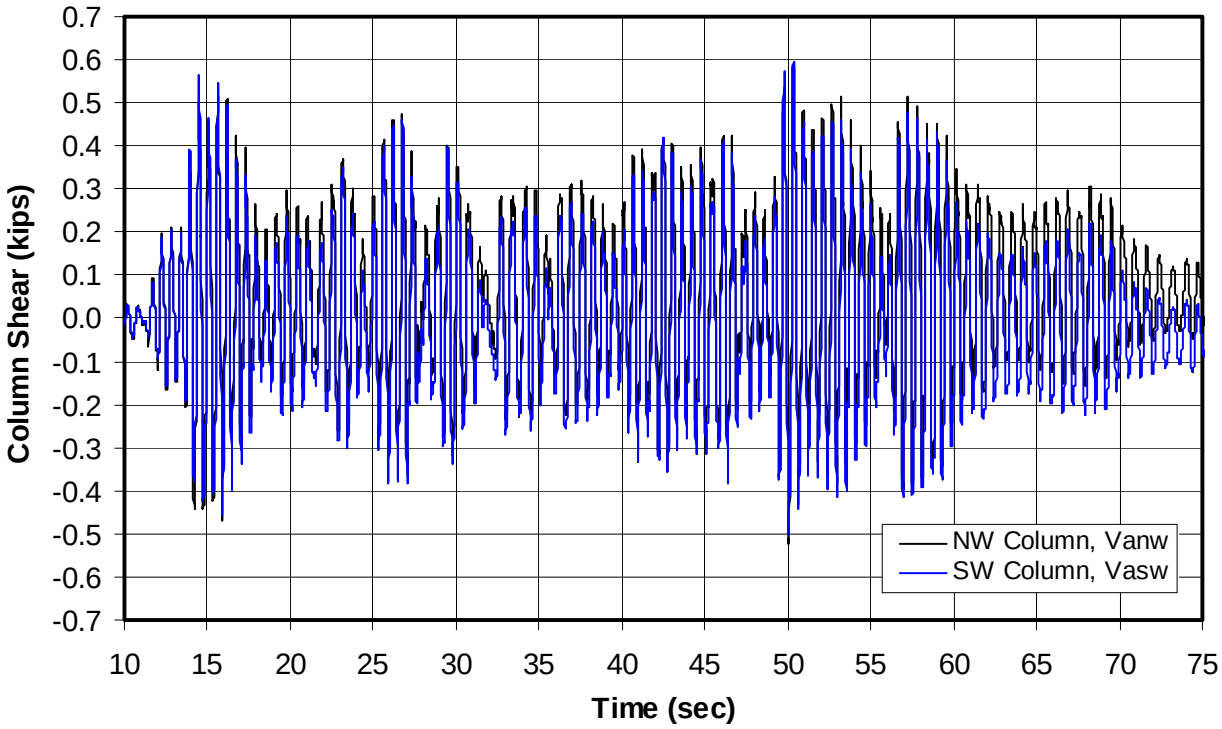

Figure 8-44. Shear for first-story
west panel columns, 8% SE32, 13–18 seconds.

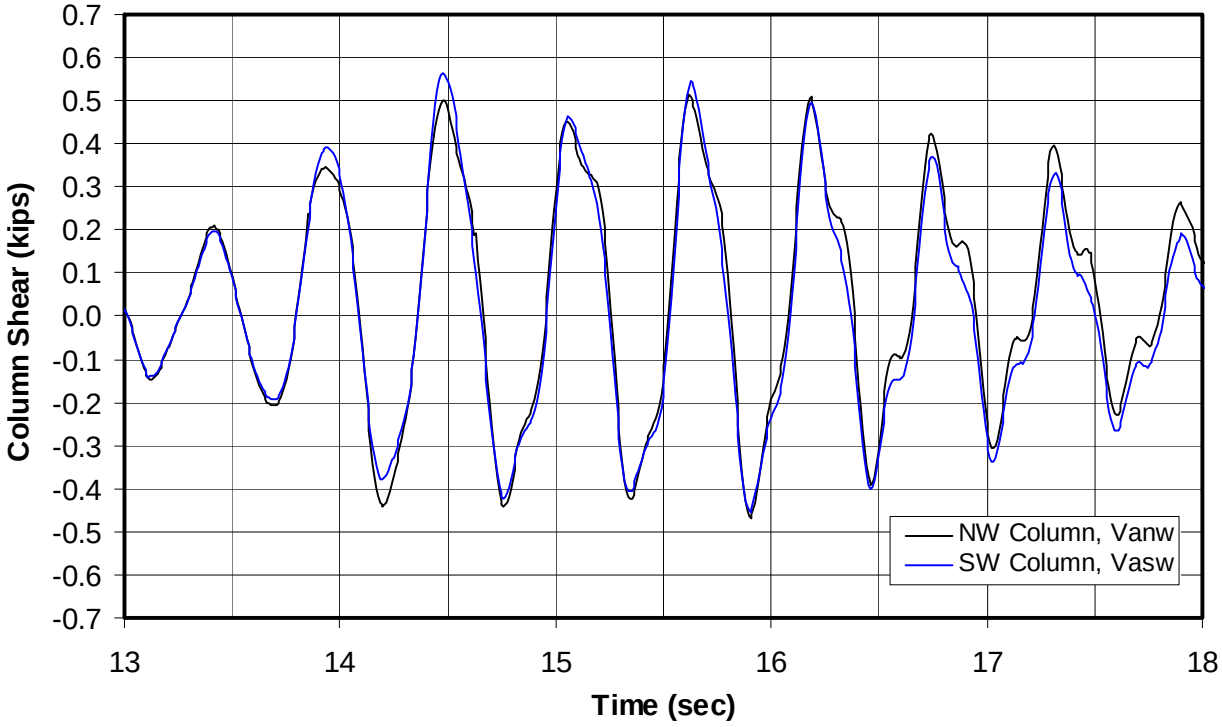

For the cycle between 14.4 and 15 seconds, the total positive column shear is 1.07 kips (Figure 8-44), which is 10% of the panel story shear of 10.28 kips (Figure 8-33). In the negative direction, the total column shear is 0.87 kips, which is 9% of the panel story shear of 10.02 kips. Table 8-16 predicted a total shear panel lateral capacity at strap yield (the model in this test is below yield) of 19.64 kips, and a lateral capacity of the strap alone of 16.62 kips, indicating a total column capacity at strap yield of 3.02 kips, which is 15% of the total. Since the measured data indicate 10% of the capacity was carried by the columns and the predicted analysis is based on assuming the columns are fully fixed, one estimate is that the columns have a fixity of 60 to 65%. These data could also be used to define a rotational spring that could be used to represent the column fixity in an analytical model.

8.9 Nonlinear seismic test

Following the 8% SE32 test, the model was tested with the full filtered SE32 record. This test was expected to cause significant nonlinear response in the shear panels. The test would provide a basis for evaluating if the cold-formed steel design recommendations developed in this program do in fact lead to ductile shear panel performance. The test should result in significant yielding of the diagonal straps and columns, and perhaps minor yielding of the anchors, but not in damage that could lead to brittle failure, such as joint or anchor failures. (Section 8.2 described the various modes of failure that would be tested in this shake table test.)

8.9.1 Measured acceleration response

The acceleration and displacement data were again examined during the linear portion of the 100% SE 32 test, to confirm that the same data channels best represented the response of the model. The acceleration measured at A23x was still much greater than at the other two second-floor slab accelerometers (A21x and A22x). The out-of-plane and torsional response was again very small. The in-plane displacements measured at the second floor (D22x and D24x) were consistent with each other, confirming little torsional response. The accelerations recorded on the first floor were double integrated and corrected for offsets, to provide displacement records that could be compared with recorded displacements. The displacements integrated from the A21x and A22x accelerometers were much less than the measured displacements at D22x and D24x. The displacements from the A23x accelerometer agreed very well with the measured displace-

ments, so the A23x record was taken as most representative of the second-floor acceleration. The first-floor acceleration measured at the A13x accelerometer, directly below A23x, agreed well with the acceleration measured at A12x and with the displacement data. Therefore, as in the linear test (8% SE32) the A13x and A23x acceleration data were determined to be most representative of the model response in this nonlinear test.

Figure 8-45 plots the measured acceleration at the TESS, first-story slab (A13x), and second-story slab (A23x). Very small out-of-plane or torsional response was seen in either the 8% or 100% SE32 tests. Some high-frequency, high-acceleration spikes were seen in the accelerometer data for the first- and second-floor levels, but the displacement data do not contain these spikes, indicating the high accelerations were due to snapping of the out-of-plane threaded rods. Figure 8-46 and Figure 8-47 zoom in on the same motions at 9–13 seconds and 13–18 seconds, respectively.

Figure 8-45. Accelerations at the TESS, first story, and second story in the 100% SE32 test.

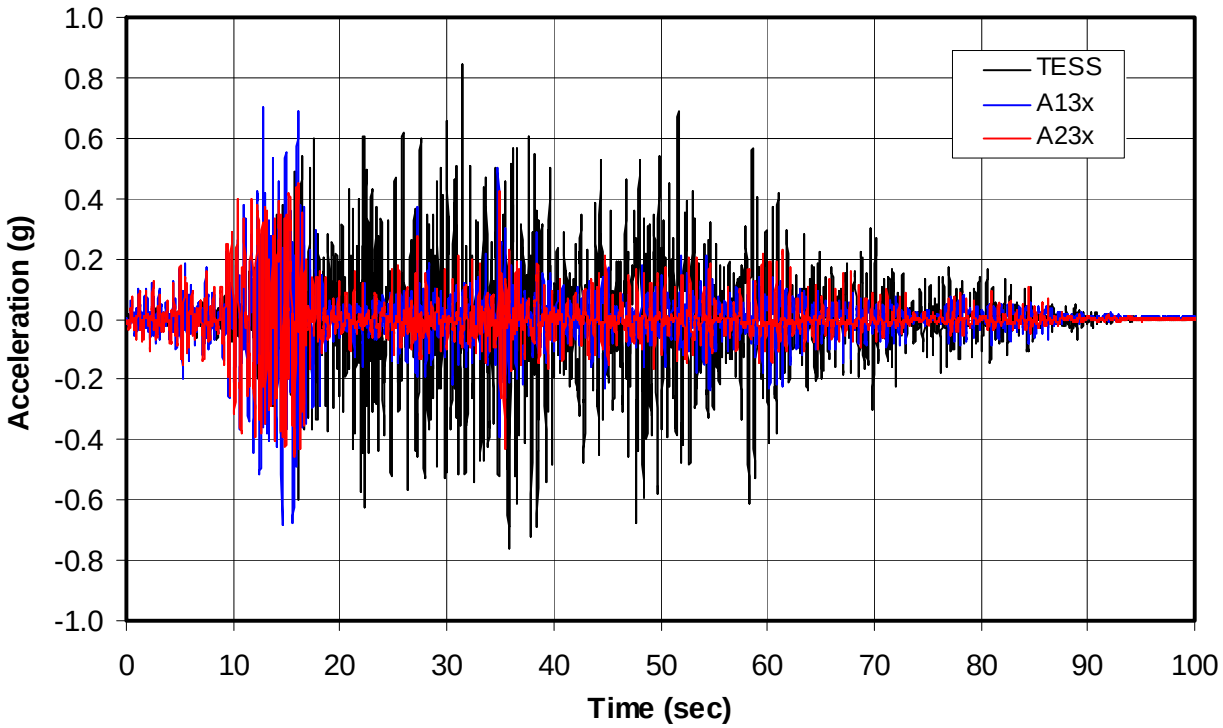

Figure 8-46. Accelerations at the TESS, first story, and second story in SE32 test, 9–13 sec.

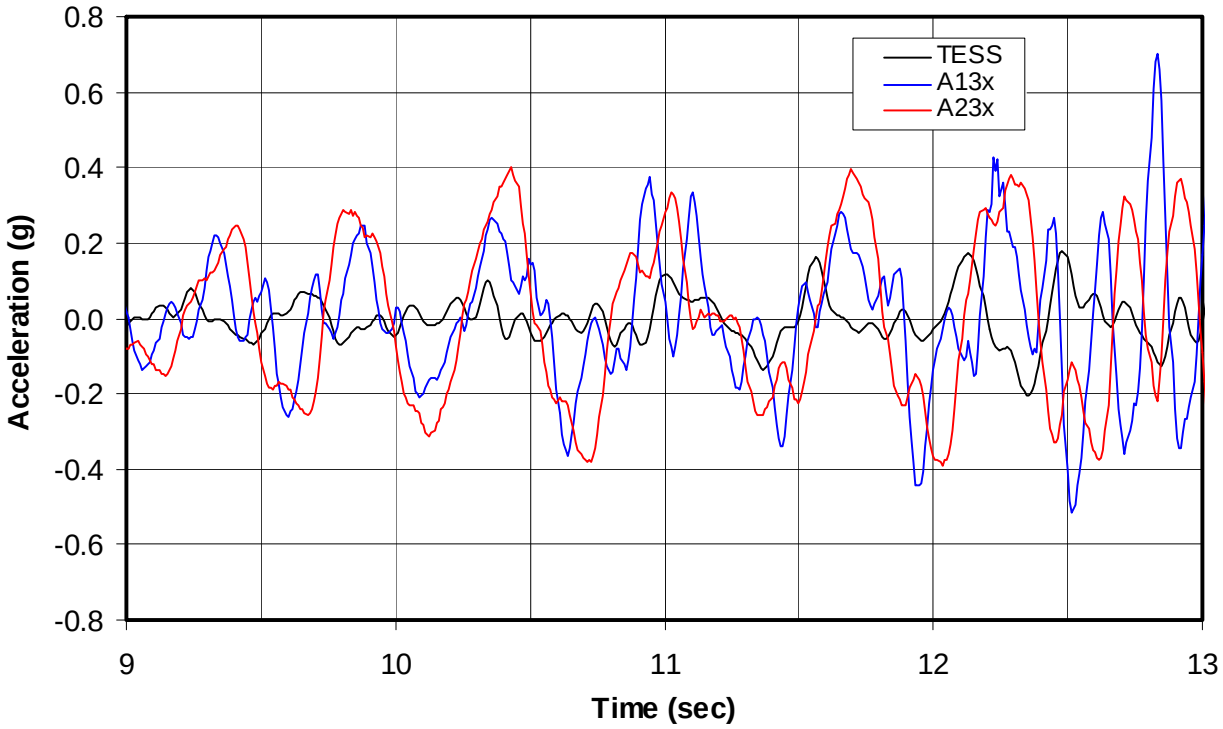

Figure 8-47. Accelerations at the TESS, first story, and second story in SE32 test, 13–18 sec.

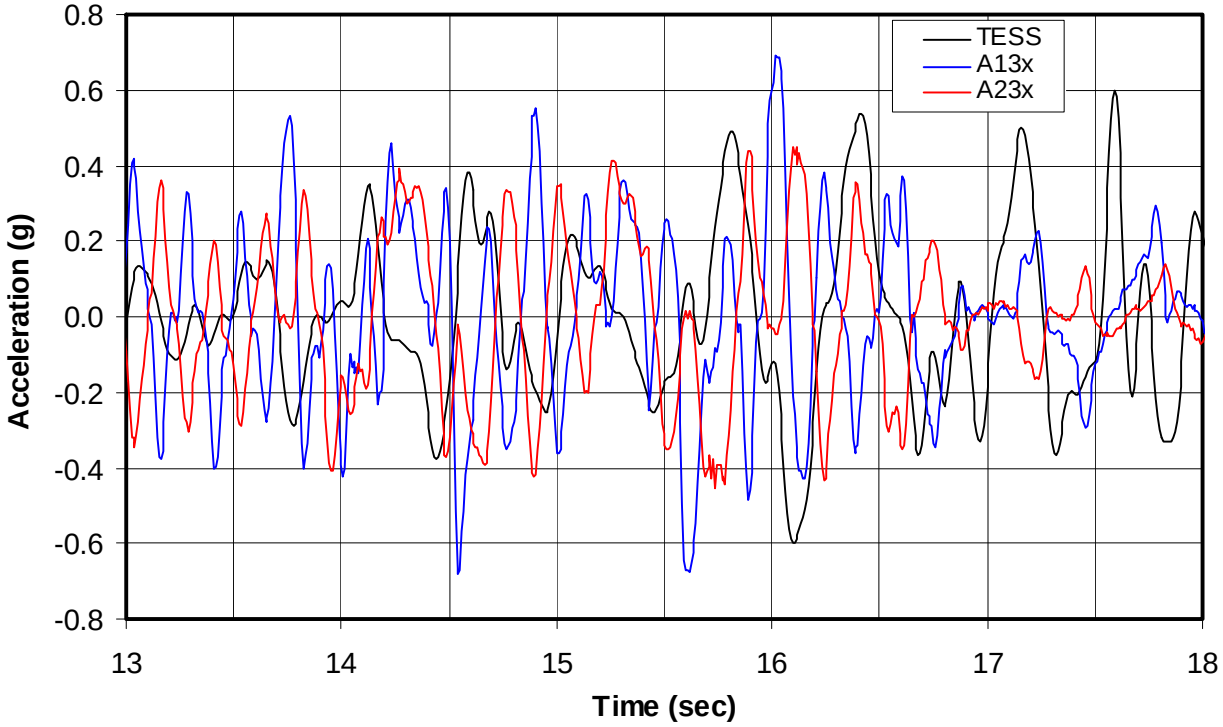

Figure 8-46 shows that the TESS motions are initially amplified significantly at the first-floor slab (A13x), and even more at the second floor (A23x). The model behavior is still fairly elastic at the beginning of the interval shown in Figure 8-46. At 12 seconds, the first-floor accelerations begin to exceed the second-floor values because of the greater amplification of the model in its second mode. Later, modal testing showed that, after this test, the model softened to the point that the first-mode frequency had fallen to 0.5 Hz. At 12 seconds, the diagonal straps are beginning to yield so that the first mode period increases, and after 13 seconds the first-mode response is not excited as much as the second mode. The second-mode frequency also begins to decrease at 12 seconds.

Figure 8-46 and Figure 8-47 show the TESS shake table motion oscillates significantly at periods corresponding to the period of the second mode of vibration of the model (0.2 seconds, or 5 Hz). The TESS motions were significantly influenced by the response of the model in the 100% SE32 test, and the TESS appears to have overcorrected in trying to prevent unwanted motions. Still, the objective of the test was accomplished, with significant nonlinear response and large lateral deformations. The actual achieved motions of the TESS and response of the model can be well documented, and the actual support motion can be used in the DRAIN2DX analysis to provide an evaluation of the ability to predict large deformation demand and capacity. Figure 8-47 shows that after 17 seconds, the diagonal straps have yielded and elongated to such an extent that the model has softened to the point that it is essentially isolated from the higher-frequency motions of the TESS. After this point, Figure 8-47 and Figure 8-45 show that the TESS accelerations are greater than the response accelerations at either the first or second floors of the model, measured at A13x and A23x, respectively.

8.9.2 Measured displacement response

Figure 8-48 shows the displacements for the entire 100% SE32 test, measured at the base beam, first-floor level, and second floor level. Figure 8-49 plots these displacements between 9 and 18 seconds, including the linear portion of the test before 12 seconds and the time of greatest model deformation. These displacements define the behavior of the model better than the accelerations. The base-beam, first-floor, and second-floor displacements are again averages of the measured displacements at these levels as explained in the linear test results.

Figure 8-48. Displacements at the base beam, first floor, and second floor.

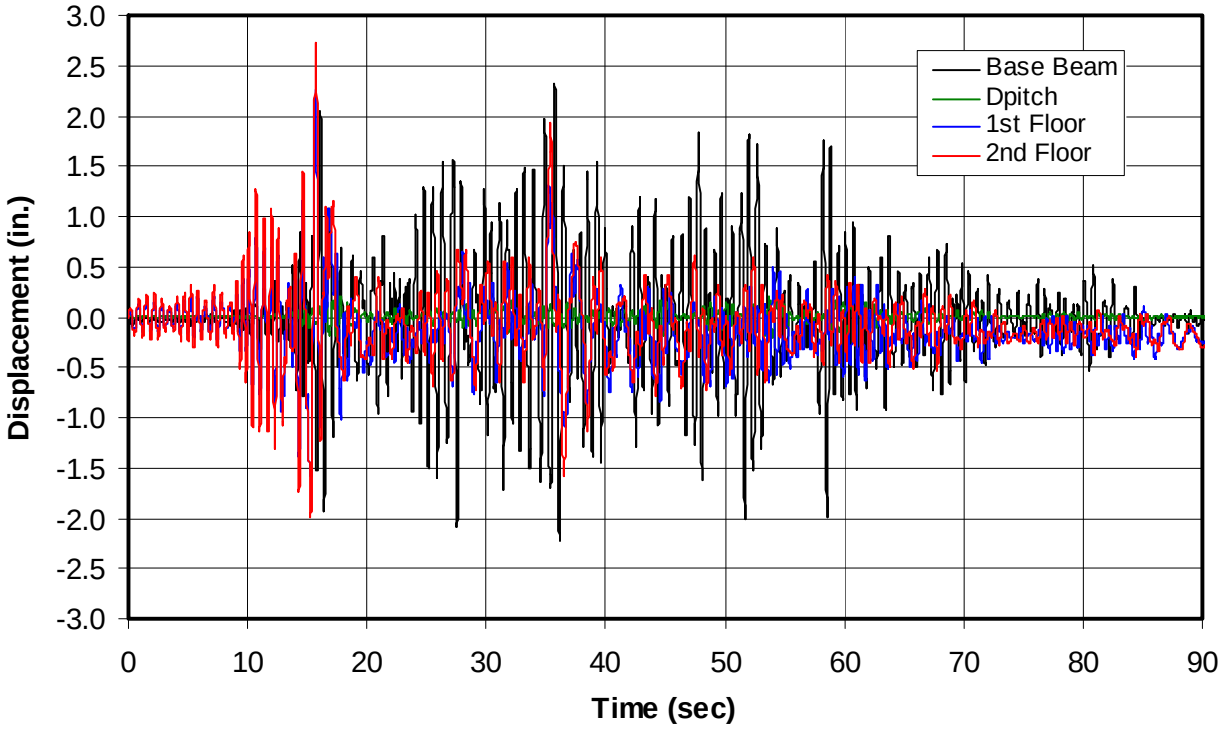

Figure 8-49. Displacements at the base beam, first floor, and second floor, 9–18 seconds.

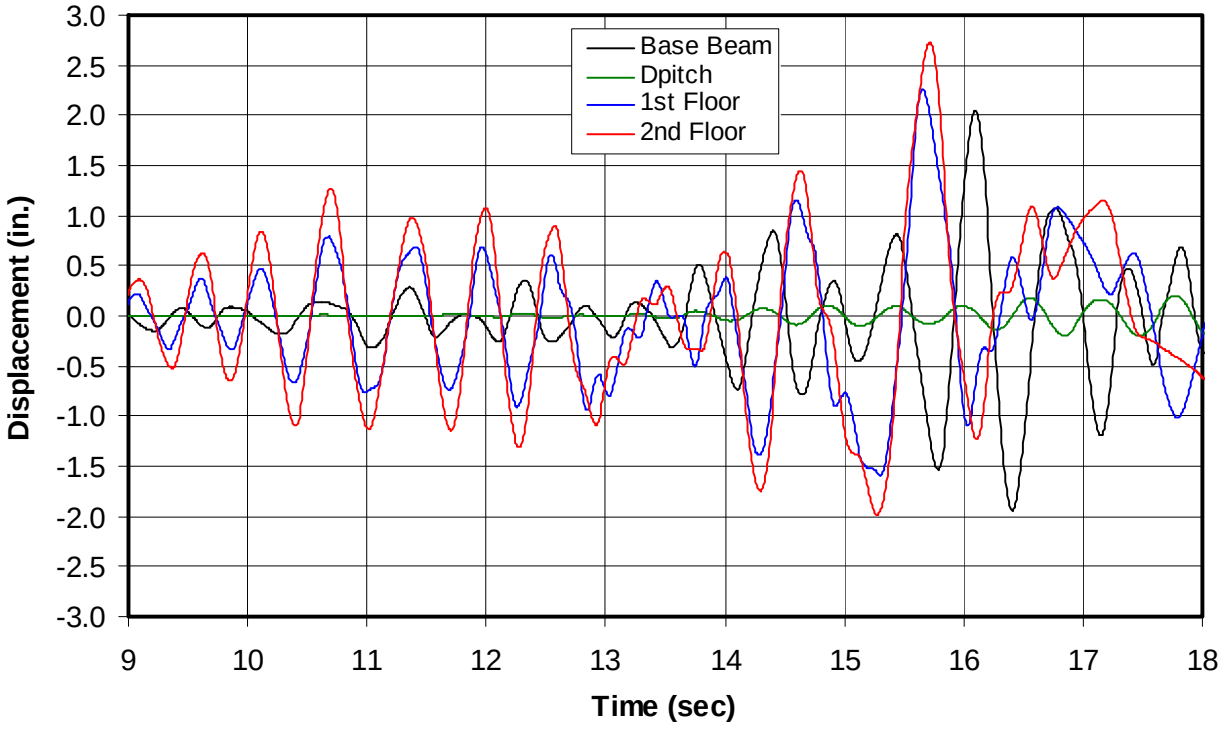

The pitch displacements, D_{pitch}, are also plotted in these figures. Figure 8-49 shows that the pitch displacements become quite large after 14 seconds. Figure 8-50 plots the first- and second-floor relative displacements, calculated from the measured displacement data according to Equations 8-1 and 8-2. Figure 8-51 plots the story drifts for both the first and second story, between 11 and 18 seconds, where the largest story drifts occur. The largest first-story drift is 3.43 in. at 15.728 seconds, and the largest second-story drift is 1.07 in. slightly later, at 15.752 seconds. This large first-story drift is the most critical deflection parameter defining the behavior of the model. The deformed model shape is plotted at 15.728 seconds in Figure 8-52. This peak first-story drift is almost nine times greater than the peak first-story drift in the 8% SE32 test (0.387 in.). Figure 8-52 shows that the peak drift was measured at a time when the first- and second-story floors were displaced to the right, while the base beam was displaced to the left. At this same time, the base beam was pitched counter-clockwise, indicating that the TESS and base beam was moving out-of-phase with the displaced shape of the model.

Figure 8-50. Relative displacements and first-story drift for the 100% SE32 test.

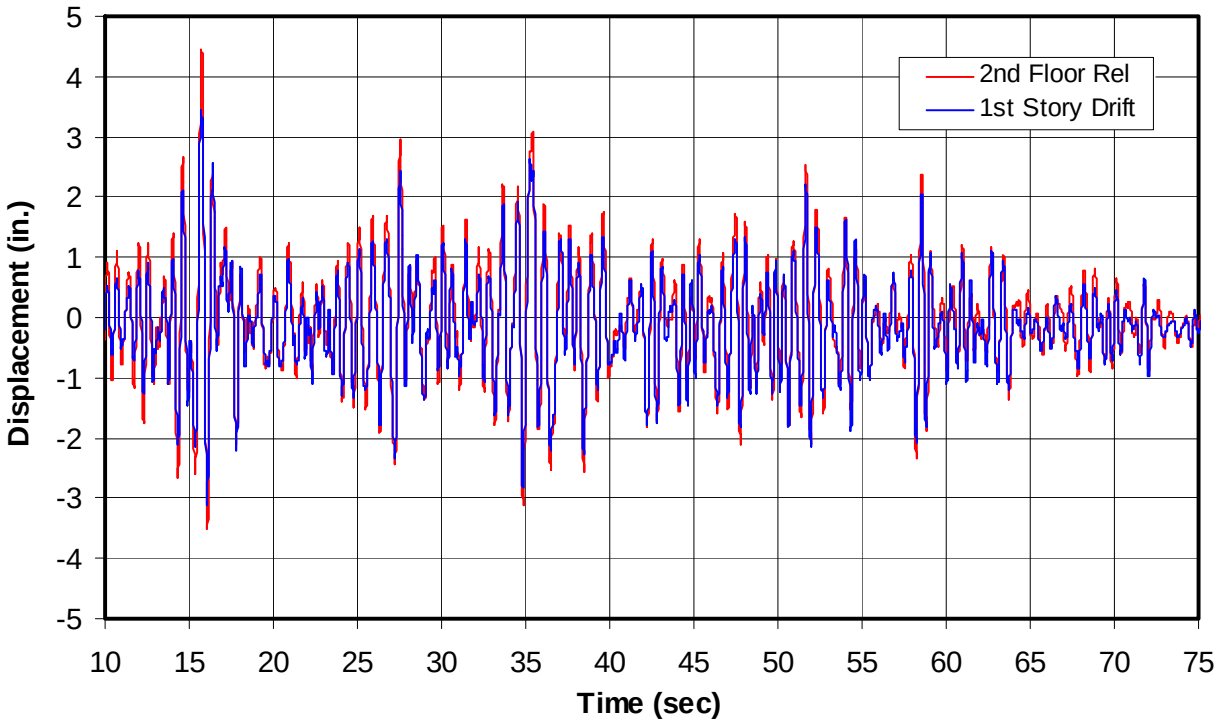

Figure 8-51. First- and second-story drifts for 100% SE32, 11 to 18 seconds.

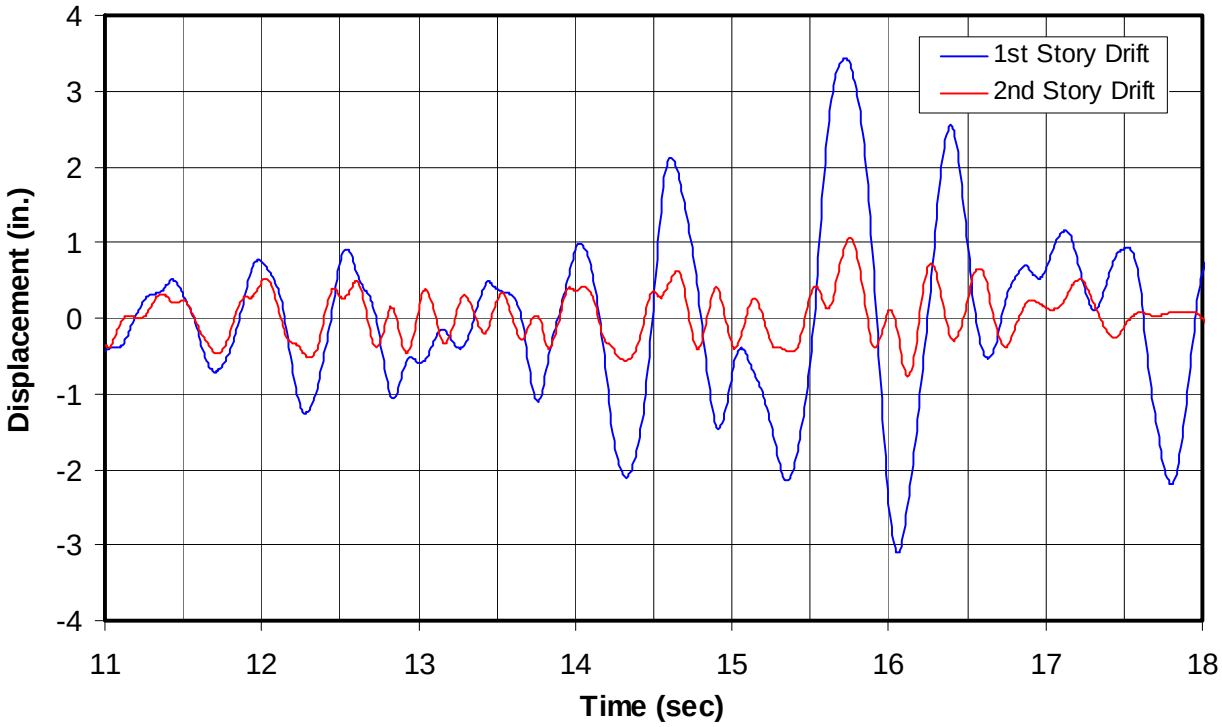

All shake table model tests were recorded with two digital camcorders, recording in a frame mode so that the video file consisted of individual photographs taken every 1/30th of a second. Figure 8-53, shows an overall view of the model taken from the east-northeast corner at approximately 15.7 seconds in the 100% SE32 test, near the time of largest model deformation shown in Figure 8-52. At this time the model was deformed to the left, which is to the south in the same direction that is to the right in Figure 8-52. The picture shown in Figure 8-53 should be very close to the shape that has been amplified by a factor of 10 in Figure 8-52. The first-story drift can best be seen in this picture by noting how the diagonal strap from the bottom-right to top-left corner of the panels are taut while they are slack in the opposite direction. Figure 8-53 shows how the diagonal straps at the second story remained almost taut, consistent with the small second-story drifts plotted in Figure 8-51. Figure 8-54 was taken by the other camcorder from the opposite west-southwest corner, having a perspective similar to Figure 8-52. This picture zooms in on the first story and it has almost the same perspective and the amplified deformed shape shown in Figure 8-52. Here the diagonal straps between the bottom-left to top-right corners were taut, while they were slack with multiple ripples in the opposite direction.

Figure 8-52. Model displacement and deformation
in the 100% SE32 test at 15.728 seconds.

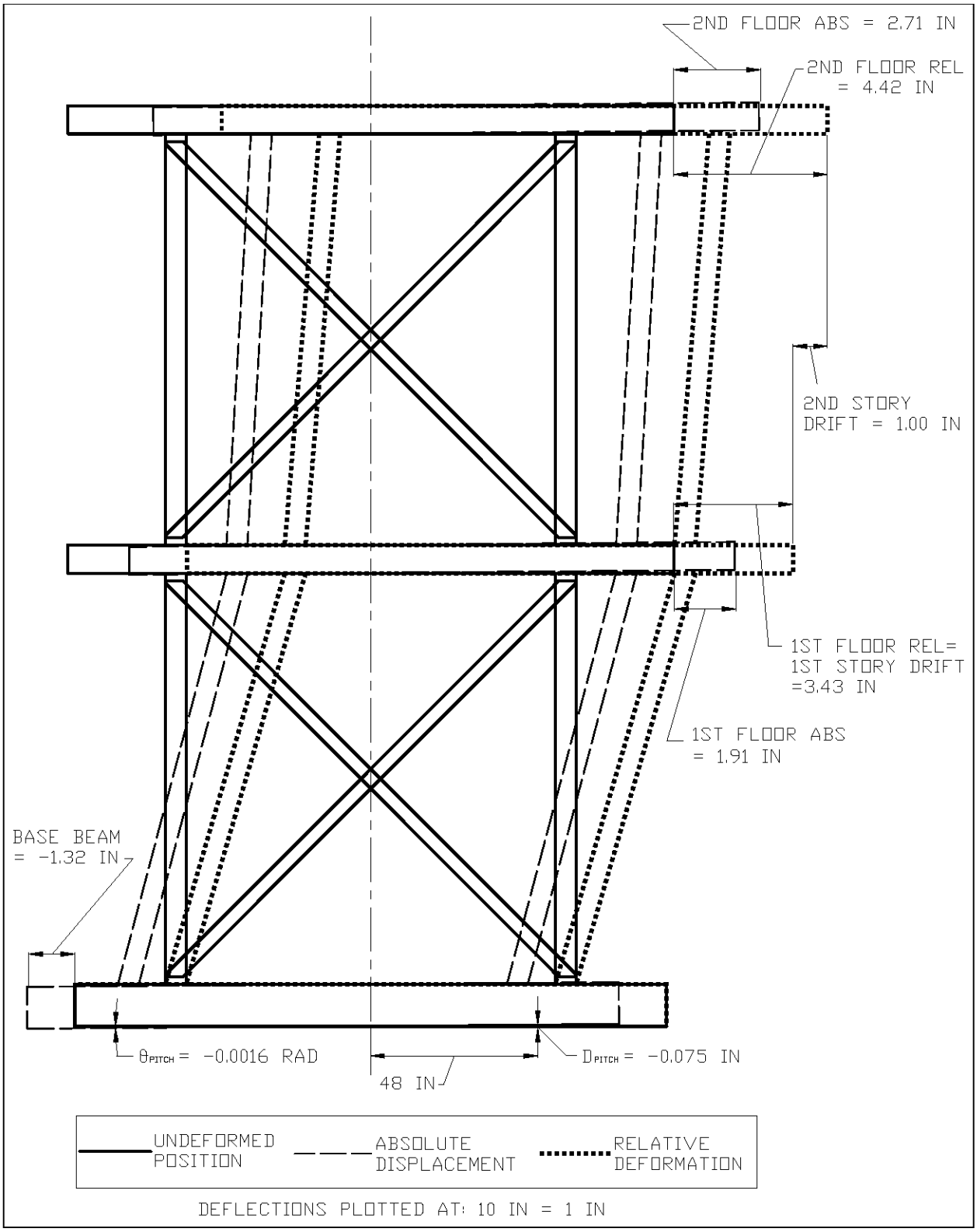

Figure 8-53. Overall view at largest positive cycle, 100% SE32 test near 15.7 sec.

Figure 8-54. First-story view at largest positive cycle, 100% SE32 test near 15.7 sec.

Inertia forces and applied lateral forces (base shear) at both story levels were calculated from the floor accelerations shown in Figure 8-45 through Figure 8-47. These forces were used to plot story shear versus story drift for both stories in Figure 8-55. This plot shows that the story shear and especially story drift was much larger at the first story. Figure 8-55 shows that the greatest first-story shear per shear panel was 20.6 kips, and the greatest second-story shear was 13.1 kips. The greatest first-story shear occurred at 14.55 seconds and the greatest second-story shear occurred during the next major cycle at 15.74 seconds. The first-story shear was 57% greater than the greatest reached at the second story. Figure 8-56 shows plots of the story shear versus story drift during the largest first-story drift cycle that occurred between 15.52 seconds and 16.25 seconds. The largest second-story shear occurred during this cycle, but the largest first-story shear occurred during the previous cycle. These plots indicate that nonlinear deformation occurred in both the first and second story, but much greater deformations occurred in the first story.

Figure 8-55. Story shear versus story drift for both stories for the 100% SE32 test.

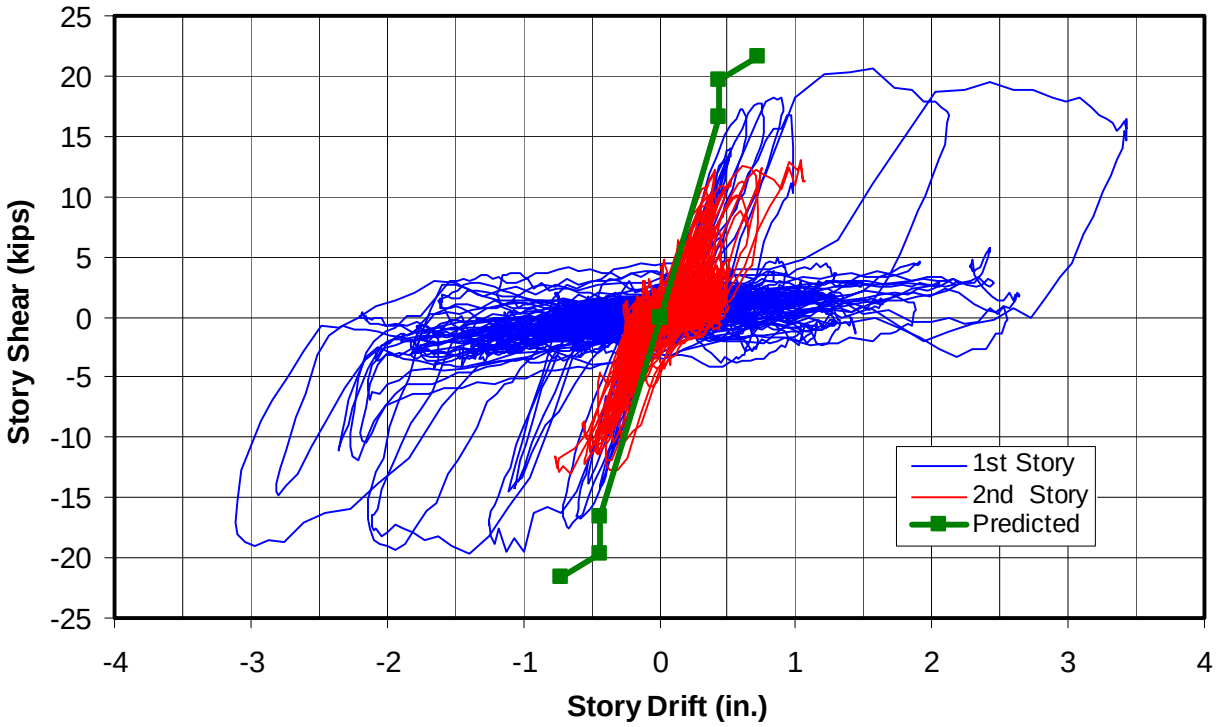

Figure 8-56. Story shear versus story drift
for 100% SE32 test, 15.52–16.248 seconds.

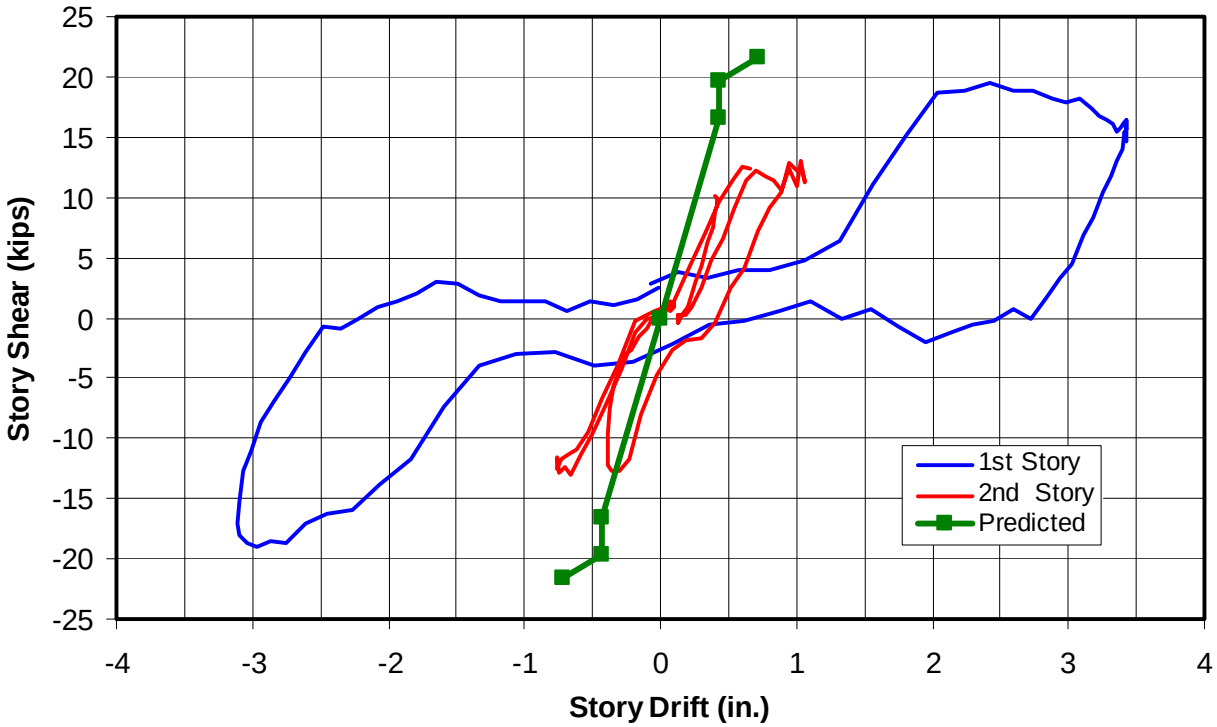

Both Figure 8-55 and Figure 8-56 plot the predicted lateral load versus deformation along with the measured data. The first-story panels reached the estimated lateral capacity of the panels from the diagonal straps alone at strap yielding at about 0.5 in. lateral deformation. Then at 1 in. drift in both directions, the panel applied story shear increased measurably, and this increase is attributed primarily to the contribution of the columns acting as moment frames. Further observation on the contribution of the columns can be made based on an examination of the column strain gage data in the following section. The plots of story shear versus story drift in Figure 8-55 and Figure 8-56 are very similar to the lateral load versus lateral deflection presented in Chapter 7. The relatively wide hysteretic plot of the single cycle shown in Figure 8-56 reveals substantial contribution of the columns acting as a moment frame.

8.9.3 Measured strains

Figure 8-57 plots strains measured at selected first-story diagonal strap gages and from one second-story diagonal strap gage. This figure shows that the first-story straps yielded repeatedly at increasing amplitudes between 10 and 16 seconds in the 100% SE32 test. Soon after 16 seconds, the

strains reached final elongation levels with only relatively small elastic variations for the remainder of the test. These data show that the diagonal straps did not yield or elongate further after 16.1 seconds. Figure 8-58 shows strains measured on diagonal straps that were oriented from the bottom-north panel corner to the top-south corner (NS orientation) on the first-story shear panels. Each of these sensors measured the greatest strain up to that time from among all the gages installed on the first-story panels in the NS direction. These strains are plotted between 10 and 16.5 seconds, when all the strap yielding and elongation took place. Figure 8-16 shows that the S2xz, S10xz, and S12xz first-story gages would all experience tensile elongation when the model was racked to the right (south). Figure 8-58 also plots the average strain of all NS-oriented strain gages on the first story (NSAvg). Similarly, Figure 8-59 plots strains measured at all the critical strain gages on straps oriented in the bottom-south to top-north (SN) orientation), along with the average of all gages in this direction (SNAvg).

Figure 8-57. Strains measured at several first-story and one second-story diagonal strap.

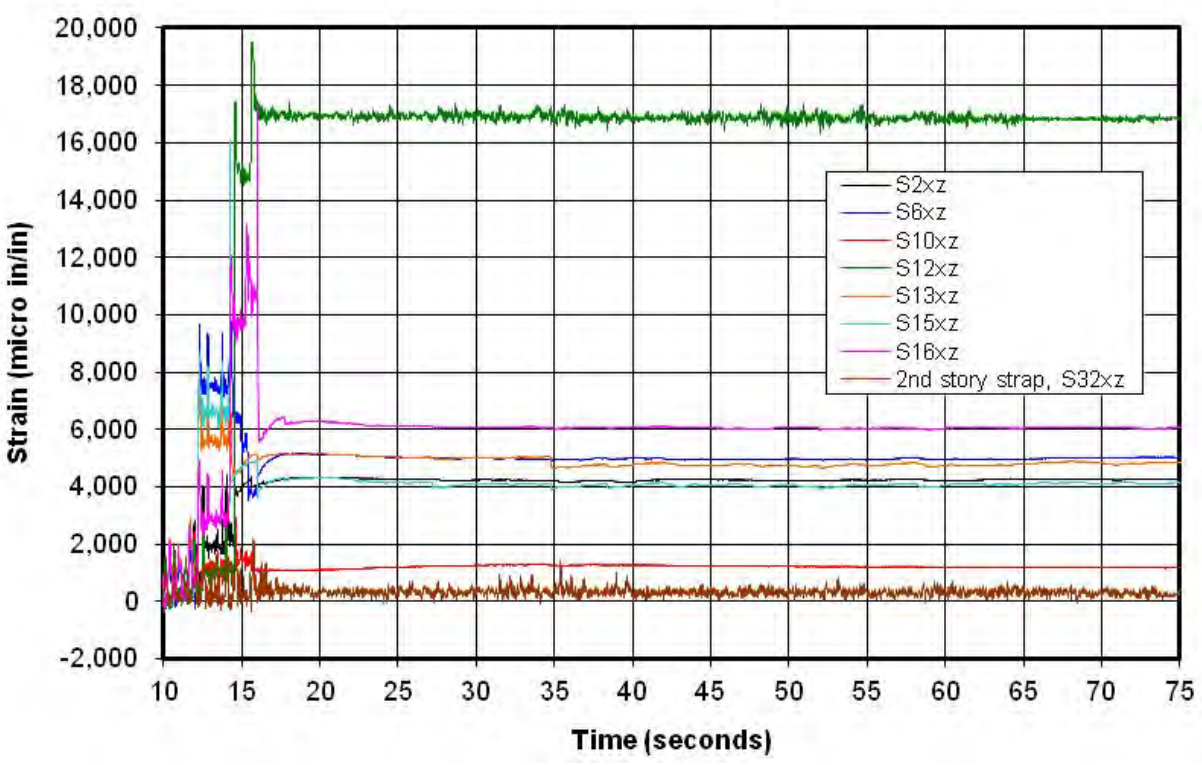

Figure 8-58. Strain measured at selected bottom-north to top-south first-story straps, 10– 16.5 seconds.

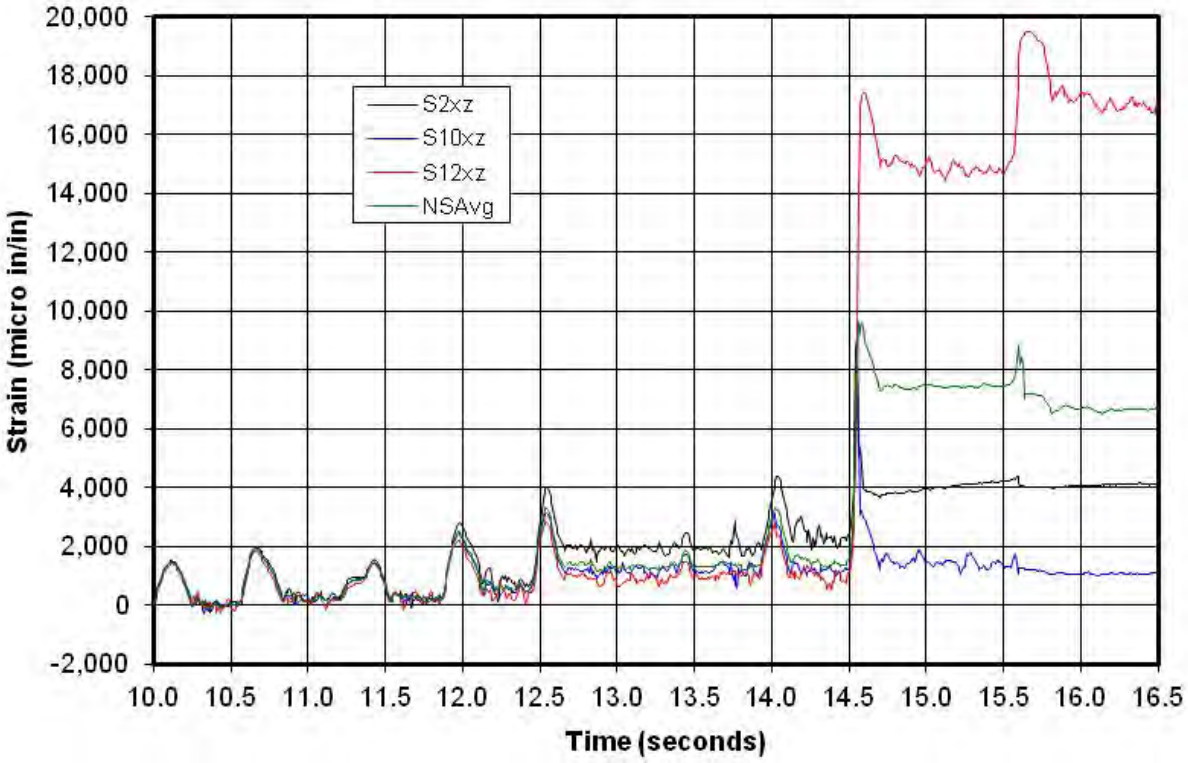

Figure 8-59. Strain measured at selected bottom-south to top-north first-story straps, 10–16.5 seconds.

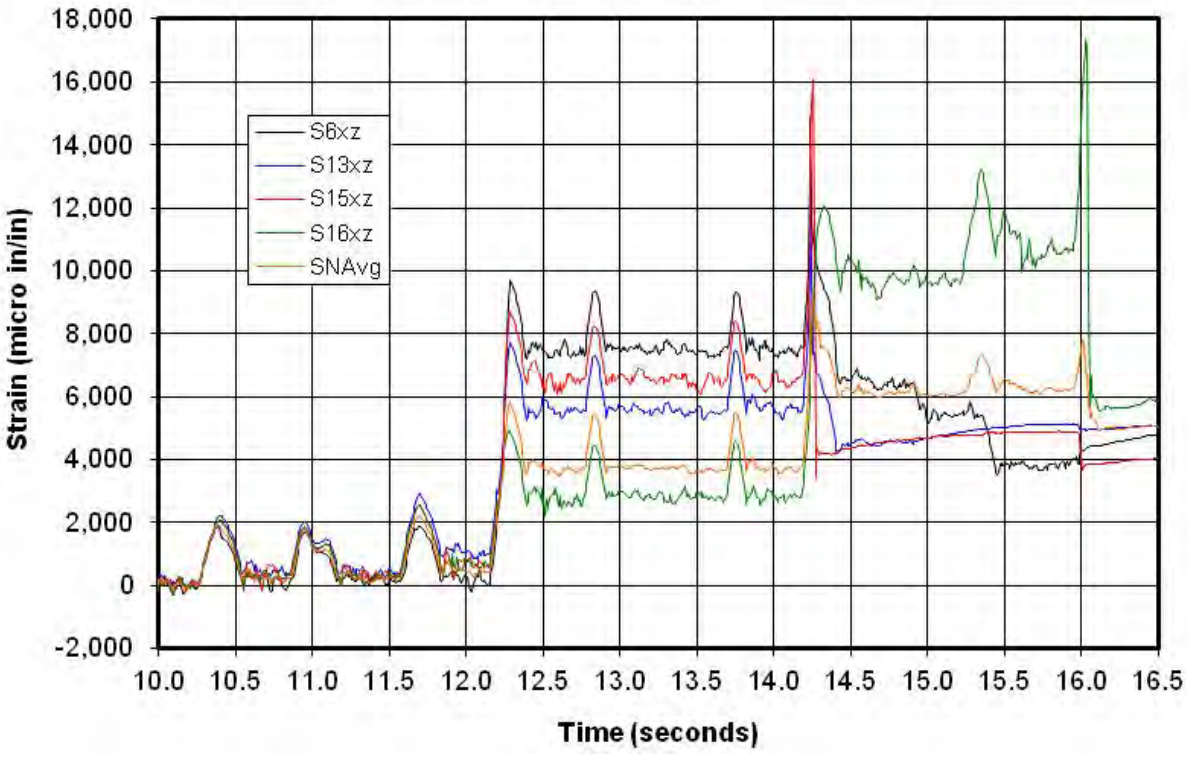

The strap coupon data plotted in Figure 8-22 show the straps begin to yield at 1,700 microinches/in., fully yield at 2,900 microinches/in. (see Table 8-6) and strain harden at 15,000 microinches/in. (0.015 in./in. in Figure 8-22). The strain plots for the first-floor straps in Figure 8-57 show these straps have yielded across their entire lengths, and many may have begun to strain harden having reached peak strains over 15,000 microinches/in. The straps would be expected to yield across their entire lengths before they begin to strain harden. This observation is consistent with the amount of elongation seen in the straps during and after the test. Comparison with the coupon data suggests the straps reached peak stresses up to 57.4 ksi, but not close to fracturing.

Comparison of the diagonal strap strain data shown in Figure 8-57 through Figure 8-59 with the strap coupon data in Figure 8-22 reveal that all the model damage related to elongation of the diagonal straps took place between 10.4 and 16.1 seconds. Table 8-18 summarizes each higher level of strain measured in the first-story straps, plus the average of all strains measured in the same direction during the same model deformation cycle. For example, the first evidence of diagonal strap yielding was seen at 10.4 seconds, with a peak measured strain at S13xz of 2,210 microinches/in. (see Figure 8-59). At this time the average of all strain gages in the SN direction was 1,930 microinches/in., and the first-story model lateral deformation, δ_s, at that time was calculated according to the following modification of Equation 5-2:

$$\delta_s = -SNAvg\left(\frac{H^2+W^2}{W}\right) \qquad \text{(Eq 8-10)}$$

The sign before Equation 8-10 is positive for the NS direction and negative for SN. Table 8-18 also provides an estimate of the strap stress for the average of all strain gage readings, based on the stress versus strain coupon data plotted in Figure 8-22. This stress can be used to estimate the panel capacity based on Equation 5.1. Table 8-18 provides average offset amplitudes for all strain gages in a given direction. In the SN direction the offset average was 200 microinches/in. This offset is a measure of the permanent elongation of the strap until further yielding takes place in a later cycle.

Table 8-18. Summary of Shake Table Model Diagonal Strap Yielding.

Strain Gauge Name	Time of Peak Strain (sec)	Peak Amplitude (mico in/in)	NSAvg (mico in/in)	SNAvg (mico in/in)	Lateral Defl, δ_s (in.)	1st Story Drift (in.)	Strap Stress, F_s (ksi)	Offset Amplitude (mico in/in)
S13xz	10.4	2210		1930	-0.46	-0.61	47.3	200
S10xz	10.7	2010	1930		0.46	0.64	47.3	200
S13xz	11.7	2910		2210	-0.52	-0.71	50.3	400
S2xz	12.0	2810	2510		0.59	0.77	51.9	600
S6xz	12.3	9690		5810	-1.37	-1.26	54.0	3700
S2xz	12.5	4020	3330		0.79	0.91	53.4	1300
S2xz	14.0	4400	3350		0.79	0.99	53.5	1400
S15xz	14.3	16110		9060	-2.14	-2.11	54.5	6000
S12xz	14.6	17440	9640		2.28	2.12	54.5	7400
S12xz	15.6	19520	8880		2.10	3.43	54.5	6600
S16xz	16.0	17320		7800	-1.84	-3.11	54.0	5100

The first-story lateral deformation, δ_s, can be compared with the measured story drifts shown in Figure 8-51. Values of measured story drift from Figure 8-51 are included in Table 8-18 for comparison. The values of measured story drift are consistent with but slightly greater than the values calculated based on the strain gage data. The overall story drifts are generally greater than the lateral deformation due to strap elongation alone, because the joints near the ends of the columns and anchors deform small amounts relative to the large values in the straps.

Figure 8-60 plots the strain data from the second-story shear panel diagonal straps, where the greatest strains were measured in the NS (S32xz) and SN orientation (S33xz). Also shown is the average of all the strain gages in both orientations of the diagonal straps (see locations of all gages in Figure 8-16). This plot shows that these straps clearly yielded at least in the NS direction (positive story shear), because the strains exceed 1,700 microinches/in., but some of the straps may have just begun to yield. The second-story drift plotted in Figure 8-51 is fairly large, reaching 1.06 in. at 15.76 seconds, but the amplitude is much less in the negative direction, reaching only -0.76 in. at 16.13 seconds. These values agree with both the time and amplitude of strains plotted in Figure 8-60. This information on diagonal strap strain gage measurements defines the nonlinear behavior of the shake table model.

Figure 8-60. Strain measured at greatest and average NS and SN second-story straps, 15.6–16.2 seconds.

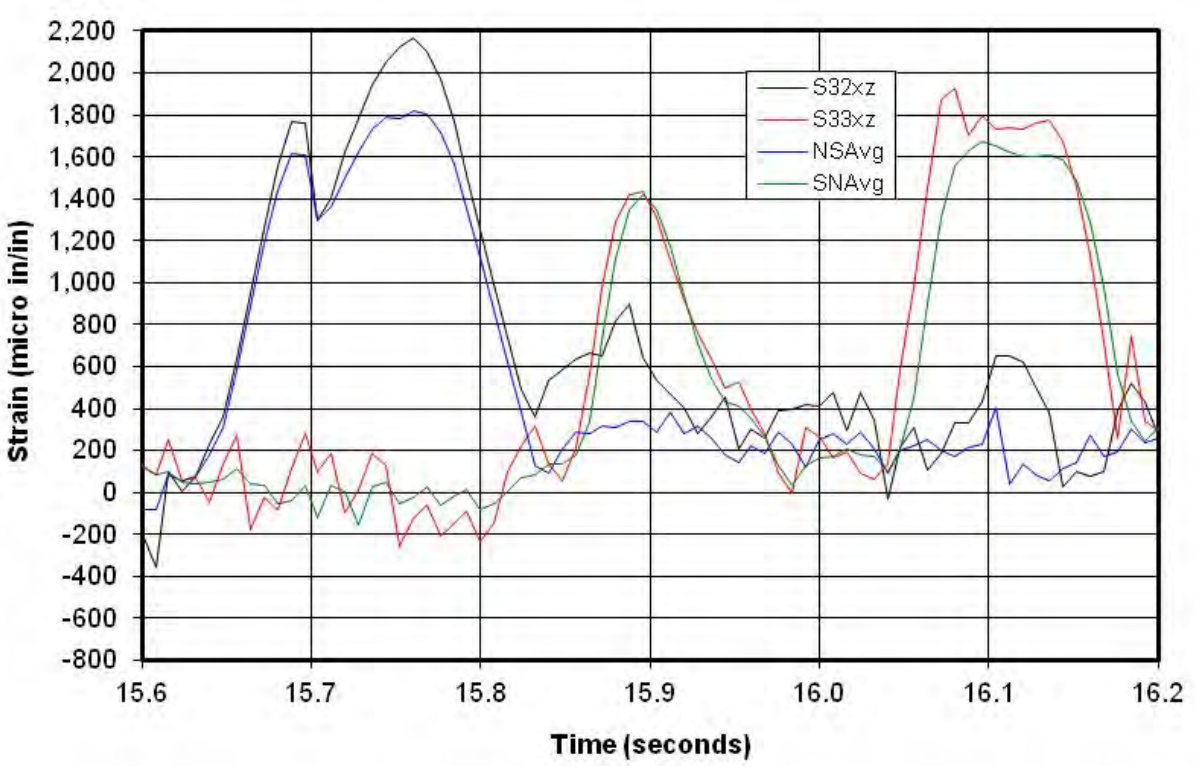

Figure 8-61 plots strains measured on the northwest column, which like for the 8% SE32 tests have been reduced by 256 microinches/in. to account for the effects of gravity. This plot shows the effects of gravity were overcome, and small tensile strains were measured at the locations of the strain gages. Scaling these strains to the location of the anchors suggests the columns would have yielded in compression. For example, the strain measured at S23z at 15.72 seconds (plotted in Figure 8-63) scales to -1,837 microinches/in. at the bottom of the top anchor leg of the southwest column. Since the column coupon data in Figure 8-22 show that it begins to yield at 1,300 microinches/in., these columns likely yielded in compression near their anchors. The greatest tensile strain of 489 microinches/in. was measured at S22z at 36.48 seconds, and this equates to 1,078 microinches/in. when scaled to the top of the bottom anchor leg, suggesting that the columns never yielded in tension. Post-test visual observations indicate that the columns did permanently buckle locally, agreeing with minor compression yielding. Figure 8-62 plots the same corrected strain data for the 12–18 second region of these records.

Both Figure 8-61 and Figure 8-62 show that the strains measured at S17z have a permanent positive increase of 200 microinches/in. beginning at either 15.6 or 16.4 seconds. This indicates that the columns may have yielded in tension at the S17z strain gage location, even though the positive tensile strains are well below the amplitude that should cause yielding. Figure 8-62 shows the same pattern of strain oscillations as explained in the linear 8% SE32 test results. Figure 8-63 plots similar strain measurements for the southwest column for the 12–18 second region, showing slightly greater measurements than on the northwest column. This figure shows a positive tensile offset at S22z of 300 microinches/in. and a negative compressive offset at S21z of 200 microinches/in. at 16 seconds, suggesting column yielding in both tension and compression at this time.

Figure 8-61. Strain measurements
on the first-story northwest column, 100% SE32 test.

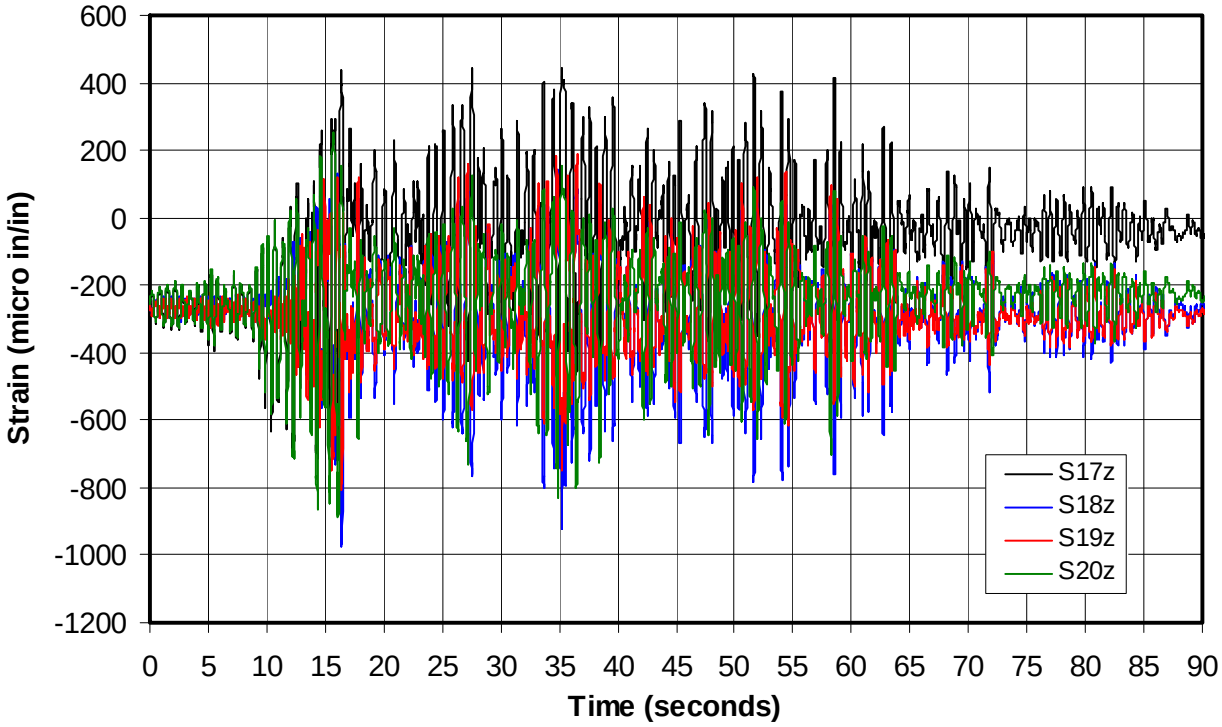

Figure 8-62. Strains on the first-story northwest column, 12–18 seconds.

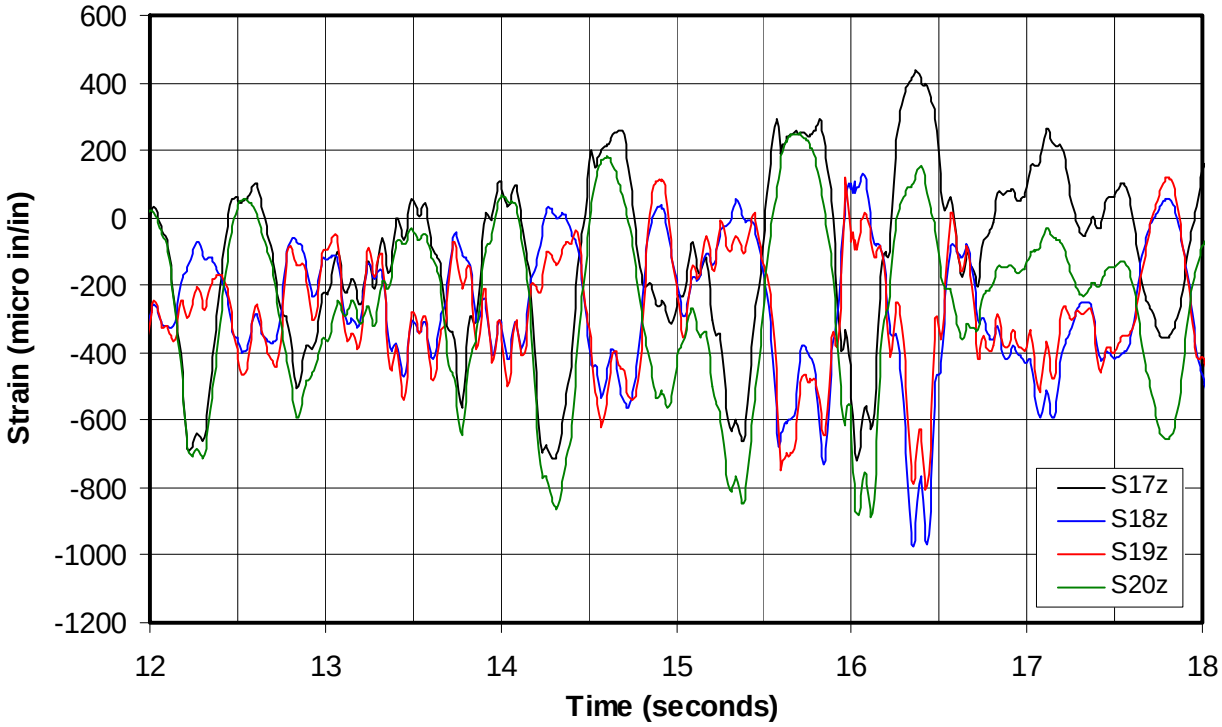

Figure 8-63. Strains on the first-story southwest column, 12–18 seconds.

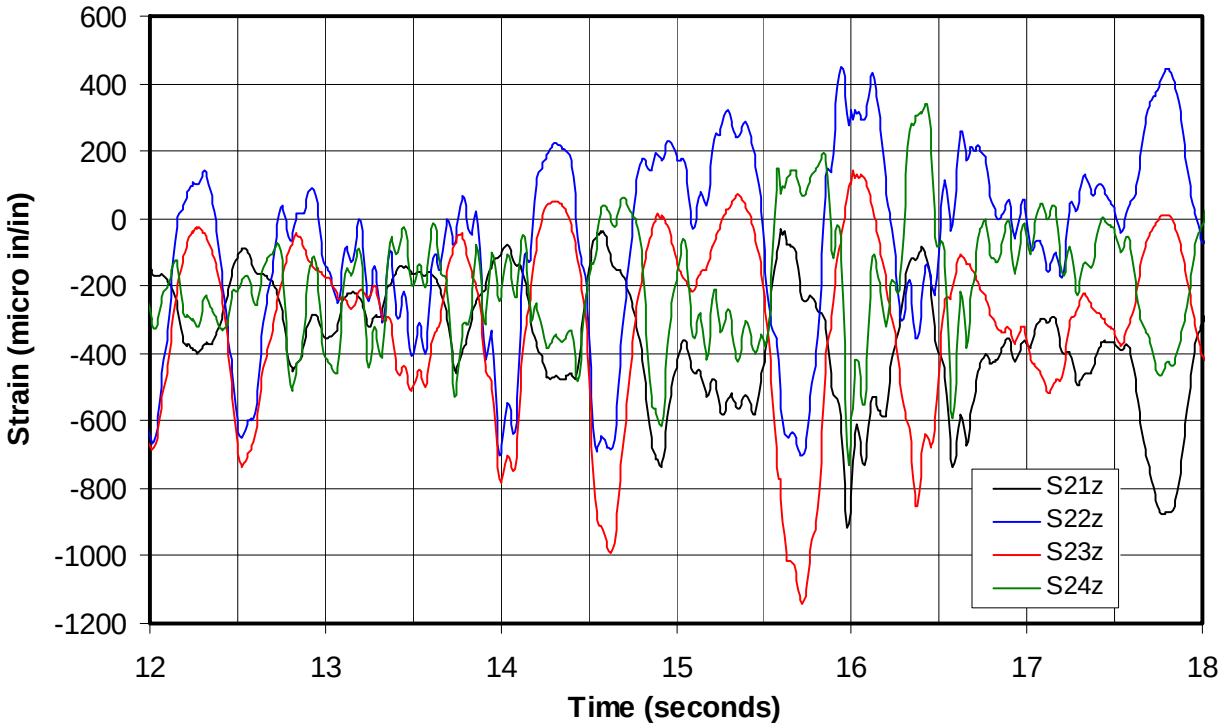

8.9.4 Column axial load, moments and shears

The column strains are again used to estimate the column axial load, load carried in shear by the columns, and column moments at their tops and bottoms. Only the columns at the west first-story shear panel were instrumented, and Equation 8-6 defines how the strain measurements were used to calculate the axial load in the northwest column, P_{aNW}. The axial load applied to the southwest column, P_{aSW}, was calculated in a similar way using the strain measurements from it. Figure 8-64 plots the applied axial load for both the north and south columns of the first-story west shear panel. The previous section describes permanent strain offsets (yielding) of 200–300 microinches/in., measured at strain gages S17z, S21z, and S22z at 16 seconds. The load calculated based on these strains should not include the effects of these offsets. The axial loads plotted in Figure 8-64 do not correct for the strain offsets, so that axial loads plotted after 16 seconds include a small error. However, the diagonal strap strain gage data showed most of the nonlinear response of the model had already taken place by 16 seconds, indicating that accurate loads after this point were less important.

Figure 8-64. Axial load for first-story west panel columns 100% SE32, 11–18 seconds.

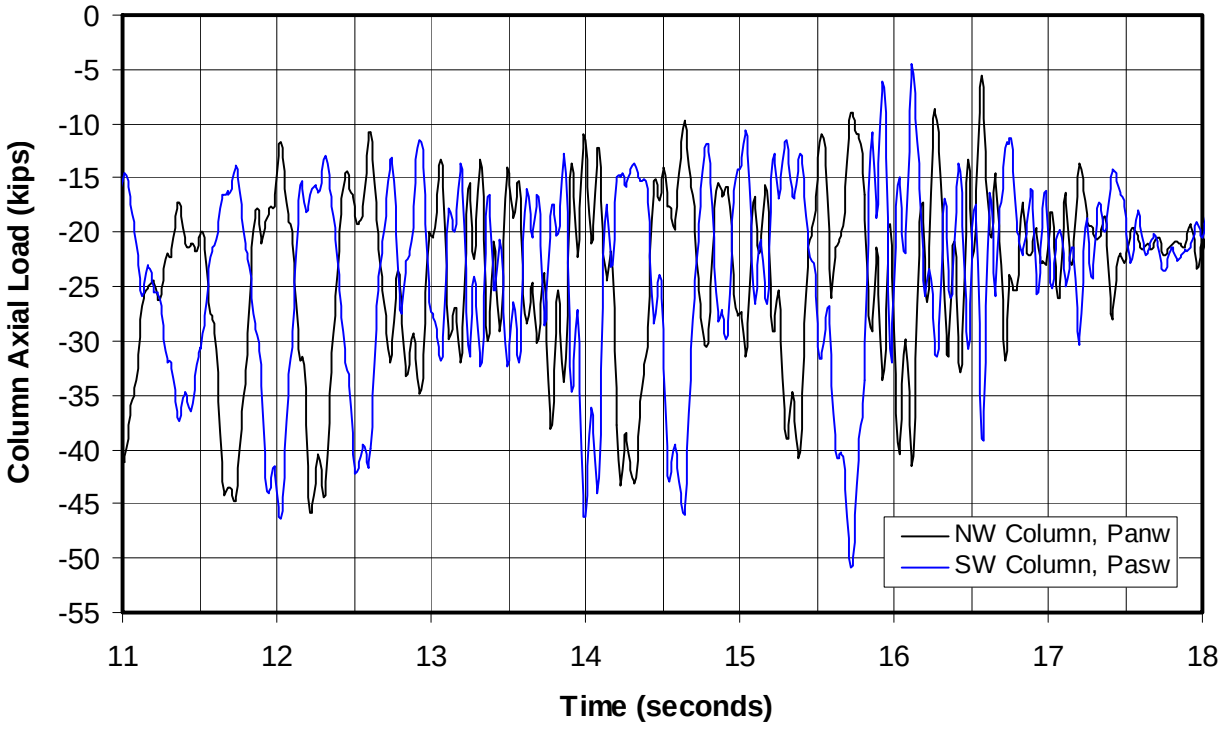

Figure 8-64 shows that the column axial loads oscillate about the 26 kip static gravity load per column. This figure shows that the overall column cross-section remains in compression throughout the test, reaching the smallest compression force of 4.4 kips at 16.1 seconds in the southwest column. Figure 8-64 also shows that the maximum compressive force in the columns is almost twice the static load, reaching a peak value of 50.8 kips at 15.7 seconds in the southwest column. Incidentally, this peak axial load in the southwest column is exactly the same as the spreadsheet-calculated column axial load at strap ultimate, P_{vumax}, shown in Table 8-8. After 16 seconds this plot erroneously shows the axial force oscillating about 21 kips (it should still be 26 kips) due to the permanent offset in the column strain measurements.

Figure 8-65 plots the moments applied to the top and bottom of both the north and south columns of the first-story west shear panel, calculated according to Equation 8-7. The same sign convention for moments is used as in the section 8.8 so the relative magnitudes can be easily compared.

Figure 8-65. Moment for first-story west shear panel columns, 100% SE32, 10–18 seconds.

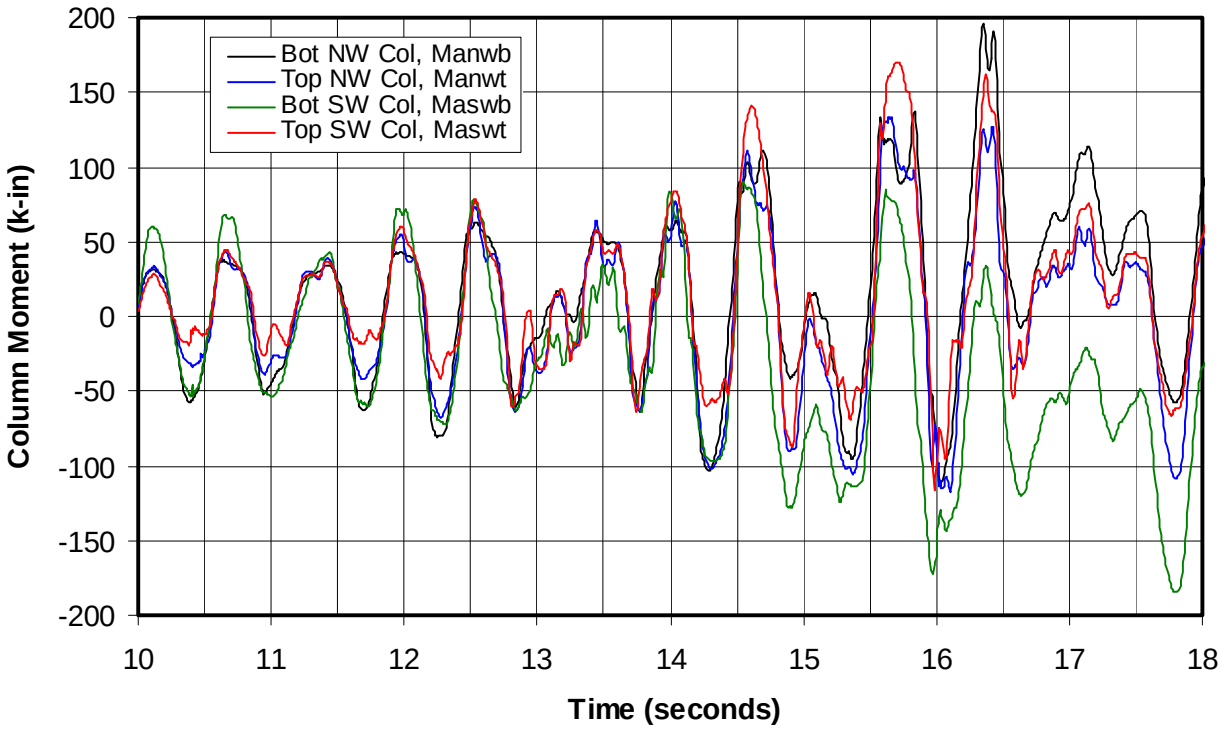

Before 12 seconds, the moments at the bottom of the columns are consistently greater for the southwest column, and also for the northwest column

when the model is deformed to the left (north), resulting in negative moments in Figure 8-65. The applied moments at the bottom of the columns are expected to be larger while the columns are behaving linearly, but after 12 seconds moments at the column tops equal or exceed values at the bottom, indicating that the columns have reached their yield capacities at their bottoms and that no greater moment resistance can be developed. After 16 seconds, the moments are inaccurate at both the bottom northwest column, M_{anwb}, and bottom southwest column, M_{aswb}, where they no longer oscillate about zero. This offset is due to the permanent offset in the column strains

Figure 8-66 plots the applied shear at the north and south columns of the first-story west shear panel. After 16 seconds, the shears at both columns are inaccurate where the northwest column shear, V_{anw}, is offset positively and the southwest column shear, V_{asw}, is offset negatively. The greatest shear prior to these offsets was at 15.7 seconds, where the northwest column reached 2.13 kips and the southwest column reached 2.08 kips.

Figure 8-66. Shear for first-story west shear panel columns, 100% SE32, 12–18 seconds.

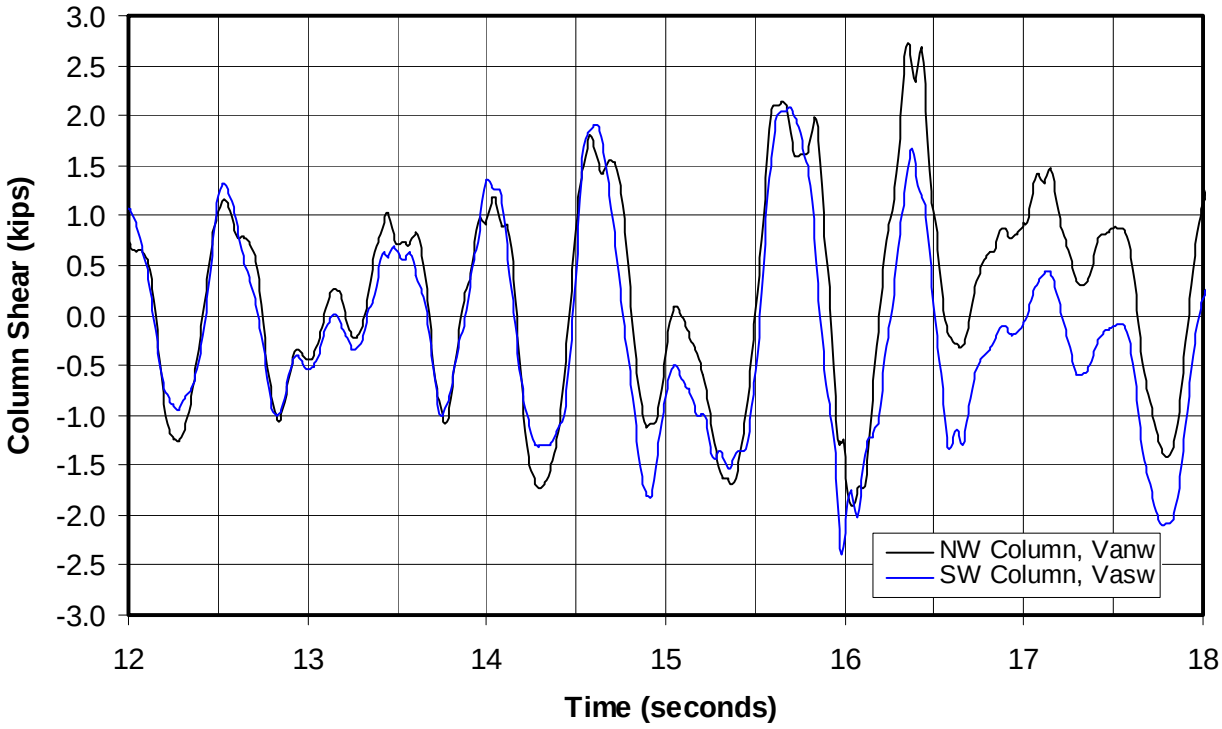

Figure 8-55 and Figure 8-56 plotted the story shear per shear panel, calculated based on the inertia forces defined by the model acceleration and

weight. This story shear at the first story carried by the columns is the total for the northwest and southwest columns, shown in Figure 8-66; and the portion carried by the diagonal straps is the amount in Figure 8-55 and Figure 8-56 minus the total carried by the two columns. For the cycle between 15.52 and 16.248 seconds shown in Figure 8-56, the total positive column shear was 4.21 kips at 15.7 seconds (Figure 8-66), which is 22% of the panel story shear of 19.45 kips (Figure 8-56). In the negative direction, the peak negative column shear at the southwest column is 2.40 kips at 15.98 seconds, but the calculated shear based on the columns strains is already offset by 0.5 kips in the negative direction, so a corrected estimate of the shear at this column is 1.9 kips. The peak negative shear at 16.04 seconds for the northwest column is 1.91 kips, giving a total negative shear at both columns of 3.81 kips, which is 20% of the negative panel story shear of 19.07 kips (Figure 8-56). The percentage of shear carried by the columns grew 10 and 9% in the positive and negative directions, respectively, in the linear 8% SE32 test to the values of 22 and 20% in this 100% SE32 test. This is because the contribution of the straps only increased from the linear 8% SE32 test to the point that the straps fully yielded, while the columns remained elastic almost to the full amplitude of the nonlinear 100% SE32 test. The added contribution of the columns after strap yielding can be seen graphically in the story shear (lateral load) versus story drift plot shown previously in Figure 8-55. A bilinear approximation or envelope of the panel capacity shown in that figure suggests the straps had fully yielded at 0.6 seconds.

8.10 Shake table model damage observations following cyclic tests

Following the 100% SE32 nonlinear test the natural frequency of the model was 0.5 Hz, based on random-motion shake table tests. In the low-level random tests only, the model columns at the first floor would have contributed to the stiffness of the model because the diagonal straps were significantly elongated and slack. Therefore, the model stiffness was much lower, explaining the decrease in the first mode of vibration frequency from 1.65 Hz to 0.5 Hz. The model was next tested using sinusoidal motions at the model new natural frequency of 0.5 Hz, in order to cause even greater deformation of the model. However, these tests resulted in relatively minor increased lateral deformation. The model behaved as a 0.5 Hz SDOF oscillator with a 115.1 kip mass at the top of the first-story columns. The model acceleration needed to produce lateral deformation large enough to further elongate the diagonal straps can be approximated by determining the acceleration of the oscillator that is large enough to produce

absolute first-floor displacements equal to the greatest measured displacements in 100% SE32 test. This approximation is fairly crude because it assumes that the dynamics of the model and the ratio of the greatest first-story drift over the absolute displacements in the 100% SE32 test are proportional to the same ratio in the 0.5 Hz sinusoidal tests. The expression below can be used to calculate this approximate acceleration, a_{SDOF}:

$$a_{SDOF} = \frac{d_{1stFloor}(2\pi f_{SDOF})^2}{386 in/sec^2/g} \quad \text{(Eq 8-11)}$$

where

$d_{1stFloor}$ = the peak absolute displacement from the 100% SE32 test. Close inspection of Figure 8-48 and Figure 8-49 show this is 2.26 in. at 15.656 seconds.

f_{SDOF} = 0.5 Hz as measured in the random shake table test described above.

At this low frequency of 0.5 Hz, Equation 8-11 shows that the model acceleration that would lead to the diagonal straps becoming taut again is only 0.058 g, which is much less than the higher frequency and much higher accelerations (see Figure 8-47) that produced the inertia forces (see Figure 8-55). The 115 kip model responding as a SDOF oscillator at 0.058 g would apply lateral forces of only 3.33 kips per shear panel. These forces are much less than the lateral forces required to further elongate the diagonal straps. These forces are actually even less than the restoring forces from the columns approximated from the column strain gages (i.e., 4.2 kips in the positive direction or 3.8 kips in the negative direction). When testing with sinusoidal motions at 0.5 Hz, there would be a sudden impact loading increase in force in the diagonal straps when their slack is overcome, but this force would almost certainly not be enough to exceed the full lateral capacity that still is available in the straps and columns. At the very small accelerations of only 0.058 g, the velocities would also be small. As the amplitude of the sinusoidal base motions at 0.5 Hz were increased, the straps "caught" the oscillating mass, so that sinusoidal motions at 0.5 Hz never did amplify significantly in the model. If higher-frequency sinusoidal or other shake table motions were used to excite the model, the low-frequency lightly damped 0.5 Hz model would isolate the model from these motions. Therefore, the only way to deform the model further with shake table base motions appeared to be use of higher-frequency motions whose displacement amplitudes exceeded the existing first-story de-

formation of the model. Because of the stroke limitations of the TESS in the in-plane direction (2.75 in. or 5.5 in. peak to peak), this could only have been done using very artificial motions of the shake table. In a single half-cycle test, the TESS could have been offset completely in one in-plane direction and then quickly displaced close to the full 5.5 in., thereby exceeding the first-story drift equivalent to the slack diagonal straps. In such a test the TESS and model base beam would have moved quickly, and the SDOF model would have been isolated from these motions, slowly tailing behind until the straps tightened. This would have caused larger deformation of the model in the one direction tested, with first-story deformations perhaps as great as 5 in. This process could have been repeated in the other direction, but the test would provide little value for comparing the DRAIN 2DX analysis with the nonlinear response of the model. Therefore, the 100% SE32 test was judged to have produced the best experimental results to compare its measured large deformation with the DRAIN 2DX analysis. The test was also very useful to evaluate the ductile performance of the model under large nonlinear deformations.

Several observations of the performance of the model can be made from pictures taken after the 0.5 Hz sinusoidal tests were completed. These sinusoidal tests did cause minor additional damage to the column (local buckling) and column anchors. Figure 8-53 and Figure 8-54 provided the best overall view of the deformed model at the greatest lateral deformation. These figures show significant elongation in the diagonal straps that are taut in one direction and slack in the other. The columns and anchors did experience somewhat greater damage at the south column of the west shear panel and the south column of the east panel. Figure 8-67 shows the bottom of the southeast column facing west toward the interior of the model. Local elastic buckling can be seen near the column knockout near the top of this photograph. When the model was deformed laterally to the south (left in Figure 8-67) the diagonal strap connected to the top of this column would be loaded in tension, applying compressive forces to this column. At this same time the column would be deformed in bending so that the compression side of the column is the face shown with the knock-out in Figure 8-67. Deformation to the south is the same direction as positive drift in Figure 8-51 and Figure 8-52. Figure 8-51 and Figure 8-52 show the model reaches a peak positive first-story drift in the 100% SE32 test at 15.728 seconds.

Figure 8-67. Bottom of southeast column facing west, showing local column buckling and anchor and column bending at top of the anchor.

The columns of the east shear panel were not instrumented, but Figure 8-16 shows the that S22z strain gage was on the south face of the south-west column, and this column would have been similarly loaded at the same point in time as the southeast column. The top of the knockout shown Figure 8-67 is 12 in. above the bottom of the column, so the S22z strain gage was centered 16 in. above the top of a similar knock-out in the southwest column. Figure 8-63 shows that the S22z strain gage shows a negative (compressive) peak strain measurement near 15.728 seconds (peak value of -702 microinches/in. at 15.72 seconds). Since the knockouts are closer to the bottom of the columns, the compression strains near

them would be greater than at S22z. They would have been further increased due to the stress concentration around these knockouts.

Local column bending can also be seen in Figure 8-67 at the center of the column south face directly above where it is welded to the horizontal top edge of the anchor angle. Close inspection of Figure 8-67 shows that the top of the angle is bent to the north at both the east and west faces of the column. This minor local inelastic deformation of both the column and the anchor is part of the intended behavior of the anchor-to-column connection configuration under load when the connected diagonal strap is in tension. Even if the diagonal strap material has a yield strength equal to its maximum value, F_{symax}, the column-to-angle connection must resist the load applied without fracture. Still, the local yielding and deformation shown in Figure 8-67 is good because it would dissipate energy in large seismic events. The load path facilitated through the strap-to-column and column-to-anchor connection configurations is intended to permit large nonlinear deformation without risk of brittle failure.

A shear panel can be designed with diagonal straps on either one or both faces. When the panel racks laterally in an earthquake, the diagonal straps in tension load the face of the column to which they are connected in shear. Like the welded connection shown in Figure 8-67, these connections should be centered below the top of the anchors so that a direct load path exists between the application of shear load to the column face and the resistance provided by the anchor. The column face then only needs to resist these shear forces locally in tension. It is critical that much of the strap is connected to the outside stud of the column (left stud in Figure 8-67) because this stud is welded to the anchor. It is also important that the column intermittent welds at the ends of the columns are placed at the column ends, behind the track, so that loads applied to the other studs at the strap welds will be carried directly between the studs in tension into the exterior stud that is in turn welded to the anchor, or in compression through the studs and groove welds that connect them.

The load path between the strap-to-column connection, along the column face where the corner of the column is welded with a vertical groove weld to the edge of the anchor edge, is all very rigid and will behave elastically in seismic motions. Some of the lateral load in the column coming from the strap connected to the interior column studs will carry this load in tension through the weld to the anchor into the horizontal portion of the an-

gle at the bottom of this connection, which is in turn carried directly into the concrete foundation or diaphragm in friction or is carried to the anchor bolts through this bottom portion of the angle in tension. A portion of this load is also carried in compression into the interior anchor at the interior side of the column. These portions of the load path are also fairly rigid, especially in tension to the exterior anchor, but much of the load will be carried into the anchor above these horizontal portions of the angle. Most of the remaining lateral load will be carried to the foundation or diaphragm through the vertical welds between the exterior anchor angle and the exterior stud, or to the horizontal weld along the top edge of the angle. These vertical welds are 3.5 in. tall in Figure 8-67 and the horizontal weld is 6 in. long (i.e., depth of the panel). The load path or stress flow between the column and the anchor is dependent on the relative stiffness of the column face welded to the anchor and the vertical leg of the anchor. The vertical leg of the anchor is stiffened with a triangular in-plane vertical stiffener plate, which is positioned at the center of the anchor in the out-of-plane direction as shown in Figure 8-67. This stiffener plate is very rigid in carrying lateral load in tension and also uplift forces down into the anchor bolts. The ductility in this joint is introduced by the flexural deformation of the vertical leg of the angle and the face of the column to which it is welded. The tensile force from the straps pulls through the column corners and applies bending load to the vertical edges of the angles. This causes them to deform in bending and even yield if the full maximum strength exists in the straps. However, the anchor welds, stiffening plate, and anchor bolts are designed to support significant yielding in this vertical leg of the anchor without loss of capacity. These anchors will only deform in the direction that the tension-only straps pull. The vertical legs of the anchors on the interior side of the columns could possibly also be loaded to the point of yielding, through the columns in horizontal compression, but only after significant deformation of the more rigid tensile load path to the exterior anchors.

The anchor bolts are placed very close to this stiffener plate to provide a relatively direct and rigid load path between the stiffener plate and anchor bolts. A small amount of flexural deformation could take place in the horizontal leg of the anchor near the anchor bolts, due to prying action, but even this deformation would be ductile if it were to exceed the yield capacity of the anchor.

Figure 8-68 shows the bottom of the southwest column facing northeast, and Figure 8-69 zooms in on the same column anchor connection at the top of the anchor angle. The diagonal strap-to-column weld connections were undamaged at all these connections even though the weld lengths were the minimum needed to develop the capacity of the straps. The discussion prior to Table 8-11 explained that the maximum strap force, P_{su}, was actually slightly greater than the welded connection capacity in order to test the ability of these welds to perform at their design limit, thereby verifying the welded connection design recommendations. The bottom-right corner of Figure 8-67 shows this connection at the bottom of the southeast column, and left side of Figure 8-68 shows it at the bottom of the southwest column.

The discussion prior to Table 8-13 explained that the height of the angles, H_A, was only 3.5 in. so that the total angle weld strength, P_A, would barely exceed the maximum applied tensile force per anchor angle ($P_{vymax}/2 + P_M$) at the first-floor anchors. Therefore, this 100% SE32 test verified the weld design recommendations for these anchor connections.

Figure 8-68. Bottom of southwest column facing northeast, showing local column buckling and anchor and column bending at top of the anchor.

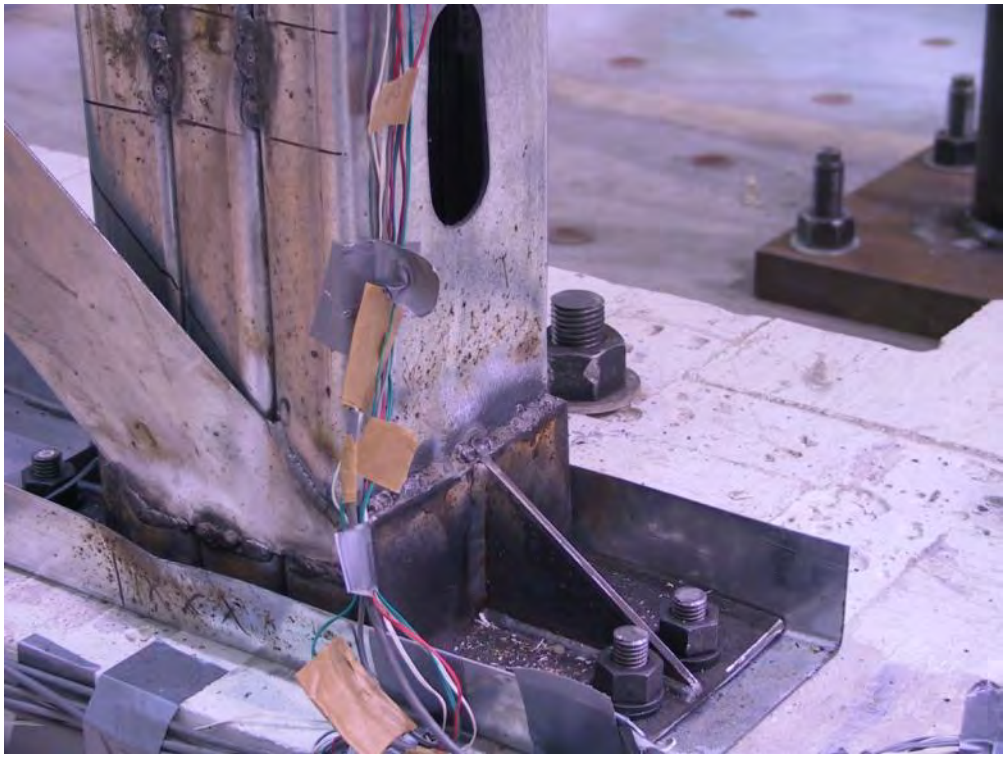

Figure 8-69. Zoomed in view of the vertical anchor leg
and stiffener plate at the bottom of the southwest column, facing northeast.

Figure 8-68 and Figure 8-69 show that bending of the vertical leg of the anchor and column where it is welded to the top of the anchor is greater here than it was at the southeast column. When the attached strap is in tension, it pulls the top corners of the vertical leg of the angle so that it deforms in bending, while the center of the anchor and attached column is held back by the stiffener plate. Then when the model racks back in the other direction, the column is loaded with large compressive forces, and it buckles locally near the stiffener plate because the relatively thin column steel has already been deformed out in the direction of the stiffener plate. However, there is no risk of buckling the entire column because of the bracing that comes from the column shape and the support of the vertical leg of the angle.

The 100% SE32 shake table test of a two-story model provided significant nonlinear response that could be compared with the ability to analytically predict both the deformation-based demand and capacity using the DRAIN 2DX analysis for cold-formed steel construction. This test also provided data to validate the cold-formed steel seismic design provisions that are presented in Part II of this report. The cyclic tests presented in an earlier chapter together with the shake table test presented in this chapter demonstrate that cold-formed steel shear panels can be designed to re-

spond in a ductile way, effectively resisting the lateral loads applied to them at very large lateral drifts. This provides the justification needed for use of the recommended response modification coefficient, R, of 4. Because of the significant contribution of the column moment frames, the R coefficient could arguably be increased to 5, but a coefficient of 4 is still conservatively recommended.

9 Special Design Considerations for Seismic Loads

The philosophy underlying building design for seismic loads may be unknown to or misunderstood by some structural engineers, even those practicing in regions of significant seismic activity. Familiarity with special design considerations for seismic loads can help to clarify certain code specifications and identify potential design errors that may, on the surface, appear to comply with the code.

Wind loads are well understood by structural engineers. Statistics on wind velocities are recorded regularly and have been for nearly 100 years. Once the design return period for wind is decided by code officials — usually 300-, 700-, or 100-year wind velocities (ICC 2011, Figures 1609A through 1609C) — the horizontal and vertical wind pressures can be calculated for design from simple equations that appear in the building code. The structural engineer includes these forces with dead, live, and other loads, and designs the building to remain elastic under the factored load combinations. The design resistance is reduced by a resistance factor, ϕ, to account for uncertainties in material properties. The load and resistance factors take the place of factors of safety used in earlier codes.

Incorporating seismic resistance specifications within this design framework is difficult for two reasons: (1) the effective seismic loads on the building that would arise due to the "design earthquake" are much greater than all of the other referenced loads and (2) they occur less frequently than the design wind load. If buildings were designed to remain elastic under the design earthquakes, the design forces would be as much as eight times greater than those currently used. This would place a large economic burden on society for the purpose of addressing seismic forces that have only a very small probability of occurring during a building's life cycle.

The current design codes are based on a maximum considered earthquake (MCE) earthquake with a return period of 2,475 years. Such an earthquake has a 2% probability of exceedance in 50 years. These forces can be compared to wind loads that have a 700-year return period.

Earthquake ground motions are both horizontal and vertical, causing building deformation and inertial loading in both directions. All of the building's mass contributes to the seismic inertial forces that occur. The dynamic response of the building amplifies ground motion, producing greater inertia forces than might be calculated by simply multiplying the ground acceleration by the building mass.

The design base shear used for building design has a coefficient, R, that appears in the denominator. This is called the *response modification coefficient*. If this coefficient were taken as 1.0, that would represent the force for which the building would have to be designed in order for the building to remain elastic under the design earthquake. In the current seismic design provisions, this coefficient may be as large as 8 for some structural systems. So it is obvious that a great deal of damage will occur in these buildings when a large earthquake occurs.

The value of R that is specified for a building type depends on

- the redundancy of the vertical load-carrying system
- the redundancy of the horizontal load-carrying system
- the expected overstrength of the building
- the ductility capacity of the building type
- the building occupancy type
- acceptable risk.

Shown in Figure 9-1 are idealized models of building frames, the first using cold-formed steel members with diagonal straps for cross-bracing. The diagonal straps resist lateral forces. The member joints themselves behave as pinned connections. The gravity frames also behave as if all of the connections are pinned. Therefore, the diagonal straps must provide all of the stability against collapse under gravity loads and also resist horizontal forces arising from wind or earthquakes. As a result, if the diagonal straps fracture or lose their lateral load-carrying capability, the building may readily collapse. This type of structural system is referred to as a *bearing wall system*.

Figure 9-1. Idealized models of building frames.

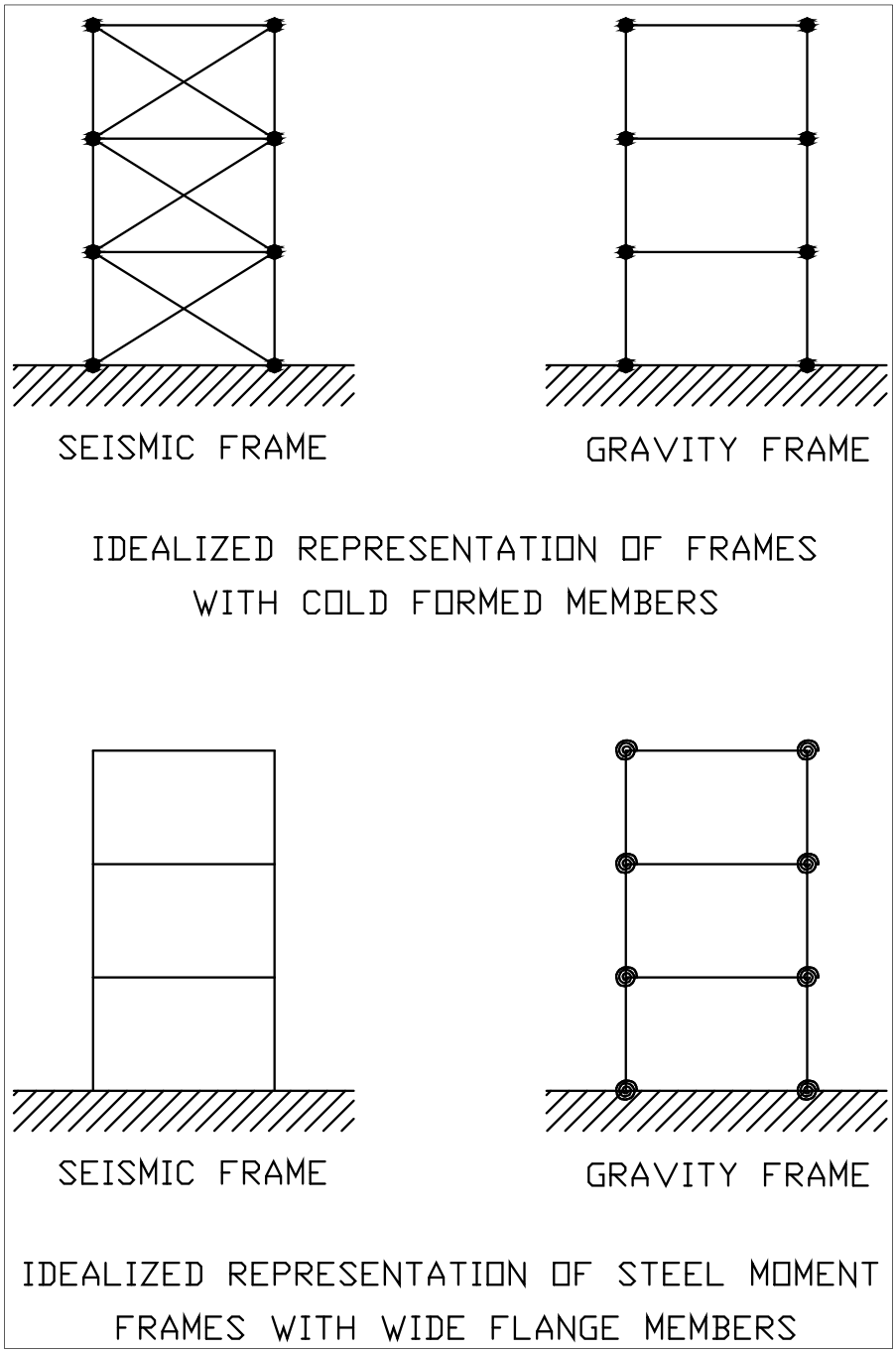

For a moment frame, all of the lateral forces are resisted by frame action, which results in shear and moment developing in the beams and columns under wind or earthquake loads. Usually only two or three frames in each direction are designed as moment frames. The rest are gravity frames. The schematic of a typical gravity frame is shown in the bottom drawings of Figure 9-1. Although the beam-to-column connections are assumed to be

pinned, they can actually develop significant moments. The mechanism for this is shown in Figure 9-2. The web shear connections, acting alone or in composite behavior with the floor slab, are able to develop significant moment resistance. As a result, the building will be able to stand up under gravity loads even if all of the moment connections in the moment frame fail during the earthquake. Thus, there is much redundancy against gravity loads in the moment frame building.

Figure 9-2. Schematic drawing showing unintended moment resistance in gravity frames with wide flange members.

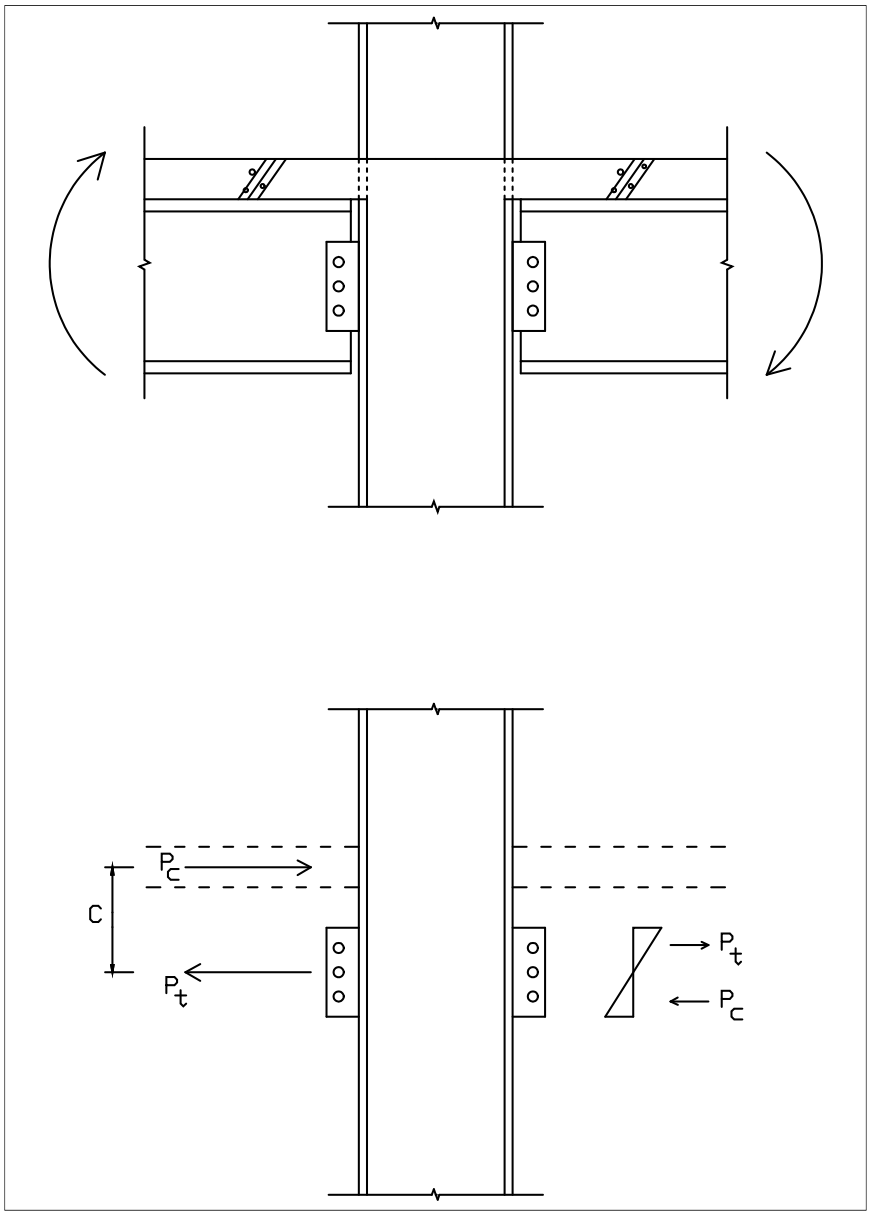

There is a rule of thumb in seismic design that is only approximately true, but which is useful for describing the function of ductility in seismic design. If a horizontal force, Q_E, taken from the elastic response spectrum of an earthquake is applied to a structure, an elastic displacement that can be called δ_E will occur. This means that if the earthquake actually occurred, the maximum deflection would be δ_E. If the structure is only designed to withstand a force of $Q_y = Q_E/\mu$ where μ is greater than 1.0, then the maximum displacement during the earthquake will be $\mu\delta_y$ where δ_y is the yield displacement that would occur if a static force is applied equal to Q_y; and μ is the *ductility factor*, which is the maximum displacement divided by the yield displacement. As a result, the larger the ability of a structure to experience lateral displacement beyond yield without failure, the greater is its ductility capacity. The larger the ductility capacity of a structure, the smaller is the seismic design force that can be used in its seismic design without risk of catastrophic failure.

Based on this discussion, one could infer that the response modification coefficient, R, is equal to the ductility factor, μ. This is not the case, however, because the actual effective strength of a building should always be greater that the design strength. This extra strength comes from many sources, including architectural partitions, stairway structures, piping, cladding, moment redistribution resulting from redundancy, material overstrength, material strain hardening, and gravity frames. The most important of these are the last three.

The total (inelastic) lateral strength of a typical cold-formed steel building may be two times greater than the design value while the total strength of a moment frame building may be six times greater than the design. This assumes that only material overstrength, strain hardening, gravity frames, and moment redistribution are considered. This extra strength beyond design means that the displacement experienced by the building under the design earthquake will be less than $R\delta_y$, because the strength is greater than Q_y. This is also why the deflection amplification factor C_d is needed and why C_d is always less than R. The strength for design is $Q_y = Q_E/R$, but the expected displacement is only $\delta_{max} = C_d\delta_y$, not $R\delta_y$.

So for a given building system, the value of R is greater if its ductility capacity is greater. The value of C_d will be smaller than R as a function of the expected overstrength. For a special moment frame, the large value for R (equal to 8) is because it has a large ductility capacity, great redundancy

for gravity loads, and it is expected to possess substantial overstrength. The value of C_d is small compared to R because it has large overstrength. For the cold-formed steel frame, the ductility capacity is large but the redundancy against collapse under gravity loads is small. As a result, R equals 4 for a cold-formed steel frame. Because the overstrength for a cold-formed steel frame is not substantial, the value of C_d equal to 3.5 is only slightly smaller than R.

10 Summary and Recommendations

This chapter concludes Part I of this technical report, which documents the technical basis for effective seismic design using cold-formed steel materials. Below is a summary of the results and areas for further research.

10.1 Summary

Previous cold-formed steel research and seismic design guidance developed by the AISI may not produce the desired ductile performance for load-bearing applications. Cold-formed steel has high strength variability, and light-gage materials are vulnerable to local buckling. Together, these characteristics can lead to brittle failures and collapse of buildings constructed with these materials. In the 1990s, USACE observed poor detailing and construction practices, which led to a moratorium on the use of cold-formed steel for load-bearing construction.

This report reviews previous CFS design research by others; presents a design philosophy encompasses special considerations for seismic loading; defined shear panel configurations; develops a design model and test panel specimens; defines material properties; defines test panel configurations and tests results that demonstrate ductile behavior; develops seismic design recommendations; and verifies those recommendations through shake table testing. Preliminary design recommendations emerging from USACE-funded research led to the lifting of the Corps moratorium on CFS construction. The data produced by the studies documented in Part I of this report serve as the basis for the detailed CFS design recommendations presented in Part II, which follows the conclusion of this chapter.

10.2 Recommendations

The test panels and design recommendations provided in this report focused on shear panels with diagonal straps as the primary lateral-load-resisting element. Other configurations that were considered in Chapter 2 used full-panel steel sheets as the lateral-load-resisting element. Further research on the G and H panel configurations is recommended. Those configurations use welded connections to fasten a steel sheet to the panel framing. The weld strength should always exceed the strength of the sheet material, so that an increase in strength of the steel sheet should require a

proportionately greater strength in the welded connection to the sheet. Chapter 2 presented two configurations: (1) the G configuration, in which the columns are built up from studs, similar to the C1 test panels; and (2) the H configuration, in which the columns are hollow structural sections (HSS). Effective design with either configuration should result in panels with greater overstrength than any of the diagonal strap configurations, because as the sheet yields, the diagonal tension field should widen, increasing the panel strength. These panels should also dissipate more energy, because as the panel deforms in the opposite direction after a peak excursion, the sheet will be buckled perpendicular to the tension field and the buckles will be forced to straighten out, picking up some load in the process. This should result in the load versus deflection hysteretic plots being less pinched than the diagonal-strap panels. The steel sheet welded to both the columns and heavy track that is braced by the anchors would also add to the column moment frame stiffness, further increasing the energy dissipation after a peak excursion. The steel sheet must be pulled taut before welding to the frame. Below are more thoughts about promising configurations using these two panel types that warrant further investigation.

10.2.1 Panel G

The panel G configuration uses columns built up from studs and anchors similar to those used in the panel C1 configuration. The sheet should be welded around its entire perimeter to the columns at the sides and to the track at the top and bottom. The track should be very heavy, and would be braced at the interior of the columns with the column anchors. The diagonal tension field should develop at close to a 45 degree angle, so panels that have an aspect ratio of 1 would be most efficient. Panels that are slightly taller, will result in increased bending load applied to the columns, while shorter panels will apply greater loads to the tracks. Even the heavy tracks should not be loaded significantly in bending. Initially the tension field will be relatively narrow, but it would widen as the sheet yields and elongates. This would result in greater loading of even the unbraced portions of the track. Therefore, it is likely that panels which are slightly taller than they are wide (i.e., aspect ratio greater than 1) would be more effective. The earlier test panels demonstrated that the diagonal straps should not be spot welded to the interior studs. Therefore, the interior studs resist only a relatively small portion of the gravity loads. For panels that have an aspect ratio much greater than 1, a mid-height horizontal compression member should be installed that should reduce bending loads on the col-

umns. As stated in Chapter 2, a method is needed to define the width of the diagonal tension field. Therefore, the research needed would require both analytical studies (e.g., Abaqus finite element analysis) and experimental testing of shear panels to define this width. The tension field width would be influenced by the thickness of the sheet and relative stiffness of the sheet and panel framing. Panels with varying dimensions of sheet thickness, frame thickness and stiffness, and aspect ratios, with and without mid-height compression members should be designed and tested. The maximum strength of the steel sheet material must be considered. Guidelines would need to be developed for designing panels of this type in a proportionate way so that the steel sheet yields significantly without any brittle failures of the sheet welded connections, columns, tracks, or anchors.

10.2.2 Panel H

The H configuration panel is identical to the panel G, except it uses HSS members for the columns. These columns would be thicker than the G columns that are built up from studs. The greater thickness would make these columns less vulnerable to tearing at the welded connections to the sheet and anchors. The heavier columns would also be less vulnerable to local buckling.

PART II:
DESIGN RECOMMENDATIONS
AND
EXAMPLE

11 Seismic Design Recommendations for Shear Walls (Diagonal Strap Systems)

The seismic design recommendations provided here may be used for all occupancy categories as defined in ASCE/SEI 7-10, "Minimum Design Loads for Buildings and Other Structures" (ASCE/SEI 7-10, Table 1.5-1), subject to the limitations presented in this chapter.

Seismic design with cold-formed steel has two problems that are inherent with the material itself: (1) light gage thickness and (2) variability in material strength. The objective of seismic design recommendations is to ensure ductile building system performance in the large seismic event and elastic response in the small seismic event or wind loading. Ductile building performance requires that selected ductile components yield but continue to carry loads and absorb energy through significant plastic response. At the same time, potentially brittle failure modes such as column buckling or connection failure must be prevented. The design challenge for cold-formed steel is to ensure that building components, and in particular shear panel components, be proportioned relative to each other and detailed so that the ductile response is ensured. In these design recommendations, ductile response is accomplished by ensuring that the diagonal straps yield and respond plastically through significant displacement, without risk of column buckling or damage to brittle connections.

Seismic design recommendations are provided on three levels:

1. Tabular data for prototype shear panels in terms of the maximum story shear and maximum and minimum gravity load as defined in this chapter. The shear panel configurations and data are provided in Appendix C.
2. Detailed seismic design recommendations using shear panels with diagonal straps as the primary lateral-load-resisting element. The recommendations are documented in this chapter, and an example application of the recommendations is given in Chapter 12[5].

[5] The spreadsheet program used in the example problem is available through the Network for Earthquake Engineering Simulation (NEES) Data Repository (http://nees.org/warehouse) as an engineering support tool for shear panel design.

3. A test procedure and acceptance criteria for other shear panel configurations, which are provided in Appendix D.

The design recommendations presented here are directly related to ASCE/SEI 7-10, *Minimum Design Loads for Buildings and Other Structures*. The technical basis for unique CFS seismic design recommendations is the topic of Part I of this report. These recommendations also incorporate material from the references listed below:

- *AISI Manual: Cold-Formed Steel Design* (AISI 2008)
- "Cold-Formed Steel Light-Frame Construction" (ICC 2011)
- *Recommended Seismic Provisions for New Buildings and Other Structures* (NEHRP 2009)
- "Standard Specification for Steel Sheet, Carbon, Metallic- and Nonmetallic-Coated for Cold-Formed Framing Members" (ASTM 2013b)
- *Steel Construction Manual* (AISC 2011)
- "Specification for Structural Steel Buildings" (AISC 2010a)
- "Seismic Provisions for Structural Steel Buildings" (AISC 2010b)
- *Guide for Design of Anchorage to Concrete: Examples Using ACI 318 Appendix D* (ACI 2011b)

Figure 11-1 is a process flowchart for seismic design using cold-formed steel shear walls. Chapter 12 explains an example problem showing the application of the recommendations presented in this chapter.

Figure 11-1. Flowchart for cold-formed steel shear panel seismic design.

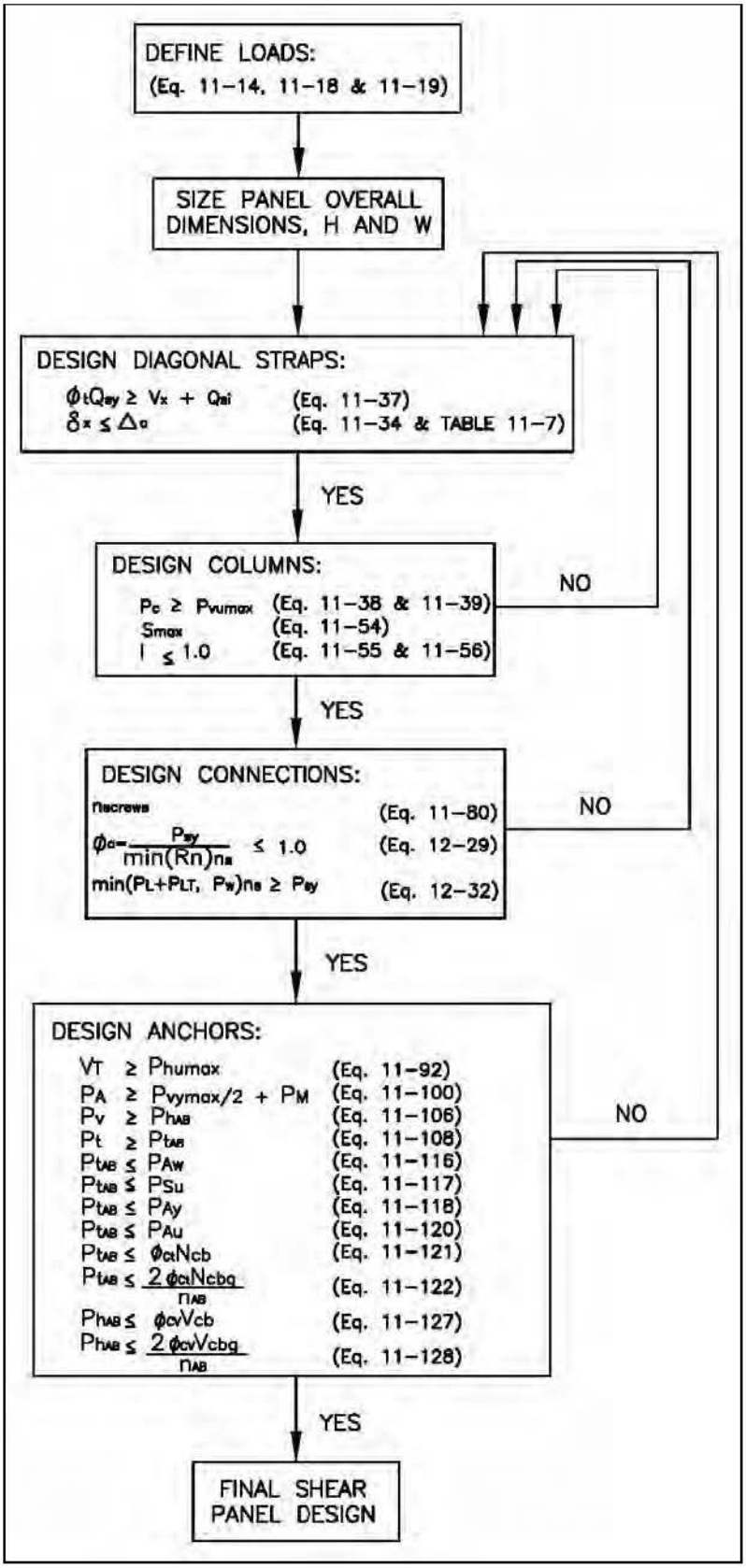

11.1 Risk category

The risk category of a building shall be determined in accordance with Table 1.5-1 of ASCE/SEI 7-10. The risk categories are based on the risk to human life, health, and welfare associated with building damage or failure by nature of their occupancy or use (ASCE/SEI 7-10, section 1.5.1). The categories vary from least critical (category I) to the most critical (category IV).

11.2 Importance factors

Seismic importance factors, I_e, are defined for buildings based on their risk category in ASCE/SEI 7-10, Table 1.5-2). These importance factors are summarized in Table 11-1 for seismic loads only.

Table 11-1. Seismic importance factors based on ASCE/SEI 7-10 risk category.

Risk Category (ASCE/SEI 7-10, Table 1.5-1)	Seismic Importance Factor, I_e
I	1.00
II	1.00
III	1.25
IV	1.50

11.3 Defining ground motion

Seismic ground motions shall be defined according to ASCE/SEI 7-10, section 11. This paragraph defines spectral response accelerations, S_s and S_1, for 0.2 and 1 second, respectively, in Figures 22-1 through 22-6 on U.S. Geological Survey (USGS) website http://earthquake.usgs.gov/hazards/designmaps/. Site classifications (A through F) shall be determined based on soil properties as defined in ASCE/SEI 7-10, Chapter 20. But if soil properties are not known, Site Class D shall be used. From the site classifications, values of site coefficients (F_a and F_v) are determined for the mapped spectral response acceleration values in ASCE/SEI 7-10, Table 11.4-1 and Table 11.4-2. These tables are reproduced below as Table 11-2 and Table 11-3.

Table 11-2. Values of F_a as a function of site class and mapped 0.2-second period maximum considered earthquake spectral response acceleration.[6]

Site Class	Mapped Risk-Targeted Maximum Considered Response (MCER) Spectral Response Acceleration Parameter at Short Period				
	SS ≤ 0.25	SS = 0.50	SS = 0.75	SS = 1.00	SS ≥ 1.25
A	0.8	0.8	0.8	0.8	0.8
B	1.0	1.0	1.0	1.0	1.0
C	1.2	1.2	1.1	1.0	1.0
D	1.6	1.4	1.2	1.1	1.0
E	2.5	1.7	1.2	0.9	0.9
F	a[7]	a	a	A	A

Table 11-3. Values of F_v as a function of site class and mapped 1-second period maximum considered earthquake spectral response acceleration.[8]

Site Class	Mapped Risk-Targeted Maximum Considered Response (MCER) Spectral Response Acceleration Parameter at 1-s Period				
	S1 ≤ 0.1	S1 = 0.2	S1 = 0.3	S1 = 0.4	S1 ≥ 0.5
A	0.8	0.8	0.8	0.8	0.8
B	1.0	1.0	1.0	1.0	1.0
C	1.7	1.6	1.5	1.4	1.3
D	2.4	2.0	1.8	1.6	1.5
E	3.5	3.2	2.8	2.4	2.4
F	a[9]	a	a	a	a

The maximum considered earthquake (MCE_R) spectral response acceleration for short periods (S_{MS}) and at 1 second (S_{M1}), adjusted for site class effects, are calculated as follows (ASCE/SEI 7-10, Eq 11.4-1 and 11.4-2):

$$S_{ms} = F_a S_S \quad \text{(Eq 11-1)}$$

and

$$S_{M1} = F_v S_1 \quad \text{(Eq 11-2)}$$

[6] Use straight-line interpolation for intermediate values of S_S.

[7] a indicates site-specific ground motion procedure set forth in ASCE/SEI 7-10, Chapter 21, are to be used.

[8] Use straight-line interpolation for intermediate values of S_1.

[9] a here has the same meaning as for Table 11-2.

These values define the elastic spectra and are reduced to define design earthquake spectral response acceleration at short periods, S_{DS}, and at 1-second period, S_{D1}, as follows (ASCE/SEI 7-10, Eq 11.4-3 and 11.4-4):

$$S_{DS} = \frac{2}{3} S_{MS} \quad \text{(Eq 11-3)}$$

and

$$S_{D1} = \frac{2}{3} S_{M1} \quad \text{(Eq 11-4)}$$

From these terms, a design response spectrum is developed (ASCE/SEI 7-10, section 11.4.5 and Figure 11-4-1). (See Figure 12-1 for an example of a response spectrum plot for building in the design example.) For the natural period of the structure, T, this spectrum defines values of effective acceleration. The three regions of this spectrum are defined as follows:

For periods less than or equal to T_0, the design spectral response acceleration, S_a, shall be (ASCE/SEI 7-10, Eq 11.4-5):

$$S_a = S_{DS}\left(0.4 + 0.6\frac{T}{T_0}\right) \quad \text{(Eq 11-5)}$$

For periods greater than or equal to T_0 and less than or equal to T_S, the design spectral response acceleration, S_a, shall be taken as equal to S_{DS}.

For periods greater than T_S and less than or equal to T_L, the design spectral response acceleration, S_a, shall be (ASCE/SEI 7-10, Eq 11.4-6):

$$S_a = \frac{S_{D1}}{T} \quad \text{(Eq 11-6)}$$

For periods greater than T_L, S_a shall be (ASCE/SEI 7-10, Eq 11.4-7):

$$S_a = \frac{S_{D1} T_L}{T^2} \quad \text{(Eq 11-7)}$$

where:

T = the fundamental period of the structure in seconds,
T_0 = $0.2 S_{D1}/S_{DS}$, and
T_S = S_{D1}/S_{DS}.

T_L = long-period transition period, in seconds, shown in ASCE/SEI 7-10, Figure 22-12 through Figure 22-16.

11.4 Seismic design category

Each structure shall be assigned a seismic design category based on its risk category and design earthquake spectral response accelerations, S_{DS} and S_{D1}, as indicated in Table 11-4 and Table 11-5 (reproduced from ASCE/SEI 7-10, Tables 11.6-1 and 11.6-2).

Table 11-4. Seismic design category based on short period response acceleration parameter.

Value of S_{DS}	Risk Category	
	I or II or III	IV
$S_{DS} < 0.167g$	A	A
$0.167g \le S_{DS} < 0.33g$	B	C
$0.33g \le S_{DS} < 0.50g$	C	D
$0.50g \le S_{DS}$	D	D

Table 11-5. Seismic design category based on 1-second-period response acceleration parameter.

Value of S_{DS}	Risk Category	
	I or II or III	IV
$S_{D1} < 0.067g$	A	A
$0.067g \le S_{D1} < 0.133g$	B	C
$0.133g \le S_{D1} < 0.20g$	C	D
$0.20g \le S_{D1}$	D	D

11.5 Structural design criteria

The basic lateral and vertical seismic-force-resisting systems considered here are diagonal-strap configurations (Panels A3, C1, and D2) shown in Appendix B. These are considered bearing-wall systems. The format of Table 12.2-1 (ASCE/SEI 7-10) is used in Table 11-6 to present the response modification coefficient, R, and deflection amplification factor, C_d. These values are used to calculate the base shear and design story drift. The overstrength factor, Ω_0, used in ASCE/SEI 7-10 is not included here because shear panel overstrength is accounted for by $\Omega_0 Q_E$ (in Equation 11-

17). This is the maximum lateral capacity of the shear panel based on the maximum estimated ultimate stress of the panel diagonal straps.

Table 11-6. Design coefficients and factors for seismic-force-resisting systems.

Seismic-Force-Resisting System	Response Modification Coefficient, R	Deflection Amplification Factor, C_d	Structural System Limitations Including Structural Height, h_n, (ft) Limits[10]				
			A&B	C	D	E	F
Bearing Wall System							
Light-gage cold-formed steel wall systems using flat strap bracing	4	3.5	NL	NL	65	65	65

The response modification coefficient, R, in the direction under consideration at any story shall not exceed the lowest value for the seismic-force-resisting system in the same direction considered above that story, excluding penthouses. Other structural systems (dual systems) may be used in combination with these cold-formed steel panels, but then the smallest R value for all systems in the direction under consideration must be used for determining the loads applied to the entire structure in that direction (ASCE/SEI 7-10, section 12.2.3), and the design shall comply with other requirements of ASCE/SEI 7-10, section 12.2.3. Another structural system may be used in the orthogonal direction with different R values, and the lowest R value for that direction only shall be used in determining loads in that orthogonal direction (ASCE/SEI 7-10, section 12.2.2).

11.6 Structural configuration and redundancy

ASCE/SEI 7-10 presents recommendations on diaphragm flexibility, configuration irregularities, and redundancy (ASCE/SEI 7-10, section 12.3). Diaphragms are considered flexible if the maximum lateral deformation of the diaphragm exceeds twice the average story drift of the associated story (ASCE/SEI 7-10, section 12.3.1.3).

A redundancy factor, ρ, shall be defined for all structures in each of the two orthogonal directions based on the extent of structural redundancy in the lateral-force-resisting system. For structures in seismic design categories B and C, the value for ρ shall be taken as 1.0. For structures in catego-

[10] NL = not limited. For metric units, use 20 m for 65 ft. Heights are measured from the base of the structure, which is the level at which the horizontal seismic ground motions are considered to be imparted to the structure.

ries D, E, and F, values for ρ shall be taken as 1.3 unless one of the following conditions is met, in which case ρ shall be taken as 1.0 (ASCE/SEI 7-10, section 12.3.4.2):

1. Each story resists more than 35% of the base shear in the direction of interest and the removal of an individual strap or connection thereto would not result in more than a 33% reduction in story strength, nor would the removal result in an extreme torsional irregularity Type 1b as defined in ASCE/SEI 7-10 (see ASCE/SEI 7-10, Table 12.3-3).
2. The structure is regular in plan at all levels and the seismic-force-resisting systems consist of at least two bays of seismic-force-resisting perimeter framing on each side of the structure in each orthogonal direction at each story resisting more than 35% of the base shear.

11.7 Load combinations

Consideration of combinations of loads in the two orthogonal directions is not needed.

The effects of gravity loads and seismic forces shall be combined in accordance with the factored load combinations as indicated below (ASCE/SEI 7-10, section 2.3.2).

$$1.2D + 1.0E + L + 0.2S \quad \text{(Eq 11-8)}$$

and

$$0.9D + 1.0E \quad \text{(Eq 11-9)}$$

where

D = the dead load
E = the earthquake load
L = the live load; the load factor on L in Equation 11-8 shall equal 0.5 for all occupancies in which L_o in ASCE/SEI 7-10 (ASCE/SEI 7-10, Table 4-1) is less than or equal to 100 psf (4.79 kN/m^2), with the exception of garages or areas occupied as places of public assembly
S = the snow load, which shall be taken as either the flat roof snow load (p_f) or the sloped roof snow load (p_s).

The earthquake load or seismic load effect for use in Equation 11-8 shall be determined in accordance with Equation 11-10 (ASCE/SEI 7-10, section 12.4.2):

$$E = E_h + E_v \quad \text{(Eq 11-10)}$$

The seismic load effect for use in Equation 11-9 shall be determined in accordance with Equation 11-11 (ASCE/SEI 7-10, section 12.4.2):

$$E = E_h - E_v \quad \text{(Eq 11-11)}$$

The effect of horizontal seismic loads, E_h, shall be defined as follows (ASCE/SEI 7-10, section 12.4.2.1):

$$E_h = \rho Q_E \quad \text{(Eq 11-12)}$$

The effect of vertical seismic loads, E_v, shall be defined as follows (ASCE/SEI 7-10, section 12.4.2.2):

$$E_v = 0.2 S_{DS} D \quad \text{(Eq 11-13)}$$

where

ρQ_E = the maximum horizontal force that could be resisted by the bracing
ρ = the redundancy factor
Q_E = the effect of horizontal seismic forces
$0.2 S_{DS} D$ = the vertical spectral acceleration effect of the seismic load
S_{DS} = the design spectral response acceleration at short periods
D = the effect of dead load.

The effects of gravity load (dead, live, and snow load) and seismic forces shall be combined as follows when the effect of gravity and vertical seismic loads are additive, by combining Equations 11-8, 11-10, 11-12, and 11-13 (ASCE/SEI 7-10, section 12.4.2.3):

$$(1.2 + 0.2 S_{DS}) D + \rho Q_E + L + 0.2 S \quad \text{(Eq 11-14)}$$

The effects of gravity load and seismic forces shall be combined as follows when the effect of gravity and seismic loads counteract each other, by

combining Equations 11-9, 11-11, 11-12, and 11-13 (ASCE/SEI 7-10, sections 2.2, 2.3.2, and 12.4.2.3):

$$(0.9 - 0.2S_{DS})D + \rho Q_E + 1.6H \quad \text{(Eq 11-15)}$$

The load factor on H shall be set equal to zero in Equation 11-15 if the structural action due to H counteracts that due to seismic loading. The term H in Equation 11-15 is the load due to lateral earth pressure, ground water pressure, or pressure of bulk materials when these pressures add to the effects of horizontal earthquake forces (ASCE/SEI 7-10, sections 2.2, 2.3.2, and 12.4.2.3).

For both expressions in Equations 11-14 and 11-15, the total horizontal force is ρQ_E. This force alone defines the total lateral load that must be resisted by the shear panel diagonal straps, and these elements should be sized based on this force.

The effect of horizontal seismic loads, E_{mh}, shall be defined as follows to account for diagonal strap overstrength:

$$E_{mh} = \Omega_o Q_E \quad \text{(Eq 11-16)}$$

where

Ω_0 = the system overstrength.

The term $\Omega_0 Q_E$ calculated in Equation 11-16 (ASCE/SEI 7-10, section 12.4.3.1) need not exceed the maximum force that can be developed in the diagonal straps based on the maximum estimated ultimate strength of these elements. This is expressed as follows:

$$\Omega_0 Q_E \leq Q_u = F_{sumax} n_s b_s t_s \frac{W}{\sqrt{H^2+W^2}} \quad \text{(Eq 11-17)}$$

where

F_{sumax} = the maximum ultimate stress of the diagonal straps, which equals 1.5 F_{su} for ASTM A1003/A 1003M Structural Grade 33 Type H (ST33H), Structural Grade 230 Type H [ST230H] steel (F_{su} = 310 MPa and 45 ksi), and 1.25 F_{su} for ASTM A1003/A

1003M Structural Grade 50 Type H (ST50H), Structural Grade 340 Type H [ST340H] steel (F_{su} = 448 MPa and 65 ksi)

n_s = the number of diagonal straps

b_s = the width of the diagonal straps

t_s = the thickness of the diagonal straps

W = the overall panel width

H = the overall panel height (see Figure 11-2 for a schematic panel drawing showing W and H).

Figure 11-2. Schematic of cold-formed steel shear panel model.

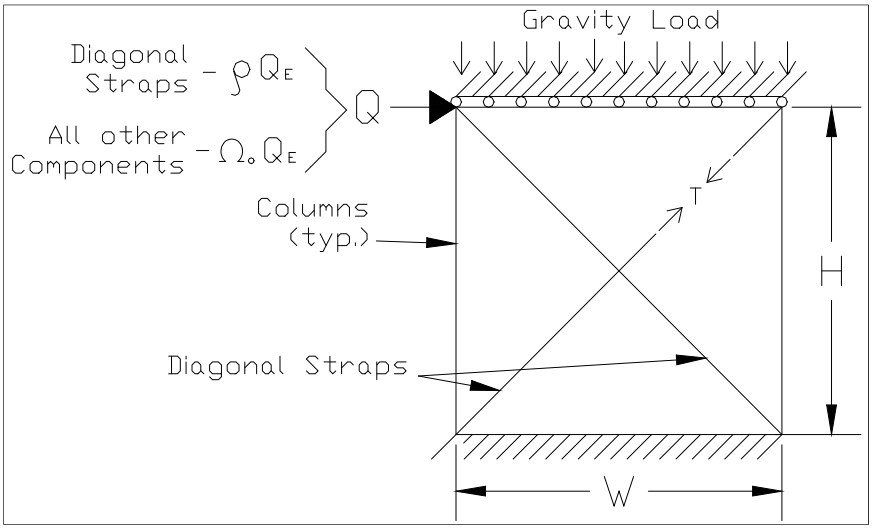

The effects of gravity load (dead, live, and snow load) and seismic forces shall be combined as follows to account for diagonal strap overstrength when the effect of gravity and seismic loads are additive by combining Equations 11-8, 11-10, 11-13, and 11-16:

$$(1.2 + 0.2S_{DS})D + \Omega_o Q_E + L + 0.2S \qquad \text{(Eq 11-18)}$$

The effects of gravity load and seismic forces shall be combined as follows to account for diagonal strap overstrength when the effect of gravity and seismic loads counteract each other by combining Equations 11-9, 11-11, 11-13, and 11-16:

$$(0.9 - 0.2S_{DS})D + \Omega_o Q_E + 1.6H \qquad \text{(Eq 11-19)}$$

For both expressions in Equations 11-18 and 11-19, the total horizontal force is $\Omega_0 Q_E$. Except for H in Equation 11-19, every other term in these equations represents vertical loads. The shear panel systems should be an-

alyzed based on the most critical load combination defined by either Equation 11-18 or 11-19. Each panel component (including all connections), other than the diagonal straps, should be designed based on these loads.

11.8 Deflection, drift limits, and building separation

The design story drift, Δ, shall not exceed the allowable story drift, Δ_a, as obtained from Table 11-7 (ASCE/SEI 7-10, Table 12.12-1), for any story. The design story drift shall be computed as the difference of deflections at the center of mass at the top and bottom of the story under consideration, as determined by Equation 11-34 (ASCE/SEI 7-10, section 12.8.6). For structures with significant torsional deflections, the maximum drift shall include torsional effects. All portions of the structure shall be designed and constructed to act as an integral unit in resisting seismic forces unless separated structurally by a distance sufficient to avoid damaging contact under total deflection as defined in ASCE/SEI 7-10, section 12.12.3.

Table 11-7. Allowable story drift, Δ_a (in. or mm).

Structure	Risk Category		
	I or II	III	IV
Light-framed wall systems using flat strap bracing (diagonal strap shear walls)	$0.020h_{sx}$[11]	$0.015h_{sx}$	$0.010h_{sx}$

11.9 Equivalent lateral force procedure

ASCE/SEI 7-10 presents three permitted analytical procedures for defining the structural response (ASCE/SEI 7-10, Table 12.6-1), but only the equivalent lateral analysis (ASCE/SEI 7-10, section 12.8) is presented here. Only this procedure is presented because of the following: (1) its simplicity; (2) it can be used for all light-frame construction in all seismic design categories; and (3) typical cold-formed steel structures will likely be low-rise construction so that first mode response will dominate the seismic response of the structures. However, if deemed beneficial, the modal response spectrum analysis procedure presented in ASCE/SEI 7-10, section 12.9) could be used. The next three sections of this chapter present the determination of base shear, period, and vertical distribution of lateral forces using the *equivalent lateral force procedure*.

[11] h_{sx} is the story height below Level x.

11.9.1 Seismic base shear

Using the equivalent lateral force procedure, the seismic base shear, V, in a given direction shall be determined according to the following equation (ASCE/SEI 7-10, Eq 12.8-1):

$$V = C_s W \quad \text{(Eq 11-20)}$$

where:

C_s = the seismic response coefficient
W = the effective seismic weight (ASCE/SEI 7-10, section 12.7.2).

The seismic response coefficient, C_s, shall be determined according to the following equation (ASCE/SEI 7-10, Eq 12.8-2):

$$C_s = \frac{S_{DS}}{\left(\frac{R}{I_e}\right)} \quad \text{(Eq 11-21)}$$

The value for C_s is calculated according to Equation 11-21, and need not exceed the following (ASCE/SEI 7-10, Eq 12.8-3 and 12.8-4):

$$C_s = \frac{S_{D1}}{T\left(\frac{R}{I_e}\right)} \text{ for } T \le T_L \quad \text{(Eq 11-22)}$$

$$C_s = \frac{S_{D1} T_L}{T^2\left(\frac{R}{I_e}\right)} \text{ for } T > T_L \quad \text{(Eq 11-23)}$$

where

T = the fundamental period of the structure determined below.
T_L = the long-period transition period, shown in ASCE/SEI 7-10 (ASCE/SEI 7-10, Figures 22-12 through Figure 22-16) but shall not be less than (ASCE/SEI 7-10, Eq 12.8-5):

$$C_s = 0.044 S_{DS} I_e \geq 0.01 \quad \text{(Eq 11-24)}$$

Also, for structures located where S_1 is greater than or equal to 0.6g (ASCE/SEI 7-10, Eq 12.8-6):

$$C_s = \frac{0.5 S_1}{\left(\frac{R}{I_e}\right)} \quad \text{(Eq 11-25)}$$

11.9.2 Period determination

The fundamental period of the building, T, in the direction under consideration shall be defined using the structural properties and deformational characteristics of the resisting elements in a properly substantiated analysis (ASCE/SEI 7-10, section 12.8.2). Alternatively, T is permitted to be taken as the approximate fundamental period, T_a, determined in accordance with the following requirements. The fundamental period, T, shall not exceed the product of the coefficient for upper limit on calculated period, C_u, from Table 11-8 (ASCE/SEI 7-10, Table 12.8-1) and the approximate fundamental period, T_a, determined as follows:

$$T_a = C_t h_n^x \quad \text{(Eq 11-26)}$$

where

C_t = constant = 0.02 (English) or 0.0488 (metric) for cold-formed steel shear panels with diagonal straps (ASCE/SEI 7-10, Table 12.8-2, for all other structural systems)

h_n = the structural height in feet (English) or meters (metric) which is the vertical distance from the base to the highest level of the seismic-force-resisting system of a structure. For pitched or sloped roofs, the structural height is from the base to the average height of the roof

x = 0.75 (ASCE/SEI 7-10, Table 12.8-2, for all other structural systems).

Table 11-8. Coefficient for upper limit on calculated period.

Design Spectral Response Acceleration at 1 second, S_{D1}	Coefficient C_u
$S_{D1} < 0.1g$	1.7
$0.1g \le S_{D1} < 0.15g$	1.7
$0.15g \le S_{D1} < 0.2g$	1.6
$0.2g \le S_{D1} < 0.3g$	1.5
$0.3g \le S_{D1} < 0.4g$	1.4
$0.4g \le S_{D1}$	1.4

11.9.3 Vertical distribution of lateral seismic forces

The vertical distribution of lateral seismic force, F_x (kip or kN), induced at any level shall be determined from the following equations (ASCE/SEI 7-10, section 12.8.3, Eqs 12.8-11 and 12.8-12):

$$F_x = C_{vx} V \quad \text{(Eq 11-27)}$$

and

$$C_{vx} = \frac{w_x h_x^k}{\sum_{i=1}^{n} w_i h_i^k} \quad \text{(Eq 11-28)}$$

where

C_{vx} = the vertical distribution factor
V = the total design lateral force or shear at the base of the structure (kip or kN)
w_i and w_x = the portion of the total effective seismic weight of the structure (W) located or assigned to Level i or x
h_i and h_x = the height (ft or m) from the base to Level i or x
k = an exponent related to the structure period as follows:
for structures having a period of 0.5 sec or less, k = 1
for structures having a period of 2.5 sec or more, k = 2
for structures having a period between 0.5 and 2.5 seconds, k shall be 2 or shall be determined by linear interpolation between 1 and 2.

The horizontal distribution of seismic story shear in any story, V_x (kip or kN), shall be determined from the following equation (ASCE/SEI 7-10, section 12.8.4, Eq 12.8-13):

$$V_x = \sum_{i=x}^{n} F_i \quad \text{(Eq 11-29)}$$

where

F_i = the portion of the seismic base shear, V (kip or kN) induced at Level i.

The seismic design story shear, V_x (kip or kN), shall be distributed to the various shear panels in the story under consideration based on the relative lateral stiffness of the panels and the diaphragm.

11.9.4 Torsion

For buildings with flexible diaphragms (ASCE/SEI 7-10, section 12.3.1.1), the distribution of forces to the vertical elements (shear panels) shall account for the position and distribution of masses supported (i.e., distribute forces based on tributary area of the shear panels. For diaphragms that are not flexible (ASCE/SEI 7-10, sections 12.3.1.2 and 12.3.1.3), the distribution of lateral seismic forces shall take into account the effects of torsional moment, M_t, resulting from the location of masses relative to the center of rigidity (inherent torsional moment) of the lateral-force-resisting frame in both orthogonal directions (ASCE/SEI 7-10, section 12.8.4.1). This torsional moment shall include the effects of accidental torsional moment, M_{ta}, caused by an assumed offset of the mass. This offset shall equal 5% of the dimension of the structure orthogonal to the direction of the applied seismic force (ASCE/SEI 7-10, section 12.8.4.2). Structures assigned to seismic design category C, D, E, or F, which have Type 1a or 1b torsional irregularity or extreme torsional irregularity (ASCE/SEI 7-10, Table 12.3-1), shall include an amplification of accidental torsion as defined in ASCE/SEI 7-10 (ASCE/SEI 7-10, section 12.8.4.3). Similar to the lateral seismic forces, the torsional moments, M_t, are distributed along the floors of the building according to the vertical distribution factor given in Equation 11-28.

The torsional resistance comes from each of the shear panels, and the resistance from each panel is proportional to the square of the distance from the center of resistance to the plane of the panel. For a given panel, the additional shear force due to torsion, Q_{si}, can be expressed as:

$$Q_{si} = k_{si}\Delta_{si} = k_{si}\rho_i\theta \qquad \text{(Eq 11-30)}$$

where

k_{si} = the shear stiffness of shear panel i, and is defined as follows:

$$k_{si} = En_s b_s t_s \left(\frac{W^2}{(H^2+W^2)^{3/2}}\right) \qquad \text{(Eq 11-31)}$$

Δsi = the additional lateral in-plane shear deflection due to torsion of panel i
ρi = the distance from the center of resistance to panel i, perpendicular to the plane of the panel
θ = the torsional rotation of the building at the floor level above the panel
E = the modulus of elasticity of steel, which is 29,000 ksi (200,000 MPa)
n_s = the number of diagonal straps in each direction
b_s = the width of the diagonal straps
t_s = the thickness of the diagonal straps
W = the overall panel width
H = the overall panel height (see Figure 11-2 for a schematic panel drawing showing W and H).

The torsional moment resistance, M_{tr}, for all the shear panels is given by:

$$M_{tr} = \sum_{i=1}^{n} \rho_i Q_{si} = \sum_{i=1}^{n} \rho_i^2 k_{si} \theta \qquad \text{(Eq 11-32)}$$

Equation 11-32 shows that the torsional resistance from each panel is proportional to $\rho_i^2 k_{si}$. The total torsional moment resistance, M_{tr}, is set equal to the M_t, and the additional shear force due to torsion, Q_{si}, is calculated using Equations 11-30 and 11-32. Note that the torsional rotation, θ, in these equations does not need to be solved for and can be treated as a constant. Also the panel shear stiffness, k_{si}, is not needed if all the panels can be assumed to be equal or if their relative stiffness can be determined.

11.9.5 Structural overturning resistance

The structure shall be designed to resist overturning effects caused by the seismic forces determined from Equation 11-27. At any story, the increment of overturning moment in the story under consideration shall be distributed to the various vertical-force-resisting elements in the same proportion as the distribution of the horizontal shears to those elements (ASCE/SEI 7-10, section 12.8.5).

The overturning moments at Level x, M_x (kN-m or kip-ft), shall be determined from the following equation:

$$M_x = \sum_{i=x}^{n} F_i (h_i = h_x) \qquad \text{(Eq 11-33)}$$

where

F_i = the portion of the seismic base shear, V, induced at Level i
h_i and h_x = the height (ft or m) from the base to Level i or x.

Foundations designed for the foundation overturning design moment, M_f (kip-ft or kN-m), at the soil/foundation interface, determined using Equation 11-33 at the foundation level, may be reduced by 25% for foundations of structures that satisfy both of the following conditions (see ASCE/SEI 7-10, section 12.13.4):

1. The structure is designed in accordance with the Equivalent Lateral Force Analysis as set forth in ASCE/SEI 7-10, section 12.8.
2. The structure is not an inverted pendulum or cantilevered column type structure.

Overturning effects at the soil/foundation interface may be reduced by 10% for foundations of structures designed in accordance with the modal analysis requirements of ASCE/SEI 7-10 sections 12.9 and 12.13.4).

11.9.6 Story drifts

Story drifts shall be calculated based on the application of design seismic forces to a mathematical model of the structure. The model shall include the stiffness and strength of all elements that are significant to the distribution of forces and deformations in the structure, and it shall represent the spatial distribution of the mass and stiffness of the structure. The design story drift, Δ, shall be computed as the difference in the deflections at the center of mass at the top and bottom of the story under consideration. The deflections of Level x, δ_x (in. or mm), shall be determined according to the following equation (ASCE/SEI 7-10, Eq 12.8-15):

$$\delta_x = \frac{C_d \delta_{xe}}{I_e} \qquad \text{(Eq 11-34)}$$

where

δ_{xe} = the deflections determined by an elastic analysis (in. or mm) based on the forces defined in Equation 11-27.

For determining compliance with the story-drift limitations in Table 11-7, the deflections of Level x, δ_x (in. or mm), shall be calculated as expressed in Equation 11-34. For the purposes of this drift analysis only, the computed fundamental period of the structure, T, in seconds, may be used without the upper-bound limitations specified in Table 11-8 (ASCE/SEI 7-10, section 12.8.6.2), when determining drift-level seismic-design forces.

11.9.7 P-delta effects

The story drifts and member forces and moments due to P-delta effects shall be determined in accordance with ASCE/SEI 7-10, section 12.8.7. The design story drift, Δ (in. or mm), shall be increased by the incremental factor relating to the P-delta effects if required by the following recommendations. The P-delta effects on story shears and moments, the resulting member forces and moments, and the story drifts induced by these effects do not need to be considered when the stability coefficient, θ, as determined by the following equation, is equal to or less than 0.10:

$$\theta = \frac{P_x \Delta I_e}{V_x h_{sx} C_d} \quad \text{(Eq 11-35)}$$

where

P_x = the total vertical design load at and above Level x (kip or kN), where no individual load factors needs to exceed 1.0 in computing P_x

Δ = the design story drift occurring simultaneously with V_x (in. or mm)

V_x = the seismic shear force acting between Level x and x-1 (kip or kN).

The stability coefficient, θ, shall not exceed θ_{max}, which is determined as follows:

$$\theta_{max} = \frac{0.5}{\beta C_d} \leq 0.25 \quad \text{(Eq 11-36)}$$

where

β = the ratio of shear demand to shear capacity for the story between Level x and x - 1. This ratio may conservatively be taken as 1.0.

When the stability coefficient, θ, is greater than 0.10 but less than or equal to θ_{max}, the incremental factor related to P-delta effects, a_d, can be determined by rational analysis (NEHRP 2009, Part 2 "Commentary," section C12.8.7). Alternatively, the P-delta effects can be accounted for by multiplying the drifts and member forces by 1.0/(1 - θ). When θ is greater than θ_{max}, the structure is potentially unstable and shall be redesigned.

11.10 Cold-formed steel seismic requirements

All boundary members, chords, and collectors shall be designed to transfer seismic forces originating in other portions of the structure to the shear panels, in accordance with ASCE/SEI 7-10, section 12.10.2. Connections for diagonal strap-to-column and column-to-anchor and shear panel anchorage, and collectors shall have adequate strength to account for the effects of material overstrength as indicated in these recommendations.

The pullout resistance of screws shall not be used to resist seismic forces.

Shear panels shall be anchored such that the bottom and top tracks are not required to resist uplift forces by bending of the track or track web. Both flanges of studs shall be braced to prevent lateral torsional buckling (IBC 2003, section 2211.4.3).

Provision shall be made for pretensioning or other methods of installing tension-only diagonal straps in order to guard against loose straps (AISI S213-07-C/SI-09-C, section C4).

The recommendations presented here require all-steel design, and does not permit the use of plywood sheathing or oriented strand board in cold-formed steel shear panels.

Shear panel design shall be based on the cold-formed steel shear design recommendations presented here. This design requires that shear panels be adequately anchored at their top and bottom to a floor diaphragm. Shear panels in the two orthogonal directions must be anchored to the same diaphragm at each floor level to tie the two orthogonal lateral load-resisting systems together. Shear panels above the ground floor must have shear panels in the same direction at every floor level below them.

Using the following recommendations, the diagonal straps are sized to resist the total horizontal loads at each floor level as defined in Equations 11-

12 and 11-13, based on trial shear panel locations and aspect ratios. Then the greater loads defined in Equations 11-18 and 11-19 shall be used to size the shear panel columns. Finally, the panel connections and anchors are designed according to the recommendations that follow.

11.11 Diagonal strap design

The diagonal straps are designed to resist the seismic story shears, V_x, given in Equation 11-29 that have been increased by the additional shear force due to torsion (Q_{si} in Equation 11-30). The shear panels shall be configured and diagonal straps designed so that the lateral shear panel design strength, $\phi_t Q_{sy}$ satisfies the following equation:

$$\emptyset_t Q_{sy} = \emptyset_t \sum_{i=1}^{n} \left[n_{si} b_{is} t_{is} F_{sy} \left(\frac{W_i}{\sqrt{H_i^2 + W_i^2}} \right) \right] \geq V_x + Q_{si} \quad \text{(Eq 11-37)}$$

where

ϕ_t = the resistance factor for tensile members, 0.90 (ASI 2007a, Appendix A, section C2)
n = the number of shear panels in the building frame for which the shear forces V_x and Q_{si} are applied
n_{si} = the number of diagonal straps (panel faces with straps) for shear panel i
b_{si} = the width of the diagonal straps in shear panel i
t_{si} = the thickness of the diagonal straps in shear panel i
F_{sy} = the design yield strength of the diagonal straps
W = the width of shear panel i
H = the height of shear panel i

This equation assumes the diagonal straps are the sole lateral-load-resisting element. It defines the lateral design capacity of the diagonal straps assuming they are tension only members and their design strength is defined by the AISI Specification S100-2007 (AISI 2007a, Appendix A, Equation C2-1). The number of shear panels, panel width, height, and strap size and strength shall be designed to meet the requirements of Equation 11-37. All diagonal strap material must be ASTM A 1003/A 1003M, Type H steel (ASTM 2013b). Diagonal straps may not use rerolled steel, because the rerolling strain hardens the material, increasing material

strength variability and reducing elongation (see Chapter 4 for a discussion of this concern).

11.12 Column design

The columns may be hollow structural sections (HSS) or can be built up from studs. The columns of the Panel A and C configurations are built up with cold-formed steel studs. These studs must be oriented to form a closed cross-section as shown on the Test Panels A3 and C1 drawings in Appendix A. Individual studs must be welded to each other with a weld thickness equal to the thickness of the studs. The welds are intermittent, with a length and spacing that will ensure composite behavior of the column.

Structural tubing column design (Panel D configuration, Drawing D2 in Appendix A of this report) follows the same procedure, but consists of a single member that is a closed section by itself. The equations in these recommendations are used such that the number of studs making up this column is one.

11.12.1 Column applied loads

Loads applied to the columns are defined based on Equation 11-18, where the effects of gravity load and seismic forces are additive and diagonal strap overstrength is accounted for. Only that portion of gravity loads applied to the tributary area of the shear panel columns is included in the design of these columns. However, the full horizontal seismic force, $\Omega_0 Q_E$, applied to the shear panel and resisted by the diagonal straps, will add a vertical component to the columns, increasing axial load. This horizontal load is based on the actual designed area of the diagonal straps as defined in Equation 11-17. The total column axial load at the maximum ultimate stress in the diagonal straps, P_{vumax} is:

$$P_{vumax} = \frac{GL_{max}}{2} + F_{sumax} n_s b_s t_s \left(\frac{H}{\sqrt{H^2+W^2}}\right) \qquad \text{(Eq 11-38)}$$

where

GL_{max} = the maximum gravity load per shear panel, i.e., from $(1.2 + 0.2S_{DS})D + \Omega_o Q_E + L + 0.2S$ in Equation 11-18

F_{sumax} = the maximum estimated ultimate stress in the diagonal straps, which equals to 1.5 F_{su} for ASTM A1003/A1003M, Type H,

Grade 33 steel (F_{su} = 45 ksi and 310 MPa), and 1.25 F_{su} of Grade 50 steel (F_{su} = 65 ksi and 448 MPa) (ASTM 2013b; Larsen 1998).

11.12.2 Column axial capacity

The columns shall be designed such that their design strength, P_c, exceeds the total axial applied load, P_{vumax}. (Equation 11-38). Column capacity is determined based on AISI provisions. The design axial strength, $P_{c,}$ shall be determined based on the AISI Standard S100-07 (AISI 2007a, section C4 "Concentrically Loaded Compression Members"). This guidance is applied to columns built-up with cold-formed steel studs or individual structural tubing members. The design strength equals the resistance factor times the nominal axial strength, P_n, determined as follows for columns built-up with cold-formed steel studs or individual structural tubing members (ibid.):

$$P_c = \phi_c P_{cn} = \phi_c A_e F_{cn} \quad \text{(Eq 11-39)}$$

where

ϕ_c = the resistance factor for compression, which equals 0.85.
A_e = the effective area at the stress F_{cn}
F_{cn} = the nominal strength of the column, determined as follows:

for $\lambda_c \leq 1.5$,

$$F_{cn} = \left(0.658^{\lambda_c{}^2}\right) F_{cy} \quad \text{(Eq 11-40)}$$

for $\lambda_c > 1.5$,

$$F_{cn} = \left(\frac{0.877}{\lambda_c{}^2}\right) F_{cy} \quad \text{(Eq 11-41)}$$

where

$$\lambda_c = \sqrt{\frac{F_{cy}}{F_e}} \quad \text{(Eq 11-42)}$$

and

F_e = the elastic flexural buckling stress for closed cross-sections as defined in the following equation:

$$F_e = \frac{\pi^2 E}{\left(\frac{KH}{r}\right)^2} \quad \text{(Eq 11-43)}$$

where

E = the modulus of elasticity, equal to 29,000 ksi
K = the effective length factor
H = the laterally unbraced height of the column
F_{cy} = the design yield strength of the column
r = the radius of gyration of the full, unreduced column cross section, calculated as follows:

$$r = \sqrt{I/Ac} \quad \text{(Eq 11-44)}$$

The effective area, A_e, is calculated as follows for columns built up from cold-formed steel studs such that they form a closed section, or structural tube columns (AISI 2007a, C4.1):

$$A_e = A_c - nt_c(w-b) \quad \text{(Eq 11-45)}$$

where

A_c = the nominal column area
n = the number of studs making up the column, or equal to 2 when using structural tube columns
t_c = the thickness of the stud material used in the built-up columns or thickness of the structural tube column
w = the flat width of the stud web making up the built-up columns, or the width of the structural tubing face perpendicular to the plane of the panel.

Assuming the outside radius of the stud or tube corners is twice the thickness, t, then w may be calculated as follows:

$$w = b_c - 4t_c \quad \text{(Eq 11-46)}$$

where

b_c = the depth of the studs making up the built-up columns, or the structural tubing width perpendicular to the plane of the panel

b = the effective width and shall be determined as follows (AISI 2007, B2.2):

For $0.50 \geq \frac{d_h}{w} \geq 0, and \frac{w}{t_c} \leq 70$ and the distance between centers of holes ≥ 0.5w and ≥ $3d_h$,

$$b = w - d_h \text{ when } \lambda \leq 0.673 \quad \text{(Eq 11-47)}$$

$$b = \frac{w\left[1 - \frac{0.22}{\lambda} - \frac{0.8d_h}{w} + \frac{0.085d_h}{w\lambda}\right]}{\lambda} \text{ when } \lambda > 0.673 \quad \text{(Eq 11-48)}$$

In all cases, $b \leq w = d_h$

where

d_h = the diameter of holes

λ = a slenderness factor defined as follows (AISI 2007, B2.1):

$$\lambda = \sqrt{\frac{f}{F_{cr}}} \quad \text{(Eq 11-49)}$$

where

f = the stress in compression element, which for compression members is taken equal to F_{cn} defined in Equations 11-40 and 11-41 (AISI 2007, C4).

$$F_{cr} = k\frac{\pi^2 E}{12(1-\mu^2)}\left(\frac{t_c}{w}\right)^2 \quad \text{(Eq 11-50)}$$

where

k = the plate buckling coefficient, equal to 4 for the studs making up the built-up columns or structural tube columns
μ = Poisson's ratio for steel, equal to 0.30.

11.12.3 Column bending and composite behavior

The column anchor design provisions presented later in these recommendations will create a moment connection. The primary purpose of the anchor design is to resist shear and uplift forces. However, this anchor design will also allow the columns to act as a moment frame, providing limited structural redundancy and widening of the hysteretic load-deflection envelopes of the shear panel. This will allow the panels to absorb more energy under cyclic loading conditions, which reduces building accelerations in an earthquake. Columns built up from studs must be designed to act as a composite cross section in order to provide this moment capacity. This requires welding between the studs that provide the shear transfer needed to develop the maximum moment in the columns. When one diagonal strap is in tension, the full gravity load on the shear panel may be carried in a single column, with the other column having no axial load. The maximum moment in a column will occur when it has no axial load. Therefore the welds shall be designed for the full moment capacity of the columns. This design requirement will allow the shear panel columns to continue providing bending resistance beyond the lateral yield deflection of the columns. These welds shall resist the maximum shear between the studs, which will be between the studs closest to the column neutral axis. This shear, q, is defined as follows:

$$q = \frac{V_c Q}{I_c} \qquad \text{(Eq 11-51)}$$

where

V_c = the maximum column shear due to column moment only
Q = the moment of the column cross-sectional area on one side of the critical weld about the critical weld plane
I_c = the moment of inertia of the column due to bending in the plane of the shear panel.

The maximum column shear, V_c, due to the maximum column moment, M_c, only is determined as follows:

$$V_c = \frac{2M_c}{H} = \frac{2F_{cy}I_c}{Hc} \quad \text{(Eq 11-52)}$$

where

F_{cy} = the yield strength of the column. This strength is not increased for column material overstrength because weld failure is controlled by the column material strength, so that any material overstrength would result in proportionately greater weld strength.

c = the distance to the column neutral axis to the extreme fiber in the plane of the shear panel.

The moment of the column cross-sectional area on one side of the critical weld about the critical weld plane, Q, is defined as follows:

$$Q = \int_A ydA = A\bar{y} \quad \text{(Eq 11-53)}$$

where

A = the area of column cross-section on one side of the critical weld plane closest to the column neutral axis

$\bar{y}$ = the distance from the neutral axis of the column cross-sectional area on one side of the critical weld plane to the critical weld failure plane.

Built-up columns are fabricated by welding individual studs together to form a closed cross-section using flare V-groove welds. The same weld size and spacing shall be used between all studs in the built-up column. These welds are design according to AISI (AISI 2007a, section E2.5, “Flare Groove Welds”), assuming double shear. The maximum spacing between centers of intermittent welds, s_{max}, is determined as follows:

$$s_{max} = 1.5\emptyset_G t_c F_{cu} \frac{L}{q} \quad \text{(Eq 11-54)}$$

where

ϕ_G = the resistance factor for flare groove welds, equal to 0.55
t_c = the stud thickness of the built-up columns
F_{cu} = the ultimate strength of the column steel
L = the length of intermittent groove welds
q = the maximum shear determined in Equation 11-51.

Intermittent welds shall be made at both the top and bottom ends of the columns, regardless of the maximum center-to-center spacing, s_{max}.

11.12.4 Column combined axial and moment capacity

The combination of axial load and bending shall be evaluated using Equations C5.2.2-1, C5.2.2-2, and C5.2.2-3 of the AISI Specification (AISI 2007a, section C5.2.2, "Combined Compressive Axial Load and Bending, LRFD and LSD Methods"). Moment is only considered in the strong direction of the panels (M_x in these equations) because the column anchors are much more flexible in their weak direction, so that the panels will not resist loads in this direction. The combination of axial load and moment on the columns shall be evaluated based on the following interaction equations (modifications of AISI 2007a, Eq C5.2.2-1, C5.2.2-2, and C5.2.2-3):

$$I = \frac{\bar{P}}{\varphi_c P_n} + \frac{C_{mx}\bar{M}_x}{\varphi_b M_{nx}\alpha_x} \leq 1.0 \qquad \text{(Eq 11-55)}$$

$$I = \frac{\bar{P}}{\varphi_c P_{no}} + \frac{\bar{M}_x}{\varphi_b M_{nx}} \leq 1.0 \qquad \text{(Eq 11-56)}$$

When $\frac{\bar{P}}{\varphi_c P_n} \leq 0.15$, then Equation 11-57 may be used in lieu of Equations 11-55 and 11-56.

$$I = \frac{\bar{P}}{\varphi_c P_n} + \frac{\bar{M}_x}{\varphi_b M_{nx}} \leq 1.0 \qquad \text{(Eq 11-57)}$$

where

$\bar{P}$ = the required compressive axial strength, which is similar to Equation 11-38 but based on the maximum yield strength of the strap rather than the slightly more conservative maximum ultimate strength.

Since the straps must be fabricated from ASTM A1003/A1003M, Type H steel (ASTM 2013b), the straps will never be rerolled, so that the strap stress will never reach maximum ultimate stress, making the maximum yield strength a reasonable upper limit. The required compressive strength is calculated as follows:

$$\bar{P} = \frac{GL_{max}}{2} + F_{symax} n_s b_s t_s \left(\frac{H}{\sqrt{H^2+W^2}}\right) \quad \text{(Eq 11-58)}$$

where

F_{symax} = maximum estimated yield stress in the diagonal straps, which equals 2 F_{sy} for ASTM A1003/A1003M, Type H, Grade 33 steel (F_{sy} = 33 ksi and 228 MPa) and 1.5 F_{sy} for Grade 50 steel (F_{sy} = 50 ksi and 345 MPa) (Larsen 1998)

$\Phi_c P_n$ = P_c, which equals the column axial design strength defined in Equation 11-39

C_{mx} = a coefficient set equal to 0.85 for compression members in frames subject to joint translation (AISI 2007, section C5.2.2)

$\bar{M}_x$ = the required flexural strength, set equal to the applied moment at maximum estimated strap yield strength, δ_{symax}, defined in Equation 11-59.

This equation assumes the columns are 50% fixed at their top and bottom by the panel anchors. Tension in the diagonal straps is responsible for the large axial load component of Equations 11-55 and 11-56, and this tension force will tend to counteract the moments applied to these columns, so that the 50% fixity of the columns is a reasonable limitation. This moment is also conservatively based on the maximum panel lateral deflection at which the diagonal strap will yield. The moment includes the column bending and P-delta effect of axial load. For the P-delta calculation in Eq 11-56, the vertical load, P_{vumax}, is a summation of the vertical loads from all columns whose lateral load resistance is provided by this column. The applied moment, The applied moment, $\bar{M}_x$, is defined as follows:

$$\bar{M}_x = \frac{(50\%)6EI_c\delta_{symax}}{H^2} + \bar{P}\delta_{symax} \quad \text{(Eq 11-59)}$$

where

δ_{symax} = the maximum estimated lateral panel deflection at the maximum estimated yield strength of the diagonal straps (F_{symax}), and is defined as follows:

$$\delta_{symax} = \frac{F_{symax}}{E}\left(\frac{H^2+W^2}{W}\right) \quad \text{(Eq 11-60)}$$

Φb = the resistance factor for bending, equal to 0.95 (AISI 2007a, section C5.2.2)

where

M_{nx} = the column nominal flexural strength, and this is defined as follows (modification of AISI 2007a, Equation C3.1.1-1):

$$M_{nx} = F_{cy}\frac{I_c}{c} \quad \text{(Eq 11-61)}$$

$$\alpha_x = 1 - \frac{\bar{P}}{P_{Ex}} > 0 \quad \text{(Eq 11-62)}$$

$$P_{Ex} = \frac{\pi^2 E I_c}{(K_x H)^2} \quad \text{(Eq 11-63)}$$

$$P_{no} = A_e F_{cy} \quad \text{(Eq 11-64)}$$

11.12.5 Column shear capacity

The trial column design must be checked for shear capacity. The diagonal straps fasten to the columns near their connection to the tracks and column anchor. Therefore the column must either have adequate shear capacity for the maximum horizontal seismic force, $\Omega_0 Q_E$, applied to the shear panel, or the column shear capacity must be augmented with other components. The column shear design strength, V_c, shall be determined as follows for columns built up with cold-formed steel studs or individual structural tubing members (AISI 2007a, section C3.2.1, "Shear Strength of Webs without Holes"):

$$\phi_v V_n = \phi_v A_w F_v \quad \text{(Eq 11-65)}$$

For $\frac{h_c}{t_c} \leq \sqrt{\frac{Ek_v}{F_{cy}}}$:

$$F_v = 0.60F_{cy} \quad \text{(Eq 11-66)}$$

For $\sqrt{\frac{Ek_v}{F_{cy}}} < \frac{h}{t} \leq 1.51\sqrt{\frac{Ek_v}{F_{cy}}}$:

$$F_v = \frac{0.60\sqrt{Ek_vF_{cy}}}{h_c/t_c} \quad \text{(Eq 11-67)}$$

For $\frac{h}{t} > 1.51\sqrt{\frac{Ek_v}{F_{cy}}}$:

$$F_v = \frac{0.904Ek_v}{h_c/t_c} \quad \text{(Eq 11-68)}$$

where

ϕ_v = the resistance factor for shear, equal to 0.95
V_n = the nominal column shear strength
A_w = the area of the column in shear

Only that portion of the column web that has a diagonal strap attached will be loaded in shear and available to resists these loads, expressed as follows:

$$A_w = n_s h_c t_c \quad \text{(Eq 11-69)}$$

where

h_c = the column depth, equal to the number of studs, n times the column stud flange width, b_f, for columns built up from studs or depth of the tube in the direction of the shear panel for structural tube columns
F_v = the column nominal shear stress
k_v = the column shear buckling coefficient, calculated in accordance with AISI S100-07 (AISI 2007a, section C3.2.1)

However, in the case of the shear panels, the diagonal straps apply shear load directly to the column faces, which are loaded in shear. This direct load transfer would be similar to a very large value of k_v. Therefore, Equation 11-66 is always used to define the shear capacity of the panel columns.

The example design in the following chapter shows that the columns normally will have insufficient shear capacity by themselves, and require additional shear capacity from their anchorage detail (see "Anchor Load Assumptions," section 11.14.1 of this report, for anchorage shear design details).

11.13 Connection design

Diagonal strap-to-column connections can be constructed using either screws or welds. As the following sections indicate, practical screwed connections are more difficult than welds for meeting connection design requirements.

11.13.1 Connection design assumptions and applied loads

This paragraph provides design assumptions that define loading and load-path issues for cold-formed steel shear panel diagonal strap-to-column connections. These loads are based only on the maximum lateral force, $\Omega_0 Q_E$. This force results from the right-hand term in Equation 11-17, $\Omega_0 Q_E$, which accounts for diagonal strap material overstrength. The maximum estimated ultimate force in the diagonal straps (in the axis of the straps), P_{sumax}, is:

$$P_{sumax} = F_{sumax} n_s b_s t_s \qquad \text{(Eq 11-70)}$$

The diagonal strap-to-column connections must be designed to resist the forces defined by Equation 11-70. Panel design will require the use of angle section anchors as described under "Panel Anchors" (section 11.14) because of the shear-transfer requirements. These anchors will also transfer loads between the column and beams above and below, or floor slab (i.e., diaphragm above and below), thereby eliminating the need for load transfer with a column-to-track connection. In low seismic zones it may be possible to transfer the shear forces with a column-to-track connection only, without anchors. However, it is considered more reasonable to use fewer shear panels rather than many with low lateral-load capacity. Therefore all shear panel design recommendations presented here require the use of anchors.

11.13.2 Screwed fastener connection design

Self-tapping screwed connection capacity definition shall follow the AISI Standard S100-07 (AISI 2007a, section E4 "Screw Connections"). Screws shall be installed and tightened in accordance with the manufacturer's recommendations. Screw connections loaded in shear can fail in one mode or in combination of several modes. These modes are screw shear, edge tearing, tilting and subsequent pullout of the screw, and bearing of the joined materials. The commentary for AISI S100 (2007b, section E4.3) gave further explanation and illustration of these modes of failure.[12] The minimum distance between the centers of screws shall not be less than three times their nominal diameter (AISI 2007a, section E4.1). The minimum distance from the center of a screw to the edge of a connected part perpendicular to the direction of loading (edge distance) shall not be less than 1.5 times the nominal screw diameter (AISI 2007a, section E4.2). The AISI provisions focus on the tilting and bearing modes of failure. Two cases are given depending on the ratio of the connected member thicknesses. The screw head will be in contact with the diagonal strap, and the strap will normally be thinner than the column. However, when the strap is the same thickness or thicker than the column, tilting becomes a more critical mode of failure. The AISI section E4 guidance on design shear strength per screw, P_s, applied to diagonal strap-to-column screw connections is summarized here. The design shear (AISI 2007a, section E4.3.1) and pull-over per screw (AISI 2007a, section E4.4.2), P_s shall be calculated as follows:

$$P_s = \emptyset_s min(P_{ns} and P_{nov}) \quad \text{(Eq 11-71)}$$

where the nominal shear strength per screw, P_{ns}, shall be determined as follows:

For $t_c/t_s \leq 1.0$, P_{ns} shall be taken as the smallest of

$P_{ns} = 4.2\sqrt{t_c^3 d}\, F_{cu}$ column tilting mode of failure (Eq 11-72)

$P_{ns} = 2.7 t_s d F_{sumax}$ diagonal strap bearing mode of failure (Eq 11-73)

[12] The Commentary section of the 2007 revision of AISI S100 (AISI 2007b) does not include these illustrations.

$P_{ns} = 2.7 t_c d F_{cu}$ column bearing mode of failure (Eq 11-74)

For $t_c/t_s \geq 2.5$, P_{ns} shall be taken as the smaller of

$P_{ns} = 2.7 t_s d F_{sumax}$ diagonal strap bearing mode of failure (Eq 11-75)

$P_{ns} = 2.7 t_c d F_{cu}$ column bearing mode of failure (Eq 11-76)

For $1.0 < t_c/t_s < 2.5$, P_{ns} shall be determined by linear interpolation between the two cases above

where

ϕ_s = the screw resistance factor for shear, equal to 0.5
d = the nominal screw diameter
t_s = the thickness of the diagonal strap or member in contact with the screw head or washer
t_c = the thickness of the column or member not in contact with the screw head or washer
F_{sumax} = the maximum estimated ultimate strength of the diagonal straps, which are the members in contact with the screw heads or washers, which equals 1.5 F_{su} for ASTM A 1003/A 1003M, Type H, Grade 33 steel (F_{su} = 45 ksi and 310 MPa), and 1.25 F_{su} for Grade 50 steel (F_{su} = 65 ksi or 448 MPa)
F_{cu} = the tensile strength of the columns, which are the members not in contact with the screw head or washer, and equals 45 ksi, 65 ksi and 58 ksi, for Grade 33, Grade 50, and ASTM A500, Grade B HSS structural tube steel, respectively.

The nominal shear strength per screw, P_{ns}, may also be determined by AISI Tables IV-9a and IV-9b (AISI 2008) for connections to various sheet thicknesses for sheets with ultimate strengths of 45 ksi (310 MPa) and 65 ksi (448 MPa), ASTM A 1003/A 1003M, Type H, Grade 33 and 50, respectively (ASTM 2013b). These tables may only be used if the grades of the materials being connected are the same.

The nominal shear strength per screw, P_{ns}, may also be limited by end distance of a connected part as defined by AISI (2007b, Appendix A, section E4.3.2), where the distance to the end is parallel to the direction of the ap-

plied force (e.g., near the end of a strap). This strength is calculated as follows:

$$P_{ns} = t_s e F_{sumax} \quad \text{(Eq 11-77)}$$

where

e = the distance in the line of the applied force, from the center of a screw to the end of the connected part (diagonal strap for the shear panels).

The nominal shear strength of the screws, P_{ss}, shall be determined based on manufacturer's data (AISI 2007b, section E4.3.3), which must be based on tests according to AISI section F1.1.

The nominal pull-over strength, P_{nov}, shall be calculated as follows (AISI 2007b, section E4.4.2, "Pull-Over"):

$$P_{nov} = 1.5 t_s d'_w F_{sumax} \quad \text{(Eq 11-78)}$$

where

d'_w = effective pull-over diameter determined in accordance with

a. For a round head, hex head, or hex washer head screw with an independent and solid steel washer beneath the screw head:

$$d'_w = d_h + 2t_w + t_s \leq d_w \quad \text{(Eq 11-79)}$$

where

d_h = screw head diameter or head washer head integral washer diameter
t_w = steel washer thickness
d_w = steel washer diameter

b. For a round head, a hex head, or hex washer head screw without an independent washer beneath the screw head:

$d'_w = d_w$ but not larger than 0.5 in. (12.7 mm)

c. For a domed (non-solid and independent) washer beneath the screw head, it is permissible to use d'_w as calculated in Equation 11-79, with d_h, t_w, and t_s (t_1) as defined in AISI S100-07, Figure E4.4.2(3). In this equation, d'_w cannot exceed ⅝ in. (16 mm).

The modes of failure expressed in Equations 11-72 through 11-78 are defined alongside or before the equations. The connection-applied loads are based on the maximum estimated ultimate strength of the strap (F_{sumax} in Equation 11-70), which recognizes that as the applied load increases with increasing strap strength, the connection capacity also increases similarly for modes of failure based on this strength. However, for modes of failure based on the column strength (Equations 11-72, 11-74, and 11-76) or screw shear capacity based on manufacturer's data (P_{ss}), no increase is permitted.

Finally, the minimum number of screws required at each diagonal strap-to-column connection, n_{screws}, is calculated as follows:

$$n_{screws} \geq \frac{P_{sumax}}{n_s P_s} \quad \text{(Eq 11-80)}$$

11.13.3 Block shear rupture strength

The design shear strength along a potential shear rupture plane between fasteners of connected members, R_n, shall be determined in accordance with AISI S100-07 (AISI 2007a, Appendix A, section E5.3 "Block Shear Rupture") as follows:

$$R = \emptyset_R R_n \quad \text{(Eq 11-81)}$$

where

$\emptyset_R$ = the shear rupture resistance factor, equal to 0.65
R_n = the nominal block shear rupture strength, determined as the lesser of Equations 11-82 and 11-83:

$$R_n = 0.6F_{sy}A_{gv} + F_{su}A_{nt} \quad \text{(Eq 11-82)}$$

$$R_n = 0.6F_{su}A_{nv} + F_{su}A_{nt} \quad \text{(Eq 11-83)}$$

where

A_{gv} = the gross area subject to shear
A_{nv} = the net area subject to shear
A_{nt} = the net area subject to tension.

AISI S100-07 (AISI 2007a, Appendix A, section E3.2 "Rupture in Net Section (Shear Lag)"), defines the provisions for this mode of failure. However, for the diagonal strap-to-column screw connections used in these panel configurations, shear rupture rather than this mode will limit the connection capacity.

The shear and tensile rupture strength are based on the diagonal strap ultimate strength of the member in the joint being evaluated. The maximum applied load on this joint is based on the yield strength of the same member, P_{sy}. This will be much less than the maximum estimated strap axial force, P_{su}. The maximum force in the members is not critical, but rather is the minimum ratio of strap ultimate strength over yield strength (F_u/F_y) because the rupture strength capacity is dependent on F_u and the maximum applied force is dependent on F_y. This guidance requires that ASTM A1003/A1003M Type H steels be used for the straps (ASTM 2013b). Type H steels are defined as high-ductility materials in ASTM A1003/A1003M. These are designated as ST50H, ST40H, ST37H, and ST33H for structural-grade, high-ductility steel with design yield strengths of 50, 40, 37, and 33 ksi, respectively. Note B in Table 2 of the ASTM A 1003/A 1003M specification requires a minimum F_u/F_y ratio of 1.08 for Type H steels. Therefore the strap yield strength, P_{sy}, may be defined simply based on the ultimate strength of these materials. This requirement is expressed as follows:

$$R_{ns} \geq P_{sy} \quad \text{(Eq 11-84)}$$

where

$$P_{sy} = \frac{F_{su}}{1.08} n_s b_s t_s \quad \text{(Eq 11-85)}$$

When the strap-to-column rupture strength is evaluated based on Equation 11-84, the resistance factor in Equation 11-81 may be increased to 1.0, because of the ASTM minimum material requirement of F_u/F_y stated above. However, the 1.08 ratio for F_u/F_y will often be too small to make screwed connections practical, and the designer may be forced to use

welded connections. The example design presented in Chapter 12 illustrates this difficulty.

11.13.4 Welded connection design

Welded design follows AISI guidance (AISI 2007a, section E2 "Welded Connections"), which covers connections of members in which the thickness of the thinnest member is 3/16 in. (4.76 mm) or less. Arc welds shall be made in accordance with AWS D1.3 and its commentary (AWS 2008). Resistance welds shall be made in accordance with the procedures in AWS C1.1. (AWS 2012)

Welded diagonal strap-to-column connections require fillet welds (AISI 2007b, section E2.4 "Fillet Welds"). The welds at the sides of the straps will be loaded in the longitudinal direction, and welds at the ends of the straps will be loaded in the transverse direction. The weld thickness should be equal to the thickness of the strap material. Ultimate failure of fillet-welded joints has usually been found to occur by the tearing of the sheet steel adjacent to the weld. In most cases, the higher strength of the weld material prevents weld shear failure, so this recommendation is based on sheet tearing (AISI 2007b, section E2.4 "Fillet Welds"). The AISI commentary further explains that research demonstrates that weld throat failure does not occur for materials thinner than 0.10 in. (ibid.), and the AISI Specification S100-07 (AISI 2007a) requires the welded connection capacity be determined based on the strength of the weld material only for welds thicker than 0.10 in. The shear strength of welded diagonal strap-to-column connections shall be determined based on the AISI Specification S100-07 (AISI 2007a) and these are summarized below. The design shear strength for loading in the longitudinal direction, P_L, shall be determined as follows:

For L/t < 25

$$P_L = \phi_{L1} P_n = \phi_{L1} \left(1 - \frac{0.01L}{t}\right) LtF_u \quad \text{(Eq 11-86)}$$

For L/t ≥ 25

$$P_L = \phi_{L2} P_n = \phi_{L2} 0.75 tLF_u \quad \text{(Eq 11-87)}$$

where

ϕ_{L1} = 0.60
L = the length of longitudinal fillet weld

t = the least value of the thicknesses of the diagonal straps (t_s) or columns (t_c) being welded
F_u = the design ultimate strength of the thinner material being welded (F_{su} or F_{cu})
ϕ_{L2} = 0.50.

The design shear strength for loading in the transverse direction, P_T, shall be determined as follows:

$$P_T = \phi_T P_n = \phi_T t L F_u \quad \text{(Eq 11-88)}$$

where

ϕ_T = 0.65.

For fillet welds to both strap and column material thicker than 0.10 in. (2.54 mm), the design shear strength for both longitudinal and transverse loading due to weld failure, P_W, shall not exceed the following (AISI 2007b, section E2.4)[13]:

$$P_w = 0.75 \emptyset_w t_w L F_{xx} \quad \text{(Eq 11-89)}$$

where

ϕ_w = 0.60
t_w = the effective throat, equal to 0.707 times the least of (1) the thickness of the strap, t_s, (2) the thickness of the weld against the strap in the axis of the strap thickness, which should normally equal the thickness of the strap, or (3) the thickness of the weld along the column in the axis of the strap, which should normally equal or exceed the strap thickness. (A larger effective throat shall be permitted if measurement shows that the welding procedure to be used consistently yields a larger value of t_w. Figure E2.4-1 (AISI 2007b) illustrates these weld thicknesses and limitations.)

[13] AISI commentary (AISI 2007b) indicated that this equation is needed to cover the possibility of weld failure through the throat of the weld material, because research showed that for high strength welded members, weld throat failure could occur for welded materials thicker than 0.10 in.

F_{xx} = the tensile strength of electrode classification (AISI 2007b, section E2.2.1.2).

The fillet weld longitudinal and transverse shear strengths are based on the ultimate strength of the thinner member (normally the diagonal strap) of the joint. The maximum applied load on this joint is based on the yield strength, P_{sy}, of the same member. Similar to the rupture strength, the maximum force in the members is not critical, but rather is the minimum ratio of F_u/F_y because the weld strength capacity is dependent on F_u and the maximum applied force is dependent on F_y. Weld connections shall be evaluated based on the following equation, where the applied strap yield strength, P_{sy}, is defined according to Equation 11-70:

$$[min(P_L + P_T, P_w)]n_s \geq P_{sy} \quad \text{(Eq 11-90)}$$

11.14 Panel anchors

Panel anchors must be installed on both sides of the shear panel columns because the columns by themselves have inadequate shear capacity. Furthermore, if the columns were simply fastened to the track, the track would be loaded in bending, due to uplift. The track is very weak in bending and should not be relied on to restrain the columns. Anchors consisting of angle iron sections with a stiffening plate shall be welded to both sides of the columns at both their tops and bottoms to provide the required panel anchorage. A stiffening plate shall be welded to each angle and the angles shall be drilled with through holes and anchored to the supporting diaphragm above and below the shear panel using embedded anchor bolts or bolts through intermediate floor diaphragms. See Chapter 12 (Figure 12-4 through Figure 12-15) for examples of this anchor configuration.

The columns (see section 11.12.5) and anchors together must have adequate capacity to resist the horizontal forced defined by Equation 11-91. The vertical leg of the angle iron anchors must extend beyond the critical shear plane. For screwed fastener connections, the critical shear plane is along the horizontal row of screws closest to the track in the diagonal strap-to-column connection. For welded connections, the critical shear plane is along the strap-to-column weld near the track. The anchor angle iron legs are welded to the columns along the top of the vertical leg and along the vertical edge of these legs to the corners of the columns. These

welds force this face of the column to act in a composite fashion with the angle vertical legs.

11.14.1 Anchor load assumptions

The most critical load condition for anchors is when the effects of gravity load and seismic forces counteract each other. This condition is expressed in Equation 11-19. The selected angle and stiffener plate anchors shall resist the applied shear and uplift forces. These anchors also provide limited moment resistance. The configuration of these anchors (see Figure 12-4 through Figure 12-15 for examples) gives them strength and stiffness to resist shear and uplift forces where they anchor the columns to the diaphragms. The anchors should remain elastic against these forces. However, moments will be applied to the column anchors by two means. At small deformations, the greatest moment in the column anchors will come from eccentric loading of the anchor through the diagonal strap tension. At larger panel deformation, the columns will displace in-plane and this will apply moments to the anchors as they resist rotation. The legs of the angles in the anchors should be designed for the horizontal force when the diagonal strap it at its maximum ultimate stress, P_{humax} (see Equation 11-91). However, these legs may yield and deform in-elastically under the maximum moment applied through eccentric loading from the strap and bending of the columns, when the straps and columns are at their maximum estimated stress. As the legs deform, their load path will more effectively carry the loads that result from the maximum estimated strap force and column bending. These recommendations are written to permit inelastic ductile response in the column anchors, which will actually improve ductile system behavior and improve design economy under these extreme load conditions.

$$P_{humax} = \Omega_0 Q_E = F_{sumax} n_s b_s t_s \left(\frac{W}{\sqrt{H^2+W^2}}\right) \qquad \text{(Eq 11-91)}$$

11.14.2 Anchor bending capacity

The legs of the anchor angles will be loaded in bending by the horizontal loads applied by the panel diagonal straps. The faces of the columns carry a portion of this load in shear down to the base of angles and transfer the load to horizontal legs of the angles (see Equation 11-65). The vertical legs of the anchor angles together with the out-of-plane faces of the column will together carry a portion of this load in bending to the bottom of the angle and stiffener plate. The critical bending plane of this angle and col-

umn section will be along a diagonal line from the top center of the angle next to the fillet weld to the stiffener down to where the vertical leg of the angle begins to thicken at the radii intersection with the horizontal leg of the angle. The vertical legs of the angles and the face of the columns will carry this load together in bending as a composite section because they are welded to each other along both the top and sides of the vertical leg of the angles. Figure 12-4 through Figure 12-5 show example anchor configurations that aid the visualization of this load path from the straps to the anchor bolts.

The total design shear strength, V_T, from the column loaded in shear and the vertical legs of the angles loaded in bending must exceed the maximum shear panel horizontal seismic force, P_{humax}. All anchors are made using two angles, on either side of the column, so that V_T may be expressed as:

$$V_T = V_C + P_{Ah} \geq P_{humax} \quad \text{(Eq 11-92)}$$

where

V_c = the column shear capacity determined according to Equation 11-65

P_{Ah} = the horizontal load capacity of the vertical legs of the angles on both sides of the columns and the faces of the columns to which the angles are welded based on the composite bending capacity of these two components, defined as follows:

$$P_{Ah} = 2\frac{M_A}{L_A}n_s \quad \text{(Eq 11-93)}$$

M_A = the design moment capacity of a single leg of angle acting in composite with the face of the column to which it is welded, based on AISI/AISC 360-10 section F1 and F7, for a single angle leg and portion of the column defined as follows (AISC 2010a, section F7):

$$M_A = \emptyset_b F_{Ay} Z_A \quad \text{(Eq 11-94)}$$

Φ_b = the bending resistance factor equal to 0.90 (AISC 2010a, section F1)

F_{Ay} = angle yield strength, normally ASTM A36, 36 ksi (AISC 2011, Part 2: “General Design Considerations,” Table 2-4)

Z_A = the plastic section modulus of the critical section vertical leg of the angle and attached column, at a diagonal angle from the top of the stiffener to the point angle along the outside corner of the column just above where the angle begins to thicken at the fillet where the two legs of the angle join, defined as follows:

$$Z_A = \frac{W_A(t_A+t_c)^2}{4} \quad \text{(Eq 11-95)}$$

W_{Ab} = the width of the angle along the critical bending plane defined as follows:

$$W_{Ab} = \sqrt{{d_{Ah}}^2 + {d_{Av}}^2} \quad \text{(Eq 11-96)}$$

d_{Ah} = the horizontal moment arm for angle leg loaded in bending, defined as follows:

$$d_{Ah} = \frac{b_c}{2} - t_{wA} - \frac{t_s}{2} \quad \text{(Eq 11-97)}$$

t_{wA} = the thickness of the weld connecting the anchor stiffener plate to the anchor angle

t_s = the thickness of the anchor stiffener plate

d_{Av} = the vertical height of the angle that is vulnerable to bending failure, which is defined as follows:

$$d_{Av} = H_A - k \quad \text{(Eq 11-98)}$$

H_A = the width of the angle leg that is oriented vertically along the side of the column

k = the anchor angle thickness, t_A plus the leg-to-leg fillet radii of the angle shown in AISC (2011), Part 1, “Dimensions and Properties,” Table 1-7

t_A = the angle thickness

L_A = the angle moment arm, perpendicular to the critical bending plane defined by W_{Ab}, defined as follows:

$$L_A = \frac{d_{Av}}{W_{Ab}} L_{Av} \quad \text{(Eq 11-99)}$$

L_{Av} = the vertical moment arm, which equals the vertical distance from the critical shear plane, at the last row of screws or horizontal weld that connects the diagonal strap to the columns, to point on the angle vertical leg where it begins to thicken at the radii intersection with the horizontal leg (k defined above).

11.14.3 Column-to-anchor angle weld design

The angles can yield significantly through many cycles with no loss of shear and uplift resistance (but some loss of moment resistance). The welds along the top edge of the angles to the columns will be fillet welds, while the welds along the sides of the angles along the corners of the columns will be flare bevel groove welds (see Figure E2.5-2 of AISI 2007b). The maximum fillet weld thickness between anchors and columns are limited to the values shown in Table 11-9, when the minimum thickness of the component welded (the column) is greater or equal to 3/16 in. For columns with thickness less than 3/16 in., no maximum weld thickness is identified in AISI provisions (AISI 2007b, section E2.5 and Figure E2.5-4)[14]. The maximum angle thickness shall be based on the column-to-anchor weld thickness as indicated in Table 11-10.

Table 11-9. Maximum column-to-anchor fillet weld thickness (AISC 2010a, section J2b).

Column Material Thickness, t_c	Maximum Weld Thickness, t_w
3/16 in. (4.8 mm) ≤ t < ¼ in. (6 mm)	$t_w = t_c$
t ≥ ¼ in. (6 mm)	t_w = tc – 1/16 in. (2 mm)

Table 11-10. Maximum angle thickness based on column-to-anchor fillet weld thickness (AISC 2010a, Table J2.4).

Weld Thickness, t_w	Maximum Angle Thickness, t_A
1/8 in. (3 mm)	1/4 in. (6 mm)
3/16 in. (5 mm)	1/2 in. (13 mm)
1/4 in. (6 mm)	3/4 in. (19 mm)
5/16 in. (8 mm)	1-1/8 in. (29 mm)[15]

[14] The AISI Specification in fact provides guidance for Flare Groove Welds (E2.5), where the weld thickness is greater than twice the thickness of the thinner connected member—double shear design in Figure E2.5-4.

[15] Maximum thickness of standard angles shown in the *Steel Construction Manual* (AISC 2011).

The column-to-angle weld design strength, P_A, shall exceed the total uplift force applied to one angle at one side of the column due to uplift and bending. This is expressed as follows:

$$\frac{P_{vymax}}{2} + P_M \leq P_A = P_T + P_G \qquad \text{(Eq 11-100)}$$

where

P_A = the total vertical design capacity of the column-to-angle weld
P_T = the design strength of the transverse loaded fillet weld at the horizontal column-to-angle weld (Equation 11-88)
P_G = the design strength of the longitudinal loaded flare bevel groove weld at the vertical column-to-angle welds at the corner of the columns (Equation 11-101 or 11-102). The design strength for this column-to-angle weld shall be determined based on AISI guidance (AISI 2007a, section E2.5, "Flare Groove Welds"). The application of this guidance to the design of column-to-angle welds is determined as follows:

For $t_c \leq t_w < 2t_c$ (single shear)

$$P_G = 0.75\emptyset_G t_c L F_{cu} \qquad \text{(Eq 11-101)}$$

For $t_w \geq 2t_c$ (double shear)

$$P_G = 1.5\emptyset_G t_c L F_{cu} \qquad \text{(Eq 11-102)}$$

where

ϕ_G = the resistance factor for flare groove welds, equal to 0.55
t_c = the thickness of the column material
L = the length of the flare bevel groove weld
F_{cu} = the ultimate strength of the column steel
P_{vymax} = the net anchor vertical load at the maximum yield stress in the diagonal straps, expressed by:

$$P_{vymax} = F_{symax} n_s b_s t_s \left(\frac{H}{\sqrt{H^2+W^2}}\right) - \frac{GL_{min}}{2} \qquad \text{(Eq 11-103)}$$

where

GL_{min} = the minimum gravity load per shear panel, i.e., $(0.9 - 0.2S_{DS})D$, in Equation 11-19

P_M = the tensile force per anchor, beyond half the net anchor vertical load, P_{vymax}, that must be available to develop the design yield stress in the columns through combined tension and bending, which is determined by Equation 11-104. This assumes the anchor bolts are sufficiently tightened to provide a moment restraint:

$$P_M = \frac{M_{Rem}}{h_c} \quad \text{(Eq 11-104)}$$

where M_{Rem} is the moment capacity remaining in the column at which the maximum column fiber stress reaches its design yield value when subjected to both this moment and the maximum diagonal strap yield stress, P_{symax}. This capacity is defined as follows:[16] [17]

$$M_{Rem} = \left(F_{cy} - \frac{P_{vymax}}{A_c}\right)\left(\frac{I_c}{h_c - c}\right) \quad \text{(Eq 11-105)}$$

11.14.4 Anchor bolt design

The anchor bolts that fasten the column anchors to the reinforced concrete beam or slab are designed next. The same detail used in the anchors at the base of the columns shall be used in the anchors at the top of the columns. The anchor bolts shall be sized based on the bolt shear strength, P_v, tensile strength, P_t, and cone failure design strength, P_c. The anchor bolt shear design strength, P_v, (AISC 2010a, section J3.7, "Combined Tension and Shear in Bearing-Type Connections") shall exceed the applied shear load per bolt, P_{hAB}. This is expressed as follows:

---

[16] Note that the actual remaining moment capacity of the column can be greater than expressed by this equation because the actual column yield stress can be greater than the design yield stress. However, the anchor welds that are designed based on this expression are limited by the ultimate strength of the column material, so overstrength in the column yield will also result in greater strength in the anchor connection. This equation may also underestimate the loads applied to the anchor itself and anchor bolts. Still, this expression is sufficiently conservative, due to the significant overstrength accounted for in the diagonal strap (Equation 11-103) and the overstrength that will be present in both the anchor material and anchor bolts.

[17] The moment of inertia, I_c, in Equation 11-105 is divided by $h_c - c$, rather than c, because $h_c - c$ is the distance from the neutral axis to the outside extreme fiber of the column, which will be most critically stressed when the diagonal strap is in tension.

$$P_v \geq P_{hAB} = \frac{P_{humax}}{n_{AB}} \quad \text{(Eq 11-106)}$$

where

$$P_v = \emptyset_{tv} F_{nv} \frac{\pi}{4} d_{AB}^2 \quad \text{(Eq 11-107)}$$

n_{AB} = the total number of anchor bolts in the anchors on both sides of the column
ϕ_{tv} = the tensile and shear resistance factor, equal to 0.75 (AISC 2010a, section J3.7)
F_{nv} = the nominal shear strength of the anchor bolts (AISC 2010a, Table J3.2 "Nominal Strength of Fasteners and Threaded Parts,") ksi (MPa)
d_{AB} = the diameter of the anchor bolts
P_{humax} = the maximum shear panel horizontal force defined by Equation 11-91.

The anchor bolt tensile design strength, P_t, shall exceed the applied tensile force per bolt, P_{tAB}.[18] This is expressed as follows:

$$P_t \geq P_{tAB} \quad \text{(Eq 11-108)}$$

where

P_t = the anchor bolt tensile strength (ϕR_n in ANSI/AISC 360-10, section J3.7), determined as follows:

$$P_t = \emptyset R_n = \emptyset_{tv} F'_{nt} \frac{\pi}{4} d_{AB}^2 \quad \text{(Eq 11-109)}$$

[18] Consideration has been given to increasing the applied tensile force per anchor bolt, P_{tAB} to account for the effects of out-of-plane prying action at these joints, between stiffener plates and the anchor bolts in accordance with AISC *Steel Construction Manual* (AISC 2011, Part 9, pp 9-10 to 9-13). However, the anchor bolts are placed as close as possible to the stiffener plates to minimize this effect; prying in this out-of-plane direction is a minor secondary effect. Furthermore, the vertical leg of the anchor angles will be much more vulnerable to yielding between corners of the columns and the stiffener plates. The vertical leg yielding and deformation will act as a fuse to limit the deformation of the horizontal leg of the angle and thereby minimize prying action.

where

F'_{nt} = the nominal tensile stress modified to include the effects of shear stress, ksi (MPa), in accordance with ANSI/AISC 360-10 (AISC 2010a, section J3.7 and Table J3.2), as follows:

$$F'_{nt} = 1.3F_{nt} - \frac{F_{nt}}{\varphi_{nt}F_{nv}} f_{rv} \leq F_{nt} \quad \text{(Eq 11-110)}$$

where

F_{nt} = the nominal tensile stress for the bolts, ksi (MPa), ANSI/AISC 360-10 (AISC 2010a, Table J3.2)

F_{nv} = the nominal shear stress for the bolts, ksi (MPa), ANSI/AISC 360-10 (AISC 2010a, Table J3.2)

f_{rv} = the required shear stress, defined as follows:

$$f_{rv} = \frac{P_{hAB}}{\pi/4 d_{AB}^2} \quad \text{(Eq 11-111)}$$

The applied tensile force per anchor bolt, P_{tAB}, is calculated as follows:

$$P_{tAB} = \frac{P_{symax}L_s - \left(\frac{GL_{min}}{2}\right)\left(\frac{h_c}{2} + W_A\right) + M_{Rem}}{(d_c + h_c + W_A)\left(\frac{n_{AB}}{2}\right)} \quad \text{(Eq 11-112)}$$

where P_{symax} is the maximum yield strength of the diagonal strap(s) in the shear panel, in the axis of the strap. This is determined as follows:

$$P_{symax} = F_{symax} n_s b_s t_s \quad \text{(Eq 11-113)}$$

where

L_s = the distance between the where the centerline of the diagonal strap-to-column connection crosses the outside vertical plane of the column to the inside edge of the interior anchor of the same column, perpendicular to the axis of the strap. This is the lever arm that is multiplied by P_{symax} to apply a moment about the inside corner of the interior anchor about which the anchor would rotate if the anchor bolts failed, defined as follows:

$$L_s = \frac{WS_v}{\sqrt{W^2+(H-2S_v)^2}} + (h_c + W_A)\left(\frac{H-2S_v}{\sqrt{W^2+(H-2S_v)^2}}\right) \quad \text{(Eq 11-114)}$$

where

S_v = the vertical distance between where the centerline of the diagonal strap-to-column connection crosses the outside vertical plane of the column, to the top of the column top connections or bottom of the column bottom connections

W_A = the width of the anchor (angle section) in the in-plane direction of the shear panel

d_c = the horizontal distance between the face of the column to the anchor bolt(s) at the exterior of the column.

n_{AB} = the number of anchor bolts per column (either 2 or 4), symmetrically placed to both the interior and exterior of the columns (see Figure 12-4 through Figure 12-15 for examples).

The anchor bolts should be placed as close to each other as possible in the out-of-plane direction (i.e., on either side of the anchor stiffer plate) so as to minimize bending stress on the anchor angle, deformation of the angle, or prying action. Equation 11-115 provides the minimum distance between these anchor bolts. For anchors with two anchor bolts (n_{AB} = 2), only one anchor bolt is placed on each side of the column and $d_{c\text{-}c}$ is the twice the distance between the center of the anchor bolt and center of the stiffener plate in the out-of-plane direction.

$$d_{c-c\,\min} = OD + 2t_{wA} + t_S \quad \text{(Eq 11-115)}$$

where

OD = the outside diameter of the anchor bolt washer, for the anchor bolt of diameter, d_{AB} (AISC 2011, Part 7, "Design Considerations for Bolts," Table 7-14)

t_{wA} = the thickness of the angle to stiffener weld

t_S = the thickness of the stiffener plate.

11.14.5 Anchor angle thickness and anchor angle to stiffener weld

Trial anchor angle, selected based on Equation 11-92, must be checked for capacity between the stiffener plate and anchor bolt. Four modes of failure are possible: (1) weld failure between the stiffener plate and angle; (2)

shear rupture failure of the stiffener base metal along the weld to the angle; (3) shear yielding of the angle between the stiffener weld and bolt; and (4) shear rupture of the angle between the stiffener weld and bolt. The capacity of the stiffener plate to angle weld is defined as follows (AISC 2010a, Table J2-5):

$$P_{tAB} \leq P_{Aw} = 0.60\Phi_w F_{xx} t_{Aw} L_{Aw} \quad \text{(Eq 11-116)}$$

where

Φ_w = the weld shear loaded resistance factor, equal to 0.75
t_{Aw} = the fillet weld thickness between the stiffener plate and angle. The minimum effective thickness used to calculate the fillet weld strength in Equation 11-116 is 0.707 times the nominal weld thickness, t_{Aw} (see the definition for fillet weld effective throat, t_w in AISI 2007b (section E2.4, Fillet Welds, p 91)
L_{Aw} = the effective length of the weld between the stiffener plate and angle. The effective length of this weld is taken as less than the width of the angle minus the angle thickness and radii of the angle fillet (W_A – k), recognizing that the load will be concentrated near the anchor bolt. The edge distance between the anchor bolt and the end of the anchor and the outside diameter of the bolt washers (OD), will all influence the effective length.

The shear rupture capacity of the stiffener base metal along the weld to the angle is defined as follows (AISC 2010a, section J4.2, Eq. J4-4):

$$P_{tAB} \leq P_{Su} = 0.60\Phi_{su} F_{Su} t_{Aw} L_{Aw} \quad \text{(Eq 11-117)}$$

where

Φ_{Su} = the shear rupture resistance factor, equal to 0.75
F_{Su} = the ultimate strength of the stiffener steel.

The shear yielding capacity of the angle between the stiffener weld and anchor bolts is defined as follows (AISC 2010a, section J4.2, Eq J4-3):

$$P_{tAB} \leq P_{Ay} = 0.60\Phi_{sy} F_{Ay} t_A L_{Ay} \quad \text{(Eq 11-118)}$$

where

Φ_{sy} = the shear yielding resistance factor, equal to 1.00
L_{Ay} = the effective length of critical yield and rupture surface of the angle between the stiffener plate and anchor bolt. This length is taken as the smaller of the twice the anchor bolt washer outside diameter and the washer outside diameter plus the edge distance from the bolt to the edge of the anchor, defined as follows:

$$L_{Ay} = min(2OD, OD + W_A - d_c) \quad \text{(Eq 11-119)}$$

The shear rupture capacity of the angle between the stiffener weld and anchor bolts is defined as follows (AISC 2010a, section J4.2, Eq J4-4):

$$P_{tAB} \leq P_{Au} = 0.60\Phi_{su}F_{Au}t_AL_{Ay} \quad \text{(Eq 11-120)}$$

where

F_{Au} = the ultimate strength of the angle steel.

11.14.6 Cast-in anchor bolt breakout strength in tension

Panel anchors must be attached to the foundation or floor and roof diaphragms using cast-in anchors (or through-bolts for intermediate floor diaphragms and roof diaphragms as defined in the next section). The nominal concrete breakout strength in tension, N_{cb}, of a single anchor or N_{cbg} of a group of anchors shall not exceed the following specifications (ACI 2011a, Appendix D: "Anchoring to Concrete," section D.5.2.1).

For one anchor bolt on each side of the column (i.e., $n_{AB} = 2$):

$$P_{tAB} \leq \Phi_{ct}N_{cb} = \Phi_{ct}\frac{A_{Nc}}{A_{Nco}}\psi_{ed,N}\psi_{c,N}\psi_{cp,N}N_b \quad \text{(Eq 11-121)}$$

For two anchor bolts on each side of the column (i.e., $n_{AB} = 4$):

$$P_{tAB} \leq \frac{2\Phi_{ct}N_{cbg}}{n_{AB}} = \frac{2\left(\Phi_{ct}\frac{A_{Nc}}{A_{Nco}}\psi_{ec,N}\psi_{ed,N}\psi_{c,N}\psi_{cp,N}N_b\right)}{n_{AB}} \quad \text{(Eq 11-122)}$$

where

Φ_{ct} = the concrete anchor strength reduction factor for concrete breakout, side-face blowout, pullout, or pryout under tension loads, equal to 0.75, when supplementary reinforcement is present (Condition A) (ACI 2011a, Appendix D, section D.4.3.c)

A_{Nc} = the projected concrete failure area of a single anchor or group of anchors that shall be approximated as the base of the rectilinear geometrical figure that results from projecting the failure surface outward 1.5 h_{ef} (effective embedment depth of the anchor bolts) from the centerlines of the anchor, or in the case of a group of anchors, from a line through a row of adjacent anchors. A_{Nc} shall not exceed nA_{Nco} where n is the number of anchors in the group that resist tension, and equals $N_{AB}/2$. The following expression is used to calculate A_{Nc} (ibid.):

$$A_{Nc} = \left(c_{a1} + 1.5h_{ef}\right)\left(c_{a2} + d_{c-c} + 1.5h_{ef}\right) \qquad \text{(Eq 11-123)}$$

where

c_{a1} = the edge distance from the anchor bolts outside the columns to the edge of the concrete diaphragm in the plane of the shear panel. If c_{a1} is greater than or equal to 1.5 h_{ef}, then c_{a1} is set equal to 1.5 h_{ef}.

h_{ef} = the effective embedment depth of the anchor bolts.

c_{a2} = the edge distance from the anchor bolt closest to the edge of the concrete diaphragm in the out-of-plane direction of the shear panel. If c_{a2} is greater than or equal to 1.5 h_{ef}, then it is set equal to 1.5 h_{ef}.

d_{c-c} = the actual center-to-center distance between two anchor bolts at the outside of the column when the number of anchor bolts on both sides of the column, n_{AB}, equals four. If there is a single anchor bolt on each side of the column, where n_{AB} equals 2, d_{c-c} becomes 0 (zero) in Equation 11-126. Note that the expression in Equation 11-115 $d_{c-c\ min}$ applies to the case where one anchor bolt is located on both sides of the column and then it is meant to define the out-of-plane distance from the center of the stiffener to the single anchor bolt.

A_{Nco} = the projected concrete failure area of a single anchor with edge distance equal to or greater than 1.5 h_{ef}, where

$$A_{Nco} = 9h_{ef}^2 \quad \text{(Eq 11-124)}$$

$\Psi_{ed,N}$ = a modification factor for edge effects for single anchors or anchor groups loaded in tension. This term equals 1.0 if the minimum of the edge distances, c_{a1} and c_{a2}, defined above, is equal to or greater than 1.5 h_{ef}. If either of these terms is less than 1.5 h_{ef}, then $\Psi_{ed,N}$ is calculated based on the minimum of these terms as follows:

$$\psi_{ed,N} = 0.7 + 0.3\frac{C_{a,min}}{1.5h_{ef}} \quad \text{(Eq 11-125)}$$

$\Psi_{c,N}$ = a modification factor permitted for regions of where analysis indicates no cracking at service load levels. This factor may be 1.25 for cast-in anchors and 1.4 for post-installed anchors where the value for k_c used in Equation 11-126 is 17. Normally a value of 1.0 should be used, assuming some cracking of the concrete occurs.

$\Psi_{cp,N}$ = a modification factor post-installed anchors designed for untracked concrete without supplementary reinforcement to prevent splitting. This factor shall be computed in accordance with ACI 318-11, section D.5.2.7, using one of many critical edge distances defined in ACI 318-11, section D.8.6, for various types of post-installed anchors (ACI 2011a).

$\Psi_{ec,N}$ = a modification factor for anchor bolt groups loaded eccentrically in tension. This applies when two anchor bolts are at the outside of the column, when those bolts are not loaded equally. For these shear panels, the two anchor bolts would always be located the same distance from the face of the column, d_c, and therefore should be loaded equally, so that this term equals 1.0.

N_b = the basic concrete breakout strength of a single anchor in tension in cracked concrete, calculated as

$$N_b = k_c\lambda_a\sqrt{f_c'}h_{ef}^{1.5} \quad \text{(Eq 11-126)}$$

where

k_c = 24 for cast-in anchors and 17 for post-installed anchors.
λa = a modification factor for lightweight concrete; which shall be 1.0λ for cast-in or undercut anchors; 0.8λ for expansion or adhesive anchors; and 0.6λ for adhesive anchors where bond failure applies (see ACI 2011a, section D.5.5.2).
λ = a modification factor to account for lightweight concrete, equal to 0.85 for sand lightweight concrete and 0.75 for all-lightweight concrete and 1.0 for normal-weight concrete (ACI 2011a, section 8.6.1).
f_c' = the specified concrete compressive strength, in pounds per square inch, psi.

The anchor bolts shall not be installed too close to the edge of a concrete beam or slab, as defined by c_{a2} as this reduces the projected concrete failure area defined by Equation 11-123. If a shear panel is designed with only 2 anchor bolts per column (n_{AB} = 2) the diagonal straps and anchor bolts could be placed to the inside of the anchor stiffener plates. This would allow the shear panel to be placed close to the edge of the beam or slab to which it is anchored.

The anchor recommendations presented here are sufficiently conservative so that the lack of symmetry resulting from only two anchor bolts will not compromise ductile performance. The relatively large distance between the anchor bolts and column faces, d_c, should further reduce asymmetric loading of the anchor. However, if edge distance is not an issue, the use of four anchor bolts per column (n_{AB} = 4) is recommended.

11.14.7 Cast-in anchor bolt breakout strength in shear

The nominal concrete breakout strength in shear, V_{cb}, of a single anchor or V_{cbg} of a group of anchors, shall not exceed the following specifications (ACI 2011a, Appendix D, section E6.2.1).

For one anchor bolt on each side of the column, i.e., n_{AB} = 2:

$$P_{hAB} \leq \varphi_{cv} V_{cb} = \varphi_{cv} \frac{A_{Vc}}{A_{Vco}} \psi_{ed,V} \psi_{c,V} \psi_{h,V} V_b \qquad \text{(Eq 11-127)}$$

For two anchor bolts on each side of the column (i.e., n_{AB} = 4):

$$P_{hAB} \leq \frac{2\varphi_{cv}V_{cbg}}{n_{AB}} = \frac{2\left(\varphi_{cv}\frac{A_{Vc}}{A_{Vco}}\psi_{ec,V}\psi_{ed,V}\psi_{c,V}\psi_{h,V}V_b\right)}{n_{AB}} \quad \text{(Eq 11-128)}$$

where

φ_{cv} = the concrete anchor strength reduction factor for concrete breakout in shear, equal to 0.75, when supplementary reinforcement is present (Condition A) (ACI 2011a, section D.4.3.c).

A_{Vc} = the projected failure area of a single anchor or group of anchors as defined in ACI 318-11, section D.6.2.1 and Figure RD.6.2.1(b) (ACI 2011a). This figure defines this area for various combinations of edge distance, depth of anchor, depth of concrete, and single or groups of anchors. A_{Vc} shall not exceed nA_{Vco}, where n is the number of anchors in the group and equals $N_{AB}/2$. Equation 11-128 assumes the group failure area includes only the bolts on one side of a column (i.e., two bolts) because the large distance between them and the bolts on the other side of the column relative to the bolt effective embedment depth, h_{ef}.

A_{Vco} = the projected concrete failure area of a single anchor in a deep member with edge distance equal to or greater than $1.5c_{a1}$, where

$$A_{Vco} = 4.5c_{a1}^2 \quad \text{(Eq 11-129)}$$

$\Psi_{ed,V}$ = a modification factor for edge effects for single anchors or anchor groups loaded in shear. This term equals 1.0 if the minimum of the out-of-plane edge distance, c_{a2}, is greater or equal to the 1.5 times the in-plane edge distance, c_{a1}. If c_{a2} is less than $1.5c_{a1}$, then $\Psi_{ed,V}$ is calculated as follows:

$$\psi_{ed,V} = 0.7 + 0.3\frac{c_{a2}}{1.5c_{a1}} \quad \text{(Eq 11-130)}$$

$\Psi_{c,V}$ = a modification factor permitted for regions of where analysis indicates no cracking. This factor may be 1.2 for anchors in cracked concrete with reinforcement of a No. 4 bar or greater between the anchor and the edge. It may be 1.4 for anchors in concrete with reinforcement of a No. 4 bar or greater between the anchor and the edge, and with the reinforcement enclosed

within stirrups spaced at not more than 4 in. Normally a value of 1.0 should be used, assuming some cracking of the concrete occurs.

$\Psi_{h,V}$ = a modification factor for anchors located in concrete members where the depth of the member, h_a, is less than $1.5c_{a1}$, which shall be computed as follows (but shall not be less than 1.0) (ACI 2o11a, Appendix D ("Anchoring to Concrete," section D.6.2.8):

$$\psi_{h,V} = \sqrt{\frac{1.5c_{a1}}{h_a}} \quad \text{(Eq 11-131)}$$

$\Psi_{ec,V}$ = a modification factor for anchor bolt groups loaded eccentrically in shear. This applies when two anchor bolts are at the outside of the column and are not loaded equally. If diagonal straps were installed on only one face of the shear panels, two anchor bolts were installed outside each column (i.e., $n_{AB} = 4$), the eccentric loading of the bolts would equal the depth of the panel divided by 2 ($b_c/2$).

V_b = the basic concrete breakout strength of a single anchor in shear in cracked concrete, which shall equal the smaller of Equation 11-132 and 11-133:

$$V_b = \left[7\left(\frac{l_e}{d_{AB}}\right)^{0.2}\sqrt{d_{AB}}\right]\lambda_a\sqrt{f_c'}c_{a1}^{1.5} \quad \text{(Eq 11-132)}$$

l_e = the load-bearing length of the anchor for shear; and equals the length of the anchor bolt, h_{ef}, for anchors with constant stiffness over their full length; equals twice the bolt diameter (d_{AB}) for torque-controlled expansion anchors with a distance sleeve separated from expansion sleeve; and shall not exceed eight times the diameter of the anchor bolt, d_{AB}.

$$V_b = 9\lambda_a\sqrt{f_c'}c_{a1}^{1.5} \quad \text{(Eq 11-133)}$$

11.14.8 Through-bolt floor diaphragm evaluation

Panel anchors may be attached to intermediate floor diaphragms or roof diaphragms using bolts installed through holes cast or drilled through the floor or roof diaphragms. Shear reinforcing shall be installed through the area between the anchors above one column and below the column of the

story above. Positive and negative longitudinal reinforcing steel shall be installed through the joint area between the column anchors of the panels above and below. The shear and moment capacity of the beam or slab must be evaluated to ensure they can resist effects of the applied tensile force per bolt, $P_{tAB,}$ and applied shear force per bolt, $P_{hAB.}$ The shear design capacity, ϕV_n, in the region of the panel anchors shall exceed the applied shear forces expressed as follows:

$$\emptyset V_n \geq P_{tAB} \frac{n_{AB}}{2} + V_u \qquad \text{(Eq 11-134)}$$

where

ϕ = the shear strength reduction factor, equal to 0.75 (ACI 2011a, section 9.3.2.3)
V_n = the nominal shear strength determined based on guidance in ACI 318-11 (ACI 2011a, section 11.1.1, Eq 11-2).
V_u = the factored shear force applied to the beam or slab section between the column anchors from the floor or roof gravity load and vertical seismic forces.

The flexural design capacity, ϕM_n, in the region of the panel anchors shall exceed the applied moment, M_u, expressed as follows:

$$\emptyset M_n \geq M_u = P_{tAB} \frac{n_{AB}}{2} (d_c + h_c + W_A) + M_{u1} \qquad \text{(Eq 11-135)}$$

where

ϕ = the flexure strength reduction factor, equal to 0.90 (ACI 2011a, section 9.3.2.1)
M_n = the nominal flexure strength determined based on guidance in ACI 318-11 (ACI 2011a, Chapter 10).
M_{u1} = the factored moment applied to the beam or slab section between the column anchors from the floor or roof gravity load and vertical seismic forces.

Through-bolt anchors must also meet the requirements for concrete breakout strength in shear expressed by Equations 11-127 and 11-128.

12 Seismic Design Example

An example problem is presented here to demonstrate the design process presented in Chapter 11. Shear panels will be designed in the short direction of the building only to illustrate the design process. In an actual building the lateral-load-resisting system must be designed in both directions. This example is a U.S. Army barracks building of a type that will be designed for construction at Fort Lewis, located between Tacoma and Olympia, WA. This building is similar to a Corps of Engineers Prototype 3 Story Steel Stud Framed Barracks Building for Seismic Zones 0 – 2 (Matsen Ford Design 1997). A three-dimensional view of one end of this building is shown in Figure A-1 in Appendix A of this report. The reader is referred to tabular data and equations presented in Chapter 11 of this report. When needed, ASCE/SEI 7-10 (ASCE 2010) and other guidance is referenced.

12.1 Risk category

The barracks building is a Risk Category II structure (ASCE/SEI 7-10, Table 1.5-1).

12.2 Importance factors

This risk category gives the barracks building a Seismic Importance Factor, I_e, of 1.0 (see Table 12-1).

12.3 Ground motion definition

The maximum considered earthquake ground motions were determined by searching the U.S. Geological Survey website (http://geohazards.usgs.gov/designmaps/us/application.php) for Fort Lewis, WA, using ASCE/SEI 7-10 as the building code reference document, Site Soil Classification D, and Risk Category I/II/II. Based on this input, the site provided a spectral response acceleration for short periods, S_s, of 1.287 g and the spectral response acceleration for 1 second, S_1, of 0.508 g. Table 12-1 summarizes these values. The soil conditions were unknown, so a reasonable worst-case site classification of D was used. Values of site coefficients, F_a and F_v, were obtained from Table 11-2 and Table 11-3, and are shown in Table 12-1. Values for the maximum considered earthquake spectral response acceleration for short periods, S_{MS}, and at 1 second, S_{M1}, adjusted for site class effects, were calculated using Equations 11-1 and 11-2, and are shown in Table 12-1. Design

earthquake spectral response acceleration at short periods, S_{DS}, and 1 second period, S_{D1}, were calculated using Equations 11-3 and 11-4, and are shown in Table 12-1. The long-period transition period, T_L, was determined using the USGS website noted above, and has a value of 6 seconds.

Table 12-1. Earthquake ground motion definition summary for Fort Lewis.

Risk Category	II
Seismic importance factor, I_e	1.0
Short period spectral response acceleration, S_S	1.287 g
1 second spectral response acceleration, S_1	0.508 g
Site classification	D
Site coefficient, F_a	1.0
Site coefficient, F_v	1.5
Adjusted short period spectral response acceleration, S_{MS}	1.287 g
Adjusted 1 second spectral response acceleration, S_{M1}	0.762 g
Design short period spectral response acceleration, S_{DS}	0.858 g
Design short period spectral response acceleration, S_{D1}	0.508 g
T_0	0.118 seconds
T_S	0.592 seconds
Long-period transition period, T_L	6 seconds
Assumed design spectral response acceleration, S_a	0.858 g
Seismic design category	D
Response modification coefficient, R	4
Deflection amplification factor, C_d	3.5

A design response spectrum was developed from these terms, as described in Chapter 11, using Equations 11-5 through 11-7, and plotted in Figure 12-1. For the natural period of the structure, T, this spectrum defines values of effective acceleration. The natural period of the barracks building, T, will almost certainly fall between T_0 and T_S, defined in Chapter 11, so that the design spectral acceleration, S_a, will equal S_{DS}. Values for T_0 and T_S are shown in Table 12-1. After the building frame is designed, the building natural period will be calculated to ensure that it falls between T_0 and T_S, and corrections will be made if needed.

Figure 12-1. Design response spectrum for Fort Lewis, WA, barracks building.

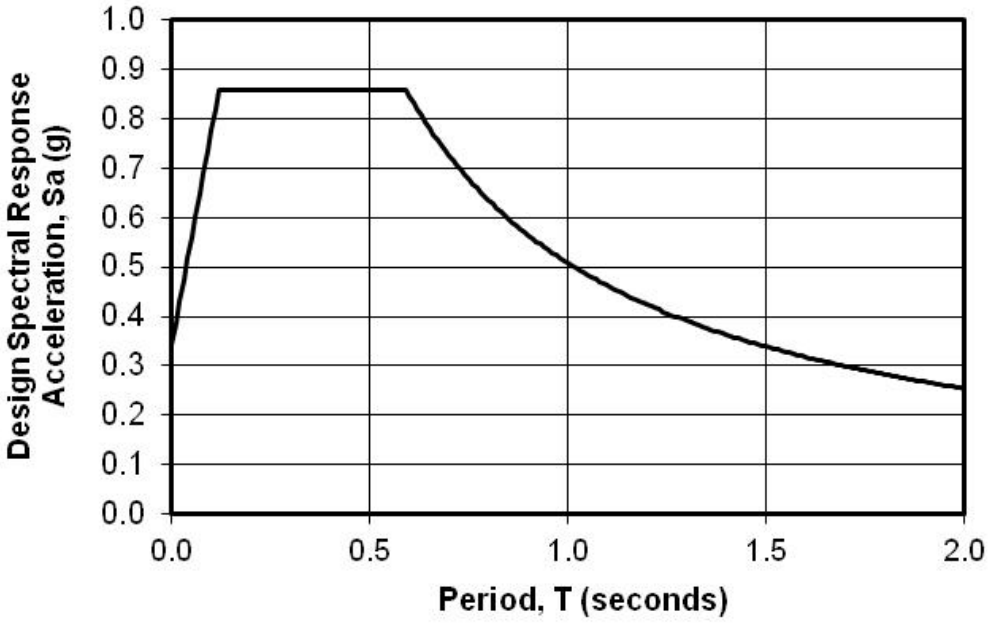

12.4 Seismic design category

The seismic design category for the barracks building was determined from Table 11-4 or Table 11-5, based on the risk category (II) and values of S_{DS} and S_{D1}. If the tables give different categories, the larger letter is chosen. For the barracks building, the seismic design category is D (see Table 12-1).

12.5 Structural design criteria

The lateral-load-resisting system of the barracks building will be designed with cold-formed steel shear panels with diagonal straps acting as the sole lateral-load-resisting elements. Values of the response modification coefficient, R, and deflection amplification factor, C_d, are taken from Table 11-6 and shown in Table 12-1.

12.6 Structural configuration and redundancy

The diaphragms of the barracks building are reinforced concrete and considered rigid. This building is in Seismic Design Category D, and the first and second floors of this three-story building will resist more than 35% of the base shear. Therefore, the braced frame requirements of ASCE/SEI 7-10, Table 12.3-3, must apply to this building if the redundancy factor, ρ, is to be kept at 1.0 (not increased to 1.3). These requirements will be kept be-

cause the removal of an individual brace or connection would not result in more than a 33% reduction in story strength, nor would it cause an extreme torsional irregularity (Type 1b defined in ASCE/SEI 7-10, Table 12.3-1). These requirements will be satisfied because the design concept for the barracks building will permit the distribution of multiple shear panels throughout the plan of the building (see Figure 12-2). Therefore, the redundancy factor was set to 1.0.

12.7 Barracks building load combinations and calculations

The effects of gravity load (dead, live, and snow) and seismic forces shall be combined as defined by Equations 11-14 and 11-15. As explained in Chapter 11, the total lateral force that must be resisted by the shear panel diagonal straps is simply defined by ρQ_E in these equations. In the case of the barracks building, this becomes Q_E because ρ equals 1.0., and the shear panel dimensions and diagonal strap design are based on the forces defined by this term.

The barracks building will be designed to act independently in the two orthogonal directions. Figure 12-2 and Figure 12-3 show schematic drawings of the barracks building. Figure 12-2 shows the plan view and long-direction elevation. Figure 12-3 shows the short-direction elevation of the building.

Figure 12-2. Barracks long-direction elevation and plan views.

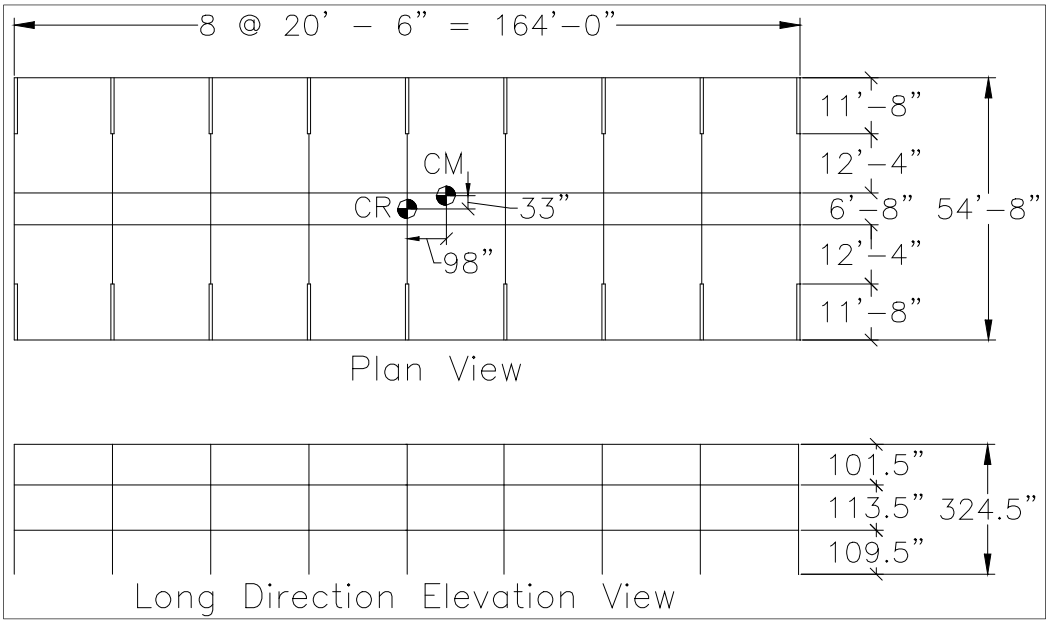

Figure 12-3. Barracks building short-direction elevation and plan views.

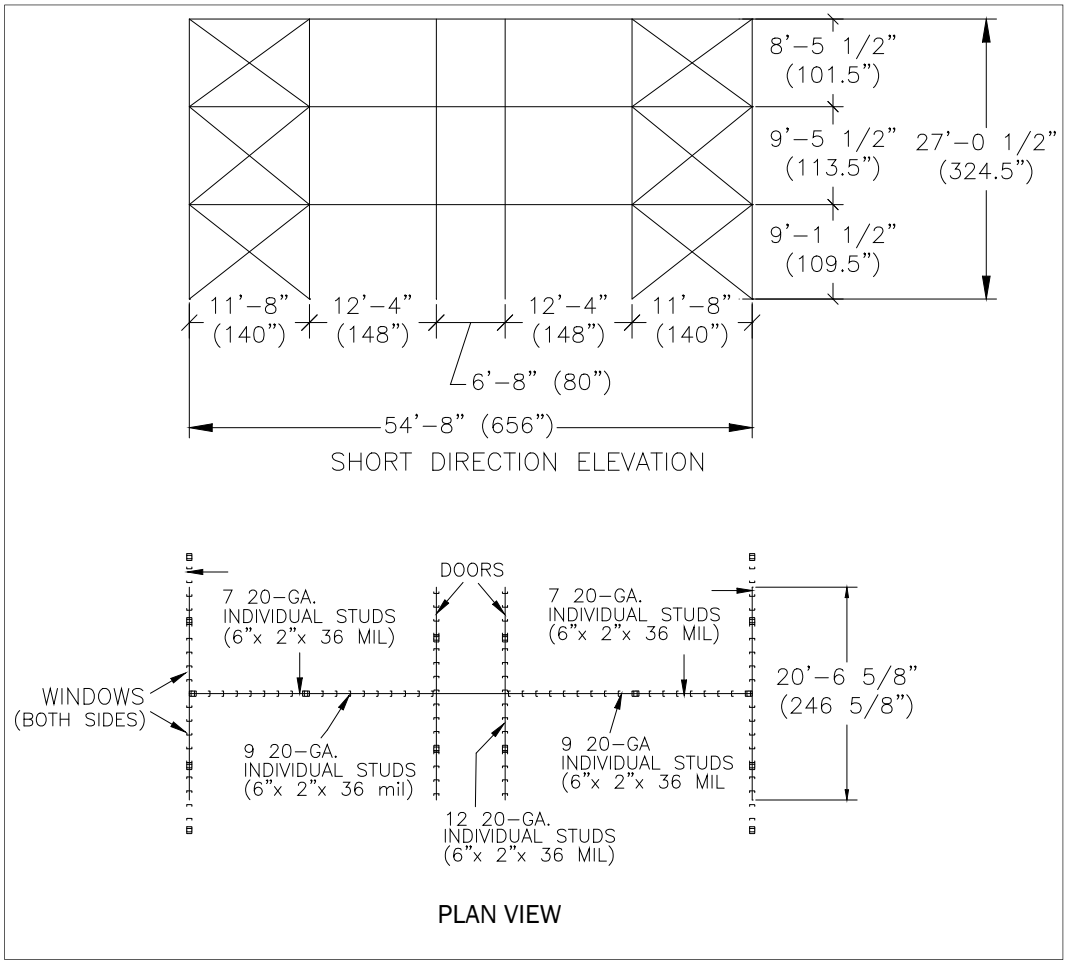

Table 12-2 and Table 12-3 summarize the weight calculations made for the entire building using a spreadsheet. These weights include roof and floor dead load (20 and 45 psf, respectively); exterior wall weight (10 psf); interior wall weight (10 psf); brick veneer weight (40 psf); and room and corridor live load (40 and 80 psf, respectively) (Matsen Ford Designs 1997, prototype drawings-Sheet C-1). The brick veneer is self-supporting for gravity loads, and for vertical and in-plane lateral seismic forces. The building lateral-load-resisting system (shear panels) resists out-of-plane lateral seismic forces from the brick veneer weight. Therefore, the short-direction shear panels resist the out-of-plane long-direction brick veneer lateral seismic forces.

Table 12-2. Barracks building, weight calculations.

Floor Level	Roof and Floor Dead Load (psf)	Floor Length (ft)	Floor Width (ft)	Floor Area (ft^2)	Total Floor Dead Load D (kips)	Story Height (ft)	Exterior Walls (psf)	Total Exterior Walls EW (kips)	Interior Walls (psf)	Total Interior Walls IW (kips)	Total Dead Load D_T= D+EW+IW (kips)	Self Supporting for gravity Brick Veneer (psf)	Long Direction Brick Veneer B_L (kips)	Short Direction Brick Veneer B_S (kips)	Short Direction Seismic Weight W_S (k-mass)
Roof															
3rd	20	164	54.7	8988	180	4.2	10	19	10	30	228	40	56	18	284
2nd	45	164	54.7	8988	404	9.0	10	39	10	64	507	40	118	39	625
1st	45	164	54.7	8988	404	9.3	10	41	10	66	511	40	122	41	634
															1543

Table 12-3. Barracks building, additional load calculations.

Floor Level	Room Live Load (psf)	Room Area (ft^2)	Corridor Live Load (psf)	Corridor Area (ft^2)	Total Floor Live Load L (kips)	Sloped Roof Snow Load p_s (psf)	Roof Area (ft^2)	Total Roof Snow Load S (kips)
Roof								
3rd	0	7892	0	1096	0	10.1	8988	91
2nd	40	7892	80	1096	403	0	0	0
1st	40	7892	80	1096	403	0	0	0

The short-direction shear panels will be placed at every bay (20 ft, 6-5/8 in. spacing) of the building, as shown in Figure 12-2, for a total of nine short-direction frames. A trial shear panel configuration will be assumed in which two shear panels are placed at every frame, as shown in Figure 12-3. That figure shows two shear panels placed against the perpendicular outside walls of the building. Shear panels will be located at each floor level, with decreasing capacity at the higher floor levels.

The ground snow load, p_g, for Fort Lewis is 20 psf (ASCE/SEI 7-10, Chapter 7 and Chapter 7 commentary). Based on ASCE/SEI 7-10, the flat-roof snow load, p_f, is calculated as follows (ASCE/SEI 7-10, Eq 7.3-1):

$$p_f = 0.7C_eC_tI_sp_g = 0.7(0.9)(1.0)(1.0)(20psf) = 12.6psf \quad \text{(Eq 12-1)}$$

where

C_e = the exposure factor (ASCE/SEI 7-10, Table 7-2), which for a terrain category C, fully exposed roof is 0.9

C_t = the thermal factor (ASCE/SEI 7-10, Table 7-3), which is taken as 1.0

I_s = the snow importance factor (ASCE/SEI 7-10, Table 1.5-2), which for Risk Category II of the barracks building is 1.0.

The sloped-roof snow load, p_s, is calculated as follows (ASCE/SEI 7-10, Eq 7.4-1):

$$p_s = C_s p_f = (0.80)(12.6psf) = 10.1psf \quad \text{(Eq 12-2)}$$

where

C_s = the roof slope factor (ASCE/SEI 7-10, Figure 7.2b), which is 0.8 for the barracks building with a cold unobstructed slippery surface and a 5/12 roof slope.

The calculation of the snow load, S, is summarized in Table 12-3.

12.8 Earthquake force definition

Seismic forces are now defined based on the equivalent lateral force procedure (see section 11.9). The seismic base shear, V, in the direction of the shear walls is given by Equation 12-3 (previously Equation 11-20):

$$V = C_s W \quad \text{(Eq 12-3)}$$

The seismic response coefficient, C_s (Equation 11-21), is calculated with the variables given in Table 12-1, which becomes:

$$C_s = \frac{S_{DS}}{R/I_e} = \frac{0.858\ g}{4/1.0} = 0.215g \quad \text{(Eq 12-4)}$$

The value of C_s need not exceed the following (using Equation 11-22 and 11-23):

$$C_s = \frac{S_{D1}}{T(R/I)} = \frac{0.508g}{0.24(4/1.0)} = 0.536g \text{ for } T \le T_L \quad \text{(Eq 12-5)}$$

$$C_s = \frac{S_{D1}T_L}{T^2\left(\frac{R}{I_e}\right)} = \frac{(0.508g)(6)}{(0.24)^2(\frac{4}{1.0})} = 13.6\ g \text{ for } T > T_L \quad \text{(Eq 12-6)}$$

but shall not be less than (using Equation 11-24):

$$C_s = 0.044 S_{DS} I_e = 0.044(0.858g)(1.0) = 0.038g \qquad \text{(Eq 12-7)}$$

The approximate fundamental period, T_a, in seconds is calculated using the following equation (based on Equation 11-26):

$$T_a = C_t h_n^x = (0.020)(27)^{0.75} = 0.24\ seconds \qquad \text{(Eq 12-8)}$$

where

C_t = 0.020 for cold-formed steel shear panels with diagonal straps
h_n = the height, which is 27 ft to the top of the shear walls for the barracks building.

This approximate period, T_a, was used for the fundamental period, T, in Equations 12-5 and 12-6 without correction.

12.9 Short-direction earthquake force definition

The effective seismic weight, W, including roof and floor dead load, exterior walls, and brick veneer perpendicular to the direction under consideration were calculated from the loads presented in Table 12-2 as follows:[19]

$$W = D_T + B = D + EW + IW + B \qquad \text{(Eq 12-9)}$$

For the short direction of the building this weight, W_S, becomes:

$$W_s = D_T + B_L = D + EW + IW + B_L \qquad \text{(Eq 12-10)}$$

where

D_T = the total dead load
B = the brick veneer weight
D = the floor and roof dead load
EW = the exterior wall weight
IW = the interior wall weight

[19] Based on ASCE/SEI 7-10, Section 12.7.2, the barracks building is not used for storage, so no live load is included in the effective seismic weight; permanent equipment is not used; and the flat snow load does not exceed 30 psf, so snow loads are not included.

B_L = the brick veneer weight in the long direction of the building carried by the shear panels in the short direction of the building.

The cumulative total weight in the short direction of the building, W_S, at the first floor is equal to 1,543 kips, as shown in Table 12-2.

The base shear in the short direction of the building, V_S, is now calculated from Equation 11-20:

$$V_S = C_S W_S = (0.215g)(1{,}543kips) = 331kips \qquad \text{(Eq 12-11)}$$

The vertical distribution of lateral seismic forces in the short direction, F_{xS}, induced at any level shall be determined using Equation 11-27. These values are determined based on the vertical distribution factor in the short direction, C_{vxS}, calculated in Equation 11-28. Values for W_{xS}, h_x, w_i, and h_i used in Equation 11-28 are given in Table 12-4.

The short-direction lateral seismic forces, F_{xS}, shown in Table 12-4 are the lateral force per frame in the short direction. There are nine frames in the short direction, n_S[20], so that lateral force per frame is calculated as follows:

$$F_{xS} = \frac{C_{vxS} V_S}{n_S} \qquad \text{(Eq 12-12)}$$

Table 12-4. Short-direction lateral seismic force calculations for barracks building.

Panel Level	Short Direction Total Weight W_S (k-mass)	Seismic Response Coefficient C_s (g)	Short Dir Base Shear V_S (kips)	Height at Floor Level h_{xS} or h_{xL} (ft)	Short Dir Vertical Distribution Factor C_{vxS}	Number Frames in Short Dir n_S	Short Dir Lateral Seismic Force/frame F_{xS} (kips)	Accidental Torsion M_{tax} (kip-ft)	Max. Add Shear due to Acc Torsion Q_{sic} (kips)	Short Dir Seismic Story Shear V_{xS} (kips)
Roof										
3rd	284			27.0	0.306	9	11.3	1074	2.6	13.9
Cumulative	284									
2nd	625			18.6	0.463	9	17.0	1627	4.0	34.9
Cumulative	909									
1st	634			9.1	0.230	9	8.5	809	2.0	45.3
Cumulative	1543	0.215	331							

[20] The symbol for the number of frames in the short direction, n_S, must not be confused with the number of faces with diagonal straps on a given shear panel, n_s.

The barracks building floor is a metal deck filled with concrete so that the diaphragm is rigid (ASCE/SEI 7-10, section 12.3.1.2). The building is very regular in plan, so the center of rigidity, C_R, in both directions should be at the center of the building. The accidental torsion is accounted for by off-setting the center of mass, C_M, 5% in both directions in plan at each floor level (see Figure 12-2). The total mass at each floor level in each direction (long and short) is multiplied by the 5% of the building dimension in that direction to calculate the accidental torsional moment, M_{ta}, at each floor level. As were the lateral seismic forces, the accidental torsional moments, M_{tax}, were distributed along the floors of the building according to the vertical distribution factor given in Equation 11-28, which is expressed as follows:

$$M_{tax} = 0.05[V_S C_{vxS}(FloorLength) + V_L C_{vxL}(FloorWidth)] \quad \text{(Eq 12-13)}$$

where

C_{vxL} = vertical distribution factor in the long direction
V_L = the base shear in the long direction.

Table 12-4 gives values for accidental torsional moments, M_{tax}, at each floor level.

The torsional resistance, M_{tr} (see Equation 11-32), is proportional to the square of the distance from the center of resistance to the plane of each panel. The torsional resistance is also proportional to the lateral stiffness of each panel. Therefore, because the barracks building is very long in one direction, the shear panels in the short direction near the ends of the building will dominate the torsional resistance. For this example, it will be assumed that all torsional resistance comes from the shear panels in the short direction. The torsional resistance from all shear panels, M_{tr}, in the short direction can be expressed as follows (based on Equation 11-32):

$$M_{tr} = \sum_{i=1}^{n} \rho_i^2 k_{si}\theta = 4[(20.5')^2 + (2x20.5')^2 + (3x20.5')^2 + (4x20.5')^2]k_{si}\theta = 4(20.5')^2(30)k_{si}\theta \quad \text{(Eq 12-14)}$$

The shear panel farthest from the center of rigidity provides the greatest torsional resistance. However, the end panels in the short direction against the exterior walls will not be loaded as heavily as the panels one bay in from the end because the end panels have only half the tributary area as

the panel one bay in. Therefore, the panels which are one bay in from the end will be the most critically loaded because of lateral loads in the short axis and the full width of that bay, and because of its large contribution to torsional resistance. The torsional resistance of the two shear panels that make up the critical short-direction frame, M_{trc}, may be expressed as follows:

$$M_{trc} = \sum_{i=1}^{n} \rho_i^2 k_{si}\theta = 2[(3x20.5)^2]k_{si}\theta = 2(20.5')^2(9)k_{si}\theta \quad \text{(Eq 12-15)}$$

Equation 12-15 shows that the critical short-direction frame provides $3/20$ of the total building torsional resistance (Equation 12-15 divided by Equation 12-14). This ratio can be used to calculate the applied torsion in the critical frame by equating the total accidental torsion, M_{ta}, and torsional resistance from all shear panels, M_{tr}, as follows:

$$M_{trc} = \frac{M_{trc}}{M_{tr}} M_{ta} = \frac{3}{20} M_{ta} \quad \text{(Eq 12-16)}$$

The additional shear force due to accidental torsion for the critical frame is now calculated by solving Equation 11-30 for Q_{sic}, as follows:

$$Q_{sic} = \frac{M_{trc}}{\rho_c} \quad \text{(Eq 12-17)}$$

Values of this additional shear force are given in Table 12-4 for each floor level.

Values of seismic story shear in the short direction, V_{xS}, are calculated by modifying Equation 11-29 to include the effects of accidental torsion as follows:

$$V_{xS} = \sum_{i=x}^{n} (F_i + Q_{sic}) \quad \text{(Eq 12-18)}$$

12.10 Long-direction earthquake force definition

The same process is repeated for the definition of earthquake forces in the long direction of the building. These results are summarized in Table 12-5. The effects from accidental torsion are not added to the frames in the long direction of the building. The frames in the short direction near the ends of the building are much more effective in resisting torsion than those in the long direction, due to their greater distance from the center of rotation (see Equation 11-32).

Table 12-5. Long-direction lateral seismic force calculations for the barracks building.

Panel Level	Long Direction Total Weight W_L (k-mass)	Seismic Response Coefficient C_s (g)	Long Dir Base Shear V_L (kips)	Height at Floor Level h_{xS} or h_{xL} (ft)	Vertical Distribution Factor C_{vxL}	Number Frames in Long Dir n_L	Long Dir Lateral Seismic Force/frame F_{xL} (kips)	Long Dir Seismic Story Shear V_{xL} (kips)
Roof								
3rd	247			27.0	0.305	2	44.0	44.0
Cumulative	247							
2nd	547			18.6	0.464	2	67.0	111.1
Cumulative	794							
1st	552			9.1	0.230	2	33.2	144.3
Cumulative	1345	0.215	289					

12.11 Diagonal strap design

From the values of seismic story shear, V_x ($V_x + Q_{si}$ in Equation 11-37), the shear panels are configured and the diagonal straps designed according to Equation 11-37. Values of the shear panel design strength, $\phi_t Q_{sy}$, are given in Table 12-6. Two identical shear panels are designed to resist the applied story shear in the short direction, V_{xS}, per shear panel ($V_x + Q_{si}$ in Equation 11-37), and these are defined in Table 12-6. Trial shear panel dimensions and diagonal strap sizes for each floor level are defined so that the design strength, $\phi_t Q_{sy}$, exceeds the applied story shear ($V_x + Q_{si}$) per shear panel using the spreadsheet program that models Equation 11-37. Table 12-6 shows trial shear panel configurations that meet this requirement for each floor of the critical frame in the barracks building example. All diagonal straps require ASTM A1003/A1003M, Type H, Grade 33 or Grade 50 steel (ST33H or ST50H) (ASTM 2013b). Panel dimensions are based on the dimensions given for shear wall Type SW-3 (Interior Load-Bearing Walls) of the barracks building drawings (Matsen Ford Design 1997, Sheet S-6). Table 12-6, and all similar panel design tables that follow, was generated by the *Excel Cold-Formed Steel Seismic Design Tool* (Wilcoski 2014). Users of this design tool should design shear panels by changing the cells with white background; cells with gray background are calculated based on the Chapter 11 design recommendations and should not be changed by the user.

Table 12-6. Diagonal strap design in the short direction.

Column Type / Figure No.	Panel Width W (in.)	Panel Height H (in.)	Strap Faces n_s (#)	Strap Width b_s (in.)	Strap Design Thickness (ga)	Strap Design Thickness t_s (in.)	Strap Initial Lat Stiffness k_s (k/in)	Yield Stress of Strap F_{sy} (ksi)	Strap Lat Yield Capacity Q_{sy} (kips)	Design Shear Strength $\phi_t Q_{sy}$ (kips)	Lat Defl at Strap Yielding δ_{sy} (in.)	Applied Story Shear V_{xS} (kips)	Elastic Lateral Defl δ_{xe} (in.)	Defl Amp Factor C_d	Seismic Import Factor I_e	Design Story Drifts $\Delta=\delta_x$ (in.)	Stability Coeff θ	Allow Story Drifts Δ_a (in.)
3rd Floor/12-4	132	101.5	1	4	14	0.0716	31	33	7.5	6.7	0.239	6.94	0.221	3.5	1.0	0.77	0.0009	2.03
3rd Floor/12-7	132	101.5	1	4	16	0.0568	25	50	9.0	8.1	0.362	6.94	0.279	3.5	1.0	0.98	0.0011	2.03
3rd Floor/12-8	132	101.5	2	4	18	0.0453	40	33	9.5	8.5	0.239	6.94	0.175	3.5	1.0	0.61	0.0007	2.03
3rd Floor/12-9*	132	101.5	1	4	16	0.0568	25	50	9.0	8.1	0.362	6.94	0.279	3.5	1.0	0.98	0.0011	2.03
2nd Floor/12-10	140	113.5	2	6	18	0.0453	53	50	21.1	19.0	0.400	17.43	0.331	3.5	1.0	1.16	0.0029	2.27
2nd Floor/12-11*	140	113.5	2	6	18	0.0453	53	50	21.1	19.0	0.400	17.43	0.331	3.5	1.0	1.16	0.0029	2.27
2nd Floor/12-12	140	113.5	2	6	18	0.0453	53	50	21.1	19.0	0.400	17.43	0.331	3.5	1.0	1.16	0.0029	2.27
1st Floor/12-13*	140	109.5	2	6	16	0.0568	69	50	26.9	24.2	0.389	22.65	0.328	3.5	1.0	1.15	0.0045	2.19
1st Floor/12-14	140	109.5	2	6	16	0.0568	69	50	26.9	24.2	0.389	22.65	0.328	3.5	1.0	1.15	0.0045	2.19
1st Floor/12-15	140	109.5	2	4	12	0.1021	83	50	32.2	29.0	0.389	22.65	0.274	3.5	1.0	0.96	0.0038	2.19

*Asterisk designates selected panels.

The diagonal straps are the sole lateral-load-resisting element, and as such they determine the story drifts. The elastic deflections, δ_{xe}, at each floor level are calculated as follows:

$$\delta_{xe} = \frac{\delta_{sy}}{Q_{sy}} \frac{V_{xS}}{n_S} \quad \text{(Eq 12-19)}$$

where δ_{sy} is the lateral deflection at diagonal strap yielding given by

$$\delta_{sy} = \frac{F_{sy}}{E}\left(\frac{H^2+W^2}{W}\right) \quad \text{(Eq 12-20)}$$

Values of δ_{xe} are given in Table 12-6 for the trial diagonal straps at each floor level in the short direction of the building. The design story drifts, Δ, are the differences in deflection at the center of mass at the top and bottom of the story under consideration. These deflections are calculated from the elastic deflection, δ_{xe}, as follows (from Equation 11-34):

$$\Delta = \delta_x = \frac{C_d \delta_{xe}}{I_e} \quad \text{(Eq 12-21)}$$

where

C_d = the deflection amplification factor given in Table 12-1 (3.5 for diagonal-strap panels)

I_e = the seismic importance factor given in Table 12-1 (1.0 for the barracks building).

Values for the design story drifts are given in Table 12-6.

Increases in design story drift, Δ related to P-delta effects are now evaluated. P-delta effects do not need to be considered if the stability coefficient, θ, is equal to or less than 0.10. The stability coefficient, θ, is defined in Equation 11-35 and values are given in Table 12-6. These values are well below 0.10, so design story drifts do not need to be increased. Values of design story drifts, Δ, must be less than the allowable story drifts, Δ_a, given in Table 11-7. For the barracks building this may be expressed as follows (from Table 11-7):

$$\Delta_a = 0.020H \qquad \text{(Eq 12-22)}$$

Values of design story drift, Δ, and allowable story drift, Δ_a, are given in Table 12-6 for each floor level for the trial panels in the short direction of the barracks building. The values in Table 12-6 show that design story drifts fall below allowable drifts. Therefore, these trial sizes meet the drift requirements.

12.12 Column design

Columns are either built up from studs (Panel A or C configuration) or are structural tubes (Panel D). The columns built up with cold-formed steel studs must have the studs oriented to form a closed cross-section as shown on the drawings for test panels A3 and C1 in Appendix A. Individual studs must be welded to each other with a weld thickness equal to the thickness of the studs. The welds are intermittent, with a length and spacing that will ensure composite behavior of the columns.

Structural tubing columns consist of a single tube that is a closed section by itself. This column will provide greater moment resistance because of the heavier anchorage detail, and will provide a greater degree of structural redundancy and widening of the shear panel hysteretic performance.

12.12.1 Column applied loads

Equation 11-18 expresses total load applied to the entire building in the short direction, where the effects of gravity load and seismic forces are additive and diagonal strap overstrength is accounted for. This equation can be expressed in terms of the total dead load, D_T; live load, L; and snow load, S; (given in Table 12-7) as follows:

$$(1.2 + 0.2S_{DS})D_T + L + 0.2S + \Omega_0 Q_E \qquad \text{(Eq 12-23)}$$

The loads expressed in Equation 12-23 are now divided between the number of frames that make up the short-direction lateral-load-resisting system. The building has a total of nine such frames. The loads are distributed based on the tributary area of each frame. Because the end bays have only half the tributary area, the loads are divided by the number of frames minus one, or also stated as the number of bays shown in Table 12-7. The vertical-load-resisting members are the shear panel columns and individual studs, and these are distributed fairly uniformly in plan throughout the building. It is assumed that vertical loads are distributed to these studs in proportion to their cross-sectional area because of the uniform distribution of columns and individual studs in throughout the building in plan. (Normally, gravity loads would be distributed based on tributary area.)

Table 12-7. Gravity load calculations.

Panel Level	S_{DS} (g)	Total Dead Load D_T=D+EW+IW (kips)	Total Floor Live Load, L (kips)	20% of Roof Snow Load, 0.2S (kips)	Short Dir # of bays n_{S-1}	# Studs in Short Dir Col	# Studs in Long Dir Col	Area/ Column Stud A_s (in^2)	Area of Short Dir Col A_{cS} (in^2)	# Ind Stud in Short & Long Dir	Area/ Indiv Stud A_s (in^2)	Area of Indiv & Long Dir Col Studs $A_{i\&cL}$ (in^2)	% Gravity Carried by Short Dir Columns (%)	Gravity /Frame Short Dir GL_{max} (kips)	Gravity /Frame Short Dir GL_{min} (kips)
3rd	0.86	228	0	18	8	8	8	0.430	3.44	68	0.270	21.80	14%	5.6	2.8
Cumulative		228	0	18										5.6	2.8
2nd	0.86	507	403	0	8	12	12	0.680	8.16	68	0.330	30.60	21%	28.9	9.7
Cumulative		736	403	18										34.6	12.6
1st	0.86	511	403	0	8	16	16	0.680	10.88	68	0.330	33.32	25%	34.0	11.5
Cumulative		1247	807	18										68.6	24.0

Table 12-8 shows trial column stud sizes. Each frame has two shear panels in the short direction of the building, and each shear panel has two columns so that the first, second, and third floor columns have four, three, and two studs, respectively. This table also summarizes the size of individual studs for the purpose of determining the area of the column studs relative to all other studs. The individual studs include the interior studs in the shear panels plus all additional individual studs making up the bearing walls in this short-direction frame of the building.

Table 12-8. Trial stud sizes and quantities for one short-direction frame.

Level	Size of Column Studs	Number of Column Studs		Size of Individual Studs	No. of Individual Studs
		Short Direction	Long Direction		
1st Floor	2" x 6" x 43 mil (18 ga)	8	8	2" x 6" x 27 mil (22 ga)	68
2nd Floor	2" x 6" x 68 mil (14 ga)	12	12	2" x 6" x 33 mil (20 ga)	68
first Floor	2" x 6" x 68 mil (14 ga)	16	16	2" x 6" x 33 mil (20 ga)	68

Table 12-7 summarizes the area calculations based on the trial stud sizes. This table shows that 25%, 21%, and 14% of the total gravity load in the tributary area of one short-direction frame is carried by the short-direction shear wall columns. The remaining gravity loads are carried by individual studs and shear panel column studs in the long direction of the building. These gravity loads are summarized in Table 12-7.

The $\Omega_0 Q_E$ term in Equation 12-23 accounts for material overstrength in the diagonal straps. The vertical component in the straps will place additional compressive loads in the columns. The total column axial load at the maximum ultimate stress in the diagonal straps, P_{vumax}, is determined from Equation 11-38 and repeated below:

$$P_{vumax} = \frac{GL_{max}}{2} + F_{sumax} n_s b_s t_s \left(\frac{H}{\sqrt{H^2+W^2}}\right) \qquad \text{(Eq 12-24)}$$

Table 12-9 gives values for P_{vumax} for each trial shear wall column at each floor in the short-direction frame of the barracks building.

Table 12-9. Column design for cold-formed steel shear panels— barracks example.

Column Type / Figure No.	Diagonal Strap Ult Stress F_{su} (ksi)	Max Ult Strap Stress F_{sumax} (ksi)	Gravity /Frame Short Dir GL_{max} (kips)	Number Shear Panels /Frame	Max Gravity Load/ Panel GL_{max} (kips)	Column Axial load at Strap Ult P_{vumax} (kips)	Column Yield Stress F_{cy} (ksi)	Column Ultimate Stress F_{cu} (ksi)	Column Design Thickness (ga)	Column Design Thickness t_c (in.)	Number of Studs /Column n	Panel Thickness /Column b_c (in.)	Col Stud Flange Width b_f (in.)	Column Depth h_c (in.)
3rd Floor/12-4	45	68	5.6	2	2.82	13.2	33	45	16	0.0568	2	6.0	2.0	4.0
3rd Floor/12-7	65	81	5.6	2	2.82	12.7	50	65	16	0.0568	2	6.0	2.0	4.0
3rd Floor/12-8	45	68	5.6	2	2.82	16.3	50	65	16	0.0568	2	6.0	2.0	4.0
3rd Floor/12-9*	65	81	5.6	2	2.82	12.7	50	65	16	0.0568	2	6.0	2.0	4.0
2nd Floor/12-10	65	81	34.6	2	17.29	36.4	50	65	14	0.0716	3	6.0	2.0	6.0
2nd Floor/12-11*	65	81	34.6	2	17.29	36.4	50	65	14	0.0716	3	6.0	2.0	6.0
2nd Floor/12-12	65	81	34.6	2	17.29	36.4	50	65	14	0.0716	4	6.0	2.0	8.0
1st Floor/12-13*	65	81	68.6	2	34.28	51.3	50	65	12	0.1021	3	6.0	2.0	6.0
1st Floor/12-14	65	81	68.6	2	34.28	51.3	46	58		0.1875	1	6.0	6.0	6.0
1st Floor/12-15	65	81	68.6	2	34.28	58.0	46	58		0.1875	1	6.0	6.0	6.0

*Asterisk designates selected panels.

12.12.2 Column axial capacity

Table 12-9 also presents trial column configurations defined in terms of their yield stress, F_{cy}; column stud or structural tubing material thickness, t_c; number of studs per column, n; panel thickness, b_c; and column depth, h_c. The panel thickness is the column width in the out-of-plane direction of the panel, and column depth is the column width in the in-plane direction of the panel. Each of the column studs are 6 in. deep with a 2 in. wide

flange, b_f. They are welded together to form a closed column section and are oriented so that the stud flanges are parallel to the plane of the shear panels (see test panels A3 and C1 in Appendix A). In this orientation, the column depth, h_c, is the number of studs per column times 2 in. Table 12-10 presents the column capacity calculations. This table gives the column nominal areas, A_c; distance to the extreme fiber, c; in-plane and out-of-plane moments of inertia; and radius of gyration. The column anchors are designed to provide moment connections at their tops and bottom, so that the effective length factor, K, becomes 0.5.

Table 12-10. Column capacity calculations for shear panels — barracks example.

Column Type / Figure No.	Nominal Column Area A_c (in^2)	Distance to Extreme Fiber c (in.)	In-Plane Mom of Inertia I_x (in^4)	In-Plane Radius of Gyration r_y (in.)	Out-of-Plane Mom of Inertia I_y (in^4)	Out-of-Plane Radius of Gyration r_x (in.)	Eff Length Factor K	Elastic Flexural Stress F_e (ksi)	λ_c	Nominal Axial Stress F_{cn} (ksi)	Knockout hole dia d_h (in.)	Flat Width w (in.)	F_{cr} (ksi)	Slenderness factor λ	Eff Width b (in.)	Eff Column Area A_e (in^2)	Column Design Strength P_c (kips)
3rd Floor/12-4	1.14	2.00	3.21	1.68	5.95	2.29	0.5	314	0.32	31.6	1.5	5.77	9.32	1.84	2.15	0.725	19.5
3rd Floor/12-7	1.14	2.00	3.21	1.68	5.95	2.29	0.5	314	0.40	46.8	1.5	5.77	9.32	2.24	1.81	0.687	27.3
3rd Floor/12-8	1.14	2.00	3.21	1.68	5.95	2.29	0.5	314	0.40	46.8	1.5	5.77	9.32	2.24	1.81	0.687	27.3
3rd Floor/12-9*	1.14	2.00	3.21	1.68	5.95	2.29	0.5	314	0.40	46.8	1.5	5.77	9.32	2.24	1.81	0.687	27.3
2nd Floor/12-10	2.15	3.21	10.29	2.19	11.14	2.28	0.5	426	0.34	47.6	1.5	5.71	15.1	1.78	2.18	1.389	56.2
2nd Floor/12-11*	2.15	3.21	10.29	2.19	11.14	2.28	0.5	426	0.34	47.6	1.5	5.71	15.1	1.78	2.18	1.389	56.2
2nd Floor/12-12	2.86	4.00	22.52	2.80	14.86	2.28	0.5	461	0.33	47.8	1.5	5.71	15.1	1.78	2.18	1.851	75.2
1st Floor/12-13*	3.06	3.21	14.46	2.17	15.63	2.26	0.5	451	0.33	47.7	1.5	5.59	32.1	1.22	2.86	2.23	90.3
1st Floor/12-14	4.27	3.00	23.8	2.36	23.8	2.36	0.5	532	0.29	44.4	1.5	5.25	123	0.60	3.75	3.99	150
1st Floor/12-15	4.27	3.00	23.8	2.36	23.8	2.36	0.5	532	0.29	44.4	1.5	5.25	123	0.60	3.75	3.99	150

*Asterisk designates selected panels.

The last two rows in Table 12-9 and Table 12-10 are for panels with columns made up of 6 x 6 x 3/16 in. hollow structural sections (HSS) structural tubing members (panel D2 configuration). The tubing material is ASTM A500/A500M Grade B (ASTM 2013c), with minimum yield stress, F_{cy}, and minimum ultimate stress, F_{cu}, values of 46 ksi and 58 ksi, respectively. Similar to the column studs, it is assumed that 1.5 in. wide holes will be drilled through the faces of the column that are out of plane to the shear panel. These holes are for electrical mechanical tubing (EMT) conduit.

The elastic flexural stress, F_e, shown in Table 12-10 is calculated based on Equation 11-43, and λ_c is calculated based on Equation 11-42. The nominal axial stress, F_{cn}, is then calculated based on either Equation 11-40 or 11-41, depending on the value of λ_c.

The effective areas, A_e, of the columns are calculated according to Equation 11-45. Values of the terms used to define this area are also given in Table 12-10. Finally, the column design strength, P_c, is calculated accord-

ing to Equation 11-39. Values of P_c are given in Table 12-10 for each trial column. Through an iterative process in the spreadsheet program, trial column configurations were defined where P_c exceeds the column axial load at the maximum ultimate stress in the diagonal straps, P_{vumax}. From these results, the column configurations marked with an asterisk in Table 12-9 and Table 12-10 were selected for the three floor levels.

12.12.3 Column bending and composite behavior

The shear panel anchor recommendations will provide moment resistance at the column ends, especially when no axial load is applied to the columns. The columns built up from studs must be designed to act as a composite cross-section. Table 12-11 gives the intermittent weld length, L (2 in. for each built-up column in Table 12-11), and maximum center-to-center intermittent weld spacing, s_{max}, needed to ensure composite behavior of the columns. This is based on Equation 11-54. Based on the values of s_{max} given in Table 12-11, actual weld spacing is selected that round down to the nearest full inch from the values shown in the table. These welds are made between all studs in the column and begin at both ends of the columns.

Table 12-11. Column intermittent weld design.

Column Type / Figure No.	Max Column Shear V_{cm} (kips)	Area on 1 Side of Crit Weld A (in^2)	Distance to Neutral Axis y (in.)	Mom of Column Area Q (in^3)	Weld Shear/ Length q (k/in)	Intermittent Weld Length L (in.)	Max o.c. Spacing s_{max} (in.)
3rd Floor/12-4	1.0	0.57	1.60	0.9	0.3	2.0	14.3
3rd Floor/12-7	1.6	0.57	1.60	0.9	0.4	2.0	13.6
3rd Floor/12-8	1.6	0.57	1.60	0.9	0.4	2.0	13.6
3rd Floor/12-9*	1.6	0.57	1.60	0.9	0.4	2.0	13.6
2nd Floor/12-10	2.8	1.43	1.61	2.3	0.6	2.0	12.1
2nd Floor/12-11*	2.8	1.43	1.61	2.3	0.6	2.0	12.1
2nd Floor/12-12	5.0	1.43	2.20	3.1	0.7	2.0	11.1
1st Floor/12-13*	4.1	2.04	1.62	3.3	0.9	2.0	11.7
1st Floor/12-14							
1st Floor/12-15							

*Asterisk designates selected panels.

12.12.4 Column combined axial and moment capacity

The combination of axial load and bending was evaluated for each trial shear panel. For each case, interaction values were determined according to Equations 11-55 and 11-56. Table 12-12 shows that the interaction values, I were below 1.0 for all but the columns in the first row, and this was not a selected panel.

12.12.5 Column shear capacity

The column design shear capacity, V_c, was calculated according Equation 11-65 for each trial column. The values are shown in the second column of Table 12-13. These are below the strap maximum estimated ultimate lateral capacity ($P_{humax} = \Omega_0 Q_E$), calculated according to Equation 11-17, with values given in the third column of Table 12-13. Therefore, the additional shear capacity from anchors is needed to resist the maximum lateral force, as shown under "Anchor shear capacity," section 12.14.1.

Table 12-12. Column combined axial and moment capacity.

Column Type / Figure No.	Required Compressive Strenth $\bar{P}$ (kips)	Column Fixity (%)	Strap Max Yield Stress F_{symax} (ksi)	Max Est Lat Defl at Strap Yield δ_{symax} (in.)	Applied Moment @δ_{symax} M_a (k-in)	C_{mx}	P_{Ex}	α_x	Effective Section Modulus S_e (in^3)	Column Nominal Moment M_{nx} (k-in)	Column Axial w/F_n=F_y P_{no}	$\bar{P}/\phi_c P_n$	Eq 11-55 Column Interaction I	Eq 11-56 Column Interaction I
3rd Floor/12-4	12.9	50%	66	0.478	19.1	0.85	356	0.96	1.60	52.9	23.9	0.665	1.000	1.017
3rd Floor/12-7	11.8	50%	75	0.543	21.1	0.85	356	0.97	1.60	80.2	34.3	0.432	0.676	0.682
3rd Floor/12-8	16.0	50%	66	0.478	20.6	0.85	356	0.96	1.60	80.2	34.3	0.585	0.826	0.818
3rd Floor/12-9*	11.8	50%	75	0.543	21.1	0.85	356	0.97	1.60	80.2	34.3	0.432	0.676	0.682
2nd Floor/12-10	34.3	50%	75	0.600	62.3	0.85	914	0.96	3.21	160.4	69.5	0.610	0.971	0.990
2nd Floor/12-11*	34.3	50%	75	0.600	62.3	0.85	914	0.96	3.21	160.4	69.5	0.610	0.971	0.990
2nd Floor/12-12	34.3	50%	75	0.600	111.8	0.85	2001	0.98	5.63	281.5	92.6	0.456	0.818	0.854
1st Floor/12-13*	48.7	50%	75	0.584	89.6	0.85	1381	0.96	4.50	225.2	111.3	0.539	0.908	0.933
1st Floor/12-14	48.7	50%	75	0.584	129.2	0.85	2273	0.98	7.93	364.9	183.5	0.323	0.647	0.685
1st Floor/12-15	54.9	50%	75	0.584	132.8	0.85	2273	0.98	7.93	364.9	183.5	0.365	0.699	0.735

*Asterisk designates selected panels.

Table 12-13. Column shear capacity.

Column Type / Figure No.	Column Shear Strength V_c (kips)	Strap Lat Ult Capacity P_{humax} (kips)
3rd Floor/12-4	4.3	15.3
3rd Floor/12-7	6.5	14.6
3rd Floor/12-8	13.0	19.4
3rd Floor/12-9*	6.5	14.6
2nd Floor/12-10	24.5	34.3
2nd Floor/12-11*	24.5	34.3
2nd Floor/12-12	32.6	34.3
1st Floor/12-13*	34.9	43.7
1st Floor/12-14	59.0	43.7
1st Floor/12-15	59.0	52.3

*Asterisk designates selected panels.

12.13 Diagonal strap-to-column connections

This section defines the applied loads and design requirements for diagonal strap connections to the panel columns.

12.13.1 Connection design assumptions and applied loads

Diagonal strap-to-column connections are designed to resist the maximum estimated ultimate force in the strap, P_{sumax}, defined by Equation 11-70. P_{sumax} values are given in the second column of Table 12-14 for each panel.

12.13.2 Screwed fastener connection design

All screws used in this example are #10 self-tapping hex-head screws, which is the largest practical size that will not interfere with drywall installation. The nominal screw diameter, d, for #10 screws is 0.190 in. (AISI 2007b, Table C-E4-1). The following fastener layout recommendations are based on text in section 11.13.2 of this report:

- Minimum distance between centers of fasteners is 3d = 0.57 in.
- For connections subjected to shear forces in only one direction, the minimum distance from centers of fasteners to the edge of a connected part perpendicular to the force is 1.5d = 0.29 in.

The design shear and pull-over per screw, P_s, was calculated for every shear panel screwed connection according to Equations 11-71 through 11-76 and 11-78, based on the thicknesses and strength of the connected members and the dimensions of the screws. Table 12-14 gives the ratio of t_c/t_s and the resulting design shear per screw, as defined by these equations. A screw head diameter, d_w, of 0.402 in.[21] was used for the screws.

[21] This dimension was measured from #10 hex washer head screws (ITW Buildex Part Number 1129000) used in test panels at ERDC-CERL. Measurement was made using a vernier caliper, and the diameter at the base of the washer head was consistently 0.402 in. ± 0.004 in. (10.2 mm ± 0.1 mm).

Table 12-14. Screwed connection design.

Column Type / Figure No.	Max Est Ult Strap Force P_{sumax} (kips)	Nominal Screw Dia d (in.)	Col/Strap Thickness Ratio (t_c/t_s)	Column Tilting Eq 11-72 P_{ns} (kips)	Strap Bearing Eq 11-73 P_{ns} (kips)	Column Bearing Eq 11-74 P_{ns} (kips)	Strap Bearing Eq 11-75 P_{ns} (kips)	Column Bearing Eq 11-76 P_{ns} (kips)	Nominal Shear P_{ns} (kips)	Screw head dia d_w (in.)	Nominal Pull-over P_{nov} (kips)	Manufacturer's Nom Shear P_{ns} (kips)	Min End Dist e (in.)	Design Shear /Screw P_s (kips)	Number Screws /Face n_{screws} (#)
3rd Floor/12-4	19.3	0.19	0.79	1.116	2.479	1.312	2.479	1.312	1.116	0.402	2.913	1.232	0.23	0.558	34.6
3rd Floor/12-7	18.5	0.19	1.00	1.613	2.369	1.895	2.369	1.895	1.613	0.402	2.785	1.232	0.27	0.616	30.0
3rd Floor/12-8	24.4	0.19	1.26	1.613	1.567	1.895	1.567	1.895	1.567	0.402	1.842	1.013	0.33	0.506	24.1
3rd Floor/12-9*	18.5														
2nd Floor/12-10	44.1	0.19	1.58	2.279	1.887	2.387	1.887	2.387	1.887	0.402	2.218	1.013	0.28	0.506	43.6
2nd Floor/12-11*	44.1														
2nd Floor/12-12	44.1	0.19	1.58	2.279	1.887	2.387	1.887	2.387	1.887	0.402	2.218	1.013	0.28	0.506	43.6
1st Floor/12-13*	55.4														
1st Floor/12-14	55.4														
1st Floor/12-15	66.4														

*Asterisk designates selected panels.

Ultimate shear values from the manufacturer's data,[22] P_u, based on the smaller thickness of the members being connected were used to calculate nominal screw shear strength, P_{ns}, according to the following equation:

$$P_{ns} = \frac{P_u}{1.25} \qquad \text{(Eq 12-25)}$$

Equation 12-25 was not included in the Chapter 11 design recommendations because the format of manufacturer's test data was not given and may need to be evaluated on a case-by-case basis, as shown in the present example. Table 12-14 provides values for this nominal shear strength, based on manufacturer's fastener shear strength and Equation 12-25. The design shear per screw, P_s, was calculated according to Equation 11-71 from the minimum of P_{ns} and P_{nov}, including P_{ns} as calculated according to Equation 12-25. Table 12-14 presents P_s based on this overall minimum nominal shear, pull-over strength, or screw shear strength. In this example problem, the manufacturer's fastener shear strength data controls the nominal fastener shear strength for all panel configurations except for the one shown on the first row of Table 12-14.

The minimum end distance for screws in the diagonal straps was defined using Equation 11-77 by setting P_{ns} equal to the minimum shear strength described in the previous paragraph and solving for end distance, e. Values for this minimum end distance are shown in Table 12-14.

[22] From ITW Buildex Catalog for #10 fasteners with #3 drill point.

Finally, the number of screws required at each diagonal strap-to-column connection, n_{screws}, was calculated according to Equation 11-80 for each trial panel configuration. These quantities are given in Table 12-14. These values are very large, and the use of larger screws or welded connections should be considered. Still, each of these connections may be constructed within the overlap area of the strap and column, and within the spacing and edge distance requirements given above in this section. The most difficult joints to lay out are those in Figure 12-4 and Figure 12-7, which are based on installing diagonal straps on only one face of the shear panel. These columns are 4 in. wide, and the straps are also 4 in. wide and oriented at an angle based on the width, W, and height, H, of the overall panels given in Table 12-6. Layouts of the fasteners were selected that keep the column critical shear plane as close as possible to the track while maximizing the net area for rupture strength evaluation. The trial layout shown in Figure 12-4 has 6 fasteners at the first row against the track, and 4, 6, 4, 6, 4, and 5 fasteners in the subsequent rows moving up the joint. Figure 12-5 is a close-up drawing of this joint, showing the fastener locations and critical rupture surface (see next section, “Block shear rupture”). These fasteners are spaced at 9/16 in. on center horizontally and 0.375 in. on center vertically, in a staggered pattern. The other diagonal strap-to-column screwed connections in Table 12-14 are laid out in a similar manner, and are shown in Figure 12-7, Figure 12-8, Figure 12-10 and Figure 12-12.

Figure 12-4. Example connection/anchorage detail— first row of Table 12-6 and Table 12-9 through 12-22.

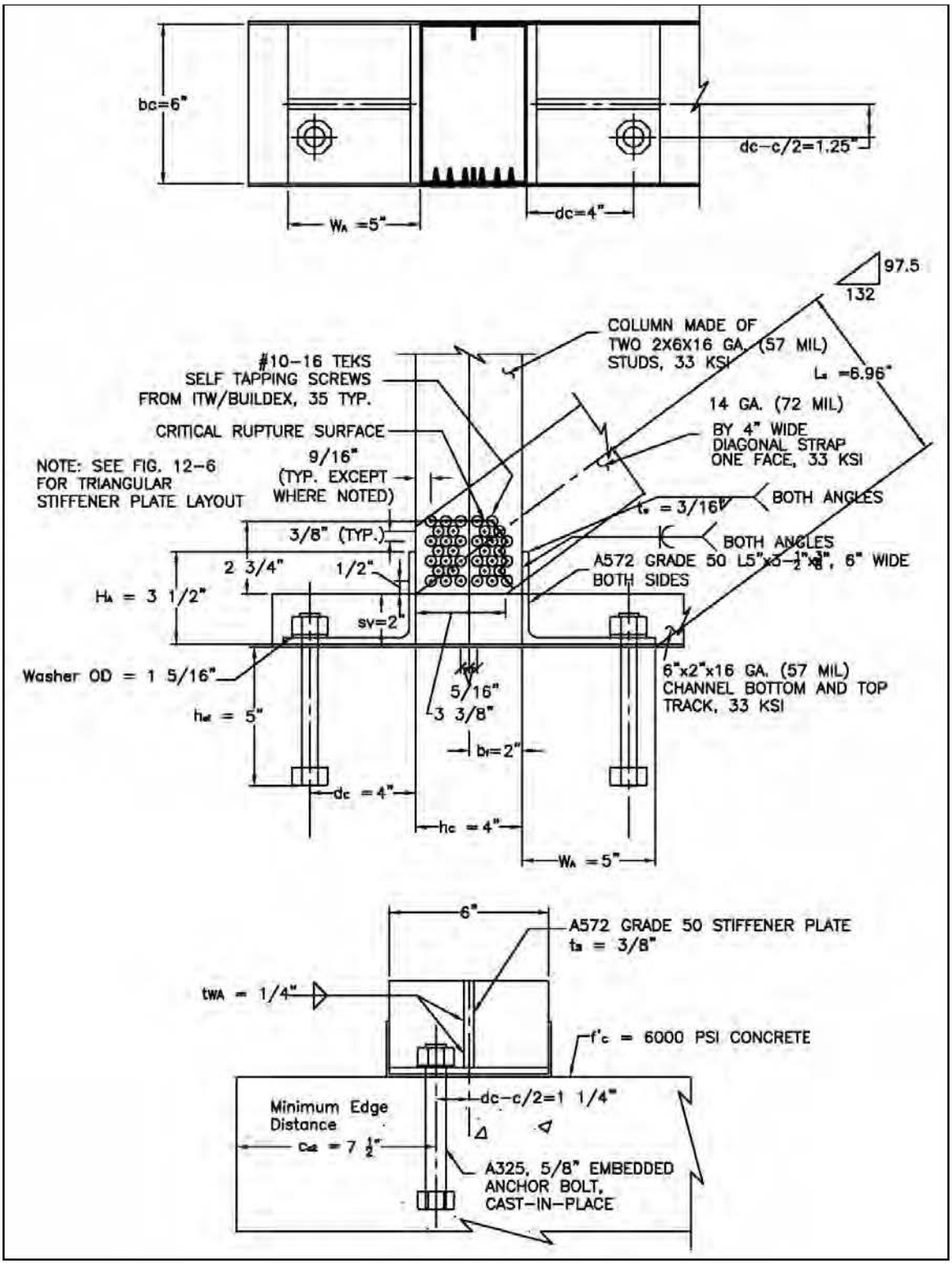

Figure 12-5. Close-up of second-row connection showing fastener locations and critical rupture surface.

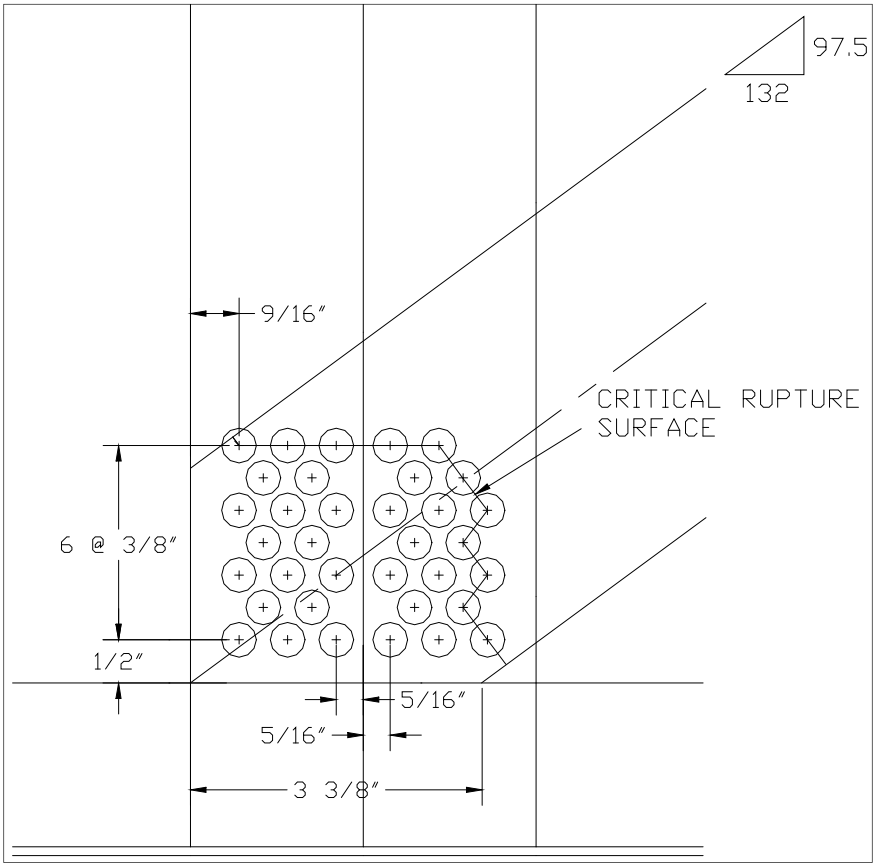

Figure 12-6. Elevation view of the second-row anchor stiffener plates.

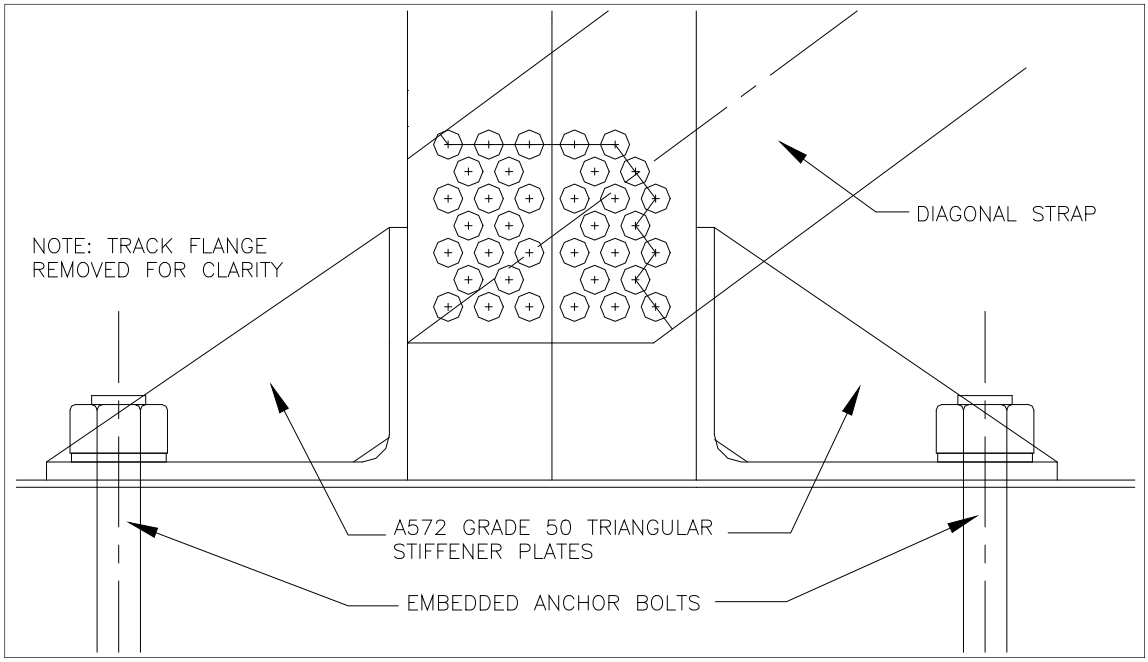

Figure 12-7. Example connection/anchorage detail—second row of Table 12-6 and Table 12-9 through 12-22.

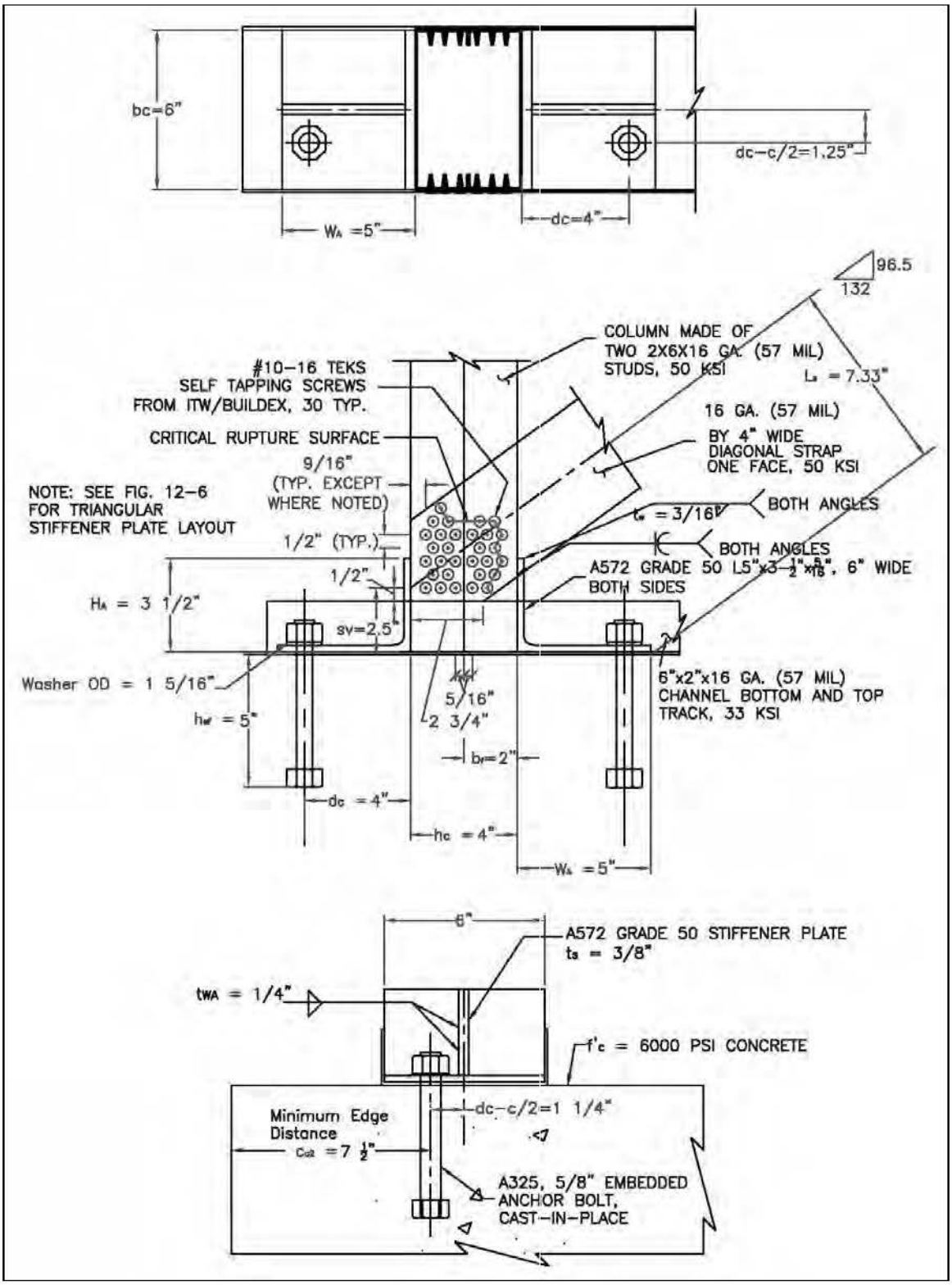

Figure 12-8. Example connection/anchorage detail—3rd row of Table 12-6 and Table 12-9 through 12-22.

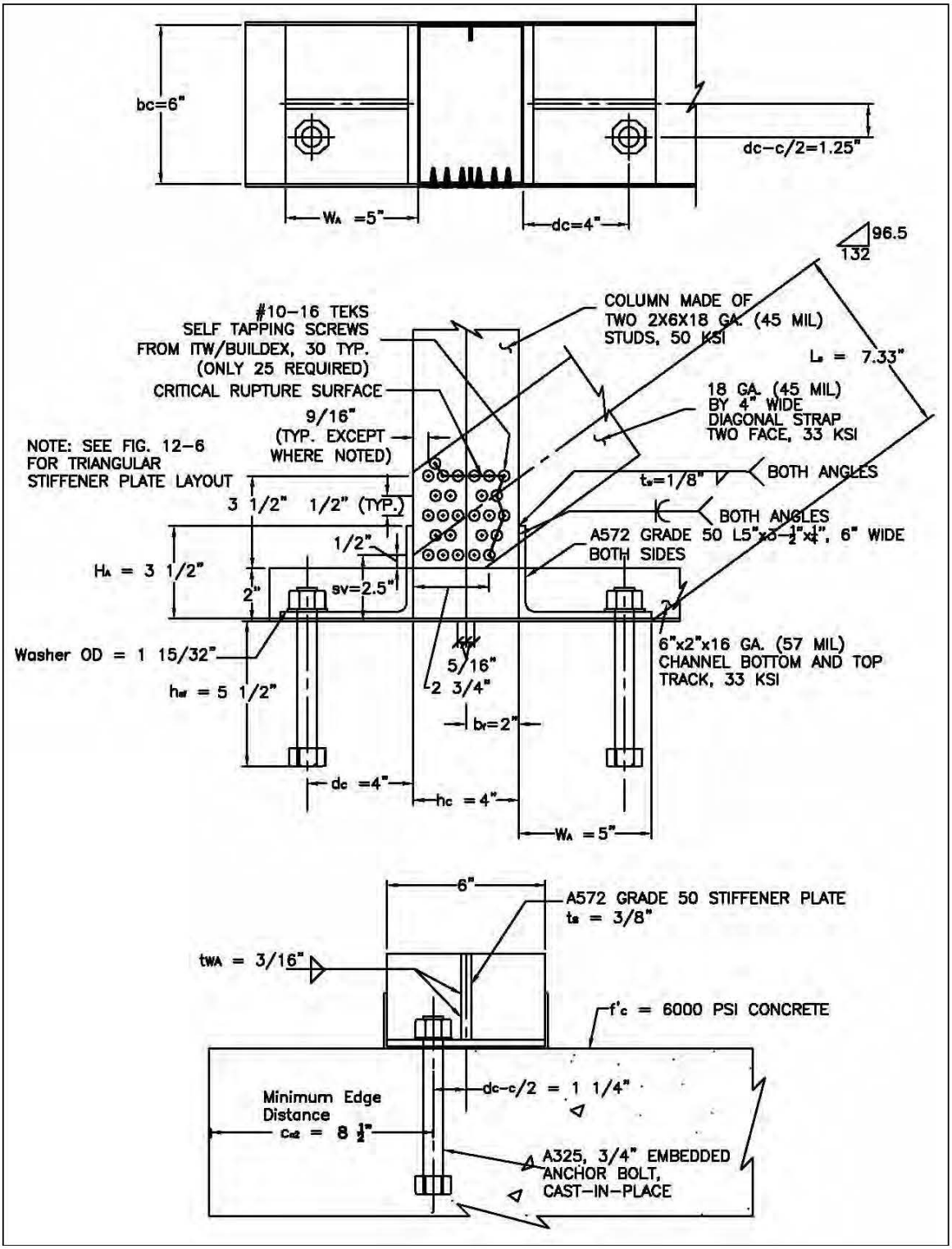

12.13.3 Block shear rupture

Figure 12-4, Figure 12-5, Figure 12-7, Figure 12-8, Figure 12-10, and Figure 12-12 show the critical diagonal strap rupture surface for trial screwed connections, for which the rupture strength was calculated. The rupture surface located along the inside edge of the columns and along a horizontal plane will be loaded at approximately a 45-degree angle to the rupture surface. Therefore, the averages of the shear and tension strength (0.8 F_{sy} and 0.8 F_{su}, respectively) are used to modify Equations 11-82 and 11-83 for the shear/tensile strength and tensile strength for the rupture surface loaded at 45 degrees, as shown in Equations 12-26 and 12-27. Values for Equations 12-26 and 12-27 are shown in Table 12-15 for each trial strap-to-column screwed connection.

$$R_n = 0.8F_{sy}A_{gvt} + F_{su}A_{nt} \quad \text{(Eq 12-26)}$$

$$R_n = 0.8F_{su}A_{nvt} + F_{su}A_{nt} \quad \text{(Eq 12-27)}$$

where

A_{gvt} = the gross area subject to shear and tension at 45 degrees
A_{nvt} = the net area subject to shear and tension at 45 degrees
A_{nt} = the net area subject to tension

The design shear rupture is calculated according to Equation 11-81 based on the trial layouts of the fasteners for each diagonal strap-to-column connection. The use of #10 screws resulted in a very large number of screws at each connection, as seen in Table 12-14 and Figure 12-4 through Figure 12-8, Figure 12-10, and Figure 12-12. The screw pattern must stay within the spacing and edge distance limitations presented in section 12.13.2. This design capacity is further modified, as shown in Equation 12-28, for the number of strap faces or straps in each direction used on the shear panels.

$$R = \emptyset_R min(R_n)n_s \quad \text{(Eq 12-28)}$$

When the strap-to-column rupture strength is evaluated based on Equation 12-28, the resistance factor may be increased to 1.0 because of the ASTM minimum material requirement on F_u/F_y (see discussion near Equations 11-84 and 11-85). The strap applied tensile force is defined in Equation 11-85.

None of the trial diagonal strap-to-column screwed connections have a rupture capacity, R, that exceeds the maximum applied load (P_{sy} in Equation 11-85), as shown in Table 12-15. The achieved resistance factor (ϕ_a) may be calculated by combining Equations 11-85 and 12-28, as shown in Equation 12-29:

$$\emptyset_a = \frac{P_{sy}}{min(R_n)n_s} \leq 1.0 \qquad \text{(Eq 12-29)}$$

Table 12-15 shows that all but one of the achieved resistance factors are above 1.0 (Figure 12-12 has the smallest, with a value of 0.926.) The trial screw locations shown in Figure 12-4 through Figure 12-8, Figure 12-10 and Figure 12-12 were defined so as to maximize the achieved resistance factor, ϕ_a, in Equation 12-29.[23] This demonstrates how difficult it is to design ductile screwed connections because the ASTM A 1003/A1003M minimum F_u/F_y ratio is only 1.08 (ASTM 2013b); therefore, all selected connections in this design example are welded.

Table 12-15. Screwed connection rupture strength.

Column Type / Figure No.	Strap Yield Force P_{sy} (kips)	Tension /Shear Gross Area A_{gvt} (in^2)	Tension /Shear Net Area A_{nvt} (in^2)	Tension Net Area A_{nt} (in^2)	Shear Ruputre Eq 12-26 Rn (kips)	Shear Ruputre Eq 12-27 Rn (kips)	Design Rupture Strength R (kips)	Achieved Resistance Factor ϕ_a
3rd Floor/12-4	11.9	0.273	0.191	0.066	10.183	9.852	6.4	1.211
3rd Floor/12-7	13.7	0.213	0.159	0.039	11.073	10.823	7.0	1.264
3rd Floor/12-8	15.1	0.144	0.101	0.051	6.096	5.933	7.7	1.272
3rd Floor/12-9*	13.7							
2nd Floor/12-10	32.7	0.297	0.231	0.046	14.842	14.950	19.3	1.101
2nd Floor/12-11*	32.7							
2nd Floor/12-12	32.7	0.300	0.236	0.087	17.644	17.905	22.9	0.926
1st Floor/12-13*	41.1							
1st Floor/12-14	41.1							
1st Floor/12-15	49.2							

*Asterisk designates selected panels.

[23]Trial screw locations were defined so that they maintain a regular pattern of screws within the overlap area of the diagonal strap and column. The number of screws per connection, n_{screws}, must meet the requirement of Equation 11-80. The overlap area between the diagonal strap and column could have been increased slightly by moving the strap up the column at the connections near the bottom of the columns, but that change would provide limited benefit because the shear rupture surface length would not be increased at all and the only benefit would be to increase the screw spacing by distributing the screws over a larger area. The greater screw spacing may increase the rupture surface area (A_{nt} and A_{nvt} in Equations 12-26 and 12-27) because fewer screws may be located along the rupture surface. However, moving the strap up the column would increase the eccentricity of diagonal strap loading of the anchor (i.e., increase S_v and L_s in Equation 11-114), resulting in larger anchor loads (i.e., increase P_{tAB} in Equation 11-112).

12.13.4 Welded connection design

Figure 12-9, Figure 12-11, and Figure 12-13 through Figure 12-15 show trial layouts of welded diagonal strap-to-column connections. The third-floor weld connection thickness, t, equals the column thickness, t_c (0.0568 in.), while the first- and second-floor welds equal the diagonal strap thickness, t_s. Details on the strap and column sizing are given in Table 12-6 and Table 12-9. The longitudinal welds are along the edges of the diagonal straps. Most of the welds have L/t ratios greater than 25, so Equation 11-87 is used to define the longitudinal weld capacity. Portions of the longitudinal welds that are broken up where they pass over the column stud junctions then have L/t ratios smaller than 25, but Equation 11-87 is still used because it conservatively results in a smaller capacity. The diagonal edges at the end of the diagonal strap are loaded close to 45 degrees so that an average of Equations 11-86 and 11-88 (or an average of Equations 11-87 and 11-88) defines the weld capacity along these diagonal edges. The longitudinal/transverse design shear, P_{LT}, is based on an average of Equations 11-86 and 11-88, and expressed here as Equation 12-30.

$$P_{LT} = \left[\emptyset_{L1}\left(1 - \frac{0.01L}{t}\right) + \emptyset_T\right]\frac{LtF_u}{2} \qquad \text{(Eq 12-30)}$$

The longitudinal/transverse design shear, P_{LT}, based on an average of Equations 11-87 and 11-88, is expressed as follows:

$$P_{LT} = 0.875\emptyset_{LT}tLF_u \qquad \text{(Eq 12-31)}$$

where

ϕ_{LT} = 0.575, which is an average of the resistance factors for longitudinal and transverse loading expressed in Equations 11-87 and 11-88.

The thickness of the welds, based on strap or column thickness, are all less than 0.10 in., except for the one shown in the last row of Table 12-16 (also shown in Figure 12-15), where the strap is 0.102 in. thick. For this case, the strength of the welded connection is calculated based on Equation 11-89. The weld used is a shielded metal arc weld (SMAW) E70XX, with an electrode tensile strength, Fxx, equals 70 ksi. Table 12-16 shows that the capacity of this last welded connection is limited by the weld capacity defined by the conservative assumptions of Equation 11-89, but the AISI

S100-2007 commentary discussion (AISI 2007b, section E2.4) indicates that this limitation is almost certainly overly conservative, and that the capacity should be limited by the those values defined by Equations 11-86 and 12-31. Still, the results reported in Table 12-16 are based on the more conservative results of Equation 11-89.

Table 12-16. Welded connection design strength.

Column Type / Figure No.	Strap Yield Force P_{sy} (kips)	Least Member Thickness t (in)	Longitudinal Weld Length L (in)	Longitudinal Weld Design Strength P_L (kips)	Long/Trans Weld Length L (in)	Long/Trans Weld Design Strength P_{LT} (kips)	Electrode Strength F_{xx} (ksi)	Weld Failure Strength P_w (kips)	Welded Conn Total Capacity $(P_L+P_{LT})n_s$ (kips)
3rd Floor/12-4	11.9								
3rd Floor/12-7	13.7								
3rd Floor/12-8	15.1								
3rd Floor/12-9*	13.7	0.0568	3.24	4.5	5.29	9.8			14.3
2nd Floor/12-10	32.7								
2nd Floor/12-11*	32.7	0.0453	4.20	4.6	8.06	11.9			33.1
2nd Floor/12-12	32.7								
1st Floor/12-13*	41.1	0.0568	4.18	5.8	8.05	15.0			41.5
1st Floor/12-14	41.1	0.0568	3.48	4.8	8.63	16.0			41.7
1st Floor/12-15	49.2	0.1021	4.80	17.3	6.14	18.1	70.0	24.9	49.8

*Asterisk designates selected panels.

Table 12-16 gives the weld thickness, and the length of welds loaded in the longitudinal and longitudinal/transverse directions. Table 12-16 also gives the design capacity of the longitudinal, longitudinal/transverse, and combined capacity ($\min(P_L + P_{LT,} Pw)n_s$) welds, expressed by the following modification of Equation 11-90 based on Equations 12-30 and 12-31 to become Equation 12-32. Comparing the total shear capacity and strap yield strength, P_{sy}, shows that these connections in Table 12-6 meet the requirements of Equation 12-32.

$$[min(P_L + P_{LT}, P_w)]n_s \geq P_{sy} \quad \text{(Eq 12-32)}$$

Figure 12-9. Example connection/anchorage detail
(fourth row of Table 12-6 and Table 12-9 through 12-22).

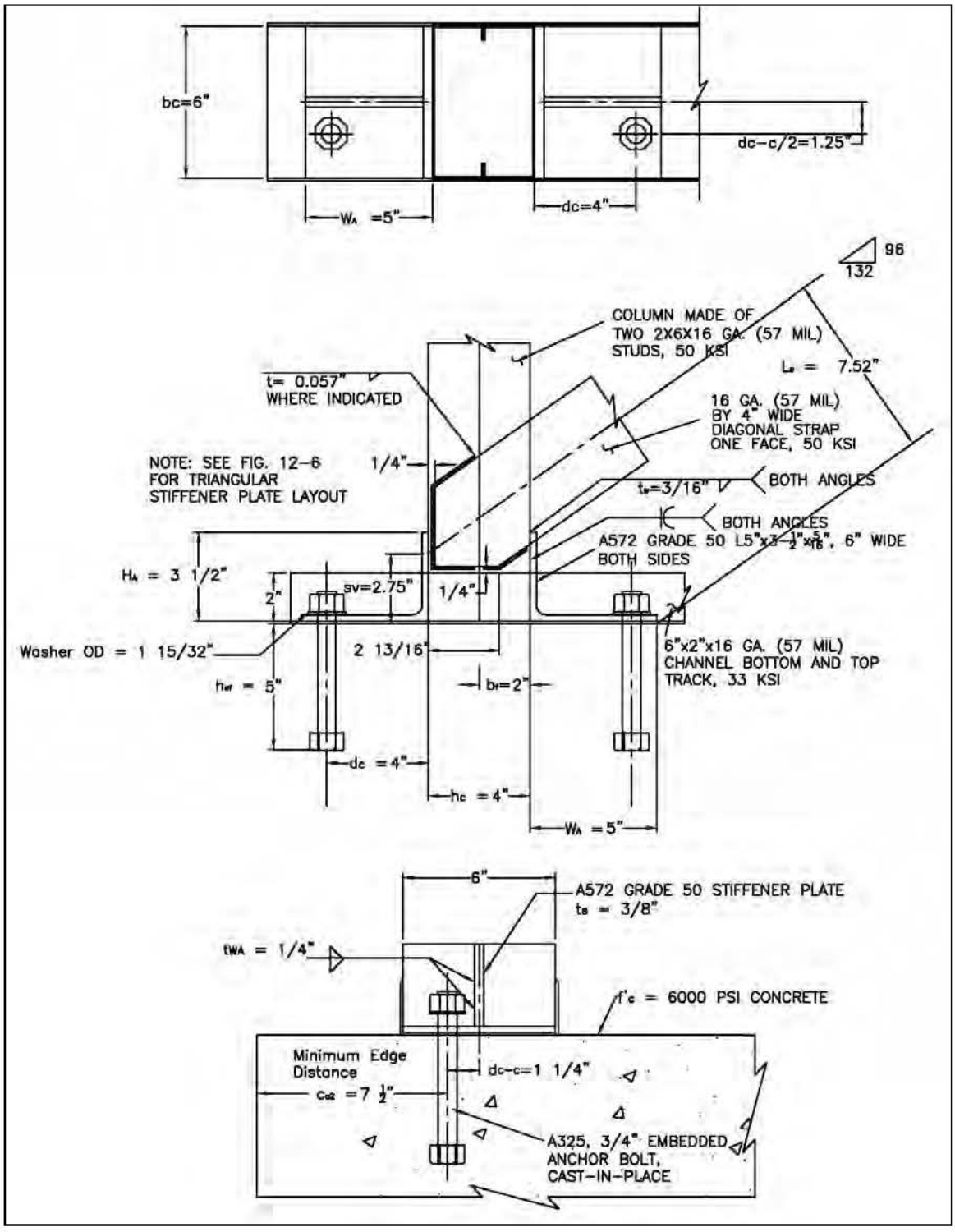

Figure 12-10. Example connection/anchorage detail – 5th row of Table 12-6 and Table 12-9 through 12-22.

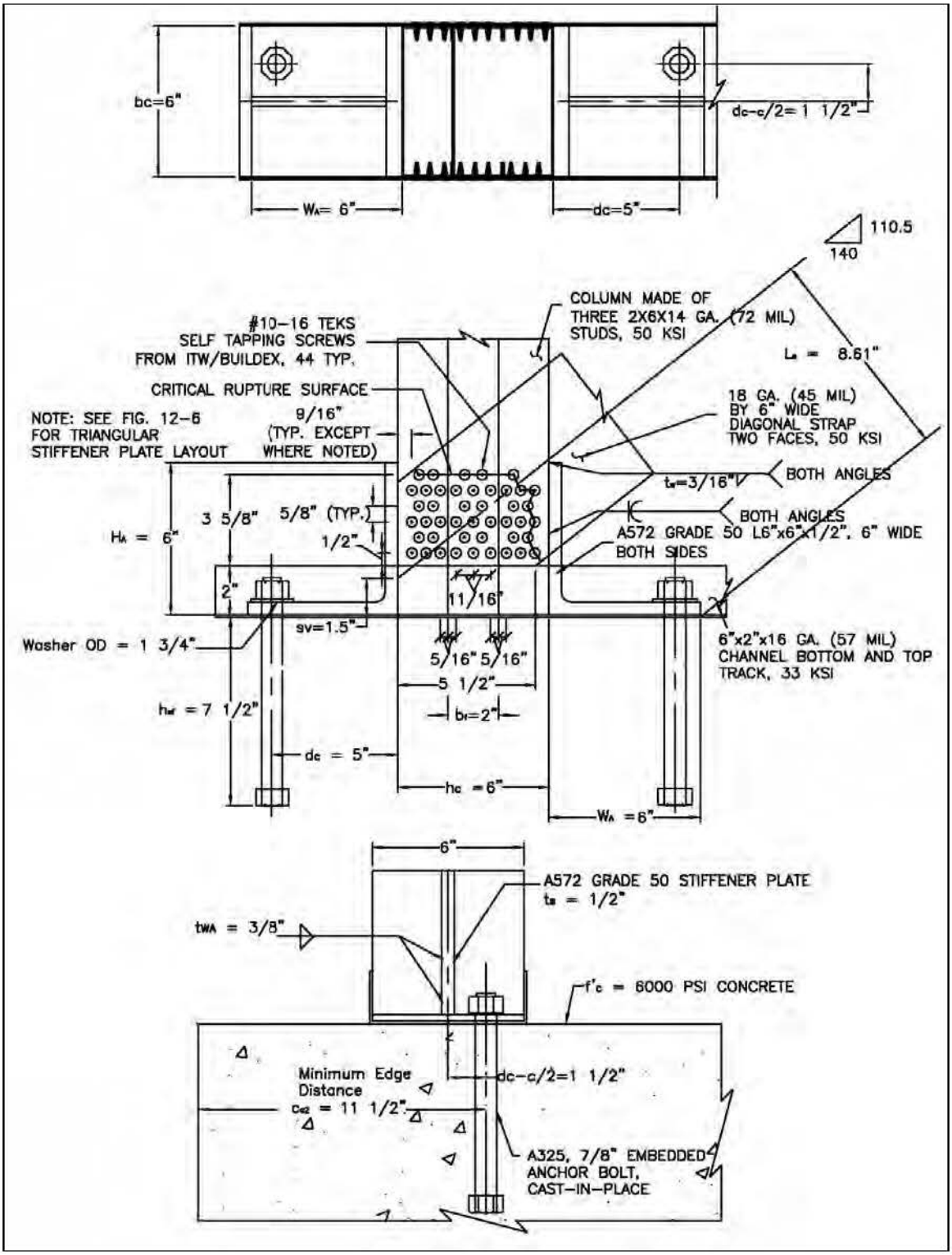

Figure 12-11. Example connection/anchorage detail
(sixth row of Table 12-6 and Table 12-9 through 12-22).

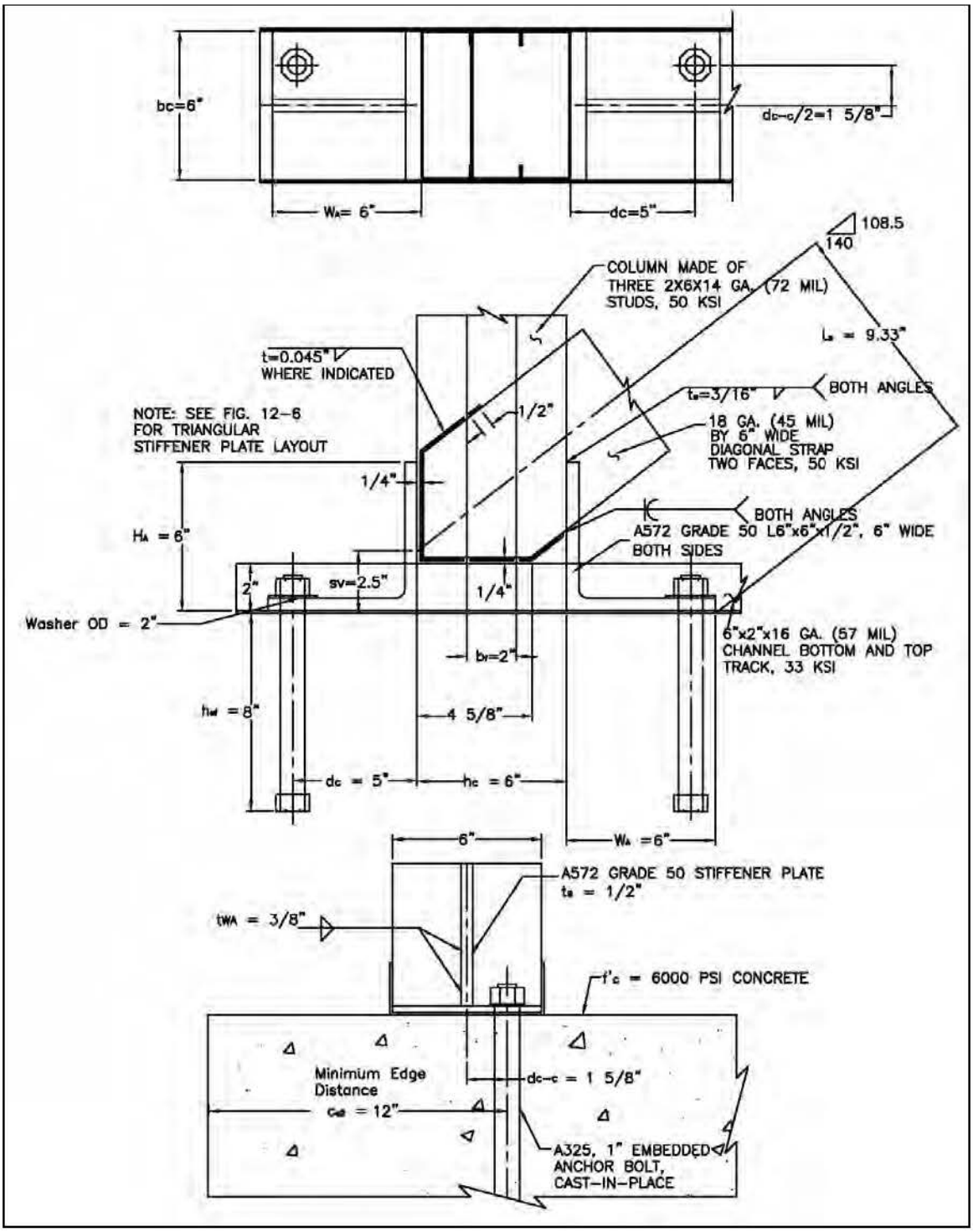

Figure 12-12. Example connection/anchorage detail
(seventh row of Table 12-6 and Table 12-9 through 12-22).

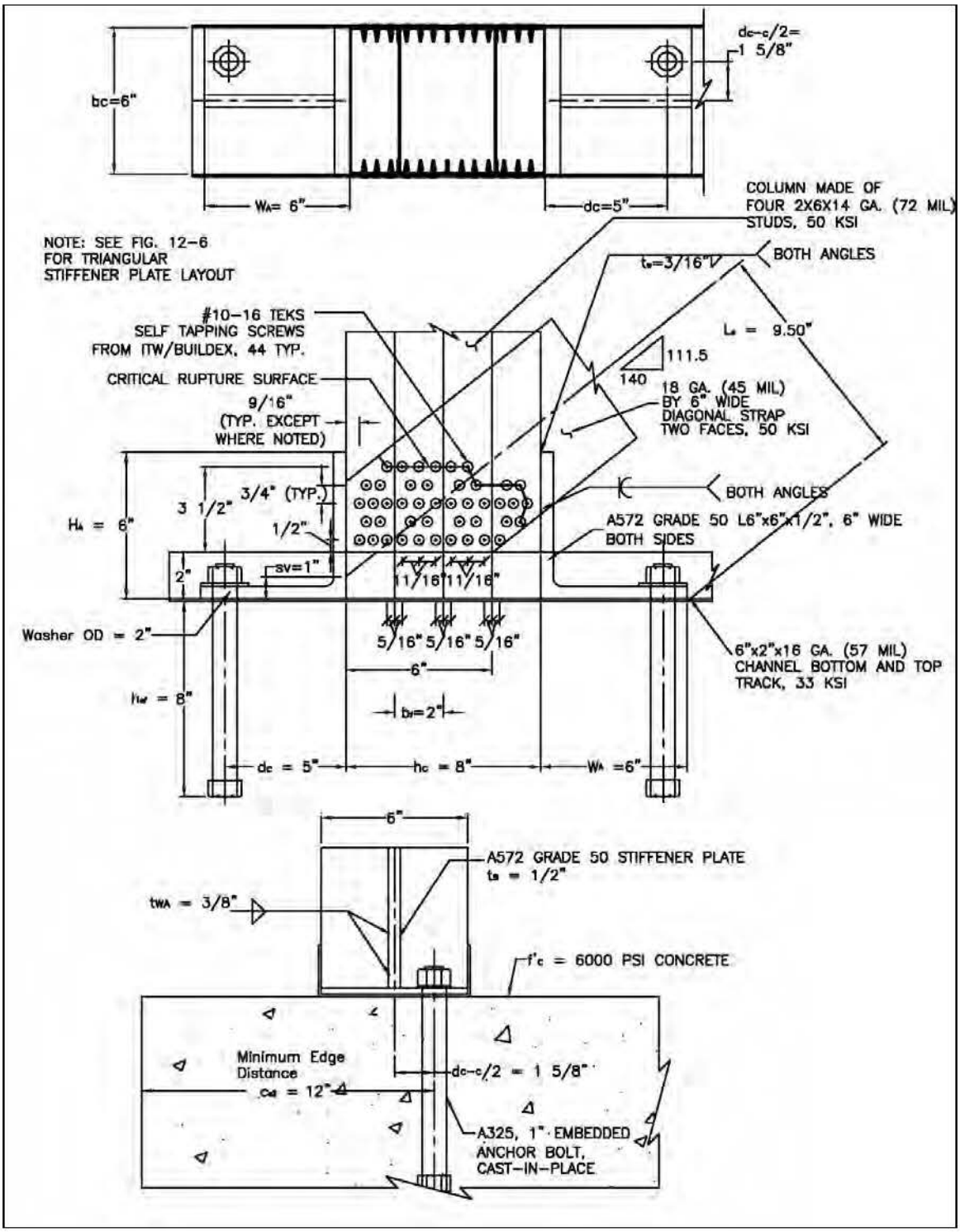

Figure 12-13. Example connection/anchorage detail
(eighth row of Table 12-6 and Table 12-9 through 12-22).

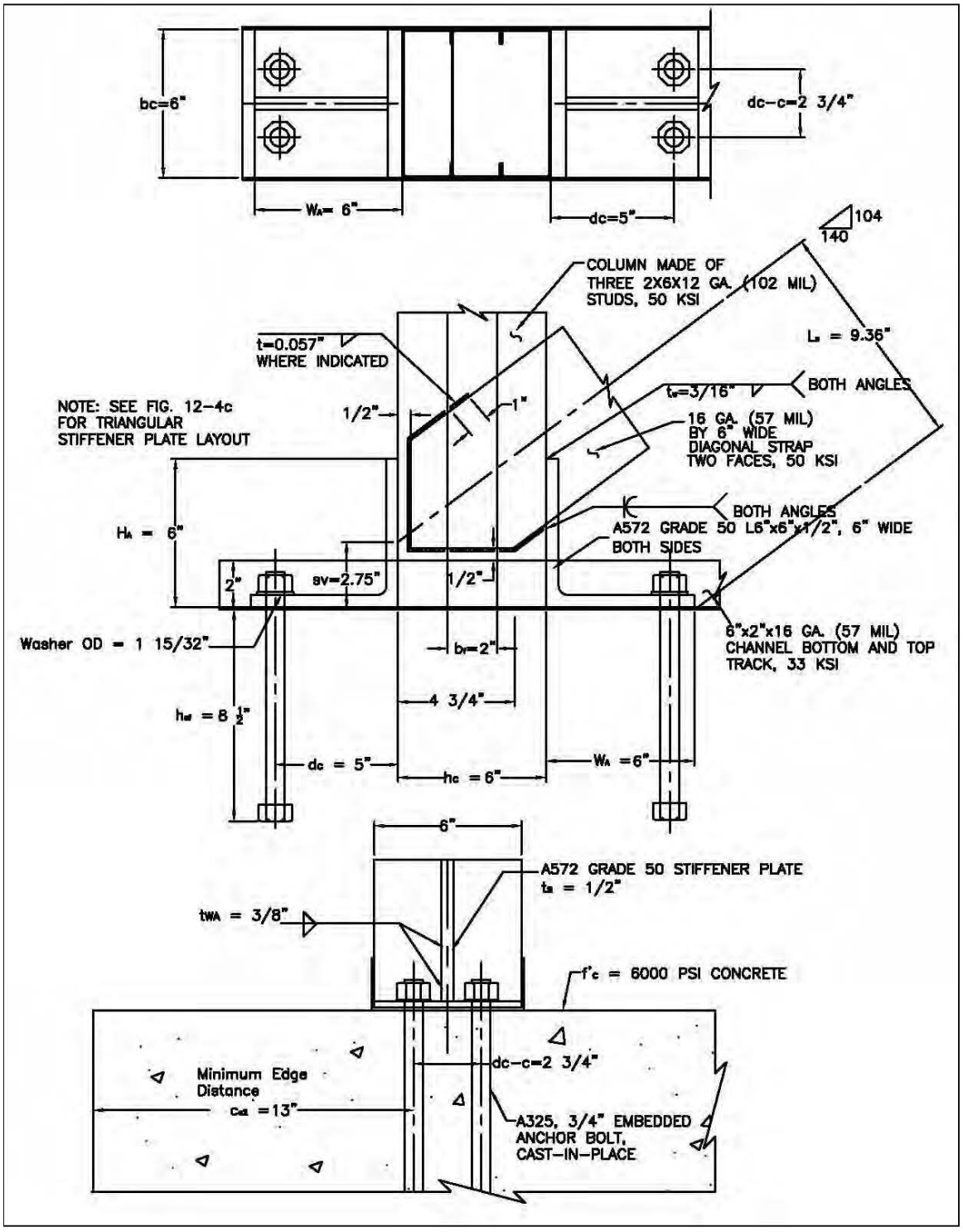

Figure 12-14. Example connection/anchorage detail
(ninth row of Table 12-6 and Table 12-9 through 12-22).

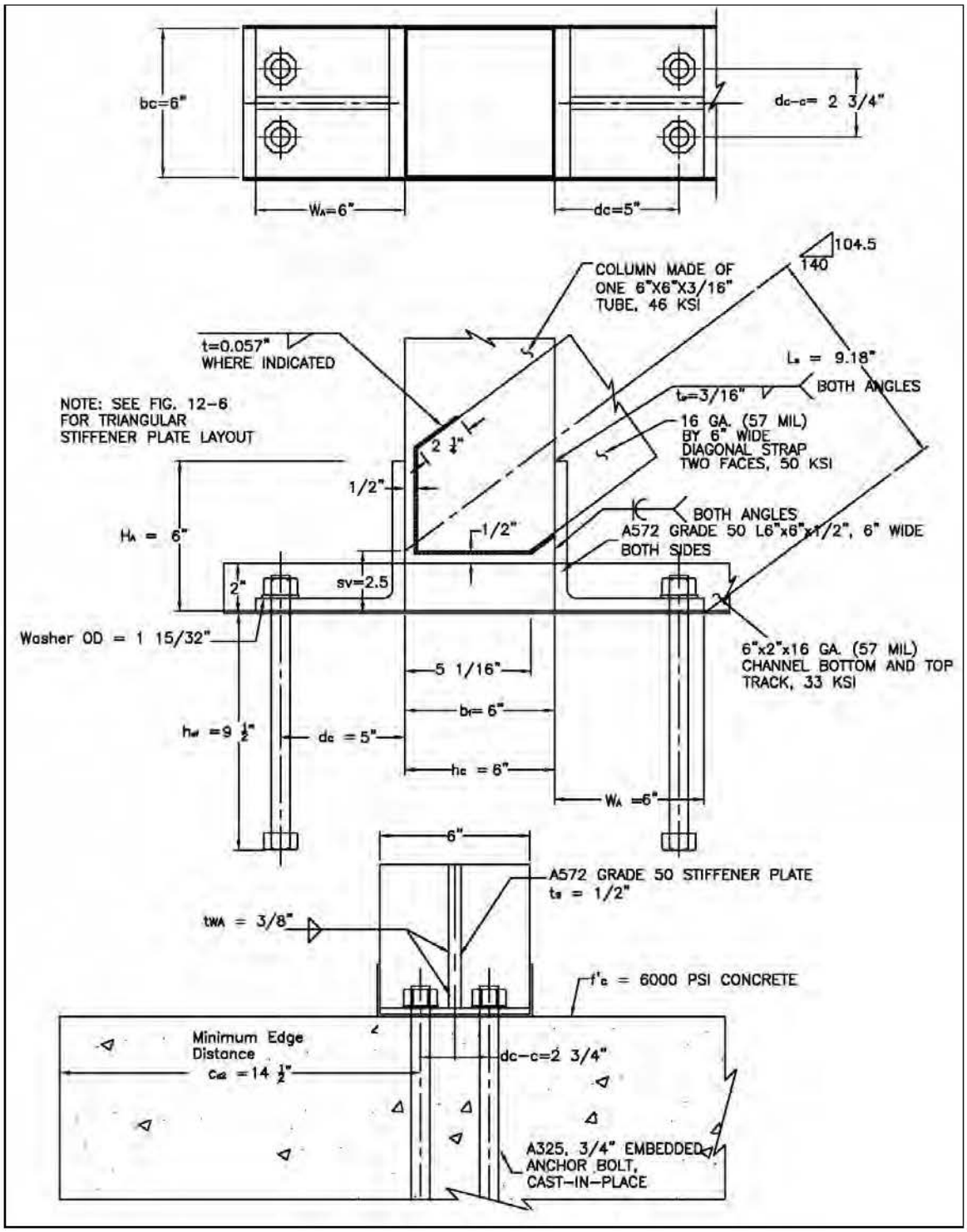

Figure 12-15. Example connection/anchorage detail
(tenth row of Table 12-6 and Table 12-9 through 12-22).

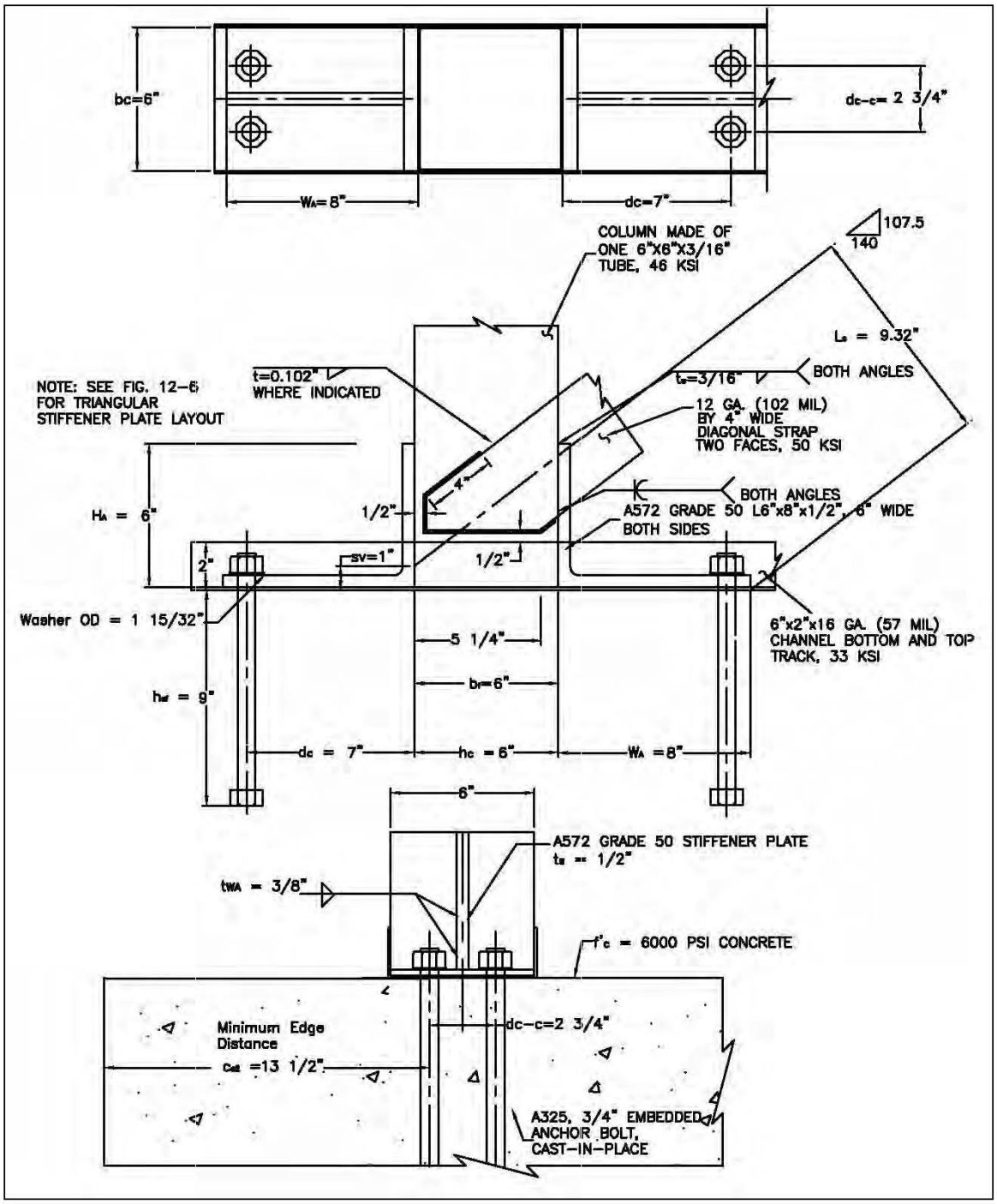

12.14 Shear panel anchors

Panel anchors must be installed on both sides of the shear panel columns. These anchors are installed at both the top and bottom of the columns to anchor the panels to the floor diaphragms both above and below the shear

panels. The anchors are needed to provide the required shear, uplift, and moment resistance from the eccentric diagonal strap loading of the anchors. The anchors will also provide limited moment resistance that will allow some moment frame action of the columns, providing system redundancy and a widening of the hysteretic load/deflection envelope. An anchor consists of an angle iron section with a stiffener plate oriented perpendicular to and welded to the legs of the angle. The stiffener plate is oriented in-plane with the panel and is located at the center of the panel in the out-of-plane direction. One leg of the anchors is welded to the columns, while the other rests inside the panel track and is bolted to the diaphragm using embedded anchor bolts (see Figure 12-4 through Figure 12-15).

12.14.1 Anchor shear capacity

All of the trial columns shown in Table 12-9 have insufficient shear capacity by themselves (see Table 12-13) and require additional capacity from their anchorage. The anchor angle vertical leg is loaded in bending, with the critical bending plane defined by Equation 11-96. Each angle leg extends beyond the critical shear plane (i.e., the H_A dimension of the angles in Table 12-17 extends above the shear plane). Figure 12-4 shows such an anchor that consists of an A572 Grade 50, 6 in. long, L 5 x 3.5 x 0.375 in. angle iron section with a 0.375 in. thick stiffener plate (shown in Table 12-20). Anchors are welded to both sides of each column at both the column tops and bottoms. The anchor bending and resulting additional horizontal capacity from the anchors on both sides of the columns are defined in Equation 11-93, and the combined column and anchor capacities are defined according to Equation 11-92. The column shear capacity, V_c, was determined earlier, in section 11.12.5, according to Equation 11-65. Table 12-17 shows the angle yield stress, width (equal to out-of-plane width of column), and thickness of the angles used in these anchors so that their combined strength, V_T, exceeds P_{humax} (Equation 11-92). Table 12-17 includes the column shear capacity presented earlier in Table 12-13 and shows that combined shear strength, V_T, exceeds P_{humax} for all the trial shear panels.

Table 12-17. Column shear and anchor bending design.

Column Type / Figure No.	Column Shear Strength V_c (kips)	Strap Lat Ult Capacity P_{humax} (kips)	Anchor Angle Yield Strength F_{Ay} (ksi)	Anchor Angle Size H_A	W_A	t_A (in)	Horiz Moment Arm d_{Ah} (in)	Angle Thickness + fillet radii k (in)	Vert Angle Height d_{Av} (in)	Width of Angle in Bending W_{Ab}	Vertical Moment Arm L_{Av}	Angle Moment Arm L_A (in)	Angle/Col Plastic Section Modulus Z_A (in3)	Angle/Col Moment Capacity M_A (k-in)	Anchor Horiz Strength P_{Ah} (kips)	Total Shear Strength V_T (kips)
3rd Floor/12-4	4.3	15.3	50	L 3.5 x 5.0 x		3/8	2.56	13/16	2.69	3.71	1.69	1.16	0.17	7.79	13.4	17.7
3rd Floor/12-7	6.5	14.6	50	L 3.5 x 5.0 x		5/16	2.56	3/4	2.75	3.76	1.75	1.19	0.13	5.77	9.7	16.2
3rd Floor/12-8	13.0	19.4	50	L 3.5 x 5.0 x		1/4	2.63	11/16	2.81	3.85	1.81	1.24	0.09	4.07	13.2	26.1
3rd Floor/12-9*	6.5	14.6	50	L 3.5 x 5.0 x		5/16	2.56	3/4	2.75	3.76	1.50	1.02	0.13	5.77	11.3	17.8
2nd Floor/12-10	24.5	34.3	50	L 6.0 x 6.0 x		1/2	2.38	1	5.00	5.54	1.50	0.64	0.45	20.34	126	151
2nd Floor/12-11*	24.5	34.3	50	L 6.0 x 6.0 x		1/2	2.38	1	5.00	5.54	1.25	0.54	0.45	20.34	152	176
2nd Floor/12-12	32.6	34.3	50	L 6.0 x 6.0 x		1/2	2.38	1	5.00	5.54	1.50	0.64	0.45	20.34	126	159
1st Floor/12-13*	34.9	43.7	50	L 6.0 x 6.0 x		1/2	2.38	1	5.00	5.54	1.50	0.64	0.50	22.58	140	175
1st Floor/12-14	59.0	43.7	50	L 6.0 x 6.0 x		1/2	2.38	1	5.00	5.54	1.50	0.64	0.65	29.43	183	242
1st Floor/12-15	59.0	52.3	50	L 6.0 x 8.0 x		1/2	2.38	1	5.00	5.54	1.50	0.64	0.65	29.43	183	242

*Asterisk designates selected panels.

12.14.2 Column-to-anchor angle weld design

Column-to-angle welds and angle sizes are selected for each trial configuration based on Table 11-9 and Table 11-10 and the angle thickness needed to provide sufficient bending capacity (see section 12.14.1). The selected weld thickness was 3/16 in. for all but one configuration of the third-floor trial panels so that heavy enough angles could be used in the anchors. This thickness is also greater than twice the thickness of the third-floor columns, so that vertical groove weld strength, P_G, is controlled by double shear at this floor (Equation 11-102)[24]. In this particular case the additional strength of double shear was not needed (see Table 12-18), but the benefit of double shear at this weld may be useful in other cases. For the first- and second-floor panels, the 3/16 in. welds permit the use of 0.5 in. thick angles for their anchors. The vertical weld strength is controlled by single shear (Equation 11-101) in first-floor columns and double shear in second-floor columns. Each of these anchors, defined in Table 12-17, meets the requirements of Equation 11-100, as shown in Table 12-18.

[24] The outside radius of the columns will be about twice the thickness of the column material, so the effective thickness of these welds will conveniently fill the gap created between the column and the angle leg.

Table 12-18. Column-to-anchor weld design.

Column Type / Figure No.	Min Gravity Load/ Panel GL_{min} (kips)	Anchor Uplift @ max Strap Yield P_{vymax} (kips)	Remaining Column Bending Cap M_{Rem} (k-in)	Tensile Force Avail/anchor P_M (kips)	Tensile Force/ Angle $P_{vymax}/2+P_M$ (kips)	Angle Horiz Weld Strength P_T (kips)	Col/Anchor Weld Thickness t_w (in)	Angle Vert Weld Strength P_G (kips)	Angle Tot Weld Strength P_A (kips)
3rd Floor/12-4	1.42	10.8	37.7	9.42	14.82	9.98	3/16	14.77	24.75
3rd Floor/12-7	1.42	9.7	66.5	16.63	21.47	14.41	3/16	21.34	35.75
3rd Floor/12-8	1.42	13.9	60.6	15.16	22.09	14.41	1/8	21.34	35.75
3rd Floor/12-9*	1.42	9.7	66.5	16.63	21.47	14.41	3/16	21.34	35.75
2nd Floor/12-10	6.28	22.5	146	24.26	35.52	18.15	3/16	46.06	64.21
2nd Floor/12-11*	6.28	22.5	146	24.26	35.52	18.15	3/16	46.06	64.21
2nd Floor/12-12	6.28	22.5	237	29.65	40.91	18.15	3/16	46.06	64.21
1st Floor/12-13*	12.0	25.5	216	36.00	48.75	25.88	3/16	32.85	58.74
1st Floor/12-14	12.0	25.5	318	52.92	65.68	42.41	3/16	53.83	96.24
1st Floor/12-15	12.0	31.7	306	50.99	66.86	42.41	3/16	53.83	96.24

*Asterisk designates selected panels.

12.14.3 Anchor bolt design

Embedded anchor bolts are used to anchor the columns to the reinforced concrete floor diaphragms. The same bolt detail is used at both the top and bottom of the columns. The anchor bolts should be positioned with a template before the concrete is cast. Alternatively, for anchors above the first floor, the same bolts that anchor the top of one panel could extend through the concrete to anchor the bottom of the panel above. Holes for these anchors could be drilled through the slab or beam after the concrete is cast. section 11.14.8 provides recommendations on through-bolt anchors. The anchor bolt strength, diameter, and position are defined so that they have adequate shear strength, P_v, and tensile strength, P_t. Then the anchor bolt length will be determined so as to meet the concrete breakout strength, N_{cb} or N_{cbg}, requirements. Table 12-19 shows that all trial anchor bolts easily meet the shear strength requirements of Equation 11-106.

The anchor bolts must provide resistance for the moment from the eccentric loading of the diagonal strap, accounting for the maximum estimated yield overstrength of the strap ($P_{symax}L_s$ in Equation 11-112). Any moment capacity beyond this is not required, but provides beneficial column moment resistance (M_{Rem} in Equation 11-105). The anchor bolt diameter, d_{AB}; strength, P_t; and horizontal distance from the column face, d_c; were determined through an iterative process. All selected anchor bolts were ASTM A325 bolts (ASTM 2014a). The anchor bolt shear and tensile strengths were determined based on Chapter 11 design recommendations,

which reference AISI/AISC 360-10, Table 3.2 (AISC 2010a), giving 68 ksi nominal shear strength for the A325 bolts (see Table 12-19). Table 12-19 shows most trial anchors used two anchor bolts per column, n_{AB}. The anchor bolts were positioned a distance from the columns, d_c, which was 1 in. less than the width of the trial anchor angles, W_A. This is the maximum distance away from the column that the anchor bolts can be placed for the selected angle width. Standard angles were selected for the anchors from AISC *Steel Construction Manual*, (AISC 2011, Part 1 "Dimensions and Properties," Table 1-7 "Angles"). Angles for the third-floor anchors were selected with their width, W_A, equal to 5 in. (i.e., L5 x 3-1/2 x 5/16 in. angle sections). Then the d_c was set to 1 in. less, equal to 4 in. for all third-floor column anchors (see Table 12-17).

Table 12-19. Shear panel anchor bolt design.

Column Type / Figure No.	# Anchor Bolts/col n_{AB}	Anchor Bolt Dia d_{AB} (in)	Applied Shear/ Bolt P_{hAB} (kips)	Bolt Nom Shear Strength F_{nv} (ksi)	Bolt Shear Design Strength P_v (kips)	Strap Max Yield Strength P_{symax} (kips)	Conn C/L Vert Dist from Base s_V (in)	Moment Arm of Dia Strap L_s (in)	Anchor Bolts to Column Face Spacing d_c (in)	Tensile Force/ Bolt P_{tAB} (kips)	Bolt Nom Tensile Strength F_{nt} (ksi)	Modified Tensile Stress F'_{nt} (ksi)	Bolt Design Strength $P_t = \phi R_n$ (kips)
3rd Floor/12-4	2	5/8	7.66	68	15.65	18.90	2.00	6.96	4.0	12.63	90	73	16.78
3rd Floor/12-7	2	5/8	7.32	68	15.65	17.05	2.50	7.33	4.0	14.35	90	75	17.23
3rd Floor/12-8	2	3/4	9.69	68	22.53	23.90	2.50	7.33	4.0	17.76	90	78	25.94
3rd Floor/12-9*	2	3/4	7.32	68	22.53	17.05	2.75	7.52	4.0	14.60	90	88	29.08
2nd Floor/12-10	2	7/8	17.14	68	30.67	40.74	1.50	8.61	5.0	27.54	90	67	30.08
2nd Floor/12-11*	2	1	17.14	68	40.06	40.74	2.50	9.33	5.0	29.25	90	78	46.23
2nd Floor/12-12	2	1	17.14	68	40.06	40.74	1.00	9.50	5.0	31.21	90	78	46.23
1st Floor/12-13*	4	3/4	10.91	68	22.53	51.16	2.75	9.36	5.0	18.85	90	73	24.32
1st Floor/12-14	4	3/4	10.91	68	22.53	51.16	2.50	9.18	5.0	21.56	90	73	24.32
1st Floor/12-15	4	3/4	13.07	68	22.53	61.26	1.00	9.32	7.0	19.31	90	65	21.47

*Asterisk designates selected panels.

The vertical distance between where the centerline of the diagonal strap-to-column connection crosses the outside vertical plane of the column, to the top of the column top connections or bottom of the column bottom connections, s_v, is illustrated in Figure 12-4 through Figure 12-15. This distance is used to calculate the moment arm of the diagonal strap, L_s, as shown in Equation 11-114, which is used in determining the anchor bolt applied tensile force according to Equation 11-112. For the third-floor anchors, the angle-to-stiffener weld, t_{Aw}, was the smaller of the maximum permitted by Table 11-9, or 0.25 in., while first- and second-floor anchors used a weld thickness of 0.375 in. This weld thickness should be the minimum that satisfies Equations 11-116 and 11-117 so that the anchor bolts can be placed as close as possible to the stiffener plate (i.e., minimum $d_{c\text{-}c}$, in Equation 11-115 and bending on the anchor angle). The top drawing of

Figure 12-4 and Figure 12-6 show the standard location and orientation of the anchor stiffener plates. Table 12-20 shows stiffener plate thicknesses, t_s, that are configured as shown in Figure 12-4 through Figure 12-15. The selected anchor bolts meet the shear strength requirement of Equation 11-106 and tensile requirement of Equation 11-108. Table 12-19 shows these requirements are met for the anchor bolts of these example panels.

12.14.4 Anchor angle thickness and angle-to-stiffener weld

The anchor angle strength must meet the requirements of Equations 11-118 and 11-120, in addition to the bending requirements of Equation 11-92 presented in Chapter 11. The strengths of the angles are based on an effective length of the critical yield and the rupture surface based on the anchor bolt washer size and distance to the edge of the angle (see Equation 11-119). Table 12-20 shows these requirements were met for all anchor angles.

The weld between the anchor angle and stiffener must have sufficient strength to satisfy Equation 11-116. The base metal capacity of the welded connection of the stiffener must also be checked according to Equation 11-117. The effective weld length, L_{Aw}, was taken as 3 in. for the third-floor anchors and 4 in. for the larger first- and second-floor anchors. Table 12-19 and Table 12-20 shows that the Equation 11-117 requirements are met for all trial anchors except the one shown in Figure 12-8, which was not selected. The asterisk, *, in Table 12-20 indicates that the anchors for the selected panels met these requirements.

Table 12-20. Anchor angle thickness and angle-to-stiffener weld strength.

Column Type / Figure No.	Angle/stiff Weld Thickness t_{Aw} (in)	Electrode Strength F_{xx} (ksi)	Effective Weld Length L_{Aw} (in)	Angle/stiff Weld Strength P_{Aw} (kips)	Yield/Rup Surface Length L_{Ay} (in)	Stiffener Base Metal Rupture P_{Su} (kips)	Angle Shear Yielding P_{Ay} (kips)	Angle/Stiff Ultimate Strength F_{Au} (ksi)	Angle Shear Rupture P_{Au} (kips)	Stiffener Plate Thickness t_S (in)	Washer Outside Diameter OD (in)	Out-of-plane Space btw Bolts d_{c-c} (in)
3rd Floor/12-4	1/4	70	3.0	16.7	2.3	21.9	26.0	65.0	25.4	3/8	1 5/16	2.5
3rd Floor/12-7	1/4	70	3.0	16.7	2.3	21.9	21.7	65.0	21.1	3/8	1 5/16	2.5
3rd Floor/12-8	3/16	70	3.0	12.5	2.5	16.5	18.5	65.0	18.1	3/8	1 15/32	2.5
3rd Floor/12-9*	1/4	70	3.0	16.7	2.5	21.9	23.1	65.0	22.6	3/8	1 15/32	2.5
2nd Floor/12-10	3/8	70	4.0	33.4	2.8	43.9	41.3	65.0	40.2	1/2	1 3/4	3.0
2nd Floor/12-11*	3/8	70	4.0	33.4	3.0	43.9	45.0	65.0	43.9	1/2	2	3.25
2nd Floor/12-12	3/8	70	4.0	33.4	3.0	43.9	45.0	65.0	43.9	1/2	2	3.25
1st Floor/12-13*	3/8	70	4.0	33.4	2.5	43.9	37.0	65.0	36.1	1/2	1 15/32	2.75
1st Floor/12-14	3/8	70	4.0	33.4	2.5	43.9	37.0	65.0	36.1	1/2	1 15/32	2.75
1st Floor/12-15	3/8	70	4.0	33.4	2.5	43.9	37.0	65.0	36.1	1/2	1 15/32	2.75

*Asterisk designates selected panels.

12.14.5 Cast-in anchor concrete breakout strength in tension

Cast-in anchors are used to anchor all the shear panels presented in this example. Post-installed anchors could also be used in accordance with the recommendations in Chapter 11 and ACI 318-11 (ACI 2011a, Appendix D). However, for many applications through-bolts may be used more economically to anchor the panels to intermediate floors and the roof diaphragm. The last section in Chapter 11 (section 11.14.8) provides through-bolt anchorage recommendations. For the cast-in anchor examples presented here, the concrete breakout strength in tension, defined by Equations 11-121 or 11-122, must exceed the applied tensile force per anchor bolt, P_{tAB} (Equation 11-112). Values for the design breakout strength for a single anchor bolt (when $n_{AB} = 2$) were calculated using Equation 11-121 for the first seven rows of Table 12-21. Similarly, design breakout strength for the two anchor bolts in tension (when $n_{AB} = 4$) were calculated using Equation 11-122 for the last three rows of Table 12-21. The effective embedment depth, h_{ef}, was adjusted so that these breakout strengths exceed the applied tensile force per bolt, P_{tAB}.

Table 12-21. Cast-in anchor concrete breakout strength in tension.

Column Type / Figure No.	Tensile Force/ Bolt P_{tAB} (kips)	Effective Embedment Depth h_{ef} (in)	In-plane Edge Distance C_{a1} (in)	Out-of-plane Edge Distance C_{a2} (in)	Actual Out-of-plane Bolt Space d_{c-c} (in)	Concrete Failure Area A_{Nc} (in^2)	Concrete Failure Area A_{Nco} (in2)	Edge Effect Modifcation Factor $\Psi_{ed,N}$	No Cracking Modifcation Factor $\Psi_{c,N}$	Post-Install Modifcation Factor $\Psi_{cp,N}$	Eccentric Modifcation Factor $\Psi_{ec,N}$	Anchor Type Factor k_c	Light Conc Modifcation Factor λ_a	Concrete Compressive Strength f'_c (psi)	Concrete Breakout Strength N_b (kips)	Design Breakout Strength $\phi_{ct}N_{cb}$ (kips)
3rd Floor/12-4	12.63	5.0	7.5	7.5	0	225	225	1.00	1.0	1.0	1.0	24	1.0	6,000	20.8	15.59
3rd Floor/12-7	14.35	5.0	7.5	7.5	0	225	225	1.00	1.0	1.0	1.0	24	1.0	6,000	20.8	15.59
3rd Floor/12-8	17.76	5.5	8.3	8.3	0	272	272	1.00	1.0	1.0	1.0	24	1.0	6,000	24.0	17.98
3rd Floor/12-9*	14.60	5.0	7.5	7.5	0	225	225	1.00	1.0	1.0	1.0	24	1.0	6,000	20.8	15.59
2nd Floor/12-10	27.54	7.5	11.3	11.3	0	506	506	1.00	1.0	1.0	1.0	24	1.0	6,000	38.2	28.64
2nd Floor/12-11*	29.25	8.0	12.0	12.0	0	576	576	1.00	1.0	1.0	1.0	24	1.0	6,000	42.1	31.55
2nd Floor/12-12	31.21	8.0	12.0	12.0	0	576	576	1.00	1.0	1.0	1.0	24	1.0	6,000	42.1	31.55
1st Floor/12-13*	18.85	8.5	12.8	12.8	2.75	720	650	1.00	1.0	1.0	1.0	24	1.0	6,000	46.1	19.14
1st Floor/12-14	21.56	9.5	14.3	14.3	2.75	891	812	1.00	1.0	1.0	1.0	24	1.0	6,000	54.4	22.38
1st Floor/12-15	19.31	9.0	13.5	13.5	2.75	803	729	1.00	1.0	1.0	1.0	24	1.0	6,000	50.2	20.74

*Asterisk designates selected panels.

In these examples, the in-plane edge distance, c_{a1}, and out-of-plane edge distance, c_{a2}, were set equal to 1.5 h_{ef}. These are the minimum edge distances that do not cause a reduction in the concrete failure area, A_{Nc}. The shear panels in these examples are oriented in the short direction of the building, whereas most panels are at the interior of the building where large edge distances should not be a problem in a heavy slab or wide beam. If large edge distances are a concern, those concerns can be reduced by increasing the embedment depth, increasing concrete strength, or using through-bolts. Figure 12-4 through Figure 12-15 show the trial anchor design for each row in Table 12-17 through Table 12-21. Figure 12-9, Figure

12-11, and Figure 12-12 show the selected anchors, which are indicated by an asterisk, *, in the first column of these tables for the third, second, and first floors respectively.

12.14.6 Cast-in anchor concrete breakout strength in shear

The concrete breakout strength in shear, defined by Equations 11-127 or 11-128, must exceed the applied shear force per anchor bolt, P_{hAB} (Equation 11-106). Values for the design breakout strength for a single anchor bolt (when $n_{AB} = 2$) were calculated using Equation 11-127 for the first seven rows of Table 12-22. Similarly, design breakout strength for the two anchor bolts in shear (when $n_{AB} = 4$) were calculated using Equation 11-128 for the last three rows of Table 12-22. The effective embedment depth, h_{ef}, was increased for only the first row of Table 12-22, because this was the only case where shear breakout strength required a longer bolt than tension.

Table 12-22. Cast-in anchor concrete breakout strength in shear.

Column Type / Figure No.	Applied Shear/ Bolt P_{hAB} (kips)	Load-bearing length l_e (in)	Concrete Failure Area A_{Vc} (in^2)	Concrete Failure Area A_{Vco} (in2)	Edge Effect Modifcation Factor $\Psi_{ed,V}$	No Cracking Modifcation Factor $\Psi_{c,V}$	$h_a<2.5C_{a1}$ Modifcation Factor $\Psi_{h,V}$	Eccentric Modifcation Factor $\Psi_{ec,V}$	Eq 11-132 Concrete Strength V_b (kips)	Eq 11-133 Breakout in Shear V_b (kips)	Design Breakout Strength $\phi_{cv}V_{cb}$ (kips)	Anchor Avail Mom Resitance $M_{colAvail}$ (k-in)	Column Moment Capacity M_{colCap} (k-in)
3rd Floor/12-4	7.66	5.0	253	253	0.90	1.0	1.0	1.0	13.3	14.3	9.01	38	53
3rd Floor/12-7	7.32	5.0	253	253	0.90	1.0	1.0	1.0	13.3	14.3	9.01	67	80
3rd Floor/12-8	9.69	5.5	306	306	0.90	1.0	1.0	1.0	16.6	16.5	11.15	61	80
3rd Floor/12-9*	7.32	5.0	253	253	0.90	1.0	1.0	1.0	14.1	14.3	9.51	67	80
2nd Floor/12-10	17.14	7.0	570	570	0.90	1.0	1.0	1.0	29.0	26.3	17.76	146	184
2nd Floor/12-11*	17.14	8.0	648	648	0.90	1.0	1.0	1.0	34.2	29.0	19.56	146	184
2nd Floor/12-12	17.14	8.0	648	648	0.90	1.0	1.0	1.0	34.2	29.0	19.56	237	281
1st Floor/12-13*	10.91	6.0	784	732	0.90	1.0	1.0	1.0	32.4	31.7	11.48	216	259
1st Floor/12-14	10.91	6.0	973	914	0.90	1.0	1.0	1.0	38.3	37.5	13.47	318	365
1st Floor/12-15	13.07	6.0	876	820	0.90	1.0	1.0	1.0	35.3	34.6	12.46	306	365

*Asterisk designates selected panels.

Figure 12-4 through Figure 12-15 show the trial anchor design for each row in Table 12-17 through Table 12-22. Figure 12-9, Figure 12-11, and Figure 12-13 show the selected anchors, which are indicated by an asterisk, *, in the first column of these tables for the third, second, and first floors, respectively.

12.15 Summary of example design problem results

Figure 12-9, Figure 12-11, and Figure 12-13 illustrate the details for the selected panels. Details for all panels are given in Table 12-6 and Table 12-9

through Table 12-22. The details of all trial panels are given in those tables, and the connection and anchor details are given in Figure 12-4 through Figure 12-15, to illustrate the variety of panel configurations that may be considered. None of the selected panels used structural tube columns (last two rows in the tables, with the details shown in Figures 12-14 and 12-15) because it was decided to use columns that are all built up from studs. However, the shear panels with structural tube columns meet all the requirements of these design recommendations.

Recommendations in Chapter 11, section 11.11 ("Diagonal strap design," p 216) require that shear panels above the ground floor have shear panels in the same direction below them, as illustrated in Figure 12-3. Through-bolt anchors at intermediate floor levels and at the roof diaphragm may often be more economical than the cast-in anchor bolts shown in the example panels (Figure 12-3). For through-bolt anchors, the anchor of the panel above should be modified to accommodate the through-bolt size and position of the heavier panels below. However, the example panels used anchor bolts to illustrate more generic shear panels that are presented for prescriptive design in Appendix C.

The spreadsheet design program used in Table 12-6 and Table 12-9 through Table 12-21 should be very useful in practical cold-formed steel seismic design (Wilcoski 2014).

References

ACI. 2011a. *Building Code Requirements for Structural Concrete and Commentary (ACI 318-11)*. Farmington Hills, MI: American Concrete Institute.

ACI. 2011b. "Guide for Design of Anchorage to Concrete: Examples Using ACI 318 Appendix D." ACI 355.3R-11. Farmington Hills, MI: American Concrete Institute, ACI Committee 355.

AISC. 2010a. "Specification for Structural Steel Buildings." ANSI/AISC 360-10. Chicago, IL: American Institute of Steel Construction.

AISC. 2010b. "Seismic Provision for Structural Steel Buildings." ANSI/AISC 341-10. Chicago, IL: American Institute of Steel Construction

AISC. 2011. *Steel Construction Manual*. 14th Edition. AISC 325-11. Chicago, IL: American Institute of Steel Construction.

AISI. 2007a. "North American Specification for the Design of Cold-Formed Steel Structural Members." AISI Specification S100-07. Washington, DC: American Iron and Steel Institute.

AISI. 2007b. "Commentary on North American Specification for the Design of Cold-Formed Steel Structural Members." AISI S100-2007-C. Washington, DC: American Iron and Steel Institute.

AISI. 2008. *AISI Manual: Cold-Formed Steel Design*. Washington, DC: American Iron and Steel Institute.

ASCE. 2010. *Minimum Design Loads for Buildings and Other Structures*. ASCE/SEI 7-10. Reston VA: American Society of Civil Engineers. doi: http://dx.doi.org/10.1061/9780784412916.

ASTM. 1995. "Standard Practice for Static Load Test for Shear Resistance of Framed Walls for Buildings." E 564-95. West Conshohocken, PA: ASTM International.

ASTM. 2013a. "Standard Specification for Steel Sheet, Zinc-Coated (Galvanized) or Zinc-Iron Alloy-Coated (Galvannealed) by the Hot-Dip Process." ASTM A653. West Conshohocken, PA: ASTM International.

ASTM. 2013b. "Standard Specification for Steel Sheet, Carbon, Metallic- and Nonmetallic –Coated for Cold-Formed Framing Members. Standard ASTM A1003/A1003M-13b. West Conshohocken, PA: ASTM International.

ASTM. 2013c. "Standard Specification for Cold-Formed Welded and Seamless Carbon Steel Structural Tubing in Rounds and Shapes." ASTM A550/A500M. West Conshohocken, PA: ASTM International.

ASTM. 2014a. "Standard Specification for Structural Bolts, Steel, Heat Tread, 120/105 ksi Minimum Tensile Strength. Standard ASTM A325. West Conshohocken, PA: ASTM International.

ASTM. 2014b. "Standard Test Methods and Definitions for Mechanical Testing of Steel Products. ASTM A370. West Conshohocken, PA: ASTM International.

ATC. 1992. "Guidelines for Cyclic Seismic Testing of Components of Steel Structures." ATC-24. Redwood City, CA: Applied Technology Council.

_____. 1995. "Structural Response Modification Factors." ATC-19. Redwood City, CA: Applied Technology Council.

_____. 1997. *A Critical Review of Current Approaches to Earthquake-Resistant Design*. ATC-34. Redwood City, CA: Applied Technology Council.

AWS. 2008. "Structural Welding Code - Sheet Steel." AWS D1.3/D1.3M:2008. Doral, FL: American Welding Society.

_____. 2012. "Recommended Practices for Resistance Welding." AWS C1.1M/C1.1:2012. Doral, FL: American Welding Society.

Caccese, Vincent, Mohamed Elgaaly, and Ruobo Chen. 1993. "Experimental Study of Thin Steel-Plate Shear Walls under Cyclic Load." *Journal of Structural Engineering* 119(2): 573–587. doi: http://dx.doi.org/10.1061/(ASCE)0733-9445(1993)119:2(573).

Driver, Robert G., Geoffrey L. Kulak, Alaa E. Elwi, and D.J. Laurie Kennedy. 1998a. "FE and Simplified Models of Steel Plate Shear Wall." *Journal of Structural Engineering* 124(2): 121–130.

Driver, Robert G., Geoffrey L. Kulak, D.J. Laurie Kennedy, and Alaa E. Elwi. 1998b. "Cyclic Test of Four-Story Steel Plate Shear Wall." *Journal of Structural Engineering* 124(2): 112–120. doi: http://dx.doi.org/10.1061/(ASCE)0733-9445(1998)124:2(112).

Elgaaly, Mohamed, Vincent Caccese, and C. Du. 1993. "Postbuckling Behavior of Steel-Plate Shear Walls under Cyclic Loads." *Journal of Structural Engineering* 119(2): 588–605. doi: http://dx.doi.org/10.1061/(ASCE)0733-9445(1993)119:2(588).

Foutch, Douglas A., and James Wilcoski. 2005. "A Rational Approach for Determining Response Modification Factors for Seismic Design of Buildings Using Current Code Provisions." *Earthquake Spectra* 21(2): 339–352.

ICC. 2011. "Cold-Formed Steel Light-Frame Construction." Section 2211 in *2012 International Building Code*. Washington, DC: International Code Council.

Larson, Jay W. 1998. In-house report. Bethlehem, PA: Bethlehem Steel Corporation.

Matsen Ford Design Associates. 1997. *U.S. Army Corps of Engineers Barracks Prototype, Department of the Army*. Prepared for the National Association of Architectural Metal Manufacturers (NAAMM), Glen Ellyn, IL. Waukesha, WI: Matsen Ford Design Associates.

NEHRP. 2009. *Recommended Seismic Provisions for New Buildings and Other Structures*. FEMA P-750. Gaithersburg, MD: National Earthquake Hazard Reduction Program.

SAC Steel Project. 1997. "SAC Testing Programs and Loading Histories" (unpublished guidance).

Serrette, Reynaud. 1997. *Additional Shear Wall Values for Light Weight Steel Framing*. Final report. Washington, DC: American Iron and Steel Institute.

USACE. 1997. *After-Action Report: Shear Wall Testing and Cold Formed Steel Design, Whole Barracks Renewal*. Fort Lewis, WA: MCA PN 41545 and PN 46748. Seattle, WA: U.S. Army Corps of Engineers, Seattle District.

_____. 1998. *Design of Cold-Formed Load Bearing Steel Systems and Masonry Veneer / Steel Stud Walls*. Technical Instructions TI 809-07. Washington, DC: Headquarters, U.S. Army Corps of Engineers, Engineering and Construction Division, Directorate of Military Programs. https://www.wbdg.org/ccb/ARMYCOE/COETI/ARCHIVES/ti809_07.pdf

Wilcoski, James. 2014. "Excel Cold-Formed Steel Seismic Design Tool." Champaign, IL: Engineer Research and Development Center. Spreadsheet available at http://nees.org/warehouse.

APPENDICES

Appendix A: Prototype Barracks Building and Cold-Formed Steel Test Panel Drawings

This appendix shows a typical three-story barracks framing layout and the six panels tested by ERDC-CERL. The elevation views are a good representation of the typical shear wall panel layout. However, the connection details have been modified since testing the earlier panels and only the details shown in test panels C1 and D2 are recommended. Designers should use the new diagonal strap-to-column connection and column anchorage details shown in the design example in Chapter 12.

Figure A-1. Prototype 3-story barracks 3-D drawing.

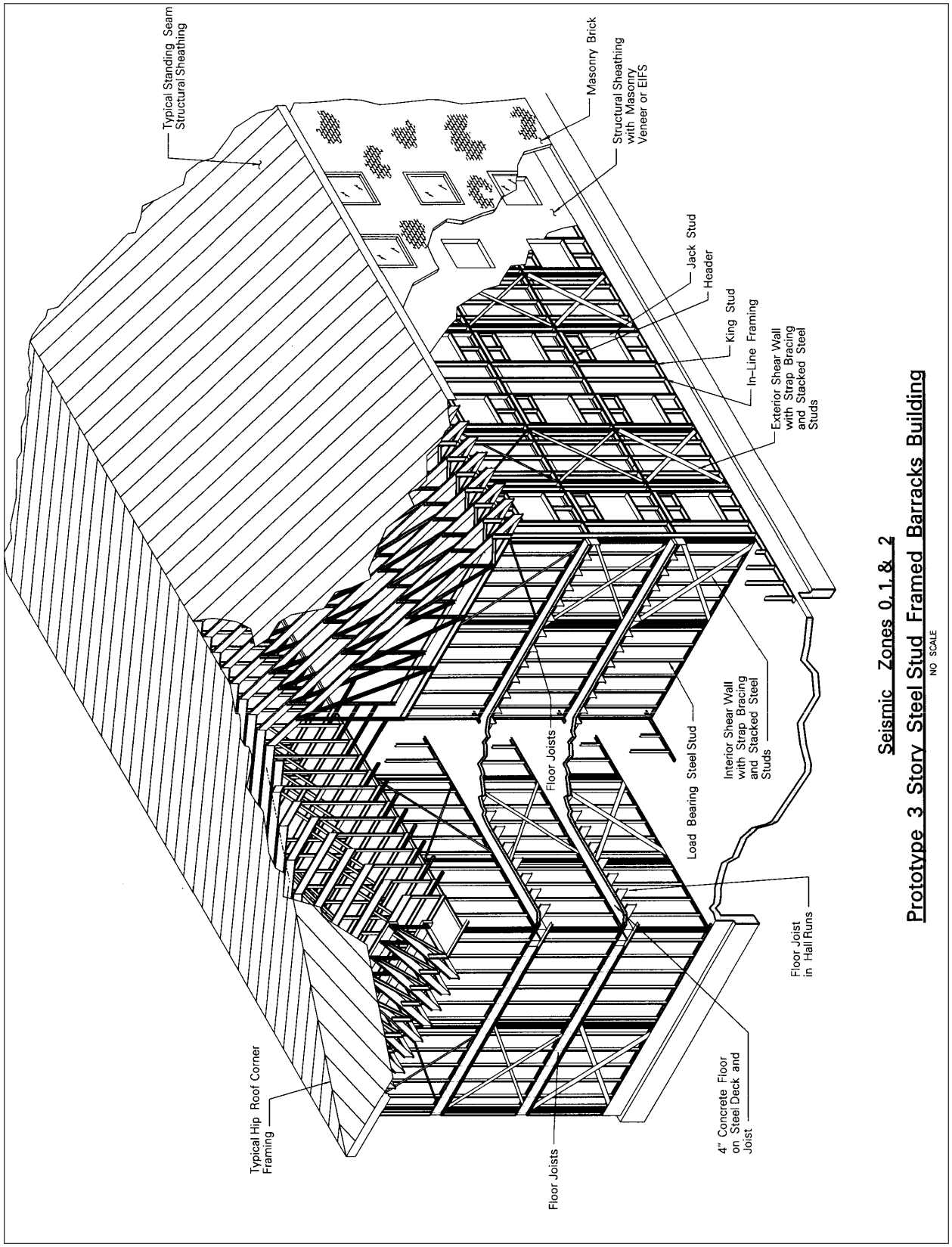

Figure A-2. Test panel A1.

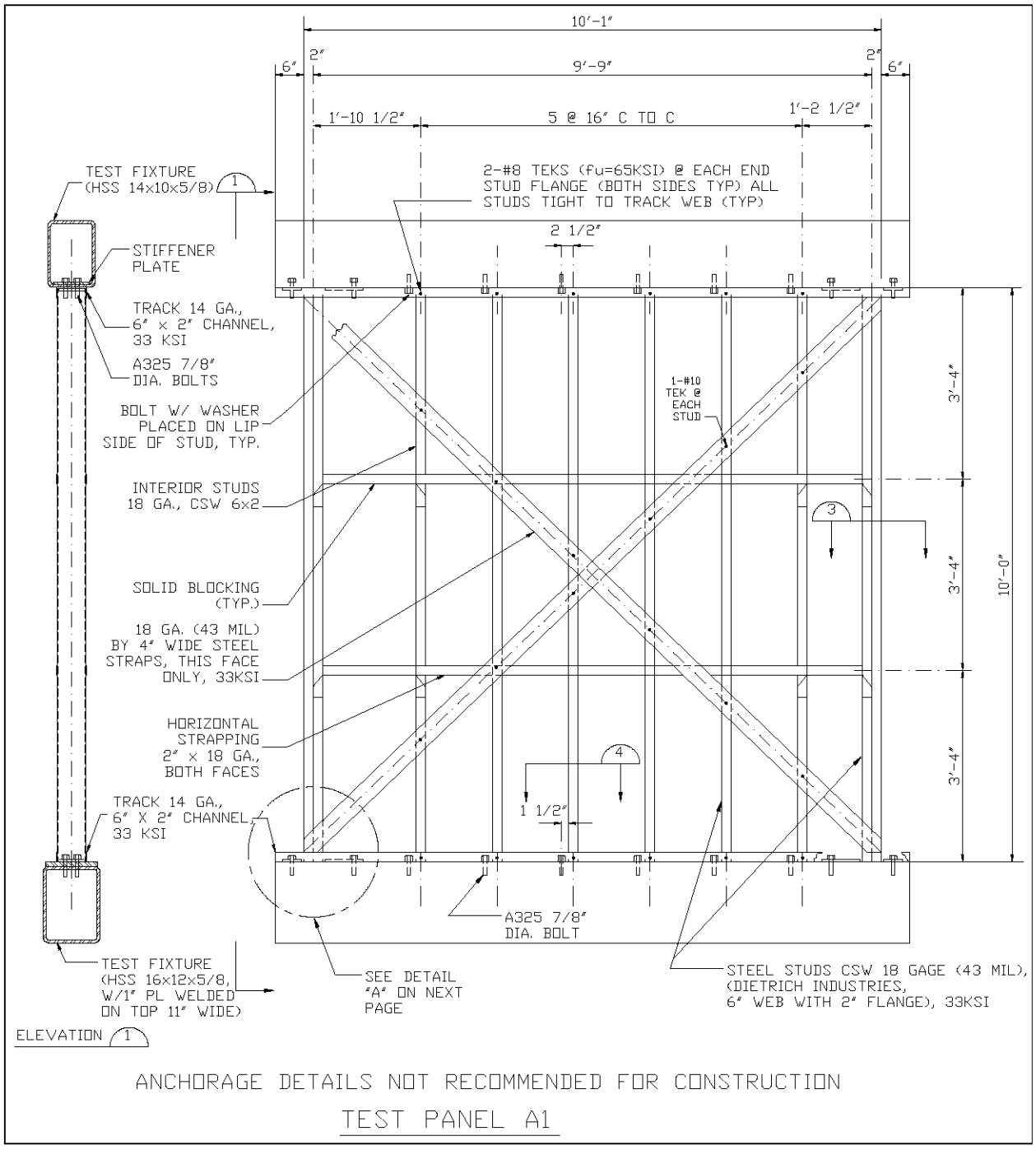

Figure A-3. Test panel A1 details.

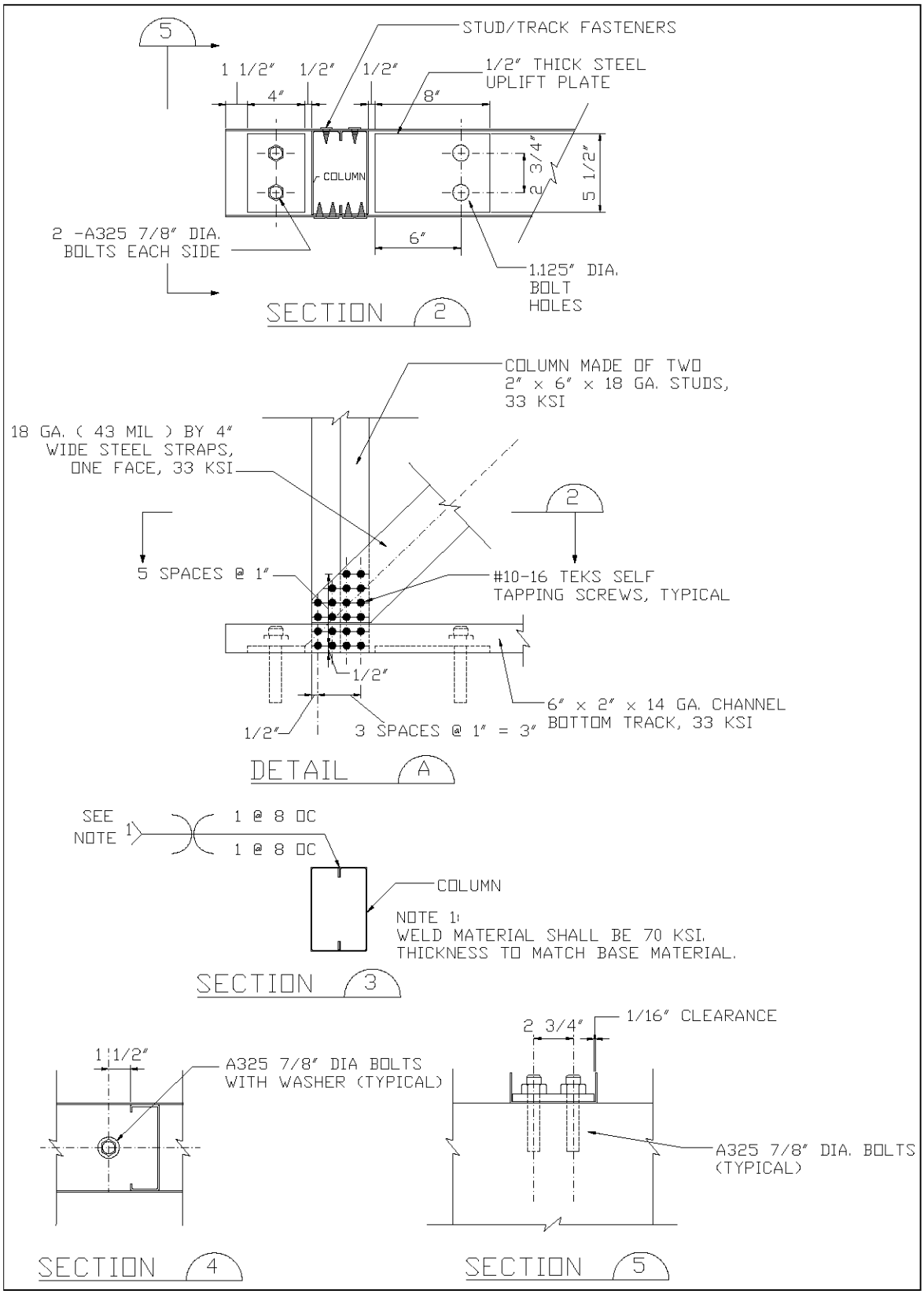

Figure A-4. Test panel A2.

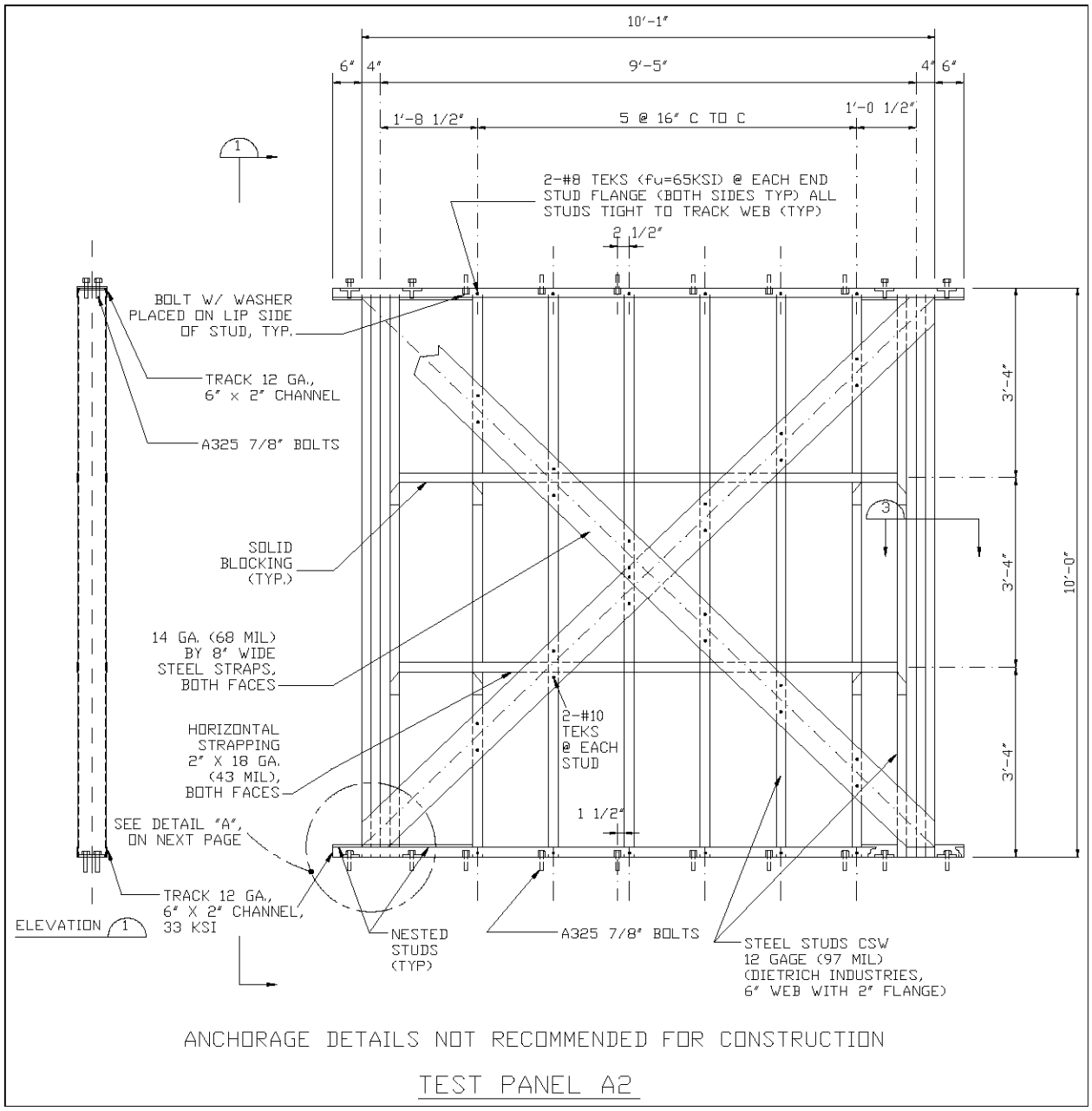

Figure A-5. Test panel A2 details.

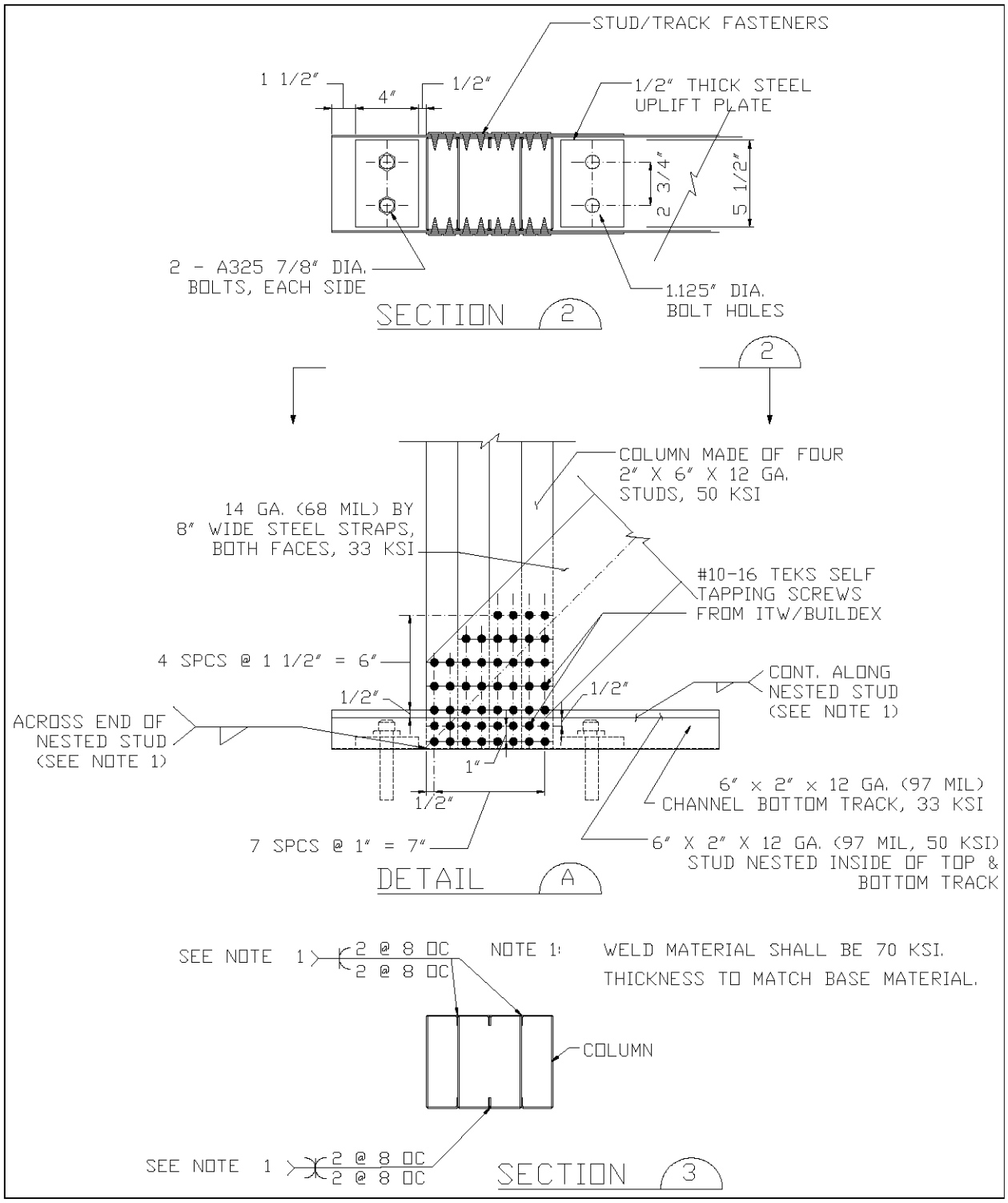

Figure A-6. Test panel A3.

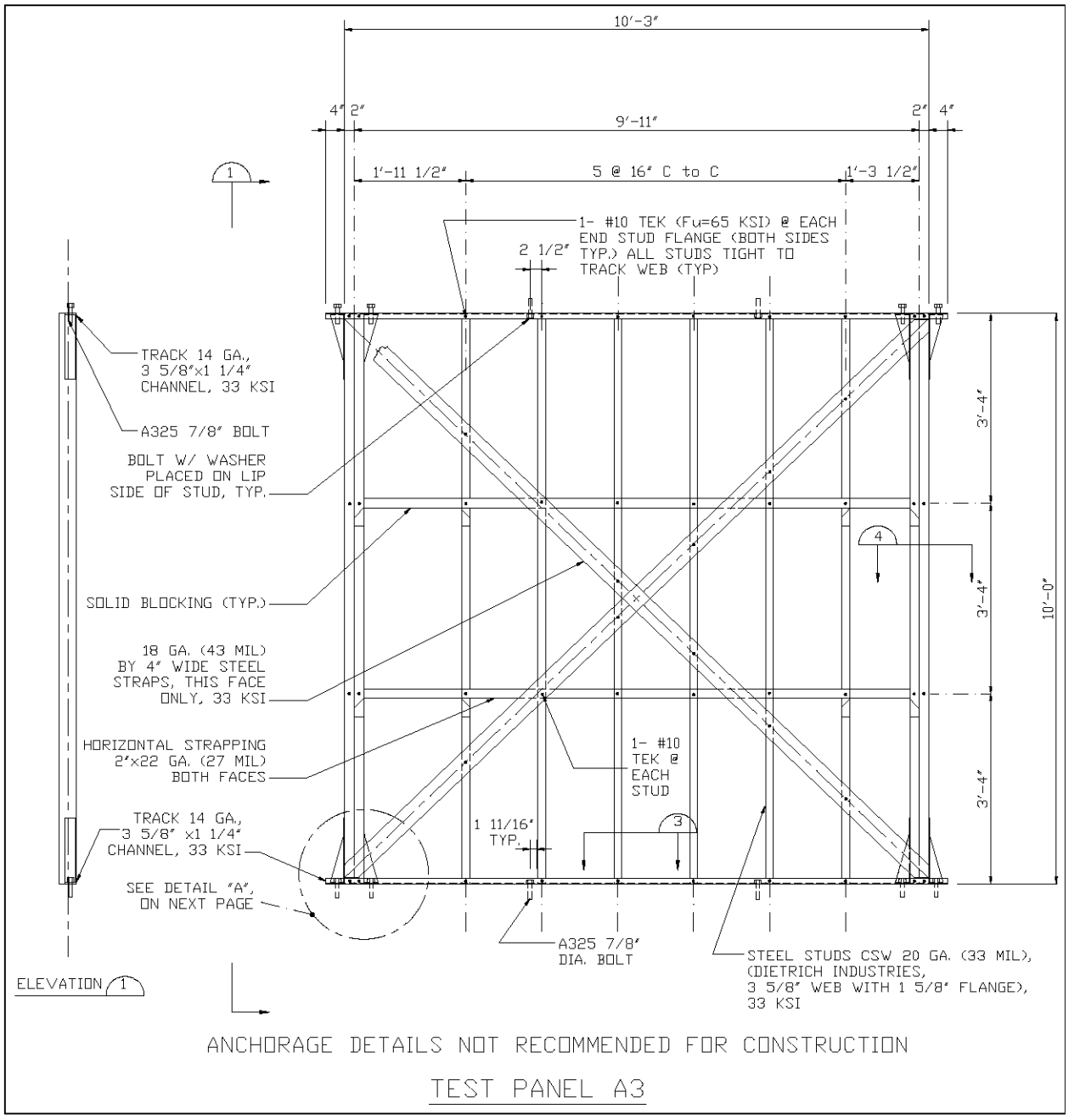

Figure A-7. Test panel A3 details.

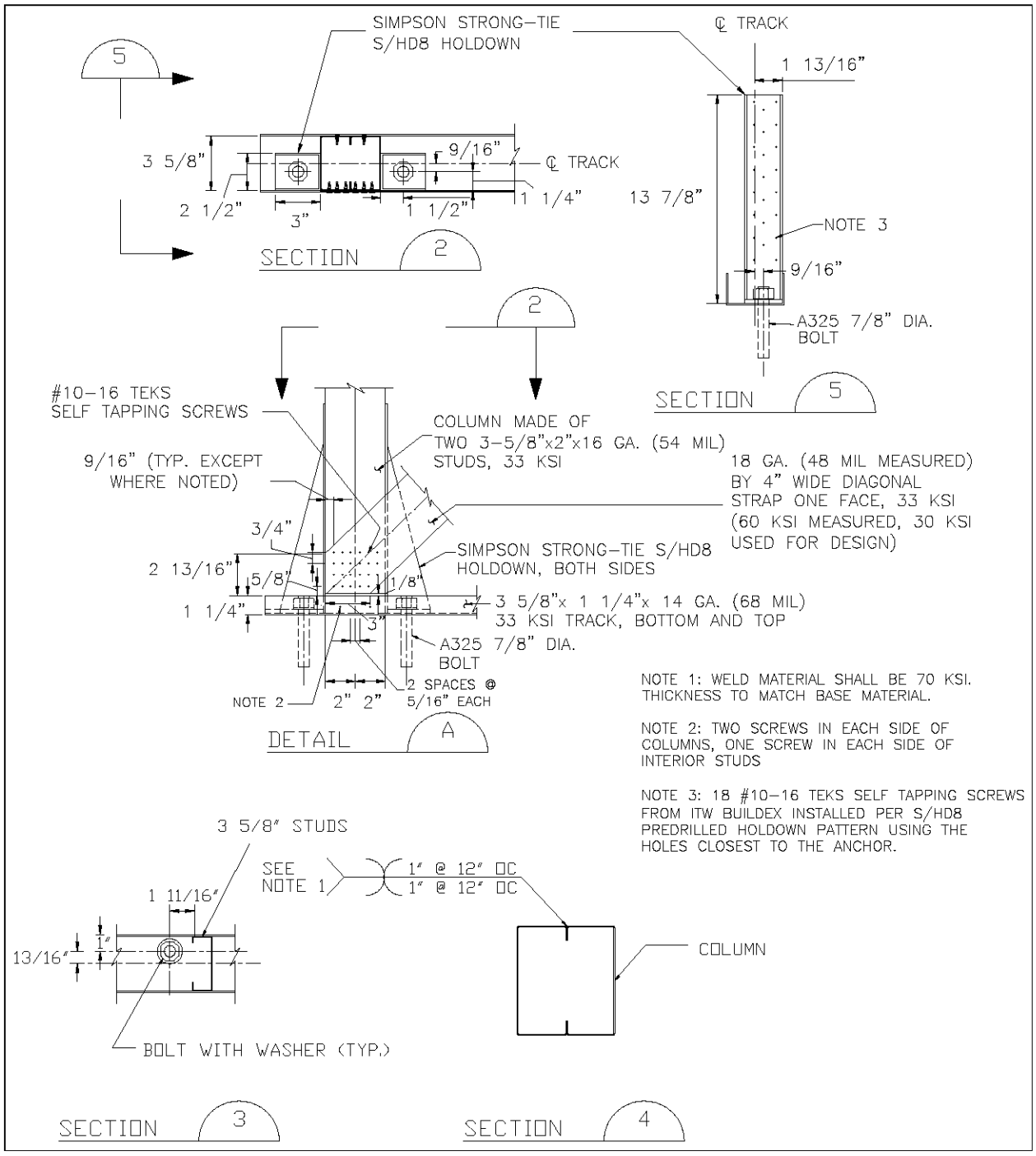

Figure A-8. Test panel C1.

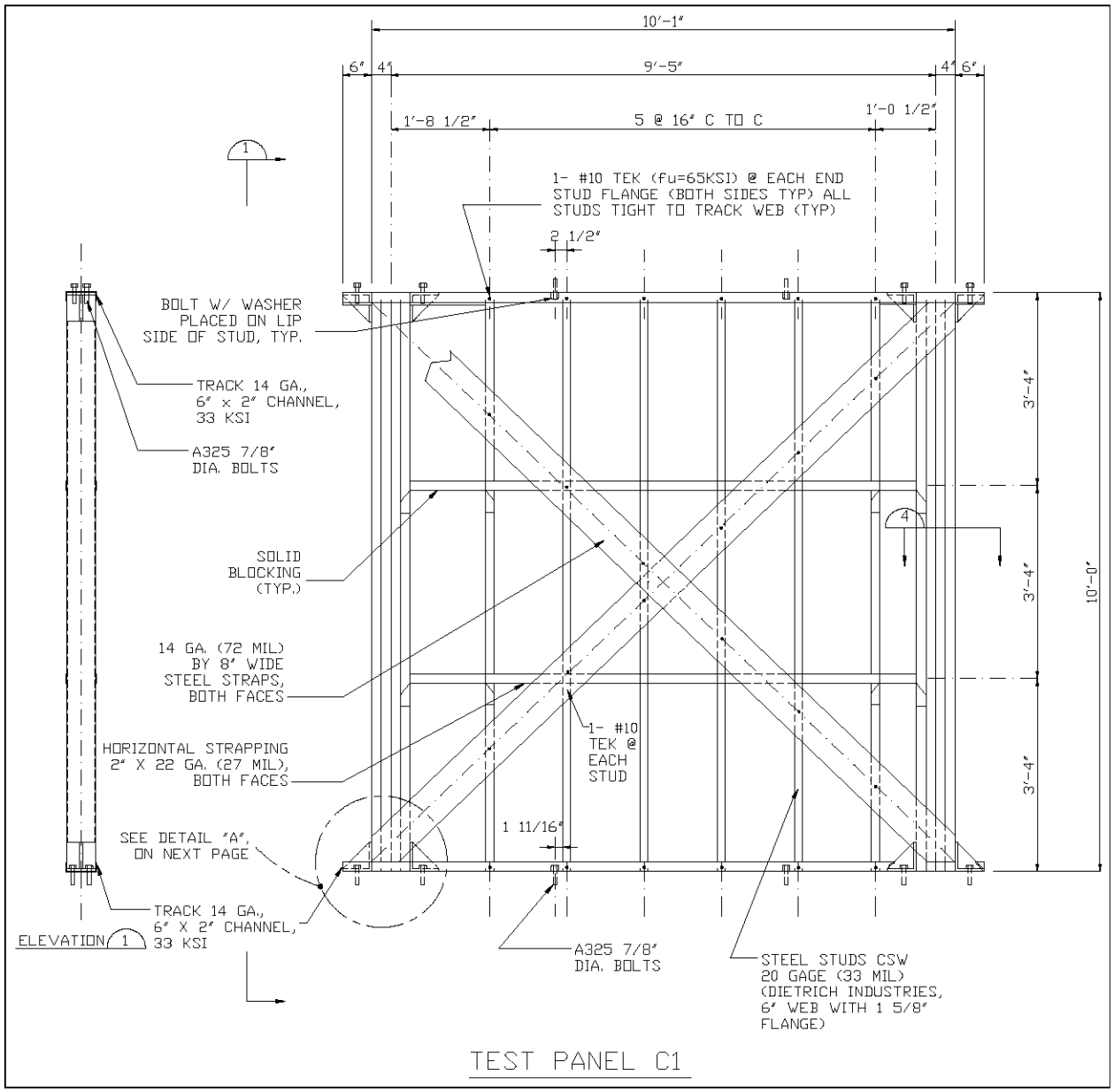

Figure A-9. Test panel C1 details.

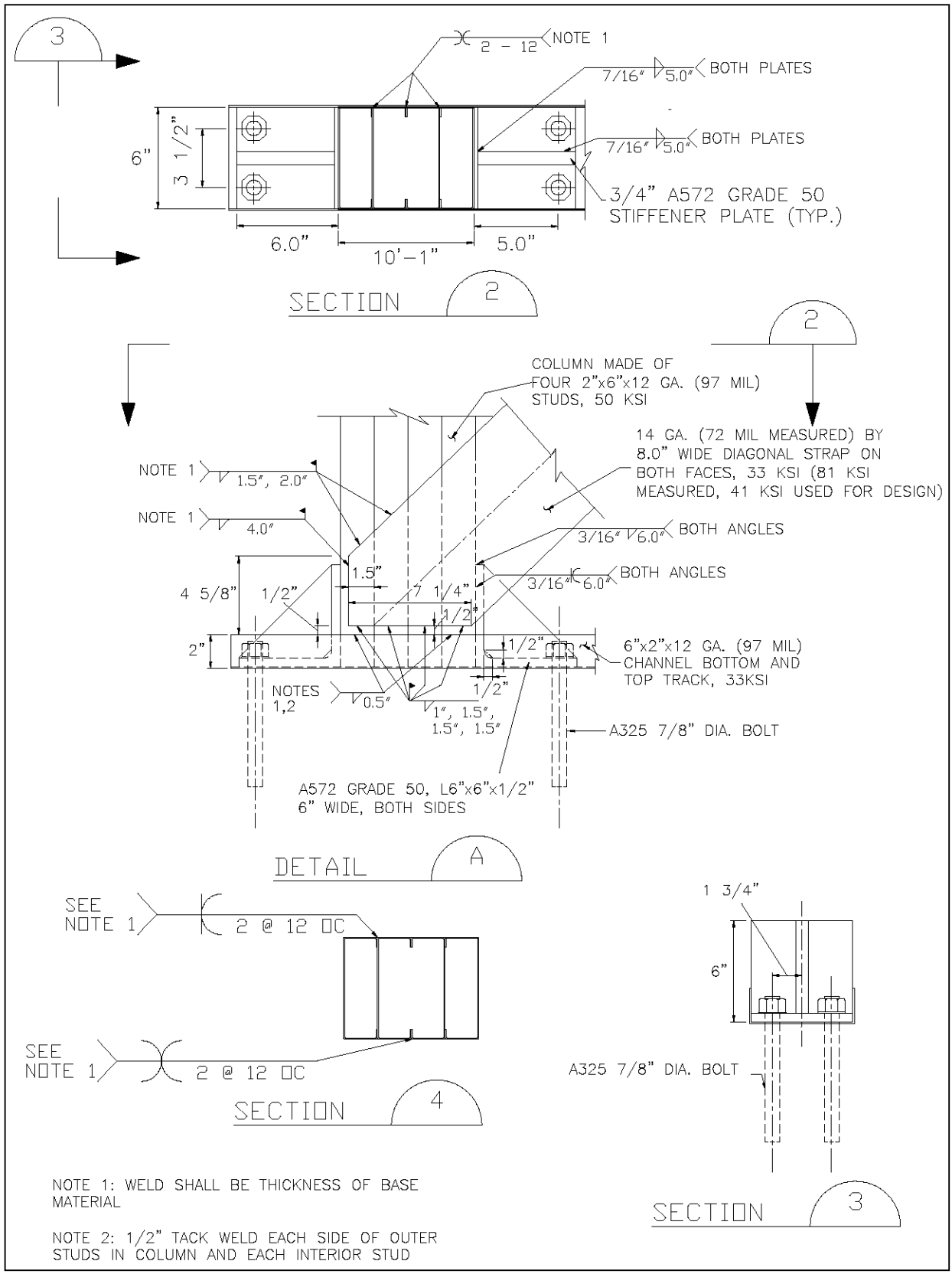

Figure A-10. Test panel D1.

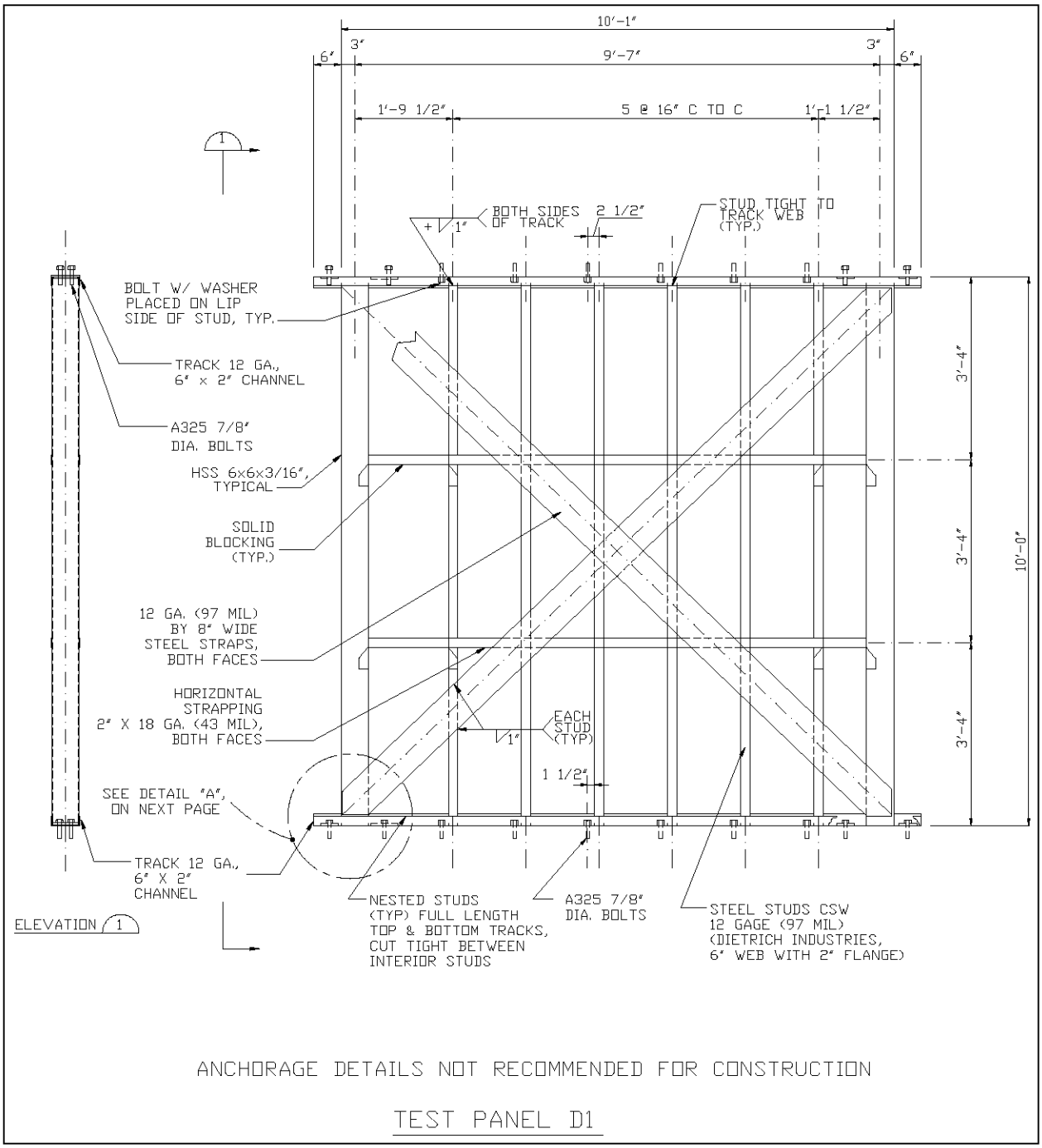

Figure A-11. Test panel D1 details.

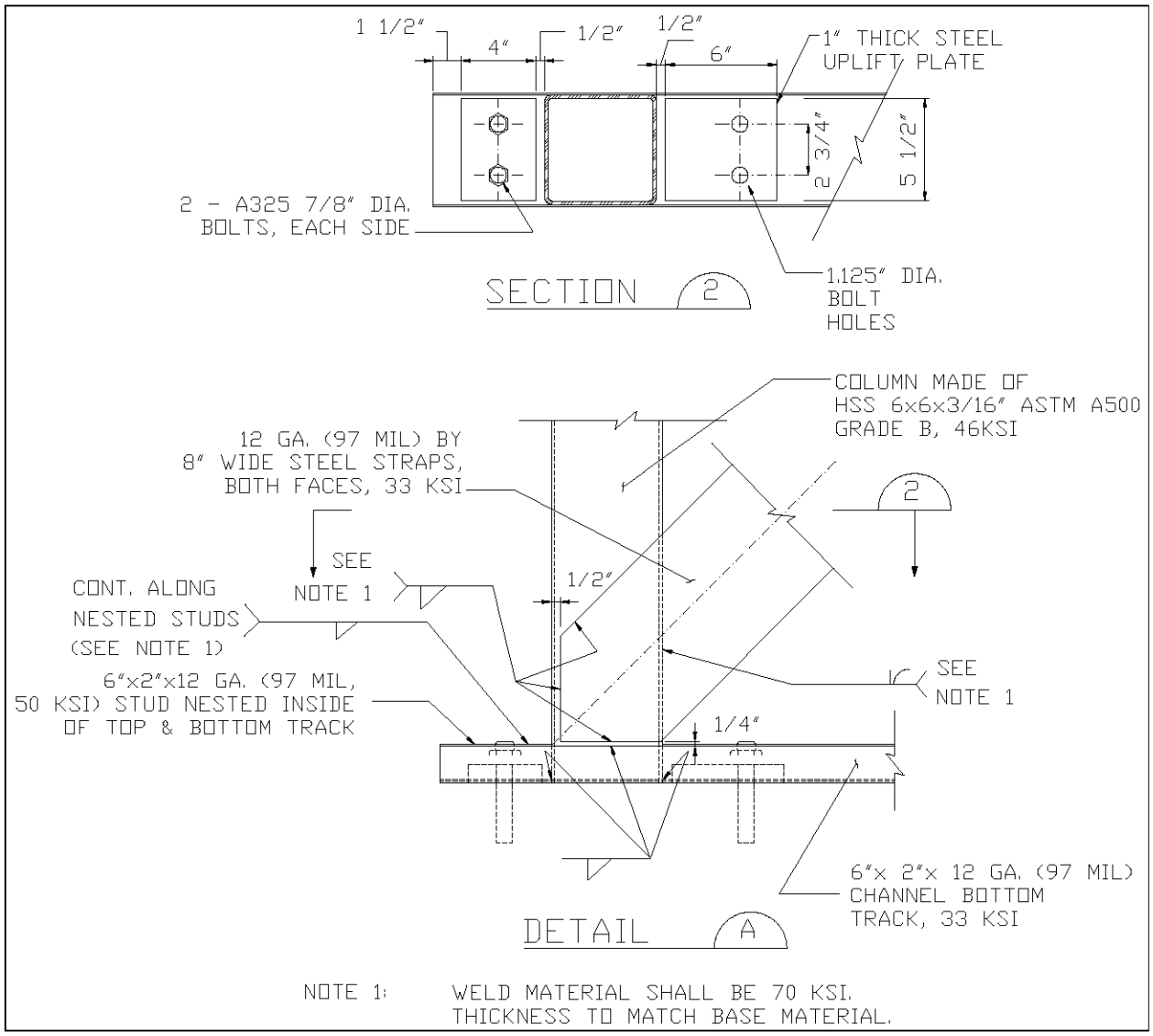

Figure A-12. Test panel D2.

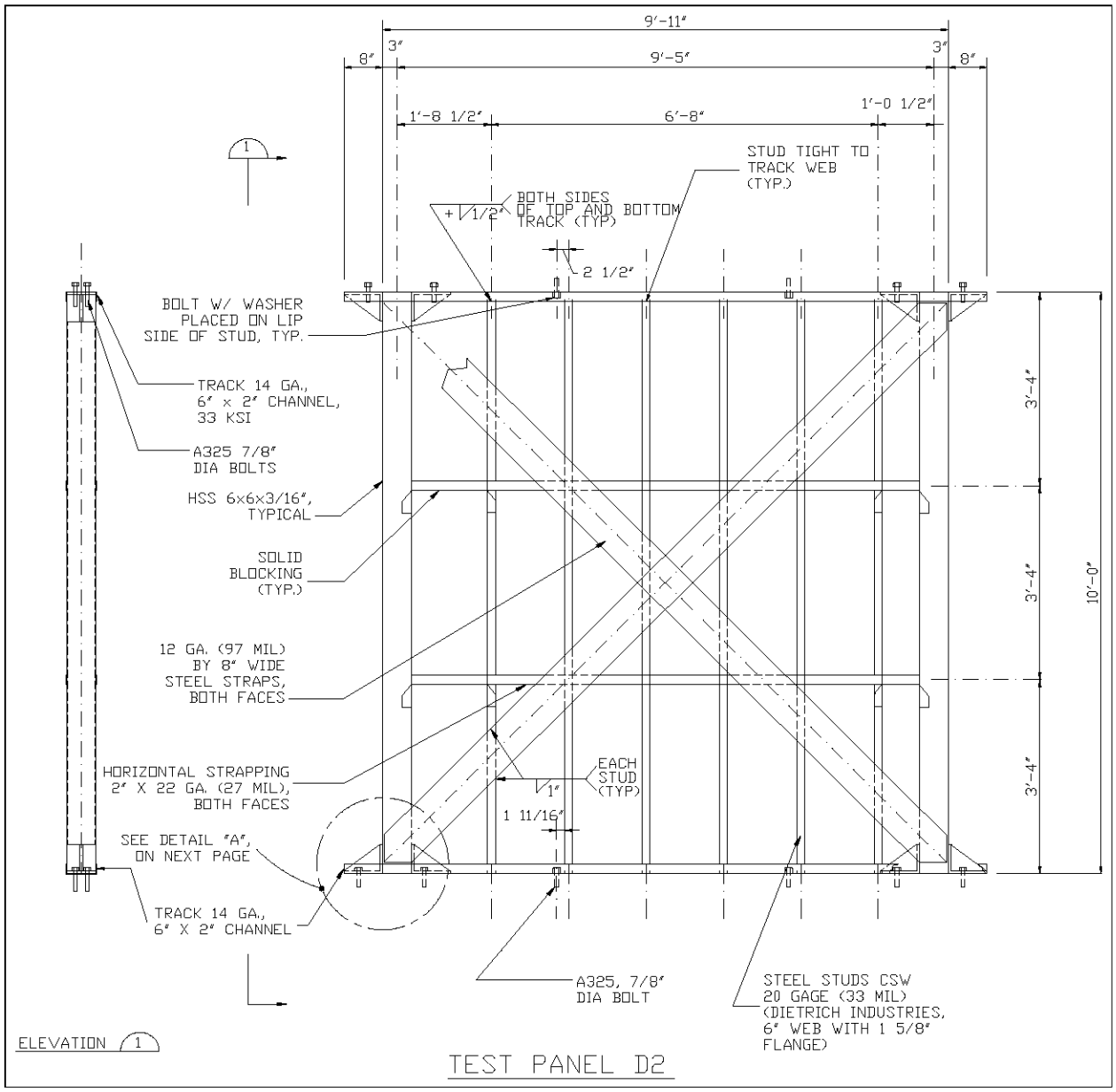

Figure A-13. Test panel D2 details.

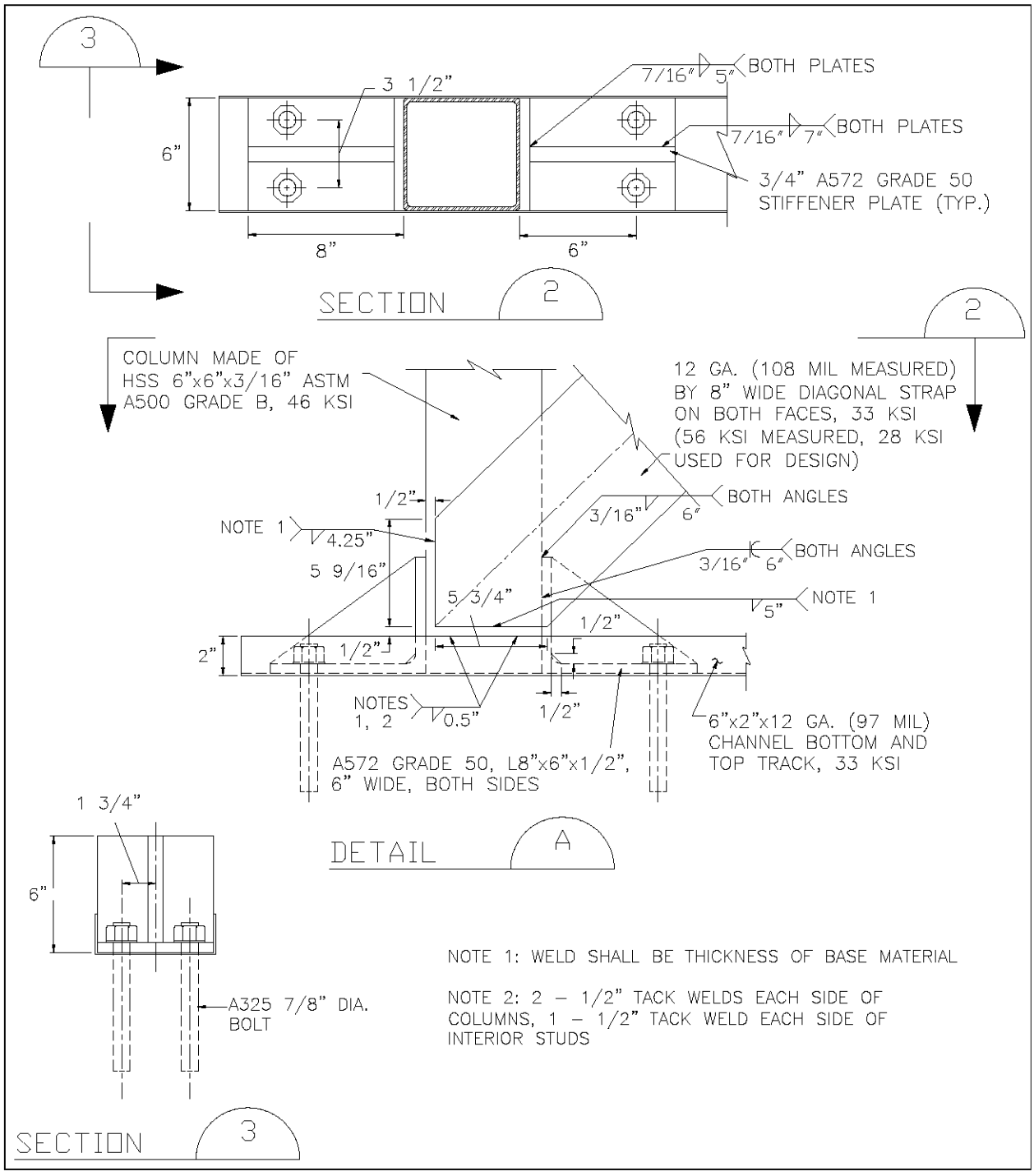

Appendix B: Cold-Formed Steel Test Observations

The following tables provide details on damage progression with respect to lateral deformation for all monotonically and cyclically loaded test panels.

Table B-1. Panel A1a monotonic observations.

Shear Deflection (in.)	Location	Failure or Other Observation
1.0	North (right) column, bottom corner	Local buckling at column knockouts – effectively redistributed loads to other portions of column cross-section.
1.4	South column, top corner	Top of tension strap began detaching, screws failed in shear at column/track connection. Column tearing in shear at column/track connection. Column began to twist at this connection because of column/track failure at the diagonal strap face of column while the other column face continued to carry shear forces to the track.
2.0	Top horizontal strap at south column	Buckling of horizontal strap.
2.1	South column, top corner	All screws at south column – top strap/column connection failed in shear.
3.5	Bottom of third stud in from north	Interior stud twisted and buckled.
3.5	North column	Buckling at two knockouts at the center and near the top of the exterior face of the north column.
3.8	First and third stud in from south column	Buckling of interior studs near their top at the diagonal and horizontal straps.
3.85	Second & third stud in from north column	Buckling of interior studs near their bottom at the diagonal and horizontal straps.
4.5	Second, third & fourth stud in from south column	Buckling of interior studs near their bottom at the horizontal strap.
4.8	North column, top corner	Column bending at the top (local buckling on the north face??).
5.0	South column, top corner	Shear failure of screws at back face of column/track connection.
5.4	North column	Buckling at two knockouts at the center and near the bottom of the interior face of the north column.
6.9	First stud in from south column – top	Screws at stud/track connection failed in shear.
7.8	Second stud in from south column – top	Screws at stud/track connection failed in shear.
8.3	Bottom of north column	Buckling at knockout at the south interior face of the north column.
9.0	Top of south column	Screws (3 or 4) failed in shear at the column/track connection.
9.7	North column, 1 ft down from top	Studs making up the column begin to separate.
10.4	Entire panel	Gross buckling of the columns and interior studs.

Table B-2. Panel A1b cyclic observations.

Shear Deflection (in.)	Location	Failure or Other Observations
0.4	Diagonal straps	Straps yield.
0.6	North and south columns	Buckling at column knockouts.
1.2	Second stud	Buckling of knockout near bottom of stud.
1.2	South column, upper corner	Column is twisting at top track (exterior face).
1.2	South column, lower corner	One screw sheared at lower south corner of column/strap connection
1.6	South column, upper and lower strap connections	Column is tearing between track flange tip and strap connection. There is large twisting at the column's midspan.
1.6	North column, upper corner	Buckling of column at the top track.
2.4	North column, upper corner	Kinking of column at top corner.
2.4	South column, upper and lower corners	Major tearing of column at track flange tip; screws, strap and track connection holding well.
2.4	South column at blocking stiffeners	Large buckling of columns at stiffeners.
2.4	6th stud	Buckling of middle knockout.
3.2	South column, upper corner	Tear halfway across column face between strap and track connections. All screws on strap side of track connection have failed. Screws on opposite side are beginning to fail.
3.2	South column, lower corner	All track screws have failed; only 2 strap screws have failed.
3.2	All studs	Twisting of interior studs near the strap connections (torsional buckling). All stud/bottom track connections have failed.
3.2	Fourth stud	Kinking of the column in the front face of stud near the knockout. Buckling of stud near the bottom track.
4.0	Bottom track	Buckling of stud flanges (front).
4.8	Bottom track	Buckling of stud flanges (back).
4.8	South column, upper corner	All track screws have failed; part of torn column still attached.
4.8	North column, upper corner	Kinking of exterior column flange (back).
5.6	Columns & interior studs	Total collapse of structure.

Table B-3. Panel A1c cyclic observations.

Shear Deflection (in.)	Location	Failure or Other Observations
0.4	Diagonal straps	Yielding of straps.
0.4	Sixth stud – top	Flange buckling in front; possible fabrication error.
0.4	South column, lower corner	Slight elastic shift in alignment of bottom track fasteners from strap connection fasteners. Column is still twisting at the connection.
0.6	North column, lower corner	See 0.4 in., south lower corner.
0.6	Fourth stud – top	Distortion around knockout.
0.6	North column	Column starting to twist at mid-height.
0.8	North column, upper corner	Local buckling of column knockout (interior face).
0.8	South column, lower corner	Permanent offset between strap and track connection.
1.2	North column, upper corner	Buckling of knockout on exterior face of column.
1.2	North column, lower corner	Buckling of column base at bottom track connection.

Shear Deflection (in.)	Location	Failure or Other Observations
1.2	South column, upper corner	Fasteners shearing in strap/column connection. Gaps are forming between the studs in the column. The top edge of the column/strap connection is pulling away from the plane.
1.2	South column, lower corner	Rotation and translation of bottom outer edge of column.
1.2	Strap on back of panel	Strap yielding on back of panel.
1.6	South column	Column has torn at top and bottom track connections.
1.6	North column, lower corner	Local deformation of top row of fasteners at joint. Pictures were taken of interior of column through the knockout.
1.6	South column, upper and lower column connections	Column is torn on face between track and strap connection.

Table B-4. Panel A2a monotonic observations.

Shear Deflection (in.)	Location	Failure or Other Observations
0.8	Diagonal strap	Buckling of strap.
2.1	North column, lower corner	Weld cracking at base (exterior front) of column at column/bottom track connection.
2.6	South column	Weld failure at lower column stiffener.
2.9	South column, upper corner	Weld fracture at column/track connection.
3.0	South column, upper corner	Fasteners breaking.
3.0	South column, lower column	Local buckling of knockout at exterior face.
3.6	North column, lower corner	Holes yielding at base of column.
4.1	Sixth stud – bottom	Stud rotated counterclockwise to the south.
4.4	North column	Local buckling of knockouts in exterior face of column.
5.3	North column, lower corner	Weld cracking at base of column (exterior face -back).
5.9	North column, lower corner	Weld failure along entire base of column/track connection.
6.2	South column, lower corner	Fasteners in column/strap connection failing in shear. Large buckling of column at track flange.
6.2	South column, upper column	Buckling of column flange at track.
7.1	First stud – top	Weld failure at nested stud connection.
7.4	North column, lower corner	Buckling of bottom track (back).
7.9	South column, upper corner	Weld failure at column/track connection.
8.2	North column, lower corner	Horizontal straps buckling.
9.2	South column, upper corner	Column is tearing at top track.
9.4	Interior studs – top	Fasteners failing in shear at top of studs (stud/track connection).
10.3	North column, lower corner	Bottom track yielding (buckling up) between sixth stud and column.
10.5	North column, lower corner	Tearing of web column at the base.
10.7	North column, upper corner	Fasteners connecting strap to studs on back shearing off.
11.2	North column, lower corner	Bottom track beginning to tear at column connection. (Front)
11.7	South column, upper corner	Column is pulling out of the connection.
12.6	Sixth stud – top	Fasteners shearing off at stud/top track connection.
13.2	Second stud	Second stud is twisting and fasteners are failing at both connections.

Shear Deflection (in.)	Location	Failure or Other Observations
14.2	South column	Local buckling of the knockouts.
14.2	South column, upper corner	Top track fractured at first column of fasteners.
Conclusion of test	North column, upper column	Weld at column/upper track connection fractured. Many fasteners at top and bottom of column sheared but the fastener heads remained affixed to the form.

Table B-5. Panel A2b trial cyclic observations (data are incomplete).

Shear Deflection (in.)	Location	Failure or Other Observations
0.5	Diagonal Straps	Buckling in both straps.
0.5	Sixth stud – bottom	Fasteners bending away from column at stud/ track connection.
0.5	Second stud – bracing	Fasteners on strap beginning to pull out.
0.5	First stud – bottom	Fasteners pulling away from base.
0.5	North column, lower corner	Slight bowing of second knockout from the bottom (exterior). Weld cracking at base of column at exterior face. Local buckling of knockouts near the bottom of the column.
0.5	North column, lower corner	Welds fracturing at top and base of column interior face. Buckling of all knockouts along exterior face.
0.5	South column, lower corner	Crack at welds in two directions into the column web (exterior).
0.5	South column, upper corner	Warping of knockouts. Local buckling of track near the back edge.
0.5	North column, upper corner	Large crack width at top of column across top weld. Buckling of top track near the back edge. Strap fasteners pulling out from studs.
6.4	North column, lower corner	Fracture through column at base.
6.4	Second stud – strap	Fasteners pulling out of studs.
6.4	North column, upper corner	Fasteners popping out of column/strap connection.
6.4	Fourth and fifth stud	Noticeable deformation of fastener holes in strap connections.
9.6	South column, upper corner	Bolts popping out of joint. Connection failure (back). Large web fracture at top of column at exterior face.
9.6	South column, lower corner	Buckling of column at base. Fasteners pulling out from column/strap connection.
9.6	Diagonal straps	Excessive buckling of bracing.
9.6	North column, upper corner	Fracture through column web on exterior face.
13.2	South column, upper corner	Column fracture completely through web. Fasteners popping out at joint
13.2	First, second, & third studs	Top fasteners in studs.
13.2	Stud –top	Failed.
15.0	South column, lower corner	Weld failure along bottom of track in nested stud. Column buckling on interior face.
15.0	Fourth & fifth studs - top	Studs twisting.

Table B-6. Panel A2b cyclic observations.

Shear Deflection (in.)	Location	Failure or Other Observations
0.6	Diagonal straps	Straps yielding.
1.2	South column, lower corner	Weld crack at stiffener front and back.
1.6	North column, upper/lower corner	Weld fracture at column.
2.4	South column, lower corner	Weld crack through stiffener.
3.2	North column, lower corner	Screw head sheared off (top row upper). Buckling of bottom track. Failure of 2 track screws at buckle point.
4.0	North column, lower corner	Buckling at column cutout. Buckling at column base.
4.8	North column, lower corner	Screw failure at top track (top row). Screw shearing at bottom track.
5.6	South column, upper corner	Fracture of column weld at top track. Tearing of column.
6.4	South column, lower corner	More weld failures at bottom of column. Column base beginning to bend.
6.4	South column, upper corner	Weld of nested stud failed.
6.4	South column	Weld fracture of column at track connection (interior).
6.4	South column, lower corner	Tearing of lower track near column intersection.
7.2	North column, lower corner	Upward buckling of track web at base of column at outer face. Tearing of track flange near weld at column base.
7.2	South column, lower corner	Fastener failure at column base. Bottom track lifting up off base beam (back).
8.0	South column, lower corner	Fasteners failing at column base (back).
8.0	Sixth stud - top	Fasteners failing at stud/strap connection.
8.0	South column, upper corner	Top track tearing at column intersection.
8.0	North column, lower corner	Fastener failed at track. Uplift of track is causing tearing of bottom track flange. Total failure of column base weld. Multiple fastener failure at north end (back).
8.8	North column - exterior	Buckling of exterior face between knockouts.
8.8	Sixth stud – top	Fastener connecting strap failed (back).
8.8	North column, upper corner	Weld tearing at column/top track connection (exterior).
9.6	North column, upper corner	Tearing of weld at column/top track connection (back).
9.6	Front diagonal strap	Various fasteners shearing at stud connections.
9.6	North column, upper corner	Four fasteners have failed in shear at top track/column connection.
9.6	North column, lower corner	Almost all fasteners in column/bottom track have failed (front).
10.4	Third stud	Fasteners shearing at stud connections.
11.2	North column, upper corner	Fasteners failing at column connection to upper stud.
11.2	Sixth stud – bottom	Fasteners failing at bracing connections.
11.2	North column, upper corner	Weld at column/top track connection failing (still maintaining some load). Fastener failed in shear at column/top track connection.
11.2	Sixth stud – bottom	Fastener failed at strap connection.
11.2	South column, upper corner	Top track tearing at column intersection (back).
11.2	Interior studs	Fasteners failing (back).
11.2	South column, upper corner	Top track tearing at top (back).

Table B-7. Panel A2c cyclic observations.

Shear Deflection (in.)	Location	Failure or Other Observations
0.4	Diagonal straps	Straps yielding.
0.6	North column, upper corner	Exterior weld crack at column/top track connection.
0.6	South column, lower corner	Weld beginning to fail at column/bottom track connection at panel exterior.
0.6	South column, lower corner	Fastener at strap/column connection failure.
1.2	North column, upper corner	Exterior weld continues to crack at column/top track connection.
1.6	Sixth stud - top	Strap fastener shear (front and back).
1.6	South column, lower corner	Bottom track beginning to buckle upwards, followed by screw failure.
2.4	North column, lower corner	Weld fracture at column/base track connection.
2.4	Track	Fasteners pulling out (back).
2.4	South column, lower corner Exterior	Weld at column/bottom track connection failed.
3.2	North column, lower corner	Base track torn from corner to fastener. Track buckling out at column intersection at back face.
3.2	South column, upper corner	Screws sheared at column/top track connection.
4.0	Diagonal strap	Strap buckling (front).
4.0	South column	Top track beginning to tear at column connections. Top weld at upper track/column connection (exterior).
4.0	South column, lower corner	Weld failure along bottom track connection (interior). Entire bottom track failing along exterior column face.
4.0	North column, upper corner	Top track buckling at column. Top track tearing along fastener line.
4.0	North column, lower corner	Welds fracturing at base. Fasteners shearing at bottom of track at back face.
4.0	Upper/north lower corners	Bending of top track away from beam at top and bottom.
4.8	North column, lower corner	Brittle weld fracture along entire base. Bottom track torn along fastener line at back face.
4.8	Sixth stud - bottom	Strap fastener failing.
5.6	Second stud	Fastener failed at strap connection.
5.6	North column, lower corner	Bottom track pulling up from beam.
5.6	North column, upper corner	Weld failure along base (exterior).
5.6	Right column	Local buckling near knockouts.
5.6	North column, lower corner	Column tearing at base near exterior weld.
5.6	South column, lower corner	Bottom track shearing and weld failure through track.
6.4	South column, upper corner	Exterior weld at upper track/column connection failed completely.
6.4	South column, lower corner	Slight buckling of column near base. Bottom track has failed (Back)
6.4	North column, lower corner	Buckling of interior track/column connection.
6.4	North column, upper corner	Column tearing near weld (exterior).
6.4	Sixth stud - top	Stud fastener to top track sheared off. Fasteners have sheared at top track – front and back face.
7.2	South column, upper corner	Fasteners failing at column connection – back face
8.0	South column, lower corner	Track is beginning to uplift from beam.
8.0	Third stud	Fastener failure at strap connection.
8.0	North column, lower corner	Column buckling at track (exterior). Column starting to gap at base.

Shear Deflection (in.)	Location	Failure or Other Observations
8.0	North column, upper corner	Fasteners shearing at track/column connection.
8.8	Third stud – strap	Fasteners shearing at strap connection.
9.6	Third stud – strap	Fasteners shearing at strap connection.
9.6	North column, lower corner	Bottom track flange beginning to tear.
9.6	South column, lower corner	Fasteners at column/strap connection failing.
10.4	North column, lower corner	Bottom track at column base has sheared. Tear continuing along the bottom track.
11.2	First stud- top	Fasteners at strap connection shearing.
12.8	Interior studs - bottom	Studs fail along bottom track at screws.

Table B-8. Panel A3a monotonic observations.

Shear Deflection (in.)	Location	Failure or Other Observations
Loading to the South – Positive Direction on Data Plots		
1.3	South column, top corner	Screws failed between column and track.
2.8	South column, top corner	Major distortion of column.
3.5	South column, top corner	Column pulled away from anchor.
4.0	South column, top corner	Screws between column and strap failing.
5.0	South column, top corner	Strap failed.
Loading to the North – Negative Direction on Data Plots		
0.7	North column, top corner	Screws failed between column and track.
1.15	South column, bottom corner	Screws failed between column and track.
2.2	South column, bottom corner	Column pulling away from strong-tie.
2.8	South column, bottom corner	Column buckling around strong-tie.
5.9	Interior	Studs buckle.
6.3	South column, bottom corner	Column pulling away from strong-tie.
10.0	South column, bottom corner	Slow progression of crushing of double stud between anchors.

Table B-9. Panel A3b cyclic observations.

Shear Deflection (in.)	Location	Failure or Other Observations
0.45	South column, bottom corner	Screws failed between column and track.
0.9	North column, bottom corner	Screws failed between column and track.
1.2	South column, top corner	Strap pulling away from column.
1.2	North column, bottom corner	Bowing of column.
1.8	South column, top corner	Buckling of column.
1.8	South column, bottom corner	Strap pulling away from column.
2.4	South column, bottom corner	Buckling of column.
2.4	North column, top corner	Buckling of column.
3.6	South column, top corner	Screws fail between strap and column.
3.6	Interior	Buckling of interior channels and partial screw pullout.

Shear Deflection (in.)	Location	Failure or Other Observations
3.6	North column, bottom corner	Screws fail between strap and column. Major tearing of column away from anchor
4.8	North column, top corner	Crushing of column against anchor.
4.8	South column, top corner	Channels of column start pulling apart.
4.8	South column, bottom corner	Screws pull out.
6.0	South column, bottom corner	Strap failure by pullout.
6.0	North column, bottom corner	Strap failure by pullout.

Table B-10. Panel A3c cyclic observations.

Shear Deflection (in.)	Location	Failure or Other Observations
0.45	North column, bottom corner	Column flexing with strap tension.
0.6	North column, top corner	Screws failed between column and track.
0.9	South column, Top/bottom corner	Screws failed between column and track.
0.9	North column, top corner	Screws failed between column and track.
1.2	North column, top corner	As connection is stressed, back of column wraps back around anchor.
2.4	North column, top/bottom corner	Screws between column and strap nearly pulling out.
3.6	North column, bottom corner	Strap net area failure at connection.
4.8	North column, top corner	Screws between column and strap pull out.
6.0	South column, bottom corner	Lots of screws showing between strap and column.
7.2	Interior	Interior studs well buckled.

Table B-11. Panel C1a monotonic observations.

Shear Deflection (in.)	Location	Failure or Other Observations
0	Unknown	Weld between track and column failed at application of vertical load.
0.5	North column, top corner	Weld between track and column failed.
0.75	South column, top corner; North column, bottom corner	Major deflection of strap (compression).
2.25	South column, bottom corner	Tearing of the strap.
3.5	South column, bottom corner	Rear strap failed.

Table B-12. Panel C1b cyclic observations.

Shear Deflection (in.)	Location	Failure or Other Observations
0.6	North column, top corner	Weld crack.
0.8	North column, bottom corner	Weld cracked on both sides
1.2	North column, bottom corner	Small cracking at top of angle/column connection.

Shear Deflection (in.)	Location	Failure or Other Observations
1.6	North column, bottom corner	First three welds cracked.
1.6	South column, bottom corner	Weld failure.
2.4	North column, top corner; North column, bottom corner	Complete tear of strap.
3.2	North column, bottom corner	Angle splitting from column.
4.8	North column, bottom corner	Complete tear at angle/column connection.

Table B-13. Panel C1c cyclic observations.

Shear Deflection (in.)	Location	Failure or Other Observations
0.3	North column, top corner	Track weld failure (front).
0.4	North column, top corner	Track weld failure (back).
0.6	North column, bottom corner	Track weld failure (front/back).
1.6	South column, bottom corner	Track weld failure (back).

Table B-14. Panel D1a monotonic observations.

Shear Deflection (in.)	Location	Failure or Other Observations
0.95	Diagonal straps	Straps yielding.
1.0	South column, upper corner	Crack forming in weld at column/top track connection. (Exterior) Track bowing away from beam.
1.37	North column, lower corner	Track pulling up.
1.6	North column, lower corner	Welds fracture at nested studs.
2.1	North column, lower corner	Bottom track tearing at weld (back). Weld at base of column fracture at exterior face.
3.8	South column, upper corner	Top track bowing away from beam.
4.0	South column, upper corner	Welds at nested stud have failed.
4.0	North column, lower corner	Track torn through to base.
4.43	North column, lower corner	Track base tearing. Track flanges bowing out between welds.
6.7	South column, lower corner	Bottom track pulling away from beam.
8.0	South column, lower corner	Weld failing at nested stud/column connection.
8.0	South column, upper corner	Top Track beginning to tear. Buckling of top track is causing it to crush against tube column.
8.46	Sixth stud - straps	Strap exhibiting a hump between welds on same stud.
9.3	North column, lower corner	Nested stud flanges are buckling against tube.
10.2	North column, lower corner - Strap	Strap tearing on back face.
10.68	North column, lower corner – Strap	Strap tom through on back.
10.68	Interior studs - bottom	Weld at base of interior stud fail.
11.24	North column, lower corner-strap	Front strap torn through on front.

Shear Deflection (in.)	Location	Failure or Other Observations
11.24	North column, lower corner	Bottom track bowing up.
11.24	Third stud	Strap weld fails.
12.0	First stud - bottom	Weld failure at strap connection.
12.5	Fifth stud - bottom	Stud buckling at base.
13.14	North column, lower corner	Bottom track buckling at base.
13.6	Interior studs - bottom	Massive buckling at stud/bottom track connections.
14.0	North column, lower corner	Weld fracture/tearing through track.
14.45	Diagonal strap	Strap weld failures at stud connections.
14.45	Base beam	Dishing effects at bolts.

Table B-15. Panel D1b cyclic observations.

Shear Deflection (in.)	Location	Failure or Other Observations
0.4	Diagonal straps	Straps yielding.
0.6	North column, upper corner	Weld begins to fail at column/top track connection at exterior face.
1.2	North column, upper corner	Welds across flanges fail at nested studs.
1.2	South column, upper corner	Welds across flanges fail at nested studs.
1.6	South column, lower corner	Welds across flanges fail at nested studs.
2.4	South column, lower corner	Bottom track beginning to uplift under outside of column.
2.4	South column, upper track	Tear in top track beginning to propagate in track near column at exterior face.
3.2	North column, lower corner	Weld begins to fail at flange of nested stud. Bottom track lifting up.
3.2	Second stud - strap	Weld at strap connection begins to fail at front and back face.
3.2	Third stud - strap	Weld failure at strap connection at back face.
4.0	North column, lower corner	Track tearing near column connection at front face. Tearing of bottom track along side at front face.
4.0	Second stud - strap	Weld at strap connection fails at front face.
4.0	North column, upper corner	Top track tearing. Flange of nested stud beginning to buckle.
4.0	South column, upper corner	Tears forming at column/top track weld connection at front and back faces. Buckling of nested stud flange due to prying action against column.
4.8	Sixth stud - bottom	Weld failure at strap connection.
4.8	Diagonal straps	Straps bowing between welds of same stud.
4.8	Second stud - bottom	Weld at strap connection failed at front and back faces.
5.6	North column, lower corner	Bottom track buckling out at column.
5.6	Sixth strap - bottom	Weld beginning to fail at strap connection.
5.6	North column, upper corner	Top track pulling away from beam.
5.6	South column, lower corner	Weld failure of column/bottom track connection at exterior face.
6.4	South column, upper corner	Weld failure of column/bottom track connection at exterior face.
6.4	North column, lower corner	Sudden weld fracture at column/bottom track connection at exterior face. Strap/column connection beginning to fail at back face. Bottom track buckling out at back face.
7.2	North column, upper corner	Strap/column connection beginning to fail. Weld failure at column/top track connection at exterior face.
7.2	Sixth stud - bottom	Stud beginning to tear near bottom track. Stud buckling at base.

Shear Deflection (in.)	Location	Failure or Other Observations
7.2	Fifth stud - bottom	Weld fails around strap.
8.0	South column, upper corner	Top track flanges beginning to buckle near column/top track connection.
8.0	Interior studs	Welds at strap/stud connection fail. Studs tearing near bottom track.
9.6	North column, lower corner	Strap beginning to tear.
9.6	North column, upper corner	Weld failure at column/top track connection at exterior face.
10.4	North column, lower corner	Strap tearing near column in two places. Weld failure near tear column/strap connection.
11.2	North column, lower corner	Sudden failure of back strap.
11.2	North column, upper corner	Strap beginning to tear.
12.0	North column, upper corner	Strap beginning to tear on back near column.
13.6	Interior studs	Local buckling near knockouts.
13.6	Diagonal straps	Three straps have failed.

Table B-16. Panel D1c cyclic observations.

Shear Deflection (in.)	Location	Failure or Other Observations
0.4	Diagonal straps	Straps yielding.
0.8	South column, lower corner	Inside weld of nested stud beginning to fracture.
1.2	South column, upper corner	Weld on top of nested stud beginning to fracture.
1.6	South column, lower corner	Tearing of bottom track at column interior.
1.6	North column, upper corner	Crack in weld at column/nested stud connection at front face.
2.4	North column, Lower Column	Weld at column/bottom track failed. Tear forming across nested stud near column connection at exterior face. Buckling of bottom track away from the nested studs. Uplift of track at column (front).
2.4	First stud	Strap weld fracturing (back).
3.2	North column, lower corner	Tear at weld propagating into bottom track.
3.2	South column, upper corner	Top track beginning to tear (exterior).
4.0	First & second stud	Welds to strap beginning to fail (back).
4.0	Third stud	Weld to strap failed (front).
4.0	North column, lower corner	Large crack through weld at the top of Bottom track near column connection at exterior face.
4.0	North column, Upper Column	Tear forming in top track at column connection at exterior face.
4.8	South column, lower corner	Bottom track beginning to lift off beam. Bottom track beginning to tear near column interior face.
4.8	First stud - bottom	Weld to bottom track beginning to fail.
4.8	South column, lower corner	Buckling of track at base.
4.8	First stud - top	Strap weld fails at back face.
5.6	North column, upper corner	Weld beginning to tear at strap/column connection at back face.
5.6	South column, lower corner	Weld at column base continues to fail.
5.6	First stud - bottom	Strap weld failure (back).
5.6	Third stud	Strap weld failure (front).
6.4	Sixth stud - top	Weld failure at strap connection at front and back face.
6.4	Fifth stud - top	Top track beginning to tear and twist at top track/stud connection.

Shear Deflection (in.)	Location	Failure or Other Observations
6.4	South column, upper corner	Top track tearing around column interior. Buckling of top track around column interior.
6.4	South column, lower corner	Small weld fracture of column/strap connection (front).
7.2	South column, lower corner	Total weld failure of column to bottom track connection at back face.
7.2	North column, upper corner	Weld failure along column/top track connection at back face.
7.2	Fourth and fifth stud	Welds to strap fails.
8.0	First stud	Strap bowing between welds on same stud. Short panel welds fail. Short panel near stud is rotating down.
8.0	Interior studs - bottom	Studs buckling near bottom track.
8.0	Second stud - strap	Strap beginning to tear (back).
8.0	First stud - bottom	Stud tearing near bottom track.
8.0	Second stud - top	Weld failing at stud/top track connection.
8.0	Fourth stud - top	Stud tearing near top track (front).
8.0	First stud - top	Stud tearing near top track (front).
8.0	Fifth stud - bottom	Stud tearing at stud/bottom track connection.
8.0	Sixth stud - top	Weld at strap connection failed (back).
8.0	Diagonal strap at fifth stud	Strap beginning to tear at stud connection on front face.
8.8	Second and third stud – top	Weld beginning to fail (track/top track connection).
8.8	Interior studs	All studs tearing along bottom track.
8.8	Diagonal strap – north column, upper corner	Strap beginning to tear at column connection (front).
9.6	North column, upper corner	Welds at strap connections beginning to tear at front & back faces.
9.6	South column, upper corner	Sudden weld failure at column/top track connection.
9.6	Interior studs	All studs tearing along top track.
9.6	South column, upper corner	Top track pulling away from beam.
12.0	North column, upper corner	Strap beginning to tear near column at back and front face.
12.8	Sixth stud at strap	Tear is propagating at first stud weld.
13.6	North column, lower corner	Two tears forming in straps near column at front face.
13.6	First stud	Short panel weld fails causing panel to swing down.

Table B-17. Panel D2a monotonic observations.

Shear Deflection (in.)	Location	Failure or Other Observations
Loading to the North – Positive Direction on Data Plot		
0.7	South column, bottom corner	Track weld failure.
0.8	North column, top corner	Track weld failure.
1.7	North column, top corner	Brittle fracture of strap.
1.9	South column, bottom corner	Brittle fracture of strap (back side).
Loading to the South – Negative Direction on Data Plot		
0.5	South column, top corner	Track weld failure.
1.2	South column, top corner	Vibration noise.

Table B-18. Panel D2b cyclic observations.

Shear Deflection (in.)	Location	Failure or Other Observations
0.4	North column, bottom corner	Track welds failed (back – north side of column).
0.6	North column, top corner	Track welds failed (back).
0.8	North column, bottom corner	Track welds failed (back – south side of column).
2.4	South column, top corner	Back strap failed.
2.4	South column, bottom corner	Front strap broke.
4.0	Unknown	Last strap broke.

Table B-19. Panel D2c cyclic observations.

Shear Deflection (in.)	Location	Failure or Other Observations
0.3	North column, top/bottom corner	Track weld failure (front and back).
2.4	North column, bottom corner	Brittle tear of strap.

Appendix C: Prototype Shear Panels for Cold-Formed Steel Seismic Design

This appendix provides tabular data for the selection of possible prototype shear panels that may be used in the seismic design of cold-formed steel structures. These panels were developed for the example problem presented in Chapter 12, using the design recommendations presented in Chapter 11. Each shear panel given in Table C-1 is defined in Figure 12-9, Figure 12-11, Figure 12-13 and Figure 12-12, as indicated in Table C-1. The panel shown in Figure 12-14 was not selected for the example problem, but meets all the requirements of these design recommendations.

Definition of terms

The prototype shear panels given in Table C-1 shall be used based on the following definition of terms. For these panels, the values of GL_{max} and GL_{min} were defined at which the demand reached the capacity for one of the limiting equations given below.

$\varphi_t Q_{sy}$ = the lateral shear panel design strength that must exceed the maximum story shear per shear panel, including the effects of torsion, defined and limited by Equation 11-37.

GL_{max} = the maximum gravity load per shear panel, defined by Equation 11-18 and limited by Equations 11-55 or 11-56.

GL_{min} = the minimum gravity load per shear panel, defined by Equation 11-19 and limited by Equations 11-100, 11-108, 11-116, 11-117, 11-118, 11-120, or 11-122.

Prototype panel load table

Table C-1 provides the tabular data needed to select prototype shear panels.

Table C-1. Prototype shear panel load capacities.

Panel Figure	Lateral Design Strength $\phi_t Q_{sy}$ (kips)	Max Gravity Load/ Panel GL_{max} (kips)	Min Gravity Load/ Panel GL_{min} (kips)
Figure 12-9	8.1	35.2	-3
Figure 12-11	19.0	36.5	-4
Figure 12-13	24.2	88.5	10
Figure 12-14	24.2	224	5

Appendix D: Seismic Qualification Procedure and Acceptance Criteria for Other Shear Panel Configurations

This appendix presents the test procedure, acceptance criteria, and documentation requirements needed to demonstrate the acceptability of cold-formed steel shear panel configurations that are different from the specific system defined in Chapter 11. Acceptable configurations are limited to cold-formed steel shear panels that use diagonal straps or full panel sheets as the lateral-load-resisting elements. The columns shall be constructed with cold-formed or hot-rolled structural steel. This procedure applies to the qualification of a prototype of the specific panel that will be used in construction. Qualification requires the testing of three specimens. All panel tests shall represent full panel system tests of all the panel components including connections and anchors.

Coupon tests of all test panel materials

Coupon tests shall be performed on all materials that may contribute to the structural performance of the test panels. At least three coupons shall be tested from each lot of each type of material. Coupons shall be prepared and tested following the provisions of ASTM A370 (ASTM 2014b). Materials that contribute to the ductility of the shear panels shall have a total elongation of at least 10% for a 2 in. gage length. All coupon test results shall be plotted in a test report, in terms of stress versus strain. All coupon test results shall also be summarized in a table in the format shown in Table D-1. The data in this table shall be the average value of the three or more coupons of the particular component.

Table D-1. Tabular format for coupon test results.

Structural Component of Coupon	Design Yield Stress (MPa or ksi)	0.2% Offset Yield Strain* (mm/mm)	0.2% Offset Yield Stress* (MPa or ksi)	Maximum Load Strain (mm/mm)	Maximum Stress (MPa or ksi)	Max Stress 0.2% Offset Yield Stress
Component #1						
Component #2						

See Chapter 4 for the definitions of 0.2% offset yield strain and stress.

Coupon test of all field panel materials

Coupon tests shall be performed on all materials that contribute to the structural performance of the field panels. The field panels shall be identical to the prototype-tested panels. At least three coupons of each material shall be tested. Coupons shall be prepared and tested following the provisions of ASTM A370 (ASTM 2014b). Materials that contribute to the ductility of the shear panels shall have a total elongation of at least 10% for a 2 in. gage length. All coupon test results shall be plotted in a test report, in terms of stress versus strain. All coupon test results shall also be summarized in a table in the format shown in Table D-1. The data in this table shall be the average value of the three or more coupons of the particular component. The field diagonal straps or full panel sheets shall have a coupon yield stress (0.2% offset) not greater than 5% above or not less than 10% below the test panel coupon yield stress (0.2% offset). The field material coupons for all other structural elements shall have coupon yield stress (0.2% offset) not less than the test panel coupon yield stress (0.2% offset).

Test configuration

Full-scale test panels shall be tested with both monotonic (push-over in one direction) and cyclic loading. The panels shall be anchored to a base beam and top beam in a manner representative of the field installation. The base beam shall resist any slippage, out-of-plane movement or rotation in any direction. Vertical load shall be applied to the shear panel through the top beam, at a level representative of potential gravity loads in the field. The amount of vertical load applied should consider the worst-case condition for the most vulnerable panel components. For example, the minimal vertical load may provide the most severe loading for the anchors, while the maximum vertical would provide the worst-case loading for column buckling. This vertical load shall be held constant throughout each test. The top beam shall be held horizontal during all tests, as this represents the field conditions when the panel is assembled in a building. Figure D-1 shows the test configuration and instrumentation plan for shear panels tested at ERDC-CERL, to illustrate the load configuration. In the ERDC-CERL tests, stroke control was used to keep the two vertical actuators at the same length, which held the top beam horizontal. The combined vertical force was held constant by using the test control system (which was done manually for earlier tests).

Figure D-1. Schematic drawing showing sensor locations.

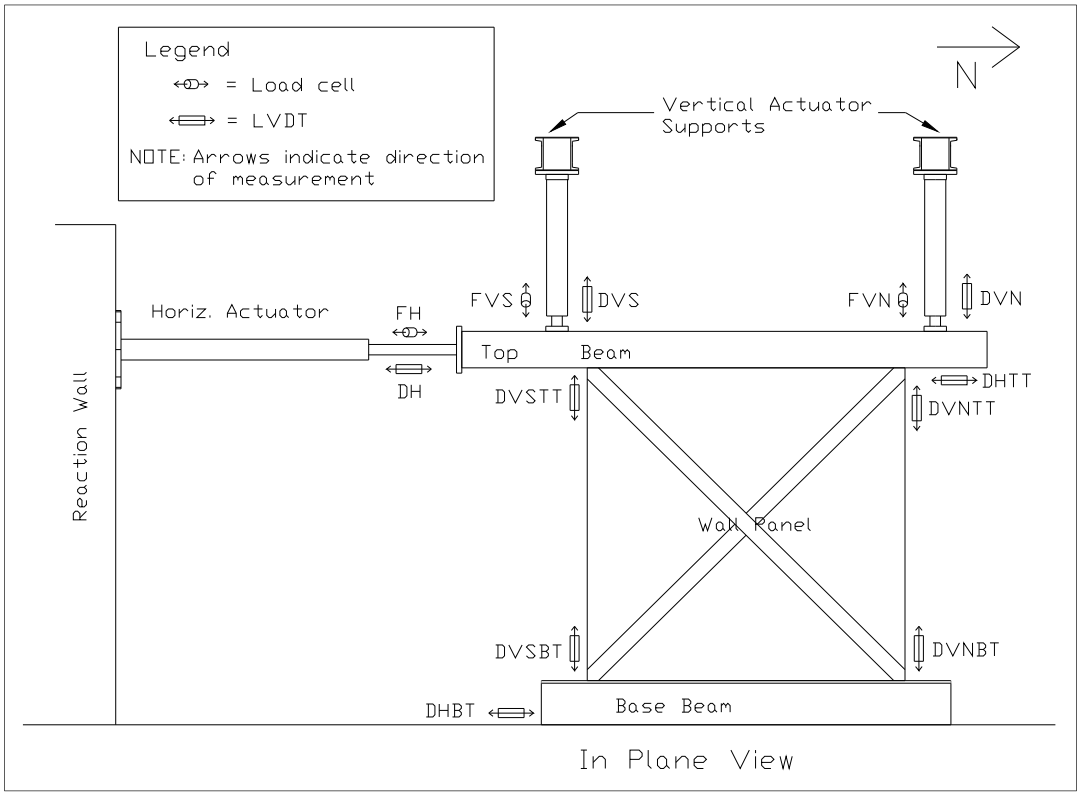

Instrumentation

Table D-2 defines the instrumentation required for all shear panel tests. Figure D-1 shows the location and orientation of all sensors, and Table D-2 describes the purpose of each sensor. The purpose of most gages is to ensure that no unwanted motion takes place and for test control. The only data used in reporting panel performance are the first, second, third, and fourth channels in Table D-2. The vertical actuator force measurements (FVS and FVN in Table D-2 and Figure D-1) are required to define total shear force when deflections reach large amplitudes, at which point the horizontal components of these forces become significant. This total shear force, TSF, is determined as follows:

$$TSF = FH - TVF\left\{sin\left[arctan\left(\frac{DH}{L}\right)\right]\right\} \quad \text{(Eq D1)}$$

where

FH = the measured horizontal actuator force (see Table D-2 or Figure D-1).

TVF = the total vertical actuator force, equal to FVS plus FVN (Table D-2 or Figure D-1).

DH = the measured horizontal displacement (Table D-2 or Figure D-1).

L = the length of the vertical actuators, with vertical load applied but no horizontal displacement.

Table D-2. Cold-formed steel shear panel instrumentation.

Channel #	Sensor Type	Measurement, Direction, Location and Symbol	Purpose
1	Load cell	Force Horizontal, FH	Horizontal actuator load measurement
2	LVDT	Deflection Horizontal, DH	Horizontal deflection, shear panel deformation
3	Load cell	Force Vertical South, FVS	Manual vertical load control (25k total load w/#5)
4	LVDT	Deflection Vertical South, DVS	Stroke (tied to #6)
5	Load cell	Force Vertical North, FVN	Load (summed with #3, for 25k total load)
6	LVDT	Deflection Vertical North, DVN	Controlled by #4 stroke feedback
7	LVDT	Defl Horiz Bot Track, DHBT	To ensure no slippage
8	LVDT	Defl Vert South Bot Track, DVSBT	To ensure no uplift
9	LVDT	Defl Vert North Bot Track, DVNBT	To ensure no uplift
10	LRDG* (20")	Defl Horiz Top Track, DHTT	Check for shear panel deformation - same as #2
11	LRDG (10")	Defl Vert South Top Track, DVSTT	Vertical panel/column deformation & rotation check
12	LRDG (10")	Defl Vert North Top Track, DVNTT	Vertical panel/column deformation & rotation check

*Linear resistance deflection gage, or cable-extension position transducer.

Test requirements

For each shear panel qualified, three specimens shall be fabricated and tested. This requirement assumes only minor variation in panel performance for a given shear panel. If large variations occur, more than three specimens shall be tested and a statistical evaluation of panel performance may be required. For panels with minor variation, one specimen shall be tested monotonically and two shall be tested cyclically, as defined below. All tests, both monotonic and cyclic, shall use stroke control, loading the panels laterally at a constant displacement per minute. The vertical load shall be held constant and the top beam shall be held horizontal throughout each test, as described previously under “Test Configuration.” Both monotonic and cyclic tests shall be conducted up to deflections that cause ultimate failure of the shear panels or reach the limits of the test equipment, but shall not be less than 10 times the lateral yield displacement of the test panel, δ_y. These deflections are very large (well beyond acceptable drift limits), but they are needed to ensure that brittle failures (sudden loss of lateral or vertical load-carrying capacity) do not occur near the useful deflection range of the panel.

Monotonic test protocol

A single specimen of each shear panel shall be loaded in one direction (monotonic) at a constant stroke rate that is slow enough to allow careful observation of panel performance and failure progression.[25] These observations shall include documentation of panel behavior through a log of observations with respect to displacement and photographs. Load versus deflection (TSF versus DH) shall be plotted to determine the measured lateral yield displacement, δ_y, and this value shall be used in defining the cyclic test protocol.

Cyclic test protocol

A minimum of two specimens of each panel configuration shall be loaded cyclically at a constant stroke rate that is slow enough to allow careful observation of panel performance and failure progression[26]. These observations shall include documentation of panel behavior through a log of observations with respect to displacement and photographs. Load versus deflection (TSF versus DH) shall be plotted to create load/deflection hysteretic envelopes. The cyclic load protocol follows a standard method, so that test results may be compared with cyclic test results of other systems. The protocol defined here is similar to SAC Phase 2 guidelines (SAC 1997) that have been modified to scale to the lateral yield deflection, as described in ATC-24 (ATC 1992). The SAC-recommended loading histories call for loading with a deformation parameter based on interstory drift angle, θ, defined as interstory displacement over interstory height. The commentary to SAC (1997) explains that the interstory drift angle of 0.005 radians corresponds to a conservative estimate of the value that would cause yield deformation. Therefore, the load protocol defined by SAC in terms of drift angle is scaled to the measured lateral yield deflection, δ_y, to define the cyclic test steps shown in Table D-3. This protocol calls for a set number of cycles at each of the deformation amplitudes shown in Table D-3. This protocol is illustrated by the deformation time history shown in Figure D-2, which is based on a lateral yield deflection, δ_y of 0.4 in. and stroke rate of 6 in. per minute.

---

[25] Monotonic tests reported in Chapter 7 used a stroke rate of 0.5 in. per minute.

[26] Cyclic tests reported in Chapter 7 used a stroke rate of 3 and 6 in. per minute. The faster stroke rate was used for panels tested cyclically beyond 10 in. (20 in. peak to peak).

Table D-3. Cyclic test load protocol.

Load Step #	SAC-2		Modified SAC Amplitude
	Number of Cycles, n	Peak Deformation, θ (radians)	
1	6	0.00375	$0.75\delta_y$
2	6	0.005	$1.0\delta_y$
3	6	0.0075	$1.5\delta_y$
4	4	0.01	$2\delta_y$
5	2	0.015	$3\delta_y$
6	2	0.02	$4\delta_y$
7	2	0.03	$6\delta_y$
8	2	0.04	$8\delta_y$
9	2	0.05	$10\delta_y$
10	2	0.06	$12\delta_y$
11	2	0.07	$14\delta_y$
12	2	0.08	$16\delta_y$
13	2	0.09	$18\delta_y$
14	2	0.10	$20\delta_y$
15	2	0.11	$22\delta_y$
16	2	0.12	$24\delta_y$
17	2	0.13	$26\delta_y$
18	2	0.14	$28\delta_y$
19	2	0.15	$30\delta_y$
20	2	0.16	$32\delta_y$

Shear panel performance documentation

Shear panel performance from both monotonic and cyclic tests shall be documented in terms of load versus deflection plots (TSF versus DH). Cyclic tests plot load versus deflection to define load-versus-deflection hysteretic envelopes. Observations of panel performance and failure progression with respect to lateral displacement shall be documented in a spreadsheet format. Photographs that document these observations shall be included in the test report. Test results for each specimen tested shall be summarized in the format shown in Table D-4. Repeatability of panel performance of a given configuration is critical so that if only two cyclic tests are conducted, the poorest performance of the two shall form the basis for design. Therefore, special consideration shall be given to large variations in panel performance, especially failure type or displacement amplitude of each type of failure. Test procedures and results shall be documented in a test report.

Figure D-2. Modified SAC cyclic test time history, with δ_y = 0.4 in. and 6 in./min stroke rate.

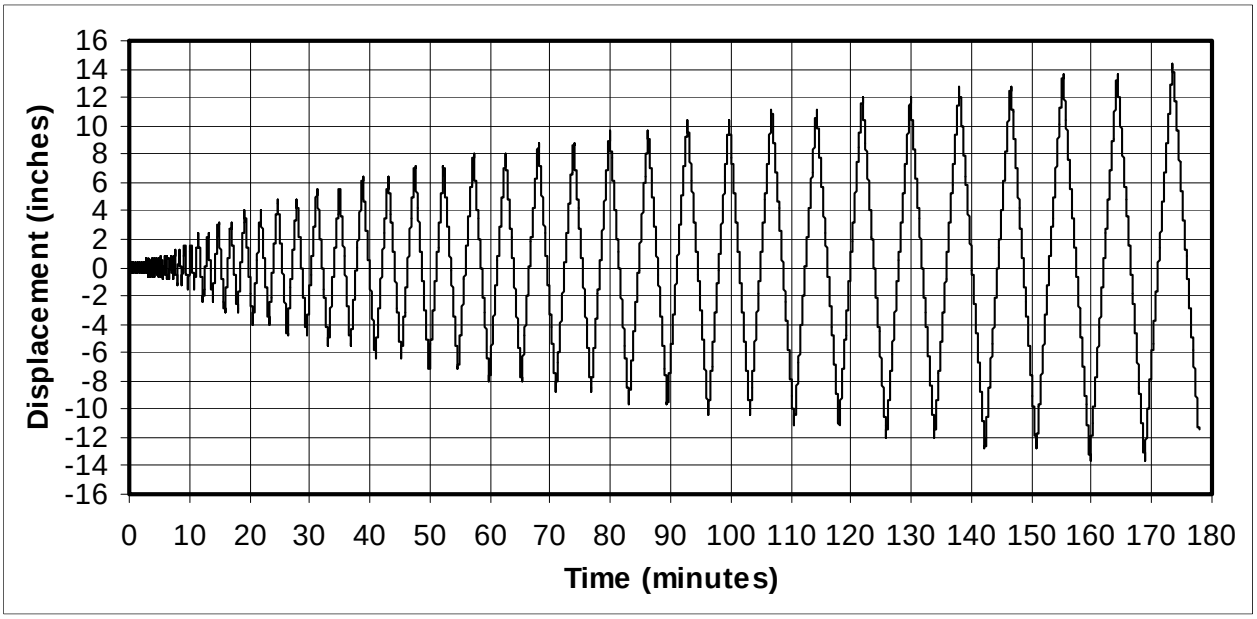

Table D-4. Summary of test panel performance (specified format).

Test Specimen	Load Type (Monotonic or Cyclic)	Load Rate (mm/min or in/min)	Linear Shear Stiffness (kN/mm) or (kips/in.)	Shear Load at δ_y Deflection (kip or kN)	Shear Deflection at Ultimate Shear Load (in. or mm)	Ultimate Shear Load (kip or kN)

Design recommendations

The measured load versus deflection data shall be used to define the design strength and stiffness of the shear panels. Resistance factors for each loading mechanism shall be defined that recognize the variation of the shear panel capacity. In other words, a panel shear capacity resistance factor, ϕ_v, shall reflect the variability of shear capacity of the tested panels. For example, ϕ_v = 0.9 if the strength variability is small and both mode and displacement of failures are consistent. The following criteria shall be defined from the shear panel cyclic test data:

1. The panel ductility, μ, the ultimate lateral deflection without loss of lateral or vertical load capacity, δ_u, over yield lateral deflection, δ_y, defined as follows:

$$\mu = \frac{\delta_u}{\delta_y} \quad \text{(Eq D2)}$$

2. The panel overstrength, Ω,[27] the maximum measured ultimate lateral panel capacity, Q_u, over the yield capacity, Q_y, defined as follows:

$$\Omega = \frac{Q_u}{Q_y} \quad \text{(Eq D3)}$$

3. The panel redundancy factor, ρ_1, of the individual shear panel tested[28]. This redundancy can be seen by comparing shear panel load/deflection data with coupon data, to determine if overstrength, Ω is due to strain hardening of the primary load-carrying element or due to the action of a secondary lateral load-resisting element. An example of this would be a panel with diagonal straps acting as the primary element with the columns effectively working to provide a significant moment frame. In this case the moment frame would provide redundancy for the shear panel. If the diagonal straps fail, this moment frame capacity would provide lateral resistance for the moment from the P-delta effect of the gravity load. This redundancy is critical to preventing building collapse for a structure whose lateral load-resisting system has failed. The panel redundancy factor, ρ_1 is calculated as follows:

$$\rho_1 = \frac{Q_u}{Q_p} = \frac{Q_p + Q_q}{Q_p} \quad \text{(Eq D4)}$$

where

Q_p = the portion of the shear panel ultimate lateral capacity carried by the primary lateral load-resisting element including the effects of strain hardening. For panels with full panel sheet(s), this contribution will increase with increasing deflection due to a widening of the panel tension field. This value can only be reasonably determined by measuring Q_c (as described below) and calculating Q_p as the difference between Q_u and Q_c.

Q_c = the portion of shear panel ultimate lateral capacity carried by the columns acting as moment frames. For panels with full

[27] This should not be confused with the system overstrength factor, Ω_0, as defined in ASCE 7-10 (ASCE 2010), Section 12.2.1.

[28] This should not be confused with the reliability factor, ρ or ρ_x, which is the extent of structural redundancy in the lateral-force-resisting system for an entire story of a building.

panel sheet(s), this value can only be obtained by testing the same exact panels with the full panel sheets removed. If these tests are not performed for full panel sheet shear panels, Q_c shall be set equal to zero.

4. The width of the cyclic test load/deflection hysteretic envelope. If the hysteretic envelope is significantly pinched (no or very little load resistance away from the peak excursions), much less energy is absorbed by the structural system so that building amplification grows. Pinched hysteretic envelopes occur when the primary lateral load-resisting element is stretched, and there is little redundant capacity from other elements to pick up load, so that little resistance is available away from the peak excursions of the load cycles. Panels with significantly pinched hysteretic envelopes, can experience high acceleration impact loading because the building will be free to sway with little resistance and then suddenly snap the lateral load-resisting element when another peak excursion is reached. This high acceleration snap can cause brittle failures. A shear panel with a great deal of redundancy within the panel, ρ_1 will tend to have a wide hysteretic envelope.

Table D-5 defines the acceptance criteria in terms of μ, Ω and ρ_1, based on data measured in the cyclic panel tests as defined by Equations D2 through D4.

Values for the system response modification coefficient, R; system overstrength factor, Ω_0; and deflection amplification factor, C_d, are defined in Table D-6. These values are used in the seismic design guidance defined in ASCE/SEI 7-10. Exceptions to these criteria shall require AISI approval or Corps of Engineers Headquarters (CEMP-ET) approval for Department of Defense construction.

Table D-5. Acceptance criteria for shear panels based on μ, Ω, and ρ_1.

Criteria	Acceptance Requirement
Panel ductility, μ	≥ 10
Panel overstrength, Ω	≥ 1.3
Panel redundancy factor, ρ_1	≥ 1.0
Hysteretic envelope width	Not required

Table D-6. Values for R, Ω_0, and C_d.

Factor	Value
System response modification coefficient, R	4
System overstrength factor, Ω_0	2
Deflection amplification factor, C_d	3.5

REPORT DOCUMENTATION PAGE

Form Approved
OMB No. 0704-0188

1. REPORT DATE (DD-MM-YYYY)	2. REPORT TYPE	3. DATES COVERED (From - To)
August 2015	Final	

4. TITLE AND SUBTITLE
Development Of Cold-Formed Steel Seismic Design Recommendations

5a. CONTRACT NUMBER

5b. GRANT NUMBER

5c. PROGRAM ELEMENT NUMBER
RDTE PE 611102T23

6. AUTHOR(S)
James Wilcoski and Douglas A. Foutch

5d. PROJECT NUMBER
CFM-E021

5e. TASK NUMBER

5f. WORK UNIT NUMBER

7. PERFORMING ORGANIZATION NAME(S) AND ADDRESS(ES)
U.S. Army Engineer Research and Development Center
Construction Engineering Research Laboratory
P.O. Box 9005
Champaign, IL 61826-9005

8. PERFORMING ORGANIZATION REPORT NUMBER
ERDC/CERL TR-15-16

9. SPONSORING / MONITORING AGENCY NAME(S) AND ADDRESS(ES)
Headquarters, U.S. Army Corps of Engineers
441 G Street NW
Washington, DC 20314-1000

10. SPONSOR/MONITOR'S ACRONYM(S)
HQUSACE

11. SPONSOR/MONITOR'S REPORT NUMBER(S)

12. DISTRIBUTION / AVAILABILITY STATEMENT
Approved for public release; distribution is unlimited.

13. SUPPLEMENTARY NOTES

14. ABSTRACT

Cold-formed steel-wall construction is a versatile and affordable technology used extensively as the gravity- and lateral-load-resisting structural system for low-rise construction. Structural design guidance for cold-formed steel members was first published in 1946, but in the 1990s the Corps of Engineers imposed a moratorium on its own use of these systems after identifying detailing and construction practices that would prevent adequate ductile performance under seismic loading. At that time, the Corps initiated the first of several applied engineering and basic research studies to investigate light-gage steel design and construction methods that provide the required ductility while conforming with applicable steel-industry specifications. That research produced design guidelines that enabled the Corps to lift its moratorium, including two updates incorporating the results of follow-on studies.

This technical report, prepared with funding support from the National Institute of Standards and Technology, compiles for the first time the complete results of three Army Research, Development, Test, and Evaluation studies on cold-formed steel design and validation. The report includes detailed, updated design recommendations for ductile structural performance in seismic events and a sample design problem to illustrate application of the recommendations.

15. SUBJECT TERMS
cold-formed steel; seismic loading; design guidelines; evaluation; structural performance; light-gage steel construction

16. SECURITY CLASSIFICATION OF:			17. LIMITATION OF ABSTRACT	18. NUMBER OF PAGES	19a. NAME OF RESPONSIBLE PERSON
a. REPORT	b. ABSTRACT	c. THIS PAGE			19b. TELEPHONE NUMBER (include area code)
Unclassified	Unclassified	Unclassified		361	